

Curso 2006/07  
**CIENCIAS Y TECNOLOGÍAS/7**  
I.S.B.N.: 978-84-7756-743-1

**JORGE PASÁN GARCÍA**

**Molecular magnetic materials:  
influence of the weak interactions in the structural  
and magnetic behaviour of malonate complexes**

**Directores**

**CATALINA RUIZ PÉREZ  
JOAQUÍN SANCHIZ SUÁREZ**



**SOPORTES AUDIOVISUALES E INFORMÁTICOS**  
**Serie Tesis Doctorales**

Este trabajo de Tesis es una realidad gracias a la financiación por parte del Ministerio de Educación y Ciencia a través de una beca predoctoral de Formación del Profesorado Universitario (ref. AP2001-3322). La investigación ha sido financiada por los proyectos del Gobierno de Canarias PI2002/175 y del Ministerio de Educación y Ciencia BQU2001-3794 y MAT2004-03112.

Las medidas presentadas en este trabajo de Tesis han sido realizadas gracias a los Servicios Generales de apoyo a la Investigación de la Universidad de La Laguna, especialmente al Servicio de Difracción de Rayos X.

## Acknowledgements

Este trabajo no habría sido posible sin que muchas personas aunaran sus esfuerzos, y no sólo por aquéllas que más han influido en el trabajo científico, sino especialmente por las que han hecho de estos cuatro años y pico de investigación una experiencia inolvidable.

En primer lugar quisiera nombrar a mis directores: a Caty, que me ha introducido en el mundo de la investigación, me ha dado la oportunidad de trabajar en su laboratorio, y con la que he compartido ciencia y vida en infinitos cafés matutinos; y a Joaquín, que me ha enseñado casi toda la química que he aprendido en estos cuatro años.

A Miguel y a Paco, porque he aprendido más de ellos de lo que pudieran creer, por su hospitalidad y por su amistad desinteresada. Estimado Miguel, gracias además, por leer y corregir esta Tesis.

A Fernando, Laura y Oscar, que han colaborado activamente en la elaboración de la Tesis, con los que he compartido congresos y Naturals, tertulias y cafés y que han sido estupendos compañeros de trabajo. También a María Laz, María Hernández y Jose Ramón, que me han animado mucho y porque lo hemos pasado bien.

A Lumi, Emilio, Xelo, Alicia (y a Pepe), Eugenia, y a Juanma por los buenos ratos que hemos pasado por Valencia y por el mundo. Y al resto de gente de Valencia, Joan, Rafa, Miguel, Alicia, Amparo, Ana, Chema...

A los profesores Juan Rodríguez y Annie Powell, por acogerme en el LLB y en la Universidad de Karlsruhe. También a Javier Campo por ayudarme con el magnetismo y enseñarme Zaragoza.

A Romén, Claudio, Sergio, Manuel, María, Dani, Cecilia, Adán, Sara... a Leonardo por el proyecto. También a Pepe, Romén, Jonay, David, Carlos... por el fútbol y porque aunque ya son muchos años, cuando nos vemos, parece que no hubiera pasado el tiempo. A Cristina y Miguel, a Rubén y Helena por haber aguantado estoicamente mis charlas magnéticas.

A mi madre y a mi hermana porque han sido un apoyo constante y a mi padre por una filosofía de vida.

Y finalmente, tengo que agradecer a Marina el compartir este proyecto de vida en el que nos hemos embarcado, y que haya sido un continuo estímulo para concluir este trabajo de Tesis.

*“Si buscas resultados distintos, no hagas siempre lo mismo”*

*Albert Einstein*

*“Nothing shocks me. I’m a scientist”*

*Indiana Jones*



*A mis padres*

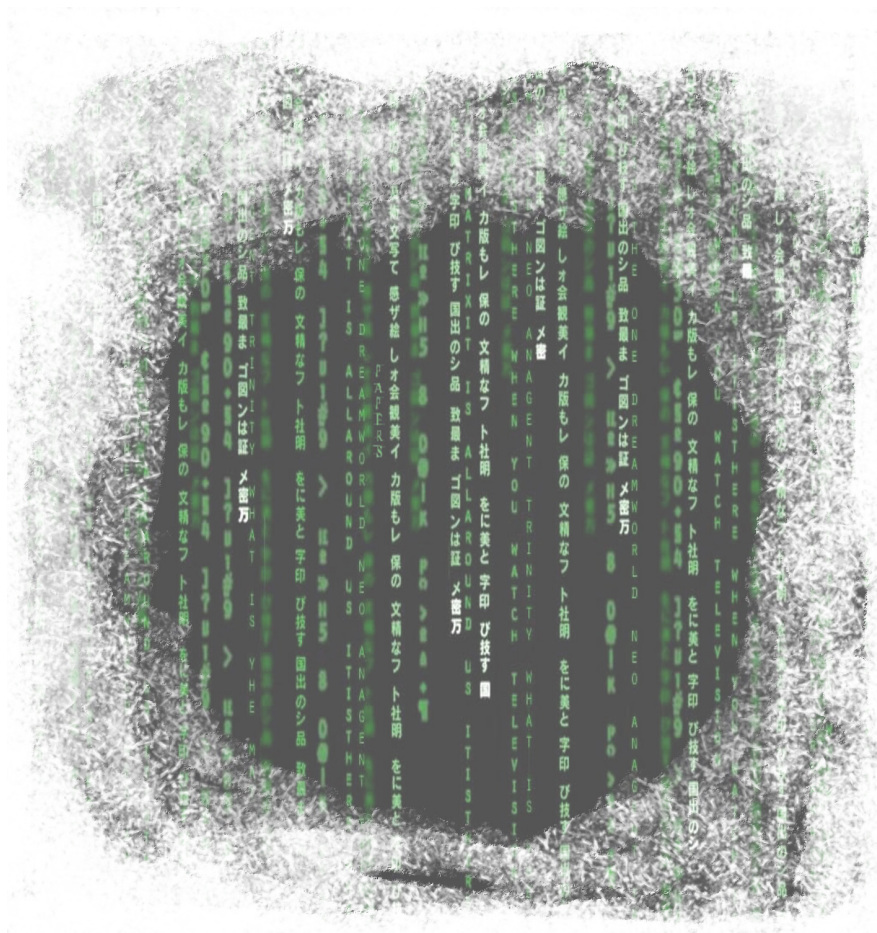
---

---

# Index

---

---



---

|                                                                                                  |           |
|--------------------------------------------------------------------------------------------------|-----------|
| <b>GLOSSARY</b>                                                                                  | <b>x</b>  |
| <b>INTRODUCTION</b>                                                                              | <b>1</b>  |
| <b>1. Molecular magnetic materials</b>                                                           | <b>3</b>  |
| <b>2. Coordination Polymers: a Way towards Tunable Magnets</b>                                   | <b>4</b>  |
| 2.1. Modules as Building Blocks                                                                  | 5         |
| 2.2. Synthetic Methods: Molecular Self-Assembly                                                  | 8         |
| <b>3. Flexible Aliphatic Dicarboxylates</b>                                                      | <b>10</b> |
| 3.1. The Malonic Acid                                                                            | 10        |
| 3.2. New Malonate-Based Coordination Networks:<br>Design and Application                         | 12        |
| <b>4. References</b>                                                                             | <b>14</b> |
| <b>OBJECTIVES</b>                                                                                | <b>17</b> |
| <b>CHAPTER I. PHENYLMALONATE COMPLEXES</b>                                                       | <b>21</b> |
| <b>I.1. Copper(II)-Phenylmalonate (1)</b>                                                        | <b>23</b> |
| I.1.1. Introduction                                                                              | 23        |
| I.1.2. Synthesis                                                                                 | 23        |
| I.1.3. Description of the Structure                                                              | 24        |
| I.1.4. Magnetic Properties                                                                       | 28        |
| I.1.5. Conclusion                                                                                | 32        |
| I.1.6. References                                                                                | 33        |
| <b>I.2. Pyrimidine (2) and Pyrazine (3) Copper(II)-Phenylmalonate<br/>Complexes</b>              | <b>34</b> |
| I.2.1. Introduction                                                                              | 34        |
| I.2.2. Synthesis                                                                                 | 34        |
| I.2.3. Description of the Structure                                                              | 35        |
| I.2.4. Magnetic Properties                                                                       | 39        |
| I.2.5. Conclusion                                                                                | 44        |
| I.2.6. References                                                                                | 45        |
| <b>I.3. 3-Cyanopyridine (4) and 4-Cyanopyridine (5) Copper(II)-<br/>Phenylmalonate Complexes</b> | <b>46</b> |

---

|                                                                                                                                           |           |
|-------------------------------------------------------------------------------------------------------------------------------------------|-----------|
| I.3.1. Introduction                                                                                                                       | 46        |
| I.3.2. Synthesis                                                                                                                          | 46        |
| I.3.3. Description of the Structure                                                                                                       | 47        |
| I.3.4. Magnetic Properties                                                                                                                | 50        |
| I.3.5. Conclusion                                                                                                                         | 55        |
| I.3.6. References                                                                                                                         | 55        |
| <b>I.4. Nicotinamide (6) and Isonicotinamide (7) Copper(II)-Phenylmalonate complexes</b>                                                  | <b>56</b> |
| I.4.1. Introduction                                                                                                                       | 56        |
| I.4.2. Synthesis                                                                                                                          | 56        |
| I.4.3. Description of the Structure                                                                                                       | 57        |
| I.4.4. Magnetic Properties                                                                                                                | 60        |
| I.4.5. Conclusion                                                                                                                         | 63        |
| I.4.6. References                                                                                                                         | 63        |
| <b>I.5. 3-Fluoropyridine (8), 3-Chloropyridine (9), 3-Bromopyridine (10), and 3-Iodopyridine (11) Copper(II)-Phenylmalonate complexes</b> | <b>65</b> |
| I.5.1. Introduction                                                                                                                       | 65        |
| I.5.2. Synthesis                                                                                                                          | 65        |
| I.5.3. Description of the Structure                                                                                                       | 66        |
| I.5.4. Magnetic Properties                                                                                                                | 70        |
| I.5.5. Conclusion                                                                                                                         | 74        |
| I.5.6. References                                                                                                                         | 74        |
| <b>I.6. 2,4'-Bipyridine (12) Copper(II)-Phenylmalonate complex</b>                                                                        | <b>76</b> |
| I.6.1. Introduction                                                                                                                       | 76        |
| I.6.2. Synthesis                                                                                                                          | 76        |
| I.6.3. Description of the Structure                                                                                                       | 77        |
| I.6.4. Magnetic Properties                                                                                                                | 82        |
| I.6.5. Conclusion                                                                                                                         | 84        |
| I.6.6. References                                                                                                                         | 85        |
| <b>I.7. 4,4'-Bipyridine (13) Copper(II)-Phenylmalonate complex</b>                                                                        | <b>86</b> |
| I.7.1. Introduction                                                                                                                       | 86        |
| I.7.2. Synthesis                                                                                                                          | 86        |
| I.7.3. Description of the Structure                                                                                                       | 86        |
| I.7.4. Magnetic Properties                                                                                                                | 90        |



---

|                                                                                         |            |
|-----------------------------------------------------------------------------------------|------------|
| I.7.5. Conclusion                                                                       | 91         |
| I.7.6. References                                                                       | 92         |
| <b>I.8. 2,2'-Bipyrimidine (14) and 1,10-Phenantroline (15)</b>                          |            |
| <b>Copper(II)-Phenylmalonate complexes</b>                                              | <b>93</b>  |
| I.8.1. Introduction                                                                     | 93         |
| I.8.2. Synthesis                                                                        | 93         |
| I.8.3. Description of the Structure                                                     | 94         |
| I.8.4. Magnetic Properties                                                              | 98         |
| I.8.5. Conclusion                                                                       | 100        |
| I.8.6. References                                                                       | 101        |
| <b>I.9. 2,2'-Bipyridine (16) Copper(II)-Phenylmalonate complex</b>                      | <b>102</b> |
| I.9.1. Introduction                                                                     | 102        |
| I.9.2. Synthesis                                                                        | 102        |
| I.9.3. Description of the Structure                                                     | 102        |
| I.9.4. Magnetic Properties                                                              | 106        |
| I.9.5. Conclusion                                                                       | 106        |
| I.9.6. References                                                                       | 106        |
| <br>                                                                                    |            |
| <b>CHAPTER II. METHYLMALONATE COMPLEXES</b>                                             | <b>107</b> |
| <b>II.1. Copper(II)-Methylmalonate (17)</b>                                             | <b>109</b> |
| II.1.1. Introduction                                                                    | 109        |
| II.1.2. Synthesis                                                                       | 109        |
| II.1.3. Description of the Structure                                                    | 109        |
| II.1.4. Magnetic Properties                                                             | 112        |
| II.1.5. Conclusion                                                                      | 115        |
| II.1.6. References                                                                      | 115        |
| <b>II.2. Pyrazine (18) and 4,4'-bipyridine (19) Copper(II)-Methylmalonate complexes</b> | <b>117</b> |
| II.2.1. Introduction                                                                    | 117        |
| II.2.2. Synthesis                                                                       | 117        |
| II.2.3. Description of the Structure                                                    | 118        |
| II.2.4. Magnetic Properties                                                             | 122        |
| II.2.5. Conclusion                                                                      | 124        |
| II.2.6. References                                                                      | 125        |

---

|                                                                                               |            |
|-----------------------------------------------------------------------------------------------|------------|
| <b>II.3. 4-Cyanopyridine (20) Copper(II)-Methylmalonate complex</b>                           | <b>126</b> |
| II.3.1. Introduction                                                                          | 126        |
| II.3.2. Synthesis                                                                             | 126        |
| II.3.3. Description of the Structure                                                          | 127        |
| II.3.4. Magnetic Properties                                                                   | 130        |
| II.3.5. Conclusion                                                                            | 132        |
| II.3.6. References                                                                            | 132        |
| <b>II.4. 3-Iodopyridine (21) and 2,4'-bipyridine (22) Copper(II)-Methylmalonate complexes</b> | <b>133</b> |
| II.4.1. Introduction                                                                          | 133        |
| II.4.2. Synthesis                                                                             | 133        |
| II.4.3. Description of the Structure                                                          | 134        |
| II.4.4. Magnetic Properties                                                                   | 138        |
| II.4.5. Conclusion                                                                            | 140        |
| II.4.6. References                                                                            | 141        |
| <b>II.5. 2,2'-bipyrimidine (22) Copper(II)-Methylmalonate complexes</b>                       | <b>142</b> |
| II.5.1. Introduction                                                                          | 142        |
| II.5.2. Synthesis                                                                             | 142        |
| II.5.3. Description of the Structure                                                          | 143        |
| II.5.4. Magnetic Properties                                                                   | 145        |
| II.5.5. Conclusion                                                                            | 147        |
| II.5.6. References                                                                            | 148        |
| <b>II.6. 2,2'-bipyridine (24) Copper(II)-Methylmalonate Complex</b>                           | <b>149</b> |
| II.6.1. Introduction                                                                          | 149        |
| II.6.2. Synthesis                                                                             | 149        |
| II.6.3. Description of the Structure                                                          | 150        |
| II.6.4. Magnetic Properties                                                                   | 154        |
| II.6.5. Conclusion                                                                            | 154        |
| II.6.6. References                                                                            | 154        |
| <b>II.7. 4,4'-Bipyridine Copper(II)-Methylmalonate Complexes (19, 25 and 26)</b>              | <b>156</b> |
| II.7.1. Introduction                                                                          | 156        |
| II.7.2. Synthesis                                                                             | 156        |
| II.7.3. Crystallographic Analysis                                                             | 157        |

---

|                                                                              |            |
|------------------------------------------------------------------------------|------------|
| II.7.4. Description of the Structure                                         | 158        |
| II.7.5. Magnetic Properties                                                  | 166        |
| II.7.6. Conclusion                                                           | 169        |
| II.7.7. References                                                           | 170        |
| <b>II.8. 1,2-bis(4-pyridyl)ethene (27) Copper(II)-Methylmalonate Complex</b> | <b>171</b> |
| II.8.1. Introduction                                                         | 171        |
| II.8.2. Synthesis                                                            | 171        |
| II.8.3. Description of the Structure                                         | 172        |
| II.8.4. Magnetic Properties                                                  | 175        |
| II.8.5. Conclusion                                                           | 177        |
| II.8.6. References                                                           | 177        |
| <br>                                                                         |            |
| <b>CHAPTER III. ETYLMALONATE COMPLEXES</b>                                   | <b>179</b> |
| <b>III.1. Copper(II)-Ethylmalonate (28, 29 and 30)</b>                       | <b>181</b> |
| III.1.1. Introduction                                                        | 181        |
| III.1.2. Synthesis                                                           | 182        |
| III.1.3. Description of the Structure                                        | 184        |
| III.1.4. Magnetic Properties                                                 | 197        |
| III.1.5. Conclusion                                                          | 201        |
| III.1.6. References                                                          | 201        |
| <b>III.2. Sodium(I)-Copper(II)-Ethylmalonate (31 and 32)</b>                 | <b>203</b> |
| III.2.1. Introduction                                                        | 203        |
| III.2.2. Synthesis                                                           | 203        |
| III.2.3. Description of the Structure                                        | 204        |
| III.2.4. Magnetic Properties                                                 | 211        |
| III.2.5. Conclusion                                                          | 212        |
| III.2.6. References                                                          | 212        |
| <b>III.3. 2,2'-bipyrimidine Copper(II)-Ethylmalonate (33)</b>                | <b>214</b> |
| III.3.1. Introduction                                                        | 214        |
| III.3.2. Synthesis                                                           | 214        |
| III.3.3. Description of the Structure                                        | 215        |
| III.3.4. Magnetic Properties                                                 | 217        |
| III.3.5. Conclusion                                                          | 219        |
| III.3.6. References                                                          | 219        |

---

|                                                                                     |            |
|-------------------------------------------------------------------------------------|------------|
| <b>III.4. 2,2'-bipyridine (34) and 1,10-phenantroline (35)</b>                      |            |
| <b>Copper(II)-Ethylmalonate Complexes</b>                                           | <b>220</b> |
| III.4.1. Introduction                                                               | 220        |
| III.4.2. Synthesis                                                                  | 220        |
| III.4.3. Description of the Structure                                               | 221        |
| III.4.4. Magnetic Properties                                                        | 225        |
| III.4.5. Conclusion                                                                 | 225        |
| III.4.6. References                                                                 | 225        |
| <br>                                                                                |            |
| <b>CHAPTER IV. STRUCTURAL AND MAGNETIC DISCUSSION</b>                               | <b>227</b> |
| <b>IV.1. Structural Discussion</b>                                                  | <b>229</b> |
| IV.1.1. Introduction                                                                | 229        |
| IV.1.2. Analysis of the Crystal Data                                                | 229        |
| IV.1.2.1. Space Groups                                                              | 229        |
| IV.1.2.2. Chirality                                                                 | 230        |
| IV.1.2.3. R-malonate Conformations                                                  | 234        |
| IV.1.2.4. Water Motifs                                                              | 237        |
| IV.1.3. The Copper(II)-R-malonate System                                            | 239        |
| IV.1.4. References                                                                  | 244        |
| <b>IV.2. Magneto-structural discussion</b>                                          | <b>245</b> |
| IV.2.1. Nature of the Magnetic Interaction                                          | 245        |
| IV.2.2. Magnitude of the Magnetic Interaction                                       | 246        |
| IV.2.3. Magneto-structural relationships in square grid layered<br>Cu(II) complexes | 247        |
| IV.2.4. References                                                                  | 254        |
| <br>                                                                                |            |
| <b>CHAPTER V. PERSPECTIVES</b>                                                      | <b>255</b> |
| <b>V.1. Molecular Magnetic Materials</b>                                            | <b>257</b> |
| V.1.1. Introduction                                                                 | 257        |
| V.1.2. Along the Thesis-work line: Copper(II)-Benzylmalonate (36)                   | 257        |
| V.1.3. The substituent as an 'active' part of the ligand                            | 262        |
| V.1.3.1. 2-Hydroxy-2-phenylmalonate (37)                                            | 262        |
| V.1.3.2. Ketomalonic acid (38)                                                      | 268        |

|                                                                                                           |            |
|-----------------------------------------------------------------------------------------------------------|------------|
| V.1.3.3. [Cu <sub>4</sub> (pz) <sub>4</sub> (OH-ppac) <sub>2</sub> (H <sub>2</sub> O) <sub>4</sub> ] (39) | 274        |
| V.1.4. References                                                                                         | 278        |
| <b>V.2. Porous Materials</b>                                                                              | <b>281</b> |
| V.2.1. References                                                                                         | 284        |
| <b>V.3. Chiral Materials</b>                                                                              | <b>285</b> |
| V.3.1. References                                                                                         | 285        |
| <br>                                                                                                      |            |
| <b>CONCLUSION</b>                                                                                         | <b>287</b> |
| <br>                                                                                                      |            |
| <b>EXPERIMENTAL</b>                                                                                       | <b>291</b> |
| <br>                                                                                                      |            |
| <b>ÍNDICE</b>                                                                                             | <b>295</b> |
| <br>                                                                                                      |            |
| <b>RESUMEN</b>                                                                                            | <b>305</b> |
| <br>                                                                                                      |            |
| <b>ANNEXE</b>                                                                                             | <b>321</b> |

## Glossary

Abbreviations used in this Thesis:

|                         |                                            |            |                          |
|-------------------------|--------------------------------------------|------------|--------------------------|
| H <sub>2</sub> mal      | Malonic acid                               | nic        | Nicotinamide             |
| H <sub>2</sub> Phmal    | Phenylmalonic acid                         | isonic     | Isonicotinamide          |
| H <sub>2</sub> Memal    | Methylmalonic acid                         | 3-Fpy      | 3-Fluoropyridine         |
| H <sub>2</sub> Etmal    | Ethylmalonic acid                          | 3-Clpy     | 3-Chloropyridine         |
| H <sub>2</sub> ox       | Oxalic acid                                | 3-Brpy     | 3-Bromopyridine          |
| H <sub>2</sub> Bzmal    | Benzylmalonic acid                         | 3-Ipy      | 3-Iodopyridine           |
| H <sub>2</sub> Ketomal  | Ketomalonic acid                           | 2,4'-bpy   | 2,4'-Bipyridine          |
| OH-H <sub>2</sub> Phmal | 2-Hydroxy-2-phenylmalonate                 | 4,4'-bpy   | 4,4'-Bipyridine          |
| OH-ppac                 | 2-Hydroxy-2-phenyl-2-(1-pyrazolyl)-acetate | 2,2'-bipym | 2,2'-Bipyrimidine        |
| pym                     | Pyrimidine                                 | 2,2'-bpy   | 2,2'-Bipyridine          |
| pyz                     | Pyrazine                                   | phen       | 1,10-Phenantroline       |
| 3-CNpy                  | 3-Cyanopyridine                            | bpe        | 1,2-Bis(4-pyridyl)ethene |
| 4-CNpy                  | 4-Cyanopyridine                            | Pz         | Pyrazole                 |

A list of the compounds presented in this Thesis with the Section where they are presented:

| Formula                                                                      | Number | Section |
|------------------------------------------------------------------------------|--------|---------|
| {[Cu(H <sub>2</sub> O) <sub>3</sub> ][Cu(Phmal) <sub>2</sub> ]} <sub>n</sub> | 1      | I.1     |
| [Cu(pym)(Phmal)] <sub>n</sub>                                                | 2      | I.2     |
| [Cu(pyz)(Phmal)] <sub>n</sub>                                                | 3      | I.2     |
| [Cu(3-CNpy)(Phmal)] <sub>n</sub>                                             | 4      | I.3     |
| [Cu(4-CNpy)(Phmal)] <sub>n</sub>                                             | 5      | I.3     |
| [Cu(nic)(Phmal)(H <sub>2</sub> O)] <sub>n</sub>                              | 6      | I.4     |
| [Cu(isonic)(Phmal)(H <sub>2</sub> O)] <sub>n</sub>                           | 7      | I.4     |
| [Cu(3-Fpy)(Phmal)] <sub>n</sub>                                              | 8      | I.5     |
| [Cu(3-Clpy)(Phmal)] <sub>n</sub>                                             | 9      | I.5     |
| [Cu(3-Brpy)(Phmal)] <sub>n</sub>                                             | 10     | I.5     |
| [Cu(3-Ipy)(Phmal)] <sub>n</sub>                                              | 11     | I.5     |
| [Cu(2,4'-bpy)(Phmal)(H <sub>2</sub> O)] <sub>n</sub>                         | 12     | I.6     |
| [Cu(4,4'-bpy)(Phmal)] <sub>n</sub> ·2nH <sub>2</sub> O                       | 13     | I.7     |
| [Cu(2,2'-bipym)(Phmal)] <sub>n</sub>                                         | 14     | I.8     |
| [Cu(phen)(Phmal)] <sub>n</sub> ·3nH <sub>2</sub> O                           | 15     | I.8     |
| [Cu(2,2'-bpy)(Phmal)(H <sub>2</sub> O)]·2H <sub>2</sub> O                    | 16     | I.9     |
| [Cu(Memal)(H <sub>2</sub> O)] <sub>n</sub>                                   | 17     | II.1    |
| [Cu(pyz)(Memal)] <sub>n</sub>                                                | 18     | II.2    |

| <b>Formula</b>                                                                                                                                                               | <b>Number</b> | <b>Section</b> |
|------------------------------------------------------------------------------------------------------------------------------------------------------------------------------|---------------|----------------|
| $[\text{Cu}(4,4'\text{-bpy})(\text{Memal})]_n$                                                                                                                               | 19            | II.2           |
| $[\text{Cu}(4\text{-CNpy})(\text{Memal})(\text{H}_2\text{O})]_n$                                                                                                             | 20            | II.3           |
| $[\text{Cu}(3\text{-Ipy})(\text{Memal})(\text{H}_2\text{O})]_n$                                                                                                              | 21            | II.4           |
| $[\text{Cu}(2,4'\text{-bpy})(\text{Memal})(\text{H}_2\text{O})]_n \cdot 3\text{H}_2\text{O}$                                                                                 | 22            | II.4           |
| $[\text{Cu}_2(2,2'\text{-bipym})(\text{Memal})_2(\text{H}_2\text{O})_2] \cdot 3\text{H}_2\text{O}$                                                                           | 23            | II.5           |
| $[\text{Cu}(2,2'\text{-bpy})(\text{Memal})(\text{H}_2\text{O})] \cdot 2\text{H}_2\text{O}$                                                                                   | 24            | II.6           |
| $\{[\text{Cu}(4,4'\text{-bpy})_2][\text{Cu}(4,4'\text{-bpy})_2(\text{Memal})(\text{NO}_3)(\text{H}_2\text{O})]\}_n \cdot n\text{NO}_3 \cdot 4n\text{H}_2\text{O}$            | 25            | II.7           |
| $[\text{Cu}(4,4'\text{-bpy})_2(\text{Memal})(\text{H}_2\text{O})]_n \cdot n\text{H}_2\text{O}$                                                                               | 26            | II.7           |
| $[\text{Cu}(\text{bpe})(\text{Memal})]_n \cdot 3n\text{H}_2\text{O}$                                                                                                         | 27            | II.8           |
| $\{[\text{Cu}(\text{H}_2\text{O})_4][\text{Cu}(\text{Etmal})_2(\text{H}_2\text{O})]\}_n$                                                                                     | 28            | III.1          |
| $[\text{Cu}(\text{Etmal})(\text{H}_2\text{O})]_n$                                                                                                                            | 29            | III.1          |
| $[\text{Cu}(\text{Etmal})(\text{H}_2\text{O})]_n \cdot 1.65n\text{H}_2\text{O}$                                                                                              | 30            | III.1          |
| $\text{Na}_6[\text{Cu}(\text{Etmal})_2(\text{H}_2\text{O})]_3 \cdot 5\text{H}_2\text{O}$                                                                                     | 31            | III.2          |
| $\{\text{Na}_3[\text{Cu}_3(\text{H}_2\text{O})_3][\text{Cu}_3(\text{Etmal})_6(\text{H}_2\text{O})_3]\}_n \cdot n\text{H}_2\text{O} \cdot n(\text{EtO})_2 \cdot n\text{NO}_3$ | 32            | III.2          |
| $[\text{Cu}_2(2,2'\text{-bipym})(\text{Etmal})_2(\text{H}_2\text{O})_2] \cdot 6\text{H}_2\text{O}$                                                                           | 33            | III.3          |
| $[\text{Cu}(2,2'\text{-bpy})(\text{Etmal})(\text{H}_2\text{O})] \cdot 3\text{H}_2\text{O}$                                                                                   | 34            | III.4          |
| $[\text{Cu}(\text{phen})(\text{Etmal})(\text{H}_2\text{O})] \cdot 3\text{H}_2\text{O}$                                                                                       | 35            | III.4          |

---

---

# Introduction

---

---





## 1. Molecular magnetic materials

The molecular magnetic materials exhibiting spontaneous magnetization are based on molecules rather than on metallic or ionic lattices.<sup>1</sup> Interesting advantages are obtained from this molecule-based approach compared with the ‘classical’ magnets. Among them, the low density, transparency and the possibility of combining different physical properties in a single material are the most remarkable ones. To design these molecule-based magnetic materials one must assemble the magnetic molecular units in such a way that the interaction between the local spin centres at the scale of the molecular unit leads to a non-zero spin value.<sup>2</sup>

Different strategies can be followed to achieve this goal: (i) all the interactions between the nearest neighbours are ferromagnetic; thus, all the spins tend to align parallel and a ferromagnetic transition is expected at the critical temperature ( $T_c$ ); (ii) antiferromagnetic interactions are dominant between nearest neighbours, but owing to a non compensation of the local spins, the resulting spin is different from zero. This system is a ferrimagnet and a magnetically ordered state is expected below  $T_c$ ; (iii) all the spins are identical and coupled antiferromagnetically, but they present a small canting; thus, a non zero resulting spin is observed. A weak ferromagnetic transition is expected at  $T_c$ ; and (iv) a non-zero resulting spin may arise from complicated spin structures involving both ferro- and antiferromagnetic interactions, as well as possible spin canted structures. Examples of these situations can be found in the recent literature.<sup>3,4</sup> In fact, in the past few years our understanding of magnetic molecular materials has enjoyed an enormous growth and several remarkable breakthroughs were made from many diverse areas of science and technology.<sup>3,4</sup>

The most relevant discoveries are: (a) the findings of bulk ferri- and ferromagnets with critical temperatures above room temperature; (b) the discovery of spin-crossover materials with large hysteretic effects above room temperature; (c) the finding of an electrochemical or a photomagnetic modulation of the magnetic behaviour in a molecular solid; (d) the discovery of single-molecule (and single-chain) magnets with a significant relaxation barrier enabling them to act as a molecule-based magnet; (e) the detection of quantum tunneling of the magnetization in high-spin clusters with a large magnetic anisotropy and a negative zero field splitting in the ground spin state; (f) the finding of large magneto-resistance effects for molecular magnetic solids; (g) the development of magnetic materials with potential applications for spintronics; (h) the development of multifunctional magnetic molecular compounds where magnetism coexists with other properties such as chirality, conductivity,

optical, etc.; (i) the rational preparation of nanoporous magnetic molecular materials with sensing and recognition properties; (j) the processing and patterning on surfaces of molecule-based magnetic materials at the nanoscale level, such as dots, wires, rings, etc.; (k) the realization of nanosized molecular objects produced by self-assembling techniques and (l) the development of new physical characterization techniques (microSQUID arrays, STM-EPR, etc.). All such important contributions essentially concerning Molecular Magnetism, Materials Science and Crystal Engineering show the huge potential of this new class of magnetic materials.

Molecule-based magnetic materials exhibit a wide variety of bonding and structural motifs. These include isolated molecules (zero-dimensional, 0D), and those with extended bonding within chains (1D), layers (2D), and 3D network structures. However, magnetically ordered molecular systems require extended interactions linking the molecules within the crystalline lattice. Thus, we need to control, not only the primary structure of these molecules, but also the secondary and ternary ones. Along this line, although the crystal engineering has recently experienced an enormous growth,<sup>5,6</sup> the knowledge about the crystal packing of the molecules is still at its first infancy. However, considering the molecular magnet as a regular net of spin carriers separated by molecular connectors, the modulation of the 3D-network and hence, its magnetic properties by modifying the connectors is not a very difficult task. Most likely, this is one of the advantages of the molecule-based magnets compared with the ‘classical’ ones. An understanding of the relationship existing between molecular arrangements in the solid and the intermolecular magnetic interactions is essential for the development of this field. The modulation of the molecular building-blocks also allows to the molecule-based materials the possibility to acquire an additional property leading to multifunctional materials or developing “smart materials” with them. As a consequence of the increasing importance of the molecule-based materials, numerous materials science laboratories worldwide are strongly engaged in the development of new, improved magnetic molecular materials.

## **2. Coordination Polymers: a Way towards Tunable Magnets**

The fact that the solid-state architecture determines the properties is the leading force for the design of solid-state materials through a controlled assembly of molecular components.<sup>7</sup> The crystal structure can be determined by the strength and directionality of covalent and non-covalent intermolecular interactions. Thus, coordination polymers represent the paradigm of the crystal engineering.<sup>8,9</sup> They are infinite frameworks which are constructed by metal ions

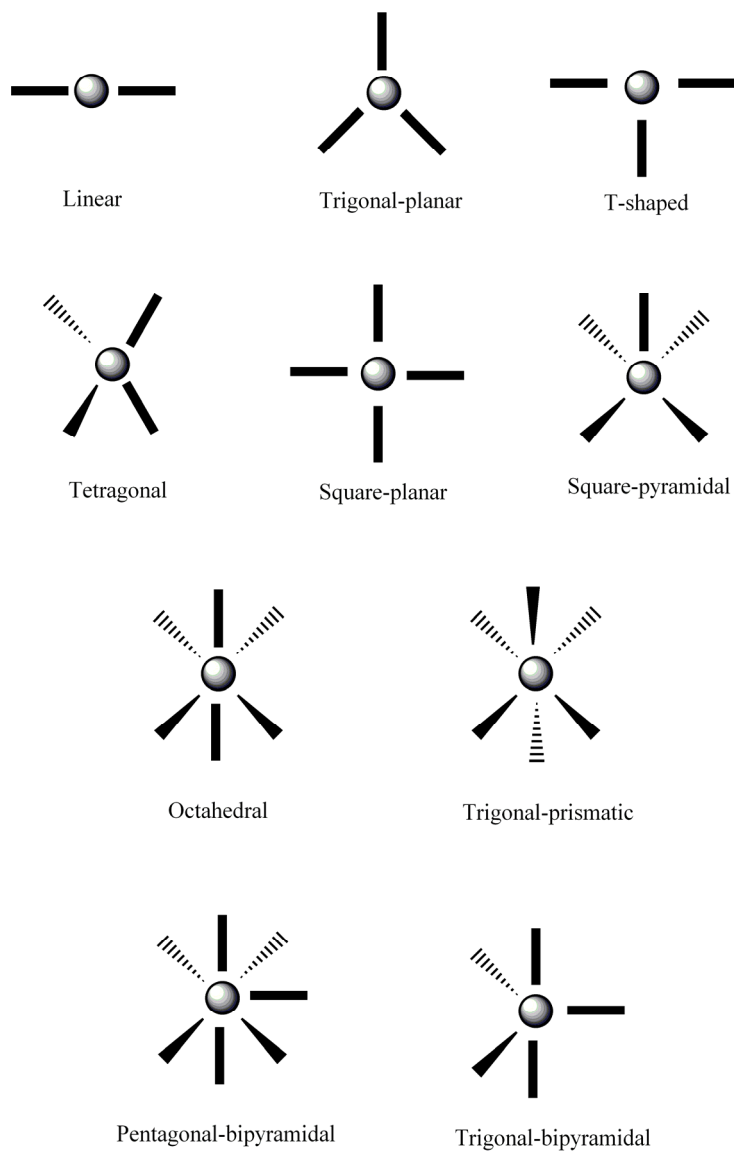
and organic ligands *via* more or less covalent metal-ligand interactions (coordinative bonds). They can be regarded as a series of points (nodes) of certain geometry which are connected through organic ‘spacers’.<sup>10</sup> The ‘nodes and spacers’ are preselected having in mind their ability for self-assembling and, according to a previous rational design in order to obtain the desired function. However, an accurate prediction of the overall crystal structure is usually not possible due to the weak but numerous non-covalent interactions involving the ligands, anions, cations as well as solvent molecules. These weakly coordinating anions influence not only the local structure of metal ions but also the overall framework and so, they can be regarded as framework regulators. It is worth noting that protic solvent molecules are involved in hydrogen bonding, forming a complementary linking network.

In comparison to assemblies of discrete metal complexes, coordination polymers have advantages aiming at building: (i) a stable framework, which could lead to microporous functions such as zeolites and activated carbons; (ii) a prefixed arrangement of paramagnetic centres, which is related to magneto-structural studies; (iii) diverse framework motifs (chains, ladders, helices, fish-bones, square and rectangular grids, bilayers, honeycombs, pillared-layers, diamondoid cells, among others). Finally, coordination polymers are of utmost relevance because of their physical and chemical properties and the applications to materials science as catalytic, conductive, luminescent, magnetic, spin transition, non-linear optics or porous materials.<sup>7-19</sup>

## 2.1. Modules as Building Blocks

- *Transition metal ions as nodes* (Scheme 1). The use of transition metal ions as nodes in the construction of coordination polymers offers substantial advantages when compared with purely organic compounds which are organized by non-covalent interactions. The covalent metal-ligand bonds (coordinative interactions) are stronger than the hydrogen bonds and they offer a greater directionality than other weak interactions such as  $\pi$ - $\pi$  stacking, etc. In addition, different stereochemistries (e.g. linear, trigonal-planar, T-shaped, tetrahedral, square-planar, square-pyramidal, trigonal-bipyramidal, octahedral, trigonal-prismatic, pentagonal-bipyramidal and their distorted forms), depending on the metal element as its valence, are provided for the construction of polymeric architectures. For instance, copper(II) is one of the best examples at this respect given the well known plasticity of its coordination sphere as a function of the reaction conditions (nature of the solvent, counteranions, type and denticity of the ligands, etc). These features associated to the facility that its complexes crystallize [an inspection of the crystal data base of inorganic

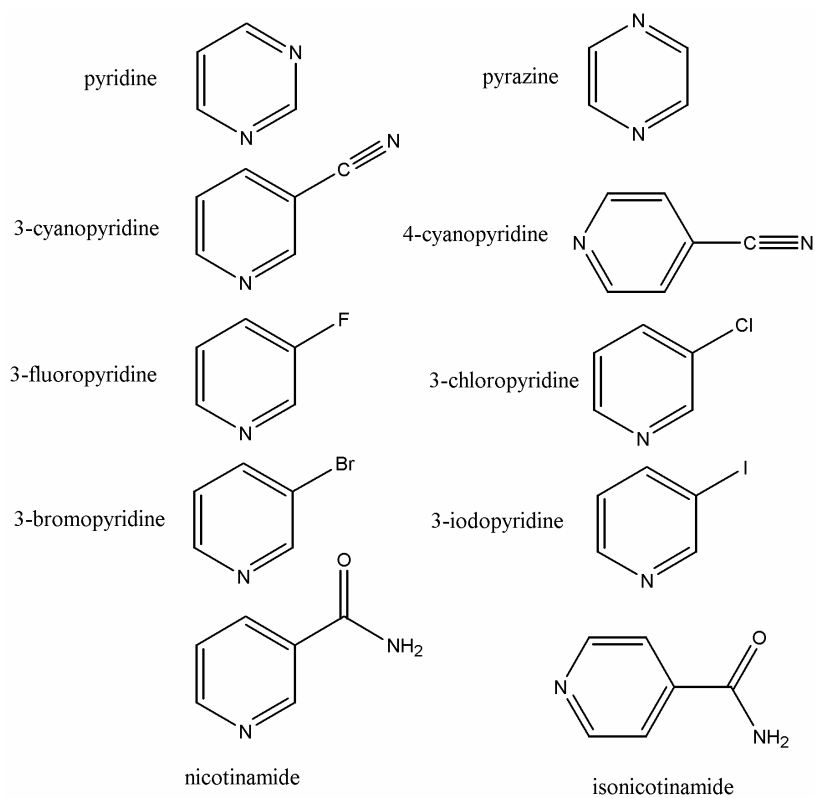
compounds shows that the number of known crystal structures of the copper(II)-containing species exceeds those of other systems] make this divalent cation an extremely useful node.



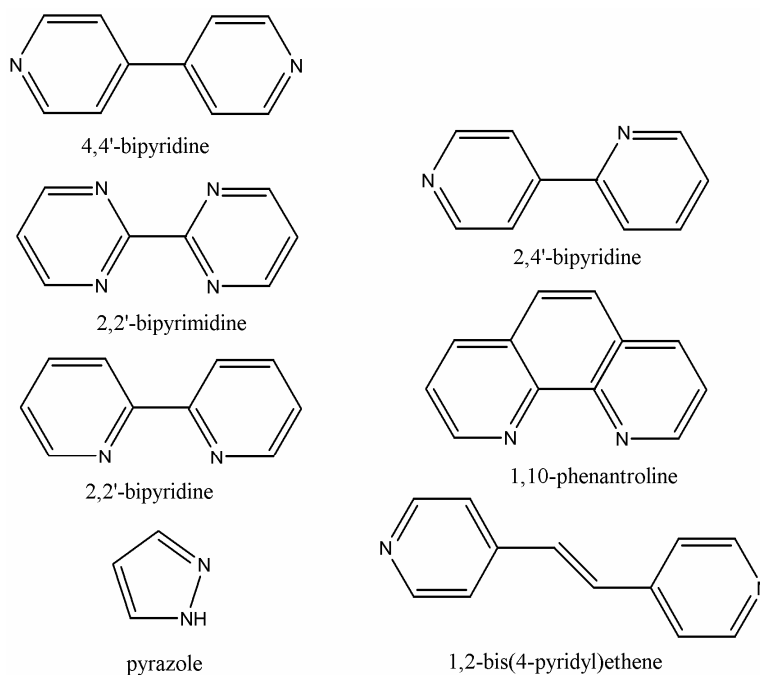
Scheme 1

- *Organic ligands as connectors.* We are referring to organic ligands used in the construction of coordination polymers which act as bridges between metal ions. Of special importance are the rigid ligands since they allow a certain control of the assembly process.

The diversity of organic components accounts for the variety of structural topologies. The rational selection of organic ligands is done having in mind the tuning the physical properties and recent efforts have been made concerning the use of extended bridging ligands as appropriate spacers.<sup>20-24</sup> Although organic ligands are in general neutral molecules, di-, tri-, tetra- and hexacarboxylate molecules with a central phenyl ring are representative anionic linkers. The neutral organic ligands which are used in this thesis are shown in Scheme 2.



Scheme 2a



Scheme 2b

- *Metal clusters and polynuclear complexes as nodes or connectors.* Multidentate linkers such as carboxylate-type ligands provide rigid frameworks due to their ability to aggregate metal ions into polynuclear units, which are referred to as secondary building units (SBUs).<sup>13</sup> The SBUs are sufficiently rigid because the metal ions are locked into their positions by the carboxylate groups. Thus, instead of using a transition metal ion at a network node, the SBUs provide nodes with specific functionalities which are able to establish connections with the adjacent SBUs through an organic ligand or act as connectors between metal ions. In several clusters with terminal ligands, their coordination sites may be opened to allow the study of metal site reactivity, feature which is also observed in the chemistry of the lanthanide ions.

## 2.2. Synthetic Methods: Molecular Self-Assembly

Self-assembly is a process in which components, either separated or linked, spontaneously form ordered aggregates.<sup>25</sup> Thus, if synthesis generates molecules, self-assembly makes ordered ensembles of molecules. Several reasons make scientifically interesting the self-assembly process: (i) it is important in life. Lipid membranes, protein aggregates, structured nucleic acids and many others that are formed by self-assembly;<sup>26</sup> (ii) it provides synthetic

routes to a range of materials with regular structures as molecular crystals, liquid crystals, etc.;<sup>6</sup> (iii) it occurs widely in systems of components larger than molecules, and there is a great potential for its use in materials and condensed matter science; (iv) it seems to offer one of the most general strategies now available for generating nanostructures. Concerning molecular self-assembly, the coordinative interactions required for the preparation of coordination polymers are increasingly considered as appropriate for self-assembly.<sup>27</sup> Requisites for the self-assembly of a rationally designed coordination polymer involves the presence of the adequate 'nodes' and 'connectors' which recognize each other to form the ordered aggregates. The 'right' arrangement according to our predictions of the adequate nodes with the functionalized connector is the main difficulty to obtain a coordination polymer with the desired physical properties. Two strategies are available to overcome this problem: (i) the one-pot synthesis which consist of mixing the right chemicals and hoping that the desired product will be formed (although it is based on serendipity, most of the interesting materials are produced in this way); and (ii) the rational approach where a synthetic route is envisaged to obtain the desired product through a straightforward self-assembly process.

The strategy that we will use in this Thesis is a merge of both of them. One-pot synthesis is adequate to obtain certain knowledge about the chemical behaviour of the connectors in the presence of the nodes. Then, the design of a rational strategy is needed to perform the required modifications of the ligands, to incorporate and to take advantage of additional forces to the coordinative and electrostatic ones such as hydrogen bonds,  $\pi$ - $\pi$  stacking and van der Waals interactions (C-H $\cdots\pi$ , for instance) and to control the complex formation by playing on different parameters (temperature, pH, type of solvent, for instance) which would lead to the desired material.

Among the synthetic methods involving self-assembly, two of the most widely used are the slow diffusion and the hydro(solvo)thermal procedures; let us finish this paragraph by a brief comment on these two techniques of crystal growing: (i) *The Slow Diffusion Method*. Slow diffusion of reactants is frequently used to get X-ray quality crystals of highly insoluble systems. For that, one of the simplest, cheapest and effective device is an H-shaped tube. Its use precludes a fast precipitation which normally would afford the desired product as a fine powder. (ii) *The Hydro(solvo)thermal Method*. The hydrothermal method, which is well established for the synthesis of zeolites, has been increasingly used to prepare coordination polymers in spite of being regarded as 'a black box'. This method, typically carried out in the temperature range 120-260 °C under autogenous pressure, exploits the

self-assembly of the product from soluble precursors. The reduced viscosity of water under these experimental conditions enhances the diffusion processes so that, solvent extraction of solids and crystal growth from solution are favoured. Since differential solubility problems are minimized, a variety of simple precursors may be introduced, as well as a number of organic and/or inorganic structure-directing agents. Under such non-equilibrium crystallization conditions, metastable kinetic phases (namely unprecedented structural networks) are most likely to be isolated. This method, although being widely used, has as main disadvantages low degrees of control and flexibility when compared to the previous slow diffusion technique.

### 3. Flexible Aliphatic Dicarboxylates

The impressive work which has been carried out with the rigid oxalato (the simplest dicarboxylate ligand) as a bridge concerning both homo- and heterometallic complexes in Magnetochemistry,<sup>28</sup> induced us to explore the use of other dicarboxylate-type ligands with a greater conformational freedom.

In fact, the conformational flexibility of the aliphatic dicarboxylates is reflected by the diversity of their connecting modes affording novel frameworks. In general, aliphatic carboxylates show the following features when looking at their complexing ability: (i) bidentate and monodentate coordination modes; (ii) *cis-cis*, *trans-trans*, or *cis-trans* orientations; (iii) tricoordinated oxygen-atom connectivity; (iv) pillaring of the metal-oxygen layers or networks; and (v) the generation of secondary building units (SBUs) by acting as capping agents through their carboxylate moieties. Many compounds containing the  $[\text{OOC}(\text{CH}_2)_n\text{COO}]^{2-}$  dianion have been prepared and characterized.<sup>29</sup> In some of these carboxylate complexes, metal-oxide dimers (0D), chains (1D), or layers (2D) are linked or pillared by dicarboxylate ions to give higher dimensional frameworks.

#### 3.1. The Malonic Acid

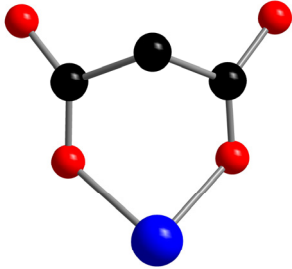
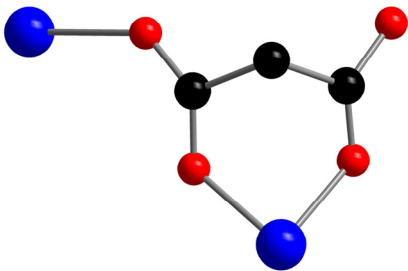
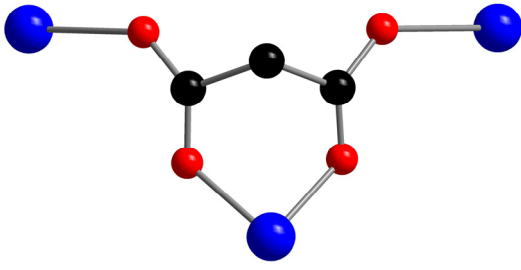
1,3-Propanedioic acid (commonly known as malonic acid) is well known in coordination chemistry because of the versatility of its fully deprotonated form as a ligand towards metal ions. As far as the applicability is concerned, it deserves to be noted that the malonate complexes of both transition metal ions and heavier rare earth elements have been used in the fluorescent probe technique, in solid fluorescent and biological active materials and also in modifiers of polyethylene. Therefore, studies of the new complexes with malonic acid are welcome from both fundamental and applied points of view.



The malonate anion is a dicarboxylic ligand with a singular behaviour which retains some of the advantages of the oxalate ligand but with a greater flexibility which is derived from the presence of the methylene group. The malonate anion has the ability to coordinate in a bidentate conformation, but the bis-bidentate behaviour analogue to that usually exhibited by the oxalate is precluded by geometric reasons. In addition, it has some degree of flexibility to act as a pillaring unit in a bis-monodentate conformation usually found in dicarboxylate ligands with longer aliphatic chains such as succinic or glutaric acids.

Concerning the coordination modes of the malonate in its metal complexes (Table 1), there are three basic schemes: (i) bidentate; (ii) bidentate and monodentate; and (iii) bidentate and bis-monodentate.

**Table 1.** Coordination modes of the malonate ligand

|                                                                                     | Metal ion | Ref.                 |
|-------------------------------------------------------------------------------------|-----------|----------------------|
|   | Cu(II)    | 30-38                |
|                                                                                     | Co(II)    | 39, 40               |
|                                                                                     | Mn(II)    | 41, 42               |
|                                                                                     | Ni(II)    | 40, 43               |
|                                                                                     | Zn(II)    | 44                   |
|  | Cu(II)    | 30, 32-35, 38, 45-48 |
|                                                                                     | Mn(II)    | 41, 49               |
|  | Cu(II)    | 34, 50-54            |
|                                                                                     | Co(II)    | 45, 55, 56           |
|                                                                                     | Mn(II)    | 53, 57, 58           |
|                                                                                     | Ni(II)    | 56                   |
|                                                                                     | Zn(II)    | 51, 52               |

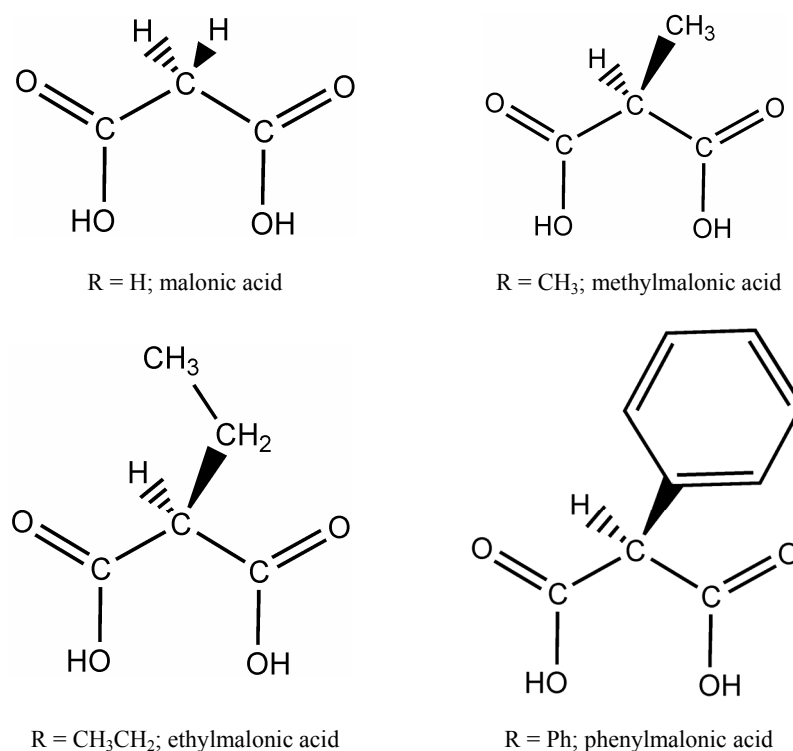
Apart from these coordination modes chelating monodentate modes have been observed with heavier elements,<sup>59</sup> but are less frequent with *3d* metal ions. The malonate ligand occupies one or two coordination sites at the metal ion and its dinegative charge contributes to neutralize the positive charge of the metal centre. The inclusion of other ligands in the coordination sphere of the metal ion is not precluded in the presence of malonate and these complementary ligands (also referred to as coligands) can adopt bridging or blocking roles contributing to the interconnection or isolation of the spin carriers, respectively. Thus, combining the malonate with other bridging and/or blocking ligands we have been able to prepare mono-,<sup>38</sup> di-,<sup>36,38</sup> tri-,<sup>38</sup> and tetranuclear species,<sup>48</sup> as well as one-,<sup>38,47,54,60</sup> two-,<sup>48</sup> and three-dimensional networks.<sup>48,58</sup>

Considering the malonate dianion as a bridging ligand which can mediate magnetic interactions and in the framework of our research work with malonate-bridged copper(II) complexes, we have observed that the carboxylate-malonate bridge is able to mediate significant ferromagnetic interactions between the copper(II) ions.<sup>36-38,47,48,54,61</sup> From a magnetic point of view, we have found that the parameters governing the magnetic interaction between metal centres are the *anti-syn* conformation of the carboxylate-bridge and the relative position of this bridge respect to the copper(II) ions in square pyramidal environment [equatorial-equatorial (a relatively strong magnetic interaction), equatorial-apical (a weak magnetic interaction) and apical-apical (a negligible magnetic interaction). Inside this division, two additional structural parameters become important: the value of the dihedral angle  $\beta$  between the mean basal planes of the interacting copper(II) ions and the distortion value ( $\tau$ )<sup>22</sup> [ $\tau = 0$  and 1 for square pyramidal and trigonal bipyramidal copper(II) environments, respectively].<sup>61</sup>

### **3.2. New malonate-based coordination networks: design and application.**

The design of crystal structures requires the rational synthesis taking into account not only of the local interactions, or supramolecular synthons, but a greater appreciation of the whole three-dimensional structure of a crystal. The intermolecular interactions guide the arrangement of the constituent building blocks of a material and the extended structure of those building blocks is responsible for the physical properties of the designed crystalline array. The synergy between these two aspects is the key for the successful design of molecular networks.

At this respect and in the light of our previous results, modifications of the malonic acid which can give us some degree of control over the intermolecular interactions could enhance the structural and physical properties of the malonate-copper(II) complexes. Keeping this in mind, we have started a systematic study on the complex formation between copper(II) and substituted malonate ligands where one of the two hydrogen atoms of the methylene carbon atom is replaced by an alkyl or aryl substituent (see Scheme 3).



Scheme 3

Several points are important when looking at this series in the context of magneto-structural investigations: the solubility in polar and non polar solvents, the hydrophobic character, steric hindrance, electron donor or acceptor effects,  $\pi$ - $\pi$  stacking and new conformations/coordination modes of the substituted malonate are the main ones. So for instance, the presence of a phenyl ring in the malonate skeleton provides the possibility of developing graphitic-like interactions between neighbouring units adding a supramolecular exchange pathway to that through the bridging carboxylate-malonate bridge. In a certain manner, this interaction can play also a role in molecular recognition, which is an important topic in supramolecular chemistry that has been widely examined.<sup>62-68</sup> As far as the

hydrophobicity is concerned; this point is relevant when thinking at the host-guest chemistry with open frameworks of malonate complexes.

In summary, the present work will show the strong influence of these subtle chemical modifications of the malonate skeleton on the structure and magnetic properties of the resulting malonate-containing copper(II) complexes.

## 4. References

- 1 F. Palacio in *Magnetic Molecular Materials*, D. Gatteschi, O. Kahn, J. S. Miller and F. Palacio, eds. Kluwer Academic Publishers, Dordrecht, **1991**.
- 2 O. Kahn in *Magnetic Molecular Materials*, D. Gatteschi, O. Kahn, J. S. Miller and F. Palacio, eds. Kluwer Academic Publishers, Dordrecht, **1991**.
- 3 *Magnetism: Molecules to Materials*, Vols. I-V, J. S. Miller and M. Drillon, eds., Wiley-VCH, Weinheim, **2005**.
- 4 *Polyhedron*, **2005**, *24*, issues 16-17.
- 5 D. Braga, L. Brammer and N. R. Champness, *CrystEngComm* **2005**, *7(1)*, 1.
- 6 (a) G. R. Desiraju, *J. Mol. Struct.* **2003**, *656*, 5. (b) G. R. Desiraju, *Crystal Engineering. The Design of Organic Solids*, Elsevier, Amsterdam, **1989**.
- 7 M. J. Zaworotko, *Chem. Comm.* **2001**, 1.
- 8 C. Janiak, *Dalton Trans.* **2003**, 2781.
- 9 B. Moulton and M. J. Zaworotko, *Chem. Rev.* **2001**, *101*, 1629.
- 10 B. F. Abrahams, M. J. Hardie, B. F. Hoskins, R. Robson and E. E. Sutherland, *Chem. Comm.* **1994**, 1049.
- 11 S. Kitagawa and M. Munakata, *Trends Inorg. Chem.* **1993**, *3*, 437.
- 12 M. Munakata, *Adv. Inorg. Chem.* **1998**, *46*, 173.
- 13 A. J. Blake, N. R. Champness, P. Hubberstey, W.-S. Li, M. A. Withersby and M. Schröder, *Coord. Chem. Rev.* **1999**, *183*, 117.
- 14 M. Eddaoudi, D. B. Moler, H. Li, B. Chen, T. M. Reineke, M. O'Keeffe and O. M. Yaghi, *Acc. Chem. Res.* **2001**, *34*, 319.
- 15 O. R. Evans and W. Lin, *Acc. Chem. Res.* **2002**, *35*, 511.
- 16 P. J. Hagrman, D. Hagrman and J. Zubieta, *Angew. Chem. Int. Ed.* **1999**, *38*, 2638.
- 17 S. Kitagawa and M. Kondo, *Bull. Chem. Soc. Jpn.* **1998**, *71*, 1739.
- 18 M. J. Zaworotko, *Chem. Soc. Rev.* **1994**, 283.
- 19 S.R. Batten and R. Robson, *Angew. Chem. Int. Ed.* **1998**, *37*, 1460.
- 20 S. Banfi, L. Carlucci, E. Caruso, G. Ciani and D. M. Proserpio, *Dalton Trans.* **2002**, 2714.
- 21 K. Biradha and M. Fujita, *Chem. Comm.* **2001**, 15.
- 22 M. A. Withersby, A. J. Blake, N. R. Champness, P. A. Cooke, P. Hubberstey and M. Schröder, *J. Am. Chem. Soc.* **2000**, *122*, 4044.
- 23 M. Fujita, Y. J. Kwon, O. Sasaki, K. Yamaguchi and K. J. Ogura, *J. Am. Chem. Soc.* **1995**, *117*, 7287.
- 24 N. G. Pschirer, D. M. Ciurtin, M. D. Smith, U. H. Bunz and H.-C. zur Loye, *Angew. Chem. Int. Ed.* **2002**, *41*, 583.
- 25 G. M. Whitesides and M. Boncheva, *PNAS* **2002**, *99(8)*, 4769.
- 26 B. Alberts, D. Bray, J. Lewis, M. Raff, K. Roberts and J. D. Watson, *Molecular Biology of the Cell*, Garland, New York, **1994**.
- 27 (a) J. M. Lehn, *NATO ASI Ser. E* **1996**, *320*, 511. (b) B. Olenyuk, J. A. Whiteford, A. Fechtenkotter and P. J. Stang, *Nature*, **1999**, *398*, 796.
- 28 (a) O. Kahn, *Molecular Magnetism*, Wiley-VCH Verlag GmbH, Weinheim, Germany, **1993**. (b) S. Decurtins, R. Peloux, G. Antorena and F. Palacio, *Coord. Chem. Rev.* **1999**, 841. (c) M. Pilkington and S. Decurtins in *Comprehensive Coordination Chemistry II. From Biology to Technology*; J. A. McCleverty and T. J. Meyer, eds., Elsevier-Pergamon, Amsterdam,

- 2004**, Vol. 7, p 214. (d) M. Gruselle, C. Train, K. Boubekeur, P. Gredin and N. Ovanesyan, *Coord. Chem. Rev.* **2006**, in press (doi:10.1016/j.ccr.2006.03.020).
- 29 C.N.R. Rao, S. Natarajan and R. Vaidhyanathan, *Angew. Chem. Int. Ed.* **2004**, *43*, 1466.
- 30 D. Chattopadhyay, S. K. Chattopadhyay, P. R. Lowe, C. H. Schwalbe, S. K. Mazumder, A. Rana and S. Ghosh, *Dalton Trans.* **1993**, 913.
- 31 (a) S. K. Chawla, M. Arora, K. Nattinen, K. Rissanen and J. V. Yakhmi, *Polyhedron*, **2004**, *23*, 3007. (b) G.-H. Cui, J.-R. Li, T.-L. Hu and X.-H. Bu, *J. Mol. Struct.* **2005**, *738*, 183. (c) I. G. Filippova, *Koord. Khim. (Russ. Coord. Chem.)* **2000**, *26*, 295. (d) L. Gasque, R. Moreno-Esparza, E. Mollins, J. L. Briansó-Peñalva, L. Ruiz-Ramírez and G. Medina-Dickinson, *Acta Cryst. Sect. C* **1998**, *C54*, 1848. (e) L. Gasque, R. Moreno-Esparza, E. Mollins, J. L. Briansó-Peñalva, L. Ruiz-Ramírez and G. Medina-Dickinson, *Acta Cryst. Sect. C* **1999**, *C55*, 158. (f) R. W. Hay, A. Danby and P. Lightfoot, *Polyhedron*, **1997**, *16*, 3261. (g) S. Kawata, S. Kitagawa, H. Machida, T. Nakamoto, M. Kondo, M. Katada, K. Kikuchi and I. Ikemoto, *Inorg. Chim. Acta* **1995**, *229*, 211. (h) W.-L. Kwik, K.-P. Ang, H.S.-O. Chan, V. Chebolu and S. A. Koch, *Dalton Trans.* **1986**, 2519. (i) Z.-Z. Lin, F.-L. Jiang, L. Chen and M.-C. Hong, *Jiegou Huaxue (Chinese J. Struct. Chem.)* **2004**, *23*, 993. (j) A. Pajunen and E. Nasakkala, *Finn. Chem. Lett.* **1977**, 189. (k) H.-Y. Shen, W.-M. Bu, D.-Z. Liao, Z.-H. Jiang, S.-P. Yan and G.-L. Wang, *Inorg. Chem. Comm.* **2000**, *3*, 497. (l) L. Sieron, *Acta Cryst. Sect. E* **2004**, *E60*, m297. (m) E. Suresh and M. M. Bhadbhade, *Acta Cryst. Sect. C* **1997**, *C53*, 193. (n) Y. Xiong, M. Tong, T. An and H. T. Karlsson, *Acta Cryst. Sect. C* **2001**, *C57*, 1385. (o) W. Zhao, J. Fan, T. Okamura, W.-Y. Sun and N. Ueyama, *New J. Chem.* **2004**, *28*, 1142.
- 32 I. G. Filippova, V. Kh. Kravtsov and M. Gdanets, *Koord. Khim. (Russ. Coord. Chem.)* **2000**, *26*, 860.
- 33 P. Naumov, M. Ristova, B. Soptrajanov, M. G. B. Drew and S. W. Ng, *Croat. Chem. Acta* **2002**, *75*, 701.
- 34 V. T. Yilmaz, E. Senel and C. Thone, *Trans. Met. Chem.* **2004**, *29*, 336.
- 35 V. T. Yilmaz, E. Senel and C. Kazak, *Sol. State Sci.* **2004**, *6*, 859.
- 36 Y. Rodríguez-Martín, J. Sanchiz, C. Ruiz-Pérez, F. Lloret and M. Julve, *Inorg. Chim. Acta* **2001**, *326*, 20.
- 37 Y. Rodríguez-Martín, J. Sanchiz, C. Ruiz-Pérez, F. Lloret and M. Julve, *CrystEngComm* **2002**, *4*, 631.
- 38 C. Ruiz-Pérez, J. Sanchiz, M. Hernández-Molina, F. Lloret and M. Julve, *Inorg. Chem.* **2000**, *39*, 1363.
- 39 D.-D. Lin, Y. Liu and D.-J. Xu, *Acta Cryst. Sect. E* **2003**, *E59*, m771.
- 40 X.-D. Wang, L.-C. Li, D.-Z. Liao, Z.-H. Jiang, S.-P. Yan and P. Cheng, *J. Coord. Chem.* **2004**, *57*, 1577.
- 41 S. Sain, T. K. Maji, G. Mostafa, T.-H. Lu and N. R. Chaudhuri, *Inorg. Chim. Acta* **2003**, *351*, 12.
- 42 (a) L. Shen, *Acta Cryst. Sect. C* **2003**, *C59*, m128. (b) Z.-X. Wang, X.-H. Zhou, W.-T. Yu and Y.-J. Fu, *Z. Kristallogr.* **2000**, *215*, 423. (c) Q.-Z. Zhang and C.-Z. Lu, *Acta Cryst. Sect. E* **2004**, *E60*, m1778.
- 43 J. G. Liu and D. J. Xu, *Acta Cryst. Sect. E* **2004**, *E60*, m541.
- 44 W. Zhao, J. Fan, T. Okamura, W.-Y. Sun and N. Ueyama, *J. Sol. State Chem.* **2004**, *177*, 2358.
- 45 S. Konar, P. S. Mukherjee, M. G. B. Drew, J. Ribas and N. R. Chaudhuri, *Inorg. Chem.* **2003**, *42*, 2545.
- 46 (a) A. Tosik, L. Sieron and M. Bukowska-Strzyewska, *Acta Cryst. Sect. C*, **1995**, *C51*, 1987. (b) A. Pajunen and E. Nasakkala, *Finn. Chem. Lett.* **1977**, 100.
- 47 J. Sanchiz, Y. Rodríguez-Martín, C. Ruiz-Pérez, A. Mederos, F. Lloret and M. Julve, *New J. Chem.* **2002**, *26*, 1624.
- 48 (a) Y. Rodríguez-Martín, C. Ruiz-Pérez, J. Sanchiz, F. Lloret and M. Julve, *Inorg. Chim. Acta* **2001**, *318*, 159. (b) Y. Rodríguez-Martín, M. Hernández-Molina, F. S. Delgado, J. Pasán, C. Ruiz-Pérez, J. Sanchiz, F. Lloret and M. Julve, *CrystEngComm*, **2002**, *4*, 440.
- 49 Y.-G. Wei, S.-W. Zhang, M.-C. Shao, Q. Liu and Y.-Q. Tang, *Polyhedron* **1996**, *15*, 4303.
- 50 (a) H.-Y. Bie, J.-H. Yu, K. Zhao, J. Lu, L.-M. Duan and J.-Q. Xu, *J. Mol. Struct.* **2005**, *741*, 77. (b) T.-F. Liu, H.-L. Sun, S. Gao, S.-W. Zhang and T.-C. Lau, *Inorg. Chem.* **2003**, *42*,

4792. (c) S. Sain, T. K. Maji, G. Mostafa, T.-H. Lu and N. R. Chaudhuri, *New J. Chem.* **2003**, *27*, 185.
- 51 X. Zhang, C. Lu, Q. Zhang, S. Lu, W. Yang, J. Liu and H. Zhang, *Eur. J. Inorg. Chem.* **2003**, 1181.
- 52 Q. Liu, Y.-Z. Li, Y. Song, and Z. Xu, *J. Sol. State Chem.* **2004**, *177*, 4701.
- 53 Y.-Q. Zheng and E.-B. Ying, *J. Coord. Chem.* **2005**, *58*, 453.
- 54 C. Ruiz-Pérez, M. Hernández-Molina, P. Lorenzo-Luis, F. Lloret, J. Cano and M. Julve, *Inorg. Chem.* **2000**, *39*, 3845.
- 55 (a) P. Lightfoot and A. Snedden, *Dalton Trans.* **1999**, 3549. (b) Y.-H. Xue, D.-D. Lin and D.-J. Xu, *Acta Cryst. Sect. E* **2003**, *E59*, m750.
- 56 Y.-Q. Zheng and H.-Z. Xie, *J. Coord. Chem.* **2004**, *57*, 1537.
- 57 (a) T. Lis and J. Matuszewski, *Acta Cryst. Sect. B* **1979**, *35*, 2212. (b) S. Konar, S. C. Manna, E. Zangrando, T. Mallah, J. Ribas and N. R. Chaudhuri, *Eur. J. Inorg. Chem.* **2004**, 4202. (c) Q. Liu, B. Li, Z. Xu, X. Sun, K.-B. Yu and Y.-Z. Li, *J. Coord. Chem.* **2003**, *56*, 771. (d) T. K. Maji, S. Sain, G. Mostafa, T.-H. Lu, J. Ribas, M. Monfort and N. R. Chaudhuri, *Inorg. Chem.* **2003**, *42*, 709.
- 58 Y. Rodríguez-Martín, M. Hernández-Molina, J. Sanchiz, C. Ruiz-Pérez, F. Lloret and M. Julve, *Dalton Trans.* **2003**, 2359.
- 59 (a) C. Hornick, P. Rabu and M. Drillon, *Polyhedron* **2000**, *19*, 259. (b) P. Rabu, J. M. Rueff, Z. L. Huang, S. Angelov, J. Souletie and M. Drillon, *Polyhedron* **2001**, *20*, 1677.
- 60 C. Ruiz-Pérez, J. Sanchiz, M. Hernández-Molina, F. Lloret and M. Julve, *Inorg. Chim. Acta* **2000**, *298*, 202.
- 61 J. Pasán, F. S. Delgado, Y. Rodríguez-Martín, M. Hernández-Molina, C. Ruiz-Pérez, J. Sanchiz, F. Lloret and M. Julve, *Polyhedron* **2003**, *22*, 2143.
- 62 (a) S. O. H. Gutschke, D. J. Price, A. K. Powell and P. T. Wood, *Angew. Chem. Int. Ed.* **2001**, *40*, 1920; (b) R. Kuhlman, G. L. Schimek and J. W. Kolis, *Inorg. Chem.* **1999**, *38*, 194.
- 63 M. C. Etter, *J. Phys. Chem.* **1991**, *95*, 4601.
- 64 S. K. Burley and G. A. Petsko, *Science* **1985**, *229*, 23.
- 65 J. Singh and J. M. Thornton, *FEBS Lett.* **1985**, *191*, 2989.
- 66 C. A. Hunter, J. Singh and J. M. Thornton, *J. Mol. Biol.* **1990**, *211*, 595
- 67 L. F. Lindoy and I. M. Atkinson, *Self-Assembly in Supramolecular Chemistry*, Royal Society of Chemistry, Cambridge, UK, **2000**.
- 68 I. Dance, *Supramolecular Inorganic Chemistry*, in G. R. Desiraju, ed., *The Crystal as a Supramolecular Entity*, John Wiley & Sons, Chichester, UK, **1996**.

---

---

# Objectives

---

---



The fundamental aim of this Thesis is the preparation and characterization of new magnetic molecular materials with magnetic ordering which could be used in future applications. In order to reach this goal, this investigation has been based on the previous work of our research group dealing with the use of the malonic acid as organic linker between transition metal ions. Along this line, a good number of coordination polymers were prepared and magneto-structurally characterized which have been the main subject of three previous thesis works. Fine results were obtained through well-defined strategies to obtain materials with interesting structural and magnetic properties. So, we decide to go a step beyond and introduce modifications in the malonate ligand itself. These modifications were oriented to get a certain degree of control over the self-assembly process. Thus, one of the hydrogen atoms of the methylene group of the malonic acid was substituted by aryl (phenyl) or alkyl (methyl or ethyl) groups. These groups can establish weak interactions ( $\pi$ -type, hydrophobic, steric repulsion, etc.) which can modify the structural behaviour of the malonate ligand. This influence on the self-assembly process, on the crystal packing and hence, on the magnetic properties will be investigated.

Although the choice of the copper(II) ions as the spin carrier is not the most appropriate one to obtain materials which exhibit spontaneous magnetization at high temperatures, it is an interesting probe for future design of molecular magnets. The preparation of copper(II) complexes with these substituted-malonate ligands, their structural characterization and the investigation of their magnetic properties are the main subjects of this Thesis. Finally, some ideas about future modifications of these ligands which could afford better results along with some interesting by-side results are reported.



---

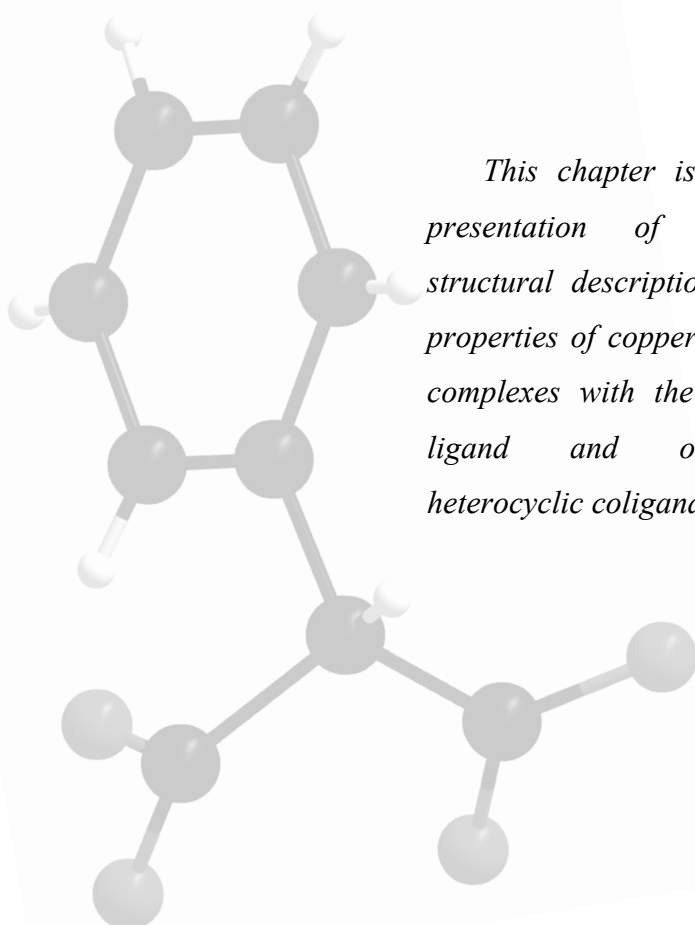
---

## Chapter I.

# Phenylmalonate Complexes

---

---



*This chapter is devoted to the presentation of the synthesis, structural description and magnetic properties of copper(II) coordination complexes with the phenylmalonate ligand and other N-donor heterocyclic coligands.*

## I.1. Copper(II)-Phenylmalonate (1)

### I.1.1. Introduction

There motivation for the preparation of this complex concerns the possibility to found other conformations than those observed for malonate–copper(II) complexes. The preparation of this phenylmalonate complex is the first step in a systematic study with substituted malonate ligands. The presence of a phenyl ring on the methylene carbon group could induce different conformations of the malonate bridging modes due to geometrical constraints and it would make possible specific attractive interactions between phenyl rings that would contribute to the overall stability of the resulting compound. Their role in supramolecular chemistry and more specifically, in molecular recognition, has now been widely examined.<sup>1-7</sup>

The magnetic properties could be very interesting since all the copper(II)-malonate complexes exhibit ferromagnetic interactions through the *anti-syn* carboxylate bridge.<sup>8</sup> Finally, the presence of  $\pi$ -type and hydrophobic interactions in the Phmal-containing complexes are expected to lead to the formation of two-dimensional carboxylate-bridged networks.

### I.1.2. Synthesis

$\{[\text{Cu}(\text{H}_2\text{O})_3][\text{Cu}(\text{Phmal})_2]\}_n$  (**1**). Copper(II) acetate (1 mmol, 200 mg) was dissolved in warm methanol (20 cm<sup>3</sup>) under stirring. Phenylmalonic acid (1 mmol, 180 mg) was added and the resulting pale blue solution was evaporated to dryness in a rotatory evaporator. The green solid obtained is thoroughly washed with acetone to remove the acetic acid. Then, it was dissolved in water (25 cm<sup>3</sup>) and the solution was allowed to evaporate at room temperature. Prismatic blue single crystals of **1** were grown after a few days. Crystallographic data are listed in Table I.1. Yield *ca.* 65%. Anal. calc. for C<sub>18</sub>H<sub>18</sub>O<sub>11</sub>Cu<sub>2</sub> (**1**): C, 40.23; H, 3.38. Found: C, 40.18; H, 3.39%.

**Table I.1.** Crystallographic data for **1**

| <b>1</b>                                                    |                                                                     |
|-------------------------------------------------------------|---------------------------------------------------------------------|
| Formula                                                     | C <sub>18</sub> H <sub>18</sub> O <sub>11</sub> Cu <sub>2</sub>     |
| FW                                                          | 537.4                                                               |
| Crystal system                                              | Monoclinic                                                          |
| Space group                                                 | <i>P</i> 2 <sub>1</sub> / <i>n</i>                                  |
| <i>a</i> /Å                                                 | 12.1329 (9)                                                         |
| <i>b</i> /Å                                                 | 10.4929 (9)                                                         |
| <i>c</i> /Å                                                 | 15.2841 (17)                                                        |
| $\beta$ /°                                                  | 98.315 (8)                                                          |
| <i>V</i> /Å <sup>3</sup>                                    | 1925.4 (3)                                                          |
| <i>Z</i>                                                    | 4                                                                   |
| $\mu$ (Mo K $\alpha$ ) /cm <sup>-1</sup>                    | 22.72                                                               |
| <i>T</i> /K                                                 | 293 (2)                                                             |
| $\rho_{\text{calc}}$ /g cm <sup>-3</sup>                    | 1.854                                                               |
| $\lambda$ /Å                                                | 0.71073                                                             |
| Index ranges                                                | -17 ≤ <i>h</i> ≤ 17,<br>-14 ≤ <i>k</i> ≤ 12,<br>-11 ≤ <i>l</i> ≤ 21 |
| Indep. reflect. (R <sub>int</sub> )                         | 5292 (0.0424)                                                       |
| Obs. reflect. [ <i>I</i> > 2 $\sigma$ ( <i>I</i> )]         | 3823                                                                |
| Parameters                                                  | 352                                                                 |
| Goodness-of-fit                                             | 1.003                                                               |
| <i>R</i> [ <i>I</i> > 2 $\sigma$ ( <i>I</i> )]              | 0.0414                                                              |
| <i>R</i> <sub>w</sub> [ <i>I</i> > 2 $\sigma$ ( <i>I</i> )] | 0.0831                                                              |
| <i>R</i> (all data)                                         | 0.0732                                                              |
| <i>R</i> <sub>w</sub> (all data)                            | 0.0932                                                              |

### I.1.3. Description of the Structure

The crystal structure of the complex  $\{[\text{Cu}(\text{H}_2\text{O})_3][\text{Cu}(\text{Phmal})_2]\}_n$  (**1**) consists of a two-dimensional arrangement of copper(II) ions which is made up of  $2_1$  chains with regular alternation of bis(phenylmalonato)cuprate(II) anions and triaquacopper(II) cations that are linked through a double  $\mu$ -oxo bridge (Fig. I.1). These  $2_1$  chains run parallel to the  $b$  axis (Fig. I.2) and the resulting layers are stacked parallel to the  $[101]$  direction. These layers are well separated from each other, the interlayer distance being  $8.187(2)$  Å. The interlayer space is filled by the phenyl rings that create hydrophobic layers (Fig. I.3) where offset face-to-face  $\pi$ - $\pi$  stacking between the phenyl rings occurs, the shortest distance between the mean planes of adjacent phenyl rings being  $3.495(3)$  Å. The centre to centre distance between adjacent phenyl rings is  $3.954(5)$  Å, a value which is a bit longer than the average distances in  $\pi$ - $\pi$  interactions between pyridine-like groups previously reported.<sup>9</sup> Intralayer hydrogen bonds involving coordinated water molecules and phenylmalonate oxygen atoms, [ $\text{O}(\text{w})\cdots\text{O}$  distances ranging from  $2.672(4)$  Å to  $2.830(3)$  Å] contribute to stabilize the structure.

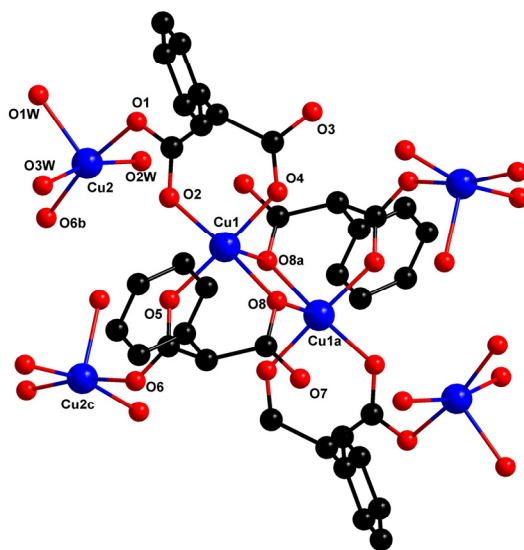


**Fig. I.1** A view of a fragment of the carboxylate-bridged copper(II) chains linked by the double  $\mu$ -oxo bridge. The numbering of the carbon atoms is omitted for clarity.

The two crystallographically independent copper(II) ions [Cu(1) and Cu(2)] have slightly distorted square pyramidal surroundings. Four coplanar carboxylate oxygen atoms [O(2), O(4), O(5), and O(8)] define the basal plane at Cu(1) [copper to oxygen bond lengths

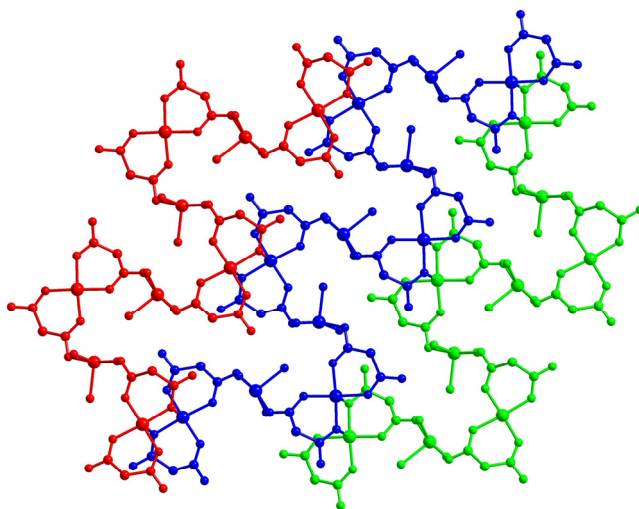


**Fig. I.2.** Sheet-like arrangement of three  $2_1$  chains running parallel to the  $b$  axis. The phenyl groups of the Phmal ligand are omitted for clarity.

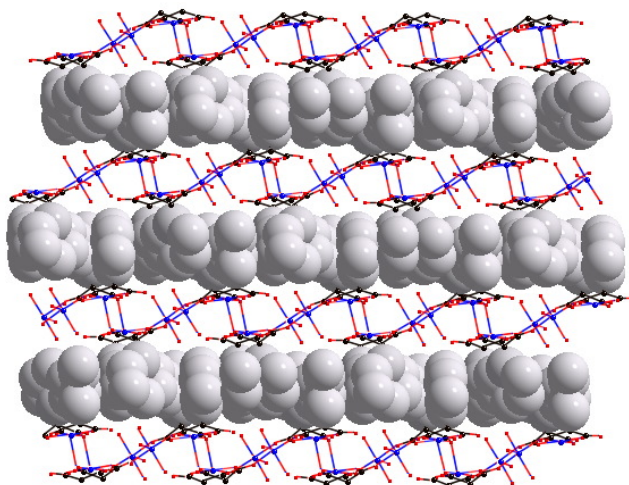


**Fig. I.3.** A view of the structure of complex **1** along the  $b$  axis showing the interlayer  $\pi$ - $\pi$  interactions

varying in the range 1.915(2)-1.945(2) Å], whereas the apical position is occupied by the symmetry-related carboxylate oxygen atom O(8a) [2.433(2) Å for Cu(1)-O(8a); (a) =  $-x + 1, -y + 1, -z + 2$ ]. Cu(1) is shifted by 0.0282(4) Å from the mean basal plane towards O(8a) (see Table I.2). The difference between the length of the axial and equatorial bonds (0.503 Å) is in agreement with the  $R_L$ - $R_S$  value (0.51 Å) reported by Hathaway.<sup>10</sup> The angles subtended at Cu(1) by the chelating phenylmalonate groups are 93.20(8) and 91.39(8)°. Two

water molecules, [O(2w) and O(3w)], and two carboxylate-oxygen atoms [O(1) and O(6b); (b) =  $-x + 3/2, y + 1/2, -z + 5/2$ ], build the basal plane at Cu(2), whereas the apical position is filled by another water molecule [O(1w)]. The equatorial copper to oxygen bond distances [1.952(2) to 1.980(2) Å] are shorter than the apical one [2.120(2) Å]. Cu(2) is shifted by 0.2130(3) Å from the mean basal plane towards O(1w). The calculated values of the  $\tau$  factor<sup>11</sup> are 0.02, and 0.06 for Cu(1) and Cu(2), respectively. These values indicate a quasi perfect square pyramidal environment in both copper(II) ions.

**Table I.2.** Selected bond lengths (Å) and bond angles (°) for compound **1**<sup>a,b</sup>

| <i>Bond Lengths</i> |           |                   |            |
|---------------------|-----------|-------------------|------------|
| Cu(1)–O(2)          | 1.926(2)  | Cu(2)–O(1)        | 1.952(2)   |
| Cu(1)–O(4)          | 1.915(2)  | Cu(2)–O(1w)       | 2.120(2)   |
| Cu(1)–O(5)          | 1.919(2)  | Cu(2)–O(2w)       | 1.978(2)   |
| Cu(1)–O(8)          | 1.945(2)  | Cu(2)–O(3w)       | 1.961(3)   |
| Cu(1)–O(8a)         | 2.433(2)  | Cu(2)–O(6b)       | 1.980(2)   |
| <i>Bond angles</i>  |           |                   |            |
| Cu(1)–O(8)–Cu(1a)   | 97.38(7)  | O(1)–Cu(2)–O(1w)  | 92.99(10)  |
| O(2)–Cu(1)–O(4)     | 93.20(8)  | O(1)–Cu(2)–O(2w)  | 89.40(9)   |
| O(2)–Cu(1)–O(5)     | 84.48(8)  | O(1)–Cu(2)–O(3w)  | 92.65(12)  |
| O(2)–Cu(1)–O(8a)    | 99.13(8)  | O(1)–Cu(2)–O(6b)  | 168.59(8)  |
| O(2)–Cu(1)–O(8)     | 175.64(8) | O(1w)–Cu(2)–O(2w) | 101.90(12) |
| O(4)–Cu(1)–O(5)     | 177.04(9) | O(1w)–Cu(2)–O(3w) | 93.12(13)  |
| O(4)–Cu(1)–O(8)     | 90.87(8)  | O(1w)–Cu(2)–O(6b) | 98.41(10)  |
| O(4)–Cu(1)–O(8a)    | 87.13(8)  | O(2w)–Cu(2)–O(3w) | 164.72(12) |
| O(5)–Cu(1)–O(8)     | 91.39(8)  | O(2w)–Cu(2)–O(6b) | 88.53(9)   |
| O(5)–Cu(1)–O(8a)    | 95.05(8)  | O(3w)–Cu(2)–O(6b) | 86.49(12)  |
| O(8)–Cu(1)–O(8a)    | 82.62(7)  | Cu(2)–O(1)–C(1)   | 116.7(2)   |
| Cu(1)–O(8)–C(12)    | 126.2(2)  | Cu(2c)–O(6)–C(10) | 129.1(2)   |
| Cu(1a)–O(8)–C(12)   | 110.4(2)  |                   |            |

<sup>a</sup> Estimated standard deviations in the last significant digits are given in parentheses.

<sup>b</sup> Symmetry code: (a)  $-x + 1, -y + 1, -z + 2$ ; (b)  $-x + 3/2, y + 1/2, -z + 5/2$ ; (c)  $-x + 3/2, y - 1/2, -z + 5/2$ .

The two phenylmalonate ligands simultaneously adopt bidentate [through O(2) and O(4) and O(5) and O(8)] and monodentate [through O(1) and O(6)] coordination modes at Cu(1) and Cu(2), respectively, affording the  $2_1$  chain with regular alternating of Cu(1) and Cu(2) atoms. In addition, one of two phenylmalonate groups [O(5)/O(8)] acts as a monodentate ligand [through the O(8) atom] towards a symmetry-related copper atom [Cu(1a)] from an adjacent chain (Fig. I.1); the  $2_1$  chains being thus linked by double  $\mu$ -oxo bridges. The bridging  $\text{Cu}_2\text{O}_2$  network is strictly planar owing to the inversion centre, and the a Cu(1)⋯Cu(1a) separation is 3.3042(5) Å. The value of the angle at the oxo bridge Cu–O–Cu is 97.38(7)°. The phenyl groups point always to the stacking direction of the layers [10-1]. The average values for the C–O bond distances and O–C–O bond angles are 1.251(3) Å and 122.2(3)° respectively. Two slightly different carboxylate bridges [O(1)C(1)O(2) and O(6)C(10)O(5)] that exhibit the *anti-syn* conformation and link equatorial positions of the

two copper atoms involved, alternate regularly within each chain. The values of the intrachain copper-copper separation through these carboxylate bridges are 4.6511(5) [Cu(1)⋯Cu(2)] and 5.0736(7) Å [Cu(1)⋯Cu(2c); (c) = -x + 3/2, y - 1/2, z + 5/2]. The values of the bond angles at the bridging O(1) and O(6) atoms are 116.7(2)° and 129.1(2)°, respectively. The values of the dihedral angle between the equatorial plane at Cu(1) and those of the O(1)C(1)O(2) and O(6)C(10)O(5) bridging carboxylates are 15.0(2) and 28.6(2)°, respectively. These values are far from the corresponding values between the equatorial plane at Cu(2) and the O(1)C(1)O(2) and O(6b)C(10b)O(5b) carboxylate planes, which are 82.67(12) and 89.9(2)°, respectively. The value of the angle between the two mean basal planes of the two crystallographically independent copper(II) ions is 87.62(7)°, indicating a quasi orthogonality between them. Curiously, the two Phmal ligands have different conformation: that containing O(2)/O(3) has the boat conformation whereas O(5)/O(8) exhibits the envelop one.

Let us finish this part with a comparison of the structure of **1** with that of the chain compound  $\{[\text{Cu}(\text{H}_2\text{O})_3][\text{Cu}(\text{mal})_2(\text{H}_2\text{O})]\}_n$  (mal = dianion of malonic acid).<sup>12</sup> This structure is made up of neutral uniform chains of copper(II) ions where the  $[\text{Cu}(\text{mal})_2(\text{H}_2\text{O})]^{2-}$  unit acts as a bis-monodentate ligand through malonate-oxygen atoms in *trans* positions of the two malonate ligands towards  $[\text{Cu}(\text{H}_2\text{O})_3]^{2+}$  entities. Both copper atoms have square pyramidal surroundings and the two carboxylate-malonate bridges exhibit the *anti-syn* conformation but one of them connects two equatorial copper sites and the other one links an equatorial with one axial site. In the case of compound **1**, one can observe an alternating arrangement of bis(phenylmalonato)cuprate(II) and triaquacopper(II) units, the former being linked to the latter as bimonodentate ligands through two *cis*-malonato oxygen atoms. The carboxylate-bridge in the resulting chain of **1** also has the *anti-syn* conformation but it connects equatorial positions of adjacent copper atoms. The presence of the phenyl ring introduces a non polar part and it exerts thus a strong influence on the resulting structure. In addition to the differences in the chelating/monodentate coordination mode of mal and Phmal within the copper(II) chain, the phenylmalonate in **1** is involved in  $\pi$ - $\pi$  interactions between the phenyl rings to build a hydrophobic intralayer space which accounts for the *cis* arrangement of the phenyl groups in each  $[\text{Cu}(\text{Phmal})_2]^{2-}$  unit. The phenylmalonate ligands of the  $[\text{Cu}(\text{Phmal})_2]^{2-}$  units tend to align their aromatic rings in the same direction, preventing the occupation of one of the axial positions of the copper(II) coordination sphere. As the other axial position is readily available, the lack of steric effects allows bulky groups to be introduced leading to the formation of the  $[\text{Cu}_2(\text{Phmal})_4]^{4-}$  dinuclear species through

double  $\mu$ -oxo(carboxylate) bridge. This dimerization has never been observed in other malonate-bridged complexes. The chains are interconnected through these units leading to a 2D system. The intrachain magnetic interaction in **1** is ferromagnetic as in  $\{[\text{Cu}(\text{H}_2\text{O})_3][\text{Cu}(\text{mal})_2(\text{H}_2\text{O})]\}_n$ , but in addition, these chains are also ferromagnetically coupled through the double  $\mu$ -oxo bridges in **1** (see below), the phenylmalonate allowing to increase the structural and magnetic dimensionality with respect to parent malonate-bridged copper(II) complexes.

#### I.1.4. Magnetic Properties

The magnetic properties of compound **1** under the form of  $\chi_M T$  vs.  $T$  plot ( $\chi_M$  being the molar susceptibility per copper(II) ion) are shown in the Figure I.4.  $\chi_M T$  at room temperature is  $0.42 \text{ cm}^3 \text{ mol}^{-1} \text{ K}$ , a value which is as expected for a magnetically isolated

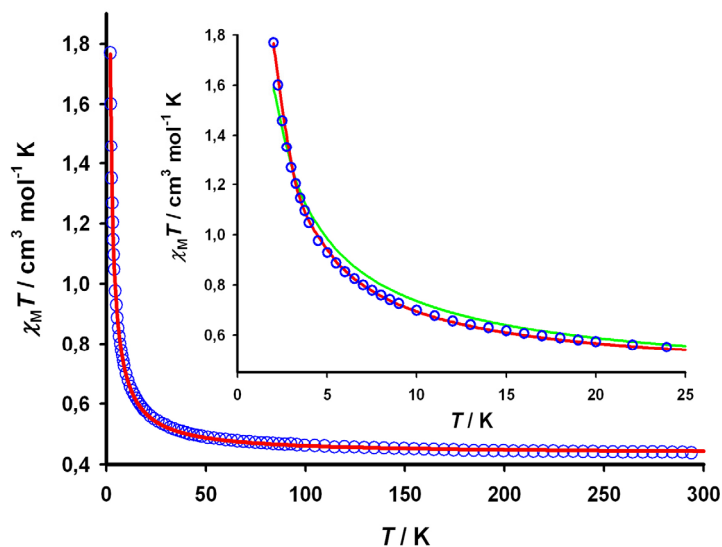


**Fig. I.4.** Thermal dependence of the  $\chi_M T$  product for **1**: (o) experimental data and (—) best fit curve. The inset shows the fits with  $\theta = 0$  (—) and  $0.70 \text{ K}$  (—) in the low temperature range (see text).

spin doublet. Upon cooling,  $\chi_M T$  increases smoothly until 50 K and then it undergoes a sharp increase to reach a value of  $1.77 \text{ cm}^3 \text{ mol}^{-1} \text{ K}$  at 2.0 K. Magnetization measurements show that the experimental data lies always above the theoretical Brillouin curve for a magnetically isolated  $S = \frac{1}{2}$  spin system, the saturation value being 1.05 BM (Fig. I.5). This behaviour is indicative of an overall ferromagnetic coupling between the copper(II) ions.

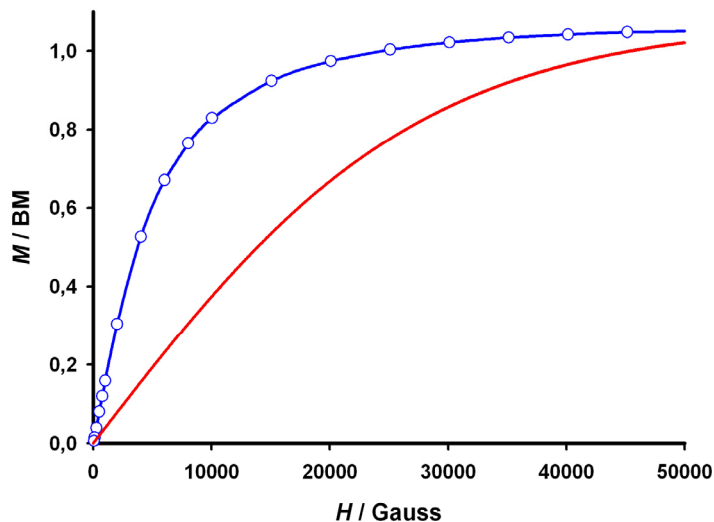


Fig. I.5. Magnetization ( $M$ ) vs. applied field ( $H$ ) plot. The red line is the Brillouin function for a magnetically isolated  $S = 1/2$  spin.

Two exchange pathways are operative in the structure of **1**: the carboxylate bridge in the *anti-syn* conformation within the  $2_1$  copper(II) chain and the double  $\mu$ -oxo(carboxylate) bridge between the chains. The carboxylate-bridged copper(II) chain may be considered as a regular chain, because of the occurrence of the same conformation in both carboxylate bridges and the similarity between the angles in the bridging skeleton, (see Scheme I.1). The magnetic data of **1** can be analyzed through the Baker and Rushbrooke numerical expression for a ferromagnetically coupled uniform copper(II) chain,<sup>13</sup> once the interchain magnetic interactions are neglected:

$$\chi_M = (N\beta^2 g^2 / 4kT)(A/B)^{2/3}$$

$$A = 1.0 + 5.7979916 y + 16.902653 y^2 + 29.376885 y^3 + 29.832959 y^4 + 14.036918 y^5$$

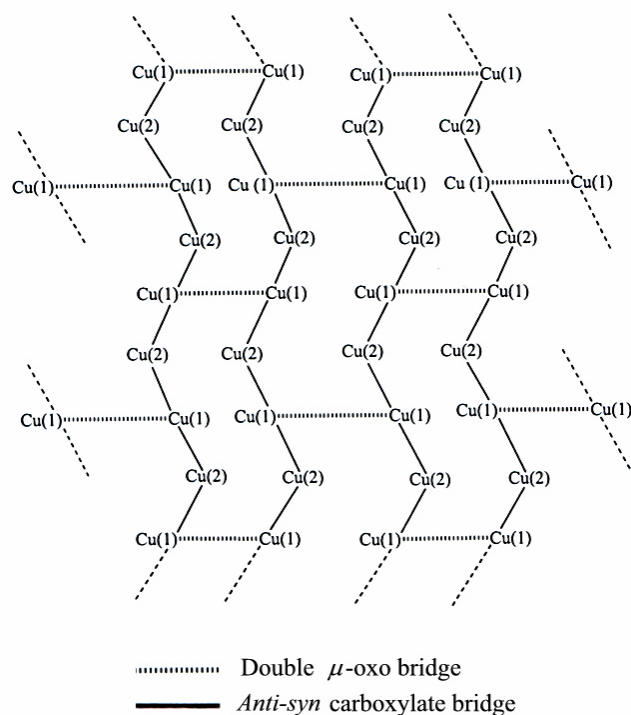
$$B = 1.0 + 2.7979916 y + 7.0086780 y^2 + 8.6538644 y^3 + 4.5743114 y^4$$

$$\hat{H} = -J \sum_i \hat{S}_i \cdot \hat{S}_{i+1}$$

with  $y = J/2kT$ .  $J$  is the intrachain magnetic coupling parameter, and the other symbols have their usual meanings. Best least-square fit parameters are  $J = +5.9(1) \text{ cm}^{-1}$ ,  $g = 2.11(1)$  and  $R = 2.0 \times 10^{-3}$ .  $R$  is the agreement factor defined as  $\sum_i [(\chi_M T)_{\text{obs}}(i) - (\chi_M T)_{\text{calc}}(i)]^2 / \sum [(\chi_M T)_{\text{obs}}(i)]^2$ . The calculated curve matches well the experimental data in the high



temperature range (above 30 K), but it lies above them in the lower temperature range (see inset of Fig. I.4). This suggests that the ferromagnetic interaction is overestimated and an additional interchain magnetic interaction is present being the double  $\mu$ -oxo bridge the most likely responsible for. Consequently, a mean-molecular field term is introduced to evaluate it. Under this approach, the best-fit parameters are  $J = +4.15(2) \text{ cm}^{-1}$ ,  $g = 2.155(1)$ ,  $\theta = 0.74(1) \text{ K}$  and  $R = 1.1 \times 10^{-4}$ . A value of the interchain coupling ( $zj$ ) of ca.  $+2.05 \text{ cm}^{-1}$  is derived from the relation  $\theta = \frac{zjS(S+1)}{3k}$ . The magnitude of this value must be taken with caution because of the inclusion in this parameter of the possible interactions through the weak  $\pi$ - $\pi$  stacking. In any case, it is clear that the two magnetic interactions ( $J$  and  $zj$ ) are ferromagnetic. The calculated curve with this last set of best-fit parameters reproduces very well the experimental data in the whole temperature range (Fig. I.4).



Scheme I.1

**Table I.3.** Relevant data for the magneto-structurally characterized double  $\mu$ -oxo carboxylate-bridged copper(II) systems

| Compound <sup>a</sup>                                                                             | $R_o / \text{\AA}$ | $\varphi / ^\circ$ | $J / \text{cm}^{-1}$          | Ref    |
|---------------------------------------------------------------------------------------------------|--------------------|--------------------|-------------------------------|--------|
| $\{\{\text{CuL}^1(\text{MeCO}_2)\}_2\}$                                                           | 2.665(4)           | 96.3(5)            | -1.84                         | 24a    |
| $\{\{\text{CuL}^2(\text{MeCO}_2)\}_2\}$                                                           | 2.577(2)           | 96.1(1)            | -1.51                         | 24a    |
| $\{\{\text{CuL}^3(\text{MeCO}_2)\}_2\}$                                                           | 2.512(5)           | 96.9(2)            | -1.33                         | 19,24b |
| $\{\{\text{CuL}^4(\text{MeCO}_2)\}_2 \cdot 2\text{H}_2\text{O}\}_n$                               | 2.498(8)           | 98.1(3)            | -1.54<br>(-2.26) <sup>b</sup> | 24b    |
| $\{\{\text{CuL}^5(\text{MeCO}_2)\}_n\} \cdot 2\text{MeOH}$                                        | 2.495(6)           | 98.3(5)            | -1.50<br>(-7.88) <sup>b</sup> | 24c    |
| $\{\{\text{CuL}^6(\text{MeCO}_2)\}_2\} \cdot \text{H}_2\text{O} \cdot \text{EtOH}$                | 2.446(2)           | 95.7(1)            | +0.63 <sup>c</sup>            | 26     |
| $\{\{\text{Cu}(\text{PhCONHCH}_2\text{CO}_2)(\text{H}_2\text{O})\}_2\} \cdot 2\text{H}_2\text{O}$ | 2.37(1)            | 101.0(5)           | -2.15                         | 20,21  |
| $\{\{\text{CuL}^7(\text{MeCO}_2)\}_2\}$                                                           | 2.490(1)           | 95.34(5)           | -0.25                         | 22     |
| $\{\{\text{Cu}(\text{tzq})_2(\text{HCO}_2)\}_2(\mu\text{-HCO}_2)_2\} \cdot 4\text{H}_2\text{O}$   | 2.331(4)           | 102.2(2)           | -0.52                         | 23     |
| Compound <b>1</b>                                                                                 | 2.433(2)           | 97.38(7)           | +1.95 <sup>d</sup>            |        |

<sup>a</sup> HL<sup>1</sup> = *N*-(5-Bromosalicylidene)-*N*-methylpropane-1,3-diamine, HL<sup>2</sup> = *N*-methyl-*N'*-(5-nitrosalicylidene)propane-1,3-diamine, HL<sup>3</sup> = *N*-methyl-*N'*-salicylidenepropane-1,3-diamine, HL<sup>4</sup> = *N*-(5-methoxysalicylidene)-*N*-methylpropane-1,3-diamine, HL<sup>5</sup> = *N,N'*-[bis(2-*o*-hydroxybenzylidene-amino)ethyl]ethane-1,2-diamine, HL<sup>6</sup> = *N*-(2-hydroxy-1,1-dimethylethyl)salicyleneamine, HL<sup>7</sup> = 7-amino-4-methyl-5-azahept-3-en-2-onate.

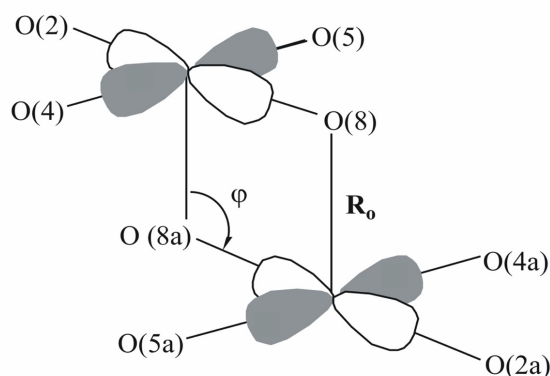
<sup>b</sup> Magnetic analysis through an alternating chain model.

<sup>c</sup> This is the only compound whose Cu<sub>2</sub>O<sub>2</sub> system is non centrosymmetric.

<sup>d</sup> This value is  $z_j$  (see text).

Let us analyze and discuss the nature and values of two magnetic couplings observed in **1**. The ferromagnetic coupling between Cu(1) and Cu(2) through the *anti-syn* carboxylate-malonate bridge in **1** is in agreement with the data reported in the literature for copper(II) complexes with this type of bridge.<sup>8,12,14</sup> Simple magnetic orbital considerations allow to understand the ferromagnetic interaction through this type of bridge. The unpaired electron of Cu(1) [the same applies for Cu(2)] is described by  $ae d(x^2-y^2)$  magnetic orbital, the  $x$  and  $y$  axes being roughly defined by the Cu(1)–O(2) and Cu(1)–O(4) bonds [Cu(2)–O(1) and Cu(2)–O(6b) at Cu(2)], and it is mainly located in the equatorial plane. As the mean basal planes of the adjacent Cu(1) and Cu(2) atoms make a dihedral angle very close to 90° [87.7(1)°], their magnetic orbitals are orthogonal and the magnetic coupling is ferromagnetic.<sup>8,15-18</sup> As far as the weak ferromagnetic coupling observed through the double  $\mu$ -oxo bridge is concerned, the comparison with previously magneto-structural results which are listed in Table I.3 provides a less clear picture. As one can see in this Table, the magnetic coupling through this type of bridge is weak and antiferromagnetic in most of the reported examples.<sup>19-23</sup> This family has in common the parallel arrangement of the  $d(x^2-y^2)$  type magnetic orbitals of the two copper(II) ions involved, each oxo atom occupying simultaneously an equatorial position at one copper atom and the axial one at the other copper atom (see Scheme I.2). The poor overlap between the two magnetic orbitals through

the out-of-plane exchange pathway allows the prediction of a weak antiferromagnetic interaction which can be ferromagnetic in the case of accidental orthogonality, the value of the angle at the oxo bridge and the basal to apical Cu–O bond length being the most important structural parameters in determining the sign and magnitude of the magnetic coupling.<sup>23,24</sup> The trigonal distortion of the copper environment seems to be another relevant parameter as already noted in the di- $\mu$ -chloro-bridged copper(II) complexes (out-of-plane exchange pathway).<sup>25</sup> In this respect, the compounds exhibiting antiferromagnetic coupling in Table I.3 have important trigonal distortions that mix the  $d_{z^2}$  orbital in the magnetic orbital of the Cu(II) ions, whereas the only case exhibiting ferromagnetic coupling has very little trigonal distortion of the Cu(II) environments ( $\tau$  being 0.09 and 0.06).<sup>26</sup> It seems that the very small trigonal distortion square pyramid of Cu(1) in **1** ( $\tau = 0.02$ ) minimizes the overlap between their magnetic orbitals through the double  $\mu$ -oxo bridge leading the ferromagnetic term to become dominant.



Scheme I.2

### I.1.5. Conclusion

Three important features of the compound presented in this section can be outlined: (i) the carboxylate-Phmal bridge is able to mediate ferromagnetic interactions between copper(II) ions through the *anti-syn* conformation as the malonate does; (ii) the inclusion of the phenyl ring in the malonate skeleton makes possible supramolecular interactions (offset  $\pi$ - $\pi$  stacking) and it allows the increase of the structural [ $\pi$ - $\pi$  stacking of the layers of copper(II) ions] and magnetic dimensionalities [intra- and interchain magnetic interactions between copper(II) ions through the Phmal ligand]; (iii) finally, the phenyl substituent induces subtle changes in the coordinating behaviour of the phenylmalonate ligand such as the bridging mode through double  $\mu$ -oxo(carboxylate).

## I.1.6. References

- 1 (a) S. O. H. Gutschke, D. J. Price, A. K. Powell and P. T. Wood, *Angew. Chem. Int. Ed.*, **2001**, *40*, 1920. (b) R. Kuhlman, G. L. Schimek and J. W. Kolis, *Inorg. Chem.*, **1999**, *38*, 194.
- 2 M. C. Etter, *J. Phys. Chem.*, **1991**, *95*, 4601.
- 3 S. K. Burley and G. A. Petsko, *Science*, **1985**, *229*, 23.
- 4 J. Singh and J. M. Thornton, *FEBS Lett.*, **1985**, *191*, 2989.
- 5 C. A. Hunter, J. Singh and J. M. Thornton, *J. Mol. Biol.*, **1990**, *211*, 595
- 6 L. F. Lindoy and I. M. Atkinson, *Self-Assembly in Supramolecular Chemistry*, Royal Society of Chemistry, Cambridge, UK, **2000**.
- 7 I. Dance, *Supramolecular Inorganic Chemistry*, in G. R. Desiraju (Editor), *The Crystal as a Supramolecular Entity*, John Wiley & Sons, Chichester, UK, **1996**.
- 8 J. Pasán, F. S. Delgado, Y. Rodríguez-Martín, M. Hernández-Molina, C. Ruiz-Pérez, J. Sanchiz, F. Lloret and M. Julve, *Polyhedron* **2003**, *22*, 2143.
- 9 C. Janiak, *J. Chem. Soc., Dalton Trans.* **2000**, 3885.
- 10 B. J. Hathaway, *Struct. Bonding (Berlin)* **1973**, *14*, 49.
- 11 A. W. Addison, T. N. Rao, J. Reedijk, J. van Rijn and G. C. Verschoor, *J. Chem. Soc., Dalton Trans.* **1984**, 1349.
- 12 C. Ruiz-Pérez, J. Sanchiz, M. Hernández-Molina, F. Lloret and M. Julve, *Inorg. Chem.* **2000**, *39*, 1363.
- 13 G. A. Baker, G. S. Rushbrooke and H. E. Gilbert, *Phys. Rev.* **1964**, *135*, A1272.
- 14 (a) C. Ruiz-Pérez, M. Hernández-Molina, P. Lorenzo-Luis, F. Lloret, J. Cano and M. Julve, *Inorg. Chem.* **2000**, *39*, 3845. (b) J. Sanchiz, Y. Rodríguez-Martín, C. Ruiz-Pérez, A. Mederos, F. Lloret and M. Julve, *New J. Chem.* **2002**, *26*, 1624. (c) Y. Rodríguez-Martín, C. Ruiz-Pérez, J. Sanchiz, F. Lloret and M. Julve, *Inorg. Chim. Acta* **2001**, *318*, 159. (d) Y. Rodríguez-Martín, M. Hernández-Molina, F. S. Delgado, J. Pasán, C. Ruiz-Pérez, J. Sanchiz, F. Lloret and M. Julve, *CrystEngComm* **2002**, *4*, 440. (e) Y. Rodríguez-Martín, C. Ruiz-Pérez, J. Sanchiz, F. Lloret and M. Julve, *Inorg. Chim. Acta* **2001**, *326*, 20. (f) Y. Rodríguez-Martín, M. Hernández-Molina, F. S. Delgado, J. Pasán, C. Ruiz-Pérez, J. Sanchiz, F. Lloret and M. Julve, *CrystEngComm* **2002**, *4*, 522. (g) F. S. Delgado, J. Sanchiz, C. Ruiz-Pérez, F. Lloret and M. Julve, *Inorg. Chem.* **2003**, *42*, 5938.
- 15 O. Kahn, *Molecular Magnetism*, VCH, New York, **1993**.
- 16 A. Rodríguez-Forteza, P. Alemany, S. Alvarez and E. Ruiz, *Chem. Eur. J.* **2001**, *7*, 627.
- 17 O. Castillo, A. Luque, F. Lloret and P. Román, *Inorg. Chim. Acta* **2001**, *324*, 141.
- 18 E. Colacio, M. Ghazi, R. Kivekäs and J. M. Moreno, *Inorg. Chem.* **2000**, *39*, 2882.
- 19 R. Hämäläinen, M. Ahlgren and U. Turpeinen, *Acta Cryst., Sect. B* **1982**, *38*, 1577.
- 20 J. N. Brown and L. M. Trefonas, *Inorg. Chem.* **1973**, *312*, 1730.
- 21 E. Dixon-Estes, W. E. Estes, R. P. N. Scaringe, W. E. Hatfield and D. J. Hodgson, *Inorg. Chem.* **1975**, *14*, 2564.
- 22 J. P. Costes, F. Dahan and J. P. Laurent, *Inorg. Chem.* **1985**, *24*, 1018.
- 23 E. Escrivá, J. Server-Carrió, L. Lezama, J. V. Folgado, J. L. Pizarro, R. Ballesteros and B. Abarca, *J. Chem. Soc., Dalton Trans.* **1997**, 2033.
- 24 (a) B. Chiari, J. H. Helms, O. Piovesana, T. Tarantelli and P. F. Zanazzi, *Inorg. Chem.* **1986**, *25*, 2408. (b) B. Chiari, J. H. Helms, O. Piovesana, T. Tarantelli and P. F. Zanazzi, *Inorg. Chem.* **1986**, *25*, 870. (c) B. Chiari, W. E. Hatfield, O. Piovesana, T. Tarantelli and P. F. Zanazzi, *Inorg. Chem.* **1983**, *22*, 1468. (d) L. K. Thompson, S. K. Mandal, S. S. Tandon, J. N. Bridson and M. K. Park, *Inorg. Chem.* **1996**, *35*, 3117. (e) A. Pasini, F. Demartin, O. Piovesana, B. Chiari, A. Cinti and O. Crispu, *J. Chem. Soc., Dalton Trans.* **2000**, 3467. (f) Y. Xie, H. Jiang, A. S. C. Chan, Q. Liu, X. Xu, C. Du and Y. Zhu, *Inorg. Chim. Acta* **2002**, *333*, 138.
- 25 M. Hernández-Molina, J. González-Platas, C. Ruiz-Pérez, F. Lloret and M. Julve, *Inorg. Chim. Acta* **1999**, *284*, 258.
- 26 A. M. Greenaway, C. J. O'Connor, J. W. Overman and E. Sinn, *Inorg. Chem.* **1981**, *20*, 1508.

## I.2. Pyrimidine (2) and Pyrazine (3) Copper(II)-Phenylmalonate Complexes

### I.2.1. Introduction

In the previous section we have shown how the introduction of a phenyl group in the methylene carbon of the malonate ligand modifies its coordination ability towards the copper(II) ions. Now, it is our purpose to continue this investigation with the introduction of a secondary ligand, rationally selected to take advantage of the singular characteristics of the phenylmalonate ligand. An aromatic N-donor ligand fulfils these requirements, being active to establish supramolecular interactions with the phenyl group of the Phmal ligand, and acting as a donor to the copper(II) ions. The question at hand which what could be a good choice? Since our first aim is to obtain high-dimensional systems, we prefer a bridging ligand instead of terminal one. Regarding at the malonate system and, as a first approximation, we pretend to emulate the three-dimensional networks obtained with cobalt(II) and zinc(II) with malonate and pyrimidine (pym) or pyrazine (pyz) ligands  $[M^{II}(L)_{1/2}(\text{mal})]_n$  [ $M^{II} = \text{Zn(II)}$  and  $\text{Co(II)}$ ;  $L = \text{pym}$  and  $\text{pyz}$ ],<sup>3</sup> which have not been prepared as copper(II) complexes. In those compounds, the layers of carboxylate (malonate)-bridged metal ions were linked through the N-donor ligands building up a three-dimensional network. In this section, we report the synthesis, structural and magnetic properties of the compounds  $[\text{Cu}(\text{pym})(\text{Phmal})]_n$  (2) and  $[\text{Cu}(\text{pyz})(\text{Phmal})]_n$  (3).

### I.2.2. Synthesis

**[Cu(pym)(Phmal)]<sub>n</sub> (2).** An aqueous solution (3 cm<sup>3</sup>) of copper(II)-phenylmalonate (0.5 mmol, 134 mg) was poured into one arm of a H-shape tube, whereas a 50/50 water/methanol

**Table I.4.** Crystallographic data for complexes 2-3

|                                                    | 2                                                                  | 3                                                                |
|----------------------------------------------------|--------------------------------------------------------------------|------------------------------------------------------------------|
| Formula                                            | C <sub>13</sub> H <sub>10</sub> O <sub>5.5</sub> N <sub>2</sub> Cu | C <sub>13</sub> H <sub>10</sub> O <sub>4</sub> N <sub>2</sub> Cu |
| FW                                                 | 345.77                                                             | 321.77                                                           |
| Crystal system                                     | Monoclinic                                                         | Monoclinic                                                       |
| Space group                                        | <i>P</i> 2 <sub>1</sub>                                            | <i>P</i> 2 <sub>1</sub> / <i>n</i>                               |
| <i>a</i> /Å                                        | 6.4460(16)                                                         | 7.019(3)                                                         |
| <i>b</i> /Å                                        | 6.4460(12)                                                         | 28.604(3)                                                        |
| <i>c</i> /Å                                        | 14.444(3)                                                          | 5.964(3)                                                         |
| $\beta$ /°                                         | 98.145(12)                                                         | 91.808(8)                                                        |
| <i>V</i> /Å <sup>3</sup>                           | 594.1(2)                                                           | 1196.8(8)                                                        |
| <i>Z</i>                                           | 2                                                                  | 4                                                                |
| $\mu(\text{Mo K}\alpha)$ /cm <sup>-1</sup>         | 18.70                                                              | 18.40                                                            |
| <i>T</i> /K                                        | 293 (2)                                                            | 293(2)                                                           |
| $\rho_{\text{calc}}$ /g cm <sup>-3</sup>           | 1.933                                                              | 1.786                                                            |
| $\lambda$ /Å                                       | 0.71073                                                            | 0.71073                                                          |
| Index ranges                                       | -9 ≤ <i>h</i> ≤ 9,<br>0 ≤ <i>k</i> ≤ 8,<br>-21 ≤ <i>l</i> ≤ 21     | -9 ≤ <i>h</i> ≤ 9,<br>-36 ≤ <i>k</i> ≤ 36,<br>-7 ≤ <i>l</i> ≤ 7  |
| Indep. reflect. ( <i>R</i> <sub>int</sub> )        | 1883 (0.0929)                                                      | 2694 (0.0753)                                                    |
| Obs. reflect. [ <i>I</i> > 2σ( <i>I</i> )]         | 1685                                                               | 2240                                                             |
| Parameters                                         | 199                                                                | 221                                                              |
| Goodness-of-fit                                    | 1.120                                                              | 1.210                                                            |
| <i>R</i> [ <i>I</i> > 2σ( <i>I</i> )]              | 0.0908                                                             | 0.0598                                                           |
| <i>R</i> <sub>w</sub> [ <i>I</i> > 2σ( <i>I</i> )] | 0.2361                                                             | 0.1323                                                           |
| <i>R</i> (all data)                                | 0.0997                                                             | 0.0740                                                           |
| <i>R</i> <sub>w</sub> (all data)                   | 0.2361                                                             | 0.1275                                                           |

solution (1 cm<sup>3</sup>) of pyrimidine (0.5 mmol, 40 mg) was added in the other one. The H-shape tube was filled with water and stored at 30 °C. Pale blue single crystals as twinned very thin plates of poor X-ray quality appeared after two weeks. Yield *ca.* 50 %. Anal. calc. for C<sub>13</sub>H<sub>10</sub>O<sub>5.5</sub>N<sub>2</sub>Cu (**2**): C, 46.23; H, 2.98; N, 8.29; Found: C, 46.18; H, 2.89; N, 8.20%.

**[Cu(pyzz)(Phmal)]<sub>n</sub> (3)**. This complex was prepared following the same procedure described for **2**, but using pyrazine (0.5 mmol, 40 mg) instead of pyrimidine, and storing the preparation at room temperature. Blue plate crystals of X-ray quality were grown after two weeks. Crystallographic data for **2** and **3** are shown in Table I.4. Yield 70 %. Anal. calc. for C<sub>13</sub>H<sub>10</sub>O<sub>4</sub>N<sub>2</sub>Cu (**3**): C, 48.52; H, 3.13; N, 8.71; Found: C, 48.48; H, 3.17; N, 8.70%.

### I.2.3. Description of the Structures

The structure of the complexes [Cu(pym)(Phmal)]<sub>n</sub> (**2**) and [Cu(pyzz)(Phmal)]<sub>n</sub> (**3**) (Figure I.6) consists of a sheet-like arrangement of (L)copper(II) (L = pym or pyzz) units bridged by phenylmalonate ligands running parallel to the *ab* (**2**) and *ac* (**3**) planes. A corrugated square grid of copper(II) atoms results (Figure I.7) where the pym or pyzz ligands are alternatively located above and below each layer and, at the same time, inversely to the position of the phenyl group of the Phmal ligand. These sheets are stacked parallel along the *c* (**2**) and *b* (**3**) axes, but in **3** the sheets are rotated 180° through the *c* direction in a twist fashion (Figure I.8) exhibiting the *ABABAB* sequence. The layers are well-separated from each other by means of hydrophobic groups (phenyl groups of the Phmal ligand and the aromatic pym or pyzz ligands) being the interlayer copper-copper separation in **3** shorter than in **2** [13.45(4) and 12.413(3) Å in **2** and **3**, respectively]. Weak  $\pi$ -type interactions play an important role in these structures as in that of **1** and they occur between the phenyl rings and the pym and pyzz ligands. Complex **2** presents most likely a face-to-face arrangement of the phenyl and pyrimidine groups with the shortest centroid-centroid distance being 3.74(3) Å and the shortest off-set angle being 28.1°. However, the aromatic groups of **3** are not located in a parallel arrangement as in **2** but forming a dihedral angle of 42.6° (between phenyl groups and pyrazine ligands) with a centroid-centroid distance of 4.330(1) Å. All these values are in agreement with previous reports on pyridyl-pyridyl interactions.<sup>1</sup>

Each copper atom exhibits a square-pyramidal environment (see Table I.5) (the  $\tau$  values<sup>2</sup> being 0.02 and 0.006 for **2** and **3**, respectively). Four phenylmalonate oxygen atoms from three different Phmal ligands build the basal plane [O(1), O(2), O(3), O(4), the average Cu–O bond distance being 1.960(6) Å] while a nitrogen atom from the pym or pyzz ligand occupies the axial position [Cu(1)–N(1) is 2.252(3) (**2**) and 2.242(1) Å (**3**)]. The copper

atom is shifted by 0.2049(10) (**2**) and 0.1416(2) Å (**3**) from the mean basal plane towards the apical position. The phenylmalonate ligand acts simultaneously as bidentate [through O(2) and O(4) with the angle subtended at the copper atom being 84.0(3)° (**2**) and 87.60(14)° (**3**)] and as bis-monodentate [through O(1) and O(3)]. The mean copper-copper separations through the phenylmalonate-carboxylate bridges within the layers are 5.121(17) and 5.122(17) Å, for **2** and **3**, respectively. These values are much shorter than the shortest interlayer metal-metal separation [13.45(4) Å (**2**) and 12.413(3) Å (**3**)].

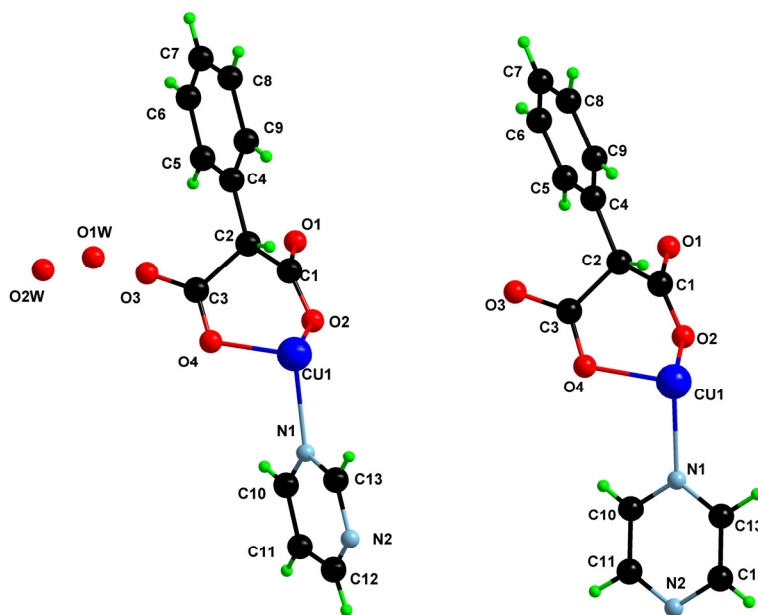


**Fig. I.6.** A view of the asymmetric units for compounds **2** (left) and **3** (right) along with their numbering scheme.

The layered structure of the complexes **2** and **3** is similar to that of **1**, however, the formation of these layers is quite different. In **1**, the layers are built by the regular alternation of  $[\text{Cu}(\text{Phmal})_2(\text{H}_2\text{O})]^{2-}$  anions and  $[\text{Cu}(\text{H}_2\text{O})_3]^{2+}$  cations (see Section 1.1) while the square grid of the copper atoms in **2** and **3** is formed repeating the neutral  $[\text{Cu}(\text{Phmal})(\text{L})]$  ( $\text{L} = \text{pym}$  or  $\text{pyz}$ ) unit. The formation of the square grid of transition metal ions in malonate-containing systems with the aid of pyridine-like ligands was previously reported.<sup>3</sup> In that case, complexes of formulae  $[\text{M}_2(\text{mal})_2(\text{L})(\text{H}_2\text{O})_2]_n \cdot n\text{H}_2\text{O}$  ( $\text{M} = \text{Zn}(\text{II})$  and  $\text{Co}(\text{II})$ ;  $\text{H}_2\text{mal} = \text{malonic acid}$ ;  $\text{L} = \text{pym}$  and  $\text{pyz}$ ) were synthesized and the structure is built up by layers of square grids of zinc and cobalt atoms which are linked through the pym and pyz ligands affording three-dimensional compounds. Despite the fact that the pym and pyz ligands bridge the layers, the main differences between the structures of these complexes

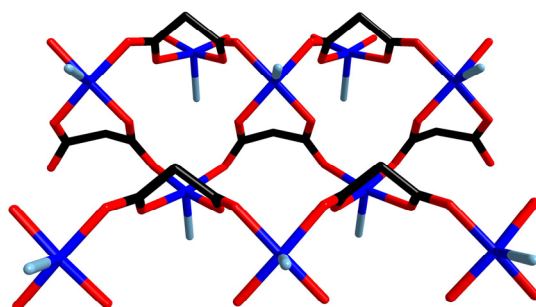


**Fig. I.7.** A central projection of the carboxylate-bridged square grid of copper(II) ions formed in **2** and **3**. The pyridine coligand and the phenyl group of the Phmal ligand have been omitted for clarity.

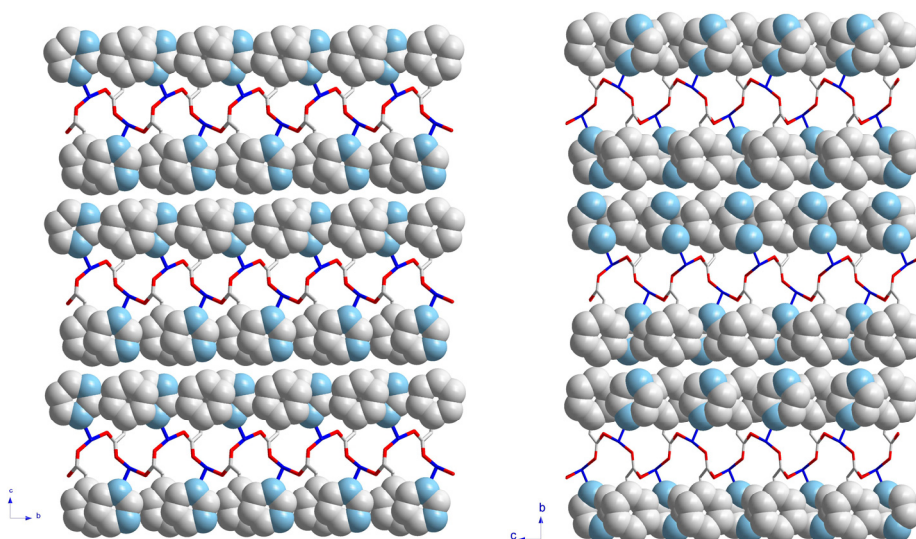


**Fig. I.8.** A view of the crystal packing along the *a* axis for **2** (left) and **3** (right).

and those of **2** and **3** are the octahedral environment at the metal ions in the Co(II) and Zn(II) complexes and the metal-metal separations, which are shorter in **2** and **3** [mean intralayer distances are 5.122 Å (**2** and **3**) and 5.357 Å in the reported malonate complexes]<sup>3</sup>.

Let us outline the fact that the pym and pyz ligands in **2** and **3** do not act as bridges between two copper atoms. This is an uncommon situation and, indeed, our goal in the use of these ligands is the reproduction of the results of the Co(II) and Zn(II) complexes with the malonate ligand (i.e. the formation of a three-dimensional complex).<sup>3</sup> From a CSD search we have found that this blocking conformation appears in other four (pym) and three



(pyz) copper(II) complexes those of twenty-five and one hundred and three which present bridging pym and pyz ligands, respectively. Moreover, if this CSD search is extended to the first-row transition metal ions, only eleven of over forty-eight complexes have a terminal pym ligand in their structure and ten over one hundred and seventy-three complexes do the same with the pyz ligand.

**Table I.5.** Selected bond lengths (Å) and bond angles (°) for compound **2** and **3**<sup>a,b</sup>

| <b>2</b>         |            |                   |            |
|------------------|------------|-------------------|------------|
| Cu(1)–O(2)       | 1.936(6)   | O(2)–Cu(1)–N(1)   | 100.7(4)   |
| Cu(1)–O(4)       | 1.944(7)   | O(4)–Cu(1)–O(1a)  | 167.4(3)   |
| Cu(1)–O(1a)      | 1.982(6)   | O(4)–Cu(1)–O(3b)  | 94.6(3)    |
| Cu(1)–O(3b)      | 1.979(7)   | O(4)–Cu(1)–N(1)   | 101.3(3)   |
| Cu(1)–N(1)       | 2.252(10)  | O(1a)–Cu(1)–O(3b) | 84.3(3)    |
| O(2)–Cu(1)–O(4)  | 84.0(3)    | O(1a)–Cu(1)–N(1)  | 91.2(3)    |
| O(2)–Cu(1)–O(1a) | 94.5(3)    | O(3b)–Cu(1)–N(1)  | 90.7(3)    |
| O(2)–Cu(1)–O(3b) | 168.6(3)   |                   |            |
| <b>3</b>         |            |                   |            |
| Cu(1)–O(2)       | 1.955(3)   | O(2)–Cu(1)–N(1)   | 102.87(14) |
| Cu(1)–O(4)       | 1.977(3)   | O(4)–Cu(1)–O(1c)  | 89.88(14)  |
| Cu(1)–O(1c)      | 1.954(3)   | O(4)–Cu(1)–O(3d)  | 171.28(14) |
| Cu(1)–O(3d)      | 1.953(3)   | O(4)–Cu(1)–N(1)   | 100.01(14) |
| Cu(1)–N(1)       | 2.242(4)   | O(1c)–Cu(1)–O(3d) | 91.65(14)  |
| O(2)–Cu(1)–O(4)  | 87.60(14)  | O(1c)–Cu(1)–N(1)  | 85.40(14)  |
| O(2)–Cu(1)–O(1c) | 171.65(14) | O(3d)–Cu(1)–N(1)  | 88.67(14)  |
| O(2)–Cu(1)–O(3d) | 89.67(14)  |                   |            |

<sup>a</sup> Estimated standard deviations in the last significant digits are given in parentheses.

<sup>b</sup> Symmetry code: (a)  $-x + 1, y + 1/2, -z$ ; (b)  $-x + 2, y + 1/2, -z$ ; (c)  $x - 1/2, -y + 1/2, z - 1/2$ ; (d)  $x + 1/2, -y + 1/2, z - 1/2$ .

We would like to finish the present structural description with a comparison of the structure of **3** with that of the previously reported malonato-copper(II) complex of formula  $[\text{Cu}_4(\text{mal})_4(\text{pyz})_2] \cdot 4\text{H}_2\text{O}$ .<sup>4</sup> This structure consists of a three-dimensional arrangement of copper(II) ions bridged by malonate and pyrazine ligands. Four copper atoms are linked through a malonate-carboxylate bridge to form small planar squares which are connected by pyrazine bridges affording a two-dimensional array. The layers are linked by malonate(carboxylate) bridges leading to a three-dimensional structure. The bidentate bis-monodentate coordination mode of the mal anion is the same of the Phmal in **3**, but the structure as a whole is quite different. Despite the fact that the pyz ligand acts as a terminal ligand in this compound, the formation of the small planar squares in **3** is avoided due to steric and hydrophobic effects of the phenyl ring. The influence of the phenyl ring leads the copper atom to adopt the role of the Co(II) and Zn(II) ions in the malonate-containing complexes.

### I.2.4. Magnetic Properties

The temperature dependence of the  $\chi_M T$  product [ $\chi_M$  being the magnetic susceptibility per copper(II) ion] for **2** in the temperature range 1.8–300 K is shown in Figure I.9.  $\chi_M T$  at room temperature is  $0.42 \text{ cm}^3 \text{ mol}^{-1} \text{ K}$ , a value which is as expected for a magnetically isolated spin doublet. Upon cooling,  $\chi_M T$  continuously increases to reach a value of  $25.9 \text{ cm}^3 \text{ mol}^{-1} \text{ K}$  at 2.15 K, and further decreases to  $17.5 \text{ cm}^3 \text{ mol}^{-1} \text{ K}$  at 1.8 K. A susceptibility maximum is observed at 2.15 K under  $H \leq 130 \text{ G}$ . This maximum disappears for  $H > 130 \text{ G}$  (Figure I.10).

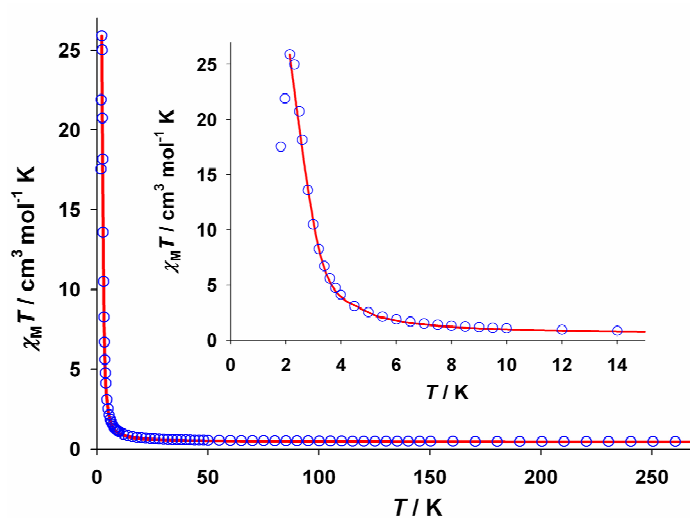


**Fig. I.9.**  $\chi_M T$  vs  $T$  plot for **2** under applied magnetic fields of 1 T ( $T \geq 12 \text{ K}$ ) and 0.01 T ( $T < 12 \text{ K}$ ): (o) experimental data; (—) best-fit curve (see text). The inset shows a detail of the low temperature region.

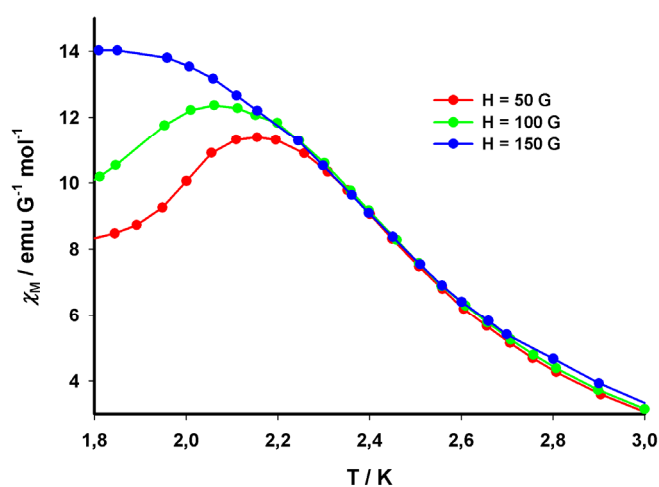


**Fig. I.10.**  $\chi_M$  vs  $T$  plot for **2** at different applied magnetic fields.

These features correspond to a metamagnetic-like behaviour which is due to the coexistence of ferro- and antiferromagnetic interactions, the latter one being overcome by an applied field larger than 130 G. The magnetization ( $M$ ) versus  $H$  plot at 1.8 K confirms this metamagnetic behaviour (Figure I.11). The abrupt increase of  $M$  at low fields and the saturation value of 1.06 BM for  $H > 3$  T, support the presence of a ferromagnetic interaction between the spin doublets. The sigmoidal shape of the magnetization plot at very low fields (see inset of Fig. I.11) with a value for the critical field ( $H_c$ ) of 130 G accounts for a very weak antiferromagnetic interaction (*ca.*  $10^{-2}$  cm $^{-1}$ ). The susceptibility maximum at  $H < H_c$  corresponds to the onset of a long range antiferromagnetic ordering. The value of the ordering temperature ( $T_c = 2.15$  K) is determined by the position of the maximum of the out-of-phase signal ( $\chi_M''$ ) (see Figure I.12).

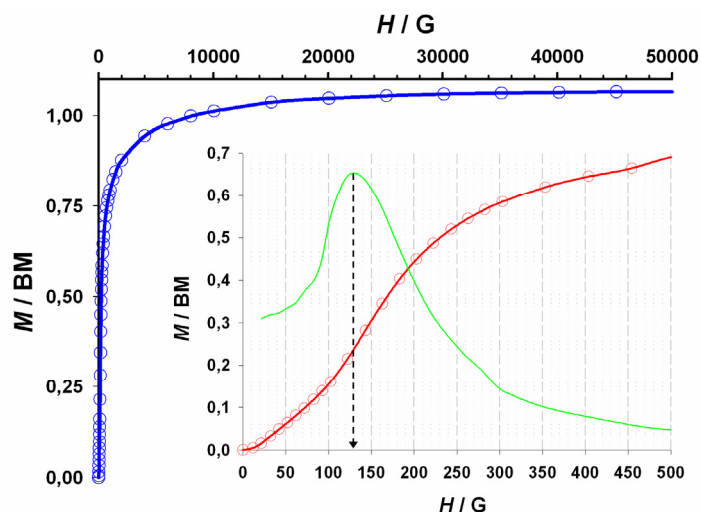


Fig. I.11. Magnetization vs.  $H$  plot at 1.8 K. The inset shows the sigmoidal shape of the magnetization in the low field region together with the  $\partial M/\partial H$  (in green).

In the light of the above magneto-structural data of **2**, its magnetic behaviour would correspond to that of a ferromagnetically coupled square grid of copper(II) ions through carboxylate-bridge in the *anti-syn* conformation, each layer interacting antiferromagnetically with the adjacent ones. Consequently, the high temperature magnetic data of **2** were analyzed through the expression of the magnetic susceptibility by Baker *et al.* derived from the high-temperature expansion series for an isotropic ferromagnetic square lattice with interacting spin doublets.<sup>5</sup> The spin Hamiltonian is defined as:

$$\hat{H} = -J \sum_i \hat{S}_i \cdot \hat{S}_{i+1}$$

and the series takes the form:

$$\chi = \left( \frac{N\beta^2 g^2}{3k_B T} S(S+1) \right) \left[ 1 + \sum_{n \geq 1} a_n \frac{x^n}{2^n} \right]$$

where  $N$ ,  $g$ ,  $\beta$  and  $k_B$  have their usual meanings,  $x = J/k_B T$ ,  $J$  is the intralayer magnetic coupling and  $a_n$  are coefficients which run up to  $n = 10$ . Least-squares fit of the experimental data in the temperature range 5–300 K leads to  $J = +5.6(1) \text{ cm}^{-1}$ ,  $g = 2.12(2)$  and  $R = 8.9 \times 10^{-5}$ . The calculated curve matches very well the experimental data in the 5-300 K temperature range. The value of  $J$  for **2** is the largest one observed in the family of carboxylate(phenylmalonate)-bridged copper(II) complexes [ $J$  ranging from  $-0.59(1)$  to  $+4.44(5) \text{ cm}^{-1}$ ]<sup>6,7</sup> and it is within the range of the previously reported magnetic interactions for the *anti-syn* carboxylate(malonate)-bridged copper(II) complexes.<sup>8,9</sup> The smaller value of  $\tau$  of the copper atom in the case of **1** when compared to other examples with the phenylmalonate ligand reduces the admixture of the  $d_{z^2}$  character in the  $d(x^2-y^2)$  magnetic orbital and reinforces the magnetic coupling through the equatorial-equatorial exchange pathway, everything being similar.

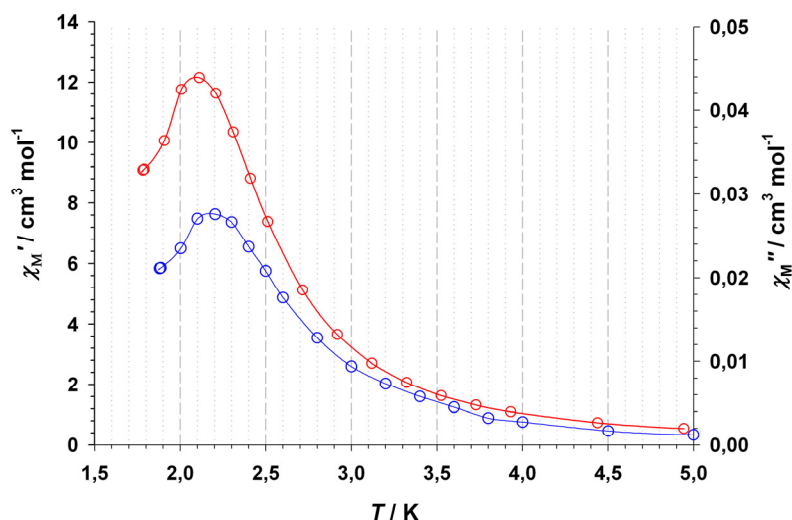


**Fig. I.12.** In-phase (red) and out-of-phase (blue) ac signals of **2** in a 1 G field oscillating at 330 Hz without dc magnetic field: (o,o) experimental data; (–) eye-guide line.

The weak antiferromagnetic interaction (*ca.*  $10^{-2} \text{ cm}^{-1}$ ) between the ferromagnetically coupled layers of **1** leads to a 3D antiferromagnetic ordering with a  $T_c$  value of 2.15 K and it accounts for the observed metamagnetic behaviour. The small magnitude of the interlayer magnetic interaction is in agreement with the large interlayer metal-metal separation and most likely it is dipolar through-space in origin, given the lack of hydrogen bonds and  $\pi$ -type interactions between the layers. This situation is similar to that observed in layered compounds of formula  $M_2(\text{OH})_3\text{X}$  [ $M = \text{Cu(II)}$  and  $\text{Co(II)}$ ;  $\text{X} = \text{organic anion}$ ] which exhibit dominant

ferromagnetic in-plane interactions, and ferro- or antiferromagnetic inter-plane interactions depending on the interlayer separation. These studies have shown that large spacing favours spontaneous magnetization.<sup>10</sup>

The magnetic properties of **3** under the form of  $\chi_M T$  vs.  $T$  plot [ $\chi_M$  being the magnetic susceptibility per copper(II) ion] are presented in Figure I.13. The value of  $\chi_M T$  at room temperature is  $0.46 \text{ cm}^3 \text{ mol}^{-1} \text{ K}$ , a value which is as expected for a magnetically isolated spin doublet. Upon cooling,  $\chi_M T$  smoothly increases to reach a maximum of  $0.55 \text{ cm}^3 \text{ mol}^{-1} \text{ K}$  at 19 K, then the  $\chi_M T$  product sharply decreases to  $0.14 \text{ cm}^3 \text{ mol}^{-1} \text{ K}$  at 2.0 K. A susceptibility maximum is observed at 3.5 K (see inset of Fig. I.13). This maximum disappears for applied fields  $H > 3 \text{ T}$  (Figure I.14). These features are very similar to that observed in **2**, and the same phenomenon is present here. A metamagnetic-like behaviour occurs in **3** due to the coexistence of ferro- and antiferromagnetic interactions, the latter being overcome for  $H > 3 \text{ T}$ . The magnetization ( $M$ ) vs  $H$  plot at 2.0 K for **3** confirms this assumption showing a sigmoidal shape with an inflexion point at  $H_c = 3.6 \text{ T}$  (Figure I.15). The linearity of the magnetization at applied fields below the inflexion point is indicative of antiferromagnetic coupling with the value of the critical field  $H_c = 3.6 \text{ T}$  accounts for the magnitude of the interaction ( $J$  being approx.  $3.6 \text{ cm}^{-1}$ ).

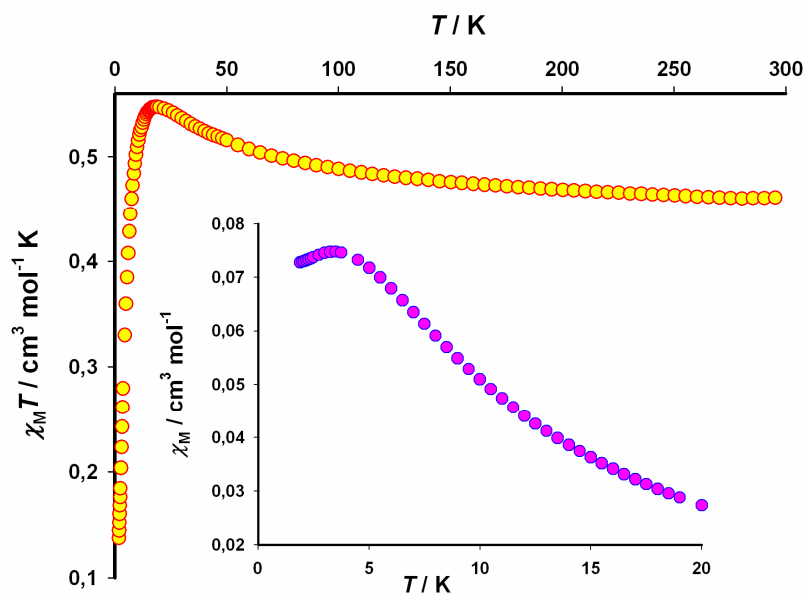


**Fig. I.13.** Thermal dependence of the  $\chi_M T$  product for complex **3** under applied magnetic fields of 1 T ( $T \geq 19 \text{ K}$ ) and 0.025 T ( $T < 19 \text{ K}$ ). The inset shows the  $\chi_M$  vs.  $T$  plot in the low temperature region.

The two coexisting ferro- and antiferromagnetic interactions are present within the square grid of carboxylate-bridged copper(II) ions in **3**, this behaviour being different from what is observed in **2**. The lack of a theoretical model to analyse a square grid of copper(II) ions magnetically coupled through two parameters different in nature, lead us to approximate this situation to ferromagnetically coupled chains which interact antiferromagnetically by means of a mean-field parameter. However, this approximation is not applicable because the antiferromagnetic coupling constant is *ca.*  $-3.6 \text{ cm}^{-1}$ , being of the same order than the ferromagnetic coupling parameter through the *anti-syn* equatorial-equatorial carboxylate bridge for **1** and **2** [ $J$  being  $+4.15(2)$  and  $+5.6(1) \text{ cm}^{-1}$ , respectively] or related malonate complexes.<sup>8</sup> This is the first observation of a malonate- or phenylmalonate-carboxylate bridge mediating antiferromagnetic interactions in copper(II) complexes.<sup>6-9</sup> The antiferromagnetic interaction become dominant in one of the bridges, according to the Kanh's model,<sup>11</sup> due to the almost perfect square pyramidal environment and the small values of the dihedral angles between the equatorial plane of the copper atom and the carboxylate bridges (see Table I.6) which favour a high overlapping between the  $d(x^2-y^2)$  magnetic orbitals of adjacent copper atoms.

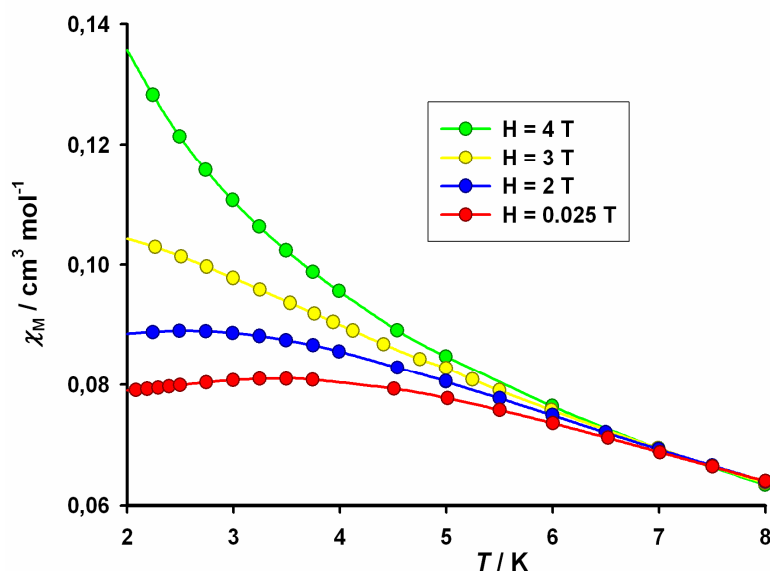
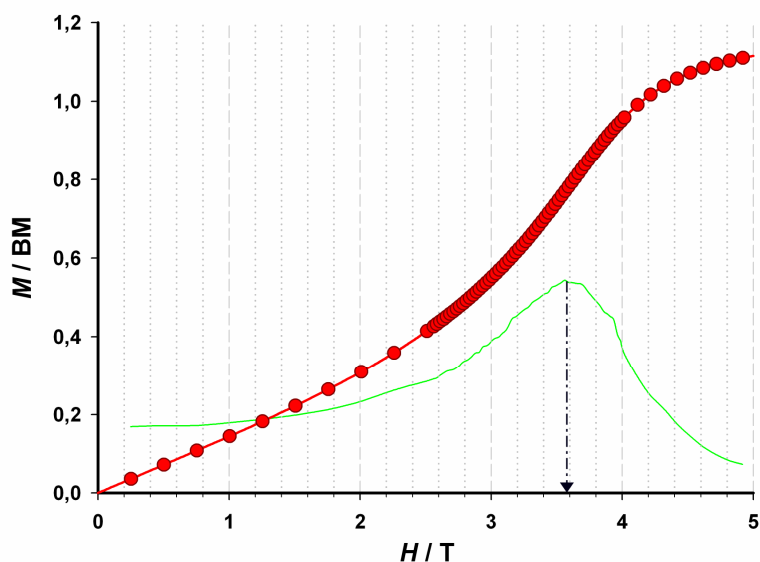


Fig. I.14.  $\chi_M$  vs  $T$  plot for **3** at different applied magnetic fields.

Fig. I.15. Magnetization vs.  $H$  plot at 1.8 K together with the  $\partial M/\partial H$  (in green).**Table I.6.** Selected structural features for complexes **2** and **3**.

|                           | <b>2</b>            | <b>3</b>              |
|---------------------------|---------------------|-----------------------|
| Cu(1)–O(1)                | 1.982(6) Å          | 1.954(3) Å            |
| Cu(1)–O(2)                | 1.936(6) Å          | 1.955(3) Å            |
| Cu(1)–O(3)                | 1.979(7) Å          | 1.953(3) Å            |
| Cu(1)–O(4)                | 1.944(7) Å          | 1.977(3) Å            |
| Cu(1)–N(1)                | 2.252(10) Å         | 2.242(4) Å            |
| $\tau$ value              | 0.02                | 0.006                 |
| Interlayer <sup>a</sup>   | 13.45(4) Å          | 12.413(3) Å           |
| Intralayer A <sup>b</sup> | 5.100(8) Å          | 5.058(3) Å            |
| Intralayer B              | 5.143(7) Å          | 5.187(3) Å            |
| Bridge A <sup>b</sup>     | 60.57(6)°–72.62(7)° | 53.915(8)°–68.299(8)° |
| Bridge B                  | 59.76(7)°–71.28(7)° | 53.749(8)°–67.081(9)° |
| $\beta^c$                 | 63.16(2)°           | 66.761(12)°           |

<sup>a</sup> Shortest copper-copper separation between two adjacent layers.

<sup>b</sup> Shortest Cu–Cu intralayer separation. A and B refer to the two crystallographically different carboxylate bridges present in the structure, which are defined univocally by the Cu–Cu separation.

<sup>c</sup> Angle between the equatorial planes of adjacent copper atoms.

### I.2.5. Conclusion

The two complexes presented in this section are very important because the number of questions that they raised is greater than the number of answers. Both compounds present almost the same layered structure, with a carboxylate-bridged square grid of copper(II) ions

separated by a hydrophilic area where the phenyl ring of the Phmal and the pym and pyz ligands are located. This is in agreement with that observed for complex **1**, the hydrophobic forces leading to the formation of well separated layers.

However, their magnetic properties are very different. Complex **2** exhibits metamagnetic-like behaviour with 3D magnetic ordering below 2.15 K. This is based on ferromagnetically coupled layers [with a coupling constant of  $+5.6(1) \text{ cm}^{-1}$ ] which interact antiferromagnetically among them [with a magnetic coupling of *ca.*  $0.01 \text{ cm}^{-1}$ , which estimated from the magnetization curve]. Complex **3** presents the coexistence of ferro- and antiferromagnetic interactions within the carboxylate-bridged copper(II) layers, a situation which is unprecedented in malonate or phenylmalonate copper(II) complexes.

Among the large number of structural features which can influence the magnetic properties, what are those which have changed from **2** to **3** to cause that dramatic variation in their magnetic properties? Could we control the magnetic properties through an adequate choice of the N-donor coligand?

## I.2.6. References

- 1 C. Janiak, *Dalton Trans.* **2000**, 3885.
- 2 A. W. Addison, T. N. Rao, J. Reedijk, J. van Rijn and G. C. Verschoor, *Dalton Trans.* **1984**, 1349.
- 3 F. S. Delgado, J. Sanchiz, C. Ruiz-Pérez, F. Lloret and M. Julve, *CrystEngComm* **2003**, *5*(48), 280.
- 4 Y. Rodríguez-Martín, M. Hernández-Molina, F.S. Delgado, J. Pasán, C. Ruiz-Pérez, J. Sanchiz, F. Lloret and M. Julve, *CrystEngComm* **2002**, *4*(73), 440.
- 5 R. Navarro, *Application of High- and Low-Temperature Series Expansions to Two-dimensional Magnetic Systems*, L. J.de Jongh, Ed., Kluwer Academic Publishers, The Netherlands, **1990**.
- 6 J. Pasán, J. Sanchiz, C. Ruiz-Pérez, F. Lloret and M. Julve, *New J. Chem.*, **2003**, *27*, 1557.
- 7 J. Pasán, J. Sanchiz, C. Ruiz-Pérez, F. Lloret and M. Julve, *Eur. J. Inorg. Chem.* **2004**, 4081; J. Pasán, J. Sanchiz, C. Ruiz-Pérez, F. Lloret and M. Julve, *Inorg. Chem.* **2005**, *44*, 7794.
- 8 J. Pasán, F. S. Delgado, Y. Rodríguez-Martín, M. Hernández-Molina, C. Ruiz-Pérez, J. Sanchiz, F. Lloret and M. Julve, *Polyhedron* **2003**, *22*, 2143.
- 9 C. Ruiz-Pérez, Y. Rodríguez-Martín, M. Hernández-Molina, F. S. Delgado, J. Pasán, J. Sanchiz, F. Lloret and M. Julve, *Polyhedron* **2003**, *22*, 2111.
- 10 V. Laget, C. Hornick, P. Rabu, M. Drillon and R. Ziessel, *Coord. Chem. Rev.* **1998**, *178-180*, 1533.
- 11 O. Kahn, *Molecular Magnetism*, VCH, New York, **1993**.



### I.3. 3-Cyanopyridine (4) and 4-Cyanopyridine (5) Copper(II)-Phenylmalonate Complexes

#### I.3.1. Introduction

The introduction of an aromatic N-donor coligand in the phenylmalonate-copper(II) system afforded layered structures due to the formation of interlayer hydrophobic areas by means of the aromatic rings which are present in the ligands. Complexes **2** and **3** described in the previous section exhibit as unique difference the position of the azine nitrogen atoms, and the magnetic behaviour of both compounds show important dissimilarities. Now, we have made an attempt to emphasize them by using coligands with bulky groups at the positions three and four of the pyridine ring. Among the variety of functional groups, we have chosen the cyano groups due to their ability to establish weak interactions between them.

#### I.3.2. Synthesis

**[Cu(3-CNpy)(Phmal)]<sub>n</sub> (4).** An aqueous solution (3 cm<sup>3</sup>) of copper(II)-phenylmalonate (0.5 mmol, 120 mg) (which was prepared as described in Section 1.1) was set in one arm of a water-fulfilled H-shape tube whereas a 50/50 water/methanol solution (1 cm<sup>3</sup>) of 3-cyanopyridine (0.5 mmol, 55 mg) was added in the other arm. Pale blue single crystals of **4** in the form of extremely thin plates were grown in the H-shape tube after one month. Yield *ca.* 50%. Anal. calc. for C<sub>15</sub>H<sub>10</sub>O<sub>4</sub>N<sub>2</sub>Cu (**4**): C, 52.10; H, 2.91; N, 8.10; Found: C, 52.05; H, 3.01; N, 8.05%.

**Table I.7.** Crystallographic data for complexes **4-5**

|                                                             | <b>4</b>                                                         | <b>5</b>                                                         |
|-------------------------------------------------------------|------------------------------------------------------------------|------------------------------------------------------------------|
| Formula                                                     | C <sub>15</sub> H <sub>10</sub> O <sub>4</sub> N <sub>2</sub> Cu | C <sub>15</sub> H <sub>10</sub> O <sub>4</sub> N <sub>2</sub> Cu |
| FW                                                          | 345.79                                                           | 345.79                                                           |
| Crystal system                                              | Monoclinic                                                       | Monoclinic                                                       |
| Space group                                                 | <i>P</i> 2 <sub>1</sub> / <i>n</i>                               | <i>P</i> 2 <sub>1</sub> / <i>n</i>                               |
| <i>a</i> /Å                                                 | 6.9188(8)                                                        | 6.924(4)                                                         |
| <i>b</i> /Å                                                 | 31.180(12)                                                       | 31.716(18)                                                       |
| <i>c</i> /Å                                                 | 6.2103(11)                                                       | 6.315(3)                                                         |
| $\beta$ /°                                                  | 93.463(15)                                                       | 92.78(5)                                                         |
| <i>V</i> /Å <sup>3</sup>                                    | 1337.3(6)                                                        | 1385.2(13)                                                       |
| <i>Z</i>                                                    | 4                                                                | 4                                                                |
| $\mu$ (Mo K $\alpha$ ) /cm <sup>-1</sup>                    | 16.53                                                            | 15.96                                                            |
| <i>T</i> /K                                                 | 293 (2)                                                          | 293(2)                                                           |
| $\rho_{\text{calc}}$ /g cm <sup>-3</sup>                    | 1.717                                                            | 1.658                                                            |
| $\lambda$ /Å                                                | 0.71073                                                          | 0.71073                                                          |
| Index ranges                                                | -9 ≤ <i>h</i> ≤ 9,<br>-43 ≤ <i>k</i> ≤ 43,<br>-8 ≤ <i>l</i> ≤ 8  | -9 ≤ <i>h</i> ≤ 9,<br>-44 ≤ <i>k</i> ≤ 44,<br>-8 ≤ <i>l</i> ≤ 8  |
| Indep. reflect. ( <i>R</i> <sub>int</sub> )                 | 3787 (0.0986)                                                    | 2650 (0.0954)                                                    |
| Obs. reflect. [ <i>I</i> > 2 $\sigma$ ( <i>I</i> )]         | 2718                                                             | 1598                                                             |
| Parameters                                                  | 239                                                              | 200                                                              |
| Goodness-of-fit                                             | 1.053                                                            | 1.073                                                            |
| <i>R</i> [ <i>I</i> > 2 $\sigma$ ( <i>I</i> )]              | 0.0578                                                           | 0.0894                                                           |
| <i>R</i> <sub>w</sub> [ <i>I</i> > 2 $\sigma$ ( <i>I</i> )] | 0.1357                                                           | 0.1503                                                           |
| <i>R</i> (all data)                                         | 0.0865                                                           | 0.1506                                                           |
| <i>R</i> <sub>w</sub> (all data)                            | 0.1458                                                           | 0.1670                                                           |

**[Cu(4-CNpy)(Phmal)]<sub>n</sub> (5).** Complex **5** was prepared following the same procedure used for **4** but replacing 3- cyanopyridine by 4-cyanopyridine (0.5 mmol, 55 mg) instead of 3-cyanopyridine. Pale blue plate single crystals appear after one month. Crystallographic

details for **4** and **5** are listed in Table I.7. Yield 50 %. Anal. calc. for  $C_{15}H_{10}O_4N_2Cu$  (**5**): C, 52.10; H, 2.91; N, 8.10; Found: C, 52.15; H, 2.85; N, 8.16%.

### I.3.3. Description of the Structures

The crystal structures of  $[Cu(3-CNpy)(Phmal)]_n$  (**4**) and  $[Cu(4-CNpy)(Phmal)]_n$  (**5**) (Figure I.16) consist of two-dimensional networks of *anti-syn* phenylmalonate-carboxylate bridged [(L)copper(II)] units (L = 3-CNpy and 4-CNpy) similar to those found for **2** and **3**. The resulting corrugated square grid of copper(II) atoms (Figure I.17) presents the 3- and 4-CNpy ligands alternatively located above and below each layer, inversely to the position of the phenyl group of the Phmal ligand, as occurred in **2** and **3**. The sheets in both compounds are extended in the *ac* plane and are stacked along the *b* axis with the odd layers rotated  $180^\circ$  exhibiting the *ABABAB* sequence (Figure I.18). These layers are well-separated by means of the aromatic groups of the Phmal and that of the 3- and 4-CNpy ligands; the interlayer copper-copper separation being 13.705(5) (**4**) and 13.985(8) Å (**5**). Weak interactions between the cyano groups play an important role in the stabilization of the structure (Figure I.19). The cyano groups of the CNpy ligands from different layers are symmetry-related (sym =  $-x, -y, 2-z$ ) and they exhibit a parallel arrangement. The distances between the midpoints of the C–N bonds are 3.5854(5) (**4**) and 3.5846(18) Å (**5**) and the angles  $C^{(1)}-N^{(1)}\dots C^{(2)}$  are  $90.513(3)^\circ$  (**4**) and  $92.643(12)^\circ$  (**5**). These values are in agreement with those reported for cyano-cyano<sup>1</sup> and carbonyl-carbonyl<sup>2</sup> interactions. Weak intralayer  $\pi$ -type interactions between the Phmal and CNpy ligands also contribute to the stabilization of the structure. The aromatic rings are disposed in a face-to-face arrangement with the shortest centroid-centroid distance and off-set angle of 4.217(5) Å and  $30.9^\circ$  (**4**) and 4.452(7) and  $29.6^\circ$  (**5**), respectively. These values are in agreement with those previously reported for pyridine-type interactions.<sup>3</sup>

Each copper atom exhibits a square-pyramidal environment (the  $\tau$  value is 0.015 and 0.018 for **4** and **5**, respectively).<sup>4</sup> Four phenylmalonate oxygen atoms [O(1), O(2), O(3), O(4)] from three different Phmal ligands build the basal plane. The copper-oxygen atoms distances in **4** are similar (see Table I.8), [mean bond distance is 1.9599(3) Å], whereas two bonds in *trans* conformation in **5** are longer [Cu(1)–O(1) and Cu(1)–O(2), the average value being 2.025(5) Å] than the other two [Cu(1)–O(3) and Cu(1)–O(4), average value of 1.892(5) Å] which are shorter than the bond distances of the copper coordination environment in **2-4**. The apical position is occupied by a nitrogen atom from the CNpy ligand [Cu(1)–N(1) distances being 2.250(3) and 2.236(7) Å for **4** and **5**, respectively]. The

copper atom is shifted by 0.1131(5) (4) and 0.1008(13) Å (5) from the basal plane towards the apical position.

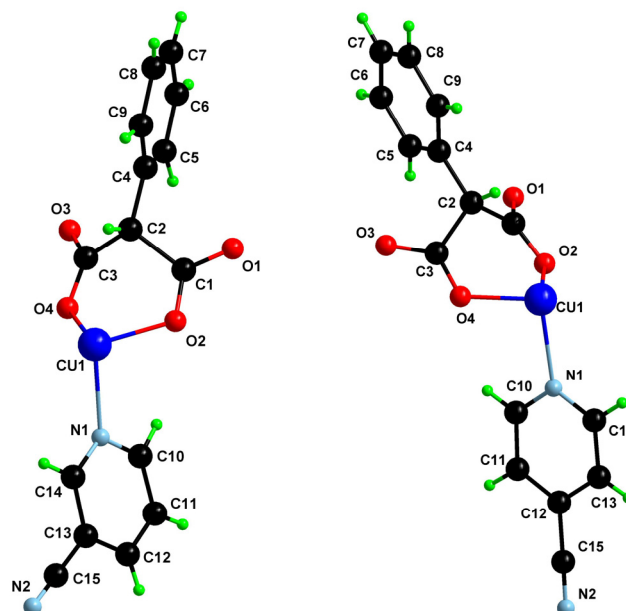


Fig. I.16. A view of the asymmetric units for compounds 4 (left) and 5 (right) along with the numbering scheme.

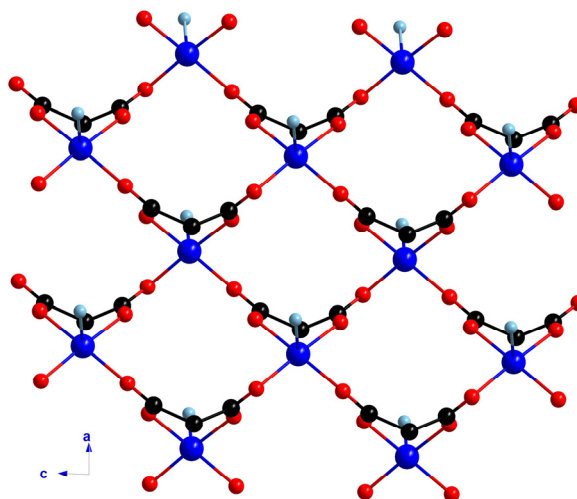
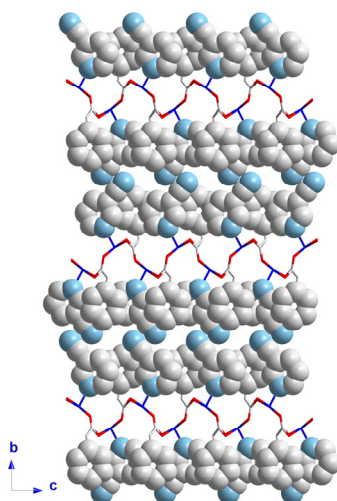


Fig. I.17. Perspective view along the *b* axis of the carboxylate-bridged square grid of copper(II) ions formed in 4 and 5. Pyridine coligands and the phenyl ring of the Phmal ligand are omitted.

The phenylmalonate acts simultaneously as bidentate [through O(2) and O(4), with the angle subtended at the copper atom being 88.16(10)° (4) and 88.3(2)° (5)] and as bis-monodentate ligand [through O(1) and O(3)]. There are two different copper-copper

separations within the layers due to the presence of two crystallographically different phenylmalonate-carboxylate bridges [O(1)–C(1)–O(2) and O(3)–C(3)–O(4)], the copper-copper distances through these bridges being 5.238(2) and 4.984(2) Å for **4** and 5.229(4) and 5.022(5) for **5**, respectively.



**Fig. I.18.** A view along the *a* axis of the crystal packing of complex **4**. The odd layers are rotated 180° in a twist fashion exhibiting the *ABABAB* sequence.

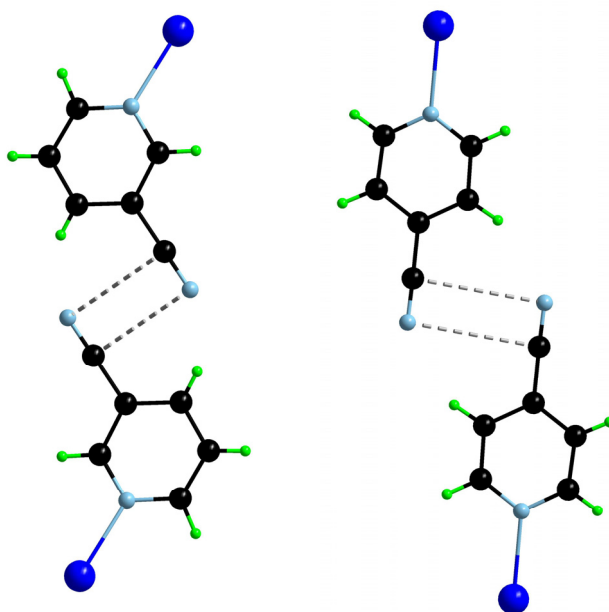


**Fig. I.19.** C–N⋯C–N interactions among the cyano groups of the cyanopyridine ligands of different layers in **4** (left) and **5** (right).

Let us finish the present structural description with a comparison of the structures **4** and **5** with those synthesized with the malonate and CNpy ligands. To our knowledge such complexes have neither been prepared with copper(II) ions, nor with other transition metal ions with the only exception of cobalt(II) ions.<sup>5</sup> The complex of formula  $[\text{Co}(\text{mal})(3\text{-CNpy})(\text{H}_2\text{O})]_n$  consist of octahedral cobalt atoms linked through *anti-syn* malonate-carboxylate bridges to build up a square-grid network. Despite of the octahedral environment of the cobalt atom in the malonate-complex, its structure and those of **4**, **5** are very similar. Main differences include intralayer  $\text{Co}\cdots\text{Co}$  separations [average value 5.3505(7) Å] longer than  $\text{Cu}\cdots\text{Cu}$  separations in **4** and **5**, interlayer metal-metal separations [10.8651(7) Å] shorter than those of **4** and **5**, and longer distances between interlayer cyano groups in the cobalt complex.

**Table I.8.** Selected bond lengths (Å) and bond angles (°) for compounds **4** and **5**<sup>a,b</sup>

| <b>4</b>         |            |                   |            |
|------------------|------------|-------------------|------------|
| Cu(1)–O(2)       | 1.976(2)   | O(2)–Cu(1)–N(1)   | 97.40(10)  |
| Cu(1)–O(4)       | 1.940(2)   | O(4)–Cu(1)–O(1a)  | 90.59(10)  |
| Cu(1)–O(1a)      | 1.968(2)   | O(4)–Cu(1)–O(3b)  | 173.68(10) |
| Cu(1)–O(3b)      | 1.955(2)   | O(4)–Cu(1)–N(1)   | 99.98(10)  |
| Cu(1)–N(1)       | 2.250(3)   | O(1a)–Cu(1)–O(3b) | 90.93(10)  |
| O(2)–Cu(1)–O(4)  | 88.16(10)  | O(1a)–Cu(1)–N(1)  | 89.84(10)  |
| O(2)–Cu(1)–O(1a) | 172.76(10) | O(3b)–Cu(1)–N(1)  | 86.16(10)  |
| O(2)–Cu(1)–O(3b) | 89.56(10)  |                   |            |
| <b>5</b>         |            |                   |            |
| Cu(1)–O(2)       | 2.021(5)   | O(2)–Cu(1)–N(1)   | 95.8(2)    |
| Cu(1)–O(4)       | 1.907(5)   | O(4)–Cu(1)–O(1c)  | 89.6(2)    |
| Cu(1)–O(1c)      | 2.030(5)   | O(4)–Cu(1)–O(3d)  | 173.3(2)   |
| Cu(1)–O(3d)      | 1.878(4)   | O(4)–Cu(1)–N(1)   | 98.6(2)    |
| Cu(1)–N(1)       | 2.236(7)   | O(1c)–Cu(1)–O(3d) | 90.7(2)    |
| O(2)–Cu(1)–O(4)  | 88.3(2)    | O(1c)–Cu(1)–N(1)  | 89.7(2)    |
| O(2)–Cu(1)–O(1c) | 174.3(2)   | O(3d)–Cu(1)–N(1)  | 88.2(2)    |
| O(2)–Cu(1)–O(3d) | 90.9(2)    |                   |            |

<sup>a</sup> Estimated standard deviations in the last significant digits are given in parentheses.

<sup>b</sup> Symmetry code: (a)  $x + 1/2, -y + 1/2, z - 1/2$ ; (b)  $x - 1/2, -y + 1/2, z - 1/2$ ; (c)  $x - 1/2, -y + 1/2, z + 1/2$ ; (d)  $x + 1/2, -y + 1/2, z + 1/2$ .

### I.3.4. Magnetic properties

The temperature dependence of the  $\chi_{\text{M}}T$  products [ $\chi_{\text{M}}$  being the magnetic susceptibility per copper(II) ion] for the complexes **4** and **5** in the temperature range 1.9-300 K are shown in Figures I.20 and I.21, respectively. The  $\chi_{\text{M}}T$  product at room temperature is 0.47 cm<sup>3</sup> mol<sup>-1</sup> K for **4** and **5**, a value which is as expected for a magnetically isolated spin doublet. This value remains constant for **4** until 150 K and then smoothly increases to reach a maximum value of 0.70 cm<sup>3</sup> mol<sup>-1</sup> K at 5.5 K; finally, it decreases sharply to a value of 0.62 cm<sup>3</sup> mol<sup>-1</sup> K at 2.0 K. This is indicative of the coexistence of ferro- and antiferromagnetic interactions.

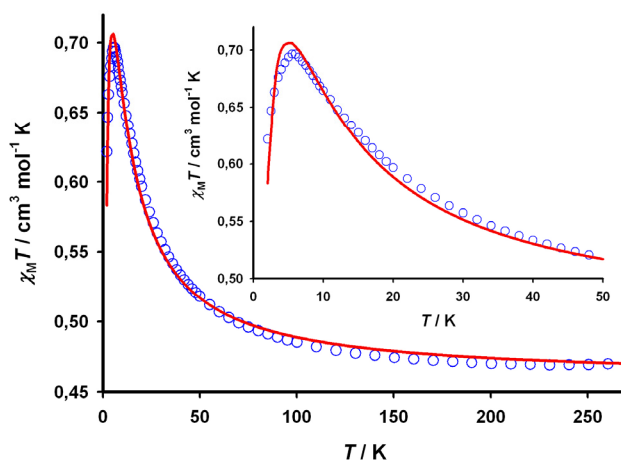


**Fig. I.20.**  $\chi_M T$  vs  $T$  plot for **4** under applied magnetic field of 1 T: (o) experimental data; (—) best-fit curve (see text). The inset shows a detail of the low temperature region.

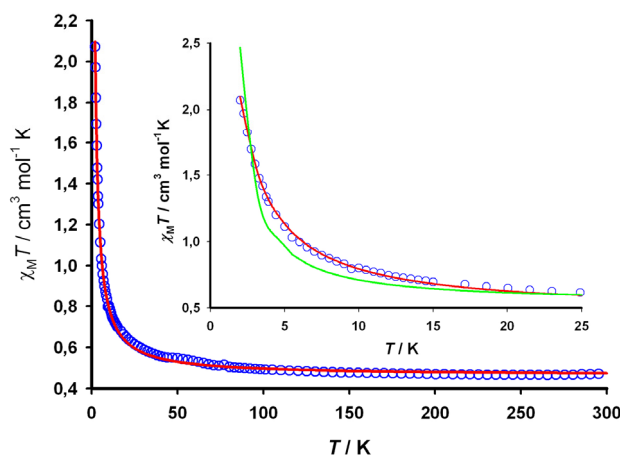


**Fig. I.21.**  $\chi_M T$  vs  $T$  plot for **5** under applied magnetic field of 1 T ( $T > 17$  K), 0.05 T ( $17$  K  $> T > 5$  K) and 0.025 T ( $T < 5$  K): (o) experimental data; (—) best-fit curve (see text). The inset shows a detail of the low temperature region: (—) fit through a two-dimensional Heisenberg model (see text).

The magnetization ( $M$ ) vs  $H$  plot for **4** at 2.0 K shows a sigmoidal shape indicating the occurrence of a metamagnetic-like behaviour (Figure I.22) with an inflexion point at  $H_c = 1.0$  T. The sharp increase after  $H_c$  to reach the saturation value of 1.10 BM at 4.0 T demonstrates the presence of ferromagnetic interactions between the spin doublets. The value of the critical field  $H_c$  accounts for an antiferromagnetic coupling of *ca.* 1  $\text{cm}^{-1}$ . This magnetic behaviour is reminiscent of that of **3** (see previous section). The situation for **5** is slightly different, the  $\chi_M T$  value at room temperature keeps almost constant up to 50 K and then  $\chi_M T$  abruptly increases to reach a value of 2.07  $\text{cm}^3 \text{mol}^{-1} \text{K}$  at 2.0 K. This indicates an

overall ferromagnetic behaviour. The magnetization curve at 2.0 K for **5** does not exhibit a sigmoidal shape and it reaches the saturation value of 1.10 BM at 3.5 T (Figure I.22).

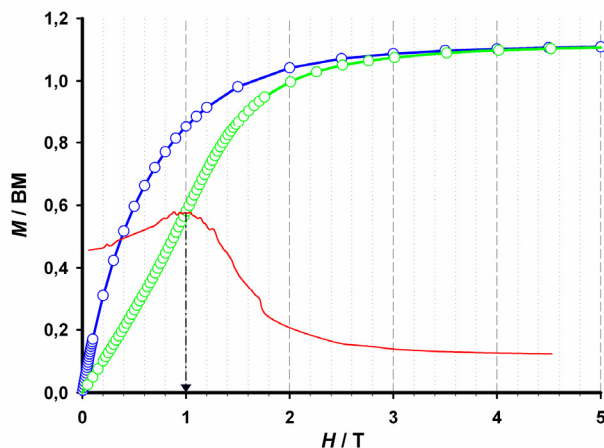


Fig. I.22.  $M$  vs  $H$  plot for **4** (green) and **5** (blue) together with the  $\partial M/\partial H$  (in red) showing the inflexion point for the sigmoidal curve for **4**.

The magnetic behaviour of **4** can be viewed as the competition of two interactions of opposite nature which operate within the carboxylate-bridged layers of copper(II) ions. Since there are two different *anti-syn* carboxylate bridges in the structure, one of them must couple the copper(II) ions ferromagnetically and the other one antiferromagnetically. Thus, from a magnetic point of view, the layers of compound **4** consist of square grids with two magnetic interactions of different nature. As there is no theoretical equation to analyse this data, it can also be seen as cross-linked AF and F chains. This situation can be analyzed through the Baker and Rushbrooke numerical expression<sup>6</sup> for a ferromagnetically coupled copper(II) chain with an additional mean-molecular field term which takes into account the AF interaction.

$$\chi_{2D} = \frac{\chi_{1D}}{1 - (2zj/Ng^2\beta^2)\chi_{1D}}$$

$$\chi_{1D} = (N\beta^2 g^2 / 4kT)(A/B)^{2/3}$$

$$A = 1.0 + 5.7979916 y + 16.902653 y^2 + 29.376885 y^3 + 29.832959 y^4 + 14.036918 y^5$$

$$B = 1.0 + 2.7979916 y + 7.0086780 y^2 + 8.6538644 y^3 + 4.5743114 y^4$$

$$\hat{H} = -J \sum_i \hat{S}_i \cdot \hat{S}_{i+1}$$

with  $y = J/2kT$ .  $J$  and  $j$  are the intra- and interchain magnetic coupling parameters, respectively;  $z = 2$ , is the number of nearest neighbours. The other symbols have their usual meanings. Best least-squares fit parameters are  $g = 2.212(4)$ ,  $J = +5.4(1) \text{ cm}^{-1}$ ,  $j = -0.70(1) \text{ cm}^{-1}$  and  $R = 2 \times 10^{-4}$ . The calculated curve is not in very good agreement with the experimental data (Figure I.20), probably because the model used is restricted to the interaction responsible for the mean field term introduced is weak enough, and in this case the difference between the ferro- and antiferromagnetic coupling parameters is less than one order of magnitude. However, the calculated AF coupling through the carboxylate bridge [ $j = -0.70(1) \text{ cm}^{-1}$ ] is in roughly agreement with the value estimated from the value of the critical field of  $H_c = 1.0 \text{ T}$ . The ferromagnetic coupling also agrees with the previous value of the magnetic coupling in **1** and **2** [ $J = +4.15(2)$  and  $+5.6(1) \text{ cm}^{-1}$ , respectively] and other related copper(II)-malonate complexes.<sup>7</sup>

The magnetic behaviour of **5** is that of a 2D Heisenberg ferromagnetic layer. The magnetic data can be analyzed by means of the expression for the susceptibility derived from a high-temperature series expansion for the isotropic ferromagnetic quadratic lattice with spin  $S = 1/2$ .<sup>8</sup> The spin Hamiltonian is defined as:

$$\hat{H} = -J \sum_i \hat{S}_i \cdot \hat{S}_{i+1}$$

and the series takes the form:

$$\chi = \left( \frac{N\beta^2 g^2}{3k_B T} S(S+1) \right) \left[ 1 + \sum_{n \geq 1} a_n \frac{x^n}{2^n} \right]$$

where  $N$ ,  $g$ ,  $\beta$  and  $k_B$  have their usual meaning,  $x = J/k_B T$ ,  $J$  is the intralayer magnetic coupling and  $a_n$  are coefficients which run up to  $n = 10$ . Best least-squares fit in the temperature range 2-300 K led to  $J = +1.00(2) \text{ cm}^{-1}$ ;  $g = 2.38(2)$  and  $R = 1.3 \times 10^{-2}$ . The poor overlap of the calculated curve over the experimental data (Fig. I.21) and a not fully satisfying agreement factor led us to use a different model to explain the magnetic behaviour. Since there are two crystallographically different carboxylate-pathways bridging the copper atoms within the layer, it is possible that they would have also different magnetic interactions. The series expansion used in the previous fit considers both exchange pathways to be equivalent; hence the new model will take into account the two bridges with different magnetic couplings. Since there is not a 2D model which can take account of a rectangular grid, we analyse the experimental data of **5** through the numerical expression for a ferromagnetically coupled copper(II) chain (main interaction) where a mean-molecular field term is introduced to evaluate the second interaction.<sup>6</sup>

$$\chi_{1D} = (N\beta^2 g^2 / 4kT) (A/B)^{2/3}$$



$$\chi_{2D} = \frac{\chi_{1D}}{1 - (2zj/Ng^2\beta^2)\chi_{1D}}$$

All the parameters here are defined above in this section ( $z = 2$  in this case). Best least-squares fit parameters are  $g = 2.093(4)$ ,  $J = +4.8(1) \text{ cm}^{-1}$ ,  $j = +0.073(3) \text{ cm}^{-1}$  and  $R = 3 \times 10^{-4}$ . In this case, the calculated curve matches very well the experimental data in the whole temperature range as can be seen in Fig. I.21. The value of  $j$  should be taken carefully since it may include some interactions between the layers through  $\pi$ - $\pi$  stacking and cyano-cyano contacts, as occurs in **2**.

**Table I.9.** Selected structural features for complexes **4** and **5**.

|                           | <b>4</b>              | <b>5</b>                |
|---------------------------|-----------------------|-------------------------|
| Cu(1)–O(1)                | 1.968(2) Å            | 2.030(5) Å              |
| Cu(1)–O(2)                | 1.976(2) Å            | 2.021(5) Å              |
| Cu(1)–O(3)                | 1.955(2) Å            | 1.878(4) Å              |
| Cu(1)–O(4)                | 1.940(2) Å            | 1.907(5) Å              |
| Cu(1)–N(1)                | 2.250(3) Å            | 2.236(7) Å              |
| $\tau$ value              | 0.015                 | 0.018                   |
| Interlayer <sup>a</sup>   | 13.705(3) Å           | 13.985(8) Å             |
| Intralayer A <sup>b</sup> | 4.984(2) Å            | 5.022(5) Å              |
| Intralayer B              | 5.238(2) Å            | 5.229(4) Å              |
| Bridge A <sup>b</sup>     | 49.694(7)°-72.921(7)° | 46.772(18)°-70.558(18)° |
| Bridge B                  | 48.941(7)°-67.752(7)° | 47.691(16)°-73.079(18)° |
| $\beta^c$                 | 71.168(6)°            | 71.725(14)°             |

<sup>a</sup> Shortest copper-copper separation between two different layers.

<sup>b</sup> Shortest Cu–Cu intralayer separation. A and B refer to the two crystallographically different carboxylate bridges present in the structure, which are defined univocally by the Cu–Cu separation.

<sup>c</sup> Angle between the equatorial planes of adjacent copper atoms.

The magnetic interactions between the copper atoms through the equatorial-equatorial *anti-syn* carboxylate bridge observed in **4** and **5** are in agreement with the data reported in the literature for copper(II) complexes with this kind of bridge.<sup>7,13</sup> The presence of two crystallographically different bridges in **4** and **5** is responsible for the occurrence of two different values for the magnetic coupling, while the different nature and magnitude of the interactions can be attributed to structural dissimilarities. On the basis of magnetic orbital considerations, it could be suggested that the distortion at the copper environment and the angle between mean basal planes of adjacent copper atoms play an important role in these differences.<sup>8-12</sup> In the light of the structural parameters displayed in Table I.9 it appears not to be enough variations to assign neither a magnetic pathway to  $J$  and  $j$  nor a single feature involved in the magnetic coupling.

### I.3.5. Conclusion

The complexes **4** and **5** exhibit little structural differences between them and also with **2** and **3**. However, they present quite a few differences magnetically. Ferro- and antiferromagnetic interactions coexist in **4**, while in **5** the magnetic behaviour is overall ferromagnetic. The position of the cyano group or the azine nitrogen atom seems to be unrelated with the appearance of carboxylate-bridges mediating AF interactions, because *para*- (**4**) and *ortho*- conformations (**3**) exhibit this kind of bridge. Thus, the variations of the nature of the magnetic interaction mediated by the carboxylate-bridges in this series of complexes must depend on very subtle structural changes, and probably they involve simultaneously several parameters.

### I.3.6. References

- 1 M. Kubicki, *Acta Cryst. Sect. B*, **2004**, B58, o255.
- 2 F. H. Allen, C. A. Baalham, J. P. M. Lommerse and P. R. Raithby, *Acta Cryst. Sect. B*, **1998**, B54, 320.
- 3 C. Janiak, *J. Chem. Soc., Dalton Trans.* **2000**, 3885.
- 4 A. W. Addison, T. N. Rao, J. Reedijk, J. van Rijn and G. C. Verschoor, *J. Chem. Soc., Dalton Trans.* **1984**, 1349.
- 5 F. S. Delgado, *PhD thesis*, **2005**.
- 6 G. A. Baker, G. S. Rushbrooke and H. E. Gilbert, *Phys. Rev.* **1964**, 135, A1272.
- 7 J. Pasán, F. S. Delgado, Y. Rodríguez-Martín, M. Hernández-Molina, C. Ruiz-Pérez, J. Sanchiz, F. Lloret and M. Julve, *Polyhedron* **2003**, 22, 2143.
- 8 R. Navarro, *Application of High- and Low-Temperature Series Expansions to Two-dimensional Magnetic Systems*, Ed. L. J. de Jongh, Kluwer Academic Publishers, Dordrecht, **1990**.
- 9 O. Kahn, *Molecular Magnetism*, VCH, New York, **1993**.
- 10 A. Rodríguez-Forteza, P. Alemany, S. Alvarez and E. Ruiz, *Chem. Eur. J.* **2001**, 7, 627.
- 11 O. Castillo, A. Luque, F. Lloret and P. Román, *Inorg. Chim. Acta* **2001**, 324, 141.
- 12 E. Colacio, M. Ghazi, R. Kivekäs and J. M. Moreno, *Inorg. Chem.* **2000**, 39, 2882.
- 13 (a) E. Colacio, J.-P. Costes, R. Kivekäs, J.-P. Laurent, J. Ruiz, *Inorg. Chem.* **1990**, 29, 4240. (b) E. Colacio, J.-M. Domínguez-Vera, J.-P. Costes, R. Kivekäs, J.-P. Laurent, J. Ruiz, M. Sundberg, *Inorg. Chem.* **1992**, 31, 774. (c) E. Colacio, J.-M. Domínguez-Vera, R. Kivekäs, J. Ruiz, *Inorg. Chim. Acta* **1994**, 218, 109. (d) P. K. Coughlin, S. J. Lippard, *J. Am. Chem. Soc.* **1984**, 106, 2328; (e) M.-C. Lim, W. Chen, H. M. Ali, *Trans. Met. Chem.* **1994**, 19, 409. (f) S. P. Perlepes, E. Libby, W. E. Streib, K. Folting, G. Christou, *Polyhedron* **1992**, 11, 923.

## I.4. Nicotinamide (6) and Isonicotinamide (7) Copper(II)-Phenylmalonate complexes

### I.4.1. Introduction

The choice to go ahead the series begun with the pyrimidine ligand with the nicotinamide and isonicotinamide ligands has been made in the aim of establish hydrogen bonds by means of the amide groups between the layers of carboxylate-bridged square-grid of copper(II) ions, once the formation of this layered systems with pyridine-like ligands seems to be reliable. At the same time, the previous sections have shown that the position of the secondary group in the azine ligand exerts some changes in the structures which affect the magnetic behaviour. Then, it is interesting to introduce the amido group in the three (nicotinamide) and four positions (isonicotinamide), and so a comparison with the previous complexes could be made.

### I.4.2. Synthesis

**Synthesis of 6.** Aqueous solution (3 cm<sup>3</sup>) of copper(II)-phenylmalonate (0.5 mmol, 120 mg) (prepared as described in Section 1.1) was introduced into one arm of a water-fulfilled H-shape tube whereas a 50/50 water/methanol solution (1 cm<sup>3</sup>) of nicotinamide (0.5 mmol, 61 mg) was added in the other arm. Pale blue single crystals as extremely thin plates of **6** appear in the H-shaped tube after 1 month at room temperature. Complex **6** always exhibits twin grow, although the single crystals of adequate size were synthesized, the twin could not be solved during the X-ray diffraction measurements. The thinnest plates of **6** exhibit the characteristic differentiation in colour areas when they are looked through polarized light (Figure I.23). Yield *ca.* 80%. Anal. found for **6**: C, 48.15; H, 4.01; N, 8.40%.

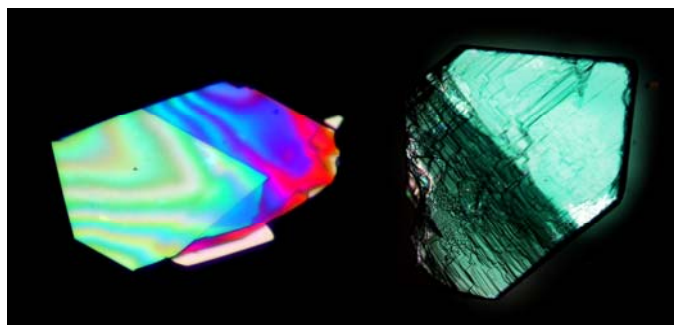


**Fig. I.23.** Microscope images of a plate micro-crystal under polarized light (left) and a crystal of adequate size for X-ray diffraction measurements formed for multiple sheets (right).

**[Cu(isonic)(Phmal)(H<sub>2</sub>O)]<sub>n</sub> (7).** Complex **7** was synthesized following the same procedure than that described for **6**, but using isonicotinamide (0.5 mmol, 61 mg) instead of nicotinamide. Thin plate-shape blue single crystals of **7** appear in the H-shaped tube after three weeks. Crystallographic details are listed in Table I.10. Yield 80 %. Anal. calc. for C<sub>15</sub>H<sub>14</sub>O<sub>6</sub>N<sub>2</sub>Cu (**7**): C, 47.18; H, 3.69; N, 7.34; Found: C, 47.11; H, 3.55; N, 7.28%.

### I.4.3. Description of the Structures

The structure of [Cu(isonic)(Phmal)(H<sub>2</sub>O)]<sub>n</sub> (**7**, Figure I.24) consists of a square grid of isonicotinamide-(aqua)copper(II) units linked through phenylmalonate carboxylate bridges running parallel to the *ab* plane, similar to that of **2-5**. The corrugated layers are stacked along the *c* direction being linked through hydrogen bonds involving the amide group of the isonicotinamide ligand (see Table I.11 and Figure I.25) affording the 3D supramolecular network. The isonic and the Phmal ligands located in *trans*-position respect to the copper atom and inversely located respect to the adjacent [Cu(isonic)(Phmal)(H<sub>2</sub>O)] units, these bulky groups being located in an hydrophobic area which separates the layers as occur in the related **2-5** complexes [the shortest interlayer copper-copper separation being 13.390(3) Å, see Figure I.26]. H-bonds between the coordinated water molecule [O(1w)] and coordinated phenylmalonate oxygen atoms [O(2) and O(4)] are found (see Table I.11). Weak intralayer  $\pi$ -type interactions between the phenyl and isonicotinamide aromatic groups contribute to the stabilization of the structure [shortest centroid-centroid separation and off-set angle being 4.773(2) Å and 29.9(3)°, respectively; values which are somewhat longer than those previously reported for this type of interactions]<sup>1</sup>.

Each copper atom exhibits a somewhat distorted octahedral environment with the parameters *s/h* and  $\phi$  being 1.32 and 56.5°, respectively (values for a ideal octahedron being *s/h* = 1.22 and  $\phi$  = 60°).<sup>2</sup> Two oxygen atoms from two different phenylmalonate ligands [O(4) and O(1a); a = -*x*, *y* + 1/2, -*z* + 1], a isonicotinamide nitrogen atom [N(1)] and a water

**Table I.10.** Crystallographic data for complex **7**

|                                                             | <b>7</b>                                                          |
|-------------------------------------------------------------|-------------------------------------------------------------------|
| Formula                                                     | C <sub>15</sub> H <sub>14</sub> O <sub>6</sub> N <sub>2</sub> Cu  |
| FW                                                          | 381.82                                                            |
| Crystal system                                              | Monoclinic                                                        |
| Space group                                                 | <i>P</i> 2 <sub>1</sub>                                           |
| <i>a</i> / Å                                                | 7.3012(10)                                                        |
| <i>b</i> / Å                                                | 7.2406(12)                                                        |
| <i>c</i> / Å                                                | 14.852(4)                                                         |
| $\beta$ / °                                                 | 104.020(11)                                                       |
| <i>V</i> / Å <sup>3</sup>                                   | 761.8(3)                                                          |
| <i>Z</i>                                                    | 2                                                                 |
| $\mu$ (Mo K $\alpha$ ) / cm <sup>-1</sup>                   | 14.69                                                             |
| <i>T</i> / K                                                | 293(2)                                                            |
| $\rho_{\text{calc}}$ / g cm <sup>-3</sup>                   | 1.665                                                             |
| $\lambda$ / Å                                               | 0.71073                                                           |
| Index ranges                                                | -10 ≤ <i>h</i> ≤ 3,<br>-10 ≤ <i>k</i> ≤ 7,<br>-16 ≤ <i>l</i> ≤ 20 |
| Indep. reflect. ( <i>R</i> <sub>int</sub> )                 | 3445 (0.0182)                                                     |
| Obs. reflect. [ <i>I</i> > 2 $\sigma$ ( <i>I</i> )]         | 3039                                                              |
| Flack parameter                                             | 0.018(11)                                                         |
| Parameters                                                  | 273                                                               |
| Goodness-of-fit                                             | 0.899                                                             |
| <i>R</i> [ <i>I</i> > 2 $\sigma$ ( <i>I</i> )]              | 0.0260                                                            |
| <i>R</i> <sub>w</sub> [ <i>I</i> > 2 $\sigma$ ( <i>I</i> )] | 0.0523                                                            |
| <i>R</i> (all data)                                         | 0.0337                                                            |
| <i>R</i> <sub>w</sub> (all data)                            | 0.0543                                                            |

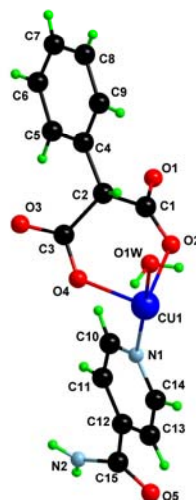


**Fig. I.24.** Asymmetric unit for **7** along with the numbering scheme.

molecule [O(1w)] build the basal plane [mean equatorial bond length being 2.0016(19) Å; see Table I.12], while two phenylmalonate oxygen atoms occupy [O(2) and O(3b)] the axial positions [mean Cu–O(ax) bond distance being 2.2902(18) Å;  $b = -x - 1, y + 1/2, -z + 1$ ].

**Table I.11.** Hydrogen bond distances and angles in **7**

| D–H···A <sup>a</sup> | D–H (Å) | H···A (Å) | D–H···A (°) | D···A (Å) |
|----------------------|---------|-----------|-------------|-----------|
| <i>Interlayer</i>    |         |           |             |           |
| N(2)–H···O(5)        | 0.67(2) | 2.28(2)   | 172.4(8)    | 2.946(4)  |
| <i>Intralayer</i>    |         |           |             |           |
| O(1w)–H···O(2)       | 0.79(3) | 1.84(2)   | 164.7(9)    | 2.616(3)  |
| O(1w)–H···O(4)       | 0.82(3) | 1.88(2)   | 178.1(9)    | 2.703(3)  |

<sup>a</sup> D and A stand for donor and acceptor, respectively.

The phenylmalonate ligand acts simultaneously as bidentate through O(2) and O(4) to Cu(1) [the angle subtended at the copper atom being 85.92(7)°] and as bis-monodentate through O(1) and O(3) to Cu(1c) and Cu(1d), respectively [ $c = -x, y - 1/2, -z + 1$ ;  $d = -x - 1, y - 1/2, -z + 1$ ]. The bidentate coordination of the Phmal ligand involves one equatorial [O(4)] and one apical [O(2)] bonds, feature which is unprecedented for R-malonato-containing copper(II) complexes,<sup>3,4</sup> although it is not uncommon for copper(II)-oxalate complexes.<sup>5,6</sup> The isonicotinamide ligand acts as monodentate ligand [through N(1)], the amide group participating in supramolecular interlayer interactions. The dihedral angle between the amide group and the pyridyl ring is 27.9(2)°.

There are two different *anti-syn* carboxylate bridges in the structure of **7**, namely O(1)–C(1)–O(2) and O(3)–C(3)–O(4), being the Cu···Cu separations 5.3362(6) and 5.3856(6) Å, respectively. Both carboxylate bridges connect one equatorial [O(1) and O(4)]

with an apical position [O(2) and O(3)] at the copper environments. The shortest interlayer copper-copper separation is 13.390(3) Å.

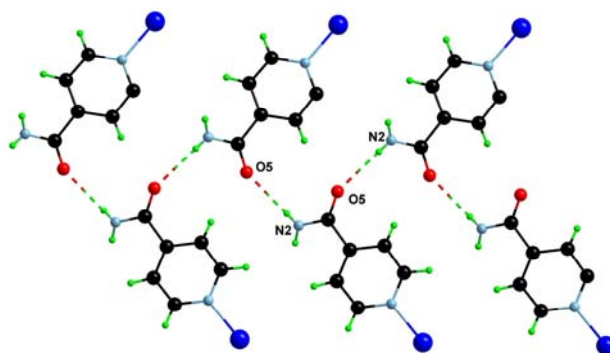


Fig. I.25. Hydrogen bonding scheme among the nicotinamide ligands of adjacent layers.

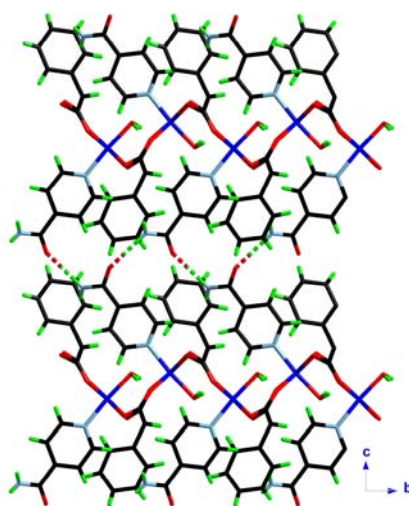


Fig. I.26. Perspective view of the crystal packing of 7 along the *a* axis.

There are more than ten structurally characterized complexes exhibiting copper(II) coordinated nicotinamide ligands, some of them including *syn-syn* carboxylate-bridges,<sup>7-9</sup> the same situation is found for the isonicotinamide ligand.<sup>10-12</sup> Most of these complexes consist of isolated molecules, only one forms extended structures through the nicotinamide ligand.<sup>7</sup>

**Table I.12.** Selected bond lengths (Å) and bond angles (°) for compound **7**<sup>a,b</sup>

| <b>7</b>         |            |                   |           |
|------------------|------------|-------------------|-----------|
| Cu(1)–O(2)       | 2.2154(17) | O(4)–Cu(1)–O(1a)  | 173.38(8) |
| Cu(1)–O(4)       | 1.9729(16) | O(4)–Cu(1)–O(3b)  | 93.65(7)  |
| Cu(1)–O(1a)      | 1.9740(16) | O(4)–Cu(1)–N(1)   | 90.43(8)  |
| Cu(1)–O(3b)      | 2.3651(18) | O(4)–Cu(1)–O(1w)  | 89.22(7)  |
| Cu(1)–N(1)       | 2.0360(19) | O(1a)–Cu(1)–O(3b) | 92.13(7)  |
| Cu(1)–O(1w)      | 2.0235(17) | O(1a)–Cu(1)–N(1)  | 86.87(7)  |
| O(2)–Cu(1)–O(4)  | 85.92(7)   | O(1a)–Cu(1)–O(1w) | 94.28(7)  |
| O(2)–Cu(1)–O(1a) | 88.27(7)   | O(3b)–Cu(1)–N(1)  | 84.94(7)  |
| O(2)–Cu(1)–O(3b) | 179.23(7)  | O(3b)–Cu(1)–O(1w) | 87.16(7)  |
| O(2)–Cu(1)–N(1)  | 94.42(8)   | N(1)–Cu(1)–O(1w)  | 172.05(8) |
| O(2)–Cu(1)–O(1w) | 93.47(8)   |                   |           |

<sup>a</sup> Estimated standard deviations in the last significant digits are given in parentheses.  
<sup>b</sup> Symmetry code: (a)  $-x, y + 1/2, -z + 1$ ; (b)  $-x - 1, y + 1/2, -z + 1$ .

#### I.4.4. Magnetic Properties

The magnetic properties of **6** and **7** under the form of a  $\chi_M T$  vs.  $T$  plots are presented in Figure I.27.  $\chi_M T$  at room temperature is  $0.44 \text{ cm}^3 \text{ mol}^{-1} \text{ K}$  for **6** and **7**, a value which is as expected for a magnetically isolated spin doublet. Upon cooling,  $\chi_M T$  remains almost constant up to 50 K, and then smoothly increases to reach a value of  $0.50$  and  $0.51 \text{ cm}^3 \text{ mol}^{-1} \text{ K}$  for **6** and **7** at 2.0 K. This behaviour is indicative of the existence of very weak ferromagnetic interactions among the copper(II) ions. The magnetization ( $M$ ) vs.  $H$  plot for **6** and **7** (inset of Figure I.27) confirms this behaviour. The  $M$  vs.  $H$  curve for both compounds is slightly above the Brillouin curve for a magnetically isolated spin doublet, the saturation value being 1.04 BM at 5.0 T.

These strong similarities in the magnetic properties of **6** and **7** encourage us to think that, although they could not be isostructural species, they have to be structurally similar or at least, from a magnetic point of view. From this point, the structure of **7** consists of *anti-syn* carboxylate-bridged square grid of copper(II) ions linking equatorial to apical positions at the metal environment. The experimental data of both complexes have been then analyzed by means of the expression for the susceptibility derived from high-temperature expansion series for the isotropic ferromagnetic quadratic lattice with local spin  $S = 1/2$ .<sup>13</sup> The spin Hamiltonian is defined as:

$$\hat{H} = -J \sum_i \hat{S}_i \cdot \hat{S}_{i+1}$$

and the series takes the form:

$$\chi = \left( \frac{N\beta^2 g^2}{3k_B T} S(S+1) \right) \left[ 1 + \sum_{n \geq 1} a_n \frac{x^n}{2^n} \right]$$

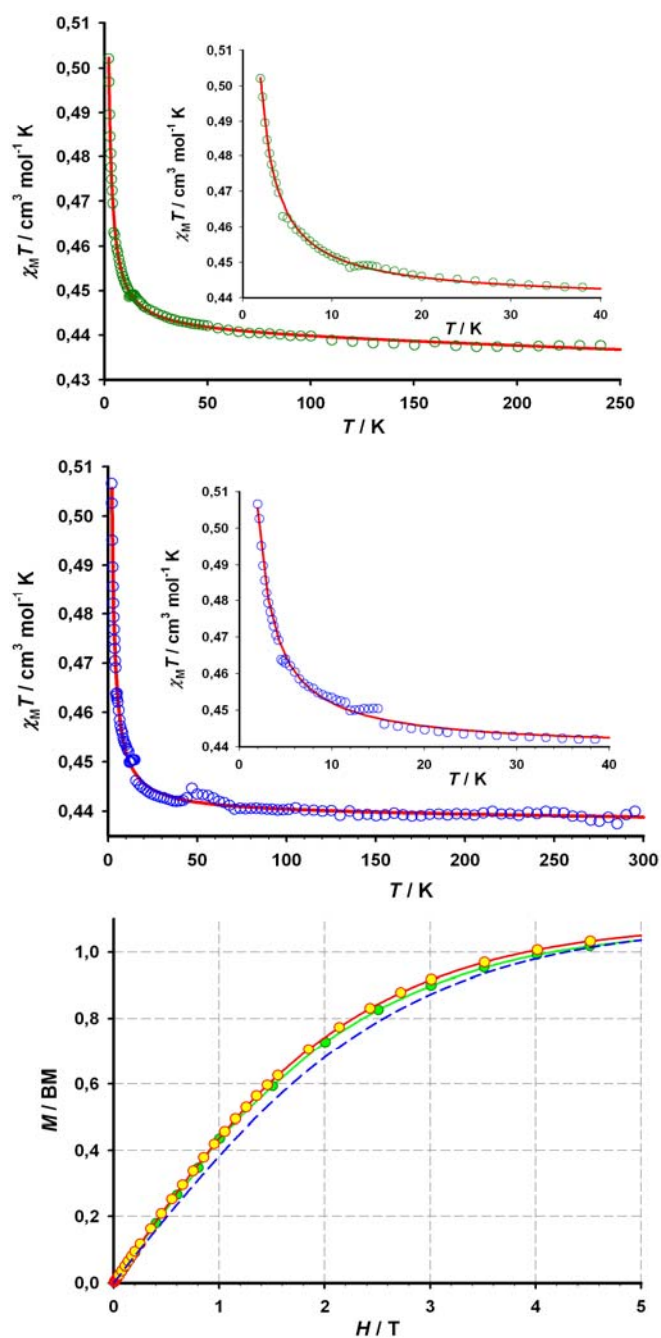


**Fig. I.27.**  $\chi_M T$  vs  $T$  plot for **6** (up) and **7** (middle) under applied magnetic field of 1 T ( $T > 16$  K), 0.1 T ( $T < 16$  K): (o) experimental data; (—) best-fit curve (see text). The inset shows a detail of the low temperature region. (Bottom)  $M$  vs  $H$  plot for **6** (green) and **7** (yellow-red) together with the Brillouin function for a magnetically isolated spin double (dashed line).



where  $N$ ,  $g$ ,  $\beta$  and  $k_B$  have their usual meaning,  $x = J/k_B T$ ,  $J$  is the intralayer magnetic coupling and  $a_n$  are coefficients which run up to  $n = 10$ . Best least-squares fit in the temperature range 2-300 K leads to  $J = +0.091(2) \text{ cm}^{-1}$ ;  $g = 2.16(2)$  and  $R = 3.1 \times 10^{-4}$  for **6** and  $J = +0.097(2) \text{ cm}^{-1}$ ;  $g = 2.16(2)$  and  $R = 7.1 \times 10^{-4}$  for **7**. The calculated curves match very well the experimental data in the whole temperature range (Figure I.27). The low values for the magnetic coupling parameters are as expected for *anti-syn* carboxylate-bridges which connect equatorial with apical positions at the metal coordination environments. The magnetic orbital of the copper(II) ion with octahedral surroundings is of the  $d(x^2-y^2)$  character (the  $x$  and  $y$  axes being roughly defined by the equatorial bonds) with some admixture of the  $d_z^2$  (which is defined by the axial bonds). According to the Kahn's model,<sup>14</sup> the magnetic orbital  $d(x^2-y^2)$  interacts with the non-magnetic one  $d_z^2$  in the apical-equatorial carboxylate-bridge, thus the magnitude of the interaction must be very weak, as occurs in **6** and **7**. Moreover, this exchange pathway produces a poor overlap between the magnetic orbitals due to the weak spin density in the apical site.<sup>15</sup> Thus, the antiferromagnetic contribution, which is proportional to the square of the overlap between the magnetic orbitals, is minimized and the resulting magnetic coupling is most likely ferromagnetic, as observed.<sup>17</sup> These values are within the range observed for this kind of bridge in other related copper(II)-malonate complexes as can be seen in Table I.13.<sup>19</sup>

**Table I.13.** Selected magneto-structural data for some equatorial-apical carboxylate-bridged malonato- and phenylmalonato-containing copper(II) complexes

| Compound <sup>a</sup>                                                                  | $J^b / \text{cm}^{-1}$ | Ref. |
|----------------------------------------------------------------------------------------|------------------------|------|
| $[\text{Cu}(\text{H}_2\text{O})_4][\text{Cu}(\text{mal})_2(\text{H}_2\text{O})_2]$     | +1.8                   | 16   |
| $\{[\text{Cu}(\text{H}_2\text{O})_4]_2[\text{Cu}(\text{mal})_2(\text{H}_2\text{O})]\}$ | +1.2                   | 16   |
| $\{[\text{Cu}(\text{H}_2\text{O})_3][\text{Cu}(\text{mal})_2(\text{H}_2\text{O})]\}_n$ | +1.9                   | 16   |
| $[\text{Cu}(\text{Im})_2(\text{mal})]_n$                                               | +1.6                   | 17   |
| $[\text{Cu}(2\text{-MeIm})_2(\text{mal})]_n$                                           | +0.4                   | 17   |
| $\{(\text{H}_2\text{bpe})[\text{Cu}(\text{mal})_2]\}_n \cdot 4n\text{H}_2\text{O}$     | +0.049                 | 18   |
| $[\text{Cu}_4(\text{mal})_4(\text{bpe})_3]_n \cdot 6n\text{H}_2\text{O}$               | +6.5                   | 18   |
| <b>6</b>                                                                               | +0.091(2)              | -    |
| <b>7</b>                                                                               | +0.097(2)              | -    |

<sup>a</sup> Abbreviations used: Im = Imidazole, 2-MeIm = 2-Methylimidazole and bpe

= 1,2-bis(4-pyridyl)ethylene.

<sup>b</sup> Values of the magnetic coupling.

The magnetic behaviour observed in **6** and **7** differs from that of the previous complexes **2-5**, despite they exhibit the same carboxylate-bridged square-grid of copper(II) ions. The fact that the nicotinamide (**6**) and the isonicotinamide (**7**) ligands occupy equatorial positions at the metal environment causes one of the oxygen atoms from the phenylmalonate ligand to fill an apical position, and then the carboxylate-bridge becomes of

the equatorial-apical type. This situation alters completely the magnetic behaviour since this kind of carboxylate-bridge is much less efficient than the equatorial-equatorial one present in complexes **2-5**.

#### I.4.5. Conclusion

The structure of the complexes **6** and **7** consists of carboxylate-bridged copper(II) layers which are linked through hydrogen bonds involving the amide groups of the nic (**6**) or isonic (**7**) ligands. This situation is what it is expected with the introduction of this kind of ligands, which are very similar to those of the complexes **2-5**. However, from a magnetic point of view **6** and **7** differ from the behaviour of **2-5** due to the fact that the square grid of carboxylate-bridged copper(II) ions involves equatorial and apical positions of the metal environments instead of the equatorial-equatorial carboxylate-bridge in complexes **2-5**. The equatorial-apical carboxylate-bridge of **6** and **7** appears as a consequence of the nic and isonic ligands occupying equatorial positions at the copper surroundings. Moreover, a water molecule enters in the coordination sphere of the metal atom, feature which is not observed in **2-5**. Summarizing, the changes due to the introduction of the amide group that we are interested in are canceled by the coligand occupying an equatorial position of the metal environment. Thus, the investigation about how different magnetic properties arise from similar structures remains open.

#### I.4.6. References

- 1 C. Janiak, *Dalton Trans.* **2000**, 3885.
- 2 E. I. Stiefel and G. F. Brown, *Inorg. Chem.*, **1972**, *11*, 434.
- 3 J. Pasán, J. Sanchiz, C. Ruiz-Pérez, F. Lloret and M. Julve, *New J. Chem.*, **2003**, *27*, 1557.
- 4 (a) D. Chattopadhyay, S. K. Chattopadhyay, P. R. Lowe, C. H. Schwalbe, S. K. Mazumder, A. Rana, and S. Ghosh, *J. Chem. Soc., Dalton Trans.* **1993**, 913. (b) I. Gil de Muro, F. A. Mautner, M. Insausti, L. Lezama, M. I. Arriortua and T. Rojo, *Inorg. Chem.* **1998**, *37*, 3243. (c) C. Ruiz-Pérez, J. Sanchiz, M. Hernández-Molina, F. Lloret, and M. Julve, *Inorg. Chim. Acta* **2000**, *298*, 245-250. (d) C. Ruiz-Pérez, J. Sanchiz, M. Hernández-Molina, F. Lloret and M. Julve, *Inorg. Chem.* **2000**, *39*, 1363. (e) C. Ruiz-Pérez, M. Hernández-Molina, P. Lorenzo-Luis, F. Lloret, J. Cano, and M. Julve, *Inorg. Chem.* **2000**, *39*, 3845. (f) C. Ruiz-Pérez, J. Sanchiz, M. Hernández-Molina, F. Lloret, and M. Julve, *Inorg. Chim. Acta* **2000**, *298*, 245. (g) Y. Rodríguez-Martín, J. Sanchiz, C. Ruiz-Pérez, F. Lloret and M. Julve, *Inorg. Chim. Acta* **2001**, *326*, 20. (h) Y. Rodríguez-Martín, C. Ruiz-Pérez, J. Sanchiz, F. Lloret and M. Julve, *Inorg. Chim. Acta* **2001**, *318*, 159. (i) J. Sanchiz, Y. Rodríguez-Martín, C. Ruiz-Pérez, A. Mederos, F. Lloret and M. Julve, *New J. Chem.* **2002**, *26*, 1624. (j) Y. Rodríguez-Martín, M. Hernández-Molina, F. S. Delgado, J. Pasán, C. Ruiz-Pérez, J. Sanchiz, F. Lloret, and M. Julve, *CrystEngComm* **2002**, *4*, 440. (k) S. Sain, T. K. Maji, G. Mostafa, T. H. Lu and N. R. Chanduri, *New J. Chem.* **2003**, *27*, 185.
- 5 (a) H. Oshio and U. Nagashima, *Inorg. Chem.* **1992**, *31*, 3295. (b) O. Castillo, A. Luque, F. Lloret and P. Román, *Inorg. Chim. Acta* **2001**, *324*, 141. (c) J. Luo, M. Hong, Y. Liang, R. Cao, *Acta Cryst., Sect. E*, **2001**, *57*, m361. (d) L. Cavalca, A. C. Villa, A. G. Manfredotti

- and A. A. G. Tomlinson, *Dalton Trans.*, **1972**, 391. (e) O. Castillo, A. Luque, M. Julve, F. Lloret and P. Román, *Inorg. Chim. Acta*, **2001**, 315, 9. (f) O. Castillo, A. Luque, P. Román, F. Lloret and M. Julve, *Inorg. Chem.* **2001**, 40, 5526. (g) J. Suárez-Varela, J. M. Domínguez-Vera, E. Colacio, J. C. Ávila-Rosón, M. A. Hidalgo and D. Martín-Ramos, *Dalton Trans.* **1995**, 2143.
- 6 O. Castillo, J. Alonso, U. García-Couceiro, A. Luque, and P. Román, *Inorg. Chem. Commun.* **2003**, 6, 803.
  - 7 B. Kozlevcar, I. Leban, I. Turel, P. Segedin, M. Petric, F. Pohleven, A. J. P. White, D. J. Williams and J. Sieler, *Polyhedron* **1999**, 18, 755.
  - 8 B. Kozlevcar, N. Leh, I. Leban, I. Turel, P. Segedin, M. Petric, F. Pohleven, A. J. P. White, D. J. Williams and G. Giester, *Croat. Chem. Acta* **1999**, 72, 427.
  - 9 I. Leban, P. Segedin and K. Gruber, *Acta Cryst., Sect. C* **1996**, C52, 1096.
  - 10 J.-P. Zhang, Y.-Y. Lin, X.-C. Huang and X.-M. Chen, *J. Am. Chem. Soc.* **2005**, 127, 5495.
  - 11 C. B. Aaheroy, A. M. Beatty, J. Desper, M. O'Shea and J. Valdés-Martínez, *Dalton Trans.* **2003**, 3956.
  - 12 I. Ucor, A. Bulut and O. Buyukgungor, *Acta Cryst., Sect. C* **2005**, C61, m218.
  - 13 R. Navarro, *Application of High- and Low-Temperature Series Expansions to Two-dimensional Magnetic Systems*, Ed. L. J. de Jongh, Kluwer Academic Publishers, Dordrecht, **1990**.
  - 14 O. Kahn, *Molecular Magnetism*, VCH, New York, **1993**.
  - 15 A. Rodríguez-Forteza, P. Alemany, S. Álvarez and E. Ruiz, *Chem. Eur. J.* **2001**, 7, 627.
  - 16 C. Ruiz-Pérez, J. Sanchiz, M. Hernández-Molina, F. Lloret and M. Julve, *Inorg. Chem.* **2000**, 39, 1363.
  - 17 J. Sanchiz, Y. Rodríguez-Martín, C. Ruiz-Pérez, A. Mederos, F. Lloret and M. Julve, *New J. Chem.* **2002**, 26, 1624.
  - 18 F. S. Delgado, J. Sanchiz, C. Ruiz-Pérez, F. Lloret and M. Julve, *Inorg. Chem.* **2003**, 42, 5938.
  - 19 J. Pasán, F. S. Delgado, Y. Rodríguez-Martín, M. Hernández-Molina, C. Ruiz-Pérez, J. Sanchiz, F. Lloret and M. Julve, *Polyhedron* **2003**, 22, 2143.

### **I.5.3-Fluoropyridine (8), 3-Chloropyridine (9), 3-Bromopyridine (10), and 3-Iodopyridine (11) Copper(II)-Phenylmalonate complexes**

#### **I.5.1. Introduction**

The strategy which is described in the previous sections is now continued with the introduction of 3-halopyridines (3-Xpy, X = F, Cl, Br and I). The formation of the carboxylate-bridged square grid of copper atoms is expected when these pyridine-like coligands are used in the synthesis as reported for the complexes 2-7. In the past few years, there has been a growing recognition that the halogen bonds offers many of the same opportunities as hydrogen bonds for forming reliable connections between molecules and ions.<sup>1</sup> Close contacts between the halogen atoms from different 3-Xpy ligands are expected to contribute to the stabilization of the layers and to induce some changes on the conformation of the carboxylate bridges. The magnetic behaviour could be most likely affected by these subtle modifications of the carboxylate-bridges, there we report the synthesis, crystal structure and magnetic properties of four new complexes based on phenylmalonate, copper(II) and 3-Xpy as coligands.

#### **I.5.2. Synthesis**

**[Cu(3-Fpy)(Phmal)]<sub>n</sub> (8).** An aqueous solution (3 cm<sup>3</sup>) of copper(II)-phenylmalonate (0.5 mmol, 120 mg) (which prepared as described in Section 1.1) was set in one arm of a water-fulfilled H-shape tube whereas a 50/50 water/methanol solution (1 cm<sup>3</sup>) of 3-fluoropyridine (0.5 mmol, 49 mg, 0.043 cm<sup>3</sup>) was added in the other arm. Pale blue sheet-like poor quality single crystals of **8** appear in the H-tube after two weeks. Yield *ca.* 20%. Anal. found for **8**: C, 48.5; H, 3.61; N, 3.05%.

**[Cu(3-Clpy)(Phmal)]<sub>n</sub> (9).** Complex **9** was prepared following the same procedure than that described for **8** but using 3-chloropyridine instead of 3-fluoropyridine (0.5 mmol, 57 mg, 0.048 cm<sup>3</sup>). Pale blue plate single crystals appear after two weeks. Yield *ca.* 60 %. Anal. calc. for C<sub>14</sub>H<sub>10</sub>O<sub>4</sub>NCICu (**9**): C, 47.34; H, 2.84; N, 3.94; Found: C, 47.05; H, 3.01; N, 3.65%.

**[Cu(3-Brpy)(Phmal)]<sub>n</sub> (10).** Complex **10** was prepared following the same procedure than that described for **8** but using 3-bromopyridine instead of 3-fluoropyridin (0.5 mmol, 79 mg,

0.048 cm<sup>3</sup>). Blue plate single crystals appear after two weeks. Yield *ca* 65 %. Anal. calc. for C<sub>14</sub>H<sub>10</sub>O<sub>4</sub>NBrCu (**10**): C, 42.07; H, 2.52; N, 3.50; Found: C, 42.15; H, 2.41; N, 3.55%.

**[Cu(3-Ipy)(Phmal)]<sub>n</sub> (11)**. Complex **11** was prepared following the same procedure than that described for **8** but using 3-iodopyridine instead of 3-fluoropyridin (0.5 mmol, 102 mg). Blue plate single crystals appear after two weeks. Crystallographic details for **9-11** are listed in Table I.14. Yield *ca* 50 %. Anal. calc. for C<sub>14</sub>H<sub>10</sub>O<sub>4</sub>NICu (**11**): C, 37.64; H, 2.26; N, 3.14; Found: C, 37.55; H, 2.15; N, 3.20%.

**Table I.14.** Crystallographic data for complexes **9-11**

|                                                             | <b>9</b>                                                        | <b>10</b>                                                       | <b>11</b>                                                       |
|-------------------------------------------------------------|-----------------------------------------------------------------|-----------------------------------------------------------------|-----------------------------------------------------------------|
| Formula                                                     | C <sub>14</sub> H <sub>10</sub> O <sub>4</sub> NCICu            | C <sub>14</sub> H <sub>10</sub> O <sub>4</sub> NBrCu            | C <sub>14</sub> H <sub>10</sub> O <sub>4</sub> NICu             |
| FW                                                          | 355.22                                                          | 399.68                                                          | 446.67                                                          |
| Crystal system                                              | Monoclinic                                                      | Monoclinic                                                      | Monoclinic                                                      |
| Space group                                                 | <i>P</i> 2 <sub>1</sub> / <i>n</i>                              | <i>P</i> 2 <sub>1</sub> / <i>n</i>                              | <i>P</i> 2 <sub>1</sub> / <i>n</i>                              |
| <i>a</i> /Å                                                 | 6.2264(11)                                                      | 6.2317(7)                                                       | 6.2604(10)                                                      |
| <i>b</i> /Å                                                 | 30.6016(17)                                                     | 31.008(6)                                                       | 31.925(5)                                                       |
| <i>c</i> /Å                                                 | 6.9804(12)                                                      | 6.9702(11)                                                      | 6.9803(6)                                                       |
| $\beta$ /°                                                  | 93.297(13)                                                      | 93.548(12)                                                      | 93.970(8)                                                       |
| <i>V</i> /Å <sup>3</sup>                                    | 1327.8(3)                                                       | 1344.3(4)                                                       | 1391.8(3)                                                       |
| <i>Z</i>                                                    | 4                                                               | 4                                                               | 4                                                               |
| $\mu$ (Mo K $\alpha$ ) /cm <sup>-1</sup>                    | 18.60                                                           | 46.11                                                           | 38.01                                                           |
| <i>T</i> /K                                                 | 293(2)                                                          | 293(2)                                                          | 293(2)                                                          |
| $\rho_{\text{calc}}$ /g cm <sup>-3</sup>                    | 1.777                                                           | 1.975                                                           | 2.132                                                           |
| $\lambda$ /Å                                                | 0.71073                                                         | 0.71073                                                         | 0.71073                                                         |
| Index ranges                                                | -7 ≤ <i>h</i> ≤ 8,<br>-42 ≤ <i>k</i> ≤ 38,<br>-9 ≤ <i>l</i> ≤ 9 | -8 ≤ <i>h</i> ≤ 8,<br>-43 ≤ <i>k</i> ≤ 37,<br>-9 ≤ <i>l</i> ≤ 9 | -8 ≤ <i>h</i> ≤ 8,<br>-39 ≤ <i>k</i> ≤ 44,<br>-9 ≤ <i>l</i> ≤ 9 |
| Indep. reflect. ( <i>R</i> <sub>int</sub> )                 | 3721 (0.0659)                                                   | 2576 (0.0640)                                                   | 3540 (0.0461)                                                   |
| Obs. reflect. [ <i>I</i> > 2 $\sigma$ ( <i>I</i> )]         | 2168                                                            | 1410                                                            | 2479                                                            |
| Parameters                                                  | 230                                                             | 191                                                             | 190                                                             |
| Goodness-of-fit                                             | 1.148                                                           | 1.062                                                           | 1.177                                                           |
| <i>R</i> [ <i>I</i> > 2 $\sigma$ ( <i>I</i> )]              | 0.0873                                                          | 0.0873                                                          | 0.0699                                                          |
| <i>R</i> <sub>w</sub> [ <i>I</i> > 2 $\sigma$ ( <i>I</i> )] | 0.1730                                                          | 0.2191                                                          | 0.1880                                                          |
| <i>R</i> (all data)                                         | 0.1533                                                          | 0.1611                                                          | 0.1013                                                          |
| <i>R</i> <sub>w</sub> (all data)                            | 0.1894                                                          | 0.2507                                                          | 0.2014                                                          |

### I.5.3. Description of the Structures

The complexes [Cu(3-Xpy)(Phmal)]<sub>n</sub> [X = Cl (**9**), Br (**10**) and I (**11**)] are isostructural species and its structure is very similar to those of complexes **2-7**. The structure of **8** could not be solved by single crystal X-ray diffraction measurements (due to the poor X-ray quality of the crystals), but powder X-ray diffraction (see Experimental) confirms that **8** is isostructural with compounds **9-11**.

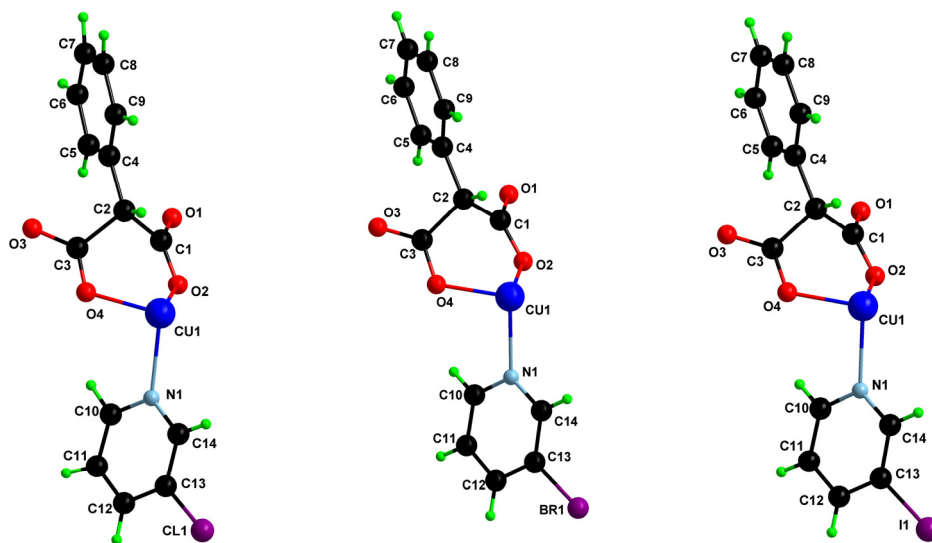


Fig. I.28. A view of the asymmetric units for **9** (left), **10** (middle) and **11** (right) along with the numbering scheme.

The structure of **9-11** (Figure I.28) is made up by a sheet-like arrangement of [CuL] units ( $L = 3\text{-Clpy}$ ,  $3\text{-Brpy}$ ,  $3\text{-Ipy}$ ) linked through phenylmalonate ligands running parallel to the *ac* plane. The resulting corrugated layer presents the X-pyridine ligands alternatively located above and below each layer, and inversely to the position of the phenyl group of the Phmal ligand. These sheets, which are stacked along the crystallographic *b* axis in the *ABABAB* sequence, have the odd layers rotated by  $180^\circ$  (Figure I.29). The layers are well separated by means of the hydrophobic groups, the pyridine-like and the Phmal ligands, the value of the shortest copper-copper interlayer separation being 13.534(7), 13.755(8) and 14.255(6) Å for **9**, **10** and **11**, respectively. The larger the Van der Waals radius of the halogen of the X-pyridine ligand is, the longer the interlayer separation. Weak interactions between the halogen atoms from different layers link the sheets to form a three-dimensional supramolecular structure (Figure I.30). The shortest contacts and angles between the halogen atoms are  $\text{Cl}\cdots\text{Cl} = 3.969(6)$  Å and  $\text{C}^{(1)}\text{-Cl}^{(1)}\cdots\text{Cl}^{(2)} = 88.726(12)^\circ$  for **9**,  $\text{Br}\cdots\text{Br} = 4.041(9)$  Å and  $\text{C}^{(1)}\text{-Br}^{(1)}\cdots\text{Br}^{(2)} = 87.916(16)^\circ$  for **10**, and  $\text{I}\cdots\text{I} = 4.245(5)$  Å and  $\text{C}^{(1)}\text{-I}^{(1)}\cdots\text{I}^{(2)} = 87.630(12)^\circ$  for **11**. These distances are slightly longer than those previously reported.<sup>2,3</sup> Weak  $\pi$ -type interactions are also present in the structure between Phmal and halogen-pyridine ligands, the shortest centroid-centroid distance and off-set angle being 4.262(6) Å and  $33.912^\circ$  for **9**, 4.238(5) Å and  $33.318(17)^\circ$  for **10** and 4.247(5) Å and  $32.603(12)^\circ$  for **11**, respectively. According to Janiak,<sup>4</sup> these values are within the range of pyridine-type interactions.

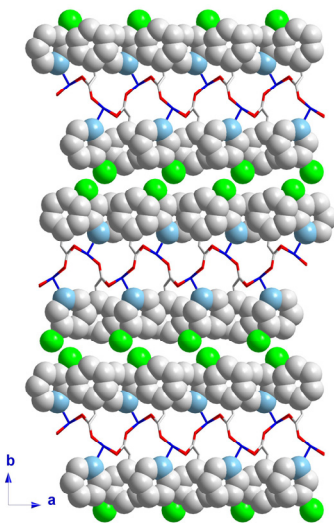


Fig. I.29. A view of the crystal packing of compounds **9**, **10** and **11**, along the *c* axis.

Each copper atom exhibits an almost perfect square-pyramidal environment, although that of complex **11** presents a somewhat more distorted surrounding than the other two (the  $\tau$  value<sup>5</sup> being 0.004, 0.003 and 0.018 for **9**, **10** and **11**, respectively). Four oxygen atoms from three different phenylmalonate ligands [O(1), O(2), O(3) and O(4); mean bond distance is 1.966(8) Å] build the basal plane while a nitrogen atom [Cu(1)–N(1) mean bond distance 2.240(9) Å] occupies the apical position. Detailed bond distances are given in Table I.15. The copper atom is shifted by 0.1180(4) (**9**), 0.1089(8) (**10**) and 0.1161(4) Å (**11**) from the mean basal plane towards the apical position.

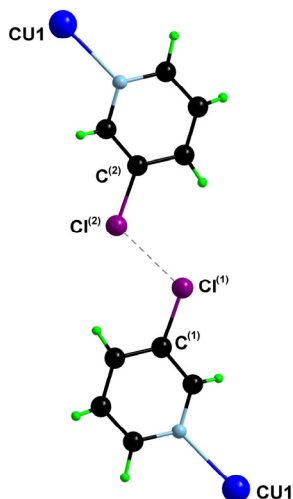


Fig. I.30. Cl...Cl interactions between 3-chloropyridine ligands of adjacent layers in **9**.

**Table I.15.** Selected bond lengths (Å) and bond angles (°) for compound **9**, **10** and **11**<sup>a,b</sup>

| <b>9</b>         |           |                   |           |
|------------------|-----------|-------------------|-----------|
| Cu(1)–O(2)       | 1.948(4)  | O(2)–Cu(1)–N(1)   | 99.9(2)   |
| Cu(1)–O(4)       | 1.991(5)  | O(4)–Cu(1)–O(1a)  | 89.38(19) |
| Cu(1)–O(1a)      | 1.959(4)  | O(4)–Cu(1)–O(3b)  | 173.8(2)  |
| Cu(1)–O(3b)      | 1.968(5)  | O(4)–Cu(1)–N(1)   | 97.1(2)   |
| Cu(1)–N(1)       | 2.239(6)  | O(1a)–Cu(1)–O(3b) | 91.61(19) |
| O(2)–Cu(1)–O(4)  | 88.1(2)   | O(1a)–Cu(1)–N(1)  | 86.9(2)   |
| O(2)–Cu(1)–O(1a) | 173.0(2)  | O(3b)–Cu(1)–N(1)  | 90.1(2)   |
| O(2)–Cu(1)–O(3b) | 91.61(19) |                   |           |
| <b>10</b>        |           |                   |           |
| Cu(1)–O(2)       | 1.942(8)  | O(2)–Cu(1)–N(1)   | 99.5(3)   |
| Cu(1)–O(4)       | 2.000(7)  | O(4)–Cu(1)–O(1c)  | 89.6(3)   |
| Cu(1)–O(1c)      | 1.956(7)  | O(4)–Cu(1)–O(3d)  | 173.3(3)  |
| Cu(1)–O(3d)      | 1.974(8)  | O(4)–Cu(1)–N(1)   | 96.4(3)   |
| Cu(1)–N(1)       | 2.239(9)  | O(1c)–Cu(1)–O(3d) | 91.9(3)   |
| O(2)–Cu(1)–O(4)  | 88.1(3)   | O(1c)–Cu(1)–N(1)  | 86.8(3)   |
| O(2)–Cu(1)–O(1c) | 173.5(3)  | O(3d)–Cu(1)–N(1)  | 90.2(3)   |
| O(2)–Cu(1)–O(3d) | 89.8(3)   |                   |           |
| <b>11</b>        |           |                   |           |
| Cu(1)–O(2)       | 1.937(5)  | O(2)–Cu(1)–N(1)   | 99.4(2)   |
| Cu(1)–O(4)       | 1.992(5)  | O(4)–Cu(1)–O(1a)  | 89.0(2)   |
| Cu(1)–O(1a)      | 1.957(5)  | O(4)–Cu(1)–O(3b)  | 172.4(2)  |
| Cu(1)–O(3b)      | 1.976(5)  | O(4)–Cu(1)–N(1)   | 96.1(2)   |
| Cu(1)–N(1)       | 2.241(6)  | O(1a)–Cu(1)–O(3b) | 91.9(2)   |
| O(2)–Cu(1)–O(4)  | 88.2(2)   | O(1a)–Cu(1)–N(1)  | 86.8(2)   |
| O(2)–Cu(1)–O(1a) | 173.5(2)  | O(3b)–Cu(1)–N(1)  | 91.5(2)   |
| O(2)–Cu(1)–O(3b) | 90.1(2)   |                   |           |

<sup>a</sup> Estimated standard deviations in the last significant digits are given in parentheses.

<sup>b</sup> Symmetry code: (a)  $x - 1/2, -y + 1/2, z - 1/2$ ; (b)  $x - 1/2, -y + 1/2, z + 1/2$ ; (c)  $x + 1/2, -y + 1/2, z + 1/2$ ; (d)  $x + 1/2, -y + 1/2, z - 1/2$ .

The phenylmalonate ligands adopts simultaneously the bidentate [through O(2) and O(4), the angle subtended at the copper atom being 88.1(3) (**9** and **10**), and 88.2(2)° (**11**)] and bis-monodentate coordination modes [through O(1) and O(3)]. Two different phenylmalonate-carboxylate bridges are present within each layer. The one with the O(1)–C(1)–O(2) groups is shorter [5.015(5), 4.999(5) and 4.995(4) Å for **9**, **10** and **11**, respectively] than that with the O(3)–C(3)–O(4) bridge [5.258(6) (**9**), 5.261(5) (**10**) and 5.289(3) Å (**11**)]. It deserves to be noted that the larger the ionic radius of the halogen present in the ligand, the shorter the copper-copper separation through the O(1)–C(1)–O(2) bridge, the reverse trend being observed through the O(3)–C(3)–O(4) bridge. In this case, these differences could be explained by means of the deviation of the phenyl ring of the Phmal ligand due to the supramolecular interaction with the halogen-derived pyridine. The values of the dihedral angle between the phenyl ring and the basal plane of the copper(II) ion are 83.14° (**9**, 3-Clpy), 83.93° (**10**, 3-Brpy) and 84.49° (**11**, 3-Ipy); the greater the deviation, the larger the distortion between the two bridges.



Let us remark that the 3-Xpy ligands have not a very common use in the coordination chemistry of the first-row transition metal ions. Of the twenty-five coordination complexes with the 3-Clpy ligand found in a CSD Database search (August 2005), only two of them exhibit the ligand coordinated to copper(II) ions.<sup>6,7</sup> In these two complexes, the 3-Clpy ligand occupies the apical position of the copper environment and it contributes to the stabilization of the structure through weak  $\pi$ -type interactions. In the case of the 3-Brpy ligand, only six complexes with this ligand coordinated to metal ions are known and among them only one with copper(II) ions.<sup>8</sup> This complex is very similar to that reported by Escuer *et al.* with the 3-Clpy ligand. Finally, there is the only compound with the 3-Ipy ligand and it is coordinated to nickel(II).<sup>9</sup> More recently, Brammer *et al.*<sup>10-15</sup> are developing supramolecular compounds based on halogen bonds between metal halides and organic halide groups and among them, they have investigated the 3-Xpy series.<sup>11</sup>

#### I.5.4. Magnetic Properties

The magnetic properties of compound **9** under the form of  $\chi_M T$  vs T plot [ $\chi_M$  being the molar susceptibility per copper(II) ion] are shown in Figure I.31.  $\chi_M T$  at room temperature is  $0.39 \text{ cm}^3 \text{ mol}^{-1} \text{ K}$ , a value which is as expected for a magnetically isolated spin doublet. Upon cooling,  $\chi_M T$  remains almost constant up to 20 K and then, it smoothly decreases to reach a value of  $0.32 \text{ cm}^3 \text{ mol}^{-1} \text{ K}$  at 1.9 K. The temperature dependence of the  $\chi_M T$  product for compounds **8**, **10** and **11** are shown in Figure I.32. At room temperature, the values of  $\chi_M T$  are  $0.46 \text{ cm}^3 \text{ mol}^{-1} \text{ K}$  for **8**, **10** and **11**. These values remain constant upon cooling until 100 K, and then smoothly increase to reach a maximum of  $0.56 \text{ cm}^3 \text{ mol}^{-1} \text{ K}$  at 11 K for **8**,  $0.66 \text{ cm}^3 \text{ mol}^{-1} \text{ K}$  at 6.5 K for **10** and at  $0.63 \text{ cm}^3 \text{ mol}^{-1} \text{ K}$  at 7.0 K for **11**. At lower temperatures, the  $\chi_M T$  curves sharply decrease to reach values of  $0.25$  (**8**),  $0.48$  (**10**) and  $0.41$  (**11**)  $\text{cm}^3 \text{ mol}^{-1} \text{ K}$  at 2.0 K. The magnetic behaviour of **9** is indicative of the existence of antiferromagnetic coupling between the copper(II) ions, however the situation for **8**, **10** and **11** is rather different, a competition between two interactions, ferro- and antiferromagnetic, being present in these complexes. The magnetization ( $M$ ) curve for **9** lies under the Brillouin function for a magnetically isolated spin  $S = 1/2$  in the entire range of the magnetic field available (0-5 T) (Figure I.33). However, the  $M$  vs.  $H$  plot for **8**, **10** and **11** shows the sigmoidal shape characteristic of a metamagnetic-like behaviour (Fig. I.33). The value of the critical field [ $H_c = 2.4$  (**8**) and 1.2 T (**10** and **11**)] obtained from the inflexion point corresponds to the antiferromagnetic interactions in these complexes [*ca.*  $2.4 \text{ cm}^{-1}$  for **8** and

1.2 cm<sup>-1</sup> for **10** and **11**]. The saturation values of the magnetization are 1.03 BM for **8** and 1.11 BM for **10** and **11** and they are reached at an applied field of 4.5 T.

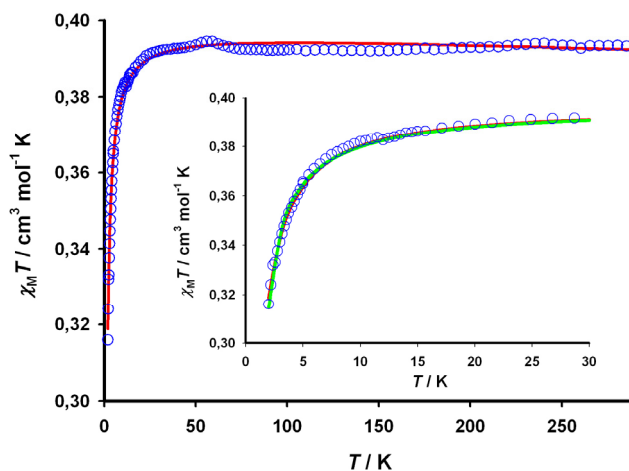


**Fig. 1.31.**  $\chi_M T$  vs  $T$  plot for **9**: (o) experimental data; (—) best-fit curve (see text). The inset shows a detail of the low temperature region: (—) alternative fit-curve (see text).

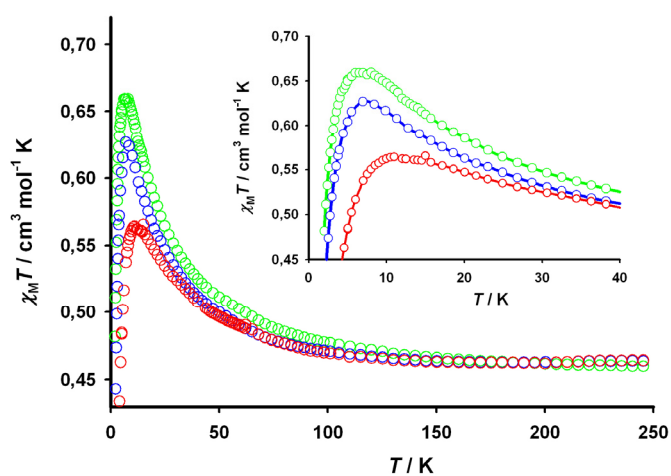


**Fig. 1.32.**  $\chi_M T$  vs  $T$  plot for **8** (red), **10** (green) and **11** (blue) under applied magnetic fields of 1 T ( $T > 15$  K) and 0.05 T ( $T < 15$  K) for **8**, 1 T ( $T > 22$  K) and 0.025 T ( $T < 22$  K) for **10** and 1 T ( $T > 22$  K) and 0.05 T ( $T < 22$  K) for **11**.

The distinct magnetic behaviour of **9** compared with all the previously reported compounds with a layered structure of carboxylate bridged copper(II) ions can be explained if the two crystallographically different carboxylate bridges within the plane couple antiferromagnetically the copper(II) ions. The two exchange pathways configure a two-

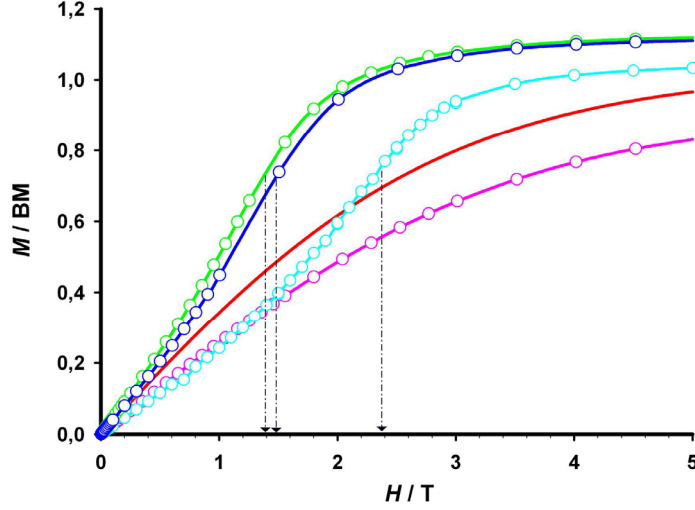


Fig. I.33.  $M$  vs  $H$  plot for **8** (pale blue), **9** (pink), **10** (green) and **11** (deep blue) together with the Brillouin function for a magnetically isolated spin double (red line).

dimensional square grid of copper atoms, behaving as 2D antiferromagnetic Heisenberg layer. The magnetic data of this system can then be analyzed by means of the Rushbrook expression for the susceptibility derived from high-temperature expansion series for the isotropic antiferromagnetic square lattice with spin  $S = 1/2$ .<sup>16</sup> The spin Hamiltonian is defined as:

$$\hat{H} = -J \sum_i \hat{S}_i \cdot \hat{S}_{i+1}$$

and the series takes the following form

$$\chi = \left( \frac{2.91 N \beta^2 g^2}{k_B T} \right) \left[ 1 + 23.33x + 147.78x^2 + 405.48x^3 + 8171.3x^4 + 64968x^5 + 15811x^6 \right]^{-1}$$

where  $N$ ,  $\beta$ ,  $g$  and  $k_B$  have their usual meanings,  $x = J/k_B T$  and  $J$  is the in-plane magnetic coupling parameter. Best least-squares fit of the experimental data leads to  $J = -0.153(1)$   $\text{cm}^{-1}$ ,  $g = 2.058(1)$  and  $R = 1.0 \times 10^{-5}$ . The calculated curve matches very well the experimental data in the whole temperature range (Figure I.31).

An additional analysis has been made to establish the difference between the two exchange pathways active in **9**. The experimental magnetic data were fitted through the Fisher eq. for an antiferromagnetically coupled regular chain of copper(II) ions with a mean-field term to take into account the second exchange pathway with  $z = 2$ .<sup>17</sup>

$$\chi_{1D} = \left( \frac{N g^2 \beta^2}{k_B T} \right) \left[ \frac{0.25 + 0.074975 x + 0.075235 x^2}{1 + 0.9931x + 0.172135 x^2 + 0.757825 x^3} \right]$$

$$\chi_{2D} = \frac{\chi_{1D}}{1 - (2zj/Ng^2\beta^2)\chi_{1D}}$$

where  $N$ ,  $\beta$ ,  $g$  and  $k_B$  have their usual meanings,  $x = |J|/k_B T$  and  $J$  and  $j$  are the magnetic coupling parameters. Best least-squares fit of the experimental data leads to  $J = -0.91(3) \text{ cm}^{-1}$ ,  $j = +0.27(3) \text{ cm}^{-1}$ ,  $g = 2.059(1)$  and  $R = 8.3 \times 10^{-5}$ . The calculated curve also matches the experimental data well (inset of Figure I.31). Although the difference between the two magnetic coupling parameters obtained in the fitting is not large enough to validate the model used, it is remarkably that they are different in nature. The largest coupling is antiferromagnetic, thus it dominates the magnetic behaviour observed in **9**.

The coupling parameter  $J = -0.153(1) \text{ cm}^{-1}$  obtained is in agreement with that expected from a carboxylate bridge in *anti-syn* conformation which links two equatorial positions of the copper(II) environment.<sup>18,19</sup> In addition, the  $J$  value obtained agrees with the fact that the magnetic coupling constant must be very small since no maximum is present in the experimental  $\chi_M$  curve. According to the Kahn's orbital model,<sup>20</sup> the counterbalance of the ferro- and antiferromagnetic contributions is so delicate that small variations of structural features can favor the overlap and then make the antiferromagnetic contribution to predominate as occur in **9**.

The magnetic behaviour of compounds **8**, **10** and **11** are very similar and reminiscent of that of **3** and **4**. Thus, there is a competition between two interactions of opposite nature which operate through the carboxylate-bridged layers of copper(II) ions. The two crystallographically different carboxylate bridges within the layers must couple the copper(II) ions ferro- and antiferromagnetically. Then, under a magnetic point of view, the layers of **8**, **10** and **11** can be seen as cross-linked AF and F chains. An analysis through the Baker and Rushbrooke<sup>21</sup> numerical expression for a ferromagnetically coupled copper(II) chain with a mean-field term to take into account the interchain interactions (similar to that made in Section 1.3.4 with the magnetic data of complex **4**) was performed, but the results are not good enough to be valid, and we conclude that the ferro- and antiferromagnetic coupling constants must be of similar magnitude. The antiferromagnetic coupling constant can be estimated from the critical field [ $H_c = 2.4$  (**8**) and 1.2 T (**10** and **11**)] being  $j \sim -2.4 \text{ cm}^{-1}$  for **8** and  $j \sim -1.2 \text{ cm}^{-1}$  for **10** and **11**. These values are similar to that obtained from the analysis of the antiferromagnetically coupled copper(II) layers in complex **9**.

There is a delicate equilibrium between the ferro- and antiferromagnetic interactions in these four complexes. The magnetic coupling parameters range in the  $|2.4 \text{ cm}^{-1}|$  span, and they are in agreement with those reported for exchange pathways through

carboxylate in *anti-syn* conformation.<sup>18,19</sup> Thus, subtle changes in the structure, such as the distortion environment, axial bond distance, planarity of the basal plane, dihedral angle of the carboxylate bridge, etc... could make the ferro- (**8**, **10** and **11**) or antiferromagnetic (**9**) contribution to predominate.

### I.5.5. Conclusion

The complexes **8-11** are isostructural with only small variations due to the distinct Van der Waals radius of the halogen of the 3-Xpy coligand [X = F (**8**), Cl (**9**), Br (**10**) and I (**11**)]. Their structures consist of square grids of copper(II) ions which are linked equatorial-equatorial *anti-syn* carboxylate-bridges. Weak halogen bonds with the adjacent layers lead to a supramolecular three-dimensional network. The four compounds exhibit different magnetic behaviours depending on which contribution, the ferro- or the antiferromagnetic one, is dominant. The weak magnetic coupling parameters observed in **8-11** ( $J$  ca.  $|2.5 \text{ cm}^{-1}|$ ) are within the reported range for an *anti-syn* carboxylate-bridge. Thus, complex **9** presents antiferromagnetic coupling, whilst **8**, **10** and **11** exhibit metamagnetic-like behaviour.

The previous sections have shown that the correlation between the magnetic properties observed and the structure of the complex is due to subtle structural changes, and a correlation between the coligand coordinated to the copper(II) ion and the magnetic behaviour cannot be made. The four complexes studied in this section confirm this statement to the point that being isostructural, the complexes exhibit different magnetic behaviours.

### I.5.6. References

- 1 P. Metrangolo, H. Neukirch, T. Pilati and G. Resnati, *Acc. Chem. Res.* **2005**, *38*, 386.
- 2 N. N. L. Madhavi, G. R. Desiraju, C. Bilton, J. A. K. Howard and F. H. Allen, *Acta Cryst. Sect. B*, **2000**, *B56*, 1063.
- 3 R. K. R. Jetti, F. Xue, T. C. W. Mak and A. Nangia, *Cryst. Eng.* **1999**, *2(4)*, 215.
- 4 C. Janiak, *J. Chem. Soc., Dalton Trans.* **2000**, 3885.
- 5 A. W. Addison, T. N. Rao, J. Reedijk, J. van Rijn and G. C. Verschoor, *Dalton Trans.* **1984**, 1349.
- 6 A. Escuer, R. Vicente, M. S. El Fallah, M. A. S. Goher and F. A. Mautner, *Inorg. Chem.* **1998**, *37*, 4466.
- 7 H. Uekusa, S. Ohba, T. Tokii, Y. Muto, M. Kato, S. Husebye, O. W. Steward, S.-C. Chang, J. P. Rose, J. F. Pletcher and I. Suzuki, *Acta Cryst. Sect. B*, **1992**, *B48*, 650.
- 8 W. Buijs, P. Comba, D. Corneli, Y. Mengerink, H. Pritzkow and M. Schickedanz, *Eur. J. Inorg. Chem.* **2001**, 3143.
- 9 E. Durcanska, M. Koman, M. Jamnicky and D. Dankova, *Z. Kristallogr.* **1995**, *210*, 367.
- 10 F. Zordan, L. Brammer and P. Sherwood, *J. Am. Chem. Soc.* **2005**, *127*, 5979.
- 11 G. Mínguez Espallargas, L. Brammer, and P. Sherwood, *Angew. Chem., Int. Ed.* **2006**, *45*, 435.
- 12 L. Brammer, F. Zordan, G. Mínguez Espallargas, S. L. Purver, L. Arroyo Marín and H. Adams, *Trans. Am. Crystallogr. Assoc.* **2004**, *39*, 114.

- 13 L. Brammer, G. Mínguez Espallargas, and H. Adams, *CrystEngComm* **2003**, 5, 343.
- 14 F. Zordan and L. Brammer, *Acta Cryst., Sect. B* **2004**, B60, 512.
- 15 F. Zordan, S. L. Purver, H. Adams and L. Brammer, *CrystEngComm* **2005**, 7, 350. [CrossRef]
- 16 G.S. Rushbrooke, G. A. Baker and P. J. Wood in *Phase Transition and Critical Phenomena*, vol. 3, C. Domb and M.S. Green, eds. Academic Press, London, **1972**.
- 17 (a) J. C. Bonner, M. E. Fisher, *Phys. Rev. A*, **1964**, 135, 640. (b) R. L. Orbach, *Phys. Rev.* **1958**, 112, 309. (c) W. E. Estes, D. P. Gavel, W. E. Hatfield, D. Hodgson, *Inorg. Chem.* **1978**, 17, 1415
- 18 A. Rodríguez-Forteza, P. Alemany, S. Álvarez and E. Ruiz, *Chem. Eur. J.* **2001**, 7, 627.
- 19 J. Pasán, F. S. Delgado, Y. Rodríguez-Martín, M. Hernández-Molina, C. Ruiz-Pérez, J. Sanchiz, F. Lloret and M. Julve, *Polyhedron* **2003**, 22, 2143.
- 20 O. Kahn, *Molecular Magnetism*, VCH, New York, **1993**.
- 21 G. A. Baker, G. S. Rushbrooke and H. E. Gilbert, *Phys. Rev.* **1964**, 135, A1272.

## I.6. 2,4'-Bipyridine (12) Copper(II)-Phenylmalonate complex

### I.6.1. Introduction

The previous sections have been devoted to the study of the influence of different pyridine-like coligands in the copper(II)-phenylmalonate system. Subtle changes in the carboxylate-bridged square grid of copper(II) ions are registered along the series, being the layered system separated by hydrophobic areas containing the phenyl rings of the phenylmalonate ligand and the pyridine-like coligands. Now, the introduction of a larger spacer would separate much more the adjacent layers producing well isolated square grids of copper atoms. The 2,4-bipyridine is a blocking ligand when coordinates to the copper(II) ion, thus it behaves as the pyridine-type coligands in the complexes **2-11**. The study of this complex is the starting point of a series of copper(II) phenylmalonate complexes with bipyridine-type as coligands. Herein we report the synthesis, structural characterization and magnetic properties of the complex  $[\text{Cu}(2,4'\text{-bpy})(\text{Phmal})(\text{H}_2\text{O})]_n$  (**12**).

### I.6.2. Synthesis

#### $[\text{Cu}(2,4'\text{-bpy})(\text{Phmal})(\text{H}_2\text{O})]_n$ (**12**).

An aqueous solution of copper(II)-phenylmalonate (0.5 mmol, 120 mg), [which was prepared as described in Section 1.1], is placed in one arm of an H-shape tube whereas a 50/50 methanol/water solution of the 2,4'-bpy (0.5 mmol, 78 mg) is introduced in the other one. A 50/50 methanol/water solution was added dropwise to fill the H tube. Single crystals of **12** as blue rods appeared within a week by slow diffusion at room temperature and they were used for all the measurements. Yield 80%. Crystallographic data for **12** are listed in Table I.16. Anal. Calcd. for  $\text{C}_{19}\text{H}_{16}\text{N}_2\text{O}_5\text{Cu}$  (**12**): C, 54.87; H, 3.69; N, 6.74. Found: C, 54.58; H, 3.76; N, 6.72.

Table I.16. Crystallographic data for complex **11**

|                                         | <b>11</b>                                                              | <b>11</b>                                                              |
|-----------------------------------------|------------------------------------------------------------------------|------------------------------------------------------------------------|
| Formula                                 | $\text{C}_{19}\text{H}_{13}\text{O}_5\text{N}_2\text{Cu}$              | $\text{C}_{19}\text{H}_{13}\text{O}_5\text{N}_2\text{Cu}$              |
| FW                                      | 412.88                                                                 | 412.88                                                                 |
| Crystal system                          | Orthorhombic                                                           | Orthorhombic                                                           |
| Space group                             | $C 2cb$                                                                | $C 2cb$                                                                |
| $a/\text{\AA}$                          | 10.1579 (7)                                                            | 10.2178 (4)                                                            |
| $b/\text{\AA}$                          | 10.3640 (8)                                                            | 10.2909 (5)                                                            |
| $c/\text{\AA}$                          | 33.313 (4)                                                             | 32.825 (2)                                                             |
| $V/\text{\AA}^3$                        | 3507.1 (6)                                                             | 3451.6 (3)                                                             |
| $Z$                                     | 8                                                                      | 8                                                                      |
| $\mu(\text{Mo K}\alpha)/\text{cm}^{-1}$ | 12.84                                                                  | 13.01                                                                  |
| $T/\text{K}$                            | 293 (2)                                                                | 100(2)                                                                 |
| $\rho_{\text{calc}}/\text{g cm}^{-3}$   | 1.642                                                                  | 1.612                                                                  |
| $\lambda/\text{\AA}$                    | 0.71073                                                                | 0.71073                                                                |
| Index ranges                            | $-14 \leq h \leq 13,$<br>$-14 \leq k \leq 13,$<br>$-46 \leq l \leq 43$ | $-14 \leq h \leq 12,$<br>$-14 \leq k \leq 11,$<br>$-46 \leq l \leq 36$ |
| Indep. reflect. ( $R_{\text{int}}$ )    | 4904 (0.085)                                                           | 4571 (0.079)                                                           |
| Obs. reflect. [ $I > 2\sigma(I)$ ]      | 4224                                                                   | 4247                                                                   |
| Flack parameter                         | -0.004(19)                                                             | 0.96(3)                                                                |
| Parameters                              | 263                                                                    | 263                                                                    |
| Goodness-of-fit                         | 1.038                                                                  | 1.132                                                                  |
| $R$ [ $I > 2\sigma(I)$ ]                | 0.0485                                                                 | 0.0678                                                                 |
| $R_w$ [ $I > 2\sigma(I)$ ]              | 0.1228                                                                 | 0.1807                                                                 |
| $R$ (all data)                          | 0.0577                                                                 | 0.0754                                                                 |
| $R_w$ (all data)                        | 0.1282                                                                 | 0.1905                                                                 |

### I.6.3. Description of the structures

The structure of **12** (Figure I.34) consists of a sheet-like arrangement of *trans*-aqua(2,4'-bipyridine)copper(II) units bridged by phenylmalonate ligands running parallel to the *ac* plane similar to that of complexes **2-11** (Figure I.35). A corrugated square grid of copper atoms results (Figure I.36) where the 2,4'-bpy terminal ligands are alternatively located above and below each layer and, at the same time, inversely to the position of the phenyl group of the Phmal ligand. These sheets are stacked parallel along the *b* axis but rotated 90° through this axis in a twisted fashion (i.e. odd units in the same position and even units rotated by 90°) exhibiting the *ABABAB* sequence. Intralayer hydrogen bonds involving the coordinated water molecule [O(1w)] and oxygen atoms from the carboxylate-malonate groups [2.615(4) and 2.633(4) Å for O(1w)⋯O(2a) and O(1w)⋯O(4b), respectively; (a) =  $x, y + 1/2, -z + 1/2$ ; (b) =  $x - 1/2, y, -z + 1/2$ ] contribute to stabilize the structure. Weak  $\pi$ -type interactions occur between the phenyl rings and the 2,4'-bpy groups, the shortest centroid⋯centroid distance being 4.154(6) Å and the shortest off-set angle being 29.6°, values which are somewhat larger than the average ones observed in  $\pi$ - $\pi$  interactions with pyridyl-like groups.<sup>1</sup>

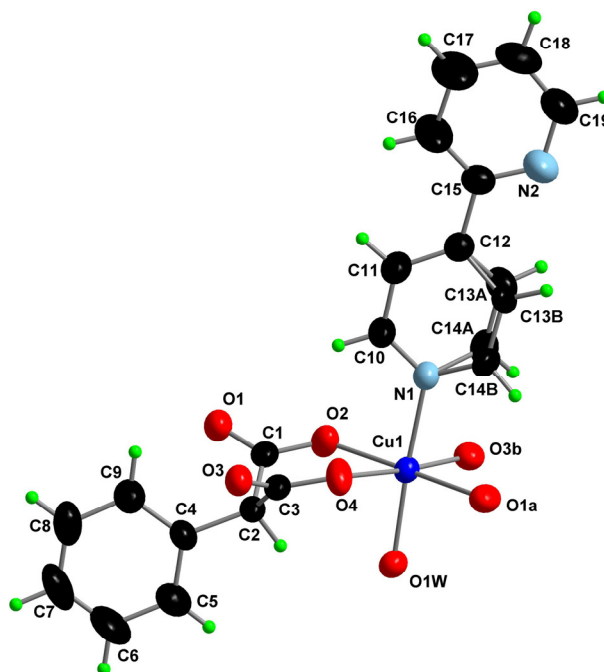
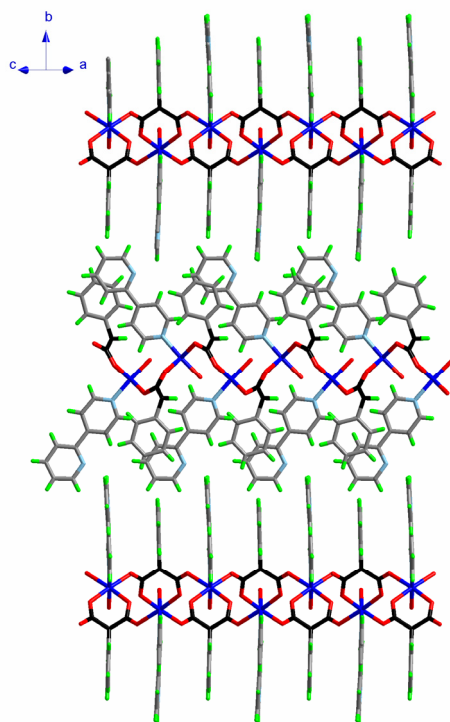


Fig. I.34. View of a fragment of the structure of **12** with the numbering scheme.





**Fig. I.35.** Crystal packing of complex **12** with the corrugated layers viewed through the [101] direction.

Each copper atom exhibits a six-coordinated environment defined by four carboxylate-phenylmalonate oxygen atoms, one 2,4'-bpy nitrogen atom and a water molecule. The  $\text{CuNO}_3$  chromophore could be described as a unusual compressed tetragonal octahedron with two short distances [2.004(2) and 2.026(3) Å for Cu(1)–O(1w) and Cu(1)–N(1), respectively] and four long ones [values ranging from 2.076(3) to 2.208(3) Å] (see Table I.17). A low temperature crystallographic study has been carried out to give a clear-cut answer to this compression. One can see in the Table I.18 that the bond distances and angles at 293 and 100 K do not vary significantly, and hence the presence of a static pseudo-Jahn-Teller disorder could be suspected.<sup>2-5</sup> The vibrational amplitudes of the ligand donor atoms along the metal-ligand bonds represented by the quantity  $\langle d^2 \rangle$  or equivalently  $\Delta\text{MSDA}^{2-5}$  are also listed in Table I.18. These values correspond to the difference in the mean-square displacements parameters (MSDAs) of a given donor atom and the Cu atom along their common vector.

$$\text{MSDA} = \frac{\sum_{i=1}^3 \sum_{j=1}^3 U_{ij} n_i n_j}{|n|^2}$$

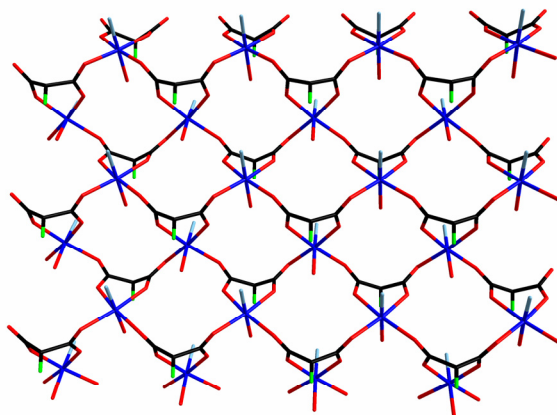


**Fig. I.36.** Central projection of the carboxylate-bridged square grid of copper(II) ions formed in **12**. The 2,4'-bipyridine coligand and the phenyl ring of the Phmal ligand have been omitted for clarity.

$$\langle d \rangle^2 = \Delta MSDA = MSDA(donor) - MSDA(Cu)$$

where  $U_{ij}$  is an element of the 3 x 3 matrix of the thermal parameters and  $n_i$  and  $n_j$  are elements of the vector describing the bond. Values of  $\Delta MSDA$  are typically found in the range of  $(10-100) \times 10^{-4} \text{ \AA}^2$ .<sup>3</sup> The values of the  $\Delta MSDA$  for O(1w) and N(1) are within this range but the four carboxylate-oxygen atoms present  $\Delta MSDAs$  in the range  $255-315 \times 10^{-4} \text{ \AA}^2$ . This disparity from the 'static' values can be attributed to the presence of a static pseudo-Jahn-Teller disorder of two of the three axes of the octahedral copper environment. The shorter bond distances corresponds with the Cu(1)-O(1w) and Cu(1)-N(1) bonds indicating that these two atoms belong to the basal plane of Cu(1). The O(2), O(4), O(1a) and O(3b) are statically disordered in pairs between the equatorial and axial positions [two different environments are found within the crystal, one with O(1w), N(1), O(2) and O(1a) in equatorial and O(4) and O(3b) in axial positions; the other with O(1w), N(1), O(4) and O(3b) in equatorial and O(2) and O(1a) in axial positions] (see Figure I.37). The analysis of the EPR spectrum at room temperature (Figure I.38) reveals three different effective  $g$  values ( $g_1 = 2.27$ ,  $g_2 = 2.20$ ,  $g_3 = 2.15$ ) indicating a rhombic environment of the copper(II) ion or, according to our approximation, averaged values of static pseudo-Jahn-Teller disorder in the crystal as they appear in the X-ray crystal structure. EPR spectra at low temperatures do not change significantly from the rhombic distortion, being the slight variations in the  $g$  values most likely associated with the spin coupling.

**Table I.17.** Selected bond lengths (Å) and angles (°) for compound **12**<sup>a,b</sup>

| <b>12</b>        |            |                   |            |
|------------------|------------|-------------------|------------|
| Cu(1)–O(2)       | 2.128(3)   | O(4)–Cu(1)–O(1a)  | 89.41(13)  |
| Cu(1)–O(4)       | 2.076(3)   | O(4)–Cu(1)–O(3b)  | 174.49(13) |
| Cu(1)–O(1a)      | 2.208(3)   | O(4)–Cu(1)–N(1)   | 90.73(12)  |
| Cu(1)–O(3b)      | 2.110(3)   | O(4)–Cu(1)–O(1w)  | 90.71(12)  |
| Cu(1)–N(1)       | 2.026(3)   | O(1a)–Cu(1)–O(3b) | 95.57(12)  |
| Cu(1)–O(1w)      | 2.004(2)   | O(1a)–Cu(1)–N(1)  | 87.13(11)  |
| O(2)–Cu(1)–O(4)  | 84.79(14)  | O(1a)–Cu(1)–O(1w) | 89.50(10)  |
| O(2)–Cu(1)–O(1c) | 174.12(14) | O(3b)–Cu(1)–N(1)  | 87.19(11)  |
| O(2)–Cu(1)–O(3b) | 90.18(13)  | O(3b)–Cu(1)–O(1w) | 91.68(11)  |
| O(2)–Cu(1)–N(1)  | 91.91(12)  | N(1)–Cu(1)–O(1w)  | 176.32(11) |
| O(2)–Cu(1)–O(1w) | 91.59(11)  |                   |            |

<sup>a</sup> Estimated standard deviations in the last significant digits are given in parentheses.  
<sup>b</sup> Symmetry code: (a)  $x, y + 1/2, -z + 1/2$ ; (b)  $x - 1/2, y, -z + 1/2$ .

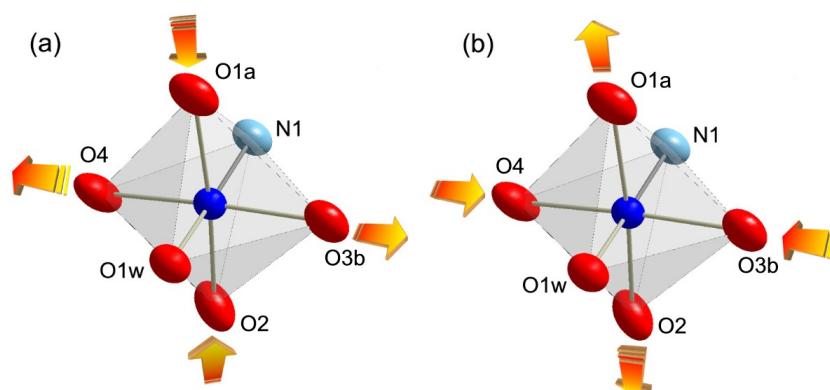


**Fig. I.37.** Two different copper(II) environments [(a) and (b)] occur in complex **12** because a static pseudo-Jahn-Teller disorder. Arrows indicate the atoms that fill equatorial (compressed) or apical (elongated) positions at the metal environment.

The phenylmalonate ligand acts simultaneously as bidentate [through O(2) and O(4); with the angle subtended to the copper atom being 84.79(14)°] and as bis-monodentate ligand [through O(1) and O(3)]. The pyridyl rings of the 2,4'-bpy ligand are quasi-planar [the dihedral angle between pyridyl rings being 4°]. The pyridyl ring formed by the N(1)–C(10)–C(11)–C(12)–C(13)–C(14) set of atoms are slightly distorted and two crystallographic positions are found for the C(13) and C(14) atoms [0.977(16) and 1.012(15) Å for C(13A)–C(13B) and C(14A)–C(14B), respectively]. These two positions are also found in the low temperature X-ray study of a different crystal; hence a static disorder within the crystal could be the responsible for this feature. The copper-copper separations through the two crystallographically independent *anti-syn* carboxylate-bridges are 5.3217(9)

and 5.4202(6) Å, values which are much shorter than the shorter interlayer Cu $\cdots$ Cu distance [15.221(2) Å].

**Table I.18.** Bond distances and calculated  $\Delta MSDA$  values for compound **12** at different temperatures.<sup>a</sup>

| Bond        | $T = 293$ K    |                                           | $T = 100$ K    |                                           |
|-------------|----------------|-------------------------------------------|----------------|-------------------------------------------|
|             | $d / \text{Å}$ | $\Delta MSDA / \text{Å}^2 \times 10^{-4}$ | $d / \text{Å}$ | $\Delta MSDA / \text{Å}^2 \times 10^{-4}$ |
| Cu(1)–O(2)  | 2.128(3)       | 269                                       | 2.111(5)       | 355                                       |
| Cu(1)–O(4)  | 2.076(3)       | 255                                       | 2.087(5)       | 301                                       |
| Cu(1)–O(1a) | 2.208(3)       | 293                                       | 2.187(5)       | 247                                       |
| Cu(1)–O(3b) | 2.110(3)       | 315                                       | 2.156(5)       | 201                                       |
| Cu(1)–O(1w) | 2.004(2)       | 59                                        | 1.992(3)       | 29                                        |
| Cu(1)–N(1)  | 2.026(3)       | 64                                        | 2.014(4)       | 36                                        |

<sup>a</sup> Symmetry operations: (a) =  $x, y + 1/2, -z + 1/2$ ; (b) =  $x - 1/2, y, -z + 1/2$ ;

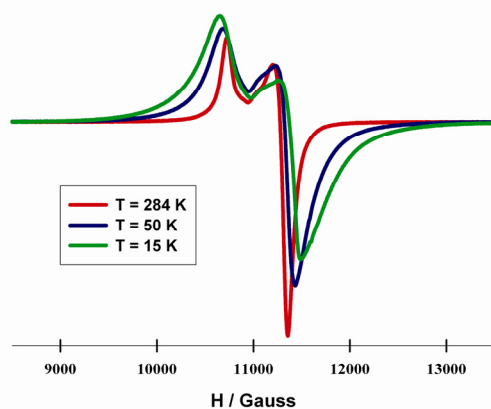


**Fig. I.38.** Q-band EPR spectra of complex **12** at different temperatures.

Let us make a comparison of the structure of **12** with that of the previously reported malonato-manganese(II) complex of formula  $[\text{Mn}(\text{mal})(\text{H}_2\text{O})(2,4\text{'-bpy})]_n$ .<sup>6</sup> This structure consists of a sheet arrangement of *trans*-aqua(2,4'-bpy)manganese(II) units bridged by malonate ligands. The square grid of manganese atoms formed is structurally identical to that of copper atoms built in **12**, while the mean difference between them is the twisted-fashion stacking of the layers in **12** that is not present in the malonato-manganese(II) compound. Despite of the similarity between these structures, that of the  $[\text{Cu}_4(\text{mal})_4(2,4\text{'-bpy})_4(\text{H}_2\text{O})_4] \cdot 8\text{H}_2\text{O}$  is very different.<sup>7</sup> Tetranuclear molecules involving a small planar square with copper(II) cations and malonate anions at each corner and edge, respectively, built up this structure. Indeed a square pyramidal environment at copper(II) cation is present while the six-coordination mode is favoured in **12**. Therefore, in the presence of the 2,4'-bpy ligand the copper(II) ion acts, structurally, as the manganese(II) cation when the malonate is substituted by the phenylmalonate ligand.

### I.6.4. Magnetic Properties

The magnetic properties of compound **12** under the form of  $\chi_M T$  vs.  $T$  plot [ $\chi_M$  being the molar susceptibility per copper(II) ion] are shown in Figure I.39.  $\chi_M T$  at room temperature is  $0.42 \text{ cm}^3 \text{ mol}^{-1} \text{ K}$ , a value which is as expected for a magnetically isolated spin doublet. Upon cooling  $\chi_M T$  remains almost constant until 30 K and then, increases to reach a value of  $0.53 \text{ cm}^3 \text{ mol}^{-1} \text{ K}$  at 2.0 K, feature which is indicative of an overall ferromagnetic coupling in **12**. The magnetization ( $M$ ) plot (Figure I.40) confirms this statement given that the  $M$  vs.  $H$  curve lies above the Brillouin curve for a magnetically isolated spin doublet.

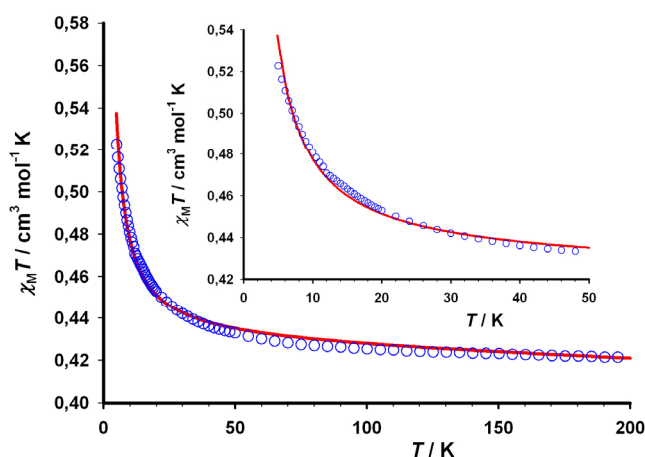


**Fig. I.39.** Thermal dependence of the  $\chi_M T$  product for **12** under applied magnetic field of 1 T ( $T > 6$  K) and 0.025 T ( $T < 6$  K): (o) experimental data; (—) best fit curve. The inset shows a detail of the low temperature region.

The structure of **12** is formed by isolated corrugated layers of *anti-syn* carboxylate bridged copper(II) ions, that exhibits an overall ferromagnetic coupling. Thus, the magnetic data were fitted by means of the high-temperature series expansion derived from the two-dimensional Heisenberg model for a  $S = 1/2$  ferromagnetic square lattice<sup>8</sup>

$$\chi = [Ng^2 \beta^2 / (3kT)] \cdot S(S+1) \cdot \left( 1 + \sum_{n=1}^{10} a_n K^n \right)$$

where  $K = J/kT$ ,  $a_n$  are the coefficients for the square lattice and  $J$  is the intralayer magnetic coupling between the local spins of the nearest-neighbors with the Hamiltonian defined as:

$$\hat{H} = -J \sum_i \hat{S}_i \cdot \hat{S}_{i+1}$$

The best fit using nonlinear regression analysis leads to  $J = +0.77(1) \text{ cm}^{-1}$ ,  $g = 2.22(1)$  and  $R = 1.2 \times 10^{-5}$ . The calculated curve matches well the experimental data in the

measured temperature range as seen in Figure I.39 and the calculated value of  $g$  is in agreement with that obtained from the EPR spectra.

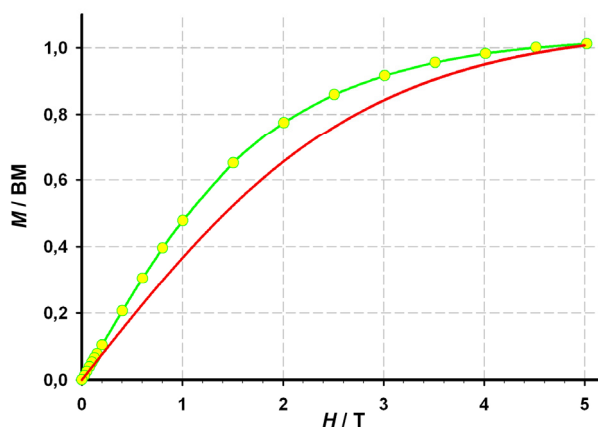
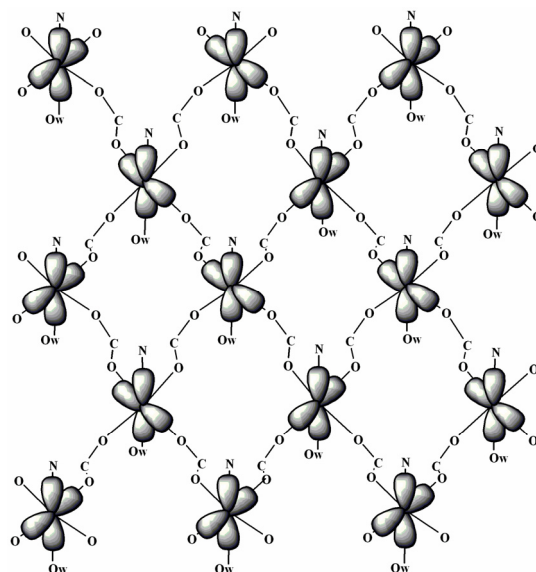


Fig. I.40. Magnetization ( $M$ ) vs applied field ( $H$ ) plot for complex **12** together with the Brillouin function for a magnetically isolated  $S=1/2$  (red line).

The analysis of the magnetic data shows that compound **12** exhibits a very small ferromagnetic coupling. The magnitude of this interaction may be explained in terms of structural features. The bidentate carboxylate group can exhibit three different coordination modes: *syn-syn*, *anti-anti* and *anti-syn*. For the two first modes from moderate to strong antiferromagnetic coupling is expected, whereas the *anti-syn* mode leads to weak coupling that can be either ferro- or antiferromagnetic.<sup>9</sup> This ability of the carboxylate group has been substantiated by DFT type calculations.<sup>10</sup> Compound **12** have copper(II) ions bridged by carboxylate groups in the *anti-syn* coordination mode and the coupling constant is very small, in agreement with the latter general rule.

In addition to the conformation of the bridge, the relative orientation of the magnetic orbitals centered in the metal ions is very unfavorable for a strong magnetic coupling. The environment of the copper(II) ion in **12** is distorted octahedral and the magnetic orbital has  $d(x^2-y^2)$  character. Each copper(II) ion is connected to other four copper(II) ions through *anti-syn* carboxylate bridges to give a bidimensional quadratic network. The magnetic coupling in this compound is very weak because the equatorial plane of the copper environment (see Scheme I.3) is perpendicular to the exchange pathway and only two of the four exchange pathways have spin density [half of the exchange pathways are inactive]. This situation is very unfavorable for a long range magnetic interaction and leads to a very weak coupling constant.



Scheme I.3

The ferromagnetic nature of the interaction may be explained attending to magnetic orbital considerations. The copper(II) ions in **12** lie in a corrugated layer and the magnetic orbitals of the metal ions form an angle of  $87.8(4)^\circ$  in the bridge (Fig. I.36), leading to an accidental orthogonality. This situation leads to a very poor overlap and it makes the antiferromagnetic contribution very small leading the ferromagnetic one to be dominant.<sup>11</sup>

### I.6.5. Conclusion

The introduction of a larger spacer such as the 2,4'-bpy ligand to form the complex **12** has partially fulfilled our expectations. Certainly, the 2,4'-bpy group acts as a blocking ligand and the structure formed is the carboxylate-bridged square grid of copper(II) ions similar to those of **2-11**, with a separation between layers of  $15.221(2)$  Å. However, the bipyridine ligand occupies an equatorial position at the copper environment as occurs in **7**, which in **12** leads to a static pseudo-Jahn-Teller disorder of the copper surroundings within the layers. This situation strongly influence the magnetic coupling which being ferromagnetic, is of lower magnitude than those of **2-5**.

Summarizing, complex **12** is a promising compound from the point of view that the structure formed is the same as that of **2-11** but with a larger spacing between the layers. The strategy can now be modified introducing other bipyridine ligands with other functionalities which will take advantages from the large spacing of the layered system.

### I.6.6. References

- 1 C. Janiak, *Dalton Trans.* **2000**, 3885.
- 2 B. J. Hathaway, *Struct. Bonding*, **1984**, 57, 55.
- 3 L. R. Falvello, *Dalton Trans.* **1997**, 4463.
- 4 M. A. Halcrow, *Dalton Trans.* **2003**, 4375.
- 5 N. K. Solanki, M. A. Leech, E. J. L. McInnes, F. E. Mabbs, J. A. K. Howard, C. A. Kilner, J. M. Rawson and M. A. Halcrow, *Dalton Trans.* **2002**, 1295.
- 6 Y. Rodríguez-Martín, M. Hernández-Molina, J. Sanchiz, C. Ruiz-Pérez, F. Lloret and M. Julve, *Dalton Trans.* **2003**, 2359.
- 7 Y. Rodríguez-Martín, M. Hernández-Molina, F. S. Delgado, J. Pasán, C. Ruiz-Pérez, J. Sanchiz, F. Lloret and M. Julve, *CrystEngComm* **2002**, 4, 440.
- 8 R. Navarro, *Application of High- and Low-Temperature Series Expansions to Two-dimensional Magnetic Systems*, de Jongh, L. J.; Ed., Kluwer Academic Publishers, The Netherlands, **1990**.
- 9 J. Pasán, F. S. Delgado, Y. Rodríguez-Martín, M. Hernández-Molina, C. Ruiz-Pérez, J. Sanchiz, F. Lloret, and M. Julve, *Polyhedron*, **2003**, 22, 2143.
- 10 A. Roríguez-Forteza, P. Alemany, S. Álvarez and E. Ruiz, *Chem. Eur. J.*, **2001**, 7, 627.
- 11 O. Kahn, *Molecular Magnetism*, VCH, New York, **1993**.



## I.7.4,4'-Bipyridine (13) Copper(II)-Phenylmalonate complex

### I.7.1. Introduction

The use of bipyridine-like groups as coligands has been proved to be a good strategy as seen in the previous section. The 4,4'-bipyridine ligand is well known<sup>1,2</sup> to act as a rod in layered systems. The efficiency of this ligand stems from its rigidity which allows some degree of control upon the steric constraints of the assembly process. The motivation to use the 4,4'-bpy ligand in the copper-phenylmalonate system is the connection of the layers system observed in the complexes **2-12** to build a robust three-dimensional network.

### I.7.2. Synthesis

**[Cu(4,4'-bpy)(Phmal)]<sub>n</sub>·2nH<sub>2</sub>O (13)**. Compound **13** is obtained by following a similar procedure to that of **12** (Section 1.6.2) but using 4,4'-bpy (0.5 mmol, 78 mg) instead of 2,4'-bpy. X-ray suitable blue rectangles of **13** appeared within a week by slow diffusion at room temperature and they were used for all the measurements. Crystallographic data are listed in Table I.19. Yield *ca* 75%. Anal. Calcd. for C<sub>19</sub>H<sub>18</sub>N<sub>2</sub>O<sub>6</sub>Cu (**13**): C, 52.59; H, 4.15; N, 6.46. Found: C, 52.30; H, 4.25; N, 6.38.

### I.7.3. Description of the Structure

The structure of complex **13** (Figure I.41) consists of chains of carboxylate(phenylmalonate)-bridged copper(II) ions which are linked through bis-monodentate 4,4'-bpy ligands to afford a sheet-like polymer growing in the *bc* plane (see Figure I.42).

Rectangles of dimensions 11.08 x 4.99 Å<sup>2</sup> are repeated within each layer, the longer edge corresponding to the 4,4'-bpy ligand (*c* axis) whereas the shorter side is defined by the phenylmalonate-carboxylate group (*b* axis). The separation between adjacent layers is 8.64 Å. The layers are not stacked parallel along the *a* axis, but forming an angle of 17.807(6)° with the normal plane vector. They are staggered in the *ABCABCABC* trend and the nearest

**Table I.19.** Crystallographic data for **12**

| <b>12</b>                                          |                                                                     |
|----------------------------------------------------|---------------------------------------------------------------------|
| Formula                                            | C <sub>19</sub> H <sub>18</sub> O <sub>6</sub> N <sub>2</sub> Cu    |
| FW                                                 | 433.86                                                              |
| Crystal system                                     | Monoclinic                                                          |
| Space group                                        | <i>P</i> 2 <sub>1</sub>                                             |
| <i>a</i> / Å                                       | 9.0837 (6)                                                          |
| <i>b</i> / Å                                       | 9.3514 (4)                                                          |
| <i>c</i> / Å                                       | 11.0831 (8)                                                         |
| <i>β</i> / °                                       | 107.807 (6)                                                         |
| <i>V</i> / Å <sup>3</sup>                          | 896.35 (10)                                                         |
| <i>Z</i>                                           | 4                                                                   |
| <i>μ</i> (Mo Kα) / cm <sup>-1</sup>                | 12.59                                                               |
| <i>T</i> / K                                       | 293 (2)                                                             |
| <i>ρ</i> <sub>calc</sub> / g cm <sup>-3</sup>      | 1.593                                                               |
| <i>λ</i> / Å                                       | 0.71073                                                             |
| Index ranges                                       | -12 ≤ <i>h</i> ≤ 12,<br>-13 ≤ <i>k</i> ≤ 12,<br>-15 ≤ <i>l</i> ≤ 13 |
| Indep. reflect. ( <i>R</i> <sub>int</sub> )        | 4940 (0.050)                                                        |
| Obs. reflect. [ <i>I</i> > 2σ( <i>I</i> )]         | 4242                                                                |
| Flack parameter                                    | 0.387(12)                                                           |
| Parameters                                         | 254                                                                 |
| Goodness-of-fit                                    | 1.025                                                               |
| <i>R</i> [ <i>I</i> > 2σ( <i>I</i> )]              | 0.0394                                                              |
| <i>R</i> <sub>w</sub> [ <i>I</i> > 2σ( <i>I</i> )] | 0.0858                                                              |
| <i>R</i> (all data)                                | 0.0525                                                              |
| <i>R</i> <sub>w</sub> (all data)                   | 0.0907                                                              |

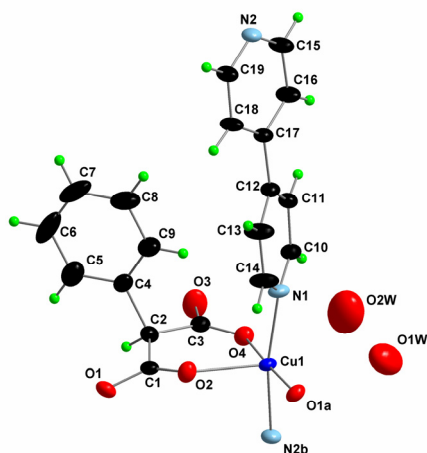


Fig. I.41. View of a fragment of the structure of **13** along with the numbering scheme.

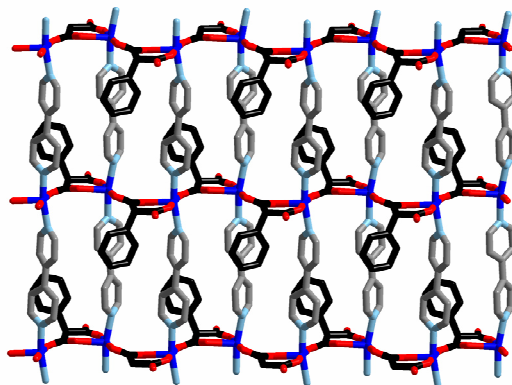
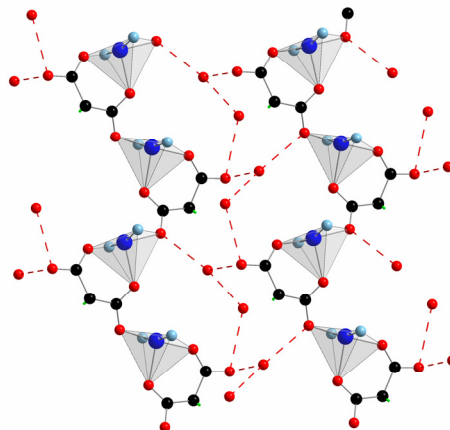


Fig. I.42. View through the [100] direction of a fragment of complex **13**. The 4,4'-bpy ligand connects chains of phenylmalonate-bridged copper(II) ions. Hydrogen atoms are omitted for clarity.

neighbours are shifted by  $c/3$  from each other. Adjacent layers are linked through hydrogen bonds involving two carboxylate-oxygen atoms [O(1) and O(3)] and the crystallization water molecules (see Figure I.43), the values of the O...O distances ranging from 2.839(5) to 3.085(6) Å. It deserves to be noted that the crystallization water molecules are placed between the layers close to the carboxylate groups due to the hydrogen bonds they form. The water molecules avoid thus the rectangular cavities because of their hydrophobic character. The  $\pi$ - $\pi$  interactions play an important role in the packing of this structure as is observed in previous sections.<sup>3,4</sup> Several intra- and interlayer C-H... $\pi$  contacts can be identified,<sup>5</sup> the shortest centroid...centroid distance being 4.8781(4) Å, a value which is close to the molecular dynamics calculations for benzene (optimum distance of 4.99 Å between two ring centres in the T-shaped orientation).<sup>6</sup> The values of the dihedral angle

between the aromatic rings range from 52.2° to 89.31°.



**Fig. I.43.** Supramolecular layers of phenylmalonate-copper(II) chains bridged through hydrogen bonds with the crystallization water molecules. Phenyl rings of Phmal, carbon atoms of 4,4'-bpy, and hydrogen atoms are omitted for clarity.

Each copper atom exhibits a somewhat distorted square pyramidal environment, the geometric  $\tau$  value being 0.13 ( $\tau = 0$  for square pyramidal and  $\tau = 1$  for trigonal bipyramidal).<sup>7</sup> Two nitrogen atoms from the 4,4'-bpy molecule [N(1) and N(2a); (a) =  $x, y, z + 1$ ] and two carboxylate oxygen atoms from the Phmal ligand [O(4) and O(1b); (b) =  $-x, y - 1/2, -z$ ] build the basal plane whereas another carboxylate oxygen atom [O(2)] occupies the apical position (selected interatomic distances and angles are listed in Table I.20). The equatorial bond lengths vary in the range 1.928(2)-2.041(2) Å and the apical bond distance is 2.185(2) Å. The copper atom is shifted by 0.0989(3) Å from the mean basal plane towards the apical position. The copper-copper separation through the phenylmalonate-carboxylate bridge is 4.9922(4) Å, a value which is much shorter than the metal-metal separation through the 4,4'-bpy ligand [11.083(1) Å].

**Table I.20.** Selected bond lengths (Å) and bond angles (°) for compound **13**<sup>a,b</sup>

| <b>13</b>        |            |                   |            |
|------------------|------------|-------------------|------------|
| Cu(1)–O(2)       | 2.185(2)   | O(2)–Cu(1)–N(2b)  | 94.72(11)  |
| Cu(1)–O(4)       | 1.928(2)   | O(4)–Cu(1)–O(1a)  | 176.69(9)  |
| Cu(1)–O(1a)      | 1.952(2)   | O(4)–Cu(1)–N(1)   | 89.26(9)   |
| Cu(1)–N(1)       | 2.041(2)   | O(4)–Cu(1)–N(2b)  | 90.60(9)   |
| Cu(1)–N(2b)      | 2.0220(19) | O(1a)–Cu(1)–N(1)  | 90.55(9)   |
| O(2)–Cu(1)–O(4)  | 89.40(8)   | O(1a)–Cu(1)–N(2b) | 88.94(9)   |
| O(2)–Cu(1)–O(1a) | 93.90(8)   | N(1)–Cu(1)–N(2b)  | 168.70(12) |
| O(2)–Cu(1)–N(1)  | 95.29(9)   |                   |            |

<sup>a</sup> Estimated standard deviations in the last significant digits are given in parentheses.

<sup>b</sup> Symmetry code: (a)  $-x, y - 1/2, -z$ ; (b)  $x, y, z + 1$ .

The phenylmalonate ligand simultaneously adopts monodentate [through O(1) to Cu(1c); (c) = -x, y + 1/2, -z] and bidentate coordination modes [through O(2) and O(4); the angle subtended at the copper atom being 89.40(8)°]. The bidentate coordination of the Phmal ligand involves one equatorial [O(4)] and one apical [O(2)] bond, feature which was previously observed in complex **7**. This situation was unprecedented for R-malonato-containing copper(II) complexes,<sup>3,8</sup> however, is not uncommon for copper(II)-oxalate complexes.<sup>9,10</sup> The preference of copper(II) ions for the nitrogen donor atoms *versus* the oxygen ones and the fact that the two 4,4'-bpy nitrogen atoms in **13** occupy *trans* positions in the coordination sphere of the copper atom account for this singularity. The pyridyl rings of the 4,4'-bpy molecule are planar but the ligand as a whole is far from being planar [the dihedral angle between the two pyridyl rings is 19.99(10)°].

As far as we know, there are two recently reported compounds whose structures are very similar to that of **13**: [Cu<sub>3</sub>(μ-ox)<sub>3</sub>(μ-4,4'-bpy)(4,4'-bpy)<sub>2</sub>]<sub>n</sub><sup>10</sup> and {[Cu(Hsal)<sub>2</sub>(4,4'-bpy)]H<sub>2</sub>O·H<sub>2</sub>sal}<sub>n</sub><sup>11</sup> (ox = oxalate dianion and H<sub>2</sub>sal = salicylic acid). The former structure is comprised of neutral layers where oxalato-bridged copper(II) chains are cross-linked by bis-monodentate 4,4'-bpy ligands. The oxalate ligand is bound to each copper atom through two oxygen atoms, one in an equatorial position [mean Cu–O<sub>eq</sub> = 1.983(9) Å] and the other in the axial one [mean Cu–O<sub>ax</sub> = 2.315 Å] as in **13**. The mean differences between both structures are that the copper(II) ion is six-coordinated in the oxalato-compound (five-coordinated in **13**) and that bis-monodentate and monodentate 4,4'-bpy groups occur in the oxalato compound (only the bis-monodentate 4,4'-bpy is present in **13**). The structure of the {[Cu(Hsal)<sub>2</sub>(4,4'-bpy)]H<sub>2</sub>O·H<sub>2</sub>sal}<sub>n</sub> complex is also two-dimensional with salicylate-bridged copper(II) chains linked by 4,4'-bpy groups. The nitrogen atoms of the 4,4'-bpy ligand in this structure occupy two *trans* equatorial positions of the copper environment as in the other compounds, whereas the three coordinated salicylate groups fill the remaining positions at the metal atom. In the light of these results, one can conclude that the appearance of the rectangular moiety in **13** is not unique, but layered motifs are ensured by the reaction of copper(II) with the appropriate bridging ligand and 4,4'-bpy.

We would like to finish the present structural description with a comparison of the structure of **13** with that of the previously reported malonato-copper(II) complex [Cu<sub>4</sub>(mal)<sub>4</sub>(H<sub>2</sub>O)<sub>4</sub>(4,4'-bpy)<sub>2</sub>]<sub>n</sub><sup>8h</sup> (H<sub>2</sub>mal = malonic acid). This structure consists of layers of tetranuclear entities of carboxylate(malonate)-bridged copper(II) ions linked by 4,4'-bpy ligands. The tetranuclear units are small squares with the copper(II) ions at the corners and the bridging-malonato ligand defining the edges. These units are linked by the 4,4'-bpy

groups to form large squares of  $15.784(1) \times 15.784(1) \text{ \AA}^2$ . Although the dimensionality of this structure as a whole is identical to that of **13**, the presence of the phenyl ring in **13** provides additional interactions (C-H $\cdots\pi$  and  $\pi$ - $\pi$  type interactions, steric effects, etc.) which account for a new coordination mode of the Phmal ligand and a hydrophobic character in the structure.

#### I.7.4. Magnetic Properties

The temperature dependence of the  $\chi_M T$  product ( $\chi_M$  being the molar susceptibility per copper(II) ion) for compound **13** is presented in the Figure I.44. The value of  $\chi_M T$  at room temperature is  $0.41 \text{ cm}^3 \text{ mol}^{-1} \text{ K}$  which is as expected for a magnetic isolated doublet. Upon cooling  $\chi_M T$  remains almost constant up to 10 K and, then, smoothly decreases to a value of  $0.34 \text{ cm}^3 \text{ mol}^{-1} \text{ K}$  at 2.0 K, indicating the occurrence of a very weak antiferromagnetic coupling between the copper(II) ions.

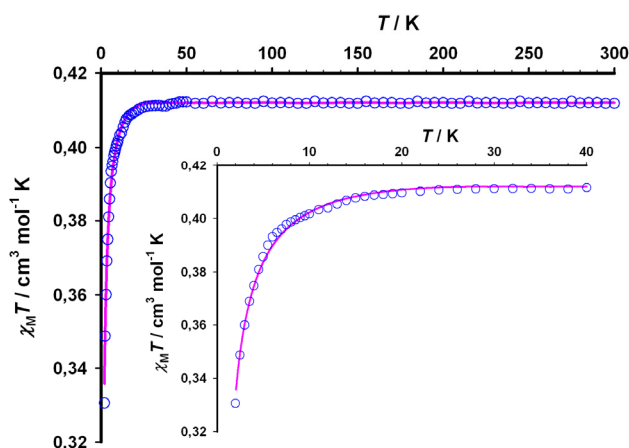


**Fig. I.44.** Thermal dependence of the  $\chi_M T$  product for **13** under applied magnetic field of 1 T: (o) experimental data; (—) best fit curve. The inset shows a detail of the low temperature region.

Two different magnetic exchange pathways between copper atoms are present in **13**: the carboxylate bridge in the *anti-syn* conformation linking apical with equatorial positions at the copper(II) atoms and the 4,4'-bpy ligand. Since the distance between copper(II) ions through the 4,4'-bpy exchange pathway is  $11.083(1) \text{ \AA}$  and the previously reported<sup>8d,12</sup> copper(II) dimers linked through this ligand refer  $J$  in the range  $-0.05$  to  $-0.1 \text{ cm}^{-1}$ , the coupling will be small compared with that of the *anti-syn* carboxylate bridge. Therefore, from a magnetic point of view, compound **13** can be seen as chains of antiferromagnetically coupled copper(II) ions and the data can be analyzed by means of the following numerical expression:<sup>13</sup>

$$\chi_M = \frac{Ng^2\beta^2}{kT} \frac{0.25 + 0.074875x + 0.075235x^2}{1.0 + 0.9931x + 0.172135x^2 + 0.757825x^3}$$

where  $x = |J|/kT$  and the Hamiltonian being defined as:

$$\hat{H} = -J \sum_i \hat{S}_i \cdot \hat{S}_{i+1}$$

The best-fit using nonlinear regression analysis leads to  $J = -0.59(1) \text{ cm}^{-1}$ ,  $g = 2.21(2)$  and  $R = 5.2 \times 10^{-5}$ . The calculated curve matches well the experimental data in the whole temperature range, as seen in Figure I.44.

The very weak magnetic interaction exhibited by compound **13** is in agreement with the *anti-syn* conformation of the carboxylate bridge, which mediates weak magnetic interactions that can be either ferro- or antiferromagnetic.<sup>14</sup> In addition to the conformation of the bridge, the relative orientation of the magnetic orbitals in **13** is very unfavourable for a strong magnetic coupling. The carboxylate bridge links an equatorial position to an axial one of adjacent copper(II) ions. The magnetic orbital for a copper(II) ion in a square pyramidal surrounding is of the  $d(x^2-y^2)$  type, but some admixture of the  $dz^2$  orbital is present due to trigonal distortion. The magnetic coupling is very small since it is the result of the interaction of a  $d(x^2-y^2)$  type orbital with a  $dz^2$  orbital, the latter with a low value of the spin density. The copper(II) ions and the carboxylate groups lie in a plane with maximum deviation of the planarity being  $0.321(2) \text{ \AA}$  for O(2), in the case of **13**. Following Kahn's orbital model,<sup>15</sup> this situation is the optimum to maximize the overlap between the magnetic orbitals of the metal ions and those of the atoms of the bridge and makes the antiferromagnetic term to dominate.

### I.7.5. Conclusion

The structure of complex **13** consists of carboxylate-bridged chains of copper(II) ions linked through rod-like 4,4'-bpy ligands. The square grid layered system observed in **2-12** is no longer obtained and thus, the main purpose in the use of the 4,4'-bpy ligand has failed. This situation has occurred because two 4,4'-bpy coligands are in equatorial positions at the copper coordination sphere avoiding the oxygen atoms of the phenylmalonate ligand to occupy them. This results in the rare conformation of the phenylmalonate which chelates one equatorial and one apical position of the copper surroundings. The antiferromagnetic behaviour observed with a coupling parameter of  $-0.59 \text{ cm}^{-1}$  is in agreement with the equatorial-apical *anti-syn* conformation of the carboxylate-bridge.

## I.7.6. References

- 1 (a) C. Janiak, *Dalton Trans.* **2003**, 2781. (b) B. Moulton and M. J. Zaworotko, *Chem. Rev.* **2001**, *101*, 1629. (c) M. J. Zaworotko, *Chem. Commun.* **2001**, 1.
- 2 (a) S. R. Batten and R. Robson, *Angew. Chem. Int. Ed.* **1998**, *37*, 1461. (b) S. R. Batten, *CrystEngComm*, **2001**, *3*, 67. (c) S. L. James, *Chem. Soc. Rev.* **2003**, *32*, 276.
- 3 J. Pasán, J. Sanchiz, C. Ruiz-Pérez, F. Lloret and M. Julve, *New J. Chem.*, **2003**, *27*, 1557.
- 4 J. Pasán, J. Sanchiz, C. Ruiz-Pérez, F. Lloret and M. Julve, *Eur. J. Inorg. Chem.* **2004**, 4081.
- 5 Examples of C-H... $\pi$  interactions: (a) C. Janiak, S. Temizdemir, S. Dechert, W. Deck, F. Girgsdies, J. Heinze, M. J. Kolm, T. G. Scharmann and O. M. Zipffel, *Eur. J. Inorg. Chem.* **2000**, 1229. (b) B. J. McNelis, L. C. Nathan and C. J. Clark, *Dalton Trans.* **1999**, 1831. (c) K. Biradha, C. Seward and M. J. Zaworotko, *Angew. Chem. Int. Ed.* **1999**, *38*, 492.
- 6 E. G. Cox, D. W. Cruickshank and J. A. S. Smith, *Proc. R. Soc. London, Ser. A* **1958**, *247*, 1-20.
- 7 A. W. Addison, T. N. Rao, J. Reedijk, J. van Rijn and G. C. Verschoor, *Dalton Trans.* **1984**, 1349.
- 8 Malonate containing Cu(II) complexes: (a) D. Chattopadhyay, S. K. Chattopadhyay, P. R. Lowe, C. H. Schwalbe, S. K. Mazumder, A. Rana, and S. Ghosh, *Dalton Trans.* **1993**, 913. (b) I. Gil de Muro, F. A. Mautner, M. Insausti, L. Lezama, M. I. Arriortua and T. Rojo, *Inorg. Chem.* **1998**, *37*, 3243. (c) C. Ruiz-Pérez, J. Sanchiz, M. Hernández-Molina, F. Lloret, and M. Julve, *Inorg. Chim. Acta* **2000**, *298*, 245-250. (d) C. Ruiz-Pérez, J. Sanchiz, M. Hernández-Molina, F. Lloret and M. Julve, *Inorg. Chem.* **2000**, *39*, 1363. (e) C. Ruiz-Pérez, M. Hernández-Molina, P. Lorenzo-Luis, F. Lloret, J. Cano, and M. Julve, *Inorg. Chem.* **2000**, *39*, 3845. (f) C. Ruiz-Pérez, J. Sanchiz, M. Hernández-Molina, F. Lloret, and M. Julve, *Inorg. Chim. Acta* **2000**, *298*, 245. (g) Y. Rodríguez-Martín, J. Sanchiz, C. Ruiz-Pérez, F. Lloret and M. Julve, *Inorg. Chim. Acta* **2001**, *326*, 20. (h) Y. Rodríguez-Martín, C. Ruiz-Pérez, J. Sanchiz, F. Lloret and M. Julve, *Inorg. Chim. Acta* **2001**, *318*, 159. (i) J. Sanchiz, Y. Rodríguez-Martín, C. Ruiz-Pérez, A. Mederos, F. Lloret and M. Julve, *New J. Chem.* **2002**, *26*, 1624. (j) Y. Rodríguez-Martín, M. Hernández-Molina, F. S. Delgado, J. Pasán, C. Ruiz-Pérez, J. Sanchiz, F. Lloret, and M. Julve, *CrystEngComm* **2002**, *4*, 440. (k) S. Sain, T. K. Maji, G. Mostafa, T. H. Lu and N. R. Chanduri, *New J. Chem.* **2003**, *27*, 185. (l) F. S. Delgado, J. Sanchiz, C. Ruiz-Pérez, F. Lloret and M. Julve, *Inorg. Chem.* **2003**, *42*, 5938.
- 9 (a) H. Oshio and U. Nagashima, *Inorg. Chem.* **1992**, *31*, 3295. (b) O. Castillo, A. Luque, F. Lloret and P. Román, *Inorg. Chim. Acta* **2001**, *324*, 141. (c) J. Luo, M. Hong, Y. Liang, R. Cao, *Acta Cryst., Sect. E*, **2001**, *57*, m361. (d) L. Cavalca, A. C. Villa, A. G. Manfredotti and A. A. G. Tomlinson, *Dalton Trans.*, **1972**, 391. (e) O. Castillo, A. Luque, M. Julve, F. Lloret and P. Román, *Inorg. Chim. Acta*, **2001**, *315*, 9. (f) O. Castillo, A. Luque, P. Román, F. Lloret and M. Julve, *Inorg. Chem.* **2001**, *40*, 5526. (g) J. Suárez-Varela, J. M. Domínguez-Vera, E. Colacio, J. C. Ávila-Rosón, M. A. Hidalgo and D. Martín-Ramos, *Dalton Trans.* **1995**, 2143.
- 10 O. Castillo, J. Alonso, U. García-Couceiro, A. Luque, and P. Román, *Inorg. Chem. Commun.* **2003**, *6*, 803.
- 11 L.-G. Zhu and S. Kitagawa, *Inorg. Chem. Commun.* **2003**, *6*, 1051.
- 12 (a) M. S. Haddad, D. N. Hendrickson, J. P. Cannady, R. S. Drago and D. S. Bieksza, *J. Am. Chem. Soc.* **1979**, *101*, 898. (b) M. Julve, M. Verdaguer, J. Faus, F. Tinti, J. Moratal, A. Monge and E. Gutiérrez-Puebla, *Inorg. Chem.* **1987**, *26*, 3520. (c) I. Castro, J. Sletten, M. L. Calatayud, M. Julve, J. Cano, F. Lloret and A. Caneschi, *Inorg. Chem.* **1995**, *34*, 4903.
- 13 W. E. Estes, D. P. Gavel, W. E. Hatfield and D. Hodgson, *Inorg. Chem.* **1978**, *17*, 1415.
- 14 J. Pasán, F. S. Delgado, Y. Rodríguez-Martín, M. Hernández-Molina, C. Ruiz-Pérez, J. Sanchiz, F. Lloret, and M. Julve, *Polyhedron*, **2003**, *22*, 2143.
- 15 O. Kahn, *Molecular Magnetism*, VCH, New York, **1993**.

## I.8. 2,2'-Bipyrimidine (14) and 1,10-Phenantroline (15) Copper(II)-Phenylmalonate complexes

### I.8.1. Introduction

The series which was started with the 2,4'-bipyridine ligand is extended now to the 2,2'-bipyrimidine and 1,10-phenantroline ligands. They are aromatic nitrogen heterocycles that in addition to their good coordinating ability (metal-ligand bonds), they can interact with the phenyl ring of the Phmal group (supramolecular interactions), making this system very appropriate to illustrate the effects of both types of interactions. Certainly, the carboxylate-bridged square grid of copper(II) ions of **2-12** cannot be formed due to the restrictions imposed by these N-donor coligands, but these complexes allow us to compare the coordination ability of the phenylmalonate respect to that of the malonate ligand.

### I.8.2. Synthesis

**{[Cu(2,2'-bpym)(Phmal)]<sub>n</sub>}** (**14**).  
2,2'-Bipyrimidine (1 mmol, 158 mg) was dissolved in 50/50 methanol/water (10 cm<sup>3</sup>) and then, an aqueous solution (15 cm<sup>3</sup>) of copper(II) phenylmalonate (1 mmol, 240 mg) was added under stirring. The solution was allowed to evaporate on a hood at room temperature. Prismatic greenish-blue single crystals were grown after a few days. Yield 60%. Analysis C<sub>17</sub>O<sub>4</sub>CuN<sub>4</sub>H<sub>12</sub>: found C 51.20, H 3.14, N 14.10; calcd. C 51.05, H 3.00, N 14.02%.

**{[Cu(phen)(Phmal)]<sub>n</sub>·3nH<sub>2</sub>O}** (**15**).

The complex **15** was synthesized by the same procedure of **14** but using 1,10-phenantroline (1 mmol, 180 mg) instead of 2,2'-bipyrimidine. Prismatic blue single crystals were grown after a few days. Yield 80%. Crystallographic data for compounds **14** and **15** are listed in

**Table I.21.** Crystallographic data for **14** and **15**

|                                                    | <b>14</b>                                                          | <b>15</b>                                                         |
|----------------------------------------------------|--------------------------------------------------------------------|-------------------------------------------------------------------|
| Formula                                            | C <sub>17</sub> H <sub>12</sub> O <sub>4</sub> N <sub>4</sub> Cu   | C <sub>21</sub> H <sub>20</sub> O <sub>7</sub> N <sub>2</sub> Cu  |
| FW                                                 | 399.85                                                             | 475.88                                                            |
| Crystal system                                     | Orthorhombic                                                       | Monoclinic                                                        |
| Space group                                        | <i>P cab</i>                                                       | <i>P 2<sub>1</sub>/n</i>                                          |
| <i>a</i> / Å                                       | 8.9331 (3)                                                         | 5.014 (3)                                                         |
| <i>b</i> / Å                                       | 11.7577(3)                                                         | 26.403 (3)                                                        |
| <i>c</i> / Å                                       | 29.8171 (4)                                                        | 14.685 (3)                                                        |
| <i>β</i> / °                                       | -                                                                  | 94.75                                                             |
| <i>V</i> / Å <sup>3</sup>                          | 3131.77 (14)                                                       | 1937.3 (12)                                                       |
| <i>Z</i>                                           | 8                                                                  | 4                                                                 |
| <i>μ</i> (Mo Kα) / cm <sup>-1</sup>                | 14.28                                                              | 11.76                                                             |
| <i>T</i> / K                                       | 293 (2)                                                            | 293 (2)                                                           |
| <i>ρ</i> <sub>calc</sub> / g cm <sup>-3</sup>      | 1.696                                                              | 1.611                                                             |
| <i>λ</i> / Å                                       | 0.71073                                                            | 0.71073                                                           |
| Index ranges                                       | -12 ≤ <i>h</i> ≤ 9,<br>-16 ≤ <i>k</i> ≤ 16,<br>-41 ≤ <i>l</i> ≤ 41 | -7 ≤ <i>h</i> ≤ 5,<br>-32 ≤ <i>k</i> ≤ 37,<br>-13 ≤ <i>l</i> ≤ 20 |
| Indep. reflect. ( <i>R</i> <sub>int</sub> )        | 4545 (0.132)                                                       | 5284 (0.051)                                                      |
| Obs. reflect. [ <i>I</i> > 2σ( <i>I</i> )]         | 2985                                                               | 2872                                                              |
| Parameters                                         | 283                                                                | 336                                                               |
| Goodness-of-fit                                    | 1.138                                                              | 1.012                                                             |
| <i>R</i> [ <i>I</i> > 2σ( <i>I</i> )]              | 0.0742                                                             | 0.0591                                                            |
| <i>R</i> <sub>w</sub> [ <i>I</i> > 2σ( <i>I</i> )] | 0.1462                                                             | 0.1098                                                            |
| <i>R</i> (all data)                                | 0.1217                                                             | 0.1376                                                            |
| <i>R</i> <sub>w</sub> (all data)                   | 0.1615                                                             | 0.1302                                                            |



Table I.21. Analysis  $C_{21}O_7CuN_2H_{20}$ : found C 52.79, H 4.32, N 5.80; calcd. C 52.99, H 4.21, N 5.89 %.

### I.8.3. Description of the Structures

The structure of  $\{[Cu(2,2'\text{-bpym})(Phmal)]\}_n$  (**14**) consists of chains of  $[Cu(2,2'\text{-bpym})(Phmal)]$  units that are linked through one phenylmalonate-carboxylate group exhibiting the *anti-syn* conformation (Figure I.45). These chains run parallel to the *a* axis and interact between them by means of  $\pi$ - $\pi$  and C-H $\cdots$  $\pi$  type interactions (Figure I.46). There are two hydrophobic cavities where 2,2'-bpym molecules and the phenyl rings from the Phmal groups are constrained. The 2,2'-bpym groups are involved in  $\pi$ - $\pi$  interactions with the shortest centroid-centroid contact being 3.798(6) Å and the shortest parallel displacement angle between pyrimidyl rings being 25.7°. These values are similar to the average ones observed in  $\pi$ - $\pi$  interactions with pyridine-like groups.<sup>1</sup> Weak C-H $\cdots$  $\pi$  interactions are also present between phenyl rings and 2,2'-bpym groups inside the chains and between phenyl groups of different chains, with the shortest H $\cdots$ centroid distance being 2.86(4) Å, and the C-H $\cdots$ centroid group almost collinear. The building units of the chain are rotated 90° through the normal axis of the planar 2,2'-bpym group in a twist fashion (i.e. odd units in the same position and even units rotated by 90°) (Fig. I.46).

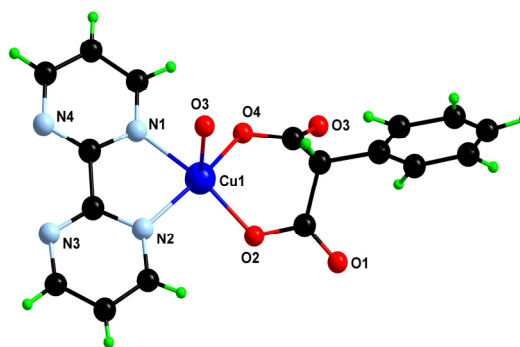
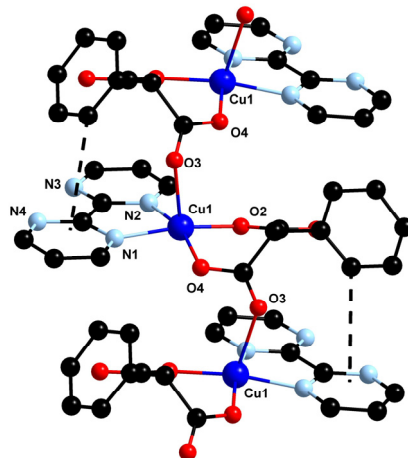


Fig. I.45. A view of a molecular fragment of **14** along with the numbering scheme.

Each copper(II) atom exhibits a slightly distorted square pyramidal surrounding, the  $\tau$  value being 0.08.<sup>2</sup> Two nitrogen atoms of the 2,2'-bpym ligand [N(1) and N(2)] and two carboxylate oxygen atoms from the Phmal ligand [O(2) and O(4)] build the basal plane, whereas the symmetry-related carboxylate oxygen atom [O(3a); (a) =  $-1/2 + x, 1/2 - y, z$ ] occupies the apical position. The equatorial bond lengths vary in the range 1.900(3)-2.003(3) Å and the apical bond distance is 2.262(3) Å (selected bond distances and angles are listed in Table I.22). The 2,2'-bpym ligand is quasi planar [the dihedral angle between



**Fig. I.46.** Fragment of the uniform chain of compound **14** showing the rotation of the units by 90° and the intrachain C–H⋯ $\pi$  interaction (dashed line).

the pyrimidyl rings being 3.5(1)°] and it acts as a bidentate ligand through two [N(1) and N(2)] of its four nitrogen atoms. This coordination mode was previously observed in several mono- and polynuclear 2,2'-bpy<sub>m</sub>-containing copper(II) complexes.<sup>3-5</sup> The outer N(3) and N(4) nitrogen atoms from the 2,2'-bpy<sub>m</sub>-ligand remain free, the N(3)⋯N(4) bite distance being somewhat greater [2.811(6) Å] than the N(1)⋯N(2) one [2.584(5) Å] due to the bidentate coordination of the 2,2'-bpy<sub>m</sub> to the copper atom. The inter-ring carbon-carbon bond length of 2,2'-bpy<sub>m</sub> in **14** [1.480(6) Å for C(13)–C(14)] is close to that found in the free ligand in the solid state [1.497(1) and 1.502(4) Å].<sup>6</sup> The Phmal adopts the boat conformation and the phenyl ring is placed perpendicular to the boat skeleton of the malonate in order to establish the weak intrachain C–H (phenyl)⋯ $\pi$  (pyrimidyl) interactions above mentioned. The shortest intrachain copper-copper separation in **14** is 4.6853(7) Å [Cu(1)⋯Cu(1c); (c) = 1/2 + x, 1/2 – y, z], a value which is much shorter than the shortest interchain metal-metal distance [7.3634(8) Å for Cu(1)⋯Cu(1d); (d) = –x, 1 – y, 1 – z].

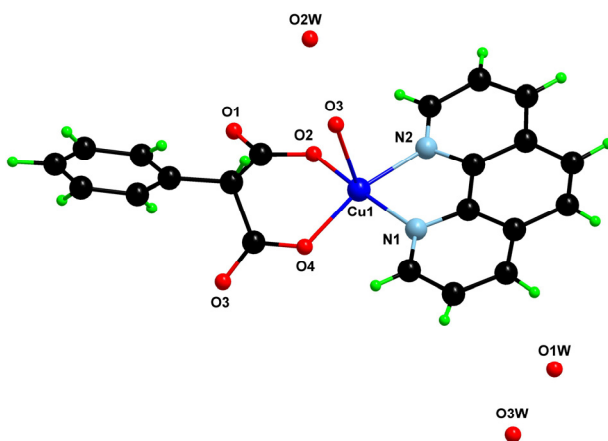
Finally, a comparison between the structure of **14** and that of the related mononuclear complex [Cu(2,2'-bpy<sub>m</sub>)(mal)(H<sub>2</sub>O)]·6H<sub>2</sub>O<sup>3</sup> shows once more the structural influence of the hydrophobic phenyl ring of the Phmal ligand. The complexation reaction between the preformed [Cu(2,2'-bpy<sub>m</sub>)]<sup>2+</sup> species and the dicarboxylate mal and Phmal ligands affords neutral hydrated mononuclear (mal) and anhydrous chain (Phmal, **14**) compounds. The structure of the former exhibits extensive hydrogen bonds involving coordinated and uncoordinated water molecules whereas carboxylate bridging and supramolecular C–H⋯ $\pi$  type interactions counterbalance the lack of hydrogen bonds in the latter one.

**Table I.22.** Selected bond lengths (Å) and bond angles (°) for compound **14** and **15**.<sup>a,b</sup>

| <b>14</b>       |            |                  |            |
|-----------------|------------|------------------|------------|
| Cu(1)–O(2)      | 1.922(3)   | O(2)–Cu(1)–O(3a) | 106.32(12) |
| Cu(1)–O(4)      | 1.900(3)   | O(4)–Cu(1)–N(1)  | 89.79(12)  |
| Cu(1)–N(1)      | 2.003(3)   | O(4)–Cu(1)–N(2)  | 162.02(14) |
| Cu(1)–N(2)      | 1.996(3)   | O(4)–Cu(1)–O(3a) | 100.05(12) |
| Cu(1)–O(3a)     | 2.262(3)   | N(1)–Cu(1)–N(2)  | 80.53(13)  |
| O(2)–Cu(1)–O(4) | 92.93(11)  | N(1)–Cu(1)–O(3a) | 85.78(12)  |
| O(2)–Cu(1)–N(1) | 166.90(14) | N(2)–Cu(1)–O(3a) | 94.33(12)  |
| O(2)–Cu(1)–N(2) | 93.31(13)  |                  |            |
| <b>15</b>       |            |                  |            |
| Cu(1)–O(2)      | 1.913(2)   | O(2)–Cu(1)–O(3b) | 92.74(10)  |
| Cu(1)–O(4)      | 1.934(2)   | O(4)–Cu(1)–N(1)  | 91.90(10)  |
| Cu(1)–N(1)      | 1.992(3)   | O(4)–Cu(1)–N(2)  | 162.66(10) |
| Cu(1)–N(2)      | 2.026(3)   | O(4)–Cu(1)–O(3b) | 101.46(9)  |
| Cu(1)–O(3b)     | 2.314(2)   | N(1)–Cu(1)–N(2)  | 81.86(11)  |
| O(2)–Cu(1)–O(4) | 92.80(9)   | N(1)–Cu(1)–O(3b) | 96.59(10)  |
| O(2)–Cu(1)–N(1) | 168.52(11) | N(2)–Cu(1)–O(3b) | 95.35(10)  |
| O(2)–Cu(1)–N(2) | 90.63(10)  |                  |            |

<sup>a</sup> Estimated standard deviations in the last significant digits are given in parentheses.  
<sup>b</sup> Symmetry code: (a)  $-1/2 + x, 1/2 - y, z$ ; (b)  $x + 1, y, z$ .

The structure of complex  $\{[\text{Cu}(\text{phen})(\text{Phmal})]\}_n \cdot 3n\text{H}_2\text{O}$  (**15**) consists of chains of  $[\text{Cu}(\text{phen})(\text{Phmal})]$  units linked through *anti-syn* carboxylate bridges and crystallization water molecules (Figure I.47). The chains run parallel to the *a* axis and they are linked by pairs along the  $[011]$  direction through hydrogen bonds involving the water molecules and non-coordinated carboxylate-oxygen atoms [the values of the  $\text{O}\cdots\text{O}$  distance ranging from 2.338(13) to 3.084(5) Å] (Figure I.48). Intrachain off-set  $\pi$ - $\pi$  interactions between phen ligands occur, the shortest centroid-centroid distance and parallel displacement angle being 3.907(4) Å and 28.6°, in agreement with previously reported values.<sup>1</sup>

**Fig. I.47.** A view of a fragment of the structure of **15** with the numbering scheme.

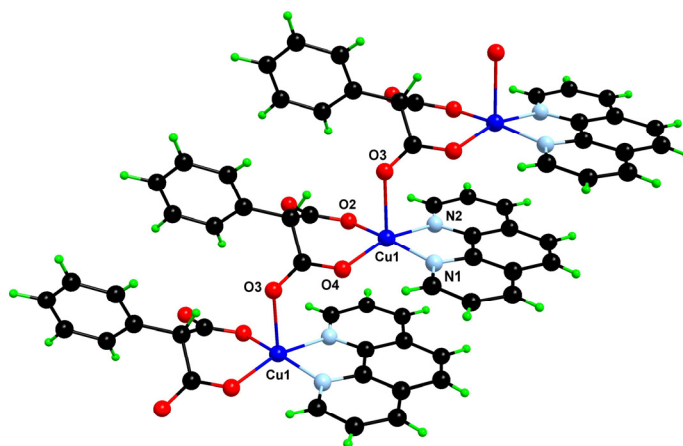


Fig. I.48. View of the uniform chain of compound **15** showing the phenylmalonate-carboxylate bridge in axial-equatorial *anti-syn* conformation.

Each copper(II) atom presents a slightly distorted square pyramidal environment with a  $\tau$  value of 0.10.<sup>2</sup> Two carboxylate oxygen atoms from the Phmal ligand, [O(2) and O(4)] and the two nitrogen atoms of phen [N(1) and N(2)] build the equatorial plane, whereas a symmetry-related carboxylate oxygen atom [O(3b); (b) =  $x + 1, y, z$ ] occupies the apical position. The equatorial bond lengths vary in the range 1.913(2)-2.026(3) Å and the apical bond amounts 2.314(3) Å (see Table I.22). The angle subtended by the planar bidentate phen ligand at the copper atom is 81.86(11)°. The bond lengths and angles of the phen ligand in **15** agree well with those reported for the free molecule.<sup>7</sup> The conformation and coordination mode of the Phmal in **15** are identical to those in **14**. However,  $\pi$ - $\pi$  stacking between phen ligands occurs in **15** instead of the C-H(phenyl)⋯ $\pi$ (N-heterocycle) type interaction which occurs in **14**. Moreover, the [Cu(phen)(Phmal)] units in **15** are not rotated by 90° in contrast to what it is observed in **14**, this modification of the crystal packing in **15** being most likely due to the crystallization water molecules which are present in the structure of this last compound. A comparison between the structure of **15** and that of the mononuclear [Cu(phen)(mal)(H<sub>2</sub>O)]·1.5H<sub>2</sub>O<sup>8</sup> complex reveals that weak  $\pi$ - $\pi$  stacking interactions between phen ligands are present in both compounds. However, the mononuclear units are grouped by pairs in the malonato-containing complex whereas a uniform chain is formed in **15**.

The shortest intrachain copper-copper separation is 5.014(3) Å [Cu(1)⋯Cu(1e); (e) =  $-1 + x, y, z$ ], a value which is much shorter than the shortest interchain metal-metal distance [7.5872(16) Å for Cu(1)–Cu(1f); (f) =  $-1/2 + x, 1/2 - y, -1/2 + z$ ].

### I.8.4. Magnetic Properties

The magnetic properties of compounds **14** and **15** under the form of  $\chi_M T$  vs.  $T$  plot [ $\chi_M$  being the molar susceptibility per copper(II) ion] are shown in Figure I.49.  $\chi_M T$  at room temperature is  $0.41 \text{ cm}^3 \text{ mol}^{-1} \text{ K}$  for both compounds, a value which is as expected for a magnetically isolated spin doublet. Upon cooling,  $\chi_M T$  remains almost constant for compound **14** up to 10 K and then, smoothly increases at lower temperatures to reach a value of  $0.44 \text{ cm}^3 \text{ mol}^{-1} \text{ K}$  at 1.9 K.  $\chi_M T$  remains constant upon cooling up to 25 K for compound **15** and then it increases at lower temperatures reaching a value of  $0.50 \text{ cm}^3 \text{ mol}^{-1} \text{ K}$  at 2.0 K. These features are indicative of an overall weak ferromagnetic coupling between the copper(II) ions in both compounds. Given that the structures of **14** and **15** consist of uniform chains where the copper(II) ions are bridged by the carboxylate-phenylmalonate group, we analyzed their magnetic properties through the numerical expression proposed by Baker and Rushbrooke<sup>9</sup> for a ferromagnetic uniform copper(II) chain:

$$\chi_M = (N\beta^2 g^2 / 4kT)(A/B)^{2/3}$$

$$A = 1.0 + 5.7979916 y + 16.902653 y^2 + 29.376885 y^3 + 29.832959 y^4 + 14.036918 y^5$$

$$B = 1.0 + 2.7979916 y + 7.0086780 y^2 + 8.6538644 y^3 + 4.5743114 y^4$$

where  $y = J/2kT$ , the spin Hamiltonian being defined as:

$$\hat{H} = -J \sum_i \hat{S}_i \cdot \hat{S}_{i+1}$$

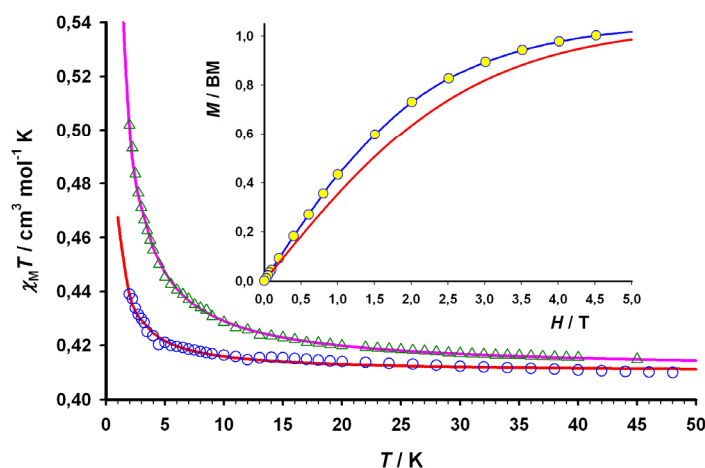


**Fig. I.49.** Experimental temperature dependence of the  $\chi_M T$  product of **14** (circles) and **15** (triangles) at  $T < 50$  K; (—) best fitting curves (see text). The inset shows the magnetization versus  $H$  plot for **15** at 2.0 K: (o) experimental data, (—) Brillouin function for a magnetically isolated spin doublet with  $g = 2.09$ .

$J$  is the intrachain magnetic coupling parameter and  $N$ ,  $g$ , and  $\beta$ , have their usual meanings. The best-fit obtained using a nonlinear regression analysis leads to  $J = +0.10(1) \text{ cm}^{-1}$ ,  $g = 2.091(1)$  and  $R = 2.6 \times 10^{-5}$  for **14** and  $J = +0.31(1) \text{ cm}^{-1}$ ,  $g = 2.092(1)$  and  $R = 2.1 \times 10^{-6}$  for **15**. The calculated curves match very well the experimental data in the whole temperature range, as seen in Figure I.49. The fact that the magnetization data of **15** at 2.0 K (see insert of Figure I.49) are clearly above the Brillouin function for a magnetically isolated spin doublet (this is also observed for the corresponding plot in **14**) confirms the ferromagnetic nature of the intrachain magnetic coupling.

The weak ferromagnetic interactions in **14** and **15** can be understood in a simple manner by analysing the exchange pathway which is involved and the relative arrangement of the magnetic orbitals. The unpaired electron of the copper(II) ion in **14** and **15** (square pyramidal environment) lies in the equatorial plane [N(1)N(2)O(2)O(4)] and it is defined by a  $d(x^2-y^2)$  type magnetic orbital [the  $x$  and  $y$  axes roughly correspond to the equatorial bonds at the copper environment]. The O(3)C(3)O(4) carboxylate bridge provides the intrachain exchange pathway in **14** and **15**: it links one equatorial position from Cu(1) [O(4)] with the axial one [O(3)] adopting the *anti-syn* bridging mode. This exchange pathway produces a very poor overlap between the magnetic orbitals due to the weak spin density in the apical site.<sup>10</sup> Thus, the antiferromagnetic contribution, which is proportional to the square of the overlap between the magnetic orbitals, is minimized and the resulting magnetic coupling is most likely ferromagnetic as observed.<sup>11</sup>

**Table I.23.** Selected magneto-structural data for some equatorial-apical carboxylate-bridged malonato- and phenylmalonato-containing copper(II) complexes

| Compound <sup>a</sup>                                                                         | $J^b / \text{cm}^{-1}$ | Ref. |
|-----------------------------------------------------------------------------------------------|------------------------|------|
| [Cu(H <sub>2</sub> O) <sub>4</sub> ][Cu(mal) <sub>2</sub> (H <sub>2</sub> O) <sub>2</sub> ]   | +1.8                   | 12   |
| {[Cu(H <sub>2</sub> O) <sub>4</sub> ] <sub>2</sub> [Cu(mal) <sub>2</sub> (H <sub>2</sub> O)]} | +1.2                   | 12   |
| {[Cu(H <sub>2</sub> O) <sub>3</sub> ][Cu(mal) <sub>2</sub> (H <sub>2</sub> O)] <sub>n</sub> } | +1.9                   | 12   |
| [Cu(Im) <sub>2</sub> (mal)] <sub>n</sub>                                                      | +1.6                   | 14   |
| [Cu(2-MeIm) <sub>2</sub> (mal)] <sub>n</sub>                                                  | +0.4                   | 14   |
| {(H <sub>2</sub> bpe)[Cu(mal) <sub>2</sub> ]} <sub>n</sub> ·4nH <sub>2</sub> O                | +0.049                 | 15   |
| [Cu <sub>4</sub> (mal) <sub>4</sub> (bpe) <sub>3</sub> ] <sub>n</sub> ·6nH <sub>2</sub> O     | +6.5                   | 15   |
| <b>6</b>                                                                                      | +0.091(2)              | -    |
| <b>7</b>                                                                                      | +0.097(2)              | -    |
| <b>14</b>                                                                                     | +0.10(1)               | -    |
| <b>15</b>                                                                                     | +0.31(1)               | -    |

<sup>a</sup> Abbreviations used: Im = Imidazole, 2-MeIm = 2-Methylimidazole and bpe = 1,2-bis(4-pyridyl)ethylene.

<sup>b</sup> Values of the magnetic coupling.

Previous examples of carboxylate (*anti-syn*)-bridged copper(II) complexes with the axial-equatorial exchange-pathway exhibit ferromagnetic couplings with values of  $J$  ranging from +0.05 to +1.9  $\text{cm}^{-1}$  (see Table I.23).<sup>12-17</sup> The intensity of the magnetic coupling is influenced by the Cu–O(axial) distance and the distortion of the metal environment; the longer the distance and the greater the distortion, the weaker the coupling is. The values of  $J$  for **14** and **15** fall in this range, but they are smaller than those with similar structural parameters [distortion and Cu–O(axial) distance]. The low value observed for the coupling constant  $J = 0.10(1) \text{ cm}^{-1}$  for **14**, could be due to the greater value of the angle between the apical oxygen to copper vector and the normal to the equatorial mean plane of the copper atom [ $7^\circ$  in **14** and only  $3.6^\circ$  in **15**]. In general, this shift influences the effectiveness of the bridge in the transmission of the magnetic coupling, because it modifies the overlap between the magnetic orbitals.

Another interesting point looking at the results listed in Table I.23 concerns compound **15** and  $\{[\text{Cu}(\text{mal})(\text{Im})]\}_n$ . Although the structural parameters of **15** are similar to those of  $\{[\text{Cu}(\text{mal})(\text{Im})]\}_n$ , the value of the ferromagnetic coupling for **15** is somewhat weaker. Most likely, the carboxylate group of the phenylmalonate is less effective in the transmission of the magnetic coupling than the carboxylate group of the malonate ligand. The magnetic coupling is essentially an electronic effect and the phenylene ring of the phenylmalonate exerts an electron-withdrawing effect that delocalizes some electron density of the copper(II) towards the aromatic ring, decreasing the electronic delocalization towards the carboxylate bridge. The decrease of the electron delocalization towards the bridge would decrease the magnitude of the magnetic coupling. This could be one of the factors that account for the weaker magnetic interaction between the copper(II) ions in **15** (and also in **14**) through the carboxylate-phenylmalonate bridge respect to the carboxylate-malonate one.

### I.8.5. Conclusion

The two complexes **14** and **15** exhibit a chain structure formed by linking  $[\text{Cu}(\text{L})\text{Phmal}]$  units through equatorial-apical *anti-syn* carboxylate bridges. The comparison with the related malonato-containing complexes reveals the strong structural role of the phenyl group in the Phmal compounds, since the malonato-containing copper(II) complexes of 2,2'-bpym and phen are mononuclear compounds. The nature of the magnetic coupling (ferromagnetic) between copper(II) ions through the phenylmalonate-carboxylate bridge is the same to that through the malonate-carboxylate, but its magnitude is somewhat weaker probably due to the electron-withdrawing effect which is exerted by the phenyl ring.

## I.8.6. References

- 1 C. Janiak, *Dalton Trans.* **2000**, 3885.
- 2 A. W. Addison, T. N. Rao, J. Reedijk, J. van Rijn and G. C. Verschoor, *Dalton Trans.* **1984**, 1349.
- 3 Y. Rodríguez-Martín, J. Sanchiz, C. Ruiz-Pérez, F. Lloret and M. Julve, *Inorg. Chim. Acta* **2001**, 326, 20.
- 4 (a) G. de Munno, G. Bruno, M. Julve and M. Romeo, *Acta Crystallogr.* **1990**, C46, 1828. (b) L. W. Morgan, W. T. Pennington, J. D. Petersen, R. R. Ruminski, D. W. Bennet and J. S. Rommel, *Acta Crystallogr.* **1992**, C48, 163. (c) G. De Munno, M. Julve, M. Verdaguer and G. Bruno, *Inorg. Chem.* **1993**, 32, 561. (d) G. De Munno, M. Julve, F. Nicolò, F. Lloret, J. Faus, R. Ruiz and E. Sinn, *Angew. Chem., Int. Ed. Engl.* **1993**, 32, 613. (e) I. Castro, J. Sletten, L. K. Glaerum, F. Lloret, J. Faus and M. Julve, *Dalton Trans.* **1994**, 2777. (f) I. Castro, J. Sletten, L. K. Glaerum, J. Cano, F. Lloret, J. Faus and M. Julve, *Dalton Trans.* **1995**, 3207. (g) S. Decurtins, H. W. Schmalle, P. Schneuwly and L. M. Zheng, *Acta Crystallogr.* **1996**, C52, 561.
- 5 (a) I. Castro, M. Julve, G. De Munno, G. Bruno, J. A. Real, F. Lloret and J. Faus, *Dalton Trans.* **1992**, 1739. (b) M. Julve, M. Verdaguer, G. De Munno, J. A. Real, G. Bruno *Inorg. Chem.* **1993**, 32, 795. (c) J. A. Real, G. De Munno, R. Chiappetta, M. Julve, F. Lloret, Y. Journaux, J. C. Colin and G. Blondin, *Angew. Chem. Int. Ed. Engl.* **1994**, 33, 1184. (d) G. De Munno, M. Julve, F. Lloret, J. Faus, . Verdaguer and A. Caneschi, *Inorg. Chem.* **1995**, 34, 157. (e) G. De Munno, M. Julve, F. Lloret, J. Cano and A. Caneschi, *Inorg. Chem.* **1995**, 34, 2048. (f) G. De Munno, M. G. Lombardi, P. Paoli, F. Lloret, M. Julve, *Inorg. Chim. Acta* **1998**, 282, 252.
- 6 L. Fernholt, C. Rømming and S. Samdal, *Acta Chem. Scand.* **1981**, A35, 707.
- 7 S. Nishigaki, H. Yoshioka and K. Nakatsu, *Acta Crystallogr., Sect. B* **1978**, 34, 875.
- 8 (a) W-L. Kwik, K-P. Ang, H. S-O. Chan, V. Chebolu and S. A. Koch, *Dalton Trans.* **1986**, 2519. (b) E. Borghi, *Gazz. Chim. It.* **1987**, 117, 557.
- 9 G. A. Baker, G. S. Rushbrooke and H. E. Gilbert, *Physical Reviews* **1964**, 135, A1272.
- 10 A. Rodríguez-Forteza, P. Alemany, S. Álvarez and E. Ruiz, *Chem. Eur. J.* **2001**, 7, 627.
- 11 O. Kahn, *Molecular Magnetism*; VCH: New York, **1993**.
- 12 C. Ruiz-Perez, J. Sanchiz, M. H. Molina, F. Lloret and M. Julve, *Inorg. Chem.* **2000**, 39, 1363.
- 13 J. Pasán, F. S. Delgado, Y. Rodríguez-Martín, M. Hernández-Molina, C. Ruiz-Pérez, J. Sanchiz, F. Lloret and M. Julve, *Polyhedron*, **2003**, 22, 2143.
- 14 J. Sanchiz, Y. Rodríguez-Martín, C. Ruiz-Pérez, A. Mederos, F. Lloret and M. Julve, *New J. Chem.* **2002**, 26, 1624-1628.
- 15 F. S. Delgado, J. Sanchiz, C. Ruiz-Pérez, F. Lloret and M. Julve, *Inorg. Chem.* **2003**, 42, 5938-5948.
- 16 Y. Rodríguez-Martín, C. Ruiz-Pérez, J. Sanchiz, F. Lloret and M. Julve, *Inorg. Chim. Acta* **2001**, 318, 159-165.
- 17 E. Colacio, J. M. Domínguez-Vera, M. Ghazi, R. Krekäs, M. Klinga and J. M. Moreno, *Eur. J. Inorg. Chem.* **1999**, 441.



## I.9. 2,2'-Bipyridine (16) Copper(II)-Phenylmalonate complex

### I.9.1. Introduction

The introduction of the 2,2'-bipyridine coligand in the phenylmalonate-containing copper(II) series allow us to compare its structure with those of the previously reported malonate complexes and to observe the changes induced by the presence of the phenyl ring in the Phmal ligand. This complex is the last example included in this chapter which was devoted to the phenylmalonate-containing complexes.

### I.9.2. Synthesis

**[Cu(2,2'-bpy)(Phmal)(H<sub>2</sub>O)]·2H<sub>2</sub>O (16).** 2,2'-Bipyridine (1 mmol, 156 mg) was dissolved in 50/50 methanol/water (10 cm<sup>3</sup>) and then, an aqueous solution (15 cm<sup>3</sup>) of copper(II) phenylmalonate (1 mmol, 240 mg) was added under stirring. The solution was allowed to evaporate on a hood at room temperature. Prismatic blue single crystals of **16** were grown after a few days. Yield *ca* 75%. Crystallographic data are listed in Table I.24. Analysis C<sub>19</sub>O<sub>7</sub>CuN<sub>2</sub>H<sub>20</sub>: found C 50.41, H 4.40, N 6.05; calcd. C 50.49, H 4.43, N 6.20%.

### I.9.3. Description of the Structures

The structure of [Cu(2,2'-bpy)(Phmal)(H<sub>2</sub>O)]·2H<sub>2</sub>O (**16**) consists of neutral [Cu(Phmal)(2,2'-bpy)(H<sub>2</sub>O)] mononuclear entities (Figure I.50) and crystallization water molecules. The molecular units are linked by hydrogen bonding involving the uncoordinated phenylmalonate oxygen atoms and the crystallization water molecules, the values of the O...O distance ranging from 2.667(3) to 2.972(4) Å (see Table I.25). A surprising two-dimensional (6,3) net results (Figure I.51) which contributes to the stabilization of the whole structure. Adjacent layers are linked by weak off-set  $\pi$ - $\pi$ -stacking interactions between pyridyl rings. The shortest off-set angle between pyridyl rings is 28.5° while the shortest

**Table I.24.** Crystallographic data for **16**

| <b>16</b>                                                   |                                                                     |
|-------------------------------------------------------------|---------------------------------------------------------------------|
| Formula                                                     | C <sub>19</sub> H <sub>20</sub> O <sub>7</sub> N <sub>2</sub> Cu    |
| FW                                                          | 451.91                                                              |
| Crystal system                                              | Orthorhombic                                                        |
| Space group                                                 | <i>P cab</i>                                                        |
| <i>a</i> /Å                                                 | 14.6113 (5)                                                         |
| <i>b</i> /Å                                                 | 16.1928 (4)                                                         |
| <i>c</i> /Å                                                 | 16.5067 (5)                                                         |
| <i>V</i> /Å <sup>3</sup>                                    | 3905.5 (2)                                                          |
| <i>Z</i>                                                    | 8                                                                   |
| $\mu$ (Mo K $\alpha$ ) /cm <sup>-1</sup>                    | 11.63                                                               |
| <i>T</i> /K                                                 | 293 (2)                                                             |
| $\rho_{\text{calc}}$ /g cm <sup>-3</sup>                    | 1.537                                                               |
| $\lambda$ /Å                                                | 0.71073                                                             |
| Index ranges                                                | -18 ≤ <i>h</i> ≤ 20,<br>-22 ≤ <i>k</i> ≤ 22,<br>-23 ≤ <i>l</i> ≤ 13 |
| Indep. reflect. ( <i>R</i> <sub>int</sub> )                 | 5537 (0.060)                                                        |
| Obs. reflect. [ <i>I</i> > 2 $\sigma$ ( <i>I</i> )]         | 3552                                                                |
| Parameters                                                  | 343                                                                 |
| Goodness-of-fit                                             | 1.043                                                               |
| <i>R</i> [ <i>I</i> > 2 $\sigma$ ( <i>I</i> )]              | 0.0429                                                              |
| <i>R</i> <sub>w</sub> [ <i>I</i> > 2 $\sigma$ ( <i>I</i> )] | 0.0837                                                              |
| <i>R</i> (all data)                                         | 0.0866                                                              |
| <i>R</i> <sub>w</sub> (all data)                            | 0.1004                                                              |

centroid-centroid contact is 3.966(4) Å, values which are slightly longer than the average values for  $\pi$ - $\pi$  interactions with pyridine-like groups previously reported.<sup>1</sup>

**Table I.25.** Hydrogen bonds in complex **16**.

| D-H...A         | D...A      | $\angle$ D-H...A | Symmetry operator <sup>a</sup> |
|-----------------|------------|------------------|--------------------------------|
| O(1w)-H...O(2w) | 2.667(3) Å | 170(4)°          | $x, y - 1, z + 1$              |
| O(1w)-H...O(3)  | 2.735(3) Å | 172(4)°          | $x + 1/2, -y, -z + 5/2$        |
| O(2w)-H...O(1)  | 2.881(4) Å | 172(6)°          | $x, y + 1/2, -z + 3/2$         |
| O(2w)-H...O(3w) | 2.763(4) Å | 171(4)°          | $x + 1, y, z$                  |
| O(3w)-H...O(3)  | 2.972(4) Å | 167(5)°          | $x - 1/2, -y + 1/2, z - 1$     |
| O(3w)-H...O(1)  | 2.815(3) Å | 158(5)°          | $x - 1/2, -y + 1, -z + 3/2$    |

<sup>a</sup> Symmetry operation concerning the acceptor atom.

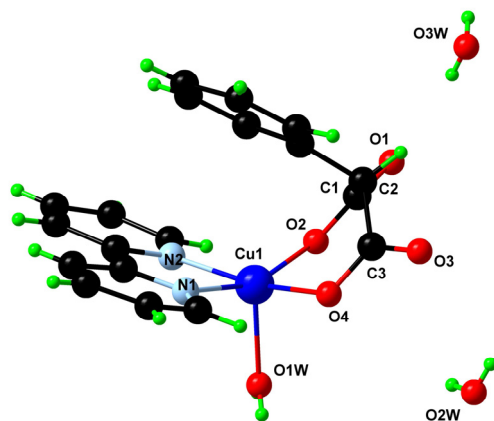


**Fig. I.50.** A view of the asymmetric unit of complex **16** along with the numbering scheme.

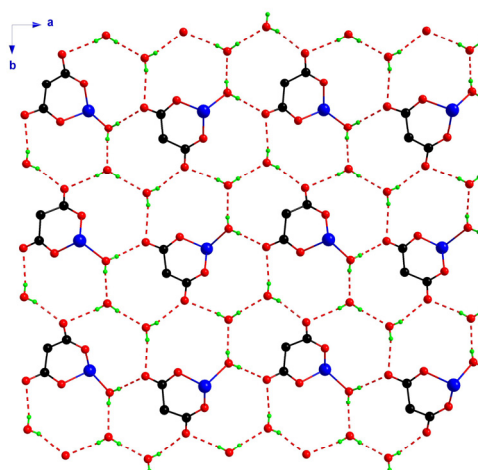


**Fig. I.51.** (6,3) pattern formed by hydrogen bonding involving the coordinated and crystallization water molecules and the malonate oxygen atoms; such a regular net contributes to the stabilization of the structure; the 2,2'-bpy ligands have been omitted for clarity.

The molecular structure of **16** is remarkably similar to that of the recently reported<sup>2,3</sup> [Cu(Bzmal)(phen)(H<sub>2</sub>O)]·3H<sub>2</sub>O and [Cu(Bzmal)(2,2'-bpy)(H<sub>2</sub>O)]·2H<sub>2</sub>O compounds (Bzmal = 2-benzylmalonate). The phenyl ring of Bzmal and Phmal is located over the N–C–C–N–Cu chelate ring in the three complexes and metalloaromaticity was pointed out to be the responsible factor for this structural feature.<sup>2</sup> A search in the Cambridge Structural Database has shown the existence of several compounds which present the same conformation (they are listed on Table I.26). The value of the dihedral angle between mean planes in complex **16** is greater ( $\alpha = 25.5^\circ$ ) than in the other compounds ( $\alpha$  ranging from  $1.2^\circ$  to  $14.5^\circ$ ) due to geometrical constraints that preclude the parallel arrangement of the phenyl group above the chelate ring. All the structures found in the CSD search have a ligand with the nitrogen atoms inside the aromatic rings (i.e. always 2,2'-bpy or phen but never N,N'-ethylenediamine). According to Janiak,<sup>1</sup> the phenyl rings do not like to stack each other but to adopt an off-set way (parallel displaced), leading thus to C–H··· $\pi$  type interactions. Therefore, we point out to this assessment as the responsible for the situation of the phenyl group above the chelate ring (i.e. displaced from the stacked position over the pyridyl groups).

**Table I.26.** Stacking parameters of some compounds found in the Cambridge Structural Database with the same conformation that complex **16**.

| Compound                                                                   | Stacking parameters <sup>a</sup>                       |                                                     |                                                      | Ref. |
|----------------------------------------------------------------------------|--------------------------------------------------------|-----------------------------------------------------|------------------------------------------------------|------|
|                                                                            | d(c <sub>1</sub> -c <sub>2</sub> ) Å /<br>$\alpha$ deg | d( $\perp$ c <sub>1</sub> -P(2))<br>Å / $\beta$ deg | d( $\perp$ c <sub>2</sub> -P(1))<br>Å / $\gamma$ deg |      |
| [Cu(L1)(L2)]SbF <sub>6</sub> ·CH <sub>2</sub> Cl <sub>2</sub> <sup>b</sup> | 3.58 / 1.2                                             | 3.49 / 13.1                                         | 3.49 / 13.2                                          | 4    |
| [Cu(L3)(L4)(L5)]                                                           | 3.49 / 7.2                                             | 3.45 / 14.3                                         | 3.38 / 8.2                                           | 5    |
| [Cu(L3)(L4)](NO <sub>3</sub> ) <sub>2</sub> ·3H <sub>2</sub> O             | 3.50 / 10.2                                            | 3.43 / 18.5                                         | 3.32 / 11.4                                          | 6    |
| catena[Cu(L4)(L6)]ClO <sub>4</sub> ·H <sub>2</sub> O                       | 3.44 / 6.46                                            | 3.37 / 8.0                                          | 3.41 / 12.1                                          | 7    |
| [Cu(L7)(L8)H <sub>2</sub> O]BF <sub>4</sub> ·3H <sub>2</sub> O             | 3.39 / 10.1                                            | 3.38 / 14.2                                         | 3.29 / 4.3                                           | 8    |
| [Cu(L9)(L8)H <sub>2</sub> O]Cl·H <sub>2</sub> O                            | 3.53 / 14.5                                            | 3.32 / 15.8                                         | 3.39 / 19.7                                          | 9    |
| [Cu(L10)(L4)H <sub>2</sub> O]·3H <sub>2</sub> O                            | 3.49 / 2.1                                             | 3.39 / 15.5                                         | 3.36 / 13.9                                          | 2    |
| [Cu(L10)(L8)H <sub>2</sub> O]·2H <sub>2</sub> O                            | 3.51 / 8.2                                             | 3.37 / 10.7                                         | 3.45 / 16.4                                          | 3    |
| [Cu(L11)(L8)H <sub>2</sub> O]NO <sub>3</sub> ·MeOH·H <sub>2</sub> O        | 3.48 / 5.2                                             | 3.41 / 15.7                                         | 3.35 / 11.3                                          | 10   |
| [Cu(L9)(L4)H <sub>2</sub> O]ClO <sub>4</sub> ·1.5H <sub>2</sub> O          | 3.38 / 8.8                                             | 3.31 / 16.6                                         | 3.24 / 11.8                                          | 11   |
| [Cu(L12)(L4)Cl]·3H <sub>2</sub> O                                          | 3.38 / 5.4                                             | 3.32 / 12.0                                         | 3.30 / 10.3                                          | 12   |
| [Cu(L12)(L8)Cl]·3H <sub>2</sub> O                                          | 3.45 / 6.7                                             | 3.41 / 5.6                                          | 3.44 / 9.2                                           | 13   |
| [Cu(L12)(L8)H <sub>2</sub> O]ClO <sub>4</sub>                              | 3.37 / 7.4                                             | 3.35 / 13.2                                         | 3.28 / 5.8                                           | 14   |
| [Cu(L9)(L13)H <sub>2</sub> O]ClO <sub>4</sub> ·H <sub>2</sub> O            | 3.42 / 3.7                                             | 3.29 / 17.1                                         | 3.27 / 16.1                                          | 15   |
| <b>16</b>                                                                  | 3.683 /<br>25.5                                        | 3.152 / 31.5                                        | 3.562 / 14.7                                         | -    |

<sup>a</sup> P(1) = Plane 1; P(2) = Plane 2; c<sub>1</sub> = Centroid of P(1); c<sub>2</sub> = Centroid of P(2);  $\alpha$  = Mean planes angle;  $\beta$  = Angle between the normal of P(1) and P(2);  $\gamma$  = Angle between the normal of P(2) and P(1).

<sup>b</sup> L1 = (S,S)-2,6-bis(4-phenyl-2-oxazolin-2-yl)pyridine; L2 = benzyloxyacetaldehyde; L3 = L-4,5-dihydroxyphenylalanine; L4 = 1,10-phenanthroline; L5 = n-propanol; L6 = L-tryptophanato; L7 = DL-2,5-dihydroxytyrosine; L8 = 2,2'-bipyridine; L9 = L-tyrosinate; L10 = 2-benzylmalonate; L11 = 3-iodo-L-tyrosinate; L12 = L-phenylalanine; L13 = 1,4,8,9-tetra-azatriphenylene.

**Table I.27.** Selected bond lengths (Å) and bond angles (°) for compound **16**<sup>a</sup>

| <b>16</b>       |           |                  |           |
|-----------------|-----------|------------------|-----------|
| Cu(1)–O(2)      | 1.954(2)  | O(2)–Cu(1)–O(1w) | 96.85(9)  |
| Cu(1)–O(4)      | 1.933(2)  | O(4)–Cu(1)–N(1)  | 91.89(8)  |
| Cu(1)–N(1)      | 2.001(2)  | O(4)–Cu(1)–N(2)  | 166.47(8) |
| Cu(1)–N(2)      | 1.998(2)  | O(4)–Cu(1)–O(1w) | 97.46(9)  |
| Cu(1)–O(1w)     | 2.143(2)  | N(1)–Cu(1)–N(2)  | 80.53(8)  |
| O(2)–Cu(1)–O(4) | 90.09(7)  | N(1)–Cu(1)–O(1w) | 104.38(9) |
| O(2)–Cu(1)–N(1) | 158.23(8) | N(2)–Cu(1)–O(1w) | 95.29(9)  |
| O(2)–Cu(1)–N(2) | 92.89(8)  |                  |           |

<sup>a</sup> Estimated standard deviations in the last significant digits are given in parentheses.

Let us finally compare this structure with that of the reported mononuclear complex  $[\text{Cu}(2,2'\text{-bpy})(\text{mal})(\text{H}_2\text{O})]\cdot\text{H}_2\text{O}$ ,<sup>13</sup> where the monomeric units are distributed in bilayers in the *bc* plane through hydrogen bonds involving the carboxylate-malonate groups and the coordinated and uncoordinated water molecules. However, the hydrophobic interactions in **16** form layers of different hydrophilic character with the aromatic rings in one and the phenylmalonate-oxygen atoms and water molecules in the other one. A remarkable difference between both compounds is the position of the methylene group: it is directed toward the coordinated water molecule in the malonate compound whereas the metalloaromaticity in the case of **16** causes the methylene C–H bond to point towards the opposite side of the coordinated water molecule.

Each copper atom in **16** exhibits a somewhat distorted square pyramidal environment with a  $\tau$  value of 0.14.<sup>14</sup> Two 2,2'-bpy nitrogen atoms [2.001(2) and 1.998(2) Å for Cu(1)–N(1) and Cu(1)–N(2), respectively] and two carboxylate-oxygen atoms from the Phmal ligand [1.954(2) and 1.933(2) Å for Cu(1)–O(2) and Cu(1)–O(4)] define its basal plane, and a water molecule fills the apical position [2.143(2) Å for Cu(1)–O(1w)] (see Table I.27). The 2,2'-bpy and Phmal groups in **16** adopt the bidentate coordination mode, the values of the angles subtended at the copper atom by them being 80.53(8) and 90.09(7)°, respectively. The 2,2'-bpy ligand is practically planar [the value of the dihedral angle between the mean pyridyl planes is 1.1(1)°] and its bond distances and angles are in agreement with those reported for the free 2,2'-bpy.<sup>15</sup> The Phmal group exhibits the boat conformation as in **1**. However, the Phmal group in this last compound exhibits simultaneously the bidentate (through two oxygen atoms of the two carboxylate groups) and bis-monodentate (through two *trans* carboxylate oxygen atoms from two Phmal ligands) coordination modes leading to a layered structure. The  $[\text{Cu}(\text{Phmal})_2]^{2-}$  units in this compound tend also to align their aromatic rings in the same direction, preventing the occupation of one of the axial positions of the copper(II) coordination sphere, while the

other apical site is filled by another  $[\text{Cu}(\text{Phmal})_2]^{2-}$  unit. This also occurs in **16** where the aromatic ring practically fills one of the axial positions of the copper coordination sphere and the other one is occupied by a water molecule. The shortest intermolecular copper-copper separation in **16** is 7.6494(5) Å  $[\text{Cu}(1)\cdots\text{Cu}(1a)$ ; (a) = -x + 2, -y, -z + 2].

#### I.9.4. Magnetic Properties

The  $\chi_{\text{M}}T$  product of compound **16** follows the Curie law in the 5-300 K temperature range. Its value is 0.365 cm<sup>3</sup> mol<sup>-1</sup> K, as expected for a magnetically isolated spin doublet of a copper(II) ion. This is in agreement with its mononuclear nature.

#### I.9.5. Conclusion

The complex **16** is mononuclear with two remarkably structural features: (i) the phenyl ring of the Phmal ligand is bent in order to be located above the chelate ring of the copper atom, feature which was unprecedented in phenylmalonate-containing complexes; (ii) the occurrence of (6,3) pattern formed through hydrogen bonds involving the malonate oxygen atoms and coordinated and uncoordinated water molecules.

#### I.9.6. References

- 1 C. Janiak, *Dalton Trans.* **2000**, 3885.
- 2 A. Castiñeiras, A. G. Sicilia-Zafra, J. M. González-Pérez, D. Choquecillo-Lazarte and J. Niclós-Gutiérrez, *Inorg. Chem.* **2003**, *41*, 6956.
- 3 W. Guan, J. Y. Sun, X. D. Zhang and Q. T. Liu, *Chem. Res. Chin. Univ.* **1998**, *19*, 5.
- 4 D. A. Evans, M. C. Kozłowski, J. A. Murry, C. S. Burgey, K. R. Campos, B. T. Connell and R. T. Staples, *J. Am. Chem. Soc.* **1999**, *121*, 669.
- 5 S. Suzuki, K. Yamaguchi, N. Nakamura, Y. Tagawa, H. Kuma and T. Kawamoto, *Inorg. Chim. Acta* **1998**, *283*, 260.
- 6 H. Masuda, O. Matsumoto, A. Odani and O. Yamauchi, *J. Chem. Soc. Jpn.* **1998**, 783.
- 7 N. Nakamura, T. Kohzuma, H. Kuma and S. Suzuki, *J. Am. Chem. Soc.* **1992**, *114*, 6550.
- 8 X. Solans, L. Ruiz-Ramírez, A. Martínez, L. Gasque and R. Moreno-Esparza, *Acta Crystallogr., Sect. C* **1992**, *48*, 1785.
- 9 F. Zhang, T. Yajima, H. Masuda, A. Odani and O. Yamauchi, *Inorg. Chem.* **1997**, *36*, 5777.
- 10 T. Sugimori, H. Masuda, N. Ohata, K. Koiwai, A. Odani and O. Yamauchi, *Inorg. Chem.* **1997**, *36*, 576.
- 11 P. S. Subramanian, E. Suresh, P. Dastidar, S. Waghmode and D. Srinivas, *Inorg. Chem.* **2001**, *40*, 4291.
- 12 X.-Y. Le, M.-L. Tong, Y.-L. Fu and L.-N. Ji, *Acta Chim. Sinica* **2002**, *60*, 367.
- 13 E. Suresh and M. M. Bhadbhade, *Acta Crystallogr., Sect. C* **1997**, *53*, 193.
- 14 A. W. Addison, T. N. Rao, J. Reedijk, J. van Rijn and G. C. Verschoor, *Dalton Trans.* **1984**, 1349.
- 15 L. L. Merrit and E. D. Schroeder, *Acta Crystallogr.* **1956**, *9*, 801.

---

---

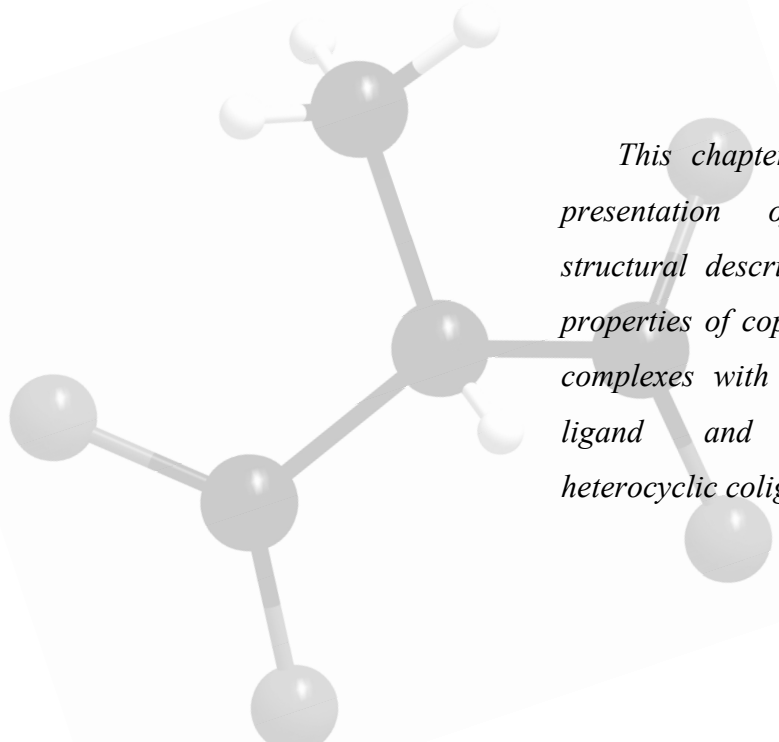
## Chapter II.

# Methylmalonate

## Complexes

---

---



*This chapter is devoted to the presentation of the synthesis, structural description and magnetic properties of copper(II) coordination complexes with the methylmalonate ligand and other N-donor heterocyclic coligands.*

## II.1. Copper(II)-Methylmalonate (17)

### II.1.1. Introduction

The first copper(II)-methylmalonate complex having water molecules as unique coligands is synthesized and magneto-structurally characterized in order to be compared with complex **1** and the copper(II)-malonate family. Compound **17** also serves as a trial to evaluate the coordination ability of the methylmalonate ligand and hence, to design the strategy for the preparation of other compounds.

### II.1.2. Synthesis

**[Cu(Memal)(H<sub>2</sub>O)]<sub>n</sub> (17).** Copper(II) nitrate (1 mmol, 230 mg) was added to an aqueous solution (10 cm<sup>3</sup>) of methylmalonic acid (1 mmol, 68 mg) and sodium carbonate (1 mmol, 106 mg) under stirring. The resulting pale blue solution was allowed to evaporate at room temperature. Prismatic blue single crystals of **17** were grown after a few days. Crystallographic data for complex **17** are listed in Table II.1. Yield *ca.* 75%. Anal. calc. for C<sub>4</sub>H<sub>6</sub>CuO<sub>5</sub> (**17**): C, 24.31; H, 3.06; Found: C, 24.13; H, 3.11 %.

**Table II.1.** Crystallographic data for complex **17**

| <b>17</b>                                                   |                                                               |
|-------------------------------------------------------------|---------------------------------------------------------------|
| Formula                                                     | C <sub>4</sub> H <sub>6</sub> O <sub>5</sub> Cu               |
| FW                                                          | 197.61                                                        |
| Crystal system                                              | Orthorhombic                                                  |
| Space group                                                 | <i>P n</i> 2 <sub>1</sub> <i>m</i>                            |
| <i>a</i> /Å                                                 | 6.203(3)                                                      |
| <i>b</i> /Å                                                 | 6.7961(12)                                                    |
| <i>c</i> /Å                                                 | 6.998(2)                                                      |
| <i>V</i> /Å <sup>3</sup>                                    | 295.01(17)                                                    |
| <i>Z</i>                                                    | 2                                                             |
| $\mu$ (Mo K $\alpha$ ) /cm <sup>-1</sup>                    | 36.33                                                         |
| <i>T</i> /K                                                 | 293(2)                                                        |
| $\rho_{\text{calc}}$ /g cm <sup>-3</sup>                    | 2.022                                                         |
| $\lambda$ /Å                                                | 0.71073                                                       |
| Index ranges                                                | -8 ≤ <i>h</i> ≤ 7,<br>-8 ≤ <i>k</i> ≤ 8,<br>-6 ≤ <i>l</i> ≤ 9 |
| Indep. reflect. ( <i>R</i> <sub>int</sub> )                 | 687 (0.0456)                                                  |
| Flack parameter                                             | 0.51(4)                                                       |
| Obs. reflect. [ <i>I</i> > 2 $\sigma$ ( <i>I</i> )]         | 638                                                           |
| Parameters                                                  | 66                                                            |
| Goodness-of-fit                                             | 1.089                                                         |
| <i>R</i> [ <i>I</i> > 2 $\sigma$ ( <i>I</i> )]              | 0.0352                                                        |
| <i>R</i> <sub>w</sub> [ <i>I</i> > 2 $\sigma$ ( <i>I</i> )] | 0.0862                                                        |
| <i>R</i> (all data)                                         | 0.0385                                                        |
| <i>R</i> <sub>w</sub> (all data)                            | 0.0872                                                        |

### II.1.3. Description of the Structure

The structure of [Cu(Memal)(H<sub>2</sub>O)]<sub>n</sub> (**17**) consists of a square grid of aquacopper(II) ions linked through methylmalonate carboxylate bridges running parallel to the *bc* plane, very similar to that observed in complexes **2-12** of Chapter I (Figure II.1 and II.2). These corrugated layers are stacked along the *a* direction with the methyl group of the methylmalonate ligand alternatively located above and below the layer (Figure II.2). Intralayer hydrogen bonds involving the coordinated water molecule and oxygen atoms from the methylmalonate ligand contribute to the stabilization of the structure [mean O–H···O distances and angles being 2.748(5) Å and 137.8(6)°, respectively]. The layers are

separated by the methyl groups of the Memal ligand, the interlayer space being occupied alternatively by a methyl group of the upper layer and another one from the layer below in a similar way as in complexes **2-12** (Figure II.3). However, the interlayer copper-copper separation [the shortest Cu...Cu separation being 6.203(3) Å] is much shorter than in the Phmal complexes [average value in **2-12** is 13.5 Å] due to the reduced dimensions of the methyl group of the Memal ligand.

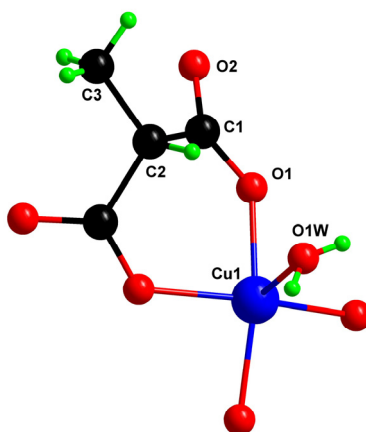


Fig. II.1. A view of a fragment of the structure of **17** with the numbering scheme.

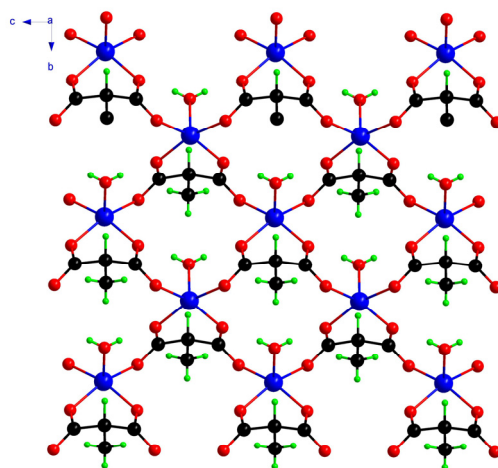
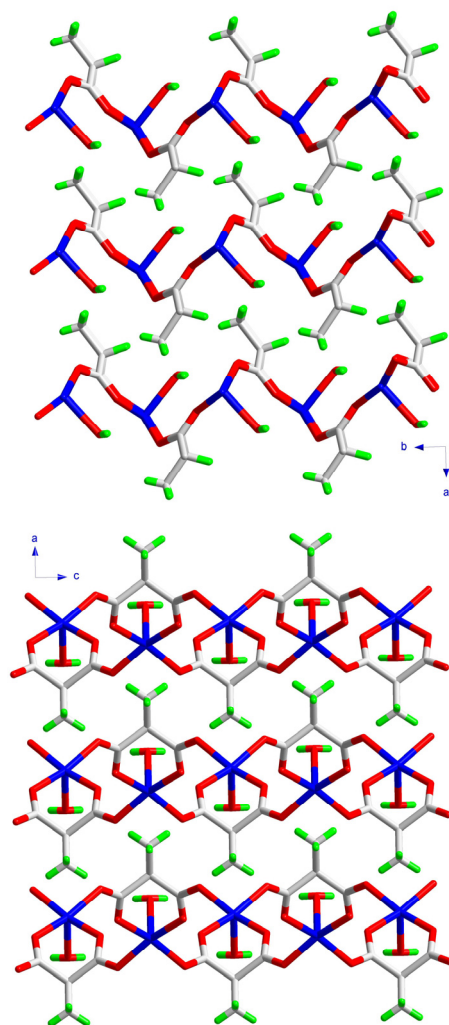


Fig. II.2. A perspective view of the carboxylate-bridged square grid of copper(II) ions formed in complex **17** along the *a* axis.





**Fig. II.3.** A view of the crystal packing of complex **17** along the *c* axis (up) and the *b* axis (bottom). The adjacent layers fit each other like zip.

Each copper atom exhibits a quasi-perfect square pyramidal environment ( $\tau$  value<sup>1</sup> being 0 due to symmetry restrictions) with an angle between the normal of the equatorial plane and the Cu-O(apical) vector of  $7.1(1)^\circ$ . Four methylmalonate oxygen atoms form this basal plane [O(1), O(1a), O(2b) and O(2c); mean bond distance  $1.960(2)$  Å; (a) =  $x, y, -z$ ; (b) =  $-x + 2, y - 1/2, -z + 1/2$ ; (c) =  $-x + 2, y - 1/2, z - 1/2$ ] while a water molecule occupies the apical position [Cu(1)–O(1w) =  $2.231(6)$  Å]. Selected bond lengths and angles are listed in Table II.2. The copper atom is shifted towards the apical position by  $0.3161(5)$  Å.

**Table II.2.** Selected bond angles (°) and lengths (Å) for **17**.

|                          |            |                   |            |
|--------------------------|------------|-------------------|------------|
| Cu(1)–O(1)               | 1.951(4)   | O(1)–Cu(1)–O(1w)  | 94.31(16)  |
| Cu(1)–O(1a) <sup>a</sup> | 1.951(4)   | O(1a)–Cu(1)–O(2b) | 161.39(14) |
| Cu(1)–O(2b)              | 1.970(3)   | O(1a)–Cu(1)–O(2c) | 86.19(15)  |
| Cu(1)–O(2c)              | 1.970(3)   | O(1a)–Cu(1)–O(1w) | 94.31(16)  |
| Cu(1)–O(1w)              | 2.231(6)   | O(2b)–Cu(1)–O(2c) | 92.0(2)    |
| O(1)–Cu(1)–O(1a)         | 89.6(2)    | O(2b)–Cu(1)–O(1w) | 104.06(15) |
| O(1)–Cu(1)–O(2b)         | 86.19(15)  | O(2c)–Cu(1)–O(1w) | 104.06(15) |
| O(1)–Cu(1)–O(2c)         | 161.39(14) |                   |            |

<sup>a</sup> Symmetry operations: (a) =  $x, y, -z$ ; (b) =  $-x + 2, y - 1/2, -z + 1/2$ ; (c) =  $-x + 2, y - 1/2, z - 1/2$

The methylmalonate ligand acts simultaneously as bidentate [through O(1) and O(1a) with the angle subtended at the copper atom being 89.6(2)°] and bis-monodentate ligand [through O(2) and O(2a)]. The hydrogen atom of the methylene group of the Memal ligand is directed towards the apical position of the copper(II) environment, as in the complexes **6-7** of the previous chapter. This configuration allows the copper basal planes to accommodate in an almost perfect perpendicular arrangement [the value of the dihedral angle between equatorial planes of adjacent copper atoms being 84.44(9)°], reducing the intralayer copper-copper separation [4.9653(12) Å].

Let us finish this structural description with a comparison of the structure of **16** with the previously reported copper(II)-malonate and -phenylmalonate complexes. The bidentate and bis-monodentate coordination modes exhibited by the Memal ligand in **17** have not been observed previously in the copper(II)-malonate<sup>2-5</sup> and the copper(II)-phenylmalonate<sup>6</sup> complexes (**1**) with water molecules as unique coligands. In the malonate-containing compounds, the trend to form the  $[\text{Cu}(\text{mal})_2]^{2-}$  entity is very favoured leading to different morphologies which are based on this unit with the aid of aquacopper(II) cations. The  $[\text{Cu}(\text{Phmal})_2]^{2-}$  units are also formed but they are condensed to build oxo-bridged  $[\text{Cu}_2(\text{Phmal})_4]^{4-}$  entities which are held together in layers with  $[\text{Cu}(\text{H}_2\text{O})_3]^{2+}$  cations. However, the situation in **17** is different. Its structure consists of layers similar to that formed in the copper(II)-Phmal complexes when a co-ligand such as pyrimidine (**2**) or 3-cyanopyridine (**4**) is present (see Chapter I). The occurrence of the methyl group in the Memal ligand would prevent the formation of the  $\text{Cu}(\text{L})_2$  unit and the close packing of the whole structure with a very short interlayer separation could finally favour the sheet-like conformation of **17**.

#### II.1.4. Magnetic Properties

The magnetic properties of complex **17** under the form of a  $\chi_M T$  vs  $T$  plot are presented in Figure II.4 [ $\chi_M$  is the magnetic susceptibility per copper(II) ion].  $\chi_M T$  at room temperature is

0.46 cm<sup>3</sup> mol<sup>-1</sup> K, a value which is as expected for a magnetically isolated spin doublet. Upon cooling,  $\chi_M T$  remains almost constant up to 30 K and then, it increases gradually to reach a value of 2.09 cm<sup>3</sup> mol<sup>-1</sup> K at 2.0 K. The  $\chi_M$  curve does not show any maximum and the magnetization ( $M$ ) vs. applied field plot (Figure II.5) shows that the saturation value of 1.03 BM is reached approximately at 2.0 T. All these features are indicative of the existence of ferromagnetic interactions between the copper(II) ions within the layers.

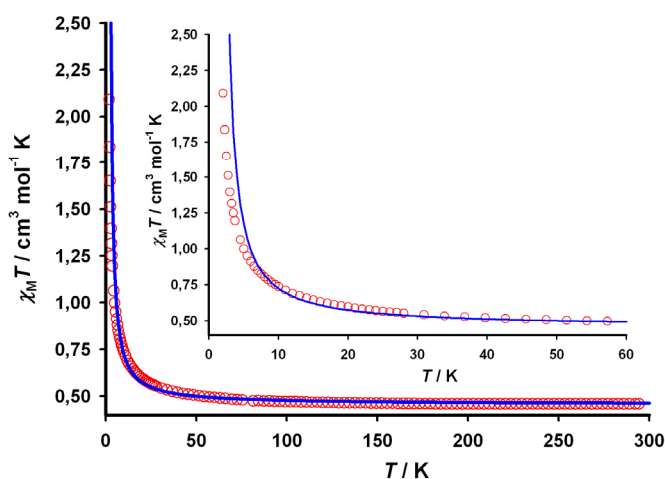


Fig. II.4.  $\chi_M T$  vs  $T$  plot for 17 under applied fields of 1 T ( $T > 66$  K) and 0.1 T ( $T < 66$  K): (o) experimental data; (—) best-fit curve (see text). The inset shows a detail of the low temperature region.

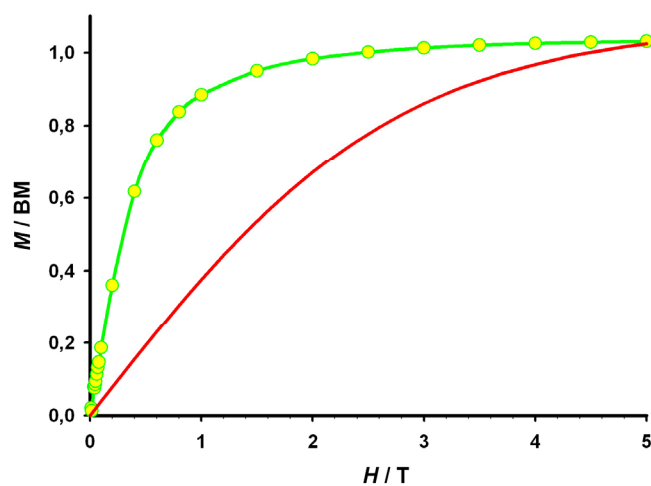


Fig. II.5.  $M$  vs  $H$  plot for 17 together with the Brillouin function for a magnetically isolated spin doublet (red line).

The structure of **17** is formed by corrugated layers of *anti-syn* equatorial-equatorial carboxylate bridged copper(II) ions, that exhibit a ferromagnetic coupling. Hence, the magnetic data can be analyzed through the high-temperature expansion series derived from the two-dimensional Heisenberg model for a  $S = 1/2$  ferromagnetic quadratic lattice:<sup>7</sup>

$$\chi_M = [Ng^2\beta^2/(3kT)] \cdot S(S+1) \cdot \left(1 + \sum_{n=1}^{10} a_n K^n\right)$$

where  $K = J/kT$ ,  $a_n$  are the coefficients for the square lattice and  $J$  is the intralayer magnetic coupling between the local spins of the nearest-neighbours with the Hamiltonian defined as:

$$\hat{H} = -J \sum_i \hat{S}_i \cdot \hat{S}_{i+1}$$

The best-fit using non-linear regression analysis gives  $J = +1.61(1) \text{ cm}^{-1}$ ,  $g = 2.203(3)$  and  $R = 5.0 \times 10^{-4}$ . The calculated curve matches the experimental data in the whole temperature range although at low temperatures the calculated curve slightly deviates from the experimental data (Figure II.4). The theoretical curve with the parameters obtained from the regression analysis lies below the experimental data [see inset of Fig. II.4] suggesting the presence of weak antiferromagnetic interactions between the layers.

The value of the magnetic coupling  $J$  obtained from the fit is in agreement with what is expected for a carboxylate-bridge in *anti-syn* conformation.<sup>8</sup> However,  $J$  is slightly lower than the values observed in other carboxylate-bridged square-grid of copper(II) ions (see Chapter I) and for equatorial-equatorial carboxylate-malonate bridged copper(II) complexes (see Table II.3).<sup>9</sup> This is the reason why complex **17** does not exhibit ferromagnetic ordering as complex **2**. Subtle structural changes, such as the distortion and bond distances at the copper environment or the value of the dihedral angle between the basal plane of the copper coordination sphere and the carboxylate pathway, account for this difference in the magnetic coupling.

The ferromagnetic nature of the interaction can be explained through magnetic orbital considerations. The magnetic orbital of the copper atom is of the  $d(x^2-y^2)$  type [the  $x$  and  $y$  axes being roughly defined by the equatorial bonds] with some admixture of the  $dz^2$  character [ $z$  is defined by the axial bond]. According to the Kahn's model,<sup>15</sup> since the angle between the equatorial planes of the carboxylate-bridged copper(II) ions is near to be perpendicular [ $84.44(9)^\circ$ ] the antiferromagnetic contribution is reduced, leading to the ferromagnetic term to dominate.

**Table II.3.** Selected magneto-structural data for some *anti-syn* equatorial-equatorial carboxylate(malonate)-bridged copper(II) complexes

| Compound <sup>a</sup>                                                                                                            | $J/\text{cm}^{-1}$ | Ref |
|----------------------------------------------------------------------------------------------------------------------------------|--------------------|-----|
| $\{\text{Cu}(\text{H}_2\text{O})_3[\text{Cu}(\text{mal})_2(\text{H}_2\text{O})]\}_n$                                             | +3.0               | 4a  |
| $\{\text{Cu}(2,2'\text{-bpy})(\text{H}_2\text{O})[\text{Cu}(2,2'\text{-bpy})(\text{mal})(\text{H}_2\text{O})]\}(\text{ClO}_4)_2$ | +4.6               | 10  |
| $[\text{Cu}_4(\text{mal})_4(2,4'\text{-bpy})_4(\text{H}_2\text{O})_4]\cdot 8\text{H}_2\text{O}$                                  | +12.3              | 11  |
| $[\text{Cu}_2(\text{mal})_2(\text{H}_2\text{O})_2(4,4'\text{-bpy})]$                                                             | +12.4              | 12  |
| $[\{\text{Cu}_3(\text{mal})_2(\text{bpa})_3(\text{H}_2\text{O})_2\}(\text{NO}_3)_2]_n$                                           | +22                | 13  |
| $[\text{Cu}_4(\text{mal})_4(\text{bpe})_3]_n\cdot 6n\text{H}_2\text{O}$                                                          | +23                | 14  |
| <b>1</b>                                                                                                                         | +4.44              | -   |
| <b>2</b>                                                                                                                         | +5.6               | -   |
| <b>4</b> <sup>b</sup>                                                                                                            | +5.4 / -0.70       | -   |
| <b>5</b> <sup>b</sup>                                                                                                            | +4.8 / +0.073      | -   |
| <b>9</b>                                                                                                                         | -0.15              | -   |
| <b>17</b>                                                                                                                        | +1.61              | -   |

<sup>a</sup> Abbreviations used: 2,2'-bpy = 2,2'-bipyridine, 2,4'-bpy = 2,4'-bipyridine, 4,4'-bpy = 4,4'-bipyridine, bpe = 1,2-bis(4-pyridyl)ethylene and bpa = 1,2-bis(4-pyridyl)ethane.  
<sup>b</sup> These complexes exhibit two different carboxylate pathways. The lower one obtained from a mean field approximation.

### II.1.5. Conclusion

Complex **17** exhibits the two-dimensional square grid of carboxylate-bridged copper(II) ions similar to that formed in phenylmalonate-containing complexes **2-12**. These compounds were synthesized in the presence of a pyridine-type coligand, the structure of the copper(II)-phenylmalonate complex with water molecules as unique coligands (**1**) being very different. The related copper(II)-malonate complexes do not form this kind of two-dimensional structure. Then, it seems that the methylmalonate ligand behaves in the presence of copper(II) ions like the phenylmalonate ligand with copper(II) and pyridine-like coligands.

From a magnetic point of view, the interaction between the spin centres in **17** is ferromagnetic as usual in related R-mal-copper(II) complexes, but of smaller size and, thus, no ferromagnetic ordering is achieved in contrast to what it is observed in **2**.

### II.1.6. References

- 1 A. W. Addison, T. N. Rao, J. Reedijk, J. van Rijn and G. C. Verschoor, *Dalton Trans.* **1984**, 1349.
- 2 (a) Y. Rodríguez-Martín, J. Sanchiz, C. Ruiz-Pérez, F. Lloret and M. Julve, *CrystEngComm* **2002**, *4*, 631. (b) I. G. Fillippova, *Koord. Khim. (Russ. Coord. Chem.)* **2000**, *26*, 295. (c) G. I. Dimitrova, A. V. Ablov, G. A. Kiosse, G. A. Popovich, T. I. Malinovski and I. F. Bourshteyn, *Dokl. Akad. Nauk SSSR* **1974**, *216*, 1055.
- 3 D. Chattopadhyay, S. K. Chattopadhyay, P. R. Lowe, C. H. Schwalbe, S. K. Mazumder, A. Rana and S. Ghosh, *Dalton Trans.* **1993**, 913.
- 4 (a) C. Ruiz-Pérez, J. Sanchiz, M. Hernández-Molina, F. Lloret and M. Julve, *Inorg. Chem.* **2000**, *39*, 1363. (b) I. G. Fillippova, V. Kh. Kravtsov and M. Gdanets *Koord. Khim. (Russ.*

- Coord. Chem.*) **2000**, *26*, 860. (c) P. Naumov, M. Ristova, B. Soptrajanov, M. G. B. Drew and S. W. Ng, *Croat. Chem. Acta* **2002**, *75*, 701.
- 5 V. T. Yilmaz, E. Senel and C. Thone, *Transition Met. Chem.* **2004**, *29*, 336.
  - 6 J. Pasán, J. Sanchiz, C. Ruiz-Pérez, F. Lloret and M. Julve, *New J. Chem.*, **2003**, *27*, 1557.
  - 7 R. Navarro, *Application of High- and Low-Temperature Series Expansions to Two-dimensional Magnetic Systems*, de Jongh, L. J.; Ed., Kluwer Academic Publishers, The Netherlands, **1990**.
  - 8 A. Rodríguez-Forteza, P. Alemany, S. Álvarez and E. Ruiz, *Chem. Eur. J.* **2001**, *7*, 627.
  - 9 J. Pasán, F. S. Delgado, Y. Rodríguez-Martín, M. Hernández-Molina, C. Ruiz-Pérez, J. Sanchiz, F. Lloret and M. Julve, *Polyhedron* **2003**, *22*, 2143.
  - 10 C. Ruiz-Pérez, M. Hernández-Molina, P. Lorenzo-Luis, F. Lloret, J. Cano and M. Julve, *Inorg. Chem.* **2000**, *39*, 3845.
  - 11 Y. Rodríguez-Martín, M. Hernández-Molina, F. S. Delgado, J. Pasán, C. Ruiz-Pérez, J. Sanchiz, F. Lloret and M. Julve, *CrystEngComm* **2002**, *4*, 522.
  - 12 Y. Rodríguez-Martín, C. Ruiz-Pérez, J. Sanchiz, F. Lloret and M. Julve, *Inorg. Chim. Acta* **2001**, *318*, 159.
  - 13 S. Sain, T. K. Maji, G. Mostafa, T. H. Lu and N. R. Chaudhuri, *New J. Chem.* **2003**, *27*, 185.
  - 14 F. S. Delgado, J. Sanchiz, C. Ruiz-Pérez, F. Lloret and M. Julve, *Inorg. Chem.* **2003**, *42*, 5938.
  - 15 O. Kahn, *Molecular Magnetism*, VCH, New York, **1993**.

## II.2. Pyrazine (18) and 4,4'-bipyridine (19) Copper(II)-Methylmalonate complexes

### II.2.1. Introduction

The previous section was devoted to the first experience with the copper(II) complexation by the methylmalonate ligand. The compound  $[\text{Cu}(\text{Memal})(\text{H}_2\text{O})]_n$  (17) has a structure of carboxylate-bridged square grid of copper(II) ions previously observed in complexes 2-12 with a intralayer ferromagnetic coupling. A similar strategy to that of the Chapter I can then be developed, introducing pyridine-like ligands which can separate the layers, as occur in complexes 2-12, or link them, as in the three-dimensional networks obtained with cobalt(II) and zinc(II) with malonate and pyrimidine (pym) or pyrazine (pyz)  $[\text{M}^{\text{II}}(\text{L})_{1/2}(\text{mal})]_n$  [ $\text{M}^{\text{II}} = \text{Zn}(\text{II})$  and  $\text{Co}(\text{II})$ ;  $\text{L} = \text{pym}$  and  $\text{pyz}$ ].<sup>1</sup> The introduction of this N-donor ligands could increase the dimensionality of the structure and the magnitude of the magnetic coupling.

The two pyridine ligands (pyrazine and 4,4'-bipyridine) which are included in this section have been selected for its ability to act as bridging ligands and as rods in layered systems.<sup>2,3</sup> Their rigidity accounts for the formation of robust structures in copper(II) complexes.<sup>4</sup> We report herein the synthesis, crystal structure and magnetic properties of two compounds based on the methylmalonate ligand, copper(II) ions and the pyrazine and 4,4'-bipyridine coligands.

### II.2.2. Synthesis

**$[\text{Cu}_2(\text{pyz})(\text{Memal})_2]$  (18).** A methanolic solution (5 cm<sup>3</sup>) of pyrazine (1 mmol, 80 mg) was added dropwise to a water solution (10 cm<sup>3</sup>) of copper(II)-methylmalonate (0.5 mmol, 90 mg) (prepared as described in Section II.1) under stirring. The pale blue solution obtained was filtered and allowed to evaporate at room

**Table II.4.** Crystallographic data for complex 18-19

|                                                    | 18                                                              | 19                                                              |
|----------------------------------------------------|-----------------------------------------------------------------|-----------------------------------------------------------------|
| Formula                                            | C <sub>6</sub> H <sub>6</sub> O <sub>4</sub> NCu                | C <sub>9</sub> H <sub>10</sub> O <sub>5</sub> NCu               |
| FW                                                 | 219.66                                                          | 275.72                                                          |
| Crystal system                                     | Monoclinic                                                      | Monoclinic                                                      |
| Space group                                        | <i>P</i> 2 <sub>1</sub> / <i>n</i>                              | <i>P</i> 2 <sub>1</sub> / <i>n</i>                              |
| <i>a</i> /Å                                        | 6.2854(2)                                                       | 7.2395(4)                                                       |
| <i>b</i> /Å                                        | 16.4373(6)                                                      | 19.4035(14)                                                     |
| <i>c</i> /Å                                        | 7.0129(2)                                                       | 7.3889(3)                                                       |
| $\beta$ /°                                         | 92.594(2)                                                       | 91.844(5)                                                       |
| <i>V</i> /Å <sup>3</sup>                           | 723.80(4)                                                       | 1037.39(10)                                                     |
| <i>Z</i>                                           | 4                                                               | 4                                                               |
| $\mu(\text{Mo K}\alpha)$ /cm <sup>-1</sup>         | 29.86                                                           | 21.10                                                           |
| <i>T</i> /K                                        | 293(2)                                                          | 293(2)                                                          |
| $\rho_{\text{calc}}$ /g cm <sup>-3</sup>           | 2.016                                                           | 1.765                                                           |
| $\lambda$ /Å                                       | 0.71073                                                         | 0.71073                                                         |
| Index ranges                                       | -8 ≤ <i>h</i> ≤ 5,<br>-19 ≤ <i>k</i> ≤ 21,<br>-8 ≤ <i>l</i> ≤ 9 | -9 ≤ <i>h</i> ≤ 9,<br>-25 ≤ <i>k</i> ≤ 21,<br>-9 ≤ <i>l</i> ≤ 9 |
| Indep. reflect. ( <i>R</i> <sub>int</sub> )        | 1590 (0.0273)                                                   | 2297 (0.0475)                                                   |
| Obs. reflect. [ <i>I</i> > 2σ( <i>I</i> )]         | 1381                                                            | 1708                                                            |
| Parameters                                         | 119                                                             | 169                                                             |
| Goodness-of-fit                                    | 1.104                                                           | 1.052                                                           |
| <i>R</i> [ <i>I</i> > 2σ( <i>I</i> )]              | 0.0298                                                          | 0.0597                                                          |
| <i>R</i> <sub>w</sub> [ <i>I</i> > 2σ( <i>I</i> )] | 0.0704                                                          | 0.1035                                                          |
| <i>R</i> (all data)                                | 0.0380                                                          | 0.0921                                                          |
| <i>R</i> <sub>w</sub> (all data)                   | 0.0738                                                          | 0.1145                                                          |

temperature. Prismatic blue single crystals of **18** were grown after a few days. Yield *ca.* 70 %. Anal. calc. for  $C_6H_6CuNO_4$  (**18**): C, 32.81; H, 2.75; N, 6.38; Found: C, 32.91; H, 2.88; N, 6.45 %.

**[Cu<sub>2</sub>(4,4'-bpy)(Memal)<sub>2</sub>(H<sub>2</sub>O)<sub>2</sub>] (19)**. An aqueous solution (5 cm<sup>3</sup>) of copper(II)-methylmalonate (1 mmol, 180 mg) was set in one arm of a water-filled H-shape tube while a methanolic solution (5 cm<sup>3</sup>) of 4,4'-bipyridine (1mmol, 156 mg) was set in the other arm. Single crystals of different colours and shapes corresponding to different phases appeared after a few weeks (see Section II.7). Prismatic pale blue single crystals of **19** which correspond to the main phase were separated mechanically. Crystallographic details for **18** and **19** are listed in Table II.4. Yield *ca* 45%. Anal. calc. for  $C_9H_{10}CuNO_5$ (**19**): C, 39.20; H, 3.65; N, 5.08; Found: C, 39.39; H, 3.71; N, 5.13 %.

### II.2.3. Description of the Structures

The crystal structures of  $[Cu_2(pyzo)(Memal)_2]$  (**18**, Figure II.6) and  $[Cu_2(4,4'-bpy)(Memal)_2(H_2O)_2]$  (**19**, Figure II.6) consist of corrugated copper(II)-methylmalonate layers, similar to that of **17**, which are linked through pyrazine (**18**) and 4,4'-bipyridine (**19**) ligands; to build up a three-dimensional network (Figure II.7). The layers are built by carboxylate-bridged copper(II) ions resulting in a square grid which grows in the *ac* plane (Figure II.8). The pyzo and 4,4'-bpy ligands are located alternatively above and below the sheets, inversely to the position of the methyl group of the Memal ligand. There are not  $\pi$ -type interactions in these structures since the shortest centroid-centroid distances between adjacent pyridyl rings are 6.285(2) (**18**) and 7.239(4) Å (**19**) [values which are much longer than the average ones for interactions between pyridyl rings].<sup>5</sup> Intralayer hydrogen bonds involving the coordinated water molecule and oxygen atoms of the methylmalonate ligand in **19** contribute to the stabilization of the structure [O(1w)–H···O(2) and O(1w)–H···O(4) distances and angles being 2.663(7) Å and 166(8)° and 2.637(6) Å and 153(8)°, respectively].



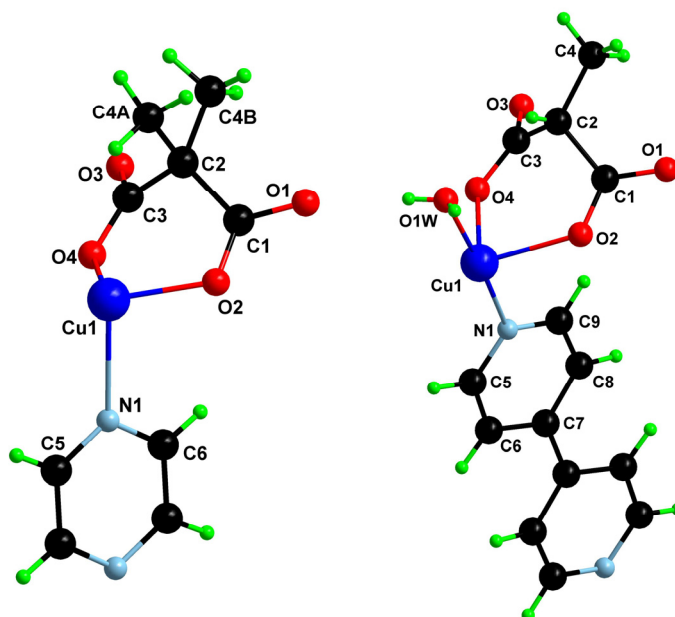


Fig. II.6. A view of molecular fragment of compounds **18** (left) and **19** (right) along with the numbering scheme.

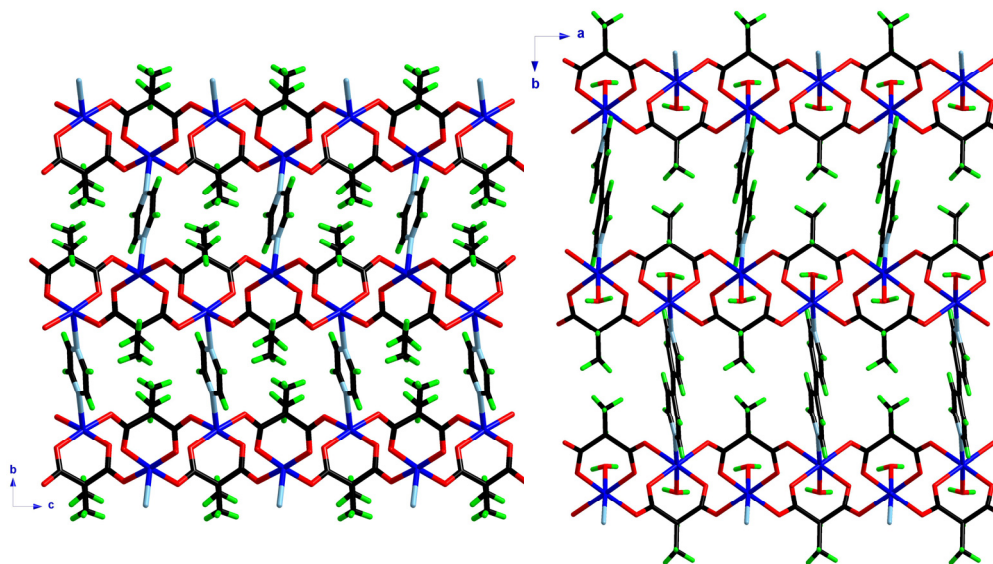


Fig. II.7. Perspective views of the crystal packing of **18** along the *a* axis (left) and **19** along the *c* axis (right).

Each copper atom in **18** exhibits an almost perfect square pyramidal environment ( $\tau$  value<sup>6</sup> being 0.006). Four methylmalonate oxygen atoms [O(1), O(2), O(3) and O(4); average bond distance is 1.962(2) Å; see Table II.5] build the basal plane whereas a nitrogen atom from a pyrazine ligand occupies the apical position [N(1); Cu–N bond distance is 2.292(2) Å]. The copper atom is shifted by 0.0767(3) Å towards the axial position. The copper atoms in **19** are six-coordinated and their environment is formed by four methylmalonate oxygen atoms, one 4,4'-bpy nitrogen atom and a coordinated water molecule. The CuNO<sub>5</sub> chromophore could be described as an unusual compressed octahedron with two short distances [1.980(4) and 2.025(4) Å for Cu(1)–O(1w) and Cu(1)–N(1), respectively] and four long ones corresponding to the oxygen atoms of the Memal ligand [values from 2.080(4) to 2.234(5) Å; see Table II.5]. This situation is reminiscent of that in [Cu(2,4'-bpy)(Phmal)(H<sub>2</sub>O)] (**12**)<sup>7</sup> (Section I.6) where a deep analysis of the vibrational amplitudes describe this compression as a static pseudo-Jahn-Teller disorder. Although the structure of **18** could not be solved at low temperature; a comparison between the data of **12** and **18** could clarify the situation. The  $\Delta$ MSDA values<sup>8-11</sup> for **12** and **18** are listed in Table II.6 and, in spite of the effect is more pronounced in **12**, the high  $\Delta$ MSDA values for the four methylmalonate oxygen atoms in **18** account for the presence of a static pseudo-Jahn-Teller disorder within the crystal. This situation correspond thus to that

**Table II.5.** Selected bond angles (°) and lengths (Å) for **18** and **19**.

| <b>18</b>         |            |                   |            |
|-------------------|------------|-------------------|------------|
| Cu(1)–O(1a)       | 1.9578(19) | O(1a)–Cu(1)–N(1)  | 88.28(9)   |
| Cu(1)–O(2)        | 1.970(2)   | O(2)–Cu(1)–O(3b)  | 88.12(8)   |
| Cu(1)–O(3b)       | 1.959(2)   | O(2)–Cu(1)–O(4)   | 89.00(8)   |
| Cu(1)–O(4)        | 1.962(2)   | O(2)–Cu(1)–N(1)   | 96.78(9)   |
| Cu(1)–N(1)        | 2.292(2)   | O(3b)–Cu(1)–O(4)  | 175.24(8)  |
| O(1a)–Cu(1)–O(2)  | 174.90(9)  | O(3b)–Cu(1)–N(1)  | 89.42(9)   |
| O(1a)–Cu(1)–O(3b) | 92.57(9)   | O(4)–Cu(1)–N(1)   | 94.68(9)   |
| O(1a)–Cu(1)–O(4)  | 89.97(8)   |                   |            |
| <b>19</b>         |            |                   |            |
| Cu(1)–O(1c)       | 2.234(5)   | O(2)–Cu(1)–O(3b)  | 89.67(16)  |
| Cu(1)–O(2)        | 2.144(4)   | O(2)–Cu(1)–O(4)   | 86.64(17)  |
| Cu(1)–O(3b)       | 2.154(5)   | O(2)–Cu(1)–N(1)   | 91.31(16)  |
| Cu(1)–O(4)        | 2.080(4)   | O(2)–Cu(1)–O(1w)  | 92.59(18)  |
| Cu(1)–N(1)        | 2.025(4)   | O(3b)–Cu(1)–O(4)  | 174.78(16) |
| Cu(1)–O(1w)       | 1.980(4)   | O(3b)–Cu(1)–N(1)  | 87.69(16)  |
| O(1c)–Cu(1)–O(2)  | 176.35(16) | O(3b)–Cu(1)–O(1w) | 92.41(18)  |
| O(1c)–Cu(1)–O(3b) | 93.33(15)  | O(4)–Cu(1)–N(1)   | 88.71(16)  |
| O(1c)–Cu(1)–O(4)  | 90.23(16)  | O(4)–Cu(1)–O(1w)  | 91.44(18)  |
| O(1c)–Cu(1)–N(1)  | 86.74(16)  | N(1)–Cu(1)–O(1w)  | 176.10(19) |
| O(1c)–Cu(1)–O(1w) | 89.36(18)  |                   |            |

<sup>a</sup> Symmetry operations: (a) =  $x - 1/2, -y + 1/2, z + 1/2$ ; (b) =  $x - 1/2, -y + 1/2, z - 1/2$ ; (c) =  $x + 1/2, -y + 1/2, z - 1/2$ .

discussed in Section I.6.3, in which the oxygen atoms of the Memal ligand act as pairs [O(1)–Cu(1)–O(2), and O(3)–Cu(1)–O(4)] in axial and equatorial positions in a disordered manner within the crystal.

The methylmalonate ligand in both compounds acts simultaneously as bidentate [through O(2) and O(4)] with the angle subtended at the copper atom being  $89.00(8)^\circ$  (**18**) and  $86.64(17)^\circ$  (**19**) and as bis-monodentate ligand [through O(1) and O(3)]. The methyl group of the Memal ligand is slightly disordered and two crystallographic positions were found for the C(4) carbon atom. The occupancy factors for these two sites was refined resulting in 0.45 and 0.55 for C(4A) and C(4B), respectively (see Figure II.6). The pyridyl rings of the 4,4'-bpy ligand in **19** are coplanar because they are symmetry-related, an inversion centre located at the middle of the central C–C bond between the pyridyl rings.

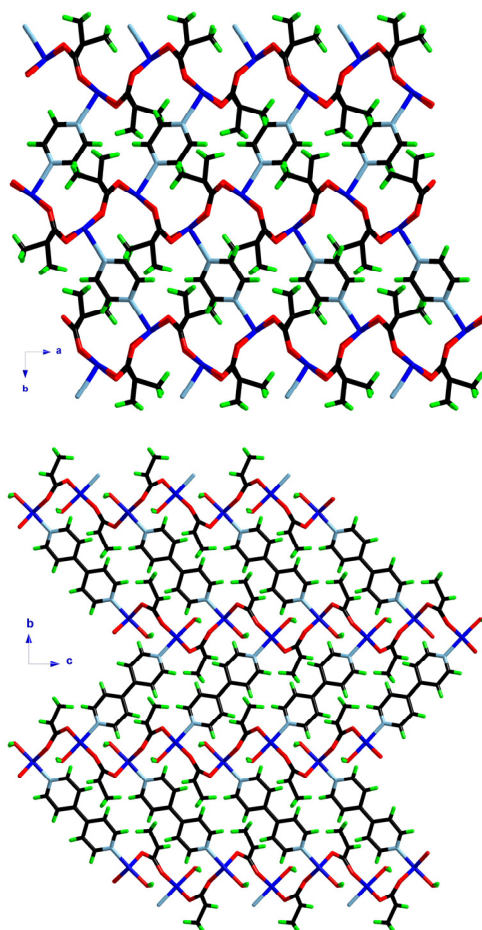


**Fig. II.8.** A view of the 3D structure of complexes **18** (up) and **19** (bottom) along the *c* and *a* axis, respectively. They show the corrugated layers of carboxylate-bridged copper(II) ions linked through pyrazine (**18**) or 4,4'-bipyridine (**19**) bridges.

The values of the copper-copper separations through the two crystallographically independent *anti-syn* carboxylate bridges are 5.0226(5) and 5.2174(5) Å for **18** and 5.2879(8) and 5.4482(8) Å for **19**. They are shorter than the shorter interlayer separations. The values for **19** are longer than those of **18** due to the fact that the carboxylate bridges in **19** link one equatorial to one apical position at the copper environment (because of the static pseudo-Jahn-Teller disorder). The carboxylate group bridges equatorial positions of the copper(II) ions in **18**. The pyrazine and the 4,4'-bpy ligands link two copper atoms of adjacent layers being the separations 7.3716(5) and 11.1261(11) Å, respectively. These values are longer than the shortest interlayer Cu...Cu distances [6.6546(5) (**17**) and 8.2709(10) Å (**19**)] because of the corrugation of the layers and the non-parallel alignment of the bridging ligands along the stacking direction of the layers [the value of the angle between the pyz and 4,4'-bpy ligands and the normal of the layer being 32.6(6) and 42.0(6)°, respectively].

**Table II.6.** Bond distances at Cu(1) and calc.  $\Delta MSDA$  values for compounds **12** and **18** at 293 K.

| Bond        | <b>18</b>        |                                             | <b>12</b>        |                                             |
|-------------|------------------|---------------------------------------------|------------------|---------------------------------------------|
|             | $d / \text{\AA}$ | $\Delta MSDA / \text{\AA}^2 \times 10^{-4}$ | $d / \text{\AA}$ | $\Delta MSDA / \text{\AA}^2 \times 10^{-4}$ |
| Cu(1)–O(1)  | 2.234(5)         | 153                                         | 2.208(3)         | 293                                         |
| Cu(1)–O(2)  | 2.144(4)         | 272                                         | 2.128(3)         | 269                                         |
| Cu(1)–O(3)  | 2.154(5)         | 99                                          | 2.110(3)         | 315                                         |
| Cu(1)–O(4)  | 2.080(4)         | 201                                         | 2.076(3)         | 255                                         |
| Cu(1)–O(1w) | 1.980(4)         | 65                                          | 2.004(2)         | 59                                          |
| Cu(1)–N(1)  | 2.025(4)         | 24                                          | 2.026(3)         | 64                                          |

#### II.2.4. Magnetic Properties

The temperature dependence of the  $\chi_M T$  product for **18** [ $\chi_M$  being the magnetic susceptibility per copper(II) ion] is presented in Figure II.9.  $\chi_M T$  at room temperature is 0.42 cm<sup>3</sup> mol<sup>-1</sup> K, a value which is as expected for a magnetically isolated spin doublet. Upon cooling,  $\chi_M T$  smoothly increases to reach a maximum of 0.51 cm<sup>3</sup> mol<sup>-1</sup> K at 17 K. Then, the  $\chi_M T$  value sharply decreases to 0.19 cm<sup>3</sup> mol<sup>-1</sup> K at 2.0 K. This behaviour is indicative of the existence in **18** of two magnetic interactions of different nature. The magnetization ( $M$ ) versus the applied field ( $H$ ) curve (inset of Figure II.9) run below the Brillouin function for an isolated spin doublet confirming the presence of antiferromagnetic interactions. However, at high applied fields a change in the linear trend is observed, which could be assigned to the beginning of the sigmoidal shape characteristic of a metamagnetic behaviour. The inflexion point of the  $M$  vs.  $H$  curve accounts for a critical field ( $H_c$ ) of ca. 3.0 T. This is in agreement

with the proposed coexistence of two magnetic interactions of different nature in complex **18**.

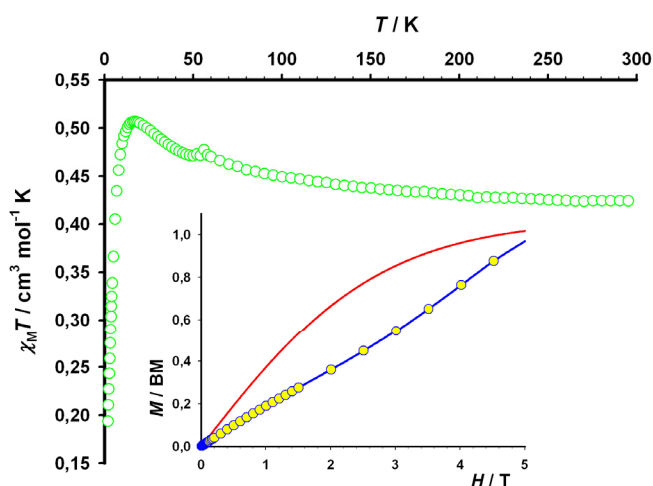
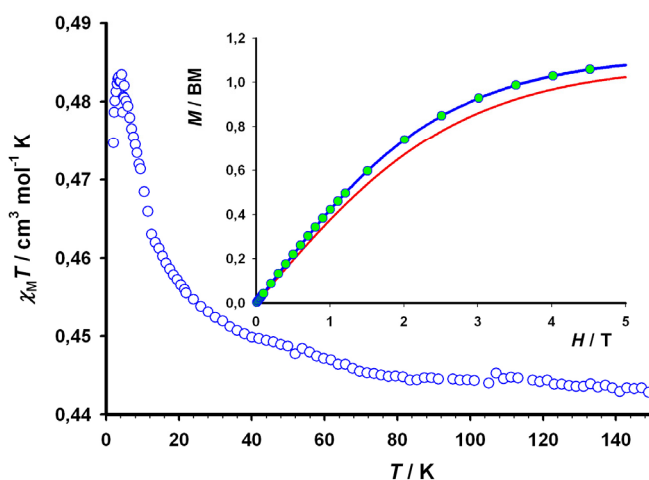


Fig. II.9.  $\chi_M T$  vs  $T$  plot for **18** under applied field of 1 T. The inset shows the  $M$  vs  $H$  curve (yellow-blue) together with the Brillouin function for a magnetically isolated  $S=1/2$  (red line).

The structure of **18** consists of a three-dimensional structure where *anti-syn* carboxylate-bridged copper(II) square grid layers are linked through pyrazine ligands. Since there are two crystallographically different carboxylate bridges; from a magnetic point of view, three different magnetic exchange pathways are active in this compound. Unfortunately, there is no model to fit the magnetic properties of this three-dimensional compound with three magnetic interactions, but their values can be roughly evaluated. Previous examples of these square grid layers of copper(II) ions are found in Chapter I, the magnetic interaction through the phenylmalonate-carboxylate bridges being either ferro- or antiferromagnetic. The nature of the magnetic interaction depends on subtle changes of the structure, and the magnitude of the coupling parameter ( $J$ ) varies in the range  $-4$  to  $+5.8$   $\text{cm}^{-1}$ . Magneto-structural studies of pyrazine-bridged copper(II) complexes reveal the occurrence of a weak antiferromagnetic coupling between the copper(II) ions through this bridge (values of  $J$  ranging from  $-2$  to  $-5$   $\text{cm}^{-1}$ ).<sup>12</sup> In this sense, the ferromagnetic interaction presents in **18** can only be attributed to the carboxylate exchange pathway, whereas the antiferromagnetic one can be due to the contributions from the pyrazine and the carboxylate bridges. The value of the critical field of the magnetization accounts for a weak antiferromagnetic interaction of ca.  $3.0$   $\text{cm}^{-1}$ , in agreement with the values reported for the pyrazine exchange pathway<sup>12</sup> and those observed for carboxylate bridges in the previous chapter.

The magnetic properties for **19** under the form of a  $\chi_M T$  vs.  $T$  plot are depicted in the Figure II.10.  $\chi_M T$  at room temperature is  $0.44 \text{ cm}^3 \text{ mol}^{-1} \text{ K}$ , a value which is as expected for a magnetically isolated copper(II) ion. Upon cooling,  $\chi_M T$  increases very smoothly to reach a maximum value of  $0.48 \text{ cm}^3 \text{ mol}^{-1} \text{ K}$  at 3.5 K. Then, it sharply decreases up to  $0.47 \text{ cm}^3 \text{ mol}^{-1} \text{ K}$  at 2.0 K. These features are indicative of the presence of magnetic interactions of different nature in the complex **19**. The magnetization curve (see inset of Figure II.10) exhibits a similar shape to that of the Brillouin function for an isolated spin doublet, lying slightly above. This situation accounts for the weak magnetic interactions present in **19**.



**Fig. II.10.**  $\chi_M T$  vs  $T$  plot for **19** under applied fields of 1 T ( $T > 10$  K) and 0.1 T ( $T < 10$  K). The inset shows the  $M$  vs  $H$  curve (green-blue) together with the Brillouin function for a magnetically isolated spin doublet (red line).

The magnetic behaviour of **19** is reminiscent of that of **18** but weaker in magnitude. This is in agreement with the structure of **19**, where the *anti-syn* carboxylate bridges are of the equatorial-apical type which is known to mediate ferromagnetic interactions,<sup>13-14</sup> but with a smaller magnetic coupling ( $J$  ranging from  $+0.049$  to  $+1.8 \text{ cm}^{-1}$ ) than the equatorial-equatorial one. Finally, the 4,4'-bipyridine mediates much weaker antiferromagnetic interactions ( $j$  ca.  $-0.05 \text{ cm}^{-1}$ ) than the pyrazine one. The two magnetic interactions in **19** are of the same order of magnitude and opposite in nature.

## II.2.5. Conclusion

The complexes **18** and **19** exhibit the predicted structure having in mind the formation of the carboxylate bridged square grids of copper(II) ions with the phenylmalonate ligand. Two rod-like ligands as the pyrazine and 4,4'-bipyridine groups link the adjacent layers to give a

robust three-dimensional structure. The methyl group is smaller than the phenyl group of the phenylmalonate ligand which is enough to avoid the connection between the layers through pyridine-type ligands.

From a magnetic point of view, the two compounds exhibit almost the same behaviour, which consist of the coexistence of two magnetic interactions of opposite nature. The magnitude of these interactions in **19** is weaker than those in **18**, a situation which is in agreement with their structural features. The magnetic coupling parameters are in accordance with the reported values for carboxylate, pyrazine and 4,4'-bipyridine bridges.

It is noteworthy to say that the introduction of a pyrimidine bridging ligand which can connect the layers mediating ferromagnetic interactions is a very interesting approach. However, despite the large number of attempts to synthesize such a complex, we did not succeed.

## II.2.6. References

- 1 F. S. Delgado, J. Sanchiz, C. Ruiz-Pérez, F. Lloret and M. Julve, *CrystEngComm* **2003**, 5(48), 280.
- 2 (a) C. Janiak, *Dalton Trans.* **2003**, 2781. (b) B. Moulton and M. J. Zaworotko, *Chem. Rev.* **2001**, 101, 1629. (c) M. J. Zaworotko, *Chem. Commun.* **2001**, 1.
- 3 (a) S. R. Batten and R. Robson, *Angew. Chem. Int. Ed.* **1998**, 37, 1461. (b) S. R. Batten, *CrystEngComm*, **2001**, 3, 67. (c) S. L. James, *Chem. Soc. Rev.* **2003**, 32, 276.
- 4 S. Noro, R. Kitaura, M. Kondo, S. Kitagawa, T. Ishii, H. Matsuzaka and M. Yamashita, *J. Am. Chem. Soc.* **2002**, 124, 2568.
- 5 C. Janiak, *Dalton Trans.* **2000**, 3885.
- 6 A. W. Addison, T. N. Rao, J. Reedijk, J. van Rijn and G. C. Verschoor, *Dalton Trans.* **1984**, 1349.
- 7 J. Pasán, J. Sanchiz, C. Ruiz-Pérez, F. Lloret and M. Julve, *Inorg. Chem.* **2005**, 44, 7794.
- 8 B. J. Hathaway, *Struct. Bonding*, **1984**, 57, 55.
- 9 L. R. Falvello, *Dalton Trans.* **1997**, 4463.
- 10 M. A. Halcrow, *Dalton Trans.* **2003**, 4375.
- 11 N. K. Solanki, M. A. Leech, E. J. L. McInnes, F. E. Mabbs, J. A. K. Howard, C. A. Kilner, J. M. Rawson and M. A. Halcrow, *Dalton Trans.* **2002**, 1295.
- 12 (a) C. P. Landee and M. M. Turnbull, *Mol. Cryst. Liq. Cryst.* **1999**, 335, 193. (b) J. Cano, P. Alemany, S. Alvarez, M. Verdaguer and E. Ruiz, *J. Am. Chem. Soc.* **1996**. (c) J. A. Real, G. de Munno, M. C. Muñoz and M. Julve, *Inorg. Chem.* **1991**, 30, 2701. (d) J. S. Haynes, S. J. Retting, J. R. Sams, J. Trotter and R. C. Thompson, *Inorg. Chem.* **1988**, 27, 1237. (e) W. Richardson and W. E. Hatfield, *J. Am. Chem. Soc.* **1976**, 98, 835.
- 13 A. Rodríguez-Forteza, P. Alemany, S. Álvarez and E. Ruiz, *Chem. Eur. J.* **2001**, 7, 627.
- 14 J. Pasán, F. S. Delgado, Y. Rodríguez-Martín, M. Hernández-Molina, C. Ruiz-Pérez, J. Sanchiz, F. Lloret and M. Julve, *Polyhedron* **2003**, 22, 2143.

## II.3. 4-Cyanopyridine (20) Copper(II)-Methylmalonate complex

### II.3.1. Introduction

The previous section have shown that the use of pyridine-like bridging ligands is a good choice to link the square grid layers of carboxylate-bridged copper(II) ions formed in **17**. We are dealing now with the separation of the layers by using the 4-cyanopyridine as coligand. The selection of the 4-CNpy group responds to comparison purposes with the related phenylmalonate complex  $[\text{Cu}(4\text{-CNpy})(\text{Phmal})]_n$  (**5**), and, in general, with the couple of CNpy-containing complexes (Section I.3). Magnetically, we expect a similar behaviour to that observed in  $[\text{Cu}(\text{Memal})(\text{H}_2\text{O})]_n$  (**17**) where ferromagnetic interactions dominate within the square grid layer.

### II.3.2. Synthesis

$[\text{Cu}(4\text{-CNpy})(\text{Memal})(\text{H}_2\text{O})]_n$  (**20**). A methanolic solution ( $5 \text{ cm}^3$ ) of 4-cyanopyridine (1 mmol, 104 mg) was added dropwise to an aqueous solution ( $10 \text{ cm}^3$ ) of copper(II)-methylmalonate (1 mmol, 180 mg) under continuous stirring. The resulting deep blue solution was allowed to evaporate at room temperature. Prismatic blue single crystals appeared after a week when almost all the solution was evaporated. Crystallographic data of **20** are listed in Table II.7. Yield *ca.* 80 %. Anal. calc. for  $\text{C}_{10}\text{H}_{10}\text{CuN}_2\text{O}_5$  (**20**): C, 39.80; H, 3.34; N, 9.28; Found: C, 39.97; H, 3.58; N, 9.34 %.

**Table II.7.** Crystallographic data for complex **20**

| <b>20</b>                               |                                                                    |
|-----------------------------------------|--------------------------------------------------------------------|
| Formula                                 | $\text{C}_{10}\text{H}_{10}\text{O}_5\text{N}_2\text{Cu}$          |
| FW                                      | 301.74                                                             |
| Crystal system                          | Orthorhombic                                                       |
| Space group                             | $Pna2_1$                                                           |
| $a/\text{\AA}$                          | 24.3070(5)                                                         |
| $b/\text{\AA}$                          | 7.1150(8)                                                          |
| $c/\text{\AA}$                          | 7.1150(18)                                                         |
| $V/\text{\AA}^3$                        | 1230.5(3)                                                          |
| $Z$                                     | 4                                                                  |
| $\mu(\text{Mo K}\alpha)/\text{cm}^{-1}$ | 17.89                                                              |
| $T/\text{K}$                            | 293(2)                                                             |
| $\rho_{\text{calc}}/\text{g cm}^{-3}$   | 1.629                                                              |
| $\lambda/\text{\AA}$                    | 0.71073                                                            |
| Index ranges                            | $-27 \leq h \leq 26,$<br>$-7 \leq k \leq 8,$<br>$-7 \leq l \leq 8$ |
| Indep. reflect. ( $R_{\text{int}}$ )    | 1867 (0.0406)                                                      |
| Obs. reflect. [ $I > 2\sigma(I)$ ]      | 1497                                                               |
| Flack parameter                         | 0.48(5)                                                            |
| Parameters                              | 196                                                                |
| Goodness-of-fit                         | 1.082                                                              |
| $R [I > 2\sigma(I)]$                    | 0.0346                                                             |
| $R_w [I > 2\sigma(I)]$                  | 0.0679                                                             |
| $R$ (all data)                          | 0.0568                                                             |
| $R_w$ (all data)                        | 0.0749                                                             |



### II.3.3. Description of the Structure

The crystal structure of  $[\text{Cu}(4\text{-CNpy})(\text{Memal})(\text{H}_2\text{O})]_n$  (**20**; Figure II.11) consists of a sheet-like arrangement of *trans*-aqua(4-cyanopyridine)copper(II) units bridged through methylmalonate ligands which are extended in the *bc* plane (Figure II.12). The structure of the layer is very similar to that of complexes **17-19** and hence, reminiscent of compounds **2-12** of Chapter I. The copper(II) ions are linked by *anti-syn* carboxylate bridges building a corrugated square grid which presents the 4-CNpy ligands alternatively located above and below the layer. The sheets are stacked along the *a* axis with the odd layers rotated by  $180^\circ$  exhibiting the *ABABAB* sequence (Figure II.13). The presence of weak cyano-cyano interactions contributes to the stabilization of the layered structure. The cyano groups of 4-CNpy ligands of adjacent layers are symmetry related through the operation  $1-x, -1-y, -0.5-z$  and they exhibit a parallel arrangement with the distances from the midpoints of the C–N bonds being  $3.8010(9)$  Å and the angle  $\text{C}^{(1)}\text{-N}^{(1)}\cdots\text{C}^{(2)}$  being  $84.99(10)^\circ$ . These values are in agreement with those reported for carbonyl-carbonyl interactions.<sup>1</sup> Weak intralayer hydrogen-bonds are also present involving the coordinated water molecule and oxygen atoms from the Memal ligand [ $\text{O}(1\text{w})\cdots\text{O}(2)$  and  $\text{O}(1\text{w})\cdots\text{O}(4)$  distances are  $2.604(13)$  and  $2.789(13)$  Å, respectively].

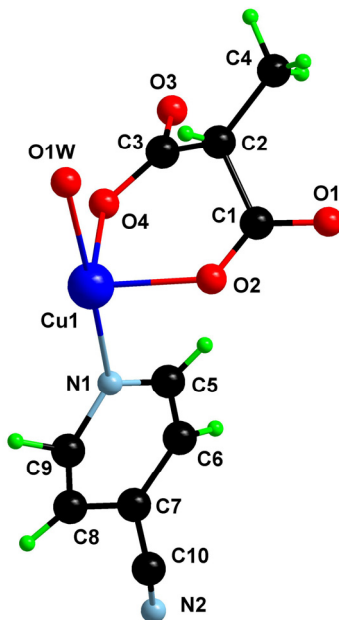
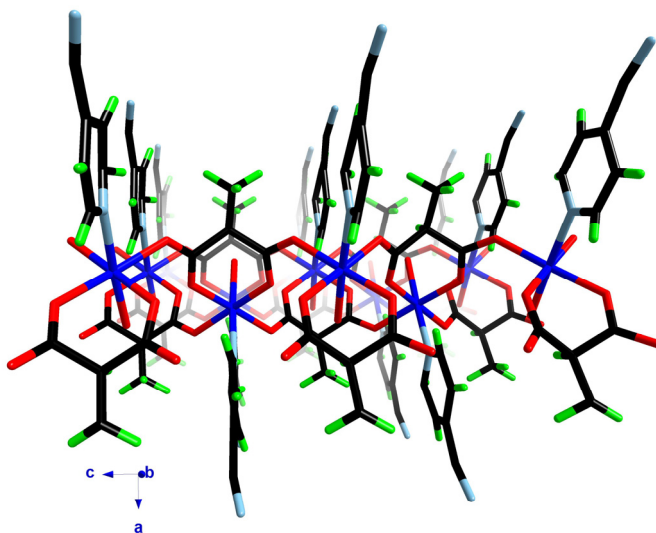


Fig. II.11. A view of the asymmetric unit of compound **20** with the numbering scheme.



**Fig. II.12.** Central projection of one layer of carboxylate-bridged square grid of copper(II) ions viewed along the *b* axis.

Each copper atom exhibits a distorted octahedral (4+2) environment with the parameters  $s/h$  and  $\phi$  being 1.31 and  $56.4^\circ$ , respectively (values for a ideal octahedron being  $s/h = 1.22$  and  $\phi = 60^\circ$ ).<sup>2</sup> Four oxygen atoms from three different methylmalonate ligands build the basal plane [average bond distance being 2.019(10) Å] whereas a nitrogen atom from a 4-CNpy ligand and a water molecule occupy the axial positions [Cu(1)–N(1) and Cu(1)–O(1w) distances are 2.237(3) and 2.323(5) Å; see Table II.8]. The methylmalonate ligand acts simultaneously as bidentate [through O(2) and O(4), with the angle subtended at the copper atom being  $87.83(13)^\circ$ ] and bis-monodentate ligand [through O(1) and O(3)]. Although there are two crystallographically different carboxylate bridges within the layers [O(2)–C(1)–O(1) and O(4)–C(3)–O(3)], the copper-copper separation through these two bridges is the same [5.227(3) Å].

Let us now compare this structure with the previously described for the complex [Cu(4-CNpy)(Phmal)]<sub>n</sub> (**5**) (Section I.3). In a general picture, both structures look very similar but they present a few notable differences. First of all, the layers are packed closer in **20** than in the Phmal complex, the shortest copper-copper separations being 11.320(2) and 13.985(8) Å, respectively. The copper environment is octahedral in **20** whereas it is square-pyramidal in **5**, because a water molecule is involved in the copper coordination environment of **20**. This can be explained attending to the location of the malonate skeleton respect to the basal plane of the copper atom (see Figure II.14), the angle between the plane

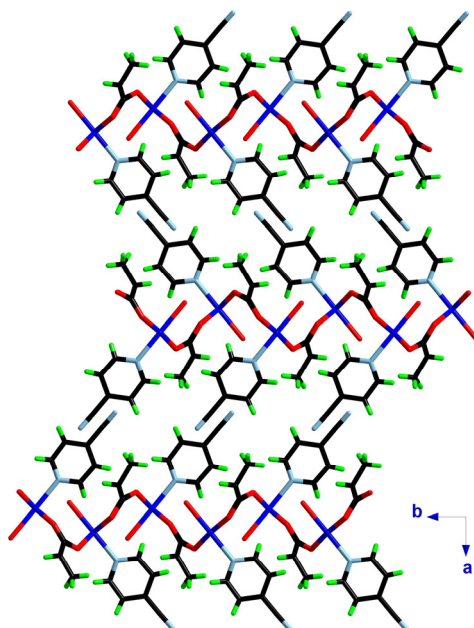


**Fig. II.13.** Perspective view of the crystal packing of complex **20** along the *c* axis. Interlayer contacts among adjacent layers occur between the cyano groups of the 4-cyanopyridine ligands.

build by the four oxygen atoms of the bidentate malonate and the basal plane at the copper atom being  $2.6(2)^\circ$  and  $28.6(1)^\circ$  for **20** and **5**, respectively. The aromatic ring of the phenylmalonate ligand in **5** participates of  $\pi$ -type interactions in the interlayer space bending the malonate skeleton to adopt the correct position. Another interesting difference fully connected with the previous discussion is the dihedral angle between the basal planes of adjacent copper atoms within the layers being  $85.45(19)^\circ$  for **20** and  $71.725(14)^\circ$  for **5**.

**Table II.8.** Selected bond angles ( $^\circ$ ) and lengths ( $\text{\AA}$ ) for **20**.

| <b>20</b>         |           |                   |           |
|-------------------|-----------|-------------------|-----------|
| Cu(1)–O(1a)       | 2.052(10) | O(2)–Cu(1)–O(3b)  | 88.8(4)   |
| Cu(1)–O(2)        | 2.031(10) | O(2)–Cu(1)–O(4)   | 87.83(13) |
| Cu(1)–O(3b)       | 2.011(9)  | O(2)–Cu(1)–N(1)   | 90.3(4)   |
| Cu(1)–O(4)        | 1.983(9)  | O(2)–Cu(1)–O(1w)  | 92.0(4)   |
| Cu(1)–N(1)        | 2.237(3)  | O(3b)–Cu(1)–O(4)  | 174.6(4)  |
| Cu(1)–O(1w)       | 2.323(5)  | O(3b)–Cu(1)–N(1)  | 85.6(4)   |
| O(1a)–Cu(1)–O(2)  | 175.0(4)  | O(3b)–Cu(1)–O(1w) | 96.1(4)   |
| O(1a)–Cu(1)–O(3b) | 93.38(11) | O(4)–Cu(1)–N(1)   | 90.2(4)   |
| O(1a)–Cu(1)–O(4)  | 89.6(4)   | O(4)–Cu(1)–O(1w)  | 88.3(4)   |
| O(1a)–Cu(1)–N(1)  | 85.4(4)   | N(1)–Cu(1)–O(1w)  | 177.2(5)  |
| O(1a)–Cu(1)–O(1w) | 92.2(4)   |                   |           |

<sup>a</sup> Symmetry operations: (a) =  $-x + 3/2, y + 1/2, z - 1/2$ ; (b) =  $-x + 3/2, y + 1/2, z + 1/2$ .

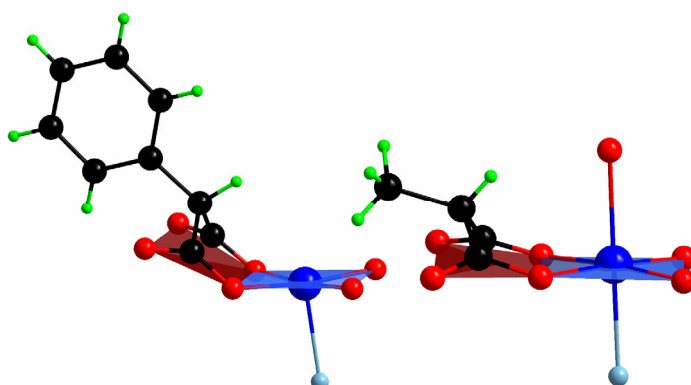


**Fig. II.14.** Comparative view between the Phmal- (left) and Memal- (right) copper(II) complexes with 4-cyanopyridine ligands: the blue plane represents the basal plane of the copper(II) environment and the red one correspond to the plane defined by the oxygen atoms of the R-mal ligand.

### II.3.4. Magnetic Properties

The magnetic properties of complex **20** are displayed in Figure II.15 under the form of a  $\chi_M T$  vs  $T$  plot [ $\chi_M$  being the magnetic susceptibility per copper(II) ion]. The room temperature value for the  $\chi_M T$  product is  $0.48 \text{ cm}^3 \text{ mol}^{-1} \text{ K}$ , and it is as expected for a magnetically isolated spin doublet. This value remains almost constant on cooling until 20 K and further smoothly increases to reach a maximum value of  $0.68 \text{ cm}^3 \text{ mol}^{-1} \text{ K}$  at 2.0 K. The magnetization curve lies slightly over the theoretical Brillouin curve for an isolated  $S = 1/2$  (Figure II.16). All these features are indicative of the presence of weak ferromagnetic interactions in this complex.

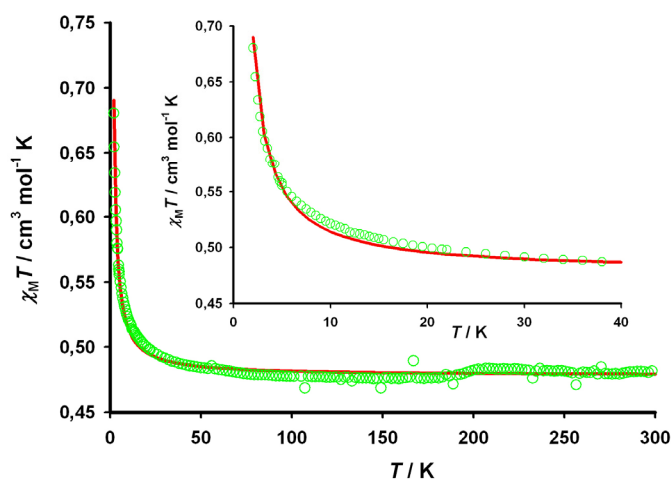


**Fig. II.15.** Thermal dependence of the  $\chi_M T$  product for complex **20** under applied fields of 1 T ( $T > 15$  K) and 0.1 T ( $T < 15$  K): (o) experimental data, (—) best fit curve. The inset shows a detail of the low temperature region.

From a magnetic point of view, the structure of **20** consists of a square grid of copper(II) ions which linked through *anti-syn* equatorial-equatorial carboxylate bridges. Although there are two crystallographically different carboxylate pathways, as a first approximation we can assign to them a unique magnetic exchange coupling ( $J$ ). Thus, the experimental magnetic data can be analyzed by means of the high-temperature expansion series derived from the two-dimensional Heisenberg model for a  $S = 1/2$  ferromagnetic square lattice.<sup>3</sup>

$$\chi_M = [Ng^2\beta^2/(3kT)] \cdot S(S+1) \cdot \left(1 + \sum_{n=1}^{10} a_n K^n\right)$$

where  $K = J/kT$ ,  $a_n$  are the coefficients for the square lattice and  $J$  is the intralayer magnetic coupling between the local spins of the nearest-neighbours with the Hamiltonian defined as:

$$\hat{H} = -J \sum_i \hat{S}_i \cdot \hat{S}_{i+1}$$

The best fit using non-linear regression analysis gives  $J = +0.25(2) \text{ cm}^{-1}$ ,  $g = 2.258(3)$  and  $R = 1.0 \times 10^{-4}$ . The calculated curve matches the experimental data in the whole temperature range with a slight deviation in the low temperature regime (see inset of Figure II.15). This agreement supports the assumption that the two carboxylate-bridges are structurally enough similar to be given by a unique coupling parameter  $J$ . The deviation could be explained taking into account weak interlayer magnetic interactions which could be operative at these temperatures.

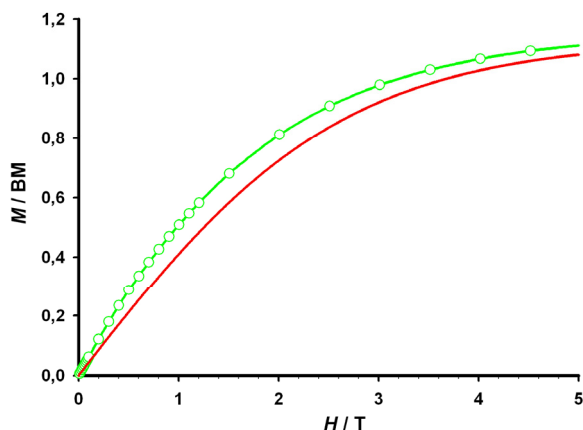


Fig. II.16.  $M$  vs  $H$  curve (green) together with the Brillouin function for a magnetically isolated spin doublet (red line).

The analysis of the magnetic data reveals that compound **20** exhibits a weak ferromagnetic coupling which is in agreement with those reported for *anti-syn* carboxylate

bridges linking equatorial positions at the copper(II) environments.<sup>4-5</sup> The relative small coupling compared with similar complexes as [Cu(Memal)(H<sub>2</sub>O)] (**17**) or [Cu(4-CNpy)(Phmal)] (**5**) is explained on the basis of the long equatorial bonds at the copper(II) environment in **20** [mean O(eq)-Cu bond distance is 2.019(10) Å] which are longer than those of **16** and **5**.

### II.3.5. Conclusion

The structure of **20** is similar to that of the related phenylmalonate complex [Cu(4-CNpy)(Phmal)]<sub>n</sub> (**5**) and it consists of square grids of carboxylate bridge copper(II) ions. However, a water molecule has entered in the coordination sphere of the copper atoms leading to a 4+2 octahedral coordination mode in **20**; moreover, the interlayer spacing is shorter in **20**. Compound **20** exhibits ferromagnetic coupling within the layers as occurs in [Cu(Memal)(H<sub>2</sub>O)]<sub>n</sub> (**17**). The magnitude of the interaction is smaller than that of **5** and **17**, due to the longer equatorial bonds present in **20**.

### II.3.6. References

- 1 F. H. Allen, C. A. Baalham, J. P. M. Lommerse and P. R. Raithby, *Acta Cryst. Sect. B*, **1998**, *B54*, 320.
- 2 E. I. Stiefel and G. F. Brown, *Inorg. Chem.*, **1972**, *11*, 434.
- 3 R. Navarro, *Application of High- and Low-Temperature Series Expansions to Two-dimensional Magnetic Systems*, de Jongh, L. J.; Ed., Kluwer Academic Publishers, The Netherlands, **1990**.
- 4 A. Rodríguez-Forteza, P. Alemany, S. Álvarez and E. Ruiz, *Chem. Eur. J.* **2001**, *7*, 627.
- 5 J. Pasán, F. S. Delgado, Y. Rodríguez-Martín, M. Hernández-Molina, C. Ruiz-Pérez, J. Sanchiz, F. Lloret and M. Julve, *Polyhedron* **2003**, *22*, 2143.

## II.4. 3-Iodopyridine (21) and 2,4'-bipyridine (22) Copper(II)-Methylmalonate complexes

### II.4.1. Introduction

The investigation of the differences caused by changing the substituent in the malonate ligand continues with the introduction of the 3-iodopyridine (3-Ipy) and 2,4'-bipyridine (2,4'-bpy) ligands. We have selected the 3-Ipy coligand to make a comparison with the halogen-pyridine group of the Section 1.5 in the previous chapter (complexes **8-11**), whereas the 2,4'-bpy group was used attempting to reproduce the anomalous structural features (static pseudo Jahn-Teller distortion) present in the  $[\text{Cu}(2,4'\text{-bpy})(\text{Phmal})(\text{H}_2\text{O})]_n$  (**12**) complex. The formation of isolated carboxylate-bridged square grids of copper(II) ions is expected, as well as the ferromagnetic interactions within the layers.

### II.4.2. Synthesis

**[Cu(3-Ipy)(Memal)(H<sub>2</sub>O)] (21).** A methanolic solution (5 cm<sup>3</sup>) of 3-Iodopyridine (1 mmol, 102 mg) was added dropwise to an aqueous solution (10 cm<sup>3</sup>) of copper(II)-methylmalonate (1 mmol) under stirring. The resulting blue solution was allowed to evaporate at room temperature. Prismatic deep blue single crystals appeared in the beaker after a few weeks, when almost all the solution has been evaporated. Yield *ca.* 60%. Anal. calc. for C<sub>9</sub>H<sub>10</sub>CuINO<sub>5</sub> (**21**): C, 26.85; H, 2.50; N, 3.48; Found: C, 26.97; H, 2.71; N, 3.56 %.

### **[Cu(2,4'-bpy)(Memal)(H<sub>2</sub>O)]·3H<sub>2</sub>O**

**(22).** An aqueous solution (5 cm<sup>3</sup>) of copper(II)-methylmalonate (0.5 mmol) was set in one arm of a water filled H-shape tube, while the other arm was filled with a methanolic solution (5 cm<sup>3</sup>) of 2,4'-bipyridine (0.5 mmol, 156 mg). Deep blue needle crystals were grown after

**Table II.9.** Crystallographic data for complex **21-22**

|                                                    | <b>21</b>                                                       | <b>22</b>                                                         |
|----------------------------------------------------|-----------------------------------------------------------------|-------------------------------------------------------------------|
| Formula                                            | C <sub>9</sub> H <sub>10</sub> O <sub>5</sub> NIcu              | C <sub>14</sub> H <sub>20</sub> O <sub>8</sub> N <sub>2</sub> Cu  |
| FW                                                 | 402.61                                                          | 407.86                                                            |
| Crystal system                                     | Monoclinic                                                      | Monoclinic                                                        |
| Space group                                        | <i>P</i> 2 <sub>1</sub> / <i>n</i>                              | <i>P</i> 2 <sub>1</sub> / <i>n</i>                                |
| <i>a</i> /Å                                        | 8.5874(13)                                                      | 17.375(4)                                                         |
| <i>b</i> /Å                                        | 7.1738(14)                                                      | 7.3305(14)                                                        |
| <i>c</i> /Å                                        | 19.093(5)                                                       | 14.247(3)                                                         |
| $\beta$ /°                                         | 99.509(15)                                                      | 111.409(15)                                                       |
| <i>V</i> /Å <sup>3</sup>                           | 1160.0(4)                                                       | 1689.4(6)                                                         |
| <i>Z</i>                                           | 4                                                               | 4                                                                 |
| $\mu(\text{Mo K}\alpha)$ /cm <sup>-1</sup>         | 45.52                                                           | 13.38                                                             |
| <i>T</i> /K                                        | 293(2)                                                          | 293(2)                                                            |
| $\rho_{\text{calc}}$ /g cm <sup>-3</sup>           | 2.294                                                           | 1.604                                                             |
| $\lambda$ /Å                                       | 0.71073                                                         | 0.71073                                                           |
| Index ranges                                       | -8 ≤ <i>h</i> ≤ 9,<br>-7 ≤ <i>k</i> ≤ 7,<br>-20 ≤ <i>l</i> ≤ 17 | -22 ≤ <i>h</i> ≤ 22,<br>-9 ≤ <i>k</i> ≤ 9,<br>-15 ≤ <i>l</i> ≤ 18 |
| Indep. reflect. ( <i>R</i> <sub>int</sub> )        | 1346 (0.0566)                                                   | 3234 (0.0803)                                                     |
| Obs. reflect. [ <i>I</i> > 2σ( <i>I</i> )]         | 1069                                                            | 1879                                                              |
| Parameters                                         | 149                                                             | 306                                                               |
| Goodness-of-fit                                    | 1.086                                                           | 1.026                                                             |
| <i>R</i> [ <i>I</i> > 2σ( <i>I</i> )]              | 0.0364                                                          | 0.0663                                                            |
| <i>R</i> <sub>w</sub> [ <i>I</i> > 2σ( <i>I</i> )] | 0.0585                                                          | 0.0839                                                            |
| <i>R</i> (all data)                                | 0.0573                                                          | 0.1420                                                            |
| <i>R</i> <sub>w</sub> (all data)                   | 0.0635                                                          | 0.1009                                                            |

one month at room temperature. Crystallographic details for compounds **21** and **22** are listed in Table II.9. Yield *ca.* 40 %. Anal. calc. for  $C_{14}H_{20}CuN_2O_8$  (**22**): C, 41.23; H, 4.94; N, 6.87; Found: C, 41.33; H, 5.09; N, 6.98 %.

### II.4.3. Description of the Structure

The structures of the compounds **21** and **22** (Figure II.17) consist of zigzag chains of *anti-syn* carboxylate-bridged copper(II) ions running along the *b* direction (Figure II.18). The pyridine-like ligands occupy one equatorial position of the copper environment avoiding the formation of the sheet-like arrangement observed in complexes **17-20**.

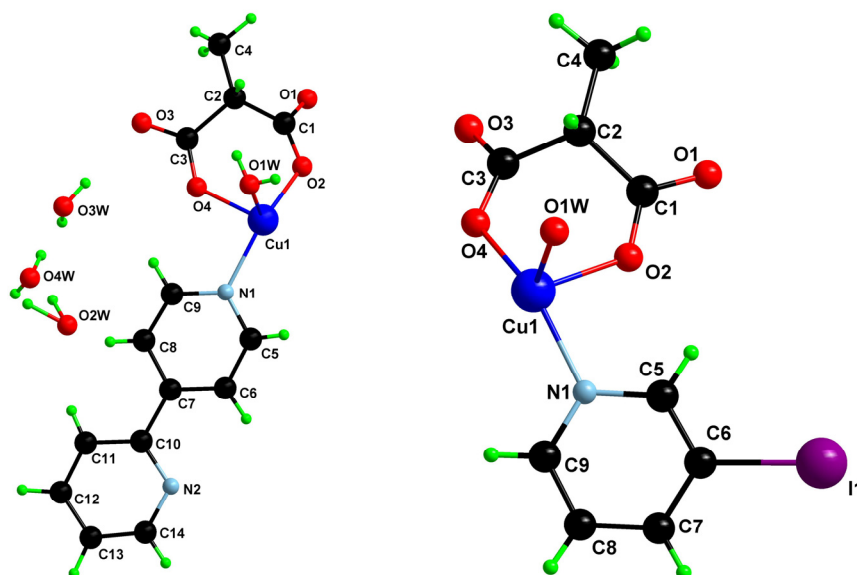
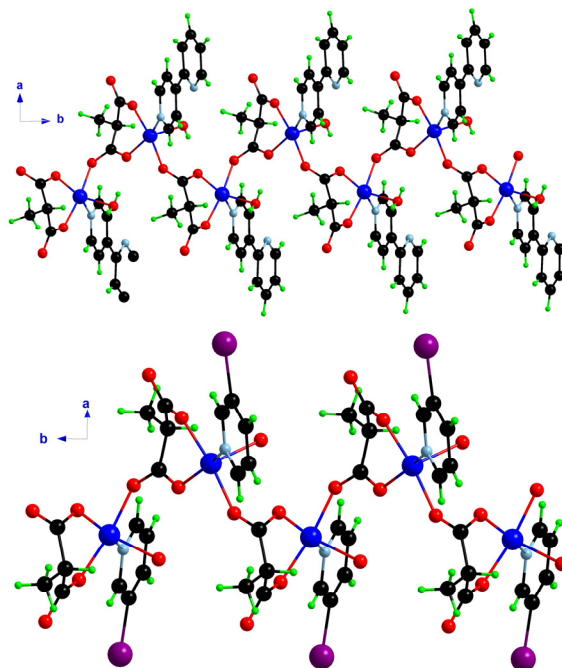


Fig. II.17. A view of the asymmetric unit for complexes **21** (left) and **22** (right) along with the numbering scheme.

The chains are grouped together in hydrophilic layers [which grow in the (001) (**21**) and (101) (**22**) planes] through hydrogen bonds involving the coordinated water molecule and coordinated and uncoordinated methylmalonate oxygen atoms [ $O\cdots O$  distances ranging from 2.677(7) to 2.729(7) Å]. The layers are pillared through the 3-Ipy (**21**) and 2,4'-bpy (**22**) ligands (Figure II.19) which are stacked through  $\pi$ - $\pi$  interactions (Figure II.20) involving alternatively aromatic ligands from two adjacent chains. The two different separations between centroids of the 3-iodopyridine rings in **21** are 3.5371(7) and 3.6610(7) Å, whereas the off-set angles are 20.39(15)° and 23.23(15)°. These values are in agreement



with those observed in pyridine-like ligands.<sup>1</sup> This is also true for the centroid–centroid distances [3.5689(7) and 3.8702(7) Å] and off-set angles [values ranging from 16.64(11)° to 28.66(11)°] between the 2,4'-bipyridine ligands in **22**. The pillared 2D sheets create interlayer 1D channels which are very small in **21** due to the small 3-iodopyridine ligand and the presence of the halogen atom, but large enough in **22** to include crystallization water molecules. These water molecules build a T5(2) pattern (following the nomenclature by Infantes *et al*)<sup>2,3</sup> which is one of the most frequent tape motifs (Figure II.21).<sup>3</sup> The water pentagons exhibit a half-chair conformation with an axial length of the tape [distance between lower and upper atoms] of 6.939(9) Å. The water tape is anchored to the host through hydrogen bonds between a water molecule [O(3w)] from the tape acting as donor and an uncoordinated methylmalonate oxygen atom [O(3)] as acceptor. Selected H-bond distances and angles are listed in Table II.10.



**Fig. II.18.** A view of the carboxylate bridged copper(II) chains of **21** (up) and **22** (bottom). Despite the different ligands, structurally the chains of both compounds are very similar.

Each copper atom in **21** and **22** exhibits a distorted square pyramidal environment [the  $\tau$  value<sup>4</sup> being 0.31 (**21**) and 0.32 (**22**)]. This feature is mainly due to steric effects of the 3-Ipy and 2,4'-bpy groups which one located in equatorial positions. Three oxygen atoms from two different methylmalonate ligands [O(2), O(3) and O(4)] and a nitrogen atom from

a N-donor ligand [N(1)] build the basal plane. The average values of the Cu(1)-O(eq) bond are 1.952(5) for **21** and 1.950(3) Å for **22**, whereas those of Cu(1)-N are 2.040(6) Å (**21**) and 2.030(4) Å for (**22**). The apical position is filled by a water molecule [O(1w)], the Cu(1)-O(1w) bond distances being 2.205(5) (**21**) and 2.233(5) Å (**22**). The methylmalonate ligands act simultaneously as bidentate [through O(2) and O(4) with the angles subtended at the copper atom being 89.6(2)° (**21**) and 89.47(13)° (**22**)] and monodentate ligands [through O(3) in **21** and O(1) in **22**].

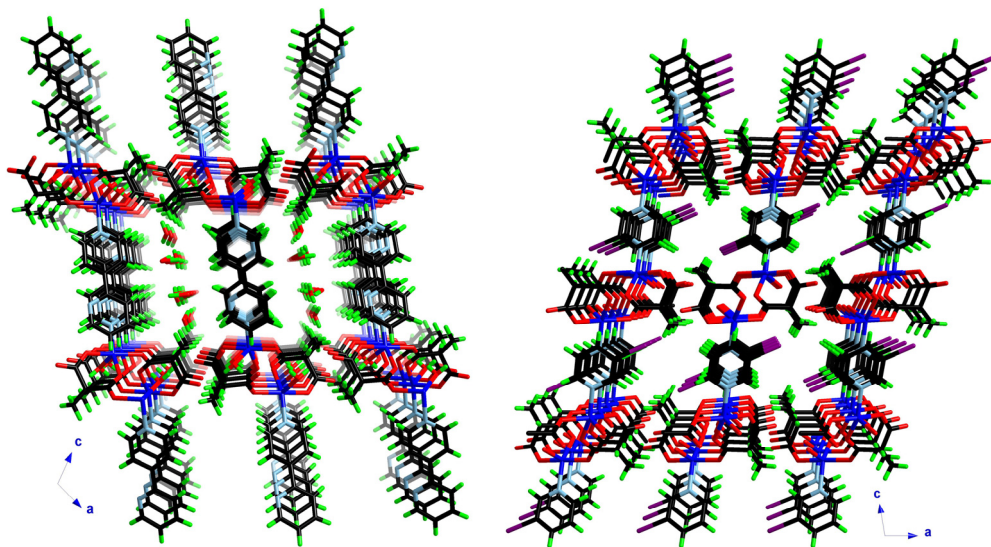


**Fig. II.19.** Central projection of the crystal packing for **21** (left) and **22** (right) along the *b* axis. The figures show the  $\pi$  stacking among the coligands and the crystallization water molecules which fill the channels of **21**.

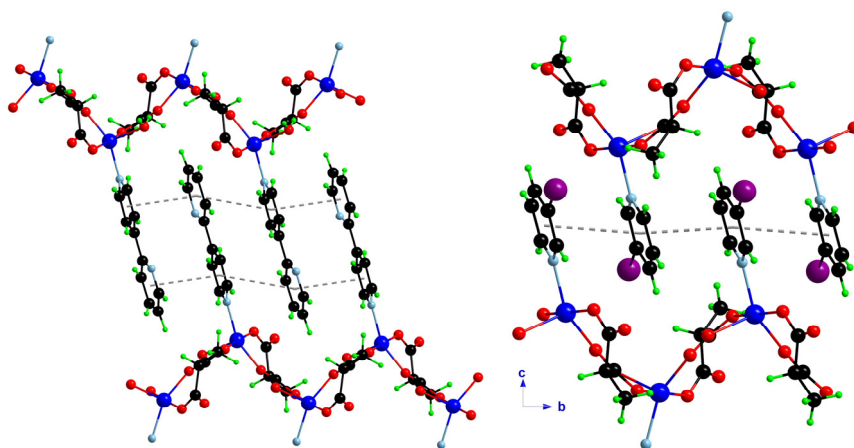


**Fig. II.20.**  $\pi$ - $\pi$  stacking among the 2,4'-bipyridine molecules in **21** (left) and among the 3-iodopyridine groups in **22** (right). The dashed lines correspond to the centroid-centroid vectors.

**Table II.10.** Hydrogen bond distances and angles in **21**

| D–H···A                      | O–H (Å)  | H···O (Å) | O–H···O (°) | O···O (Å) |
|------------------------------|----------|-----------|-------------|-----------|
| <i>T5(2) tape</i>            |          |           |             |           |
| O(2w)–H···O(4W)              | 1.00(6)  | 1.90(6)   | 156(5)      | 2.850(7)  |
| O(3w)–H···O(2W)              | 0.85(8)  | 2.09(9)   | 166(7)      | 2.922(8)  |
| O(4w)–H···O(2W)              | 0.68(7)  | 2.18(7)   | 160(6)      | 2.841(8)  |
| O(4w)–H···O(3W)              | 0.95(7)  | 1.88(7)   | 176(6)      | 2.837(8)  |
| <i>Anchorage of the tape</i> |          |           |             |           |
| O(3w)–H···O(3)               | 0.82(8)  | 2.04(8)   | 171(7)      | 2.854(8)  |
| <i>Other H-bonds</i>         |          |           |             |           |
| O(1w)–H···O(2)               | 0.69(10) | 2.18(8)   | 136(9)      | 2.730(6)  |
| O(1w)–H···O(3)               | 0.78(9)  | 2.01(8)   | 158(9)      | 2.748(6)  |

The intrachain copper-copper separation in **21** through the *anti-syn* carboxylate bridge [5.1638(16) Å] is shorter than the interchain ones [the shortest separations being 6.671(2) Å between chains separated by the 3-iodopyridine ligand and 8.0206(16) Å between H-bonded chains]. A similar situation is observed in **22** where the intrachain separation between the copper atoms through the *anti-syn* carboxylate bridge is 5.0432(12) Å while the shortest interchain separations are 7.490(2) (between H-bonded chains) and 10.067(2) Å (between chains separated by the 2,4'-bipyridine ligand).

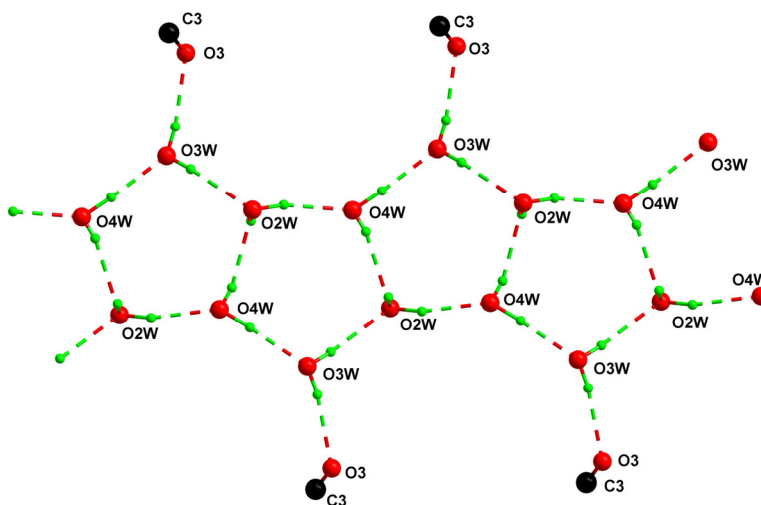


**Fig. II.21.** T5(2) pattern formed by the crystallization water molecules in the compound **21** with the numbering scheme.

Let us finish this structural description with a comparison of these structures with those synthesized with malonato or phenylmalonato-carboxylate ligands. The location of the 3-iodopyridine ligand in an equatorial position at the copper(II) environment avoids the formation of the carboxylate-bridged copper(II) layers of [Cu(3-Ipy)(Phmal)]<sub>n</sub> (**11**). The

same feature occurs with the 2,4'-bpy ligand and hence, the layers observed in  $[\text{Cu}(2,4'\text{-bpy})(\text{Phmal})(\text{H}_2\text{O})]_n$  (**12**) could not be reproduced in **22**. In the case of the malonic acid, there are not complexes with the 3-Ipy ligand to our knowledge, but several compounds with the 2,4'-bpy ligand were reported.<sup>5,6</sup> A manganese(II) complex<sup>5</sup> with similar layers as those formed in **12** (see Section I.6.2) and a copper(II) compound<sup>6</sup> exhibiting a copper environment similar to that of **22** where the 2,4'-bpy ligand occupies an equatorial position and a water molecule fills the apical one. However, the chains of **22** are bent in the malonate-containing complex to form isolated tetranuclear entities with the copper atoms in the corners, the malonate ligands in the edges and the 2,4'-bpy ligands like arms pointing outwards the unit.

**Table II.11.** Selected bond angles (°) and lengths (Å) for **21** and **22**.

| <b>21</b>                |            |                   |            |
|--------------------------|------------|-------------------|------------|
| Cu(1)–O(2)               | 1.931(5)   | O(2)–Cu(1)–O(1w)  | 94.77(19)  |
| Cu(1)–O(3a) <sup>a</sup> | 1.966(5)   | O(3a)–Cu(1)–O(4)  | 86.1(2)    |
| Cu(1)–O(4)               | 1.959(5)   | O(3a)–Cu(1)–N(1)  | 91.2(2)    |
| Cu(1)–N(1)               | 2.040(6)   | O(3a)–Cu(1)–O(1w) | 93.14(19)  |
| Cu(1)–O(1w)              | 2.205(5)   | O(4)–Cu(1)–N(1)   | 153.1(2)   |
| O(2)–Cu(1)–O(3a)         | 171.9(2)   | O(4)–Cu(1)–O(1w)  | 109.3(2)   |
| O(2)–Cu(1)–O(4)          | 89.6(2)    | N(1)–Cu(1)–O(1w)  | 97.6(2)    |
| O(2)–Cu(1)–N(1)          | 89.5(2)    |                   |            |
| <b>22</b>                |            |                   |            |
| Cu(1)–O(1b)              | 1.973(3)   | O(1b)–Cu(1)–O(1w) | 99.79(19)  |
| Cu(1)–O(2)               | 1.949(3)   | O(2)–Cu(1)–O(4)   | 89.47(13)  |
| Cu(1)–O(4)               | 1.927(3)   | O(2)–Cu(1)–N(1)   | 152.76(16) |
| Cu(1)–N(1)               | 2.030(4)   | O(2)–Cu(1)–O(1w)  | 107.20(19) |
| Cu(1)–O(1w)              | 2.233(5)   | O(4)–Cu(1)–N(1)   | 90.36(15)  |
| O(1b)–Cu(1)–O(2)         | 85.37(14)  | O(4)–Cu(1)–O(1w)  | 87.90(19)  |
| O(1b)–Cu(1)–O(4)         | 171.73(14) | N(1)–Cu(1)–O(1w)  | 100.01(19) |
| O(1b)–Cu(1)–N(1)         | 91.27(15)  |                   |            |

<sup>a</sup> Symmetry operations: (a) =  $-x + 1/2, y + 1/2, -z + 1/2$ ; (b) =  $-x + 1/2, y + 1/2, -z + 3/2$ .

#### II.4.4. Magnetic Properties

The magnetic properties of the compounds **21** and **22** under the form of  $\chi_M T$  vs.  $T$  plot ( $\chi_M$  being the molar susceptibility per copper(II) ion) are shown in Figure II.22. The  $\chi_M T$  values at room temperature are 0.48 and 0.46  $\text{cm}^3 \text{mol}^{-1} \text{K}$  for **21** and **22**, respectively. These values are as expected for a magnetically isolated spin doublet. Upon cooling,  $\chi_M T$  smoothly increases and in a sharply way at  $T < 20 \text{ K}$  to reach values of 1.13 (**21**) and 1.10  $\text{cm}^3 \text{mol}^{-1} \text{K}$  (**22**) at 2.0 K. The magnetization ( $M$ ) vs. the applied magnetic field ( $H$ ) plots for both compounds, which are depicted in Figure II.23, are clearly above the theoretical Brillouin curve for an isolated spin  $S = 1/2$ . The saturation of the magnetization is achieved for both

compounds at *ca.* 3.0 T. All these features are indicative of the presence of ferromagnetic interactions within the chains in **21** and **22**.

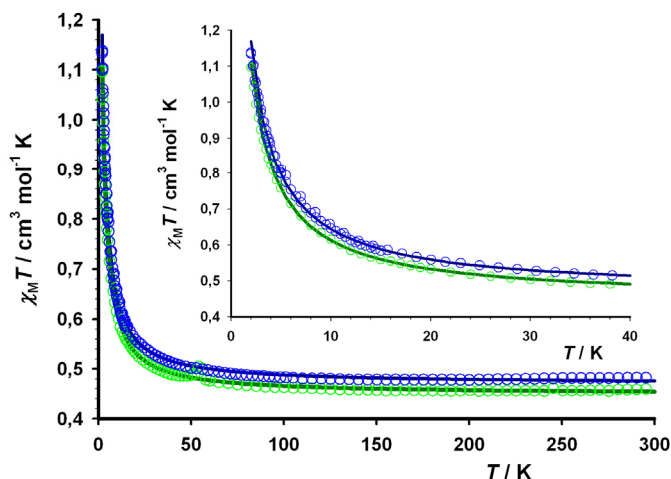


**Fig. II.22.**  $\chi_M T$  vs  $T$  plot for **21** (blue) under applied fields of 1 T ( $T > 15$  K) and 0.1 T ( $T < 15$  K) and **22** (green) under applied fields of 1 T ( $T > 20$  K), 0.1 T ( $20 > T > 15$  K) and 0.05 T ( $T < 15$  K): (o) experimental data, (—) best fit curve. The inset shows a detail of the low temperature region.

The structure of these compounds consists of chains of *anti-syn* carboxylate-bridged copper(II) ions with intrachain ferromagnetic interactions. Thus, the magnetic data are analysed by means of the numerical expression for a  $S = 1/2$  ferromagnetic uniform chain:<sup>7</sup>

$$\chi_M = (N\beta^2 g^2 / 4kT)(A/B)^{2/3}$$

$$A = 1.0 + 5.7979916 y + 16.902653 y^2 + 29.376885 y^3 + 29.832959 y^4 + 14.036918 y^5$$

$$B = 1.0 + 2.7979916 y + 7.0086780 y^2 + 8.6538644 y^3 + 4.5743114 y^4$$

$$\hat{H} = -J \sum_i \hat{S}_i \cdot \hat{S}_{i+1}$$

with  $y = J/2kT$ ,  $J$  is the intrachain magnetic coupling, and the other symbols have their usual meanings. Best least-squares fit parameters are:  $J = +2.66(2) \text{ cm}^{-1}$ ,  $g = 2.238(2)$  and  $R = 1.6 \times 10^{-5}$  for **21** and  $J = +2.62(2) \text{ cm}^{-1}$ ,  $g = 2.188(2)$  and  $R = 1.1 \times 10^{-5}$  for **22**. The calculated curves match very well the experimental data in the whole temperature range (Figure II.22). At the same time, the values of  $J$  are practically identical for the two compounds, in agreement with their structural similarity.

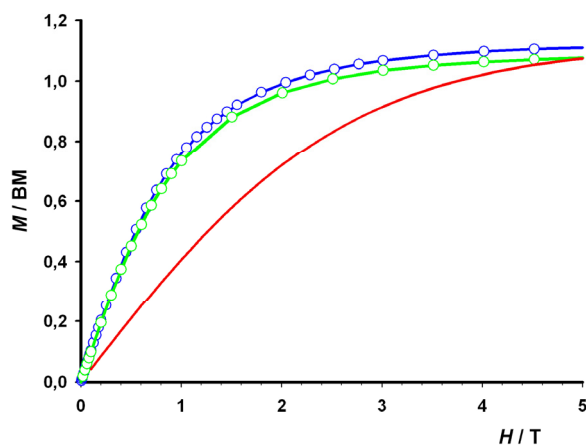


**Fig. II.23.**  $M$  vs  $H$  curve for **21** (green) and **22** (blue) together with the Brillouin function for a magnetically isolated spin doublet (red line).

The ferromagnetic nature of the magnetic interactions in **21** and **22** is in agreement with the data reported in the literature for the *anti-syn* equatorial-equatorial carboxylate bridge.<sup>8</sup> According to the Kahn's model, the magnetic coupling for two interacting copper(II) ions can be decomposed in two different contributions of opposite nature, the antiferromagnetic one being dependent on square of the overlap of the magnetic orbitals (the smaller the overlap is, the lower the AF term).<sup>9</sup> The magnetic orbitals at the copper atoms are of the  $d(x^2-y^2)$  type [the  $x$  and  $y$  axes roughly corresponding with the equatorial bonds of the copper environment] with some admixture of the  $dz^2$  character [the  $z$  axis being defined by the axial bond]. The angle between the basal planes of the magnetically coupled copper atoms are nearly orthogonal [ $84.76(12)^\circ$  and  $75.28(8)^\circ$  for **21** and **22**, respectively], then the overlap is reduced to a minimum and the ferromagnetic contribution becomes predominant.

The magnitude of the interaction can be explained having in mind some structural considerations. The carboxylate exchange pathways link two equatorial positions at the copper(II) ions. This conformation is more favourable to the magnetic coupling ( $J$  values ranging from  $+3.0$  to  $+23 \text{ cm}^{-1}$ )<sup>10-15</sup> than the equatorial-apical one. The large distortion of the square pyramidal environment in both compounds is responsible for the fact that the magnetic coupling constants for **21** and **22** lay in the lower limit of this range.

#### II.4.5. Conclusion

The structures of **21** and **22** do not correspond to the square grids of copper(II) ions which occur in the related phenylmalonate-containing complexes **11** and **12**. The pyridine

coligands are now occupying equatorial positions at the copper environment, being the resulting structure drastically modified. Complexes **21** and **22** consists of carboxylate-bridged chains of copper atoms which build a pillared two-dimensional (2D) supramolecular network by means of weak  $\pi \cdots \pi$  interactions and hydrogen bonds. The 3D network in **22** exhibits channels where water molecules are hosted, with a T5(2) pattern. Both compounds exhibit ferromagnetic interactions through the carboxylate exchange pathway.

The preference of the pyridine-like ligands for the equatorial position at the copper atom has been observed previously in this Thesis, for example in the complex **13** with the 4,4'-bipyridine as coligand. Thus, it is not surprising, although unexpected, that the square grids of copper atoms have turned into carboxylate-bridged chains due to the introduction of a terminal ligand in the basal plane of the copper atom environment.

#### II.4.6. References

- 1 C. Janiak, *Dalton Trans.* **2000**, 3885.
- 2 L. Infantes, J. Chisholm and S. Motherwell, *CrystEngComm* **2003**, 5(85), 480.
- 3 L. Infantes and S. Motherwell, *CrystEngComm* **2002**, 4(75), 454.
- 4 A. W. Addison, T. N. Rao, J. Reedijk, J. van Rijn and G. C. Verschoor, *Dalton Trans.* **1984**, 1349.
- 5 Y. Rodríguez-Martín, M. Hernández-Molina, J. Sanchiz, C. Ruiz-Pérez, F. Lloret and M. Julve, *Dalton Trans.* **2003**, 2359.
- 6 Y. Rodríguez-Martín, M. Hernández-Molina, F. S. Delgado, J. Pasán, C. Ruiz-Pérez, J. Sanchiz, F. Lloret and M. Julve, *CrystEngComm* **2002**, 4, 440.
- 7 G. A. Baker, G. S. Rushbrooke and H. E. Gilbert, *Phys. Rev.* **1964**, 135, A1272.
- 8 J. Pasán, F. S. Delgado, Y. Rodríguez-Martín, M. Hernández-Molina, C. Ruiz-Pérez, J. Sanchiz, F. Lloret and M. Julve, *Polyhedron* **2003**, 22, 2143.
- 9 O. Kahn, *Molecular Magnetism*, VCH, New York, **1993**.
- 10 C. Ruiz-Pérez, J. Sanchiz, M. Hernández-Molina, F. Lloret and M. Julve, *Inorg. Chem.* **2000**, 39, 1363.
- 11 C. Ruiz-Pérez, M. Hernández-Molina, P. Lorenzo-Luis, F. Lloret, J. Cano and M. Julve, *Inorg. Chem.* **2000**, 39, 3845.
- 12 Y. Rodríguez-Martín, C. Ruiz-Pérez, J. Sanchiz, F. Lloret and M. Julve, *Inorg. Chim. Acta* **2001**, 318, 159.
- 13 F. S. Delgado, J. Sanchiz, C. Ruiz-Pérez, F. Lloret and M. Julve, *Inorg. Chem.* **2003**, 42, 5938.
- 14 S. Sain, T. K. Maji, G. Mostafa, T. H. Lu and N. R. Chaudhuri, *New J. Chem.* **2003**, 27, 185.
- 15 J. Pasán, J. Sanchiz, C. Ruiz-Pérez, F. Lloret and M. Julve, *New J. Chem.* **2003**, 27, 1557.

## II.5. 2,2'-bipyrimidine (22) Copper(II)-Methylmalonate complexes

### II.5.1. Introduction

Once demonstrated that the presence of the methyl group in the methylmalonate ligand does not favour the formation of the square grids of carboxylate-bridged copper(II) ions as occurred with the phenylmalonate ligand, we plan to investigate the kind of structures which can arise when chelating coligands are used.

The 2,2'-bipyrimidine (2,2'-bipym) ligand is a chelating well known bridging coligand which is able to mediate from medium to strong antiferromagnetic interactions when acting as a bis-bidentate ligand.<sup>1,2</sup> Previous work with malonate and phenylmalonate ligands afforded crystal structures with different dimensionalities. Mononuclear and dinuclear structures have been reported for the mal-containing complexes,<sup>3</sup> whereas a chain is formed with the Phmal ligand (complex **14**).<sup>4</sup> Thus, the preparation of the related methylmalonate complex is necessary to investigate the influence of the methyl group in the structure.

### II.5.2. Synthesis

**[Cu<sub>2</sub>(2,2'-bipym)(Memal)<sub>2</sub>(H<sub>2</sub>O)<sub>2</sub>·3H<sub>2</sub>O (23)**. A methalonic solution (5 cm<sup>3</sup>) of 2,2'-bipyrimidine (0.5 mmol, 158 mg) was added dropwise to an aqueous solution (10 cm<sup>3</sup>) of copper(II)-methylmalonate (1 mmol) under continuous stirring. The resulting blue solution was allowed to evaporate at room temperature. Blue prismatic single crystals of **23** were grown after a few days. Crystallographic details are listed in Table II.12. Yield *ca.* 80%. Anal. calc. for C<sub>8</sub>H<sub>12</sub>CuN<sub>2</sub>O<sub>6</sub> (**23**): C, 32.49; H, 4.09; N, 9.47; Found: C, 32.54; H, 4.12; N, 9.34 %.

**Table II.12.** Crystallographic data for **23**

|                                                    |                                                                   |
|----------------------------------------------------|-------------------------------------------------------------------|
| Formula                                            | C <sub>8</sub> H <sub>12</sub> O <sub>6,5</sub> N <sub>2</sub> Cu |
| FW                                                 | 303.73                                                            |
| Crystal system                                     | Monoclinic                                                        |
| Space group                                        | C2/c                                                              |
| <i>a</i> / Å                                       | 15.057(4)                                                         |
| <i>b</i> / Å                                       | 7.250(2)                                                          |
| <i>c</i> / Å                                       | 19.958(4)                                                         |
| $\beta$ / °                                        | 91.23(7)                                                          |
| <i>V</i> / Å <sup>3</sup>                          | 2178.3(7)                                                         |
| <i>Z</i>                                           | 8                                                                 |
| $\mu$ (Mo K $\alpha$ ) /cm <sup>-1</sup>           | 20.31                                                             |
| <i>T</i> /K                                        | 293(2)                                                            |
| $\rho_{\text{calc}}$ /g cm <sup>-3</sup>           | 1.852                                                             |
| $\lambda$ / Å                                      | 0.71073                                                           |
| Index ranges                                       | -19 ≤ <i>h</i> ≤ 17,<br>-9 ≤ <i>k</i> ≤ 9,<br>-23 ≤ <i>l</i> ≤ 25 |
| Indep. reflect. (R <sub>int</sub> )                | 2392 (0.0258)                                                     |
| Obs. reflect. [ <i>I</i> > 2σ( <i>I</i> )]         | 2032                                                              |
| Parameters                                         | 214                                                               |
| Goodness-of-fit                                    | 1.153                                                             |
| <i>R</i> [ <i>I</i> > 2σ( <i>I</i> )]              | 0.0311                                                            |
| <i>R</i> <sub>w</sub> [ <i>I</i> > 2σ( <i>I</i> )] | 0.0677                                                            |
| <i>R</i> (all data)                                | 0.0420                                                            |
| <i>R</i> <sub>w</sub> (all data)                   | 0.0715                                                            |



### II.5.3. Description of the Structure

The structure of  $[\text{Cu}_2(2,2'\text{-bipym})(\text{Memal})_2(\text{H}_2\text{O})_2]\cdot 3\text{H}_2\text{O}$  (**23**, Figure II.24) consists of 2,2'-bipym bridged dinuclear entities and crystallization water molecules.

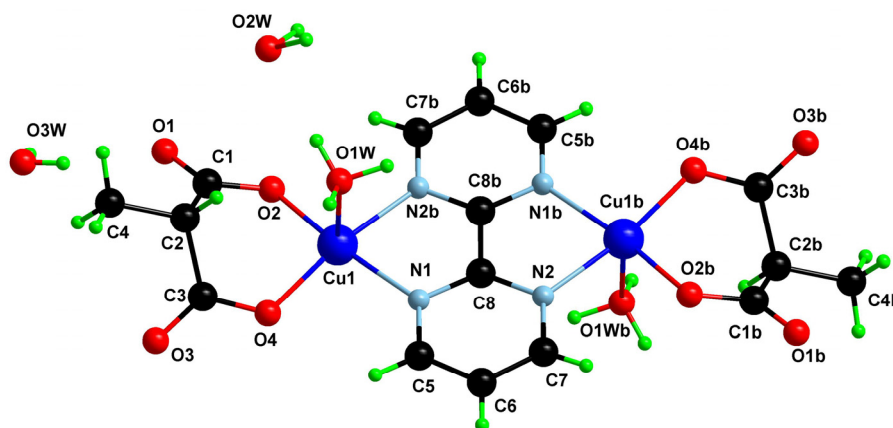


Fig. II.24. A view of a fragment of the structure of **23** with the numbering scheme.

The 2,2'-bipym bridged units are linked to form chains along the *b* direction through a very long  $\mu$ -oxo bridge involving the methylmalonate carboxylate oxygen atoms (Figure II.25). The dinuclear units are generated by an inversion centre located at the midpoint of the inter-ring carbon-carbon bond of the 2,2'-bipym ligand. The chains generate a supramolecular 2D network through H-bonds among the coordinated water molecules of adjacent chains. The interlayer space is filled with crystallization water molecules [O(2w) and O(3w)] linking the layers with an intricate H-bonded network involving the coordinated water molecules and the uncoordinated oxygen atoms from the malonate ligand [O $\cdots$ O distances ranging from 2.712(5) to 2.937(5) Å] (Figure II.26). The O(2w) water molecules are disordered in two symmetry related positions.<sup>5</sup>

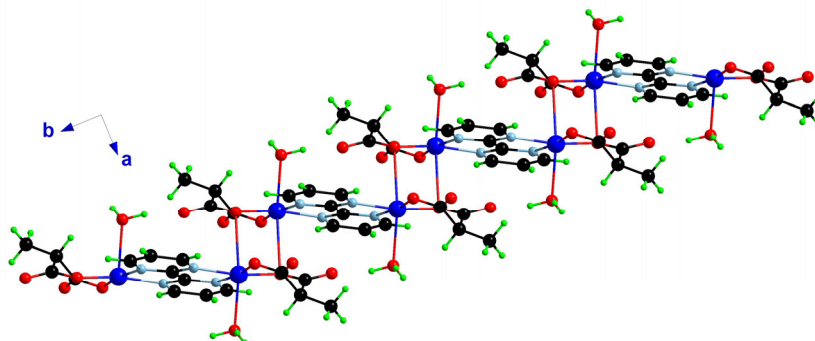
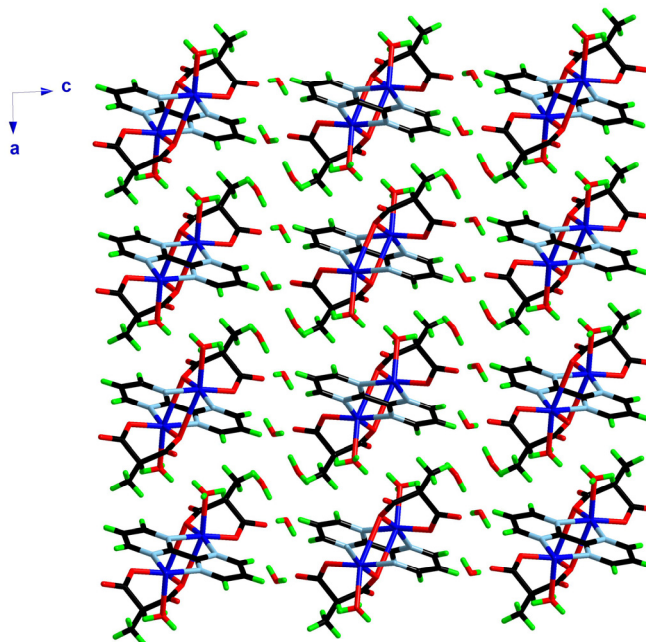


Fig. II.25. Perspective view of the  $\mu$ -oxo bridged chain of the dinuclear units of **23** running along the *b* axis.

Each copper atom can be considered basically as five-coordinated with a square pyramidal geometry [ $\tau$  value<sup>6</sup> being 0.032]. However the O(4a) [ $a = -x+1/2, -y+5/2, -z+1$ ] atom occupies the sixth coordination position leading to a 4+1+1\* type coordination [Cu(1)–O(4a) = 2.8641(17) Å]. Two methylmalonate oxygen atoms [O(2) and O(4)] and two nitrogen atoms from the 2,2'-bipym ligand [N(1) and the symmetry related N(2b);  $b = -x+1/2, -y+3/2, -z+1$ ] build the basal plane. The average equatorial bond distance is 1.976(2) Å, but the Cu–N(2,2'-bipym) bond distances are somewhat longer than the Cu–O(Memal) ones (see Table II.13). The apical position is occupied by a water molecule [Cu(1)–O(1w) 2.386(2) Å]. The copper atom is shifted towards O(1w) by 0.1303(3) Å. Finally, considering the octahedral environment with the O(1w) in O(4a) atoms in axial positions, the geometry is somewhat distorted, the O(1w)–Cu(1)–O(4a) angle being 161.44(6)°.



**Fig. II.26.** A view of the crystal packing of **23** along the  $b$  axis. Crystallization water molecules fill the intermolecular space.

The methylmalonate group acts as a bidentate ligand [through O(2) and O(4)], the angle subtended at the copper atom being 92.99(7)°. This angle for the bis(chelating) 2,2'-bipym is 81.49(6)°, the value of the bite distance N(1)⋯N(2b) being 2.655(2) Å. The dihedral angle between the basal plane of the copper environment and the mean plane of the 2,2'-bipym molecule is 4.72(5)°. The pyrimidyl rings of the 2,2'-bipym ligand are planar as occur with the ligand as a whole. The average Cu–N bond distance is 2.034(2) Å, a value

which is similar to that of other bipym-bridged dinuclear copper(II) complexes.<sup>7,8</sup> The copper-copper separation across the 2,2'-bipym ligand is 5.4512(4) Å, a value much longer than the shortest interdimer metal-metal separation through the long oxo-bridge [3.6764(3) Å].

**Table II.13.** Selected bond angles (°) and lengths (Å) for **23**.

| <b>23</b>                |            |                   |           |
|--------------------------|------------|-------------------|-----------|
| Cu(1)–O(2)               | 1.9108(17) | O(2)–Cu(1)–O(1w)  | 99.86(8)  |
| Cu(1)–O(4)               | 1.9245(15) | O(4)–Cu(1)–N(1)   | 94.25(7)  |
| Cu(1)–N(1)               | 2.0376(19) | O(4)–Cu(1)–N(2b)  | 168.90(8) |
| Cu(1)–N(2b) <sup>a</sup> | 2.0294(18) | O(4)–Cu(1)–O(1w)  | 97.52(8)  |
| Cu(1)–O(1w)              | 2.386(2)   | N(1)–Cu(1)–N(2b)  | 81.48(7)  |
| O(2)–Cu(1)–O(4)          | 93.00(7)   | N(1)–Cu(1)–O(1w)  | 84.36(8)  |
| O(2)–Cu(1)–N(1)          | 171.07(7)  | N(2b)–Cu(1)–O(1w) | 92.28(8)  |
| O(2)–Cu(1)–N(2b)         | 90.44(7)   |                   |           |

<sup>a</sup> Symmetry operations: (b) =  $-x + 1/2, -y + 3/2, -z + 1$ .

The structures of **23** and the related Phmal complex (**14**)<sup>4</sup> are very different since the 2,2'-bipym group acts as a terminal bidentate ligand in **14** and as a bis-chelating ligand in **23**. The structure of **14** consists of chains of carboxylate-bridged copper(II) ions. The Memal acts in **23** as a terminal ligand and, hence the polymerization is avoided as occurs in the related malonate-containing complex. Thus, let us compare the structure of **23** with that of the [Cu<sub>2</sub>(2,2'-bipym)(mal)<sub>2</sub>(H<sub>2</sub>O)<sub>2</sub>] $\cdot$ 4H<sub>2</sub>O complex.<sup>3</sup> Both dinuclear compounds are generated by an inversion centre located at the midpoint of then inter-ring C–C bond of the 2,2'-bipym ligand. The unique difference between them is the position of the crystallization water molecules which changes not only the supramolecular architectures they form, but the short intermolecular separation of **23**. The methyl group of the Memal ligand in **23** is the responsible factor for the different location of the crystallization water molecules. Along with the dinuclear complex, the reaction of malonic acid, 2,2'-bipym and copper(II) also yields a mononuclear compound which has been obtained from concentrated solutions due to its high solubility. Since the behaviour of the Memal resembles that of the malonate with the 2,2'-bipym as the coligand, we do not investigate the synthesis of the methylmalonate mononuclear complex.

#### II.5.4. Magnetic Properties

The thermal dependence of  $\chi_M$  for **23** is shown in Figure II.27. The curve exhibits a behaviour which is characteristic of antiferromagnetically coupled copper(II) ions with a smooth maximum of the susceptibility at about 130 K. On the light of the structural features described above, there are two exchange pathways available in **23**: (i) through the 2,2'-

bipym ligand, and (ii) through the long apical-equatorial oxo-bridge [copper-copper separation of 3.6764(3) Å]. It is well known that the 2,2'-bipym ligand strongly couples antiferromagnetically the copper(II) ions.<sup>1-4,7-11</sup> The magnetic exchange coupling through the oxo-bridge is very weak (in general, antiferromagnetic) and it depends on the apical Cu–O bond distance [which in **23** is 2.8641(17) Å].<sup>12-16</sup> The comparison of both bridges makes the latter one negligible. Thus, the experimental data can be fitted through the expression for a simple dinuclear copper(II) complex.<sup>16,17</sup> A parameter ( $\rho$ ) has been included to take into account the presence of paramagnetic impurities. The expression for the magnetic susceptibility in this case is:

$$\chi_M = (2N\beta^2 g^2 / kT) \frac{1}{[3 + \exp(-J/kT)]} (1 - \rho) + (N\beta^2 g^2 / 2kT) \rho$$

where  $J$  is the singlet-triplet gap defined by the Hamiltonian:

$$\hat{H} = -J \hat{S}_1 \cdot \hat{S}_2$$

the other symbols have their usual meanings. The least-squares fit leads to  $J = -155.6(3)$  cm<sup>-1</sup>,  $g = 2.058(2)$ ,  $\rho = 0.0043(2)$  and  $R = 2.0 \times 10^{-4}$ . The calculated curve is in agreement with the experimental one (Figure II.27).

The value of  $J$  reveals a strong antiferromagnetic coupling between the copper(II) ions separated by 5.4512(4) Å in complex **23**. The overlap between the  $d(x^2-y^2)$  magnetic orbitals centred on each metal ion [the  $x$  and  $y$  axes being defined by the equatorial bonds at the copper environment] accounts for this coupling. According to the Kahn's orbital model,<sup>18</sup> for extended bridges such as the 2,2'-bipym, the ferromagnetic term is very small and it can be neglected. Then,  $J$  is proportional to  $\Delta^2$  [ $\Delta$  = energy gap between the two singly

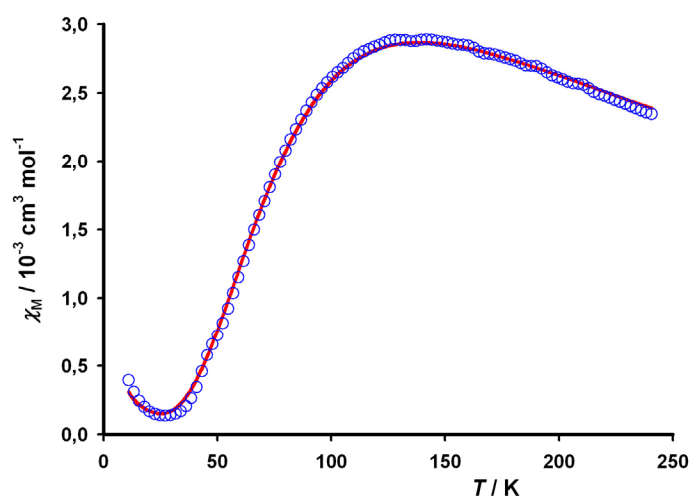


Fig. II.27.  $\chi_M$  vs  $T$  plot for **23** (blue) under an applied field of 1 T: (o) experimental data, (—) best fit curve.

occupied molecular orbitals in the dinuclear copper(II) unit]. In a previous work,<sup>8</sup> the variation of  $\Delta^2$  with some structural parameters such as the Cu–N bond distance, the dihedral angle between the basal plane at the copper atom and the 2,2'-bipym plane ( $\gamma$ ), the height of the metal atom above the basal plane ( $h_M$ ) was analyzed [see Table II.14]. The conclusion was that these are the main factors that govern the magnetic coupling.<sup>8</sup> Remarkably, small variations in the value of the Cu–N bond distances exert a great influence on  $J$ . The parameters for **23** are within the range observed and they are similar to those found on the malonato-containing complex.<sup>3</sup>

**Table II.14.** Magnetostructural data for a series of 2,2'-bipym bridged copper(II) complexes<sup>a</sup>

| Compounds                                                                                                                                                     | Cu–N | Cu–O              | $\gamma^b / ^\circ$ | $h_M^c / \text{Å}$ | Cu...Cu <sup>d</sup> / Å | $-J / \text{cm}^{-1}$ | Ref |
|---------------------------------------------------------------------------------------------------------------------------------------------------------------|------|-------------------|---------------------|--------------------|--------------------------|-----------------------|-----|
| [Cu <sub>2</sub> (L)(C <sub>4</sub> O <sub>4</sub> ) <sub>2</sub> (H <sub>2</sub> O) <sub>6</sub> ]                                                           | 2.07 | 1.96              | 11.4                | 0.096              | 5.542                    | 139                   | 8   |
| [Cu <sub>2</sub> (L)(C <sub>5</sub> O <sub>5</sub> ) <sub>2</sub> (H <sub>2</sub> O) <sub>2</sub> ] $\cdot$ 4(H <sub>2</sub> O)                               | 2.02 | 1.97              | 14.4                | 0.187              | 5.348                    | 160                   | 7   |
| [Cu <sub>2</sub> (L)(H <sub>2</sub> O) <sub>4</sub> (SO <sub>4</sub> ) <sub>2</sub> ] $\cdot$ 3(H <sub>2</sub> O)                                             | 2.04 | 1.97              | 5.1                 | 0.075              | 5.456                    | 159                   | 9   |
| [Cu <sub>2</sub> (L)(NO <sub>3</sub> ) <sub>4</sub> ]                                                                                                         | 2.01 | 1.96              | 3.5                 | 0.021              | 5.371                    | 191                   | 2   |
| [Cu <sub>2</sub> (L)(C <sub>3</sub> H <sub>2</sub> O <sub>4</sub> ) <sub>2</sub> (H <sub>2</sub> O) <sub>2</sub> ] $\cdot$ 4(H <sub>2</sub> O)                | 2.04 | 1.90              | 6.5                 | 0.118              | 5.445                    | 149                   | 3   |
| [Cu <sub>2</sub> (L)(C <sub>6</sub> H <sub>5</sub> O <sub>2</sub> N <sub>2</sub> ) <sub>2</sub> (H <sub>2</sub> O) <sub>4</sub> ] $\cdot$ 2(H <sub>2</sub> O) | 2.05 | 1.96 <sup>e</sup> | 4.3                 | 0.061              | 5.506                    | 99                    | 11  |
| <b>23</b>                                                                                                                                                     | 2.03 | 1.92              | 4.7                 | 0.130              | 5.451                    | 156                   | -   |

<sup>a</sup> L = 2,2'-bipym. Average bond distances are given for each structure in Å.

<sup>b</sup> Dihedral angle between the basal plane at the copper environment and the 2,2'-bipym plane.

<sup>c</sup> The height of the metal atom above the mean plane defined by the equatorial ligand atoms.

<sup>d</sup> Metal-metal separation across 2,2'-bipym.

<sup>e</sup> In this case, this is a Cu–N bond distance: the nitrogen atoms of the ligand are bonded to the metal atom.

## II.5.5. Conclusion

The crystal structure of **23** consists of dinuclear entities and crystallization water molecules, with a structure similar to that found for the malonate-containing copper(II) complex, but very different from the Phmal complex (**14**). Probably, the smaller size of the methyl group respect to the phenyl one and the ability of the latter to establish weak  $\pi$ -type interactions with the 2,2'-bipym ligand are responsible for the differences between **23** and **14**. Supramolecular interactions are also involved in the dissimilarities between the crystal packing of the dinuclear entities of **23** and the mal-complex. Mainly, the location of the water molecules is affected by the presence of the methyl group of the Memal ligand. From a magnetic point of view, **23** exhibits the behaviour characteristic of an antiferromagnetically coupled dinuclear copper(II) complex [ $J$  being  $-155.6(3) \text{ cm}^{-1}$ ], in agreement with previous reported values for 2,2'-bipym-bridged dinuclear copper(II) complexes.

### II.5.6. References

- 1 G. De Munno, M. Julve, F. Lloret, J. Cano and A. Caneschi, *Inorg. Chem.* **1995**, *34*, 2048.
- 2 M. Julve, G. De Munno, G. Bruno and M. Verdager, *Inorg. Chem.* **1988**, *27*, 3160
- 3 Y. Rodríguez-Martín, J. Sanchiz, C. Ruiz-Pérez, F. Lloret and M. Julve, *Inorg. Chim. Acta* **2001**, *326*, 20.
- 4 J. Pasán, J. Sanchiz, C. Ruiz-Pérez, F. Lloret and M. Julve, *Eur. J. Inorg. Chem.* **2004**, 4081.
- 5 The occupation was fixed to 0.5 due to the symmetry restrictions in the refinement (i.e. just one molecule appears in the asymmetric unit).
- 6 A. W. Addison, T. N. Rao, J. Reedijk, J. van Rijn and G. C. Verschoor, *Dalton Trans.* **1984**, 1349.
- 7 I. Castro, J. Sletten, L. K. Glærum, F. Lloret, J. Faus and M. Julve, *Dalton Trans.* **1994**, 2777.
- 8 I. Castro, J. Sletten, L. K. Glærum, J. Cano, F. Lloret, J. Faus and M. Julve, *Dalton Trans.* **1995**, 3207.
- 9 A. L. Spek, *Acta Cryst., Sect. A* **1990**, *46*, 34.
- 10 M. Julve, M. Verdager, G. De Munno, J. A. Real and G. Bruno, *Inorg. Chem.* **1993**, *32*, 795.
- 11 F. Thetiot, S. Triki, J. S. Pala, J. R. Galán-Mascaros, J. M. Martínez-Agudo and K. R. Dunbar, *Eur. J. Inorg. Chem.* **2004**, 3783.
- 12 R. Hämäläinen, M. Ahlgren and U. Turpeinen, *Acta Cryst., Sect. B* **1982**, *38*, 1577.
- 13 J. N. Brown and L. M. Trefonas, *Inorg. Chem.* **1973**, *312*, 1730.
- 14 E. Dixon-Estes, W. E. Estes, R. P. N. Scaringe, W. E. Hatfield and D. J. Hodgson, *Inorg. Chem.* **1975**, *14*, 2564.
- 15 J. P. Costes, F. Dahan and J. P. Laurent, *Inorg. Chem.* **1985**, *24*, 1018.
- 16 E. Escrivá, J. Server-Carrió, L. Lezama, J. V. Folgado, J. L. Pizarro, R. Ballesteros and B. Abarca, *Dalton Trans.* **1997**, 2033.
- 17 B. Bleaney and K. D. Bowers, *Proc. R. Soc. London Ser. A* **1952**, *214*, 451.
- 18 O. Kahn, *Molecular Magnetism*, VCH, New York, **1993**.

## II.6. 2,2'-bipyridine (24) Copper(II)-Methylmalonate Complex

### II.6.1. Introduction

The 2,2'-bipyridine molecule acts as a chelating ligand towards metal ions and in general it occupies equatorial positions of the copper(II) ions. The unusual complexes formed with the malonate ligand reported by C. Ruiz-Pérez *et al.*<sup>1</sup> are responsible for this attempt to reproduce such results with the methylmalonate ligand. In the previous chapter it was shown that the complex formed with the phenylmalonate ligand (**16**) was mononuclear but with very interesting supramolecular interactions.<sup>2</sup> Then, we are interested in comparing the crystal structures of the family of the R-malonate ligands with the 2,2'-bipyridine coligand and copper(II) ions. Thus, herein we report the synthesis, crystal structure and magnetic properties of the [Cu(2,2'-bpy)(Memal)(H<sub>2</sub>O)]·2H<sub>2</sub>O complex.

### II.6.2. Synthesis

[Cu(2,2'-bpy)(Memal)(H<sub>2</sub>O)]·2H<sub>2</sub>O (**24**). A methanolic solution (5 cm<sup>3</sup>) of 2,2'-bipyridine (0.5 mmol, 156 mg) was added dropwise to an aqueous solution (10 cm<sup>3</sup>) of copper(II)-methylmalonate (1 mmol) under continuous stirring. The resulting blue solution was allowed to evaporate at room temperature and blue needle single crystals of **24** were grown after a week. The crystallographic details are listed in Table II.15. Yield *ca* 80 %. Anal. calc. for C<sub>14</sub>H<sub>18</sub>CuN<sub>2</sub>O<sub>7</sub> (**24**): C, 43.13; H, 4.65; N, 7.18; Found: C, 43.26; H, 4.78; N, 7.73 %.

**Table II.15.** Crystallographic data for **24**

| <b>24</b>                                                   |                                                                   |
|-------------------------------------------------------------|-------------------------------------------------------------------|
| Formula                                                     | C <sub>14</sub> H <sub>18</sub> O <sub>7</sub> N <sub>2</sub> Cu  |
| FW                                                          | 389.84                                                            |
| Crystal system                                              | Monoclinic                                                        |
| Space group                                                 | <i>P</i> 2 <sub>1</sub> / <i>n</i>                                |
| <i>a</i> / Å                                                | 10.7514(3)                                                        |
| <i>b</i> / Å                                                | 7.4878(2)                                                         |
| <i>c</i> / Å                                                | 20.0786(7)                                                        |
| $\beta$ / °                                                 | 90.9690(10)                                                       |
| <i>V</i> / Å <sup>3</sup>                                   | 1616.18(8)                                                        |
| <i>Z</i>                                                    | 4                                                                 |
| $\mu$ (Mo K $\alpha$ ) / cm <sup>-1</sup>                   | 13.91                                                             |
| <i>T</i> / K                                                | 293(2)                                                            |
| $\rho_{\text{calc}}$ / g cm <sup>-3</sup>                   | 1.602                                                             |
| $\lambda$ / Å                                               | 0.71073                                                           |
| Index ranges                                                | -14 ≤ <i>h</i> ≤ 14,<br>-9 ≤ <i>k</i> ≤ 9,<br>-18 ≤ <i>l</i> ≤ 27 |
| Indep. reflect. ( <i>R</i> <sub>int</sub> )                 | 4120 (0.0582)                                                     |
| Obs. reflect. [ <i>I</i> > 2 $\sigma$ ( <i>I</i> )]         | 3103                                                              |
| Parameters                                                  | 285                                                               |
| Goodness-of-fit                                             | 1.163                                                             |
| <i>R</i> [ <i>I</i> > 2 $\sigma$ ( <i>I</i> )]              | 0.0557                                                            |
| <i>R</i> <sub>w</sub> [ <i>I</i> > 2 $\sigma$ ( <i>I</i> )] | 0.1406                                                            |
| <i>R</i> (all data)                                         | 0.0838                                                            |
| <i>R</i> <sub>w</sub> (all data)                            | 0.1618                                                            |

### II.6.3. Description of the Structure

The structure of **24** consists of discrete  $[\text{Cu}(2,2'\text{-bpy})(\text{Memal})(\text{H}_2\text{O})]$  mononuclear entities and crystallization water molecules (Figure II.28).

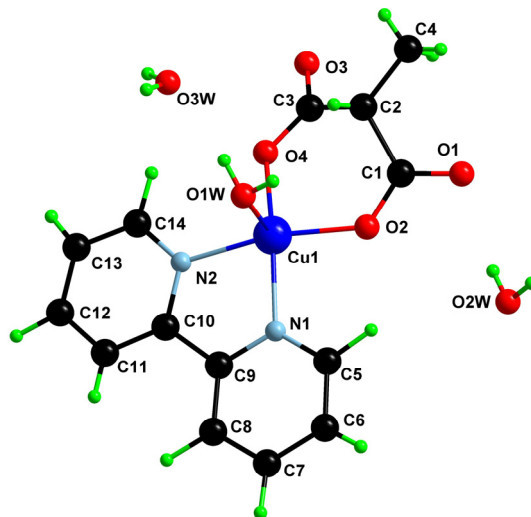


Fig. II.28. View of the asymmetric unit of complex **24** along with the numbering scheme.

These units are linked to form a chain along the  $a$  axis through an hydrogen bond which involves the coordinated water molecule [O(1w)] and the uncoordinated malonate oxygen atom [O(1)]. Selected bond distances and angles are displayed in Table II.16 (Figure II.29). H-bonds among the water molecules and the malonate oxygen atoms connect the previous chains in the  $ab$  plane (see Table II.16 and Figure II.30). Finally, H-bonded sheets are stacked through  $\pi$ - $\pi$  interactions between 2,2'-bpy ligands to yield a 3D supramolecular network (Figure II.31) [the value for the shortest centroid-centroid distance and off-set angle are 3.720(1) Å and 18.78(8)°, respectively]. The complex hydrogen bond network builds an extended water motif which can be seen in the Figure II.32. The C4 chain formed by the

Table II.16. Hydrogen bond distances and angles in **24**

| D-H...A                      | O-H (Å) | H...O (Å) | O-H...O (°) | O...O (Å) |
|------------------------------|---------|-----------|-------------|-----------|
| <i>Supramolecular chain</i>  |         |           |             |           |
| O(1w)-H...O(1a) <sup>a</sup> | 0.77(5) | 2.00(6)   | 170(5)      | 2.770(4)  |
| <i>Supramolecular sheet</i>  |         |           |             |           |
| O(1w)-H...O(3w)              | 0.80(5) | 1.94(5)   | 172(5)      | 2.742(5)  |
| O(2w)-H...O(1)               | 0.72(6) | 2.18(6)   | 172(6)      | 2.902(6)  |
| O(2w)-H...O(3wb)             | 0.89(6) | 2.04(6)   | 168(5)      | 2.927(6)  |
| O(3w)-H...O(3c)              | 0.73(6) | 2.10(7)   | 161(7)      | 2.802(5)  |
| O(3w)-H...O(3d)              | 0.86(6) | 1.93(6)   | 170(6)      | 2.786(5)  |

<sup>a</sup> Symmetry operators: (a) =  $-x + 3/2, y + 1/2, -z + 1/2$ ; (b) =  $-x + 3/2, y - 1/2, -z + 1/2$ ; (c) =  $x, y + 1, z$ ; (d) =  $-x + 1/2, y + 1/2, -z + 1/2$ .



O(3w) and O(3) atoms presents pendant tetramer clusters formed by O(3w), O(2w), O(1w) and O(1).

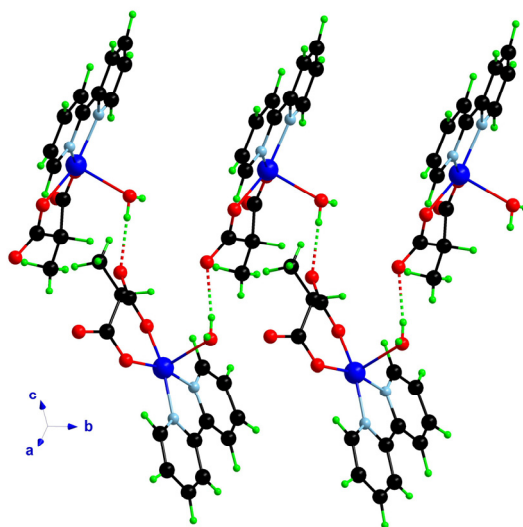


Fig. II.29. Perspective view of the hydrogen-bonded chains of [Cu(2,2'-bpy)(Memal)(H<sub>2</sub>O)] which are extended along the *b* axis.

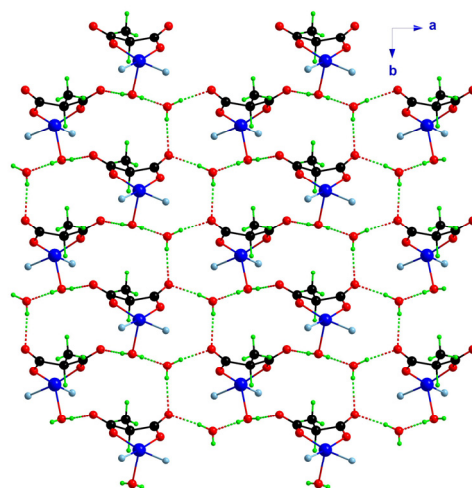
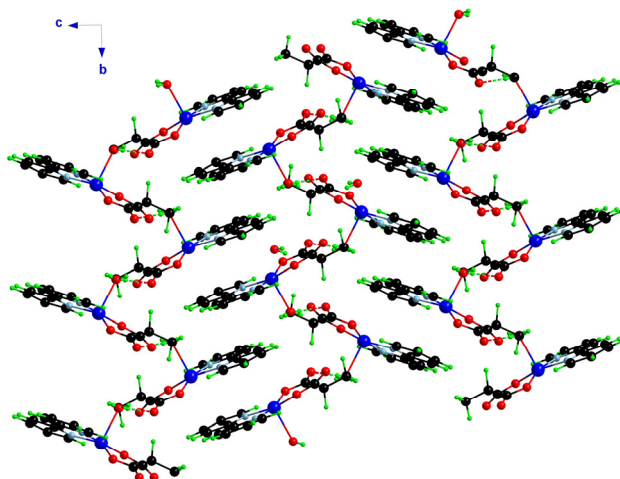


Fig. II.30. Hydrogen-bonding among the mononuclear entities of **24** forms a supramolecular sheet in the *ab* plane.

The copper atom exhibits a somewhat distorted square pyramidal environment, the  $\tau$  value being 0.017.<sup>1</sup> Two oxygen atoms from the methylmalonate ligand [O(2) and O(4), mean Cu–O bond distance is 1.920(3) Å] and two nitrogen atoms from the 2,2'-bpy ligand

[N(1) and N(2); mean Cu–N bond distance being 2.008(3) Å] build the basal plane while a water molecule occupies the apical position [Cu(1)–O(1w) is 2.274(3) Å]. The copper atom is shifted towards the apical position by 0.2411(4) Å.



**Fig. II.31.** A view along the  $a$  axis of the 3D supramolecular network formed by  $\pi$ - $\pi$  stacking of the hydrogen-bonded sheets of **24**.

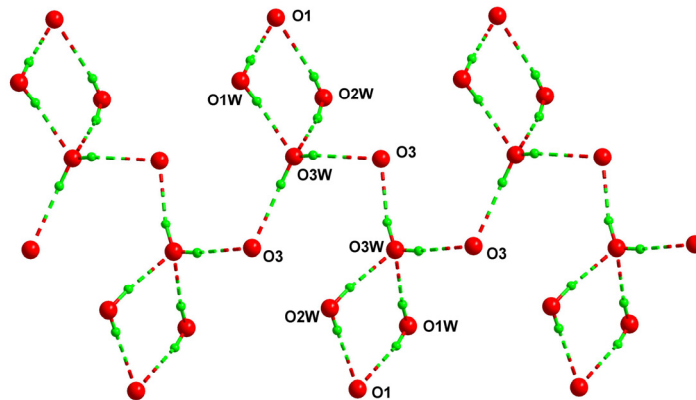


**Fig. II.32.** A view of the arrangement of the water molecules in **24**. The chain motif is formed with the inclusion of an uncoordinated malonate oxygen atom, the a pendant tetramer is connected to the chain.

The malonate and the 2,2'-bpy ligands adopt the bidentate coordination mode, the values of the angle subtended at the copper atom being 92.81(11)° and 81.18(12)°, respectively. The 2,2'-bpy ligand is nearly planar [the largest deviation from the mean plane is 0.059(4) Å], the dihedral angle between the mean planes of the two pyridyl rings being 3.8(1)°. These values are in agreement with that previously reported for malonato-containing copper(II) complexes.<sup>2-4</sup>

**Table II.17.** Selected bond angles ( $^{\circ}$ ) and lengths ( $\text{\AA}$ ) for **24**.

| <b>24</b>       |            |                  |            |
|-----------------|------------|------------------|------------|
| Cu(1)–O(2)      | 1.911(2)   | O(2)–Cu(1)–O(1w) | 97.73(12)  |
| Cu(1)–O(4)      | 1.929(3)   | O(4)–Cu(1)–N(1)  | 165.20(12) |
| Cu(1)–N(1)      | 2.012(3)   | O(4)–Cu(1)–N(2)  | 90.98(11)  |
| Cu(1)–N(2)      | 2.004(3)   | O(4)–Cu(1)–O(1w) | 97.69(12)  |
| Cu(1)–O(1w)     | 2.274(3)   | N(1)–Cu(1)–N(2)  | 81.18(12)  |
| O(2)–Cu(1)–O(4) | 92.81(11)  | N(1)–Cu(1)–O(1w) | 95.73(11)  |
| O(2)–Cu(1)–N(1) | 91.56(12)  | N(2)–Cu(1)–O(1w) | 96.99(12)  |
| O(2)–Cu(1)–N(2) | 164.16(12) |                  |            |

The structure of **24** presents some similarities with those of the complexes **21–23**. Despite of the different nuclearity (**21** and **22** are 1D complexes and **23** is a dinuclear complex), the supramolecular structure is like a mixture of these ones. If we isolate two  $\pi$ - $\pi$  stacked  $[\text{Cu}(2,2'\text{-bpy})(\text{Memal})(\text{H}_2\text{O})]$  units, it resembles the dinuclear complex **23** with the inversion centre at the midpoint of the 2,2'-bipym ligand (see Figure II.33). At the same time, the H-bonded chains along the *b* axis of **24** are somewhat similar to the chain compounds **21** and **22** (Figure II.18).

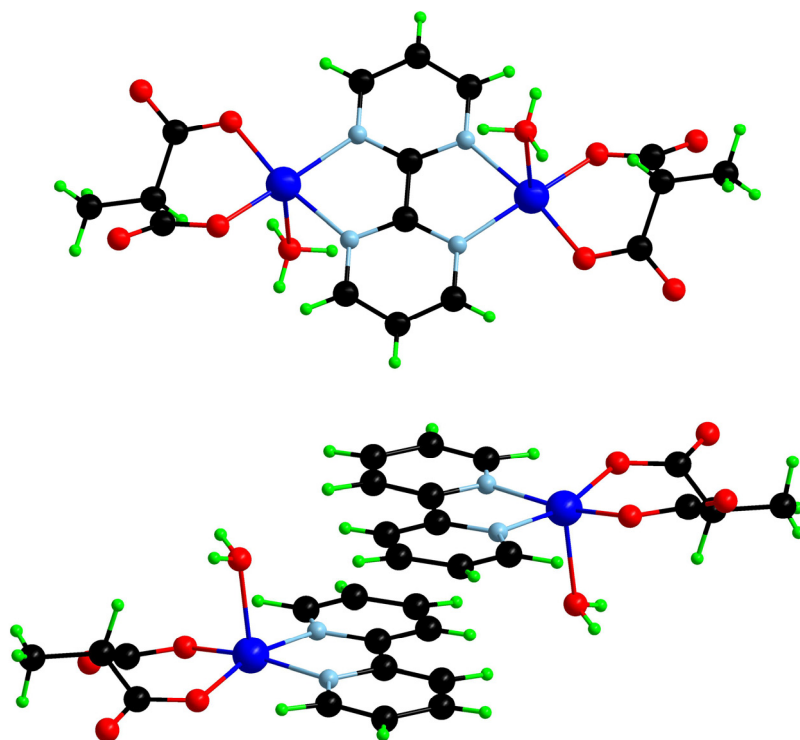


**Fig. II.33.** Comparative view of the dinuclear entity of complex **23** (up) and two  $\pi$ - $\pi$  stacked molecules of **24** (bottom).

Let us finish this structural description with a comparison of the structure of **24** with that of the previously reported  $[\text{Cu}(2,2'\text{-bpy})(\text{mal})(\text{H}_2\text{O})]\cdot\text{H}_2\text{O}$  complex.<sup>7</sup> This structure also consists of discrete mononuclear units of  $[\text{Cu}(2,2'\text{-bpy})(\text{mal})(\text{H}_2\text{O})]$  which are very similar to that of **24**. The main differences between these complexes appear in the supramolecular interactions that they undergo. The hydrogen bond between the coordinated water molecule and one uncoordinated malonate oxygen atom which builds the supramolecular chains in **24** [O(1w) and O(3); Figure II.29], only gives dinuclear entities in the mal complex. The presence of two (**23**) instead of one crystallization water molecule (mal complex) changes completely the 3D structure they build, although in both compounds it can be observed a hydrophobic area dominated by the  $\pi$ - $\pi$  type interactions among the 2,2'-bpy ligands.

It deserves to be noted that the reaction of copper(II), malonic acid and 2,2'-bpy also yields two other products whose structures consist of chains of carboxylate-bridged copper(II) ions.<sup>2</sup> The reproduction of these results with the methylmalonic acid has been unsuccessful.

#### II.6.4. Magnetic Properties

The  $\chi_{\text{M}}T$  product of compound **24** follows the Curie law in the 5-300 K temperature range. Its value is  $0.365 \text{ cm}^3 \text{ mol}^{-1} \text{ K}$ , as expected for a magnetically isolated spin doublet of a copper(II) ion. This is in agreement with its mononuclear nature.

#### II.6.5. Conclusion

The crystal structure of complex **24** consists of mononuclear copper(II) entities which are linked by supramolecular interactions to afford a three-dimensional network. This situation is similar to that of the mononuclear complexes obtained with the malonate and phenylmalonate ligands. Interestingly, a C4 pattern water motif is built through hydrogen bonds involving water molecules and uncoordinated carboxylate-oxygen atoms.

#### II.6.6. References

- 1 C. Ruiz-Pérez, M. Hernández-Molina, P. Lorenzo-Luis, F. Lloret, J. Cano and M. Julve, *Inorg. Chem.* **2000**, *39*, 3845.
- 2 J. Pasán, J. Sanchiz, C. Ruiz-Pérez, F. Lloret and M. Julve, *Eur. J. Inorg. Chem.* **2004**, 4081.
- 3 L. Infantes, J. Chisholm and S. Motherwell, *CrysEngComm* **2003**, *5(85)*, 480.
- 4 L. Infantes and S. Motherwell, *CrysEngComm* **2002**, *4(75)*, 454.
- 5 A. W. Addison, T. N. Rao, J. Reedijk, J. van Rijn and G. C. Verschoor, *Dalton Trans.* **1984**, 1349.

- 6 M. Hernández-Molina, P. A. Lorenzo-Luis, C. Ruiz-Pérez, F. Lloret and M. Julve, *Inorg. Chim. Acta*, **2001**, 313, 87.
- 7 E. Suresh and M. M. Bhadbhade, *Acta Cryst.* **1997**, C53, 193.

## II.7. 4,4'-Bipyridine Copper(II)-Methylmalonate Complexes (19, 25 and 26)

### II.7.1. Introduction

The compounds presented afterwards are like an epilogue of this chapter devoted to the methylmalonate containing complexes. They are the byproducts which appear in the synthesis of the  $[\text{Cu}_2(4,4'\text{-bpy})(\text{Memal})_2(\text{H}_2\text{O})_2]$  (**19**) complex, their structures being very different of what we are expecting along the outline of this chapter, but very interesting. The use of the rod-like 4,4'-bipyridine coligand as a pillar unit is well known and a lot of examples are present in the literature,<sup>1-6</sup> complex **19** being one of them. However, the 4,4'-bpy ligand is able to built high-dimensional networks which can be pillared by other units. This approach has been successfully used by Fujita and Kitagawa, and complexes with interesting properties in gas absorption, anion exchange and catalysis have been developed.<sup>4</sup> Although unexpected, the complex  $\{[\text{Cu}(4,4'\text{-bpy})_2][\text{Cu}(4,4'\text{-bpy})_2(\text{Memal})(\text{NO}_3)(\text{H}_2\text{O})]\}_n \cdot n\text{NO}_3 \cdot 4n\text{H}_2\text{O}$  whose synthesis, crystal structure and magnetic properties will be presented here is an example of such a strategy.

The other 4,4'-bpy-containing complex presented herein is a rare example of coordination of the malonate ligand where, instead of exhibiting bridging carboxylate as usual, acts as a bis(monodentate) ligand linking the copper atoms through the malonate carbon skeleton. Its synthesis, crystal structure and magnetic properties will be also reported.

### II.7.2. Synthesis

$[\text{Cu}_2(4,4'\text{-bpy})(\text{Memal})_2(\text{H}_2\text{O})_2]$  (**19**) and  $\{[\text{Cu}(4,4'\text{-bpy})_2][\text{Cu}(4,4'\text{-bpy})_2(\text{Memal})(\text{NO}_3)(\text{H}_2\text{O})]\}_n \cdot n\text{NO}_3 \cdot 4n\text{H}_2\text{O}$  (**25**). An aqueous solution (5 cm<sup>3</sup>) of copper(II)-methylmalonate (1 mmol, 180 mg) was set in one arm of a water-filled H-shape tube while a methanolic solution (5 cm<sup>3</sup>) of 4,4'-bipyridine (1 mmol, 156 mg) was set in the other arm. Four different kind of single crystals appeared after a few weeks, but not all of them were structurally characterised due to the poor quality of the crystals and hence they are not discussed in this work. Pale blue prisms (main product, yield *ca* 45%) and deep blue plates (minor product, yield *ca* 15%) were suitable for X-ray diffraction and they correspond to the complexes **19** and **25**, respectively.

There is a different method to obtain the complex **25** which yields only this phase and it was used to prepare the sample for both, structural and magnetic measurements. A

methanolic solution (5 cm<sup>3</sup>) of 4,4'-bpy (0.5 mmol, 78 mg) was added dropwise to an aqueous solution (10 cm<sup>3</sup>) of copper(II)-methylmalonate (0.5 mmol, 90 mg) leading to a pale blue precipitate after the addition of a few drops. The filtration of this product gives a clear blue solution which was stood to evaporate at room temperature. X-ray quality blue plates of **25** were grown after a few days (yield *ca* 10%, based on copper). The addition of a minimum amount of guanidine nitrate to the filtered solution affords better quality crystals. Anal. calc. for C<sub>44</sub>H<sub>46</sub>Cu<sub>2</sub>N<sub>10</sub>O<sub>15</sub> (**25**): C, 48.84; H, 4.28; N, 12.94; Found: C, 48.96; H, 4.34; N, 12.42 %.

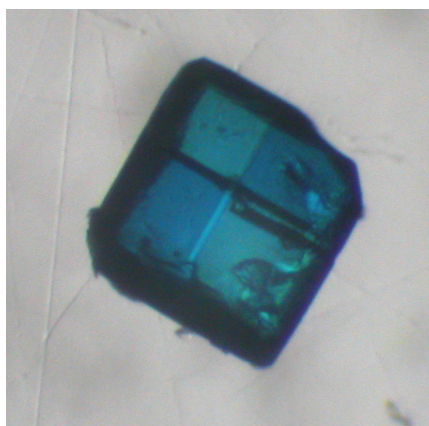


Fig. II.34. Microscope image of a 'single' crystal of complex **25**. Four regions are observed with a subtle change of colour among them.

[Cu(4,4'-bpy)<sub>2</sub>(Memal)(H<sub>2</sub>O)]<sub>n</sub>·nH<sub>2</sub>O (**26**). A hot aqueous solution (5 cm<sup>3</sup>) of 4,4'-bpy (2 mmol, 312 mg) was added dropwise to a hot aqueous solution (5 cm<sup>3</sup>) of copper(II)-methylmalonate (0.5 mmol, 90 mg). The resulting blue solution was stored at 38 °C and it provides prismatic blue single crystals of **26** after a few hours. Yield *ca* 60%. Anal. calc. for C<sub>24</sub>H<sub>24</sub>CuN<sub>4</sub>O<sub>6</sub> (**26**): C, 54.59; H, 4.58; N, 10.61; Found: C, 55.09; H, 4.67; N, 10.78 %.

### II.7.3. Crystallographic Analysis

A single crystal of **25** is shown in Figure II.34. They appear as octagonal prisms with a subtle cross on the surface which delimits four areas of different blue shades with opposite zones having the same colour. At first time, not much attention was paid to this fact which would become crucial and a well shaped high quality crystal was mounted for X-ray measurements. The cell measurement gave a tetragonal space group with good  $\sigma$ -deviations, the data reduction led to  $R_{sym} = 0.042$ . The structure was solved by direct methods using SHELXS-97<sup>7</sup> in the  $P4_2/n$  space group, but the refinement always failed. The good

experimental data ( $R_{sym}$  for triclinic space group being 0.041), the failure of the refinement and the tetragonal space group pointed out the possibility of merohedral twinning, but a few attempts to solve it were not successful.

After this, we focus on the morphology of the crystal, in the two different blue areas separated by a subtle cross. The two twin phases were evident. Carefully, we broke the crystal to separate the two areas, mounting both crystals for the X-ray measurements. The new space group was orthorhombic with the values of the cell parameters  $a, b$  and  $c$  very similar to those found in the first measurement. The structure was finally solved in the orthorhombic non-centrosymmetric  $Pc2_1n$  space group with a Flack parameter 0.019(15).<sup>8</sup> The experimental data of the other phase (the other crystal area) was refined with the atomic positions of the first phase leading to a Flack parameter near 1, supporting that the two phases are within the same crystal. Crystallographic details for complexes **25** and **26** are listed in Table II.18.

**Table II.18.** Crystallographic data for **25** and **26**

|                                         | <b>25</b>                                                                       | <b>26</b>                                                            |
|-----------------------------------------|---------------------------------------------------------------------------------|----------------------------------------------------------------------|
| Formula                                 | C <sub>44</sub> H <sub>46</sub> O <sub>15</sub> N <sub>10</sub> Cu <sub>2</sub> | C <sub>24</sub> H <sub>24</sub> O <sub>6</sub> N <sub>4</sub> Cu     |
| FW                                      | 1081.90                                                                         | 527.978                                                              |
| Crystal system                          | Orthorhombic                                                                    | Monoclinic                                                           |
| Space group                             | $Pc2_1n$                                                                        | $P2_1/n$                                                             |
| $a/\text{Å}$                            | 15.814(2)                                                                       | 7.4191(3)                                                            |
| $b/\text{Å}$                            | 15.9037(10)                                                                     | 27.4874(13)                                                          |
| $c/\text{Å}$                            | 18.4974(16)                                                                     | 11.5347(11)                                                          |
| $\beta/^\circ$                          | -                                                                               | 91.609(6)                                                            |
| $V/\text{Å}^3$                          | 4652.3(8)                                                                       | 2351.4(3)                                                            |
| $Z$                                     | 4                                                                               | 4                                                                    |
| $\mu(\text{Mo K}\alpha)/\text{cm}^{-1}$ | 9.95                                                                            | 9.77                                                                 |
| $T/\text{K}$                            | 293(2)                                                                          | 293(2)                                                               |
| $\rho_{\text{calc}}/\text{g cm}^{-3}$   | 1.529                                                                           | 1.480                                                                |
| $\lambda/\text{Å}$                      | 0.71073                                                                         | 0.71073                                                              |
| Index ranges                            | $-18 \leq h \leq 20,$<br>$-20 \leq k \leq 20,$<br>$-15 \leq l \leq 24$          | $-8 \leq h \leq 9,$<br>$-35 \leq k \leq 32,$<br>$-14 \leq l \leq 11$ |
| Indep. reflect. ( $R_{\text{int}}$ )    | 10222 (0.0519)                                                                  | 5318 (0.0495)                                                        |
| Obs. reflect. [ $I > 2\sigma(I)$ ]      | 6732                                                                            | 3164                                                                 |
| Flack parameter                         | 0.019(15)                                                                       | -                                                                    |
| Parameters                              | 669                                                                             | 316                                                                  |
| Goodness-of-fit                         | 1.064                                                                           | 1.058                                                                |
| $R$ [ $I > 2\sigma(I)$ ]                | 0.0554                                                                          | 0.0723                                                               |
| $R_w$ [ $I > 2\sigma(I)$ ]              | 0.1004                                                                          | 0.1522                                                               |
| $R$ (all data)                          | 0.1079                                                                          | 0.1345                                                               |
| $R_w$ (all data)                        | 0.1183                                                                          | 0.1764                                                               |

#### II.7.4. Description of the Structure

{[Cu(4,4'-bpy)<sub>2</sub>][Cu(4,4'-bpy)<sub>2</sub>(Memal)(NO<sub>3</sub>)(H<sub>2</sub>O)]}<sub>n</sub>·nNO<sub>3</sub>·4nH<sub>2</sub>O (**25**). The structure of **25** is a 3D-network based on a square grid of [Cu(4,4'-bpy)<sub>2</sub>]<sub>n</sub> pillared by carboxylate-methylmalonate bridged [Cu(4,4'-bpy)<sub>2</sub>(Memal)(NO<sub>3</sub>)(H<sub>2</sub>O)] units (Figure II.35). The (4,4) [Cu(4,4'-bpy)<sub>2</sub>]<sub>n</sub> grid provides channels of dimension 11 x 11 Å<sup>2</sup> along the  $a$ - and  $b$ -axes which are filled by the terminal 4,4'-bpy molecules of the pillaring units, nitrate and crystallization water molecules (Figure II.36). The pillar unit bridges adjacent 2D [Cu(4,4'-bpy)<sub>2</sub>]<sub>n</sub> networks along the  $c$  axis affording the 3D structure (Figure II.37). An intricate network of hydrogen bonds among the water and nitrate molecules contribute to the



stabilization of the structure [O $\cdots$ O distances in the range 2.56(3)–2.728(15) Å]. The terminal 4,4'-bpy groups establish hydrogen bonds with the crystallization water molecules [N(2) $\cdots$ O(4w) and N(4) $\cdots$ O(3w) being 2.869(12) and 2.845(10) Å, respectively]. They participate also in weak  $\pi$ -type interactions among them and with the [Cu(4,4'-bpy) $_2$ ] $_n$  2D-network, fixing their position in the channels (Figure II.38).

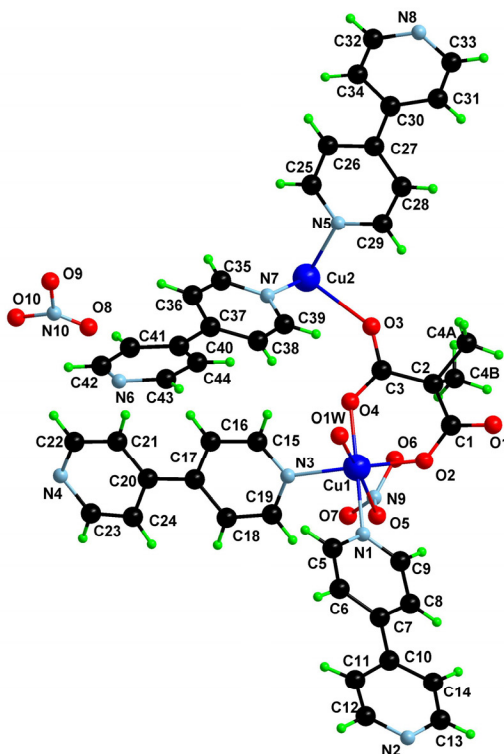
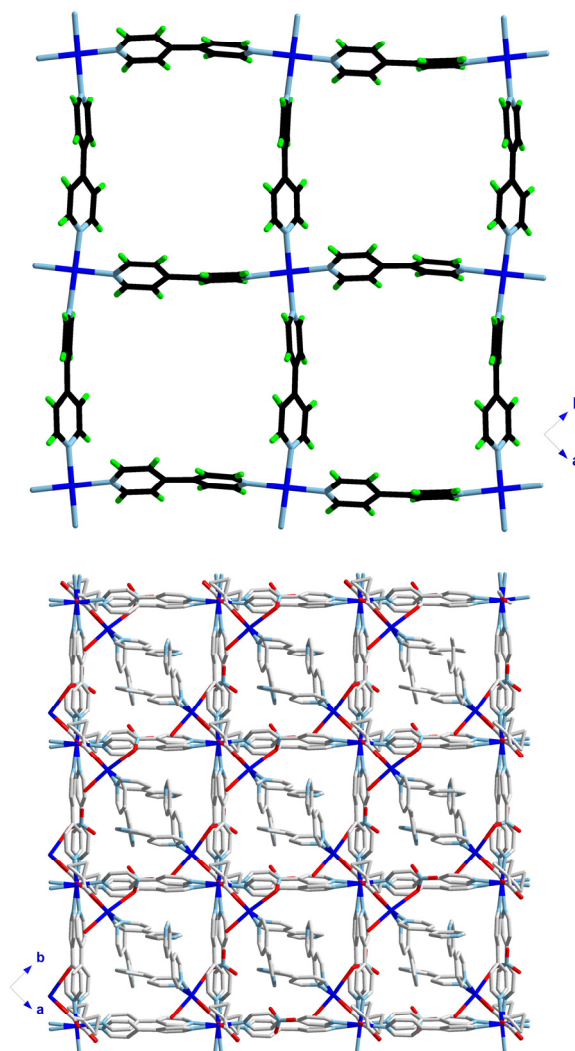


Fig. II.35. A view of the asymmetric unit of **25** along with the numbering scheme.

Each copper atom exhibits a distorted octahedral environment with the parameters  $s/h$  and  $\phi$  being 1.45 and 54.4° for Cu(1) and 1.31 and 56.2° for Cu(2) [the values for an ideal octahedron being  $s/h = 1.22$  and  $\phi = 60^\circ$ ].<sup>9</sup> Two nitrogen atoms of 4,4'-bpy ligands [N(1) and N(3); average Cu(1)–N bond distance being 2.021(4) Å; see Table II.19] and two methylmalonate oxygen atoms [O(2) and O(4); average Cu(1)–O bond distance is 1.922(3) Å] build the basal plane of Cu(1), while the axial positions are occupied by a water molecule [Cu(1)–O(1w) = 2.395(5) Å] and a nitrate-oxygen atom [Cu(1)–O(5) = 2.692(6) Å]. The environment of Cu(2) is built by four 4,4'-bpy nitrogen atoms [N(5), N(6), N(7) and N(8); average Cu–N bond distance being 2.075(4) Å] in the equatorial plane and two malonate

oxygen atoms occupying the axial positions [O(1) and O(3); mean Cu(2)–O bond distance is 2.364(3) Å].



**Fig. II.36.** A perspective view along the *c* axis of the (4,4) [Cu(4,4'-bpy)<sub>2</sub>]<sub>n</sub> grid of **25**. Only with the bridging 4,4'-bpy and the copper atoms (up) and the full crystal packing (bottom).

The methylmalonate ligand adopts simultaneously the bidentate [through O(2) and O(4) to Cu(1), the angle subtended at the copper atom being 92.30(12)°] and bis-monodentate coordination modes [through O(3) and O(1) to Cu(2) and Cu(2a), respectively;  $a = -x+3/2, y, z-1/2$ ]. The four crystallographically different 4,4'-bpy ligands present in **25** exhibit two different coordination modes. Two 4,4'-bpy molecules act as monodentate ligands towards Cu(1) being the terminal groups of the pillaring unit, while the 4,4'-bpy

group which acts as bis-monodentate ligands towards Cu(2) are responsible for the construction of the square grid. The pyridyl rings of the 4,4'-bpy ligands are planar but the ligand as a whole are far from being planar, the angles between the pyridyl rings vary in the range  $8.2(1)^\circ$  to  $25.3(2)^\circ$ , the terminal 4,4'-bpy ligands being the more planar. The terminal 4,4'-bpy ligands are situated in the channels created by the pillaring of the  $[\text{Cu}(4,4'\text{-bpy})_2]_n$  2D-network (Figure II.37). They exhibit a trend to point towards the growing direction of the channel and establish weak  $\pi$ - $\pi$  stacking interactions with adjacent terminal 4,4'-bpy groups building a zigzag tape along the channel.

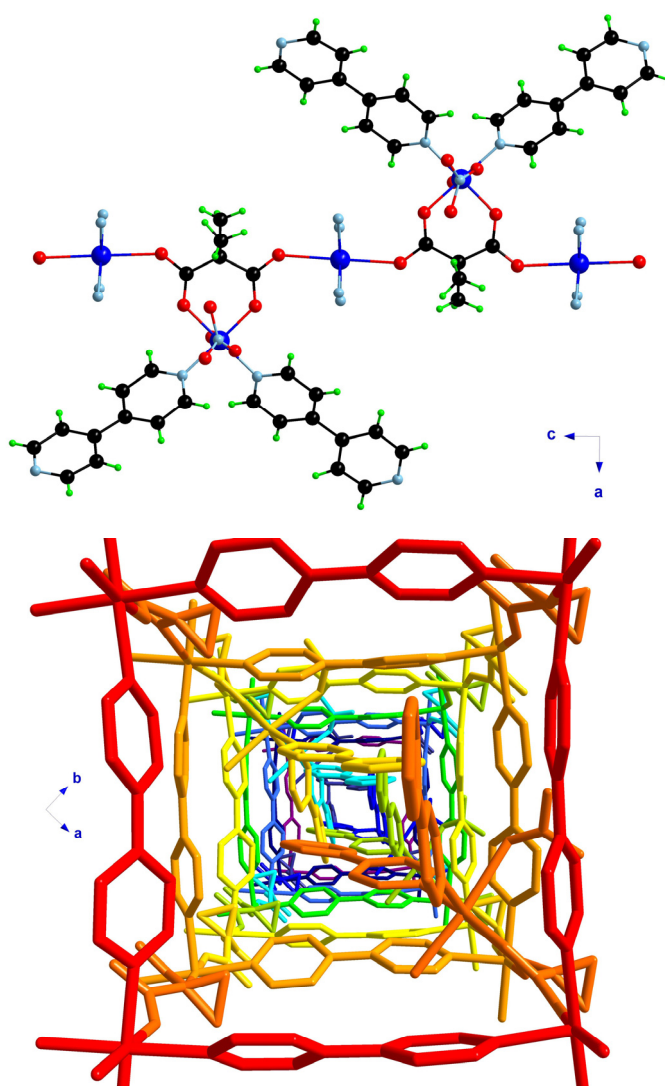


**Fig. II.37.** View along the  $b$  axis of the pillaring units which connects the parallel  $[\text{Cu}(4,4'\text{-bpy})_2]_n$  grids in the crystal structure of **25** (up) where the bridging 4,4'-bpy ligands are not showed for clarity purposes. Central projection of one of the pores of **25** along the  $c$  direction (bottom).

The copper-copper separation within the square grid of  $[\text{Cu}(4,4'\text{-bpy})_2]_n$  is the same since it involves only Cu(2), and it has a value of 11.2198(12) Å. The Cu(1)⋯Cu(2) separation through the two crystallographically independent carboxylate bridges O(3)–C(3)–O(4) and O(1)–C(1)–O(2) are 5.6430(9) and 5.6248(9) Å, respectively. The carboxylate bridges exhibit the *anti-syn* coordination mode and they link one equatorial position of Cu(1) with an apical one of Cu(2).

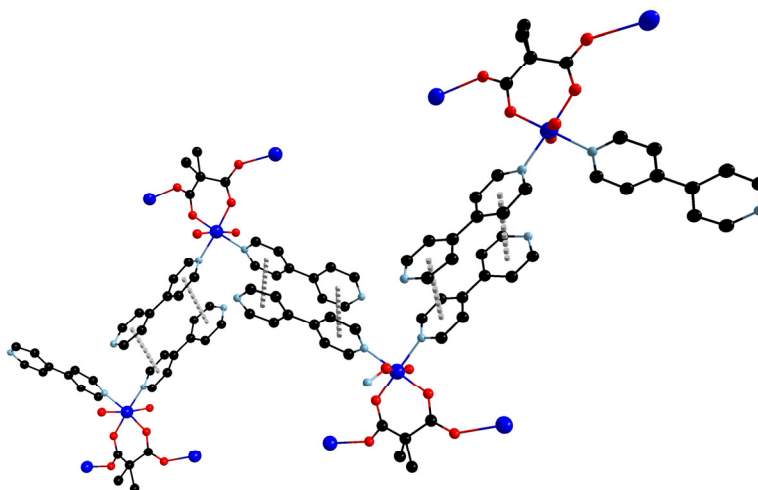


Fig. II.38.  $\pi$ - $\pi$  stacking among the pendant 4,4'-bpy terminal ligands of the pillar unit in **25**. These 4,4'-bpy ligands fill the channels of the  $[\text{Cu}(4,4'\text{-bpy})_2]_n$  grids.

The structure of **25** resembles that of the family of compounds  $[\text{Cu}(\text{A})(4,4'\text{-bpy})_2]_n \cdot n\text{H}_2\text{O}$  (A is a counterion such as  $[\text{SiF}_6]^{2-}$ ,  $[\text{GeF}_6]^{2-}$ ,  $[\text{PF}_6]^-$ ) reported Kitagawa's group.<sup>5,6</sup> The structure of the complex  $[\text{Cu}(\text{SiF}_6)(4,4'\text{-bpy})_2]_n \cdot 8n\text{H}_2\text{O}$  consists of a 3D-network based on a square grid of  $[\text{Cu}(4,4'\text{-bpy})_2]_n$  and pillars of  $\text{SiF}_6^{2-}$  anions, the same as in **25** where the pillars are the  $[\text{Cu}(4,4'\text{-bpy})_2(\text{Memal})(\text{NO}_3)(\text{H}_2\text{O})]$  units. Main differences include the cationic character of the 3D-network of **25**, and the presence of the terminal 4,4'-bpy ligands in the channels, which are filled only with crystallization water molecules in the Kitagawa's complex. The existence of a complex such as **25** shows up the robustness of the 2D  $[\text{Cu}(4,4'\text{-bpy})_2]_n$  network, which can be pillared through bulkier groups than the anions of the family  $[\text{AF}_6]^{x-}$  [A = Si and Ge (x=2) and P (x = 1)].

**Table II.19.** Selected bond angles (°) and lengths (Å) for **25** and **26**.<sup>a</sup>

| <b>25</b>        |            |                   |            |
|------------------|------------|-------------------|------------|
| Cu(1)–O(2)       | 1.908(3)   | Cu(2)–N(5)        | 2.080(4)   |
| Cu(1)–O(4)       | 1.936(3)   | Cu(2)–N(6a)       | 2.081(4)   |
| Cu(1)–N(1)       | 2.042(4)   | Cu(2)–N(7)        | 2.060(4)   |
| Cu(1)–N(3)       | 2.002(4)   | Cu(2)–N(8b)       | 2.079(4)   |
| Cu(1)–O(1w)      | 2.394(5)   | Cu(2)–O(1c)       | 2.397(3)   |
| Cu(1)–O(5)       | 2.692(6)   | Cu(2)–O(3)        | 2.331(3)   |
| O(2)–Cu(1)–O(4)  | 92.31(12)  | N(5)–Cu(2)–N(6a)  | 178.11(18) |
| O(2)–Cu(1)–N(1)  | 87.68(14)  | N(5)–Cu(2)–N(7)   | 88.82(17)  |
| O(2)–Cu(1)–N(3)  | 173.08(19) | N(5)–Cu(2)–N(8b)  | 90.97(16)  |
| O(2)–Cu(1)–O(1w) | 92.93(18)  | N(5)–Cu(2)–O(1c)  | 94.93(15)  |
| O(2)–Cu(1)–O(5)  | 86.8(2)    | N(5)–Cu(2)–O(3)   | 88.56(16)  |
| O(4)–Cu(1)–N(1)  | 173.92(19) | N(6a)–Cu(2)–N(7)  | 91.52(16)  |
| O(4)–Cu(1)–N(3)  | 87.33(14)  | N(6a)–Cu(2)–N(8b) | 88.61(16)  |
| O(4)–Cu(1)–O(1w) | 84.30(18)  | N(6a)–Cu(2)–O(1c) | 83.22(14)  |
| O(4)–Cu(1)–O(5)  | 103.4(2)   | N(6a)–Cu(2)–O(3)  | 93.26(14)  |
| N(1)–Cu(1)–N(3)  | 93.41(15)  | N(7)–Cu(2)–N(8b)  | 177.42(18) |
| N(1)–Cu(1)–O(1w) | 89.63(18)  | N(7)–Cu(2)–O(1c)  | 88.32(15)  |
| N(1)–Cu(1)–O(5)  | 82.7(2)    | N(7)–Cu(2)–O(3)   | 94.87(15)  |
| N(3)–Cu(1)–O(1w) | 93.90(18)  | N(8b)–Cu(2)–O(1c) | 89.14(15)  |
| N(3)–Cu(1)–O(5)  | 86.8(2)    | N(8b)–Cu(2)–O(3)  | 87.69(15)  |
| O(1w)–Cu(1)–O(5) | 172.2(2)   | O(1c)–Cu(2)–O(3)  | 175.32(14) |
| <b>26</b>        |            |                   |            |
| Cu(1)–O(1)       | 1.943(3)   | O(1)–Cu(1)–O(1w)  | 79.06(15)  |
| Cu(1)–O(4d)      | 1.930(3)   | O(4d)–Cu(1)–N(1)  | 88.66(14)  |
| Cu(1)–N(1)       | 2.064(4)   | O(4d)–Cu(1)–N(3)  | 90.54(15)  |
| Cu(1)–N(3)       | 2.050(4)   | O(4d)–Cu(1)–O(1w) | 114.85(16) |
| Cu(1)–O(1w)      | 2.289(4)   | N(1)–Cu(1)–N(3)   | 173.62(16) |
| O(1)–Cu(1)–O(4d) | 165.94(15) | N(1)–Cu(1)–O(1w)  | 91.66(1)   |
| O(1)–Cu(1)–N(1)  | 88.86(14)  | N(3)–Cu(1)–O(1w)  | 94.42(15)  |
| O(1)–Cu(1)–N(3)  | 90.39(15)  |                   |            |

<sup>a</sup> Symmetry operations: (a) =  $-x + 1, y + 1/2, -z + 1$ ; (b) =  $-x + 2, y + 1/2, -z + 1$ ; (c) =  $-x + 3/2, y, z + 1/2$ ; (d) =  $x + 1/2, -y + 1/2, z + 1/2$ .

**[Cu(4,4'-bpy)<sub>2</sub>(Memal)(H<sub>2</sub>O)]<sub>n</sub>·nH<sub>2</sub>O (26).** The structure of **26** consists of chains of methylmalonate bridged *trans*-bis(4,4'-bpy)aquacopper(II) units which grow along the [101] direction (Figures II.39 and II.40). These chains are linked (*i*) through hydrogen bonds involving the coordinated, the crystallization water molecule and methylmalonate oxygen atoms (see Table II.20) and (*ii*) through the  $\pi$ - $\pi$  stacking of the 4,4'-bpy ligands to form layers in the *ac* plane (see Figure II.41). The shortest centroid-centroid contact is 3.858(2) Å, being the off-set angle 14.63(12)°, in agreement with previously observed pyridyl-pyridyl contacts.<sup>10</sup> Weak  $\pi$ -type interactions connect the layers to form the supramolecular three-dimensional network [the values of the shortest centroid-centroid separation and off-set angle are 4.359(2) Å and 36.58(14)°, respectively].

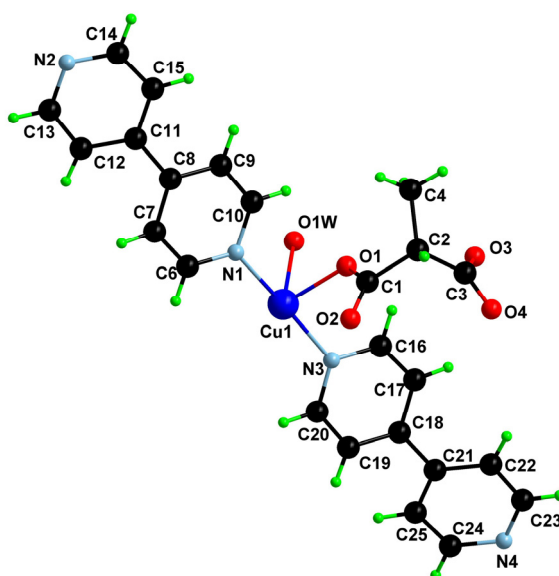


Fig. II.39. View of the asymmetric unit of **26** with the numbering scheme.

Each copper atom in **26** exhibits a somewhat distorted square pyramidal environment the  $\tau$  value being 0.13.<sup>11</sup> Two oxygen atoms from two different methylmalonate ligands [O(1) and O(4a); mean Cu–O(eq) bond distance being 1.936(3) Å; a =  $x + 1/2$ ,  $-y + 1/2$ ,  $z + 1/2$ ] and two 4,4'-bpy nitrogen atoms [N(1) and N(3); average Cu–N bond distance is 2.057(4) Å; see Table II.19] build the basal plane while a water molecule occupies the apical position [Cu(1)–O(1w) = 2.289(4) Å]. The O(1w) is located far from the ideal apical position for a square pyramidal geometry, the angle between the Cu(1)–O(1w) vector line and the normal of the basal plane being 17.65(11)°. The copper atom is shifted towards the apical position by 0.1866(7) Å.

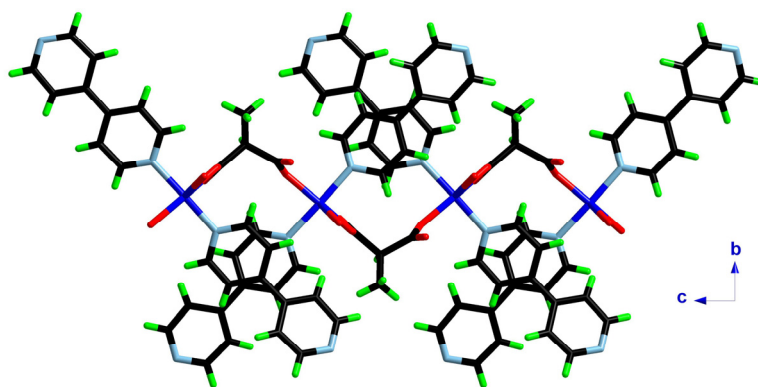
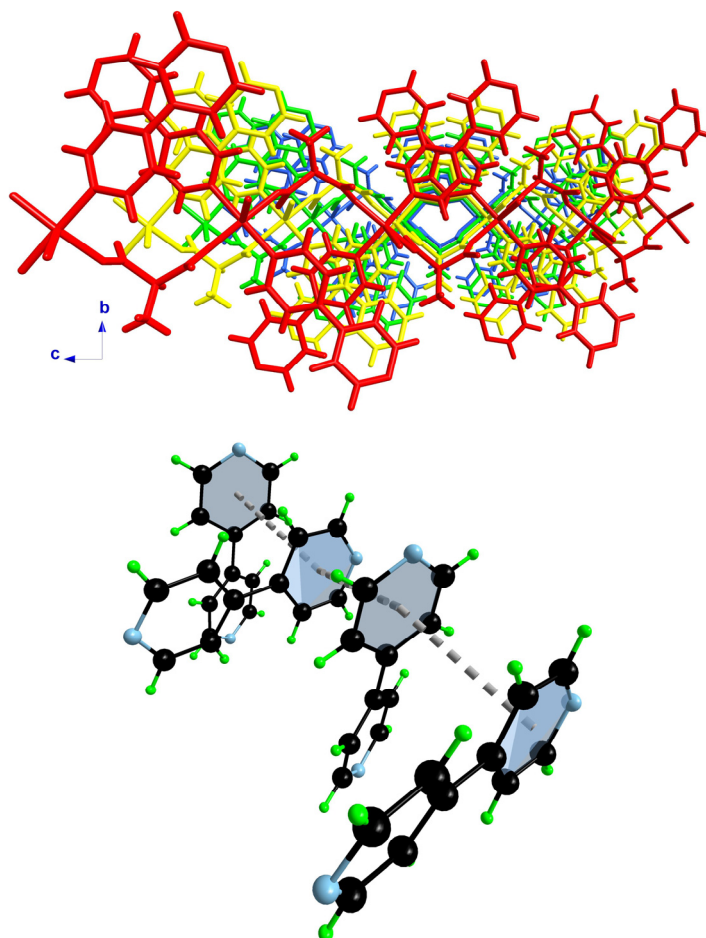


Fig. II.40. A view along the  $a$  axis of a malonato-bridged copper(II) chains formed in **26**.



**Fig. II.41.** (Up) Central projection along the  $a$  axis of the crystal packing of **26**. Different colours correspond to different chains. (Bottom)  $\pi$ - $\pi$  stacking of the 4,4'-bipyridine ligands of adjacent chains. The dashed lines represent the centroid-centroid vectors.

**Table II.20.** Hydrogen bond distances and angles in **26**.

| D ... A                      | O ... O (Å) |
|------------------------------|-------------|
| O(1w)-H...O(2a) <sup>a</sup> | 2.725(5)    |
| O(1w)-H...O(2wa)             | 2.905(7)    |
| O(2w)-H...O(4)               | 2.916(6)    |
| O(2w)-H...O(3b)              | 2.967(7)    |

<sup>a</sup> Symmetry operators: (a) =  $x + 1, y, z$ ; (b) =  $x - 1, y, z$ .

The methylmalonate ligand exhibits a *trans*-bis-monodentate coordination mode [through O(1) and O(4) to Cu(1) and Cu(1b), respectively;  $b = x - 1/2, -y + 1/2, z - 1/2$ ]. This coordination mode is unprecedented in the copper(II)-R-malonate family of complexes (Figure II.42) and it was observed previously only in two zinc(II)-malonate complexes.<sup>12,13</sup> The two crystallographically independent 4,4'-bpy molecules act as monodentate ligands

[through N(1) and N(3)] occupying *trans*-positions in the copper coordination environment. The pyridyl rings of the 4,4'-bpy molecules are planar, but the ligands as a whole are far from being planar being the dihedral angles between pyridyl rings of 27.41(18)° and 12.4(2)°. The copper-copper separation along the chain through the methylmalonate bridge [6.7757(10) Å] is shorter than the shortest interchain Cu⋯Cu distance [7.4191(10) Å].

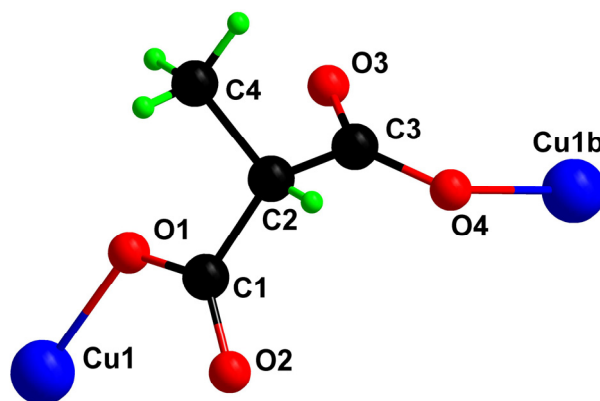


**Fig. II.42.** Conformation of the methylmalonate ligand in **26**, unprecedented in copper(II)-R-malonate complexes.

Although the compounds **19**, **25** and **26** were prepared with the same chemicals, their crystal structures are very different. The Memal:4,4'-bpy molar ratio is illustrative of these dissimilarities 2:1 (**19**), 1:4 (**25**) and 1:2 (**26**). The crystal structure is monitored by the methylmalonate ligand in **19**, and the square grids are similar to those of the [Cu(Memal)(H<sub>2</sub>O)] (**17**) complex. However, the structure in **26** is built by the 4,4'-bpy ligand and leads to the formation of the [Cu(4,4'-bpy)<sub>2</sub>]<sub>n</sub> square grid. Here the functionality of the Cu(Memal) unit reduced to be just a pillar linker. The structure of **26** could be an intermediate case with the methylmalonate as a linker of the [Cu(4,4'-bpy)<sub>2</sub>(H<sub>2</sub>O)] units, but anyway, very different from the other Memal complexes since the Cu(Memal) unit is not present in **26**.

### II.7.5. Magnetic Properties

The magnetic properties of complex **19** have been described in Section II.2.4. The thermal dependence of the magnetic susceptibility and the  $\chi_M T$  product [ $\chi_M$  being the magnetic susceptibility per copper(II) ion] for complex **25** are plotted in Figure II.43. The  $\chi_M T$  value at room temperature is 0.47 cm<sup>3</sup> mol<sup>-1</sup> K, which is as expected for a magnetically isolated spin doublet. Upon cooling,  $\chi_M T$  remains almost constant up to 40 K, and then smoothly



decreases to reach a value of  $0.34 \text{ cm}^3 \text{ mol}^{-1} \text{ K}$  at 2.0 K. This feature is indicative of the existence of antiferromagnetic interactions among the copper(II) ions in **25**.

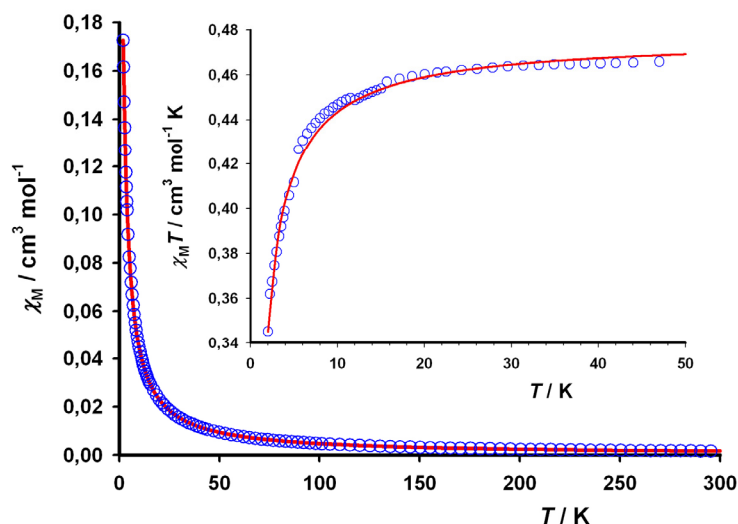


**Fig. II.43.**  $\chi_M$  vs  $T$  plot for **25** under applied fields of 1 T ( $T > 15$  K), 0.1 T ( $15 \text{ K} > T > 5$  K) and 0.02 T ( $T < 5$  K): (o) experimental data, (—) best fit curve. The inset shows a detail of the low temperature region for the  $\chi_M T$  vs  $T$  plot.

Two different magnetic exchange pathways can be identified in the crystal structure of **25**: the *anti-syn* carboxylate bridges linking apical with equatorial positions at the copper(II) ions and the 4,4'-bipyridine ligand. The copper-copper separation through the carboxylate exchange pathway is only  $5.6335(9) \text{ \AA}$ , being  $11.2198(12) \text{ \AA}$  through the 4,4'-bpy group. This feature, and the previous reported<sup>14,15</sup> values for the magnetic coupling through the 4,4'-bpy ligand ( $J$  in the range  $-0.05$  to  $-0.1 \text{ cm}^{-1}$ ), make negligible its contribution to the magnetic coupling compared with that of the carboxylate bridge. This approximation has been already used in the analysis of the magnetic behaviour of complex **13** (see chapter I). Thus, the experimental data can be analyzed by means of the numerical expression:<sup>16</sup>

$$\chi_M = \frac{Ng^2\beta^2}{kT} \frac{0.25 + 0.074875x + 0.075235x^2}{1.0 + 0.9931x + 0.172135x^2 + 0.757825x^3}$$

with  $x = |J|/kT$ , the Hamiltonian defined as  $\sum_i -JS_i S_{i+1}$  and  $J$  is the magnetic coupling constant. The best fit using nonlinear regression analysis leads to  $J = -1.23(1) \text{ cm}^{-1}$ ,  $g = 2.25(2)$ , and  $R = 9.8 \times 10^{-5}$ . The calculated curve matches well the experimental data in the whole temperature range, as seen in Figure II.43.

The weak magnetic coupling parameter obtained is in accordance with the *anti-syn* conformation of the carboxylate bridge which can mediate weak either ferro- or antiferromagnetic interactions.<sup>17-18</sup> The  $J$  value for **25** is in agreement with that of the complex **13** which exhibits a similar magnetic behaviour [ $J$  being  $-0.59(1) \text{ cm}^{-1}$ ].<sup>19</sup> The magnetic orbitals for copper(II) ions in octahedral environment are of the  $d(x^2-y^2)$  character, but with some admixture of the  $dz^2$  character [the  $x$  and  $y$  axes roughly defined by the equatorial bonds whereas the  $z$  axis corresponds to the axial bond]. The copper(II) ions and the carboxylate group lie in a plane with maximum deviation from the planarity of  $0.071(5) \text{ \AA}$  in **25** [ $0.321(2) \text{ \AA}$  for **13**]. According to the Kahn's model,<sup>20</sup> this situation is optimum to maximize the overlap between the magnetic orbitals of the metal ions and those of the atoms of the bridge, making the antiferromagnetic contribution to dominate.

The magnetic properties for **26** under the form of  $\chi_M$  and  $\chi_M T$  vs.  $T$  plots are displayed in the Figure II.44 [ $\chi_M$  being the magnetic susceptibility per copper(II) ion]. The value of  $\chi_M T$  at room temperature is  $0.43 \text{ cm}^3 \text{ mol}^{-1} \text{ K}$ , which is as expected for a magnetically isolated spin doublet. The  $\chi_M T$  value remains constant up to 20 K and then smoothly decreases to reach  $0.30 \text{ cm}^3 \text{ mol}^{-1} \text{ K}$  at 2.0 K. This feature is indicative of the presence of very weak antiferromagnetic interactions in **26**.

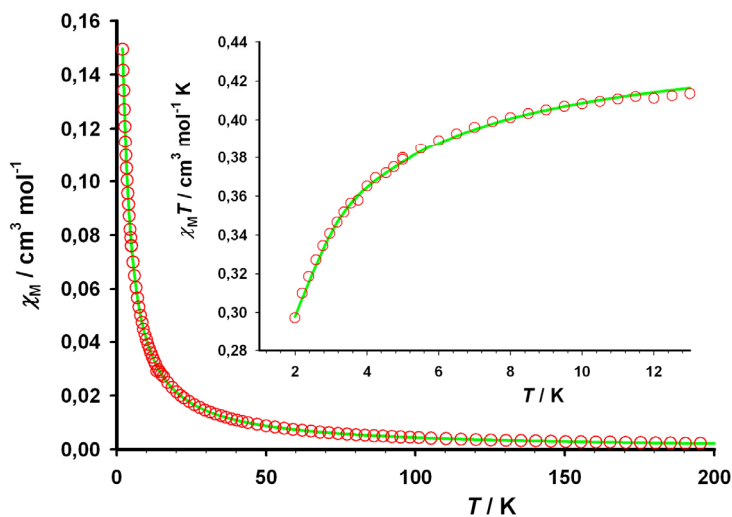


**Fig. II.44.**  $\chi_M$  vs  $T$  plot for **26** under applied fields of 1 T ( $T > 15$  K) and 0.1 T ( $T < 15$  K): (○) experimental data, (—) best fit curve. The inset shows a detail of the low temperature region for the  $\chi_M T$  vs  $T$  plot.

There exists only one possible magnetic exchange pathway in **26**, the skeleton of the malonate ligand (OCCCCO exchange pathway). A previous work supported by DFT investigations<sup>21</sup> establishes that this exchange pathway can be operative and mediates antiferromagnetic interactions. Thus, the magnetic data of **26** can be analyzed by means of the expression:<sup>16</sup>

$$\chi_M = \frac{Ng^2\beta^2}{kT} \frac{0.25 + 0.074875x + 0.075235x^2}{1.0 + 0.9931x + 0.172135x^2 + 0.757825x^3}$$

with  $x = |J|/kT$ , the Hamiltonian defined as  $\sum_i -JS_iS_{i+1}$  and  $J$  is the magnetic coupling constant. The best fit using nonlinear regression analysis leads to  $J = -1.38(1) \text{ cm}^{-1}$ ,  $g = 2.18(2)$ , and  $R = 3.3 \times 10^{-5}$ . The calculated curve matches well the experimental data in the whole temperature range (see Figure II.44).

The value for the magnetic coupling is in agreement with that reported by C. Ruiz-Pérez et al.<sup>21</sup> for the  $\{[\text{Cu}(2,2'\text{-bpy})(\text{H}_2\text{O})][\text{Cu}(2,2'\text{-bpy})(\text{mal})(\text{H}_2\text{O})]\}(\text{ClO}_4)_2$  complex ( $J$  being  $-4.2 \text{ cm}^{-1}$ ) which was supported by DFT calculations ( $J$  ca.  $-1.78 \text{ cm}^{-1}$ ). The antiferromagnetic nature of the through-malonate interaction is confirmed by **26**; where other magnetic exchange pathways (with the exception of the interchain through-space one) are not available. However, the magnitude of the interaction is questionable since the two malonate-bridges, in **26** and the reported complex, are structurally very different. Main differences involve *trans*-coordination for the copper atoms in **26** (see Figure II.42). Thus, the through-malonate exchange pathway mediates weak antiferromagnetic interactions, but with only two examples, a magneto-structural correlation cannot be made.

### II.7.6. Conclusion

The two complexes presented in this section are very interesting and also, promising. The interest of **25** comes from their unusual crystal structure, which is built from square grid of 4,4'-bpy-bridged copper(II) ions pillared by a copper(II)-malonate unit. Although the  $11 \times 11 \text{ \AA}^2$  channels formed by the 2D-network of  $[\text{Cu}(4,4'\text{-bpy})_2]$  are filled with terminal 4,4'-bpy ligands in **25**, this structure could be viewed as a first step in the preparation of rationally designed microporous materials. For example, larger pore dimensions could be achieved by the introduction of spacers such as 4,4'-azo-bis(pyridine), 4,4'-bis(pyridyl)ethylene or 4,4'-bis(pyridyl)ethane.

The methylmalonate ligand in **25** and **26** does not play a fundamental role as, for example, in complexes **18** or **19**. The copper(II) coordinated Memal acts as a pillaring unit

in **25**, whereas it is a simple spacer in **26**, it is not chelating. This is a surprising behaviour of the methylmalonate ligand and, also, of the malonate ligand, a further investigation being necessary to corroborate if this is an isolated case or well the formation of different phases is usual and one can obtain those products through simple variations of the synthetic routes.

## II.7.7. References

- 1 (a) C. Janiak, *Dalton Trans.* **2003**, 2781. (b) B. Moulton and M. J. Zaworotko, *Chem. Rev.* **2001**, *101*, 1629. (c) M. J. Zaworotko, *Chem. Commun.* **2001**, 1.
- 2 (a) S. R. Batten and R. Robson, *Angew. Chem., Int. Ed.* **1998**, *37*, 1461; (b) S. R. Batten, *CrystEngComm*, **2001**, *3*, 67. (c) S. L. James, *Chem. Soc. Rev.* **2003**, *32*, 276.
- 3 (a) C. Ruiz-Pérez, P. A. Lorenzo-Luis, M. Hernández-Molina, M. M. Laz, P. Gili and M. Julve, *Cryst. Growth Des.* **2004**, *4(1)*, 57. (b) B. Rather and M. J. Zaworotko, *Chem. Commun.* **2003**, 830. (c) J.-L. Song, A. V. Prosvirin, H.-H. Zhao and J.-G. Mao, *Eur. J. Inorg. Chem.* **2004**, 3706.
- 4 (a) M. Kondo, T. Yoshitomi, K. Seki, H. Matsuzaka and S. Kitagawa, *Angew. Chem., Int. Ed. Engl.* **1997**, *36*, 1725. (b) M. Fujita, Y. J. Kwon, S. Washizu and K. Ogura, *J. Am. Chem. Soc.* **1994**, *116*, 1151. (c) O. Ohmori and M. Fujita, *Chem. Commun.* **2004**, 1586.
- 5 S. Noro, S. Kitagawa, M. Kondo and K. Seki, *Angew. Chem. Int. Ed.* **2000**, *39*, 2082.
- 6 S. Noro, R. Kitaura, M. Kondo, S. Kitagawa, T. Ishii, H. Matsuzaka and M. Yamashita, *J. Am. Chem. Soc.* **2002**, *124*, 2568.
- 7 G. M. Sheldrick, *SHELXL-97* and *SHELXS-97*; Universität Göttingen: Göttingen, Germany, **1998**.
- 8 H. D. Flack *Acta Cryst., Sect. A* **1983**, *A39*, 876.
- 9 E. I. Stiefel and G. F. Brown, *Inorg. Chem.*, **1972**, *11*, 434.
- 10 C. Janiak, *J. Chem. Soc., Dalton Trans.* **2000**, 3885.
- 11 A. W. Addison, T. N. Rao, J. Reedijk, J. van Rijn and G. C. Verschoor, *Dalton Trans.* **1984**, 1349.
- 12 Y. Zhang, J. Li, J. Chen, Q. Su, W. Deng, M. Nishiura, T. Imamoto, X. Wu and Q. Wang, *Inorg. Chem.* **2000**, *39*, 2330.
- 13 A. D. Burrows, R. W. Harrington, M. F. Mahon and C. E. Price, *Dalton Trans.* **2000**, 3845.
- 14 Y. Rodríguez-Martín, C. Ruiz-Pérez, J. Sanchiz, F. Lloret and M. Julve, *Inorg. Chim. Acta* **2001**, *318*, 159.
- 15 (a) M. S. Haddad, D. N. Hendrickson, J. P. Cannady, R. S. Drago and D. S. Bieksza, *J. Am. Chem. Soc.* **1979**, *101*, 898. (b) M. Julve, M. Verdaguer, J. Faus, F. Tinti, J. Moratal, A. Monge and E. Gutiérrez-Puebla, *Inorg. Chem.* **1987**, *26*, 3520. (c) I. Castro, J. Sletten, M. L. Calatayud, M. Julve, J. Cano, F. Lloret and A. Caneschi, *Inorg. Chem.* **1995**, *34*, 4903.
- 16 W. E. Estes, D. P. Gavel, W. E. Hatfield and D. Hodgson, *Inorg. Chem.* **1978**, *17*, 1415.
- 17 A. Rodríguez-Forteza, P. Alemany, S. Álvarez and E. Ruiz, *Chem. Eur. J.* **2001**, *7*, 627.
- 18 J. Pasán, F. S. Delgado, Y. Rodríguez-Martín, M. Hernández-Molina, C. Ruiz-Pérez, J. Sanchiz, F. Lloret and M. Julve, *Polyhedron* **2003**, *22*, 2143.
- 19 J. Pasán, J. Sanchiz, C. Ruiz-Pérez, F. Lloret and M. Julve, *Inorg. Chem.* **2005**, *44*, 7794.
- 20 O. Kahn, *Molecular Magnetism*, VCH, New York, **1993**.
- 21 C. Ruiz-Pérez, M. Hernández-Molina, P. Lorenzo-Luis, F. Lloret, J. Cano and M. Julve, *Inorg. Chem.* **2000**, *39*, 3845.

## II.8. 1,2-bis(4-pyridyl)ethene (27) Copper(II)-Methylmalonate Complex

### II.8.1. Introduction

The previous section has shown that the introduction of a large spacer in the copper(II)-methylmalonate system could afford some different complexes with a variety of crystal structures. The 1,2-bis(4-pyridyl)ethene (bpe) is a ligand similar to the 4,4'-bpy, but somewhat larger and more flexible which it has been used in the construction of coordination polymers of high dimensionality and entangled systems.<sup>1-2</sup> Two related malonate-containing complexes have been previously reported showing the versatility of the bpe ligand.<sup>3</sup> Herein, we report the synthesis, crystal structure and magnetic properties of the  $[\text{Cu}(\text{bpe})(\text{Memal})]_n \cdot 3n\text{H}_2\text{O}$  complex.

### II.8.2. Synthesis

**$[\text{Cu}(\text{bpe})(\text{Memal})]_n \cdot 3n\text{H}_2\text{O}$  (27).** An aqueous solution (5 cm<sup>3</sup>) of copper(II)-methylmalonate (1 mmol) was set in one arm of an H-shaped glass tube while in the other arm a methanolic solution (3 cm<sup>3</sup>) of 1,2-bis(4-pyridyl)ethene (0.5 mmol, 85 mg). The H-shaped tube was filled with a 50/50 water/methanol solution. The first appearing crystals (in a few days) are blue needles (27) and after that, other phases with different crystal habits were grown. They were mechanically separated. Yield 27: 60%. Anal. calc. for  $\text{C}_{32}\text{H}_{40}\text{Cu}_2\text{N}_4\text{O}_{14}$  (27): C, 46.20; H, 4.85; N, 6.73; Found: C, 46.37; H, 4.91; N, 6.88 %. Crystallographic details for complex 27 are listed in Table II.21. The crystal structures of the other phases were not reliably resolved and, hence, they

did not appear in this work. However, we suspect with the basis of preliminary X-ray measurements that among the other phases there is the analogous compound of the pillared complex 25.

**Table II.21.** Crystallographic data for 27.

| <b>27</b>                                 |                                                                       |
|-------------------------------------------|-----------------------------------------------------------------------|
| Formula                                   | $\text{C}_{32}\text{H}_{40}\text{O}_{14}\text{N}_4\text{Cu}_2$        |
| FW                                        | 831.70                                                                |
| Crystal system                            | Monoclinic                                                            |
| Space group                               | $C 2/c$                                                               |
| $a / \text{\AA}$                          | 24.224(2)                                                             |
| $b / \text{\AA}$                          | 16.967(2)                                                             |
| $c / \text{\AA}$                          | 9.309(2)                                                              |
| $\beta / ^\circ$                          | 106.63(2)                                                             |
| $V / \text{\AA}^3$                        | 3666.3(5)                                                             |
| $Z$                                       | 4                                                                     |
| $\mu(\text{Mo K}\alpha) / \text{cm}^{-1}$ | 12.31                                                                 |
| $T / \text{K}$                            | 293(2)                                                                |
| $\rho_{\text{calc}} / \text{g cm}^{-3}$   | 1.492                                                                 |
| $\lambda / \text{\AA}$                    | 0.71073                                                               |
| Index ranges                              | $-30 \leq h \leq 31,$<br>$-20 \leq k \leq 22,$<br>$-12 \leq l \leq 8$ |
| Indep. reflect. ( $R_{\text{int}}$ )      | 4119 (0.0410)                                                         |
| Obs. reflect. [ $I > 2\sigma(I)$ ]        | 2735                                                                  |
| Flack parameter                           | -                                                                     |
| Parameters                                | 235                                                                   |
| Goodness-of-fit                           | 1.059                                                                 |
| $R [I > 2\sigma(I)]$                      | 0.0546                                                                |
| $R_w [I > 2\sigma(I)]$                    | 0.1158                                                                |
| $R$ (all data)                            | 0.1037                                                                |
| $R_w$ (all data)                          | 0.1373                                                                |

### II.8.3. Description of the Structure

The structure of **27** (Figure II.45) is a three-dimensional network based on carboxylate(methylmalonate)-bridged chains of copper(II) ions growing along the *c* axis, which are linked through bridging bpe ligands to form a layer in the *bc* plane (Figure II.46).

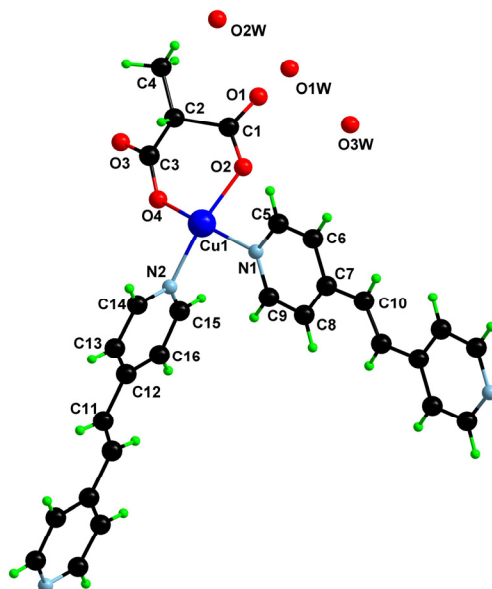


Fig. II.45. A view of a molecular fragment of complex **27** with the numbering scheme.

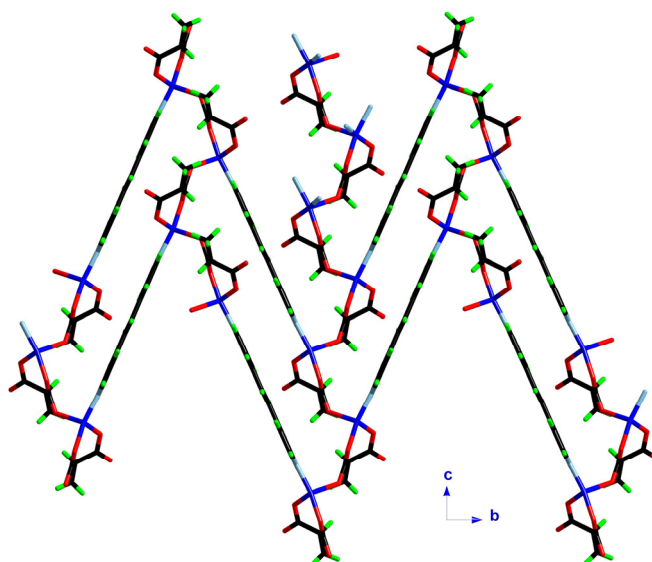


Fig. II.46. A view along the *a* axis of the 3D structure of **27**. The sheets are formed by carboxylate bridging ligands and bpe connectors.

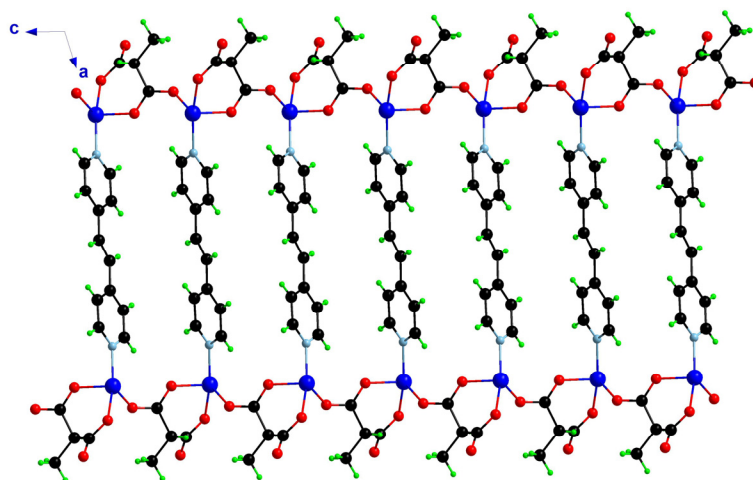


Fig. II.47. A view along the  $b$  axis to visualize the bpe linkers connecting the  $bc$  sheets along the  $a$  axis.

Other bpe ligand acting as a pillar unit connects the adjacent layers along the  $a$  axis (Figure II.47) affording the 3D-network (Figure II.48). The resulting three-dimensional structure exhibits channels along the  $c$  direction of dimensions  $15 \times 14 \text{ \AA}^2$  ( $\text{Cu}\cdots\text{Cu}$  separations) with hourglass shape with the shortest central separation being  $10 \text{ \AA}$  (Figure II.49). The methyl groups of the Memal ligand occupy this area separating the channel in two sections. Each one of these sections is filled with crystallization water molecules, which build a T6(2) water tape motif<sup>4,5</sup> along the channel growing direction [ $\text{O}\cdots\text{O}$  distances ranging from  $2.791(8)$  to  $2.938(9) \text{ \AA}$ ] (Figure II.50). Weak  $\pi$ -type interactions are present in

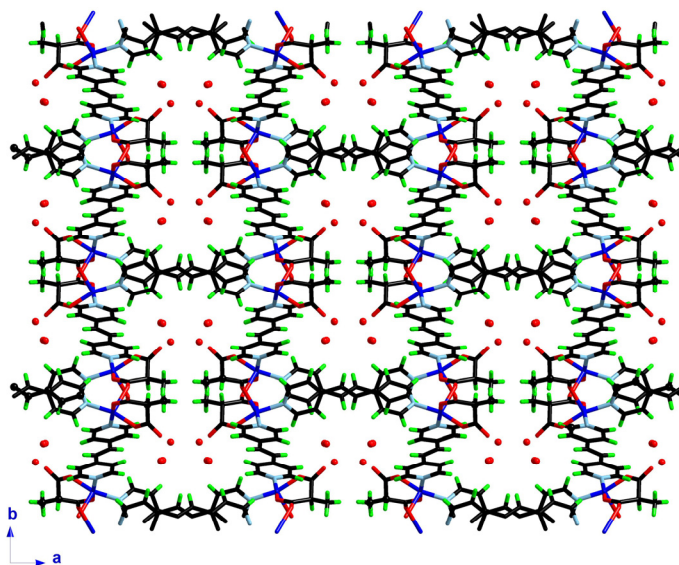
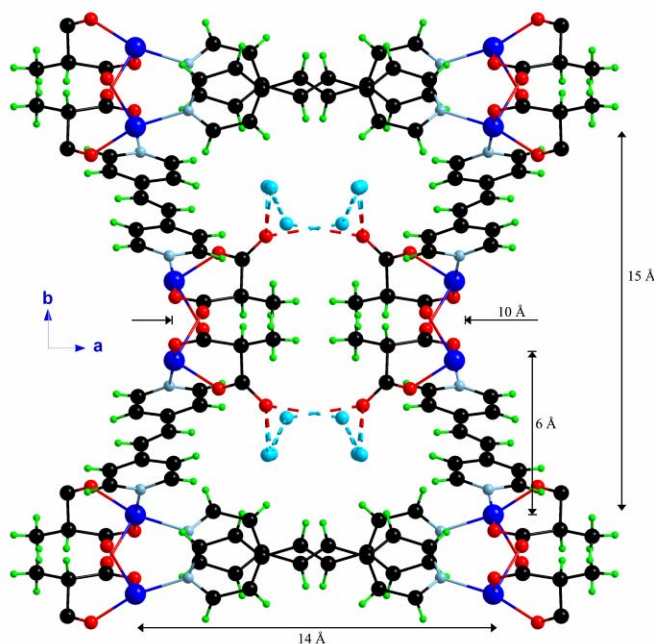


Fig. II.48. A perspective view of the three-dimensional structure of **27** along the  $c$  axis. Water molecules fill the channels of the structure.

the structure of **27**, although many of these interactions are at very long distances. This feature is not expected since the great quantity of pyridyl rings involved in this structure, the shortest contact has a centroid-centroid distance of 4.381(1) Å and the off-set angle being 34.8(1)° which are longer than those observed for related structures.<sup>6</sup>



**Fig. II.49.** A detailed view of one of the channels formed in **27** along with its dimensions.

Each copper atom exhibits a somewhat distorted square pyramidal environment with the  $\tau$  value<sup>4</sup> being 0.11. Two Memal oxygen atoms [O(2) and O(4); average Cu–O(eq) bond distance is 1.937(3) Å; see Table II.22] and two nitrogen atoms from two different bpe ligands [N(1) and N(2); average Cu–N bond distance being 2.022(3) Å] build the equatorial plane while an oxygen atom from a symmetry related Memal ligand occupies the apical position [Cu(1)–O(3) bond distance is 2.228(3) Å].

**Table II.22.** Selected bond angles (°) and lengths (Å) for **27**.

| <b>27</b>       |            |                  |            |
|-----------------|------------|------------------|------------|
| Cu(1)–O(2)      | 1.936(3)   | O(2)–Cu(1)–O(3a) | 94.95(12)  |
| Cu(1)–O(4)      | 1.938(2)   | O(4)–Cu(1)–N(1)  | 169.44(14) |
| Cu(1)–N(1)      | 2.038(3)   | O(4)–Cu(1)–N(2)  | 85.93(12)  |
| Cu(1)–N(2)      | 2.006(3)   | O(4)–Cu(1)–O(3a) | 98.77(11)  |
| Cu(1)–O(3a)     | 2.228(3)   | N(1)–Cu(1)–N(2)  | 92.76(13)  |
| O(2)–Cu(1)–O(4) | 90.50(11)  | N(1)–Cu(1)–O(3a) | 91.75(12)  |
| O(2)–Cu(1)–N(1) | 87.66(12)  | N(2)–Cu(1)–O(3a) | 102.33(12) |
| O(2)–Cu(1)–N(2) | 162.69(14) |                  |            |

<sup>a</sup> Symmetry operations: (a) =  $x, -y, z + 1/2$ ;



The methylmalonate ligand simultaneously acts as bidentate [through O(2) and O(4)]; the angle subtended at the copper atom being  $90.50(11)^\circ$  and as monodentate [through O(3)]. The two crystallographically different bpe ligands act as bis-monodentate and they are strictly planar due to inversion centres in the middle point of the ethylene bonds of both bpe ligands. There are three different bridges connecting the copper atoms. The shortest one involve the carboxylate(methylmalonate)-bridge in *anti-syn* conformation which links one equatorial position with an apical one at a distance of  $5.4706(7)$  Å. The other two bridges connects copper atoms through bpe ligands being the Cu...Cu separations  $13.3477(6)$  and  $13.4570(7)$  Å.

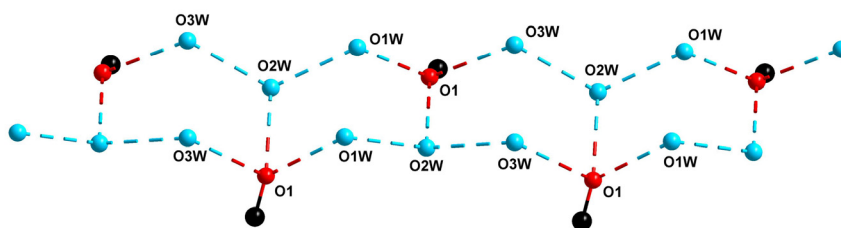


Fig. II.50. T6(2) hydrogen-bonding pattern involving water molecules and an uncoordinated malonate oxygen atom [O(1)] which fills the channels of **27**.

Finally, let us compare the structure of **27** with that of the related malonate-containing complexes  $\{(H_2bpe)[Cu(mal)_2]\}_n \cdot 4nH_2O$  (**a**) and  $[Cu_4(mal)_4(bpe)_3]_n \cdot 6nH_2O$  (**b**).<sup>3</sup> The three complexes exhibit different metal:ligand:bpe ratio; being 1:1:1, 1:2:1 and 4:4:3 for **27**, **a** and **b**, respectively. Two malonate ligands with bidentate conformation leads to the anionic  $[Cu(mal)_2]$  unit which is present in the two mal-containing compounds whereas in **27** the neutral  $[Cu(Memal)]$  unit is favoured. As a result of this situation, the complex **a** has a protonated bpe ligand as counterion. The case of **b** is different and somewhat more similar to that of **27** since a three-dimensional structure is built by the pillaring of malonate-bridged copper(II) sheets through bpe coligands. Two crystallographically different copper atoms were found in **b**, but only one is coordinated by two bpe ligands in *trans*-position occupying equatorial positions. Two bpe ligands also occupy equatorial positions at the copper atom in **27** but they are located in *cis*-position. This feature along with other structural dissimilarities leads to the formation of very different 3D-networks.

#### II.8.4. Magnetic Properties

The thermal dependence of the magnetic susceptibility and the  $\chi_M T$  product for **27** is represented in Figure II.51 [ $\chi_M$  being the magnetic susceptibility per copper(II) ion]. The

$\chi_M T$  value at room temperature is  $0.43 \text{ cm}^3 \text{ mol}^{-1} \text{ K}$ , in accordance with what is expected for a magnetically isolated copper(II) ion. Upon cooling,  $\chi_M T$  remains almost constant up to 30 K and then smoothly decreases to reach a value of  $0.32 \text{ cm}^3 \text{ mol}^{-1} \text{ K}$  at 2.0 K. This situation is indicative of the existence of weak antiferromagnetic interactions coupling the copper(II) ions.

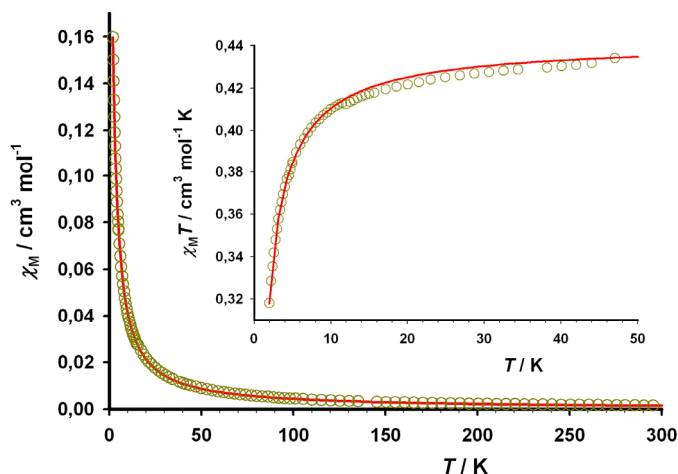


**Fig. II.51.**  $\chi_M$  vs  $T$  plot for **27** under applied fields of 1 T ( $T > 22$  K) and 0.05 T ( $T < 22$  K): (o) experimental data, (—) best fit curve. The inset shows a detail of the low temperature region for the  $\chi_M T$  vs  $T$  plot.

There are two different magnetic exchange pathways in the structure of **27**: through the *anti-syn* equatorial-apical carboxylate bridges and through the bpe coligands. It is clear that the much larger copper-copper separations across bridging bpe (more than 13 Å) when compared to the shorter values across the carboxylate bridge [5.4706(7) Å] allow us to discard the exchange pathways through the bpe coligand. Thus, from a magnetic point of view, **27** can be seen as antiferromagnetically coupled carboxylate-bridged copper(II) chains which can be analyzed by means of the expression:<sup>8</sup>

$$\chi_M = \frac{Ng^2\beta^2}{kT} \frac{0.25 + 0.074875x + 0.075235x^2}{1.0 + 0.9931x + 0.172135x^2 + 0.757825x^3}$$

with  $x = |J|/kT$ , the Hamiltonian defined as  $\sum_i -JS_i S_{i+1}$  and  $J$  is the magnetic coupling constant. The best fit using nonlinear regression analysis leads to  $J = -1.25(1) \text{ cm}^{-1}$ ,  $g = 2.27(2)$  and  $R = 2.1 \times 10^{-5}$ . The calculated curve matches well the experimental data in the whole temperature range (see Figure II.51).

The weak magnetic coupling ( $J$ ) is in agreement with the *anti-syn* conformation of the carboxylate bridge which is able to mediate weak ferro- or antiferromagnetic

interactions.<sup>9-10</sup> The  $J$  value is in accordance with that of the complexes **13** and **25**,  $J$  are  $-0.59$  and  $-1.23(1)$   $\text{cm}^{-1}$ , respectively; which exhibit the same magnetic behaviour and structural features. The magnetic orbitals for copper(II) ions with square pyramidal environments are of the  $d(x^2-y^2)$  character, but with some admixture of the  $d(z^2)$  character [the  $x$  and  $y$  axes roughly defined by the equatorial bonds whereas the  $z$  axis corresponds to the axial bond]. The copper(II) ions and the carboxylate group lie in a plane with maximum deviation from the planarity of  $0.325(2)$  Å in **27** [ $0.321(2)$  Å and  $0.071(5)$  Å for **13** and **25**, respectively]. According to the Kahn's model,<sup>11</sup> this situation is optimum to maximize the overlap between the magnetic orbitals of the metal ions and those of the atoms of the bridge, making the antiferromagnetic contribution to dominate.

### II.8.5. Conclusion

The crystal structure of **27** is three-dimensional based on carboxylate bridged copper(II) chains linked through bpe ligands. The resulting structure exhibit pores of dimensions  $15 \times 14$  Å<sup>2</sup>, which are hosts for crystallization water molecules. The results obtained with the 4,4'-bpy group have not been reproduced but a highly porous system has been synthesized. The analysis of its porous properties is not the main field of this work, but it should be further investigated. From a magnetic point of view, the copper(II) ions exhibit weak antiferromagnetic interactions through the carboxylate exchange pathways [ $J$  being  $-1.25(1)$   $\text{cm}^{-1}$ ].

### II.8.6. References

- 1 (a) M. A. Withersby, A. J. Blake, N. R. Champness, P. A. Cooke, P. Hubberstey, A. L. Realf, S. J. Teat and M. Schröder, *Dalton Trans.* **2000**, 3261. (b) S. R. Batten, J. C. Jeffery and M. D. Ward, *Inorg. Chim. Acta* **1999**, 292, 231. (c) A. Das, G. Pilet, D. Luneau, M. S. El Fallah, J. Ribas and S. Mitra, *Inorg. Chim. Acta* **2005**, 358, 4581. (d) G. Marin, V. Tudor, V. C. Kravtsov, M. Schmidtman, Y. A. Simonov, A. Muller and M. Andruh, *Cryst. Growth Des.* **2005**, 5, 279.
- 2 (a) T. K. Maji, M. Ohba and S. Kitagawa, *Inorg. Chem.* **2005**, 44, 9225. (b) C. Janiak, *Dalton Trans.* **2003**, 2781. (c) B. Moulton and M. J. Zaworotko, *Chem. Rev.* **2001**, 101, 1629.
- 3 F. S. Delgado, J. Sanchiz, C. Ruiz-Pérez, F. Lloret and M. Julve, *Inorg. Chem.* **2003**, 42, 5938.
- 4 L. Infantes, J. Chisholm and S. Motherwell, *CrystEngComm* **2003**, 5(85), 480.
- 5 L. Infantes and S. Motherwell, *CrystEngComm* **2002**, 4(75), 454.
- 6 C. Janiak, *Dalton Trans.* **2000**, 3885.
- 7 A. W. Addison, T. N. Rao, J. Reedijk, J. van Rijn and G. C. Verschoor, *Dalton Trans.* **1984**, 1349.
- 8 W. E. Estes, D. P. Gavel, W. E. Hatfield and D. Hodgson, *Inorg. Chem.* **1978**, 17, 1415.
- 9 A. Rodríguez-Forteza, P. Alemany, S. Álvarez and E. Ruiz, *Chem. Eur. J.* **2001**, 7, 627.
- 10 J. Pasán, F. S. Delgado, Y. Rodríguez-Martín, M. Hernández-Molina, C. Ruiz-Pérez, J. Sanchiz, F. Lloret and M. Julve, *Polyhedron* **2003**, 22, 2143.
- 11 O. Kahn, *Molecular Magnetism*, VCH, New York, **1993**.

---

---

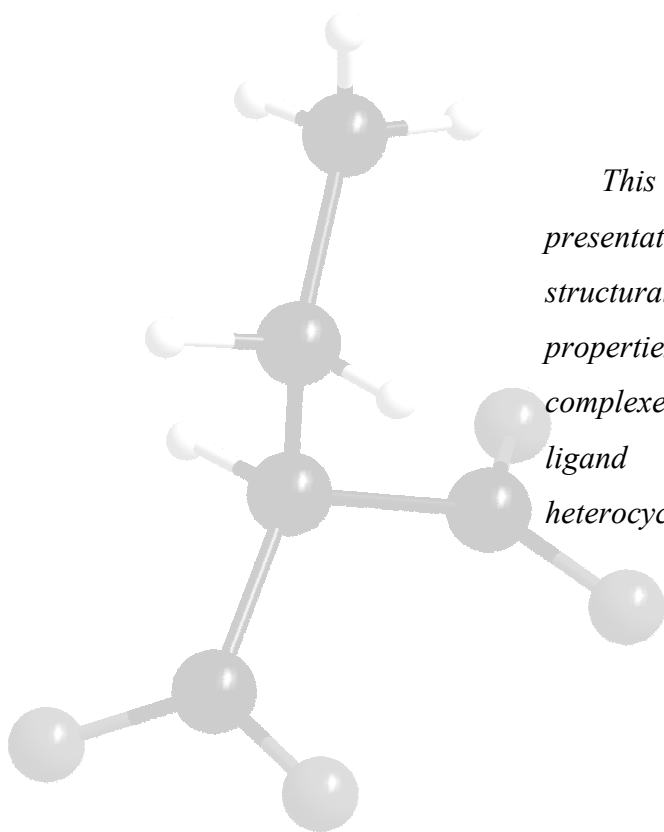
## Chapter III.

# Ethylmalonate

# Complexes

---

---



*This chapter is devoted to the presentation of the synthesis, structural description and magnetic properties of copper(II) coordination complexes with the Ethylmalonate ligand and other N-donor heterocyclic coligands.*

## III.1. Copper(II)-Ethylmalonate (28, 29 and 30)

### III.1.1. Introduction

The same strategy used in the previous chapters will be applied now for the ethylmalonate ligand. A first attempt of the synthesis of a copper(II) coordination compound with the Etmal ligand and water molecules as unique coligands was made in order to know the coordination ability of the Etmal ligand. Then, and with this knowledge in mind, a suitable choice of N-donor coligands could be made to design characteristic structures with interesting magnetic properties.

From the three complexes that have been obtained during the synthesis, all of them being solvated species but two have almost the same number of water molecules per unit cell and they can then be considered as polymorphs or pseudopolymorphs.<sup>1</sup> This situation is not uncommon since for the malonate ligand, up to five different copper(II) complexes have been synthesized with water molecules as unique coligands.<sup>2-3</sup> The crystal structures of the three Etmal-containing complexes will be investigated and compared with those of the related R-mal (R being H-, Me- or Ph-) copper(II) complexes.

Chiral coordination compounds may be obtained either by enantioselective synthesis using enantiopure chiral species (procedure which yields enantiopure samples), or by spontaneous resolution upon crystallization without any enantiopure chiral species, affording conglomerate.<sup>4</sup> A conglomerate is a mechanical and racemic mixture of chiral crystals, of which each crystal is enantiopure. Discovered as early as in 1846 by Louis Pasteur, spontaneous resolution is still a relatively rare phenomenon, and it cannot be predicted *a priori* because the laws of physics determining the processes are not yet fully understood. However, if there are preferential and extended homochiral interactions between neighbouring chiral units, the chirality would be able to extend to higher dimensionality and hence spontaneous resolution would be more likely to occur. The three complexes presented here crystallize in non-centrosymmetric space groups and two of them spontaneously resolve in chiral structures; the reasons for this preference will be treated here, although a section in chapter IV is devoted to a more general view on this aspect.

Thus, we present here the syntheses, crystal structures and magnetic properties of three copper(II) coordination complexes with ethylmalonate and water molecules as coligands.

### III.1.2. Synthesis

$\{[\text{Cu}(\text{H}_2\text{O})_4][\text{Cu}(\text{Etmal})_2(\text{H}_2\text{O})]\}_n$  (**28**),  $[\text{Cu}(\text{Etmal})(\text{H}_2\text{O})]_n$  (**29**) and  $[\text{Cu}(\text{Etmal})(\text{H}_2\text{O})]_n \cdot 1.65n\text{H}_2\text{O}$  (**30**). The three phases of the copper(II)-ethylmalonate system are synthesized in slightly different conditions. An aqueous solution (3 cm<sup>3</sup>) of copper(II) nitrate (1 mmol, 230 mg) was added to a mixture of ethylmalonic acid (1 mmol, 65 mg) and sodium carbonate (1 mmol, 106 mg) dissolved in water (10 cm<sup>3</sup>). The resulting pale blue solution was left to evaporate at room temperature and pale blue prismatic single crystals of **28** appear in the beaker after a few days (Figure III.1). Yield 85%. Anal. calc. for C<sub>5</sub>H<sub>11</sub>CuO<sub>6</sub> (**28**): C, 26.03; H, 4.80; Found: C, 26.18; H, 4.98 %.

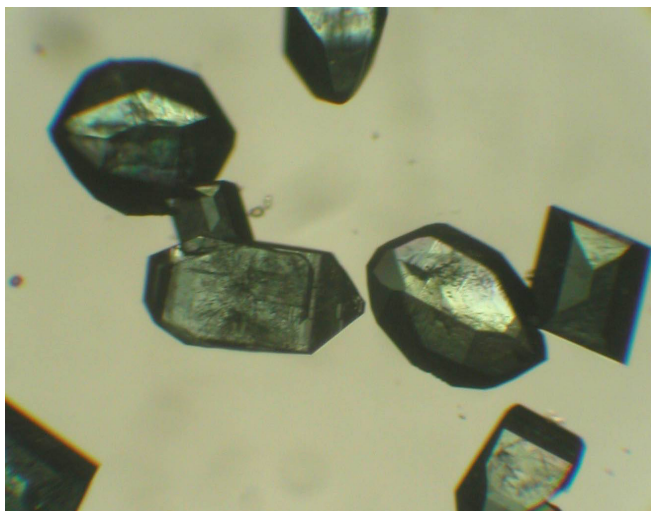


Fig. III.1. Microscope image of single crystals of complex **28**.

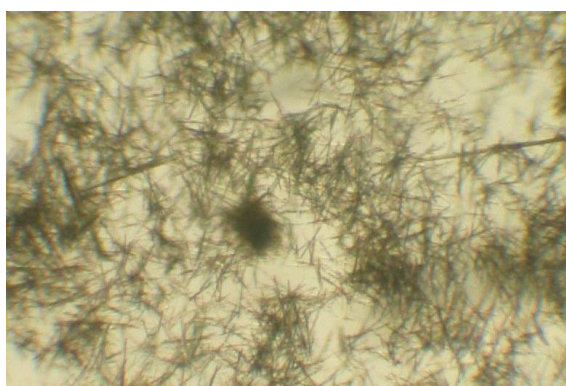
Compound **29** is obtained as **28** but in slightly acidic conditions: a 15% excess of ethylmalonic acid was added to the mixture. Single crystals of **29** as blue plates appear in the resulting pale blue solution after a few days. Yield 50%. Anal. calc. for C<sub>5</sub>H<sub>8</sub>CuO<sub>5</sub> (**29**): C, 28.37; H, 3.81; Found: C, 27.18; H, 3.78 %.

The synthesis of compound **30** is serendipitous. It appeared as blue needles the first time that compound **28** was prepared. The addition of a minimum amount of water for cleaning purposes dissolved the crystals of **30**, those of **28** remaining unsolved. In a second preparation, the needles of **30** appear as poor crystals mixed with nice prismatic ones of **30** (Figure III.2). This product was used for the magnetic measurements, the purity product being confirmed by powder X-ray diffraction. Then, compound **30** literally disappeared and, in spite of our numerous attempts, **30** has not been obtained again, yielding always

compound **28**. Then, it could be a disappearing polymorph as those reported by Bernstein et al.<sup>1</sup> Variation of the copper(II) salt, pH conditions, solvents and temperature were factors tested, but all of them appeared unsuccessful in the preparation of **30**. Anal. calc. for  $C_{10}H_{12}Cu_2O_{13.33}$  (**30**): C, 25.70; H, 2.59; Found: C, 25.85; H, 2.63 %.

**Table III.1.** Crystallographic data for complexes **28-30**

|                                           | <b>28</b>                                                              | <b>28</b>                                                             | <b>29</b>                                                              | <b>30</b>                                                             |
|-------------------------------------------|------------------------------------------------------------------------|-----------------------------------------------------------------------|------------------------------------------------------------------------|-----------------------------------------------------------------------|
| Formula                                   | $C_{10}H_{22}O_{13}Cu_2$                                               | $C_{10}H_{22}O_{13}Cu_2$                                              | $C_5H_8O_5Cu$                                                          | $C_{10}H_{22.66}O_{13.33}Cu_2$                                        |
| FW                                        | 477.36                                                                 | 477.36                                                                | 211.64                                                                 | 483.27                                                                |
| Crystal system                            | Orthorhombic                                                           | Orthorhombic                                                          | Orthorhombic                                                           | Trigonal                                                              |
| Space group                               | $C 222_1$                                                              | $C 222_1$                                                             | $C 2cb$                                                                | $P 3_2$                                                               |
| $a / \text{\AA}$                          | 9.9582(4)                                                              | 9.9825(4)                                                             | 9.770(3)                                                               | 11.5964(8)                                                            |
| $b / \text{\AA}$                          | 12.0031(6)                                                             | 11.8834(6)                                                            | 9.921(3)                                                               | -                                                                     |
| $c / \text{\AA}$                          | 14.1247(13)                                                            | 13.9937(17)                                                           | 14.477(3)                                                              | 10.5437(6)                                                            |
| $V / \text{\AA}^3$                        | 1688.32(19)                                                            | 1659.8(2)                                                             | 1403.2(7)                                                              | 1227.93(14)                                                           |
| $Z$                                       | 4                                                                      | 4                                                                     | 8                                                                      | 3                                                                     |
| $\mu(\text{Mo K}\alpha) / \text{cm}^{-1}$ | 25.85                                                                  | 26.30                                                                 | 30.81                                                                  | 26.67                                                                 |
| $T / \text{K}$                            | 293(2)                                                                 | 100(2)                                                                | 293(2)                                                                 | 293(2)                                                                |
| $\rho_{\text{calc}} / \text{g cm}^{-3}$   | 1.878                                                                  | 1.910                                                                 | 1.985                                                                  | 1.917                                                                 |
| $\lambda / \text{\AA}$                    | 0.71073                                                                | 0.71073                                                               | 0.71073                                                                | 0.71073                                                               |
| Index ranges                              | $-13 \leq h \leq 14,$<br>$-10 \leq k \leq 16,$<br>$-19 \leq l \leq 19$ | $-11 \leq h \leq 12,$<br>$-8 \leq k \leq 15,$<br>$-18 \leq l \leq 18$ | $-12 \leq h \leq 10,$<br>$-10 \leq k \leq 12,$<br>$-18 \leq l \leq 15$ | $-15 \leq h \leq 13,$<br>$-15 \leq k \leq 15,$<br>$-13 \leq l \leq 9$ |
| Indep. reflect. ( $R_{\text{int}}$ )      | 2444 (0.0234)                                                          | 1845 (0.0306)                                                         | 1409 (0.0656)                                                          | 3748 (0.0398)                                                         |
| Obs. reflect. [ $I > 2\sigma(I)$ ]        | 2117                                                                   | 1806                                                                  | 1059                                                                   | 3454                                                                  |
| Flack param.                              | 0.076(11)                                                              | 0.053(12)                                                             | 0.52(4)                                                                | 0.03(3)                                                               |
| Parameters                                | 159                                                                    | 159                                                                   | 101                                                                    | 236                                                                   |
| Goodness-of-fit                           | 0.993                                                                  | 1.073                                                                 | 1.043                                                                  | 1.210                                                                 |
| $R [I > 2\sigma(I)]$                      | 0.0251                                                                 | 0.0201                                                                | 0.0505                                                                 | 0.0599                                                                |
| $R_w [I > 2\sigma(I)]$                    | 0.0465                                                                 | 0.0486                                                                | 0.1112                                                                 | 0.1492                                                                |
| $R$ (all data)                            | 0.0356                                                                 | 0.0209                                                                | 0.0807                                                                 | 0.0676                                                                |
| $R_w$ (all data)                          | 0.0485                                                                 | 0.0490                                                                | 0.1218                                                                 | 0.1645                                                                |

**Fig. III.2.** Microscope image of crystalline material of compound **30**.

Crystallographic details for the three compounds are listed in Table III.1. The thermogravimetric analysis for compound **28** is shown in Figure III.3. The first mass loss of about 20% at ca. 110 °C is due to the lost of all the coordinated water molecules, and then the compound remains stable until 250 °C when the degradation starts.

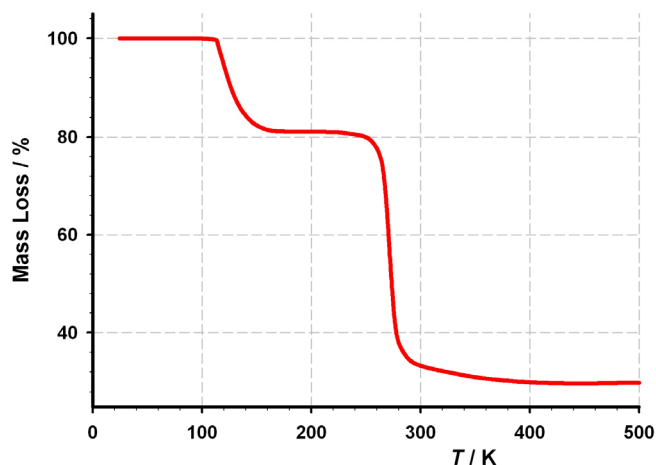


Fig. III.3. Thermogravimetric curve for complex **28** in the 30-500 K temperature range at 10 °C/min heating rate in N<sub>2</sub>.

### III.1.3. Description of the Structures

$\{[\text{Cu}(\text{Etmal})_2(\text{H}_2\text{O})][\text{Cu}(\text{H}_2\text{O})_4]\}_n$  (**28**). The structure of **28** (Figure III.4) is chiral and consists of zigzag chains with a regular alternation of  $[\text{Cu}(\text{Etmal})_2(\text{H}_2\text{O})]^{2-}$  and  $[\text{Cu}(\text{H}_2\text{O})_4]^{2+}$  units, the former being linked to the latter as bis-monodentate ligands through two *trans*-ethylmalonate oxygen atoms, these chains grow along the *c* direction (Figure III.5).

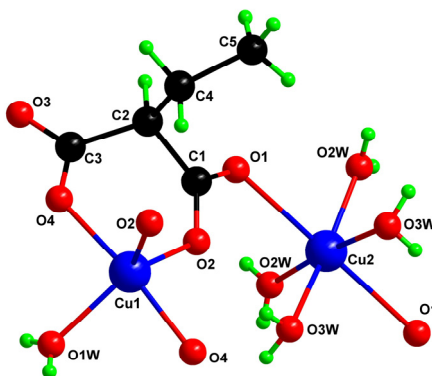
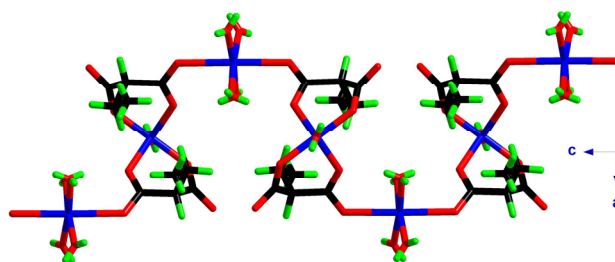


Fig. III.4. View of a fragment of the molecular structure of compound **28** along with the numbering scheme.





**Fig. III.5.** View along the *b* axis of a carboxylate-bridged copper(II) chain of **28**. The regular alternation of copper centres in trigonal bipyramidal and square pyramidal environments could be observed.

The chirality of **28** comes from the fact that all the  $[\text{Cu}(\text{Etmal})_2(\text{H}_2\text{O})]$  units exhibit the copper(II) ion coordinated in the  $\Lambda$  or  $\Delta$  conformation within the  $\Lambda$ - or  $\Delta$ -crystals. Each one of the chains is surrounded by other six ones in a close crystal packing which avoid the presence of crystallization water molecules (Figure III.6). The chains are linked through hydrogen bonds between the coordinated water molecules and coordinated and uncoordinated ethylmalonate oxygen atoms to build a supramolecular three-dimensional network (Table III.2). Figure III.7 shows the H-bonding scheme for the two repeating units along the chain. The tetraaquacopper(II) units are linked to three adjacent chains and the  $[\text{Cu}(\text{Etmal})_2(\text{H}_2\text{O})]$  units are connected to the six adjacent chains. This complex interconnection between the chains could be responsible for the insolubility of this compound in water, fact which favours its crystallization first than the other phases.

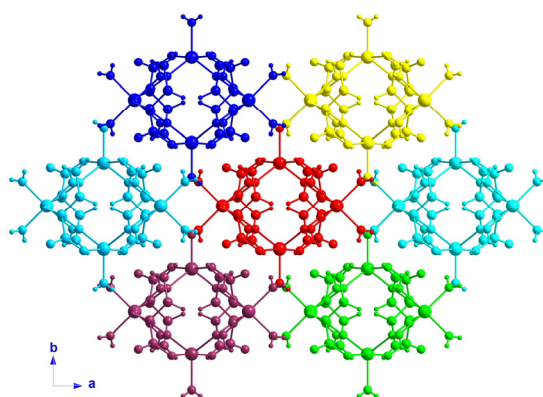


**Fig. III.6.** Perspective view of the crystal packing along the *c* axis in **28**. The different coloured entities refer to different carboxylate-bridged chains.

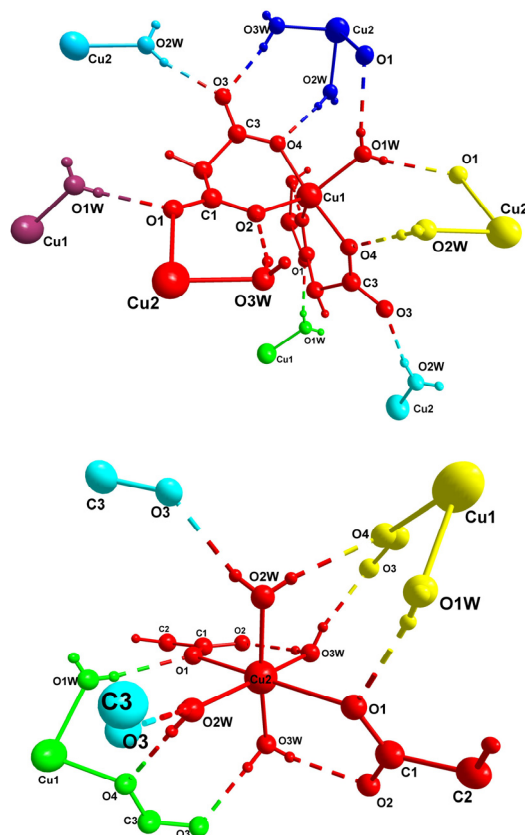


**Fig. III.7.** Hydrogen bonding environment of the  $[\text{Cu}(\text{Etmal})_2(\text{H}_2\text{O})]^{2-}$  (up) and  $[\text{Cu}(\text{H}_2\text{O})_4]$  (bottom) units. The different coloured entities refer to different carboxylate-bridged chains (with same colour code of the Fig. III.6).

**Table III.2.** Hydrogen bond distances and angles in **28**

| D–H···A <sup>a</sup> | O–H (Å) | H···O (Å) | O–H···O (°) | O···O (Å) |
|----------------------|---------|-----------|-------------|-----------|
| O(1w)–H···O(1)       | 0.62(2) | 2.09(2)   | 166(2)      | 2.704(2)  |
| O(2w)–H···O(3)       | 0.72(2) | 2.00(2)   | 166(2)      | 2.719(2)  |
| O(2w)–H···O(4)       | 0.70(2) | 2.13(2)   | 171(2)      | 2.826(2)  |
| O(3w)–H···O(2)       | 0.67(2) | 2.03(2)   | 161(2)      | 2.679(2)  |
| O(3w)–H···O(3)       | 0.74(2) | 1.95(2)   | 167(2)      | 2.675(2)  |

<sup>a</sup>D and A stand for donor and acceptor, respectively.

The two different copper atoms also exhibit different coordination environments. The Cu(1) atom from the  $[\text{Cu}(\text{Etmal})_2(\text{H}_2\text{O})]$  unit presents a trigonal bipyramidal environment with a  $\tau$  value<sup>5</sup> of 0.86, being the first example of this stereochemistry in the copper(II)-(R)malonate series (Figure III.8). Two oxygen atoms from two different ethylmalonate ligands [O(2) and O(2a);  $a = -x+2, y, -z+1/2$ ] and a coordinated water molecule [O(1w); Cu(1)–O(eq) average bond distance is 2.008(2) Å, see Table III.3] build the triangular equatorial plane. The apical positions are filled by two oxygen atoms from

two symmetry-related Etmal ligands [O(4) and O(4a), the Cu(1)–O(ap) bond distance being 1.9445(13) Å]. Each Cu(2) atom from the [Cu(H<sub>2</sub>O)<sub>4</sub>] unit exhibits a distorted octahedral environment (Figure III.8) with the parameters  $s/h$  and  $\phi$  being 1.38 and 55.0° (the values for a ideal octahedron being  $s/h = 1.22$  and  $\phi = 60^\circ$ ).<sup>6</sup> Four water molecules, symmetry related in pairs, build the equatorial plane [O(2w), O(2wb), O(3w) and O(3wb), with Cu(2)–O(eq) mean bond distance of 1.9630(16) Å; (b) =  $x, -y, -z$ ], while two oxygen atoms from two different Etmal ligands [occupy the apical positions [O(1) and O(1b); with Cu(2)–O(ap) bond distance of 2.3937(13) Å].

**Table III.3.** Selected bond angles (°) and lengths (Å) for **28**, **29** and **30**.

| <b>28</b>        |            |                   |            |
|------------------|------------|-------------------|------------|
| Cu(1)–O(2)       | 2.0200(13) | Cu(2)–O(1)        | 2.3937(13) |
| Cu(1)–O(4)       | 1.9445(13) | Cu(2)–O(2w)       | 1.9592(16) |
| Cu(1)–O(1w)      | 1.986(2)   | Cu(2)–O(3w)       | 1.9668(16) |
| O(2)–Cu(1)–O(4)  | 90.69(6)   | O(1)–Cu(2)–O(2w)  | 96.40(7)   |
| O(2)–Cu(1)–O(1w) | 122.65(4)  | O(1)–Cu(2)–O(3w)  | 88.36(7)   |
| O(4)–Cu(1)–O(1w) | 87.06(4)   | O(2w)–Cu(2)–O(3w) | 174.57(9)  |
| <b>29</b>        |            |                   |            |
| Cu(1)–O(1)       | 1.977(5)   | Cu(1)–O(3)        | 1.963(5)   |
| Cu(1)–O(2)       | 1.951(6)   | Cu(1)–O(4)        | 1.946(5)   |
| Cu(1)–O(1w)      | 2.267(6)   |                   |            |
| O(1)–Cu(1)–O(2)  | 162.1(2)   | O(2)–Cu(1)–O(4)   | 89.9(3)    |
| O(1)–Cu(1)–O(3)  | 92.5(2)    | O(2)–Cu(1)–O(1w)  | 94.1(2)    |
| O(1)–Cu(1)–O(4)  | 85.2(2)    | O(3)–Cu(1)–O(4)   | 161.4(3)   |
| O(1)–Cu(1)–O(1w) | 103.6(2)   | O(3)–Cu(1)–O(1w)  | 101.7(2)   |
| O(2)–Cu(1)–O(3)  | 86.5(2)    | O(4)–Cu(1)–O(1w)  | 96.7(2)    |
| <b>30</b>        |            |                   |            |
| Cu(1)–O(2)       | 1.945(5)   | Cu(2)–O(1)        | 1.955(5)   |
| Cu(1)–O(3)       | 1.984(5)   | Cu(2)–O(6)        | 1.950(5)   |
| Cu(1)–O(4)       | 1.973(5)   | Cu(2)–O(7)        | 1.979(5)   |
| Cu(1)–O(5)       | 1.945(5)   | Cu(2)–O(8)        | 1.976(5)   |
| Cu(1)–O(1w)      | 2.305(7)   | Cu(2)–O(2w)       | 2.310(7)   |
| O(2)–Cu(1)–O(3)  | 88.0(2)    | O(1)–Cu(2)–O(6)   | 179.1(2)   |
| O(2)–Cu(1)–O(4)  | 90.6(2)    | O(1)–Cu(2)–O(7)   | 92.1(2)    |
| O(2)–Cu(1)–O(5)  | 179.8(3)   | O(1)–Cu(2)–O(8)   | 89.6(2)    |
| O(2)–Cu(1)–O(1w) | 84.1(3)    | O(1)–Cu(2)–O(2w)  | 95.4(2)    |
| O(3)–Cu(1)–O(4)  | 161.9(2)   | O(6)–Cu(2)–O(7)   | 87.1(2)    |
| O(3)–Cu(1)–O(5)  | 92.0(2)    | O(6)–Cu(2)–O(8)   | 91.2(2)    |
| O(3)–Cu(1)–O(1w) | 91.9(3)    | O(6)–Cu(2)–O(2w)  | 84.2(3)    |
| O(4)–Cu(1)–O(5)  | 89.5(2)    | O(7)–Cu(2)–O(8)   | 161.9(2)   |
| O(4)–Cu(1)–O(1w) | 105.9(3)   | O(7)–Cu(2)–O(2w)  | 92.7(3)    |
| O(5)–Cu(1)–O(1w) | 95.8(2)    | O(8)–Cu(2)–O(2w)  | 105.2(3)   |

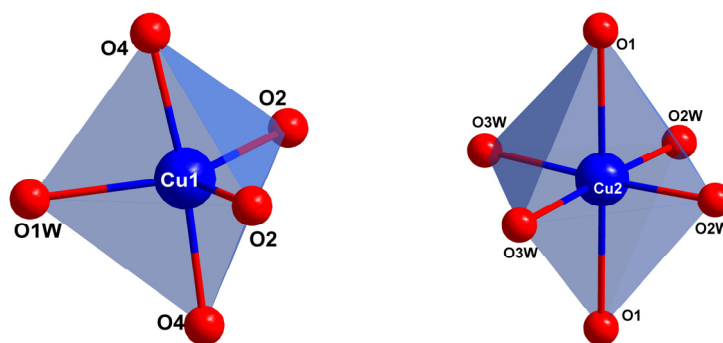


Fig. III.8. Polyhedron view of the two crystallographically different copper(II) environments present in **28**.

The ethylmalonate ligand acts simultaneously as bidentate [through O(2) and O(4) towards Cu(1); the angle subtended at the copper atom being  $90.69(6)^\circ$ ] and monodentate [through O(1) towards Cu(2) ligand]. The Etmal ligand chelates one equatorial [O(2)] and one apical position [O(4)] at the copper atom, this feature was observed previously (see compounds **7**, **12** and **13**) although it is not very common in malonate-based complexes.<sup>7</sup> Cu(1) becomes a stereochemical effective centre because two of these chelating Etmal ligands are coordinated to Cu(1) which exhibits a trigonal bipyramidal environment.

The carboxylate bridge exhibits the *anti-syn* conformation and it links one equatorial position of the trigonal bipyramid environment of Cu(1) with an apical position of the octahedral surrounding of Cu(2). The copper-copper separation through this bridge is  $5.3560(3)$  Å, a value which is slightly longer than the shortest interchain copper-copper separation [Cu(1)⋯Cu(2c) distance being  $5.3324(4)$  Å; (c) =  $x-1/2, y-1/2, z$ ]. The connection between Cu(1) and Cu(2) occurs through two hydrogen bonds Cu(1)–O(1w)–O(1)–Cu(2) and Cu(1)–O(4)–O(2w)–Cu(2);].

The structure of **28** can be compared with those of the previously reported phenylmalonate-  $\{[\text{Cu}(\text{H}_2\text{O})_3][\text{Cu}(\text{Phmal})_2]\}_n$  (**1**, section I.1) and malonate-containing  $\{[\text{Cu}(\text{H}_2\text{O})_3][\text{Cu}(\text{mal})_2(\text{H}_2\text{O})]\}_n$  complexes.<sup>3,8</sup> All the three complexes exhibit the same  $[\text{Cu}(\text{R-mal})_2]^{2-}$  motif which lead to the formation of zigzag chains with the regular alternation of the two conformational units. In the case of **1**, the apical position of the bis(phenylmalonate)copper(II) unit is not occupied by a water molecule but by another  $[\text{Cu}(\text{Phmal})_2]^{2-}$  unit through a  $\mu$ -oxo bridge leading to the chains to assemble in a two-dimensional network. The Etmal- and the mal-containing complexes are very similar, and main differences involve the coordination sphere of the copper atoms being square pyramidal in the mal complex and octahedral and trigonal bipyramidal in **28**. Remarkably, the methylmalonate ligand do not afford the bis(R-mal)copper(II) motif and the chain

structure is not observed in that case. This is an important feature that will be discussed later (section IV.1.3).

**[Cu(Etmal)(H<sub>2</sub>O)]<sub>n</sub> (29).** The structure of **29** (Figure III.9) is made up by a square grid arrangement of aquacopper(II) ions linked through ethylmalonate carboxylate bridges running in the *ab* plane (Figure III.10), very similar to that observed in [Cu(Memal)(H<sub>2</sub>O)]<sub>n</sub> (**16**; section II.1). The resulting corrugated layers are stacked along the *c* direction being the odd layers rotated by 90° in a twist fashion exhibiting the *ABABAB* sequence (Figure III.11).

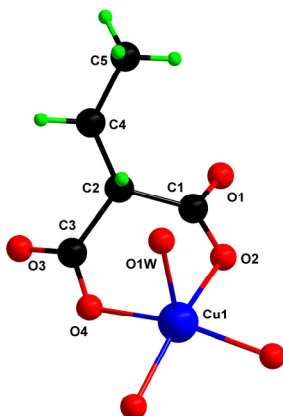


**Fig. III.9.** A view of a molecular fragment of the structure of **29** along with the numbering scheme.

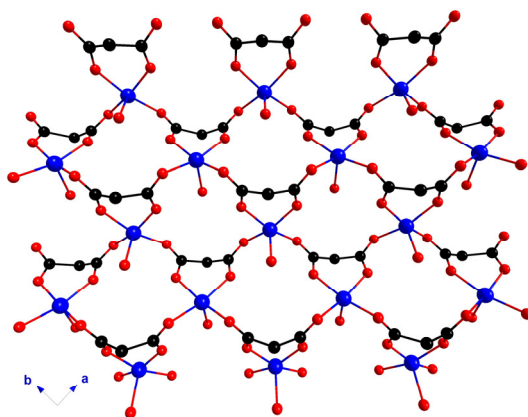


**Fig. III.10.** Central projection view of the carboxylate-bridged square grid of copper(II) ions formed in **29**. Ethyl groups of the Etmal ligands are omitted for clarity.

Each [Cu(Etmal)(H<sub>2</sub>O)] unit presents the ethylmalonate ligand and the coordinate water molecule in a *trans*-conformation inversely to the location of the adjacent units. Intralayer hydrogen bonds involving the coordinated water molecule and ethylmalonate

oxygen atoms contribute to the stabilization of the structure [O(1w)⋯O(2) and O(1w)⋯O(4) distances being 2.762(8) and 2.741(8) Å, respectively]. As the ethyl groups are not disordered, thus the packing of the crystal has to accommodate the ethyl group to close pack the layers, being this fact the origin of the presence of the twist fashion stacking. The adjacent layers insert one on each other with the ethyl groups as teeth of a gear wheel, minimizing the interlayer copper-copper separation (Figure III.11).

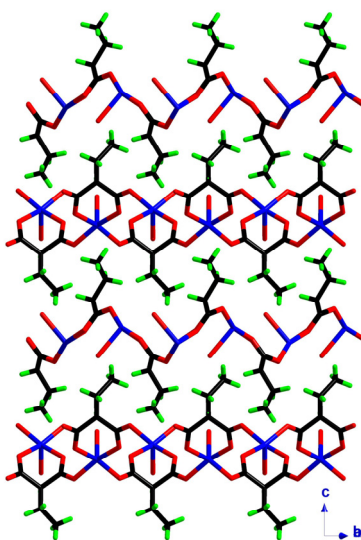


**Fig. III.11.** Perspective view of the crystal packing of the complex **29** where the alternative rotation of 90° of the layers exhibiting the *ABABAB* sequence could be observed.

Each copper atom exhibits somewhat distorted square pyramidal surroundings with a  $\tau$  value<sup>5</sup> of 0.012. Four oxygen atoms from three different ethylmalonate ligands [O(1), O(2), O(3) and O(4); mean Cu–O(eq) bond distance is 1.959(6) Å; see Table III.3] build the basal plane while a water molecule occupies the apical position [Cu–O(1w) is 2.267(6) Å]. The copper atom is shifted from the basal plane toward the apical position by 0.3102(9) Å. The ethylmalonate ligand simultaneously acts as bidentate [through O(2) and O(4); the angle subtended at the copper atom being 89.9(3)°] and bis-monodentate [through O(1) and O(3)] ligand.

There are two crystallographically independent carboxylate bridges in **29**, both exhibiting the *anti-syn* conformation and linking equatorial positions at the copper environments. The values of the Cu⋯Cu separation through these bridges are 4.971(2) and 5.0452(18) Å with an angle between the basal planes of adjacent copper atoms of

88.81(13)°. These values are shorter than the shortest interlayer copper-copper separation [6.6864(16) Å].

The comparison of the structure of **29** with that of **16** reveals a great number of similarities, both complexes being constituted by square grids of carboxylate-bridged aquacopper(II) units. The main difference is that the Memal complex does not cause the twist of one of the layer for a better insertion as occur for the ethyl group of the Etmal ligand in **29**. This is not necessary in **16** due to the smaller size of the methyl group of the Memal ligand. The shortest interlayer copper-copper separations in **16** and **29** are 6.203(3) and 6.6864(16) Å, respectively; pointing out how close is the packing of the layers in **29**.

**[Cu(Etmal)(H<sub>2</sub>O)]<sub>n</sub> · 1.65nH<sub>2</sub>O (30)**. The crystal structure of **30** (Figure III.12) is a three-dimensional network based on carboxylate-bridged aquacopper(II) units. The 3D network shows 9.5 Å diameter pores running along the 3<sub>2</sub> symmetry element parallel to the

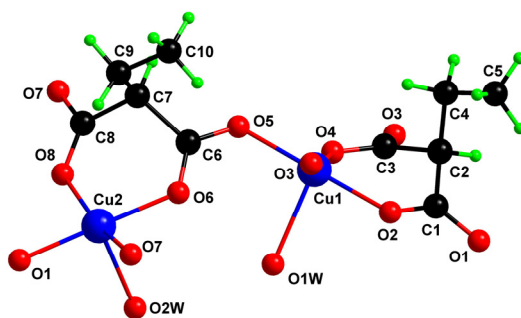


Fig. III.12. View of the asymmetric unit of the structure of **30** along with the numbering scheme.

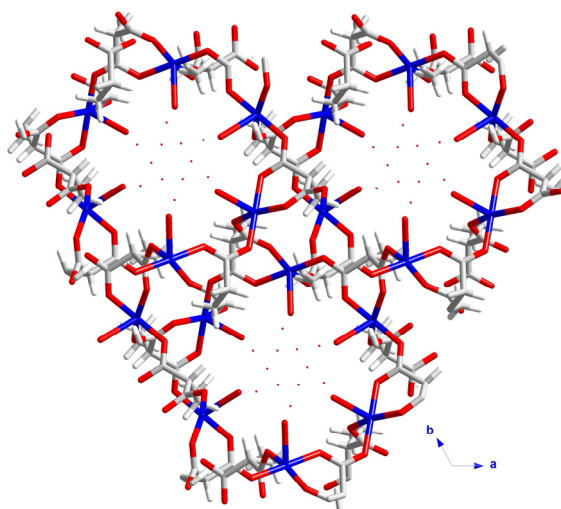
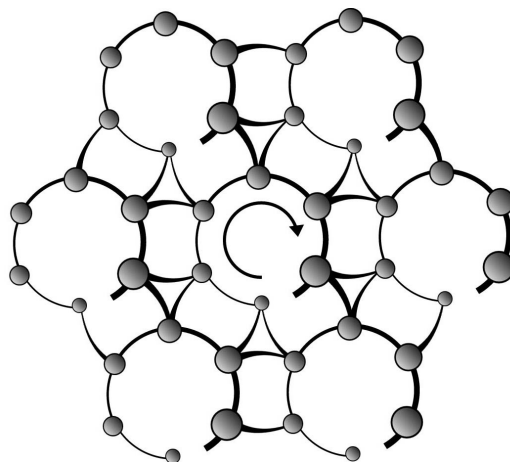
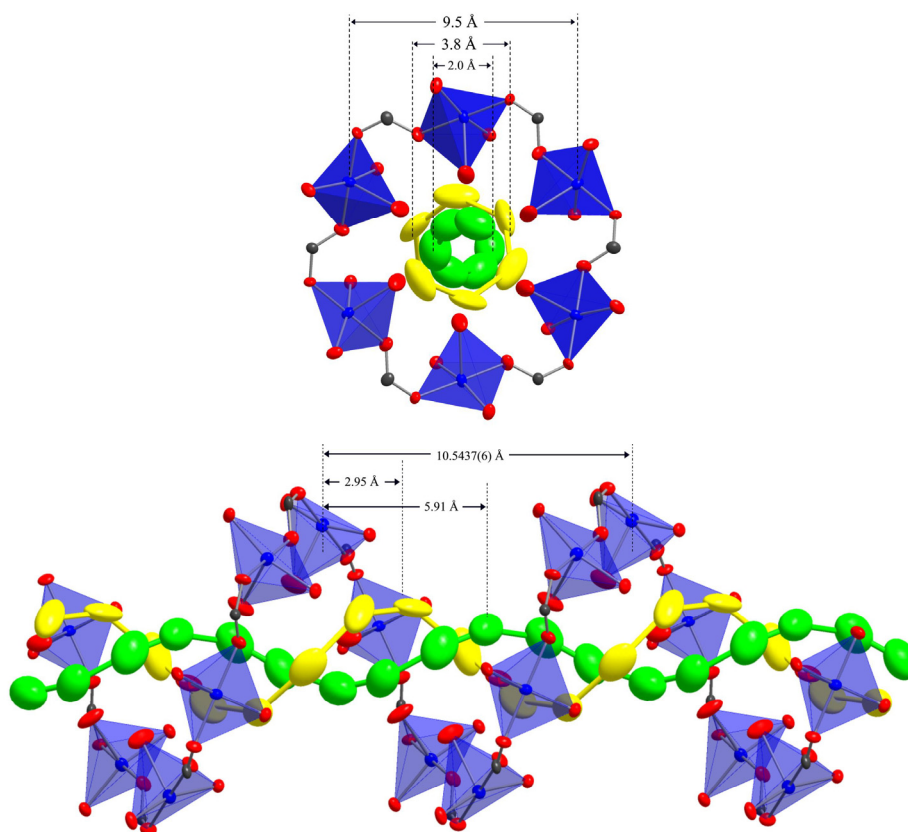


Fig. III.13. Perspective view of the 3D structure of complex **30** along the *c* axis. The pores are filled with crystallization water molecules.



Scheme III.1



**Fig. III.14.** A detailed view of the pore of **30** with its dimensions along the *c* axis (up). View of the carboxylate-bridged copper(II) helices which built up the surface of the pores and the two water helices inside them and the most relevant distances (bottom).



*c* axis (Figure III.13). The pores having the crystallization water molecules embedded are *M*-helices (left-handed) of carboxylate-bridged copper(II) ions which are interconnected through carboxylate bridges affording the three-dimensional polymer, all the carboxylate groups exhibiting the *anti-syn* coordination mode (Scheme III.1). The crystallization water molecules located inside the helix also present a screw moiety. The two helical chains of water molecules are built by inner [O(5w) and O(6w)] and outer [O(3w) and O(4w)] *M*-helices with diameters of *ca.* 2.0 and 3.8 Å, respectively (Figure III.14). The turn-lengths of the three helices are equal to the *c* axis [10.5437(6) Å] but they are shifted by 2.95 Å (outer) and 5.91 Å (inner) respect to the copper(II) helix, affording a better occupancy of the available volume of the channel (Figure III.14). The water motif is stabilized by hydrogen bonds among the water molecules inside each helix and between those from the inner and outer helices. The anchoring to the host matrix is different for the two helices due to the coiling, the inner helix establishing strong contacts with the coordinated water molecules [O(1w) and O(2w)] with distances ranging from 2.84(4) to 2.98(3) Å. The water molecules of the outer helix are connected to ethylmalonate oxygen atoms through hydrogen bonds [2.88(2) and 2.90(4) Å for O(4)⋯O(4w) and O(8)⋯O(3w), respectively] (Figure III.15). Two points are remarkable in the formation of these two helical water chains: first, the helical polymer host acts as a template for the formation of the helical chain of water molecules and secondly, the large pore is responsible for the occurrence of the two chains and the disorder of the water molecules (empty volume allows mobility of water molecules) (Figure III.16). The chiral environment of the channel and the hydrophilic anchoring positions mimic the structure of the pores encountered in some biological systems.<sup>9</sup>

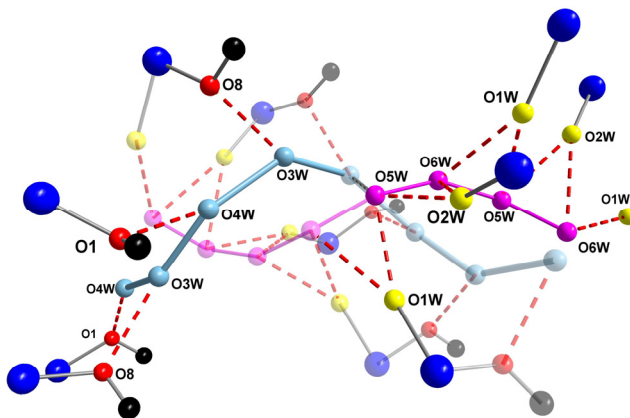
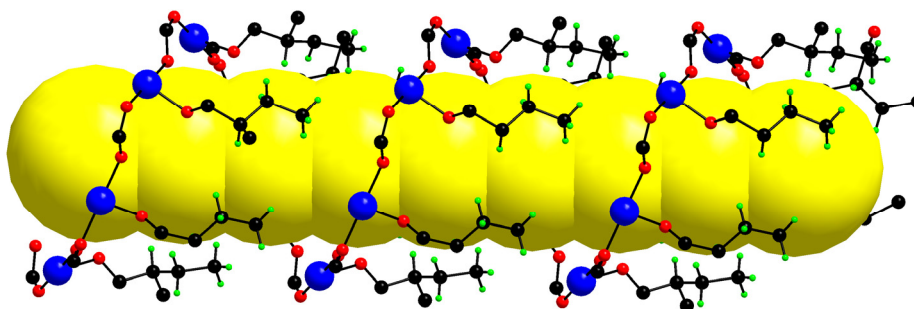
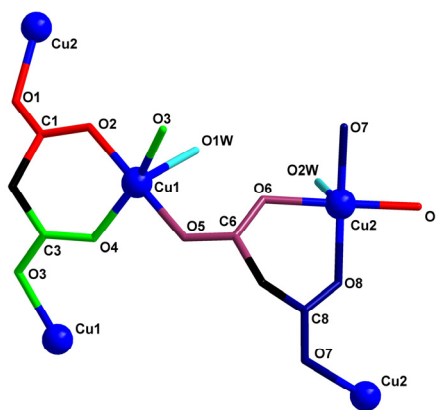


Fig. III.15. Anchoring of the two water helices to the pore surface through hydrogen bonding.



**Fig. III.16.** A representation of the void space (yellow) inside the pore which accounts for 28% of the total cell volume.

The two crystallographically independent copper(II) ions exhibit a somewhat distorted square pyramidal environment, the  $\tau$  values<sup>5</sup> being 0.30 and 0.29 for Cu(1) and Cu(2), respectively. The basal planes of Cu(1) and Cu(2) are built by four oxygen atoms from three different ethylmalonate ligands [O(2), O(3), O(4) and O(5) for Cu(1) and O(1), O(6), O(7) and O(8) for Cu(2)]; the mean values of the Cu(1)–O(eq) and Cu(2)–O(eq) bond distances are 1.962(5) and 1.965(5) Å, respectively; see Table III.3] while a water molecule [O(1w)–Cu(1) and O(2w)–Cu(2) bond distances are 2.305(7) and 2.310(7) Å, respectively] occupies the apical positions. The copper atoms are shifted towards the apical position by 0.1547(10) Å [Cu(1)] and 0.1437(9) Å [Cu(2)].



**Fig. III.17.** A view of the four crystallographically different carboxylate bridges present in complex **30** along with the numbering scheme.

The two ethylmalonate ligands adopt the same coordination mode: bidentate and bis-monodentate. Etmal(1) chelates Cu(1) through O(2) and O(4) with an angle subtended at the copper atom of 90.6(2)° while Etmal(2) bites Cu(2) through O(6) and O(8) [the bite

angle being  $91.2(2)^\circ$ ]. Etmal(1) acts as bis-monodentate through O(1) to Cu(2a) and O(3) to Cu(1b) [(a) =  $-y+2, x-y+2, z-1/3$  and (b) =  $-x+y+1, -x+2, z+1/3$ ] while Etmal(2) does it through O(5) and O(7).

There are four different carboxylate bridges (Figure III.17). All of them exhibit the *anti-syn* conformation linking equatorial positions of the copper environments (see Table III.4). The two shorter copper-copper separations involve same atoms [Cu(1)⋯Cu(1) and Cu(2)⋯Cu(2) distances being 4.8322(14) and 4.8317(14) Å, respectively] and two long carboxylate bridges [Cu(1)⋯Cu(2) separation through O(1)–C(1)–O(2) is 5.0947(12) Å and through O(5)–C(6)–O(6) is 5.0936(13) Å]. These latter carboxylate ethylmalonate bridges are responsible for the formation of the helix pore, thus it exhibits a regular alternation of Cu(1) and Cu(2) linked through the longer bridges being the angles between their basal planes  $77.45(10)^\circ$  and  $49.74(16)^\circ$  (see Table III.4).

**Table III.4.** Structural data of the carboxylate bridges present in **30**<sup>a</sup>

| Carboxylate bridge | Atoms linked | Cu⋯Cu separation / Å | $\varphi^b / ^\circ$ |
|--------------------|--------------|----------------------|----------------------|
| O(1)–C(1)–O(2)     | Cu(1)⋯Cu(2)  | 5.0947(12)           | 77.45(10)            |
| O(3)–C(3)–O(4)     | Cu(1)⋯Cu(1)  | 4.8322(14)           | 87.12(15)            |
| O(5)–C(6)–O(6)     | Cu(1)⋯Cu(2)  | 5.0936(13)           | 49.74(16)            |
| O(7)–C(8)–O(8)     | Cu(2)⋯Cu(2)  | 4.8317(14)           | 86.66(19)            |

<sup>a</sup> See Figure III.17.

<sup>b</sup> Angle between basal planes of the copper atoms.

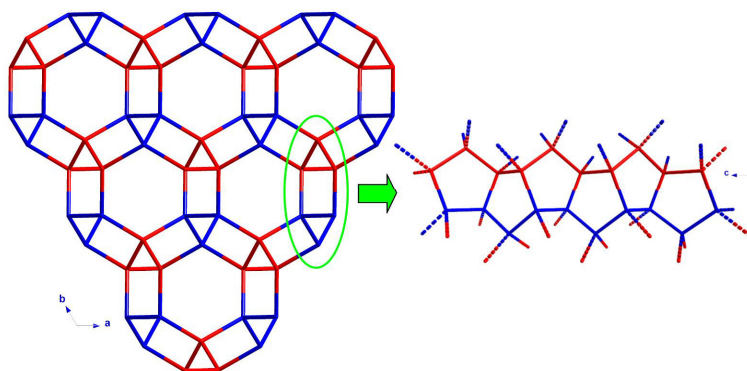


**Fig. III.18.** The (5,4) net representation of the topology of the structure of **30**. Along the *c* axis (left) the surface of the channels are constructed by chains of pentagons sharing one edge (right).

Considering the carboxylate bridges as unique connectors, each copper atom has a tetrahedral coordination sphere being linked to other four copper atoms. The mean angle between the vertices of the tetrahedron is the same for Cu(1) and Cu(2) as central atoms being  $109.3(3)^\circ$ , with a maximum deviation of  $14.7(2)^\circ$ . Then, the 3D-network can be viewed

as a (5,4) net where each pentagon of copper atoms share its edges with other eight pentagons or easily, as a tape of pentagons sharing one edge which are connected to other two in a 3 symmetry axis building the channel along the *c* direction (Figure III.18).

The structure of the pores consists of seven carboxylate-bridged copper atoms per helix turn with the ethyl groups of the Etmal ligand occupying remaining space in the wall of the pore. The coordinated water molecules reduce the size of the channel to *ca.* 5.5 Å. The total solvent-accessible volume of the channel in the unit cell is about 350 Å<sup>3</sup>, a value which accounts for 28% of the total cell volume. Thus, the pore is large enough to host organic guests and only a small number of greater chiral cavities in 3D polymers have been reported.<sup>4,9</sup>

The three ethylmalonate-containing copper(II) complexes crystallize in non-centrosymmetric space groups, the Flack parameters of **28** and **30** are close to 0.0, while in **29** is *c.a.* 0.5 (see Table III.1); thus, the structures of **28** and **30** are chiral. The crystal is homochiral because of only *M*-helices are present in the crystal structure of *M*-crystals in **30** and only  $\Delta$ -[Cu(Etmal)<sub>2</sub>(H<sub>2</sub>O)] units are present in  $\Delta$ -crystals in **28**. The ethylmalonate ligand is achiral, thus complexes **28** and **30** spontaneously resolve in enantiomorphous crystals. The initial nucleation usually leads to the formation of *P*- or *M*-crystals randomly.<sup>9</sup> However, Aoyama et al. have found in an other chiral porous coordination network constructed from achiral ligands reported in the literature [for instance the complex Cd[5-(9-anthracenyl)pyrimidine] (NO<sub>3</sub>)<sub>2</sub>(H<sub>2</sub>O)(EtOH)],<sup>10</sup> that the bulk sample is homochiral. They have suggested that crystals grow as a single colony from the first formed nucleus; therefore, the stereochemistry of the first grown nucleus dictates the stereochemistry of all the crystals. In the case of complex **28**, the two enantiomers have been found in the same crystallization; however, due to the difficulty to obtain X-ray quality crystals of **30** we cannot assure that *P*- and *M*-crystals crystallize simultaneously.

Finally, let us compare the structures of these three ethylmalonate-containing copper(II) complexes. They appear, structurally, very different, but if we recall the formulae they look very similar: {[Cu(H<sub>2</sub>O)<sub>4</sub>][Cu(Etmal)<sub>2</sub>(H<sub>2</sub>O)]}<sub>n</sub> (**28**), [Cu(Etmal)(H<sub>2</sub>O)]<sub>n</sub> (**29**) and [Cu(Etmal)(H<sub>2</sub>O)]<sub>n</sub> · 1.65nH<sub>2</sub>O (**30**). The three complexes have a 1:1 Cu:Etmal ratio, being organized in the same way in **29** and **30**. The water molecules seem to be the main difference, but compounds **28** and **30** have almost the same five molecules in different arrangements. The copper atoms and the ethylmalonate ligands have the same conformation in **29** and **30**, but the [Cu(Etmal)(H<sub>2</sub>O)] units are linked forming a two-dimensional (4,4) net in **29** and a three-dimensional (5,4) net in **30** (the copper atom acts as a planar four-node in

**29** and as a tetrahedral node in **30**). It deserves to be noted that three complexes of different dimensionality [the 1D (**28**), 2D (**29**) and 3D (**30**) networks] have been obtained from almost the same synthesis.

### III.1.4. Magnetic Properties

The magnetic properties of the three complexes will be explored consecutively due to their fundamental structural differences and their also different magnetic behaviour.

$\{[\text{Cu}(\text{Etmal})_2(\text{H}_2\text{O})][\text{Cu}(\text{H}_2\text{O})_4]\}_n$  (**28**). The thermal dependence of  $\chi_M$  and  $\chi_M T$  for **28** is shown in Figure III.19 [ $\chi_M$  is the magnetic susceptibility per copper(II) ion]. The  $\chi_M T$  value at room temperature is  $0.42 \text{ cm}^3 \text{ mol}^{-1} \text{ K}$  which is as expected for a magnetically isolated spin doublet. Upon cooling,  $\chi_M T$  remains almost constant until 25 K and then, smoothly decreases to reach a value at 2.0 K of  $0.26 \text{ cm}^3 \text{ mol}^{-1} \text{ K}$ . This is indicative that weak antiferromagnetic interactions between the copper(II) ions are present in **28**.

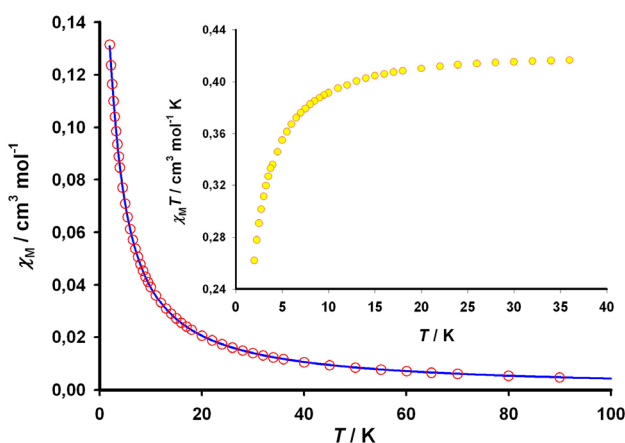


**Fig. III.19.**  $\chi_M$  vs  $T$  plot for **28** under an applied field of 0.11 T: (o) experimental data, (—) best fit curve. The inset shows a detail of the low temperature region for the  $\chi_M T$  vs  $T$  plot.

The structure of **28** consists of chains of *anti-syn* carboxylate-bridged copper(II) ions. There is only one crystallographically independent carboxylate bridge and then, only one magnetic coupling parameter will be introduced in the analysis. The magnetic data can be fitted by the Bonner-Fisher equation for a uniform chain of copper(II) ions<sup>11</sup> with intrachain antiferromagnetic coupling

$$\chi_M = \left( \frac{N g^2 \beta^2}{k_B T} \right) \left[ \frac{0.25 + 0.074975x + 0.075235x^2}{1 + 0.9931x + 0.172135x^2 + 0.757825x^3} \right]$$

where  $N$ ,  $\beta$ ,  $g$  and  $k_B$  have their usual meanings,  $x = |J|/k_B T$  and  $J$  the magnetic coupling parameter. Best least-squares fit of the experimental data leads to  $J = -1.54(2) \text{ cm}^{-1}$ ,  $g = 2.150(1)$  and  $R = 2.3 \times 10^{-5}$ . The calculated curve matches as well the experimental data in the whole temperature range (Figure III.19).

The antiferromagnetic coupling between the copper(II) ions in the chain compound **28** is in agreement with those previously reported Phmal- and Memal-containing carboxylate-bridged chains [complexes **13**, **25** and **27**; with  $J$  values of  $-0.59(1)$ ,  $-1.23(1)$  and  $-1.25(1) \text{ cm}^{-1}$ ; respectively], but this behaviour has not been observed in malonate-containing copper(II) chain complexes.<sup>12</sup> It deserves to be noted that the magnetic coupling between copper ions through the *anti-syn* carboxylate-bridge is weak and either ferro- or antiferromagnetic.<sup>13</sup>

The carboxylate exchange pathway in **28** links one equatorial position of a copper(II) ion exhibiting trigonal bipyramidal (tbp) environment with an apical position of an adjacent octahedral ( $O_h$ ) Cu(II) ion (see Figure III.4). The magnetic orbital of a copper(II) ion with a tbp surrounding is mainly of the  $dz^2$  character (the  $z$  axis being roughly defined by the axial bonds) whereas that of the copper(II) ions with octahedral surrounding is of the  $d(x^2-y^2)$  type (the  $x$  and  $y$  axis being defined by the equatorial bonds). Therefore, two non-magnetic orbitals are interacting in **28**, a situation which accounts for the weak magnetic coupling. However, some overlap between the magnetic orbitals leads to the antiferromagnetism to predominate.<sup>14</sup>

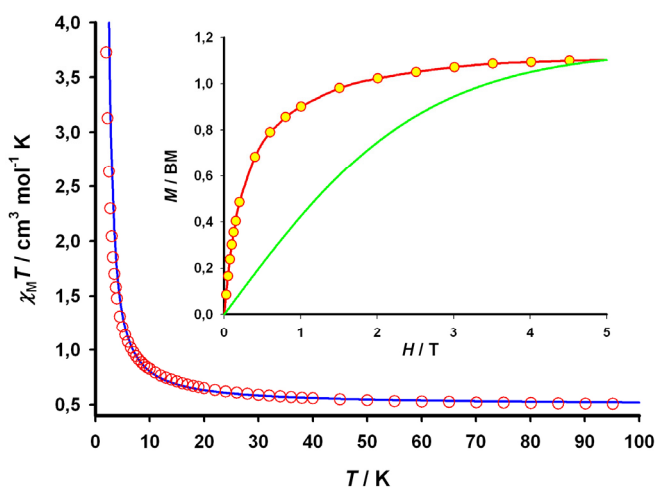


**Fig. III.20.**  $\chi_M T$  vs  $T$  plot for **29** under applied fields of 1 T ( $T > 10$  K) and 0.05 T ( $T < 10$  K): (o) experimental data, (—) best fit curve. The inset shows the  $M$  vs  $H$  plot for **29** together with the Brillouin function for a magnetically isolated spin doublet (green line).

**[Cu(Etmal)(H<sub>2</sub>O)]<sub>n</sub> (29)**. The magnetic properties for **29** in the form of a  $\chi_M T$  vs  $T$  plot are shown in Figure III.20 [ $\chi_M$  is the magnetic susceptibility per copper(II) ion].  $\chi_M T$  at room temperature is  $0.47 \text{ cm}^3 \text{ mol}^{-1} \text{ K}$ , a value which is as expected for a magnetically isolated spin doublet. Upon cooling, this value remains almost constant up to 20 K and then sharply increases to reach a value of  $3.73 \text{ cm}^3 \text{ mol}^{-1} \text{ K}$  at 2.0 K. The  $\chi_M$  curve does not exhibit any maxima and the saturation value of 1.09 BM is reached at an applied field of 3.5 T (inset of Figure III.20). These features are indicative of the existence of intralayer ferromagnetic interactions among the copper(II) ions.

The structure of **29** is formed by corrugated layers of *anti-syn* carboxylate-bridged copper(II) ions in a square grid arrangement. Although there are two crystallographically independent carboxylate bridges in **29**, their similarity induces us to consider only one magnetic exchange parameter. Thus, the experimental data can be analyzed through the high-temperature series expansion derived from the two-dimensional Heisenberg model for a  $S = 1/2$  ferromagnetic quadratic lattice.<sup>15</sup>

$$\chi = \left[ N g^2 \beta^2 / (3kT) \right] S(S+1) \left( 1 + \sum_{n=1}^{10} a_n K^n \right)$$

Where  $K = J/kT$ ,  $a_n$  are the coefficients for the square lattice and  $J$  is the intralayer magnetic coupling between the local spins of the nearest-neighbours with the Hamiltonian defined as:

$$\hat{H} = -J \sum_i \hat{S}_i \cdot \hat{S}_{i+1}$$

The best fit using a nonlinear regression analysis leads to  $J = +1.67(2) \text{ cm}^{-1}$ ,  $g = 2.30(2)$  and  $R = 1.05 \times 10^{-3}$ . The calculated curve matches well the experimental data in the whole temperature range (Figure III.20).

The value obtained for  $J$  is in agreement with the previous values for carboxylate-bridged square-grids of copper(II) ions (see previous chapters) and, in particular, it is very similar to that obtained for the complex [Cu(Memal)(H<sub>2</sub>O)] (**16**). The magnetic orbital for a copper(II) ion in square pyramidal environment is of the  $d(x^2-y^2)$  character [the  $x$  and  $y$  axes being defined by the equatorial bonds]. Following the Kahn's model,<sup>14</sup> if the magnetic orbitals of two interacting copper(II) ions are orthogonal, the ferromagnetic coupling is ensured given that the zero overlap between the magnetic orbitals vanishes the antiferromagnetic contribution. As the angle between equatorial planes of adjacent copper atoms in **29** is  $88.81(14)^\circ$ , the orthogonality is achieved and the results are as expected. The weakness of the magnetic interaction through the *anti-syn* carboxylate bridge is in agreement with the reported values for this kind of bridge.<sup>12,13</sup>

**[Cu(Etmal)(H<sub>2</sub>O)]<sub>n</sub>1.65nH<sub>2</sub>O (30).** Variable-temperature dc magnetic-susceptibility measurements were performed on a polycrystalline sample of **30** in the temperature range of 2-300 K under an applied magnetic field varying in the range 0-5 T.  $\chi_M T$  at room temperature is  $0.42 \text{ cm}^3 \text{ K mol}^{-1}$  ( $\chi_M$  is the molar magnetic susceptibility per a copper(II) ion), a value which is as expected for a spin doublet (Figure III.21). Upon cooling,  $\chi_M T$  smoothly increases till 4.0 K. Below this temperature, it sharply increases reaching a value of  $40 \text{ cm}^3 \text{ K mol}^{-1}$  at 2.95 K (see inset of Figure III.21) and then decreases linearly with  $T$ .

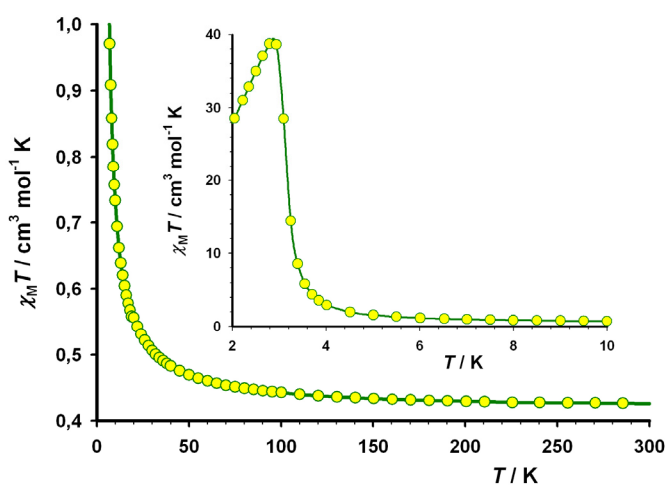


**Fig. III.21.**  $\chi_M T$  vs  $T$  plot for **30** under applied fields of 1 T ( $T > 20$  K), 0.025 T ( $5 \text{ K} < T < 10$  K) and 0.01 T ( $T < 5$  K). The inset shows a detail of the low temperature region.

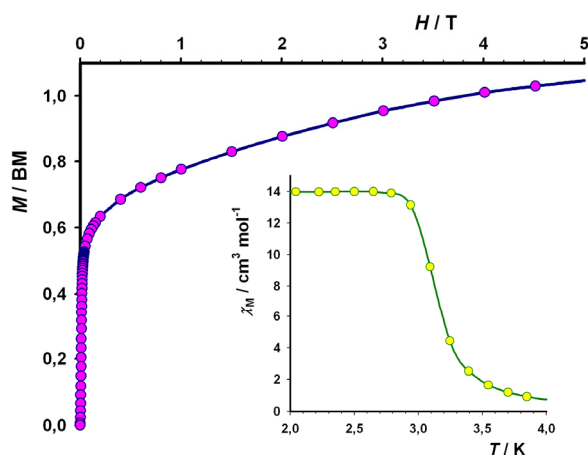


**Fig. III.22.** Magnetization ( $M$ ) vs  $H$  plot for **30** (violet). The inset shows the low temperature region for the  $\chi_M$  vs  $T$  plot for **30**.



The  $\chi_M$  versus  $T$  plot (see inset of Figure III.22) exhibits a sigmoidal shape with an inflexion point at 3.0 K. All these features indicate the occurrence of a ferromagnetic interaction between the copper(II) ions with a magnetic ordering below 3.0 K. In fact, the ac measurements show an out-of-phase signal with a maximum at 3.0 K which is frequency independent indicating a non-glassy character of the ferromagnetic state. The  $M$  versus  $H$  plot at 2.0 K (see Figure III.22) exhibits an abrupt increase at low magnetic fields and tends to a value of 1.04 BM at 5 T. However, no coercive field is observed within the experimental error.

There is not theoretical model to analyze the magnetic data of **30**, since its structure is three-dimensional and it presents up to four different exchange pathways between the copper(II) ions through carboxylate-bridges. All we can say is that the carboxylate(malonate) bridge in *anti-syn* conformation linking equatorial positions has been reported to be a weak to medium ferromagnetic exchange pathway, as occurs in **30**.<sup>12,13,16</sup>

### III.1.5. Conclusion

Three complexes has been obtained by the reaction of ethylmalonate with copper(II) in aqueous solution (**28**, **29**, and **30**). Their crystal structures are very different and they range from the one-dimensional network of **28** to the 3D-architecture of **30**. **28** is constructed from the  $[\text{Cu}(\text{Etmal})_2]$  unit exhibiting a trigonal bipyramidal coordination polyhedra, feature which is unprecedented in the R-mal copper(II) coordination compounds. However, **29** and **30** are built by carboxylate bridging of  $[\text{Cu}(\text{Etmal})]$  units, where the copper atoms act as four nodes in the resulting network. Remarkably, the three complexes crystallize in non-centrosymmetric space groups, but only **28** and **30** are chiral structures. **28** is an antiferromagnetically coupled chain, **29** exhibit intralayer ferromagnetic coupling (similar to those formed in Phmal and Memal-containing copper(II) complexes), whereas **30** presents magnetic ordering below 3.0 K.

Our results show that the strategy to design new Etmal-containing copper(II) complexes with desired morphology and magnetic properties is a very difficult task. The use of N-donor coligands is a good choice to assemble the layers of **29**, or to block some positions occupied by water molecules in **28**. However, the Etmal ligand has shown such a variety of behaviours that the structure of the resulting compound becomes unpredictable.

### III.1.6. References

- 1 J. Bernstein, *Polymorphism in Molecular Crystals*, Clarendon Press, Oxford, **2002**.
- 2 (a) G. I. Dimitrova, A. V. Ablov, G. A. Kiosse, G. A. Popovich, T. I. Nmalinouskii and I. F. Bourshteyn, *Dokl. Akad. Nauk. SSSR* **1974**, *216*, 1055; (b) Y. Rodríguez-Martín, J. Sanchiz, C. Ruiz-Pérez, F. Lloret and M. Julve *CrystEngComm* **2002**, *4*, 631. (c) D. Chattopadhyay, S. K. Chattopadhyay, P. R. Lowe, C. H. Schwalde, S. K. Mazumder, A. Rana and S. Ghosh, *Dalton Trans.* **1993**, 913. (d) V. T. Yilmaz, E. Senel and C. Thone, *Transition Met. Chem.* **2004**, *29*, 336.
- 3 C. Ruiz-Pérez, J. Sanchiz, M. Hernández-Molina, F. Lloret and M. Julve, *Inorg. Chem.* **2000**, *39*, 1363.
- 4 (a) B. Kesanli and W. Lin, *Coord. Chem. Rev.* **2003**, *246*, 305. (b) W. Lin, *J. Solid State Chem.* **2005**, *178*, 2486. (c) Y. Cui, H. L. Ngo, P. S. White and W. Lin, *Inorg. Chem.* **2003**, *42*, 652. (d) E.-Q. Gao, Y.-F. Yue, S.-Q. Bai, Z. He and C.-H. Yan, *J. Am. Chem. Soc.* **2004**, *126*, 1419.
- 5 A. W. Addison, T. N. Rao, J. Reedijk, J. van Rijn and G. C. Verschoor, *Dalton Trans.* **1984**, 1349.
- 6 E. I. Stiefel and G. F. Brown, *Inorg. Chem.*, **1972**, *11*, 434.
- 7 J. Pasán, J. Sanchiz, C. Ruiz-Pérez, F. Lloret and M. Julve, *Inorg. Chem.* **2005**, *44*, 7794.
- 8 J. Pasán, J. Sanchiz, C. Ruiz-Pérez, F. Lloret and M. Julve, *New J. Chem.*, **2003**, *27*, 1557.
- 9 (a) B. Moulton and M. J. Zaworotko, *Chem. Rev.* **2001**, *101*, 1629. (b) C. Janiak, *Dalton Trans.* **2003**, 2781. (c) H. Li, M. Eddaoudi, M. O'Keeffe and O. M. Yaghi, *Nature* **1999**, *402*, 276 and references therein. (d) N. L. Rosi, J. Eckert, M. Eddaoudi, D. T. Vodak, J. Kim, M. O'Keeffe and O. M. Yaghi, *Science*, **2003**, *300*, 1127.
- 10 (a) T. Ezuhara, K. Endo and Y. Aoyama, *J. Am. Chem. Soc.* **1999**, *121*, 3279. (b) C. J. Kepert, T. J. Prior and M. J. Rosseinsky, *J. Am. Chem. Soc.* **2000**, *122*, 5158.
- 11 (a) J. C. Bonner and M. E. Fisher, *Phys. Rev. A* **1964**, *135*, 640. (b) W. E. Estes, D. P. Gavel, W. E. Hatfield and D. Hodgson, *Inorg. Chem.* **1978**, *17*, 1415.
- 12 J. Pasán, F. S. Delgado, Y. Rodríguez-Martín, M. Hernández-Molina, C. Ruiz-Pérez, J. Sanchiz, F. Lloret and M. Julve, *Polyhedron* **2003**, *22*, 2143.
- 13 A. Rodríguez-Forteza, P. Alemany, S. Álvarez and E. Ruiz, *Chem. Eur. J.* **2001**, *7*, 627.
- 14 O. Kahn, *Molecular Magnetism*, VCH, New York, **1993**.
- 15 R. Navarro, *Application of High- and Low-Temperature Series Expansions to Two-dimensional Magnetic Systems*, de Jongh, L. J.; Ed., Kluwer Academic Publishers, The Netherlands, **1990**.
- 16 F. S. Delgado, J. Sanchiz, C. Ruiz-Pérez, F. Lloret and M. Julve, *Inorg. Chem.* **2003**, *42*, 5938.

## III.2. Sodium(I)-Copper(II)-Ethylmalonate (31 and 32)

### III.2.1. Introduction

The introduction of sodium(I) cations in the polymeric networks usually affords structures of higher dimensionality, because their affinity to occupy the available coordination sites of the ligand left by the transition metal atoms.<sup>1</sup> The use of sodium basic salts for the deprotonation of the carboxylic acid provides the Na(I) cations. As they are charged, the network has to be anionic to allow their inclusion. A malonate-containing complex with Na(I) and Cu(II) cations is known where the sodium cations influence the whole structure formed.<sup>2</sup> The two sodium(I)-containing complexes presented here were serendipitously synthesized but they illustrate how the Na(I) ions can afford new interesting crystal structures.

### III.2.2. Synthesis

**Na<sub>6</sub>[Cu(Etmal)<sub>2</sub>(H<sub>2</sub>O)]<sub>3</sub>·5H<sub>2</sub>O (31).** An aqueous solution (5 cm<sup>3</sup>) of copper(II) nitrate (1 mmol, 232 mg) was added to a aqueous solution (10 cm<sup>3</sup>) containing a mixture of ethylmalonic acid (1 mmol, 65 mg) and sodium hydroxide (0.5 mmol, 20 mg). The resulting pale blue solution was allowed to evaporate at room temperature, and pale blue prismatic single crystals of **31** were collected after a week. Yield 40 %. Anal. calc. for C<sub>30</sub>H<sub>52</sub>Cu<sub>3</sub>Na<sub>6</sub>O<sub>32</sub> (**31**): C, 28.75; H, 4.18; Found: C, 28.58; H, 4.29 %.

**{Na[Cu<sub>3</sub>(H<sub>2</sub>O)][Cu(Etmal)<sub>2</sub>(H<sub>2</sub>O)<sub>3</sub>]<sub>n</sub>·nH<sub>2</sub>O·n(EtO)<sub>2</sub>nNO<sub>3</sub> (32).** An aqueous solution (5 cm<sup>3</sup>) of copper(II) nitrate (0.5 mmol, 116 mg) was added to a mixture of ethylmalonic acid (0.5 mmol, 32 mg), malonic acid (0.5 mmol, 52 mg) and sodium hydroxide (0.5 mmol, 20 mg) in a 50/50 water/ethanol (10 cm<sup>3</sup>) solution. Prismatic pale blue single crystals appear in the resulting clear blue solution obtained after a few days of slow evaporation at room temperature. Crystallographic details for **31** and **32** are listed in Table III.5. Yield ca. 25%.

**Table III.5.** Crystallographic data for **31-32**

|                                                    | <b>31</b>                                                                          | <b>32</b>                                                                                  |
|----------------------------------------------------|------------------------------------------------------------------------------------|--------------------------------------------------------------------------------------------|
| Formula                                            | C <sub>30</sub> H <sub>52</sub> O <sub>32</sub><br>Na <sub>6</sub> Cu <sub>3</sub> | C <sub>5.66</sub> H <sub>10</sub> O <sub>6</sub> N <sub>0.16</sub><br>Na <sub>0.5</sub> Cu |
| FW                                                 | 1253.15                                                                            | 251.29                                                                                     |
| Crystal system                                     | Monoclinic                                                                         | Hexagonal                                                                                  |
| Space group                                        | <i>P</i> 2 <sub>1</sub> / <i>c</i>                                                 | <i>P</i> -6 <i>2c</i>                                                                      |
| <i>a</i> /Å                                        | 13.1564(12)                                                                        | 16.0818(3)                                                                                 |
| <i>b</i> /Å                                        | 15.654(2)                                                                          | -                                                                                          |
| <i>c</i> /Å                                        | 23.810(3)                                                                          | 10.7132(2)                                                                                 |
| $\beta$ /°                                         | 91.284(7)                                                                          | -                                                                                          |
| <i>V</i> /Å <sup>3</sup>                           | 4902.4(10)                                                                         | 2399.49(8)                                                                                 |
| <i>Z</i>                                           | 4                                                                                  | 6                                                                                          |
| $\mu$ (Mo K $\alpha$ ) /cm <sup>-1</sup>           | 14.40                                                                              | 27.53                                                                                      |
| <i>T</i> /K                                        | 293(2)                                                                             | 293(2)                                                                                     |
| $\rho_{\text{calc}}$ /g cm <sup>-3</sup>           | 1.676                                                                              | 1.050                                                                                      |
| $\lambda$ /Å                                       | 0.71073                                                                            | 0.71073                                                                                    |
| Index ranges                                       | -18 ≤ <i>h</i> ≤ 14,<br>-19 ≤ <i>k</i> ≤ 21,<br>-22 ≤ <i>l</i> ≤ 33                | -23 ≤ <i>h</i> ≤ 19,<br>-23 ≤ <i>k</i> ≤ 22,<br>-15 ≤ <i>l</i> ≤ 15                        |
| Indep. reflect.<br>( <i>R</i> <sub>int</sub> )     | 12244<br>(0.0300)                                                                  | 2669<br>(0.0982)                                                                           |
| Obs. reflect.<br>[ <i>I</i> > 2σ( <i>I</i> )]      | 7449                                                                               | 2280                                                                                       |
| Flack param.                                       | -                                                                                  | 0.48(6)                                                                                    |
| Parameters                                         | 640                                                                                | 132                                                                                        |
| Goodness-of-fit                                    | 1.034                                                                              | 0.961                                                                                      |
| <i>R</i> [ <i>I</i> > 2σ( <i>I</i> )]              | 0.0519                                                                             | 0.0648                                                                                     |
| <i>R</i> <sub>w</sub> [ <i>I</i> > 2σ( <i>I</i> )] | 0.1235                                                                             | 0.2063                                                                                     |
| <i>R</i> (all data)                                | 0.1035                                                                             | 0.0824                                                                                     |
| <i>R</i> <sub>w</sub> (all data)                   | 0.1396                                                                             | 0.2340                                                                                     |

Anal. calc. for  $C_{34}H_{60}Cu_6N_1Na_3O_{36}$  (**32**): C, 27.06; H, 4.18; N, 0.98; Found: C, 27.28; H, 4.29; N, 1.12 %.

### III.2.3. Description of the Structures

$Na_6[Cu(Etmal)_2(H_2O)]_3 \cdot 5H_2O$  (**31**). The crystal structure of **31** (Figure III.23) is three-dimensional and consists of mononuclear bis(ethylmalonate)aquacopper(II) entities linked through sodium ions building the 3D network plus crystallization water molecules (Figure III.24).

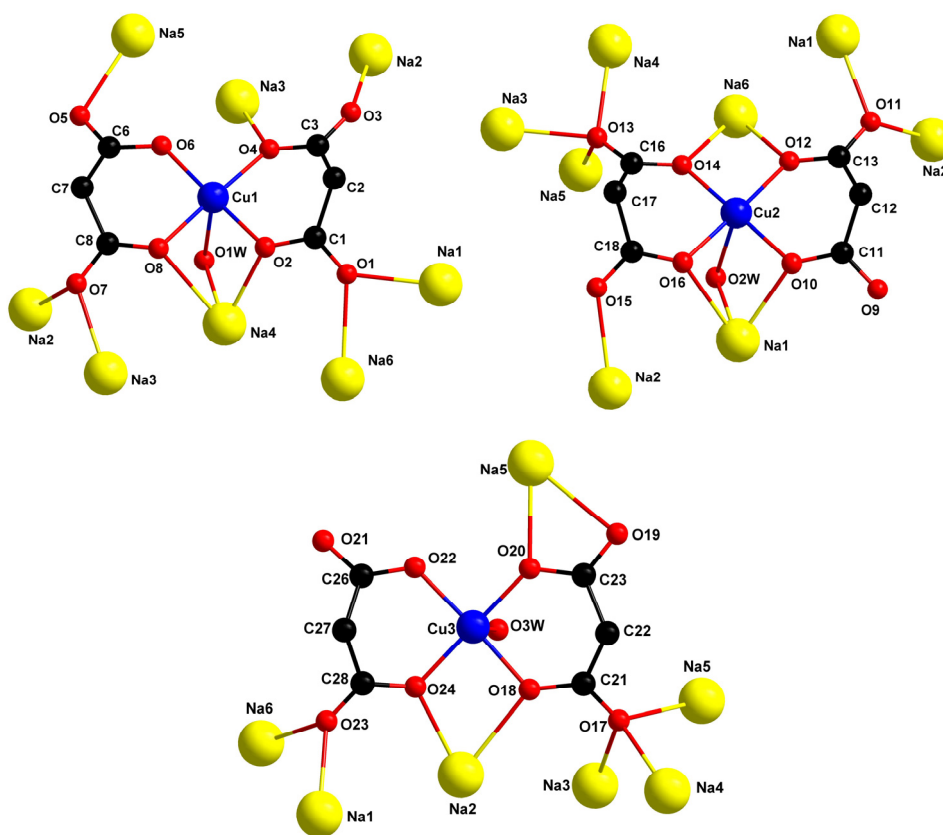


**Fig. III.23.** View of three fragments of the structure of **31** along with the numbering scheme. Each one shows a crystallographically independent mononuclear unit of **31**.

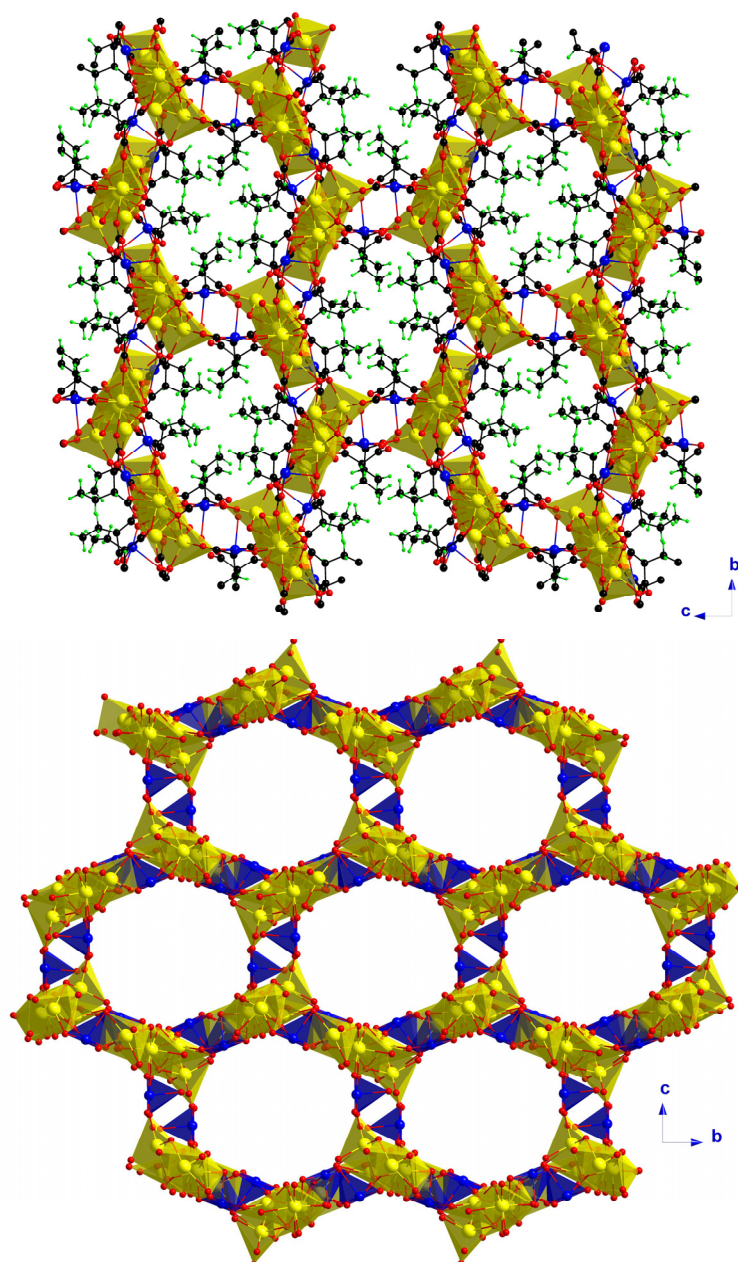


**Fig. III.24.** (Up) A perspective view along the *a* axis of the crystal packing of **31** showing the hydrophobic channels running in the *a* direction. (Bottom) The previous image but in polyhedra configuration, where the ethyl groups of the ethylmalonate ligand have been omitted.

The  $\mu$ -oxo and  $\mu$ -hydroxo bridged sodium atoms build chains along the *a* direction (Figure III.25), which are linked through the  $[\text{Cu}(\text{Etmal})_2(\text{H}_2\text{O})]^{2-}$  units in the other two directions. The resulting 3D network exhibits pores of dimension *c.a.*  $10 \times 12 \text{ \AA}^2$  along the *a*

axis which are filled by the ethyl groups of the ethylmalonate ligands avoiding the inclusion of water molecules. The crystallization water molecules [O(7w) and O(8w)] are located near the sodium atoms and anchored to the polymeric network through hydrogen bonds involving ethylmalonate oxygen atoms and coordinated water molecules (see Table III.6). Hydrogen bonds among the coordinated water molecules which also involves the Etmal oxygen atoms contribute to the stabilization of the structure [O...O distances ranging from 2.714(4) to 2.979(4) Å].

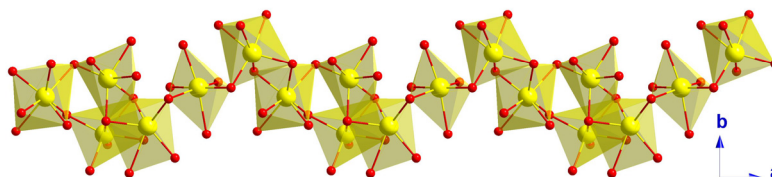


Fig. III.25. A view of three repeating units of a  $\mu$ -oxo bridged sodium(I) chain along the  $c$  direction.

The copper atoms exhibit somewhat distorted square pyramidal environments the  $\tau$  values<sup>3</sup> being 0.027, 0.009 and 0.037 for Cu(1), Cu(2) and Cu(3), respectively. Four ethylmalonate oxygen atoms form the basal plane [see Table III.7; average bond distances are Cu(1)–O(eq) 1.926(3) Å, Cu(2)–O(eq) 1.923(2) Å and Cu(3)–O(eq) 1.931(3) Å] while coordinated water molecules occupy the apical positions [the Cu(1)–O(1w), Cu(2)–O(2w) and Cu(3)–O(3w) bond distances are 2.425(3), 2.569(3) and 2.439(3) Å, respectively]. The six crystallographically independent sodium atoms exhibit five- [Na(3)], six- [Na(1), Na(2) and Na(4)] and seven- [Na(5) and Na(6)] coordinated surroundings (see Table III.7 for bond distances). The O-bridged chain of sodium atoms exhibits Na...Na separations ranging from 3.156(3) to 4.153(2) Å.

**Table III.6.** Structural data of hydrogen bonds in **31**

| D–H...A                                | O...O (Å) | D–H...A       | O...O (Å) |
|----------------------------------------|-----------|---------------|-----------|
| <i>Crystallization water molecules</i> |           |               |           |
| O(7w)...O(21)                          | 2.757(4)  | O(8w)...O(7)  | 2.928(4)  |
| O(7w)...O(3W)                          | 2.744(4)  | O(8w)...O(9)  | 2.730(4)  |
| O(7w)...O(5W)                          | 2.858(4)  | O(8w)...O(1W) | 2.714(4)  |
| O(7w)...O(6W)                          | 2.858(4)  |               |           |
| <i>Coordinated water molecules</i>     |           |               |           |
| O(1w)...O(15)                          | 2.834(4)  | O(4w)...O(3)  | 2.979(4)  |
| O(1w)...O(8w)                          | 2.714(4)  | O(4w)...O(21) | 2.771(5)  |
| O(2w)...O(5)                           | 2.910(4)  | O(5w)...O(5)  | 2.760(4)  |
| O(2w)...O(4w)                          | 2.740(4)  | O(5w)...O(7w) | 2.858(4)  |
| O(3w)...O(3)                           | 2.926(4)  | O(6w)...O(22) | 2.773(4)  |
| O(3w)...O(19)                          | 2.714(4)  | O(6w)...O(7w) | 2.858(4)  |
| O(3w)...O(7w)                          | 2.744(4)  |               |           |

Each one of the six different ethylmalonate ligands acts as bidentate to the copper atom, being also linked to the sodium atoms as monodentate ligands. The coordination scheme to the sodium atoms for each  $[\text{Cu}(\text{Etmal})_2(\text{H}_2\text{O})]$  unit are displayed in the Figure III.23; these units act as connectors of adjacent oxo-bridged sodium chains affording the 3D-network. The  $[\text{Cu}(\text{Etmal})_2(\text{H}_2\text{O})]$  units are well separated from each other, the shortest copper-copper distance being 6.7718(9) Å.

**Table III.7.** Selected bond angles (°) and lengths (Å) for **31**.

| <i>Copper atoms</i> |            |                   |            |                   |            |
|---------------------|------------|-------------------|------------|-------------------|------------|
| Cu(1)–O(2)          | 1.917(2)   | Cu(2)–O(10)       | 1.920(2)   | Cu(3)–O(18)       | 1.945(2)   |
| Cu(1)–O(4)          | 1.932(2)   | Cu(2)–O(12)       | 1.914(2)   | Cu(3)–O(20)       | 1.917(3)   |
| Cu(1)–O(6)          | 1.919(2)   | Cu(2)–O(14)       | 1.918(2)   | Cu(3)–O(22)       | 1.934(3)   |
| Cu(1)–O(8)          | 1.935(3)   | Cu(2)–O(16)       | 1.942(2)   | Cu(3)–O(24)       | 1.930(3)   |
| Cu(1)–O(1w)         | 2.425(3)   | Cu(2)–O(2w)       | 2.569(3)   | Cu(3)–O(3w)       | 2.439(3)   |
| O(2)–Cu(1)–O(4)     | 92.67(10)  | O(10)–Cu(2)–O(12) | 92.54(11)  | O(18)–Cu(3)–O(20) | 94.25(11)  |
| O(2)–Cu(1)–O(6)     | 176.53(12) | O(10)–Cu(2)–O(14) | 174.54(13) | O(18)–Cu(3)–O(22) | 177.81(11) |
| O(2)–Cu(1)–O(8)     | 85.66(10)  | O(10)–Cu(2)–O(16) | 87.52(10)  | O(18)–Cu(3)–O(24) | 85.70(11)  |
| O(2)–Cu(1)–O(1w)    | 88.67(10)  | O(10)–Cu(2)–O(2w) | 87.95(10)  | O(18)–Cu(3)–O(3w) | 80.43(11)  |
| O(4)–Cu(1)–O(6)     | 86.86(11)  | O(12)–Cu(2)–O(14) | 86.62(10)  | O(20)–Cu(3)–O(22) | 87.71(11)  |
| O(4)–Cu(1)–O(8)     | 178.16(11) | O(12)–Cu(2)–O(16) | 175.06(12) | O(20)–Cu(3)–O(24) | 175.60(12) |
| O(4)–Cu(1)–O(1w)    | 100.95(11) | O(12)–Cu(2)–O(2w) | 107.23(10) | O(20)–Cu(3)–O(3w) | 91.70(11)  |
| O(6)–Cu(1)–O(8)     | 94.86(11)  | O(14)–Cu(2)–O(16) | 93.79(10)  | O(22)–Cu(3)–O(24) | 92.27(11)  |
| O(6)–Cu(1)–O(1w)    | 94.79(11)  | O(14)–Cu(2)–O(2w) | 87.15(10)  | O(22)–Cu(3)–O(3w) | 100.51(11) |
| O(8)–Cu(1)–O(1w)    | 78.25(11)  | O(16)–Cu(2)–O(2w) | 77.71(10)  | O(24)–Cu(3)–O(3w) | 92.63(11)  |
| <i>Sodium atoms</i> |            |                   |            |                   |            |
| Na(1)–O(1)          | 2.313(3)   | Na(3)–O(4)        | 2.301(3)   | Na(5)–O(5)        | 2.376(3)   |
| Na(1)–O(10)         | 2.385(3)   | Na(3)–O(6)        | 2.805(3)   | Na(5)–O(6)        | 2.912(3)   |
| Na(1)–O(11)         | 2.328(3)   | Na(3)–O(7)        | 2.360(3)   | Na(5)–O(13)       | 2.564(3)   |
| Na(1)–O(16)         | 2.491(3)   | Na(3)–O(13)       | 2.321(3)   | Na(5)–O(17)       | 2.531(3)   |
| Na(1)–O(23)         | 2.338(3)   | Na(3)–O(17)       | 2.390(3)   | Na(5)–O(19)       | 2.634(3)   |
| Na(1)–O(2w)         | 2.446(3)   | Na(4)–O(2)        | 2.300(3)   | Na(5)–O(20)       | 2.468(3)   |
| Na(2)–O(3)          | 2.598(3)   | Na(4)–O(8)        | 2.573(3)   | Na(5)–O(6w)       | 2.348(4)   |
| Na(2)–O(7)          | 2.428(3)   | Na(4)–O(13)       | 2.321(3)   | Na(6)–O(1)        | 2.583(3)   |
| Na(2)–O(11)         | 2.401(3)   | Na(4)–O(17)       | 2.304(3)   | Na(6)–O(12)       | 2.441(3)   |
| Na(2)–O(15)         | 2.488(3)   | Na(4)–O(1w)       | 2.416(3)   | Na(6)–O(14)       | 2.407(3)   |
| Na(2)–O(18)         | 2.585(3)   | Na(4)–O(5w)       | 2.350(3)   | Na(6)–O(23)       | 2.343(3)   |
| Na(2)–O(24)         | 2.319(3)   |                   |            | Na(6)–O(4w)       | 2.669(3)   |
|                     |            |                   |            | Na(6)–O(5w)       | 2.580(3)   |
|                     |            |                   |            | Na(6)–O(6w)       | 2.540(4)   |

$\{\text{Na}[\text{Cu}(\text{H}_2\text{O})][\text{Cu}(\text{Etmal})_2(\text{H}_2\text{O})]\}_{3n} \cdot n\text{H}_2\text{O} \cdot n(\text{EtO})_2 \cdot n\text{NO}_3$  (**32**). The crystal structure of **32** (Figure III.26) consists of a three-dimensional network of carboxylate-bridged copper(II) ions which exhibits cavities and channels where the sodium cations, nitrate, ethoxol and crystallization water molecules are located (Figure III.27). The 3D network is composed by  $[\text{Cu}(\text{Etmal})_2(\text{H}_2\text{O})]^{2-}$  units which are connected to aquacopper(II) cations through carboxylate groups. Two different pores are found in the structure of **32** (Figure III.28): small triangular ones formed around a three-fold rotation axis and big hexagonal channels formed around a six-fold rotation axis, both of them running along the *c*

direction. The latter ones having a diameter of 10.8 Å are filled with the ethyl groups of the ethylmalonate ligand and the coordination water molecules located on the edge of the channel, reducing the pore diameter to 6.8 Å. The small triangular pores exhibit a diameter of 6 Å, and they are filled with the sodium cations, the nitrate and ethoxo anions and the crystallization water molecules. A nitrate group is coordinated to three sodium atoms building a planar entity which acts as a stopper along the triangular pores every 10.7132(2) Å (the *c* cell parameter), the ethoxo and crystallization water molecules disordered inside these cavities (Figure III.29).

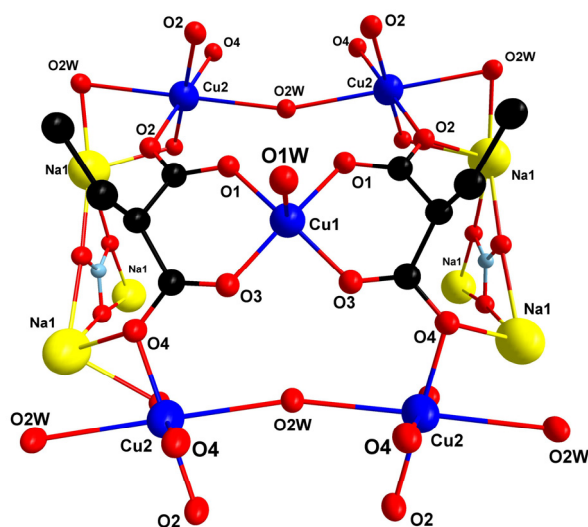


Fig. III.26. A view of a fragment of the molecular structure of complex **32** along with the numbering scheme.

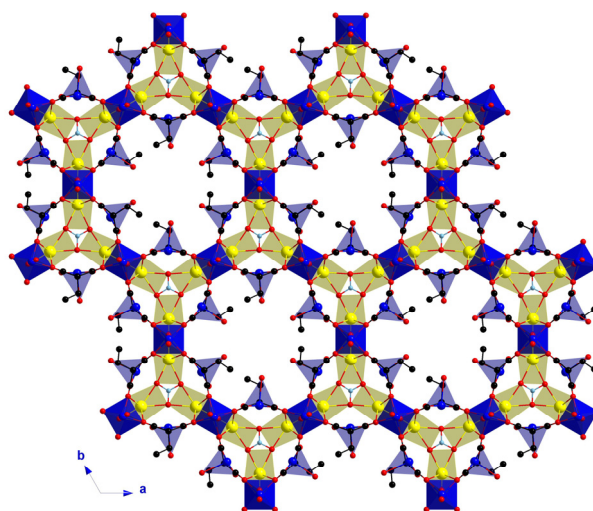
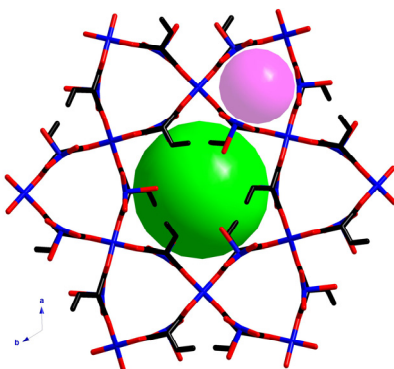
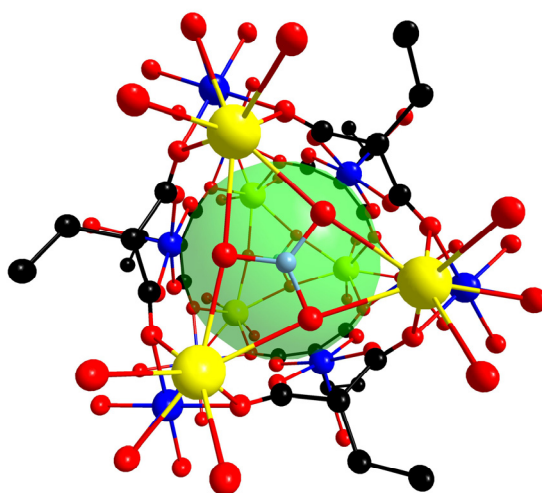


Fig. III.27. A perspective view of the 3D structure of **32** along the *c* axis with the polyhedra scheme showing the channels running in the *c* direction.





**Fig. III.28.** Sticks model view of the structure of **32** along the *c* axis. The green sphere limits the area available in the large pore whereas the pink one occupies the small cavities (see text).



**Fig. III.29.** The NO<sub>3</sub> groups act as stoppers in the small channels constructing 'pockets' filled with solvent molecules. The green sphere represents the void volume inside the pocket.

There are two different copper atoms, Cu(1) with a square pyramidal environment, [ $\tau$  value<sup>3</sup> being 0 due to symmetry reasons] and Cu(2) with a square planar surroundings and two very long apical positions [the water molecule O(2w) occupying these long apical positions at 2.7086(16) Å]. Four oxygen atoms from two [O(1), O(1a), O(3) and O(3a) for Cu(1); (a)  $x, y, -z+3/2$ ] and four [O(2), O(2b), O(4c) and O(4d) for Cu(2); (b)  $-x+2, -x+y+1, -z+1$ ; (c)  $-y+1, x-y, -z+3/2$ ; (d)  $y+1, x, z-1/2$ ] different ethylmalonate ligands build the basal plane at Cu(1) and Cu(2), respectively [average Cu–O(eq) bond distance being 1.923(8) and 1.974(6) Å, for Cu(1) and Cu(2), respectively; see Table III.8]. A water molecule occupies the apical position of Cu(1) [Cu(1)–O(1w) bond distance being 2.44(4) Å]. The sodium atom is seven-coordinated with two oxygen atoms from a nitrate molecule,

four oxygen atoms from four different ethylmalonate ligands and a water molecule building a distorted  $\text{NaO}_7$  surrounding.

The ethylmalonate ligand acts as a bidentate [through O(1) and O(3) to ward Cu(1); the angle subtended at the copper atom being  $93.07(18)^\circ$ ] and as bis-monodentate ligand [through O(2) and O(4) to ward Cu(2)]. Therefore, each Cu(1) belonging to the  $[\text{Cu}(\text{Etmal})_2(\text{H}_2\text{O})]$  unit is connected to four Cu(2) from aquacopper(II) units through carboxylate-bridges, the latter ones being linked to four different former units. The  $\text{Cu}(1)\cdots\text{Cu}(2)$  separation through the two different *anti-syn* carboxylate bridges linking equatorial positions at both copper environments being  $4.9471(19)$  Å through O(3)–C(3)–O(4) and  $4.9312(13)$  Å through O(1)–C(1)–O(2). The Cu(2) atoms are also linked among them through a very long  $\mu$ -oxo bridge involving the water molecule O(2w) occupying long axial positions at the two adjacent copper atoms [the  $\text{Cu}(2)\cdots\text{Cu}(2)$  separation being  $5.3566(16)$  Å].

**Table III.8.** Selected bond angles ( $^\circ$ ) and lengths (Å) for **32**<sup>a</sup>

| <b>32</b>         |           |                   |           |
|-------------------|-----------|-------------------|-----------|
| Cu(1)–O(1)        | 1.927(7)  | Cu(2)–O(2)        | 1.983(6)  |
| Cu(1)–O(1a)       | 1.927(8)  | Cu(2)–O(2b)       | 1.983(6)  |
| Cu(1)–O(3)        | 1.920(6)  | Cu(2)–O(4c)       | 1.965(5)  |
| Cu(1)–O(3a)       | 1.920(6)  | Cu(2)–O(4d)       | 1.965(6)  |
| Cu(1)–O(1w)       | 2.44(4)   | O(2)–Cu(2)–O(2b)  | 93.1(14)  |
| O(1)–Cu(1)–O(1a)  | 87.0(4)   | O(2)–Cu(2)–O(4c)  | 179.1(3)  |
| O(1)–Cu(1)–O(3)   | 172.6(4)  | O(2)–Cu(2)–O(4d)  | 86.13(17) |
| O(1)–Cu(1)–O(3a)  | 93.07(18) | O(2b)–Cu(2)–O(4c) | 86.13(17) |
| O(1)–Cu(1)–O(1w)  | 95.7(11)  | O(2b)–Cu(2)–O(4d) | 179.1(3)  |
| O(1a)–Cu(1)–O(3)  | 93.07(18) | O(4c)–Cu(2)–O(4d) | 94.6(4)   |
| O(1a)–Cu(1)–O(3a) | 172.6(4)  |                   |           |
| O(1a)–Cu(1)–O(1w) | 95.7(11)  |                   |           |
| O(3)–Cu(1)–O(3a)  | 86.0(4)   |                   |           |
| O(3)–Cu(1)–O(1w)  | 91.7(11)  |                   |           |
| O(3a)–Cu(1)–O(1w) | 91.7(11)  |                   |           |

<sup>a</sup> Symmetry operations: (a)  $x, y, -z+3/2$ ; (b)  $-x+2, -x+y+1, -z+1$ ; (c)  $-y+1, x-y, -z+3/2$ ; (d)  $y+1, x, z-1/2$ .

Let us compare the structure of **32** with that of the  $[\text{Cu}(\text{Etmal})(\text{H}_2\text{O})]_n \cdot 1.65n\text{H}_2\text{O}$  (**30**) complex. Both compounds exhibit a 3D-network based on carboxylate bridged copper(II) ions with a characteristic topology in which each copper atom acts as a four-connecting node. Cavities and channels are formed in the two structures, with a remarkable difference, the 1D pore in **30** exhibits an hydrophilic environment with the coordination water molecules pointing towards the channel instead of the ethyl groups which occupy the edge of the biggest channel in **32**. The smallest triangular channels of **32** exhibit also hydrophilic environments with the nitrate molecules coordinated to the sodium atoms as

stoppers and the distorted ethoxo and water molecules inside. However, two different units,  $[\text{Cu}(\text{Etmal})_2]$  and aquacopper(II) entities, are involved in **32**, while only one,  $[\text{Cu}(\text{Etmal})_2]$ , is present in **30**.

Let us finish this structural description with a comparison of the crystal structure of **31** and **32** and the related malonate-containing complex of formula  $\{[\text{Na}(\text{H}_2\text{O})_2[\text{Cu}(\text{mal})_2]]_n\}^2$ . Compounds **31** and **32** have almost the same components but different crystal structures. They are both formed by  $[\text{Cu}(\text{Etmal})_2]$  units which are linked through sodium atoms in **31** and through carboxylate bridges to aquacopper(II) cations in **32** affording 3D-networks. As a result of this coordination, pores are formed in both compounds. However, **32** exhibits an unusual feature, the presence of small pores with  $\text{Na}^+$ -coordinated nitrate molecules acting as stoppers. This situation is indicative that the presence of the nitrate groups in the structure could act as a template in the formation of **32**. The structure of the malonate-containing complex consists of layers of carboxylate-bridged  $[\text{Cu}(\text{mal})_2]$  units, which are linked through sodium atoms affording a three-dimensional network. This structure is very different from that found for the Etmal-containing complexes. However, it is noteworthy to mention the different role played by the sodium atoms in the three complexes. The sodium atoms in **31** and in the mal-complex are grouped in chains building an own entity in the structure (Figures III.24 and III.25) which links the mononuclear units in **31** and the layers in the mal-complex, whereas in **32** they simply build the  $\text{Na}_3\text{NO}_3$  entity which acts as stopper in the small pores (Figure III.26).

#### III.2.4. Magnetic Properties

The magnetic properties of complex **31** have not been studied because of the small amount of available product. **31** is a mononuclear species from a magnetic point of view and hence a Curie law behaviour is expected.<sup>4,5</sup>

The temperature dependence of the  $\chi_M T$  product [ $\chi_M$  being the magnetic susceptibility per copper(II) ion] for the complex **32** in the temperature range 2-100 K is shown in the Figure III.30.  $\chi_M T$  at 100 K is  $0.45 \text{ cm}^3 \text{ mol}^{-1} \text{ K}$  a value which is as expected for a magnetically isolated spin doublet. Upon cooling,  $\chi_M T$  smoothly increases with a continuous increment of the slope being asymptotical at 2.0 K. The value of  $\chi_M T$  at this temperature is  $1.63 \text{ cm}^3 \text{ mol}^{-1} \text{ K}$ . This behaviour is indicative of an overall ferromagnetic coupling among the copper(II) ions in **32**. The magnetization curve (inset of Figure III.30) lies over the Brillouin curve for an isolated spin of  $S = 1/2$ , fixing the previous statement.

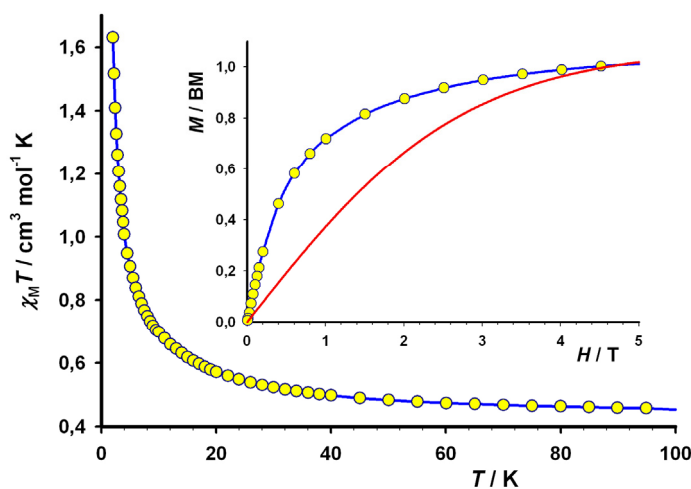


**Fig. III.30.**  $\chi_M T$  vs  $T$  plot for **32** under applied fields of 0.1 T ( $T > 10$  K) and 0.025 T ( $T < 10$  K); the blue line is only an eye-guide. The inset shows the  $M$  vs  $H$  plot for **32** together with the Brillouin function for a magnetically isolated spin doublet (red line).

The crystal structure of **32** is three-dimensional based on carboxylate-bridged copper(II) ions, hence the  $\chi_M T$  curve cannot be fitted since there is no theoretical expression which simulates the magnetic behaviour of a 3D-network of interacting copper(II) ions.<sup>5</sup> However, a ferromagnetic coupling is encountered in a related system which exhibits the *anti-syn* carboxylate bridge linking equatorial positions of the adjacent copper(II) environments as in **32**.<sup>6,7</sup>

### III.2.5. Conclusion

The two sodium-containing copper(II)-ethylmalonate complexes (**31** and **32**) are very different, basically due to the role played by the sodium atoms in the structure. On one hand, the sodium atoms in **31** build one-dimensional entities which are linked through the  $\text{Cu}(\text{Etmal})_2$  units affording the 3D network. On the other hand, the copper(II)-ethylmalonate network in **32** is three-dimensional occupying the sodium atoms the cavities of the 3D network. From a magnetic point of view, ferromagnetism occurs in complex **32**, although the size of the magnetic coupling parameter could not be determined.

### III.2.6. References

- 1 O. Fabelo, L. Cañadillas-Delgado, J. Pasán, C. Ruiz-Pérez and M. Julve, *CrystEngComm* **2006**, *8*, 338.
- 2 (a) J. C. Barnes and T. J. R., private deposition in the Cambridge Crystallographic Data Center, **1997**. CCDC reference code: RUWMUR. (b) S.-L. Deng, L.-S. Long, L.-S. Zheng

- and S. W. Ng, *Main Group Metal Chemistry*, **2002**, 25, 465. (c) H.-L. Liu, H.-Y. Mao, H.-Y. Zhang, C. Xu, Q.-A. Wu, G. Li, Y. Zhu and H.-Y. Hou, *Polyhedron* **2004**, 23, 943. (d) F. S. Delgado, C. Ruiz-Pérez, J. Sanchiz, F. Lloret and M. Julve, *CrystEngComm* accepted.
- 3 A. W. Addison, T. N. Rao, J. Reedijk, J. van Rijn and G. C. Verschoor, *Dalton Trans.* **1984**, 1349.
  - 4 R. L. Carlin, *Magnetochemistry*, Springer-Verlag, **1986**.
  - 5 O. Kahn, *Molecular Magnetism*, VCH, New York, **1993**.
  - 6 J. Pasán, F. S. Delgado, Y. Rodríguez-Martin, M. Hernández-Molina, C. Ruiz-Pérez, J. Sanchiz, F. Lloret and M. Julve, *Polyhedron* **2003**, 22, 2143.
  - 7 A. Rodríguez-Forte, P. Alemany, S. Álvarez and E. Ruiz, *Chem. Eur. J.* **2001**, 7, 627.

### III.3. 2,2'-bipyrimidine Copper(II)-Ethylmalonate (33)

#### III.3.1. Introduction

The next step in the preparation of ethylmalonate-containing copper(II) complexes is the introduction of a N-donor ligand emulating the strategy followed in the previous chapters. However, this procedure has become a difficult task. The numerous attempts made to prepare copper(II)-ethylmalonate complexes with 4,4'-bipyridine, pyrazine, pyrimidine, etc. always yield compound **28** (Section III.1). The next sections are devoted to those which the synthesis yields what is expected. Remarkably, this situation was only encountered with chelating N-donor heterocycle ligands, such as the 2,2'-bipyrimidine. Thus, herein we report the synthesis, crystal structure and magnetic properties of the  $[\text{Cu}_2(2,2'\text{-bipym})(\text{Etmal})_2(\text{H}_2\text{O})_2]\cdot 6\text{H}_2\text{O}$  complex.

#### III.3.2. Synthesis

##### $[\text{Cu}_2(2,2'\text{-bipym})(\text{Etmal})_2(\text{H}_2\text{O})_2]\cdot 6\text{H}_2\text{O}$

**(33)**. An aqueous solution (3 cm<sup>3</sup>) of copper(II) nitrate (0.5 mmol, 116 mg) was added to a water solution (10 cm<sup>3</sup>) of a ethylmalonic acid (0.5 mmol, 65 mg) and sodium carbonate (0.5 mmol, 53 mg) mixture. A methanolic solution (5 cm<sup>3</sup>) of 2,2'-bipym was added dropwise to the previous pale blue solution under continuous stirring. The final deep blue solution obtained was filtered and allowed to evaporate at room temperature. Blue needle single crystals of **33** appear after a few days. Crystallographic details are listed in Table III.9. Yield 60 %. Anal. calc. for C<sub>9</sub>H<sub>17</sub>CuNO<sub>8</sub> (**33**): C, 31.35; H, 4.97; N, 8.12; Found: C, 31.44; H, 4.69; N, 8.39 %.

**Table III.9.** Crystallographic data for complex **33**

| <b>33</b>                                                   |                                                                   |
|-------------------------------------------------------------|-------------------------------------------------------------------|
| Formula                                                     | C <sub>9</sub> H <sub>17</sub> O <sub>8</sub> N <sub>2</sub> Cu   |
| FW                                                          | 344.79                                                            |
| Crystal system                                              | Monoclinic                                                        |
| Space group                                                 | <i>P</i> 2 <sub>1</sub> / <i>n</i>                                |
| <i>a</i> /Å                                                 | 12.1440(5)                                                        |
| <i>b</i> /Å                                                 | 7.3809(2)                                                         |
| <i>c</i> /Å                                                 | 15.3115(7)                                                        |
| $\beta$ /°                                                  | 92.965(2)                                                         |
| <i>V</i> /Å <sup>3</sup>                                    | 1370.59(9)                                                        |
| <i>Z</i>                                                    | 4                                                                 |
| $\mu$ (Mo K $\alpha$ ) /cm <sup>-1</sup>                    | 16.32                                                             |
| <i>T</i> /K                                                 | 293(2)                                                            |
| $\rho_{\text{calc}}$ /g cm <sup>-3</sup>                    | 1.671                                                             |
| $\lambda$ /Å                                                | 0.71073                                                           |
| Index ranges                                                | -15 ≤ <i>h</i> ≤ 16,<br>-9 ≤ <i>k</i> ≤ 9,<br>-20 ≤ <i>l</i> ≤ 20 |
| Indep. reflect. ( <i>R</i> <sub>int</sub> )                 | 3522 (0.0773)                                                     |
| Obs. reflect. [ <i>I</i> > 2 $\sigma$ ( <i>I</i> )]         | 2693                                                              |
| Parameters                                                  | 247                                                               |
| Goodness-of-fit                                             | 1.128                                                             |
| <i>R</i> [ <i>I</i> > 2 $\sigma$ ( <i>I</i> )]              | 0.0595                                                            |
| <i>R</i> <sub>w</sub> [ <i>I</i> > 2 $\sigma$ ( <i>I</i> )] | 0.1440                                                            |
| <i>R</i> (all data)                                         | 0.0861                                                            |
| <i>R</i> <sub>w</sub> (all data)                            | 0.1690                                                            |

### III.3.3. Description of the Structure

The structure of  $[\text{Cu}_2(2,2'\text{-bipym})(\text{Etmal})_2(\text{H}_2\text{O})_2]\cdot 6\text{H}_2\text{O}$  (**33**) consists of discrete 2,2'-bipym bridged copper(II) dinuclear entities and crystallization water molecules (Figure III.31).

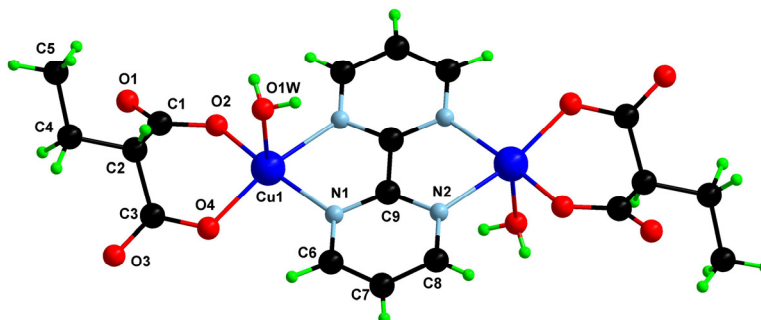


Fig. III.31. A view of a fragment of the structure of **33** along with the numbering scheme.

The dinuclear unit is generated by an inversion centre at the midpoint of the inter-ring carbon-carbon bond of the 2,2'-bipym ligand. The dinuclear entities are grouped in chains along the *b* direction through a very long  $\mu$ -oxo bridge [Cu–O separation being 3.077(2) Å] (Figure III.32).

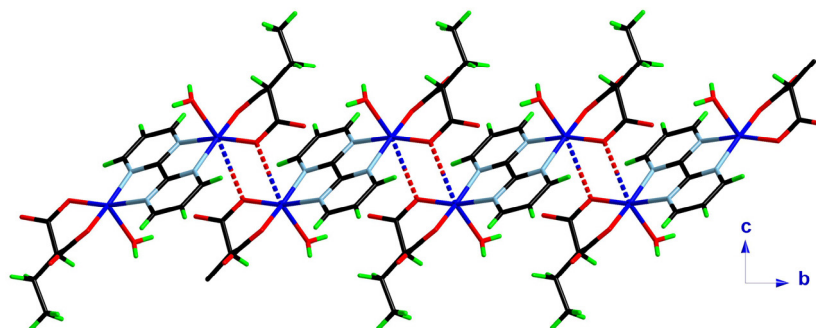


Fig. III.32. A view of the  $\mu$ -oxo bridged chain of dinuclear  $\text{Cu}_2(2,2'\text{-bipym})(\text{Etmal})_2(\text{H}_2\text{O})_2$  units running along the *b* direction.

The void space between the discrete units is filled with water molecules which establish a complex 3D supramolecular network through hydrogen bonds (see Table III.10 and Figure III.33). H-bonds among these crystallization water molecules build a hexagonal cluster (R6, according to the notation of Infantes *et. al*<sup>1</sup>) with two extra-pendant water molecules (Figure III.34). The R6 cluster exhibits the chair conformation and it is formed by three independent water molecules and their symmetry related by an inversion centre ones, feature which is common for this kind of water clusters (Figure III.34).<sup>1,2</sup>

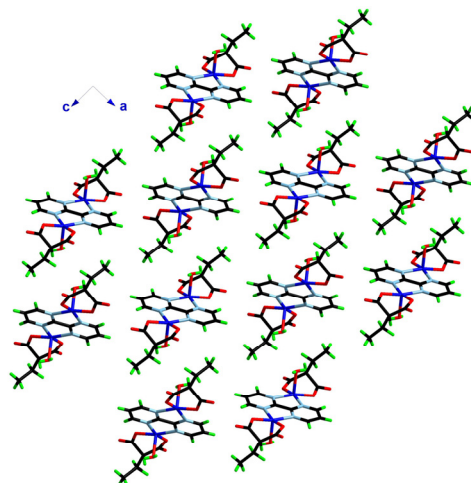


Fig. III.33 . A view along the *b* axis of the crystal packing of **33**. The crystallization water molecules have been omitted for clarity.

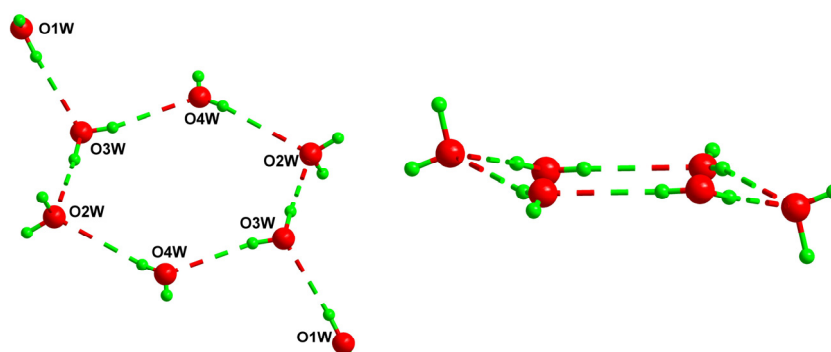


Fig. III.34. A perspective view of the hexagonal motif formed in **33** by the crystallization water molecules with the numbering scheme (up). A lateral view revealing the chair conformation of the water motif (bottom).

Each copper atom exhibits somewhat distorted square pyramidal surroundings with the  $\tau$  value<sup>3</sup> being 0.03. Two oxygen atoms from ethylmalonate ligand [O(2) and O(4); mean Cu–O(eq) bond distance being 1.921(2) Å; see Table III.11] and two 2,2'-bipyridine nitrogen atoms [N(1) and N(2a), Cu–N average bond distance is 2.045(3) Å; (a)  $-x + 1, -y + 3, -z$ ] build the basal plane while a water molecule occupies the apical position [Cu–O(1w) bond distance is 2.255(3) Å]. The copper atom is shifted toward the apical position by 0.1953(4) Å.

The ethylmalonate group acts as a bidentate ligand [through O(2) and O(4)], the angle subtended at the copper atom being 92.57(10)°. This angle for the chelating 2,2'-bipyridine is 81.25(11)°, the value of the bite distance N(1)⋯N(2a) being 2.664(4) Å. The dihedral angle between the basal plane of the copper environment and the mean plane of the



2,2'-bipym molecule is 5.76(7)°. The copper-copper separation across the 2,2'-bipym ligand is 5.4683(6) Å, a value much longer than the shortest interdimer metal-metal separation through the long oxo bridge [3.9274(6) Å].

**Table III.10.** Hydrogen bond distances and angles in **33**.

| D-H...A                      | O-H / Å  | H...O / Å | O-H...O / ° | O...O / Å |
|------------------------------|----------|-----------|-------------|-----------|
| <i>R6 Hexagonal cluster</i>  |          |           |             |           |
| O(3w)-H...O(2w) <sup>a</sup> | 0.92(11) | 1.88(11)  | 174(10)     | 2.801(6)  |
| O(3w)-H...O(4w)              | 0.70(6)  | 2.07(6)   | 164(6)      | 2.753(8)  |
| O(4w)-H...O(2w)              | 0.61(5)  | 2.27(4)   | 165(5)      | 2.862(9)  |
| O(1w)-H...O(3w)              | 0.72(6)  | 2.07(6)   | 161(6)      | 2.757(6)  |
| <i>Other H-bonds</i>         |          |           |             |           |
| O(1w)-H...O(3a) <sup>b</sup> | 0.78(6)  | 2.09(6)   | 171(6)      | 2.870(4)  |
| O(2w)-H...O(1b)              | 0.72(5)  | 2.43(5)   | 170(5)      | 3.142(4)  |
| O(2w)-H...O(2b)              | 0.72(5)  | 2.41(6)   | 133(6)      | 2.957(4)  |
| O(2w)-H...O(1)               | 0.87(6)  | 1.87(6)   | 167(5)      | 2.741(4)  |

<sup>a</sup> For a better schematic view of the formation of the cluster see Figure III.34.

<sup>b</sup> Symmetry operations: (a)  $x, y + 1, z$ ; (b)  $-x + 1/2, y - 1/2, -z + 1/2$ ;

The structure of **33** exhibit little differences with [Cu<sub>2</sub>(2,2'-bipym)(Memal)<sub>2</sub>(H<sub>2</sub>O)<sub>2</sub>].3H<sub>2</sub>O (**22**) and also with the previously reported malonate complex [Cu<sub>2</sub>(2,2'-bipym)(mal)<sub>2</sub>(H<sub>2</sub>O)<sub>2</sub>].4H<sub>2</sub>O.<sup>4</sup> However, they present quite a few differences structurally. The higher number of crystallization water molecules in **33** changes not only the supramolecular structure [allows the formation of hexameric water clusters] but also the interdimer separation through the long oxo bridge [3.9274(6) in **33** and 3.077(2) Å in **22**].

**Table III.11.** Selected bond angles (°) and lengths (Å) for **33**.<sup>a</sup>

| <b>33</b>        |            |                   |            |
|------------------|------------|-------------------|------------|
| Cu(1)-O(2)       | 1.911(2)   | O(2)-Cu(1)-O(1w)  | 100.23(13) |
| Cu(1)-O(4)       | 1.932(2)   | O(4)-Cu(1)-N(1)   | 93.58(10)  |
| Cu(1)-N(1)       | 2.036(3)   | O(4)-Cu(1)-N(2a)  | 166.32(11) |
| Cu(1)-N(2a)      | 2.055(3)   | O(4)-Cu(1)-O(1w)  | 102.91(11) |
| Cu(1)-O(1w)      | 2.255(3)   | N(1)-Cu(1)-N(2a)  | 81.25(11)  |
| O(2)-Cu(1)-O(4)  | 92.57(10)  | N(1)-Cu(1)-O(1w)  | 88.37(13)  |
| O(2)-Cu(1)-N(1)  | 168.06(11) | N(2a)-Cu(1)-O(1w) | 89.66(11)  |
| O(2)-Cu(1)-N(2a) | 90.45(11)  |                   |            |

<sup>a</sup> Symmetry operations: (a)  $-x + 1, -y + 3, -z$ .

### III.3.4. Magnetic Properties

The thermal dependence of the  $\chi_M$  value is shown in Figure III.35. The curve exhibits the characteristic behaviour of antiferromagnetically coupled copper(II) ions with a smooth maximum of the susceptibility at about 130 K. On the light of the structural features described above, the 2,2'-bipym bridging ligand is the main magnetic exchange pathway in **33**. It is well known that the 2,2'-bipym ligand strongly couples antiferromagnetically the

copper(II) ions.<sup>4-10</sup> The experimental data can then be analyzed by means of the Bleaney and Bowers expression for a dinuclear antiferromagnetically coupled copper(II) complex.<sup>11,12</sup>

$$\chi_M = (2N\beta^2 g^2 / kT) \frac{1}{[3 + \exp(-J/kT)]}$$

where  $J$  is the singlet-triplet gap defined by the Hamiltonian:

$$\hat{H} = -J \hat{S}_1 \cdot \hat{S}_2$$

and the other symbols have their usual meanings. The least-squares fit leads to  $J = -132.6(8) \text{ cm}^{-1}$ ,  $g = 2.13(2)$  and  $R = 2.0 \times 10^{-4}$ . The calculated curve is in agreement with the experimental one (Figure III.35).

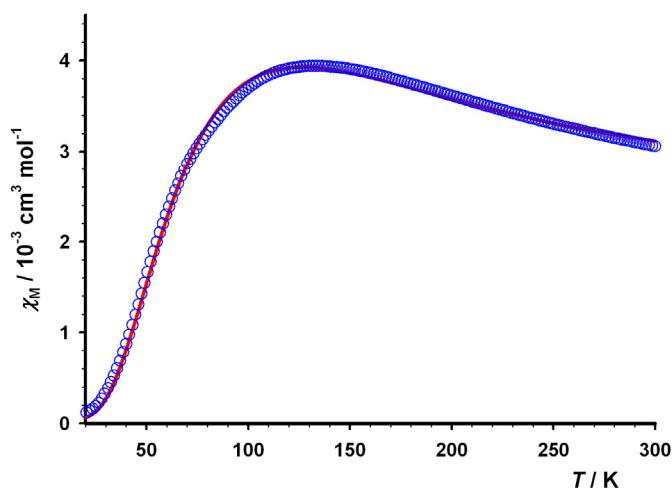


Fig. III.35.  $\chi_M$  vs  $T$  plot for **33** under an applied field of 1 T: (o) experimental data; (—) best fit curve.

The value of  $J$  reveals a strong antiferromagnetic interaction between the copper(II) ions separated by 5.4683(6) Å in **33**. The overlap between the  $d(x^2-y^2)$  magnetic orbitals centred on each metal ion [the  $x$  and  $y$  axes being defined by the equatorial bonds at the copper environment] accounts for this coupling. The influence of some structural features such as the Cu–N bond distance, the dihedral angle between the basal plane at the copper atom and the 2,2'-bipym plane, etc, in the magnitude of the magnetic coupling parameter have been investigated in a previous work (see Table III.12).<sup>7</sup> The  $J$  parameter for **33** are slightly lower than those observed for the related mal- and Memal-containing (**23**) complexes, in agreement with a subtly longer Cu...Cu separation through the 2,2'-bipym bridge.

**Table III.12.** Magnetostructural data for a series of 2,2'-bipym bridged copper(II) complexes<sup>a</sup>

| Compounds                                                                                                                                                              | Cu–N | Cu–O              | $\gamma^b/\circ$ | $h_M^c/\text{\AA}$ | Cu $\cdots$ Cu <sup>d</sup> | $-J/\text{cm}^{-1}$ | Ref. |
|------------------------------------------------------------------------------------------------------------------------------------------------------------------------|------|-------------------|------------------|--------------------|-----------------------------|---------------------|------|
| [Cu <sub>2</sub> (2,2'-bipym)(C <sub>4</sub> O <sub>4</sub> ) <sub>2</sub> (H <sub>2</sub> O) <sub>6</sub> ]                                                           | 2.07 | 1.96              | 11.4             | 0.096              | 5.542(1)                    | 139                 | 7    |
| [Cu <sub>2</sub> (2,2'-bipym)(C <sub>3</sub> O <sub>5</sub> ) <sub>2</sub> (H <sub>2</sub> O) <sub>2</sub> ] $\cdot$ 4(H <sub>2</sub> O)                               | 2.02 | 1.97              | 14.4             | 0.187              | 5.348(1)                    | 160                 | 6    |
| [Cu <sub>2</sub> (2,2'-bipym)(H <sub>2</sub> O) <sub>4</sub> (SO <sub>4</sub> ) <sub>2</sub> ] $\cdot$ 3(H <sub>2</sub> O)                                             | 2.04 | 1.97              | 5.1              | 0.075              | 5.456(1)                    | 159                 | 8    |
| [Cu <sub>2</sub> (2,2'-bipym)(NO <sub>3</sub> ) <sub>4</sub> ]                                                                                                         | 2.01 | 1.96              | 3.5              | 0.021              | 5.371(1)                    | 191                 | 5    |
| [Cu <sub>2</sub> (2,2'-bipym)(C <sub>3</sub> H <sub>2</sub> O <sub>4</sub> ) <sub>2</sub> (H <sub>2</sub> O) <sub>2</sub> ] $\cdot$ 4(H <sub>2</sub> O)                | 2.04 | 1.90              | 6.5              | 0.118              | 5.445(1)                    | 149                 | 4    |
| [Cu <sub>2</sub> (2,2'-bipym)(C <sub>6</sub> H <sub>5</sub> O <sub>2</sub> N <sub>2</sub> ) <sub>2</sub> (H <sub>2</sub> O) <sub>4</sub> ] $\cdot$ 2(H <sub>2</sub> O) | 2.05 | 1.96 <sup>e</sup> | 4.3              | 0.061              | 5.506(1)                    | 99                  | 10   |
| <b>23</b>                                                                                                                                                              | 2.03 | 1.92              | 4.7              | 0.130              | 5.451(1)                    | 156                 | -    |
| <b>33</b>                                                                                                                                                              | 2.04 | 1.92              | 5.8              | 0.195              | 5.468(1)                    | 133                 | -    |

<sup>a</sup> Average bond distances are given for each structure in  $\text{\AA}$ .

<sup>b</sup> Dihedral angle between the basal plane at the copper environment and the 2,2'-bipym plane.

<sup>c</sup> The height of the metal atom above the mean plane defined by the equatorial ligand atoms.

<sup>d</sup> Metal-metal separation across 2,2'-bipym in  $\text{\AA}$ .

<sup>e</sup> In this case, this is a Cu–N bond distance: the nitrogen atoms of the ligand are bonded to the metal atom.

### III.3.5. Conclusion

The structure of **33** consists of a isolated dinuclear 2,2'-bipym-bridged copper(II) and crystallization water molecules, with a structure similar to that found for the malonate<sup>-4</sup> and methylmalonate-containing copper(II) (**23**) complexes, but very different from the phenylmalonate complex (**14**). Magnetically, **33** exhibits a behaviour characteristic of an antiferromagnetic coupled dinuclear copper(II) complex [ $J$  being  $-132.6(8)\text{ cm}^{-1}$ ], in agreement with previous reported values for 2,2'-bipym-bridged dinuclear copper(II) complexes.

### III.3.6. References

- (a) L. Infantes and S. Motherwell, *CrystEngComm* **2002**, *4*(75), 454. (b) L. Infantes, J. Chisholm and S. Motherwell, *CrystEngComm*, **2003**, *5*, 480. (c) M. Mascal, L. Infantes and J. Chisholm, *Angew. Chem. Int. Ed.* **2006**, *45*, 32.
- (a) M. Losada and S. Leutwyler, *J. Chem. Phys.* **2002**, *117*, 2003. (b) B. K. Saha and A. Nangia, *Chem. Commun.* **2006**, 1825.
- A. W. Addison, T. N. Rao, J. Reedijk, J. van Rijn and G. C. Verschoor, *J. Chem. Soc., Dalton Trans.* **1984**, 1349.
- Y. Rodríguez-Martín, J. Sanchiz, C. Ruiz-Pérez, F. Lloret and M. Julve, *Inorg. Chim. Acta* **2001**, *326*, 20.
- M. Julve, G. De Munno, G. Bruno and M. Verdaguer, *Inorg. Chem.* **1988**, *27*, 3160.
- I. Castro, J. Sletten, L. K. Glærum, F. Lloret, J. Faus and M. Julve, *Dalton Trans.* **1994**, 2777.
- I. Castro, J. Sletten, L. K. Glærum, J. Cano, F. Lloret, J. Faus and M. Julve, *Dalton Trans.* **1995**, 3207.
- A. L. Spek, *Acta Cryst., Sect. A* **1990**, *46*, 34.
- M. Julve, M. Verdaguer, G. De Munno, J. A. Real and G. Bruno, *Inorg. Chem.* **1993**, *32*, 795.
- F. Thetiot, S. Triki, J. S. Pala, J. R. Galán-Mascaros, J. M. Martínez-Agudo and K. R. Dunbar, *Eur. J. Inorg. Chem.* **2004**, 3783.
- B. Bleaney and K. D. Bowers, *Proc. R. Soc. London Ser. A* **1952**, *214*, 451.
- O. Kahn, *Molecular Magnetism*, VCH, New York, **1993**.

### III.4. 2,2'-bipyridine (34) and 1,10-phenantroline (35) Copper(II)-Ethylmalonate Complexes

#### III.4.1. Introduction

The two final complexes of this chapter are a logical continuation of the previous section. The preparation of ethylmalonate copper(II) complexes with 2,2'-bipyridine and 1,10-phenantroline obeys to comparative reasons since their related complexes with Phmal and Memal were already reported. Here, thus, we report their synthesis, crystal structure and magnetic properties.

#### III.4.2. Synthesis

##### [Cu(2,2'-bpy)(Etmal)(H<sub>2</sub>O)]·3H<sub>2</sub>O

**(34)**. An aqueous solution (3 cm<sup>3</sup>) of copper(II) nitrate (0.5 mmol, 115 mg) was added to a water solution (10 cm<sup>3</sup>) of a ethylmalonic acid (0.5 mmol, 65 mg) and sodium carbonate (0.5 mmol, 53 mg) mixture. 2,2'-Bipyridine (0.5 mmol, 78 mg) dissolved in methanol (5 cm<sup>3</sup>) was added dropwise to the resulting pale blue solution. The resulting deep blue solution was filtered and stored at room temperature. After a few days, thin needle-shaped single crystals of **34** were grown. Yield 70 %. Analc.

calc. for C<sub>16</sub>H<sub>12</sub>CuN<sub>2</sub>O<sub>4</sub> (**34**): C, 53.40; H, 3.36; N, 7.79; Found: C, 53.26; H, 3.49; N, 7.92 %.

**[Cu(phen)(Etmal)(H<sub>2</sub>O)]·3H<sub>2</sub>O (35)**. This complex was prepared following the same synthetic procedure for **34**, but using 1,10-phenantroline (0.5 mmol, 90 mg) instead of 2,2'-bpy. Deep blue single crystals in the form of thin needles appeared after a few days. Crystallographic details for **34** and **35** are listed in Table III.13.<sup>1</sup> Yield 60%. Analc. calc. for C<sub>17</sub>H<sub>20</sub>CuN<sub>2</sub>O<sub>7</sub> (**35**): C, 47.72; H, 4.71; N, 6.55; Found: C, 47.89; H, 4.98; N, 6.71 %.

**Table II.13.** Crystallographic data for complexes **34-35**

|                                                    | <b>34</b>                                                        | <b>35</b>                                                           |
|----------------------------------------------------|------------------------------------------------------------------|---------------------------------------------------------------------|
| Formula                                            | C <sub>16</sub> H <sub>12</sub> O <sub>4</sub> N <sub>2</sub> Cu | C <sub>17</sub> H <sub>20</sub> O <sub>7</sub> N <sub>2</sub> Cu    |
| FW                                                 | 359.82                                                           | 427.84                                                              |
| Crystal system                                     | Orthorhombic                                                     | Monoclinic                                                          |
| Space group                                        | <i>P mnn</i>                                                     | <i>P2<sub>1</sub>/c</i>                                             |
| <i>a</i> /Å                                        | 13.848(2)                                                        | 9.5392(9)                                                           |
| <i>b</i> /Å                                        | 16.781(2)                                                        | 11.6835(12)                                                         |
| <i>c</i> /Å                                        | 7.6283(8)                                                        | 16.416(2)                                                           |
| $\beta$ /°                                         | -                                                                | 99.648(9)                                                           |
| <i>V</i> /Å <sup>3</sup>                           | 1772.6(4)                                                        | 1803.7(3)                                                           |
| <i>Z</i>                                           | 4                                                                | 4                                                                   |
| $\mu$ (Mo K $\alpha$ ) /cm <sup>-1</sup>           | 12.50                                                            | 12.53                                                               |
| <i>T</i> /K                                        | 293(2)                                                           | 293(2)                                                              |
| $\rho_{\text{calc}}$ /g cm <sup>-3</sup>           | 1.348                                                            | 1.553                                                               |
| $\lambda$ /Å                                       | 0.71073                                                          | 0.71073                                                             |
| Index ranges                                       | -8 ≤ <i>h</i> ≤ 18,<br>-20 ≤ <i>k</i> ≤ 22,<br>-7 ≤ <i>l</i> ≤ 9 | -12 ≤ <i>h</i> ≤ 12,<br>-15 ≤ <i>k</i> ≤ 15,<br>-20 ≤ <i>l</i> ≤ 21 |
| Indep. reflect. ( <i>R</i> <sub>int</sub> )        | 2294 (0.0682)                                                    | 4041 (0.0872)                                                       |
| Obs. reflect. [ <i>I</i> > 2σ( <i>I</i> )]         | 1638                                                             | 2590                                                                |
| Parameters                                         | 133                                                              | 244                                                                 |
| Goodness-of-fit                                    | 1.106                                                            | 1.521                                                               |
| <i>R</i> [ <i>I</i> > 2σ( <i>I</i> )]              | 0.0634                                                           | 0.1408                                                              |
| <i>R</i> <sub>w</sub> [ <i>I</i> > 2σ( <i>I</i> )] | 0.1634                                                           | 0.3882                                                              |
| <i>R</i> (all data)                                | 0.0945                                                           | 0.1892                                                              |
| <i>R</i> <sub>w</sub> (all data)                   | 0.1891                                                           | 0.4189                                                              |

### III.4.3. Description of the Structure

The structures of  $[\text{Cu}(\text{L})(\text{Etmal})(\text{H}_2\text{O})]\cdot 3\text{H}_2\text{O}$  [L being 2,2'-bpy (**34**) and phen (**35**)] consist of discrete mononuclear copper(II) entities and crystallization water molecules. The molecule is generated by a mirror plane perpendicular to the 2,2'-bpy plane in **34**, while the complete entity is crystallographically independent in **35** (Figure III.36).

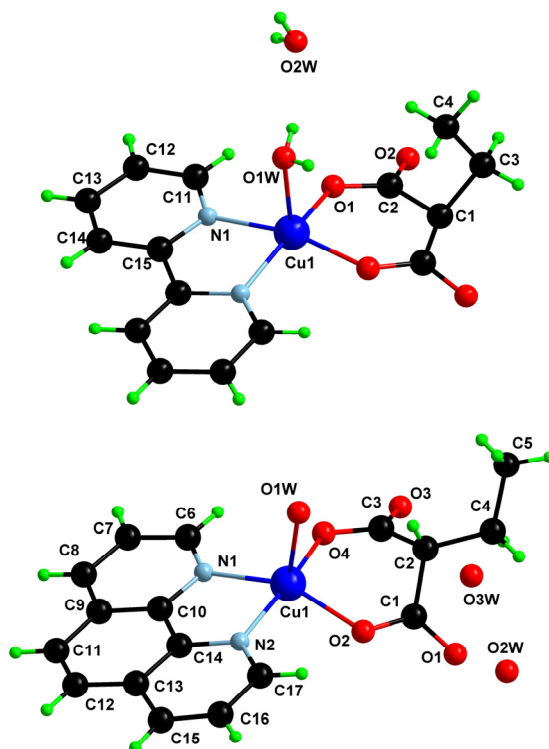
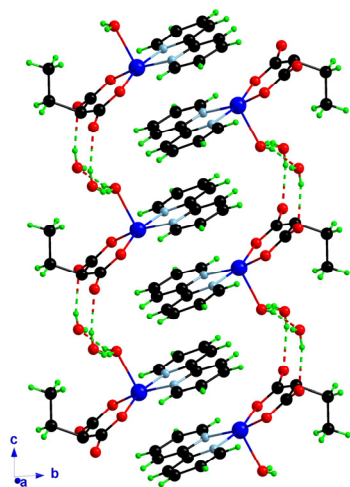
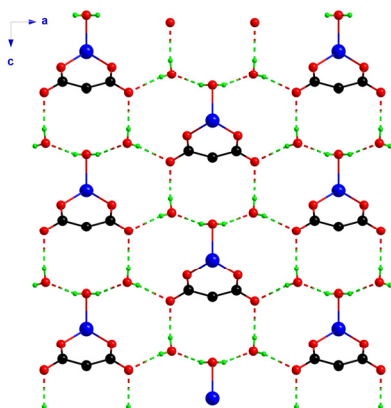


Fig. III.36. A view of a molecular fragment of the structure of complex **34** (up) and the asymmetric unit of complex **35** (bottom) along with the numbering scheme.

The  $[\text{Cu}(2,2'\text{-bpy})(\text{Etmal})(\text{H}_2\text{O})]$  units of **34** are stacked through weak  $\pi$ - $\pi$  interactions along the  $c$  direction (Figure III.37). The centroid-centroid distance and the offset angle being 3.936(2) Å and 27.3(2)°, respectively; values which are in agreement with those previously reported for pyridyl rings.<sup>2</sup> Hydrogen bonds involving the water molecules and uncoordinated ethylmalonate oxygen atoms form a supramolecular 2D network in the  $ac$  plane (Figure III.38 and Table III.14) with a surprising (6,3) appearance, reminiscent to that found for complex **16** (see Section I.9).<sup>3</sup> Since the  $\pi$ - $\pi$  stacked chains are H-bonded to all its nearest neighbours, the resulting supramolecular network is three-dimensional (Figure III.39).



**Fig. III.37.**  $\pi$ - $\pi$  stacking among the 2,2'-bipyridine ligands of adjacent hydrogen bonded chains of  $[\text{Cu}(2,2'\text{-bpy})(\text{Etmal})(\text{H}_2\text{O})]$  mononuclear units.



**Fig. III.38.** A (6,3) regular hydrogen bonded pattern involving the coordinated and uncoordinated water molecules and uncoordinated malonate oxygen atoms viewed along the  $b$  axis. 2,2'-bpy ligands and ethyl groups of the Etmal ligands are omitted for clarity.

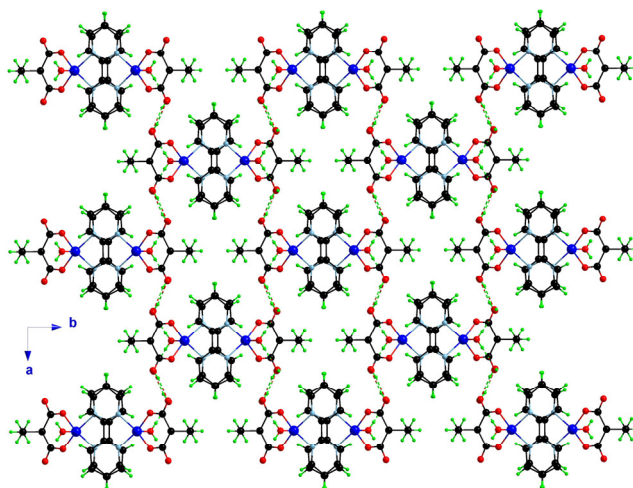


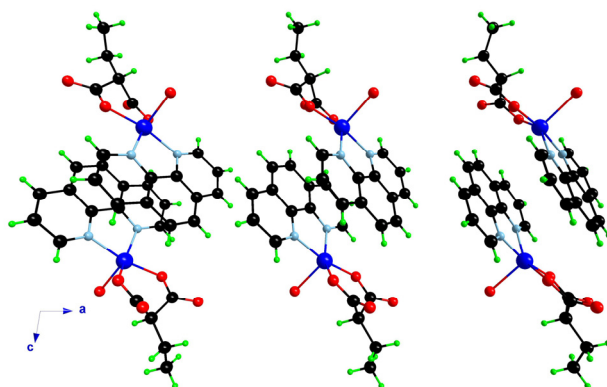
**Fig. III.39.** A perspective view along the  $c$  axis of the crystal packing of **34**. Dashed lines correspond to hydrogen bonds.

**Table III.14.** Hydrogen bond distances and angles in **34**.

| D–H···A                      | O–H (Å) | H···O (Å) | O–H···O (°) | O···O (Å) |
|------------------------------|---------|-----------|-------------|-----------|
| O(1w)–H···O(2w)              | 0.75(5) | 1.99(5)   | 162(5)      | 2.719(5)  |
| O(2w)–H···O(2a) <sup>a</sup> | 0.78(5) | 2.05(5)   | 167(5)      | 2.817(5)  |
| O(2w)–H···O(2b)              | 0.73(8) | 2.10(8)   | 164(8)      | 2.813(6)  |

<sup>a</sup> Symmetry operators: (a)  $x, y, z - 1$ ; (b)  $-x + 1/2, -y + 1/2, z - 1/2$ .

The [Cu(phen)(Etmal)(H<sub>2</sub>O)] units of **35** are grouped in pairs through weak  $\pi$ - $\pi$  interactions along the  $a$  direction (Figure III.40). The shortest centroid-centroid distance and off-set angle being 3.611(2) Å and 18.5(2)° respectively; being in accordance with previous reported values.<sup>2</sup> H-bonding involving the water molecules and uncoordinated ethylmalonate oxygen atoms build a T(5)2-like<sup>4</sup> tape motif along the  $b$  direction (Figure III.41) [O···O distances ranging from 2.692(15) to 2.883(13) Å] affording a two-dimensional network. Since the discrete units involved in the  $\pi$ - $\pi$  pair interactions belong to different layers, the complex exhibit a supramolecular 3D-network.

**Fig. III.40.** A view of the through  $\pi$ - $\pi$  stacking dinuclear units formed in **35**.

Each copper atom in **34** and **35** exhibits square pyramidal environments being the  $\tau$  value 0 for **34** (due to symmetry reasons) and 0.29 for **35**. Two ethylmalonate oxygen atoms [O(1) and O(1a) for **34** and O(2) and O(4) for **35**, average Cu–O(eq) bond length being 1.915(3) (**34**) and 1.938(7) Å (**35**); (a)  $-x, y, z$ ; see Table III.15] and two nitrogen atoms from the 2,2'-bpy (**34**) or 2,2'-bipym (**35**) ligands [N(1) and N(1a) for **34**, and N(1) and N(2) for **35**, Cu–N mean bond distance being 2.015(3) (**34**) and 2.017(9) Å (**35**)] build the basal plane while a water molecule occupies the apical position [Cu–O(1w) bond distances are 2.231(5) and 2.232(7) Å for **34** and **35**, respectively].

The ethylmalonate ligand acts in both complexes as bidentate [through O(1) and O(1a) in **34** and through O(2) and O(4) in **35**] being the angle subtended at the copper atom 93.56(17)° (**34**) and 94.4(3)° (**35**). These angles for the bidentate N-donor ligands take the

values  $80.9(2)^\circ$  for the 2,2'-bpy and  $81.4(3)^\circ$  for the phen ligand. The bite distance between the N-donor atoms are 2.614(6) and 2.630(11) Å for **34** and **35**, respectively. The shortest copper-copper separation is 5.0855(11) Å, between to  $\pi$ - $\pi$  stacked adjacent units for **34**; being 6.106(2) Å for **35** between to adjacent H-bonded entities.

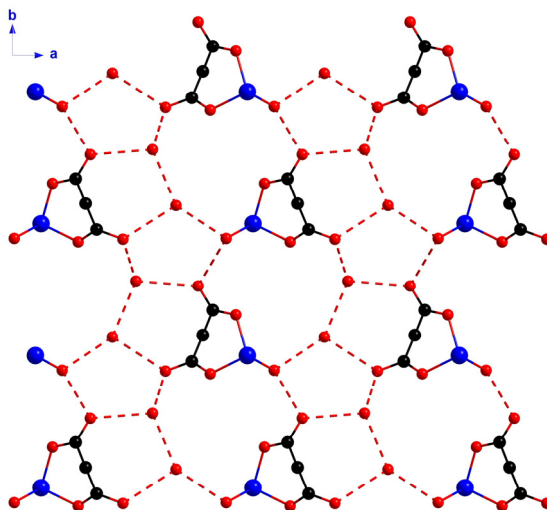


**Fig. III.41.** The water molecules and the uncoordinated ethylmalonate oxygen atoms form a T5(2)-like motif in **35** running in the *b* direction. 1,10-phenanthroline ligands and ethyl groups of the Etmal ligand are omitted for clarity.

**Table III.15.** Selected bond angles ( $^\circ$ ) and lengths (Å) for **34** and **35**.<sup>a</sup>

| <b>34</b>        |            |                   |            |
|------------------|------------|-------------------|------------|
| Cu(1)–O(1)       | 1.915(3)   | O(1)–Cu(1)–O(1w)  | 97.80(13)  |
| Cu(1)–O(1a)      | 1.915(3)   | O(1a)–Cu(1)–N(1)  | 165.49(14) |
| Cu(1)–N(1)       | 2.015(3)   | O(1a)–Cu(1)–N(1a) | 91.28(13)  |
| Cu(1)–N(1a)      | 2.015(3)   | O(1a)–Cu(1)–O(1w) | 97.80(13)  |
| Cu(1)–O(1w)      | 2.231(5)   | N(1)–Cu(1)–N(1a)  | 80.9(2)    |
| O(1)–Cu(1)–O(1a) | 93.56(17)  | N(1)–Cu(1)–O(1w)  | 95.08(13)  |
| O(1)–Cu(1)–N(1)  | 91.28(13)  | N(1a)–Cu(1)–O(1w) | 95.08(13)  |
| O(1)–Cu(1)–N(1a) | 165.49(14) |                   |            |
| <b>35</b>        |            |                   |            |
| Cu(1)–O(2)       | 1.948(7)   | O(2)–Cu(1)–O(1w)  | 100.6(3)   |
| Cu(1)–O(4)       | 1.928(7)   | O(4)–Cu(1)–N(1)   | 89.2(3)    |
| Cu(1)–N(1)       | 2.029(8)   | O(4)–Cu(1)–N(2)   | 168.3(3)   |
| Cu(1)–N(2)       | 2.006(9)   | O(4)–Cu(1)–O(1w)  | 95.0(3)    |
| Cu(1)–O(1w)      | 2.232(7)   | N(1)–Cu(1)–N(2)   | 81.4(3)    |
| O(2)–Cu(1)–O(4)  | 94.4(3)    | N(1)–Cu(1)–O(1w)  | 108.1(3)   |
| O(2)–Cu(1)–N(1)  | 150.7(3)   | N(2)–Cu(1)–O(1w)  | 94.4(3)    |
| O(2)–Cu(1)–N(2)  | 90.6(3)    |                   |            |

<sup>a</sup>Symmetry operations: (a)  $-x, y, z$ .



Despite the similarities between compounds **34** and **35**, the 2,2'-bpy complex also exhibit great resemblance with the related Phmal and Memal complexes, **16** and **24**, respectively.<sup>3</sup> The formation of a supramolecular 2D network with a (6,3)-like pattern through H-bonds is shared by the three complexes. The  $\pi$ - $\pi$  stacking between the discrete units is similar in **24** and **34**, being different in the Phmal-containing complex (**16**) due to the special conformation of the phenyl group of the Phmal ligand.

#### III.4.4. Magnetic Properties

The magnetic behaviour of **34** and **35** follows a Curie law in the 5-300 K temperature range, according to the mononuclear nature of both compounds. The values of  $\chi_M T$  for **34** and **35** are 0.42 and 0.41 cm<sup>3</sup> mol<sup>-1</sup> K, as expected for a magnetically isolated spin doublet, corresponding to *g* values of 2.11(2) and 2.09(2) for **34** and **35**, respectively.

#### III.4.5. Conclusion

The two mononuclear complexes **34** and **35** exhibit a supramolecular three-dimensional structure, due to hydrogen-bonding and  $\pi$ -type interactions. Remarkably, the two-dimensional hydrogen bond network of **34** was previously observed in the related Phmal- and Memal-containing complexes. Their magnetic properties follow the Curie law, in accordance with their mononuclear nature.

#### III.4.6. References

- 1 The high values for the goodness of fit and *R*-factors for complex **35** could be ascribed to unresolved twinning effects in the data set.
- 2 C. Janiak, *Dalton Trans.* **2000**, 3885.
- 3 J. Pasán, J. Sanchiz, C. Ruiz-Pérez, F. Lloret and M. Julve, *Eur. J. Inorg. Chem.* **2004**, 4081.
- 4 (a) L. Infantes and S. Motherwell, *CrystEngComm* **2002**, 4(75), 454. (b) L. Infantes, J. Chisholm and S. Motherwell, *CrystEngComm*, **2003**, 5, 480. (c) M. Mascal, L. Infantes and J. Chisholm, *Angew. Chem. Int. Ed.* **2006**, 45, 32.

---

---

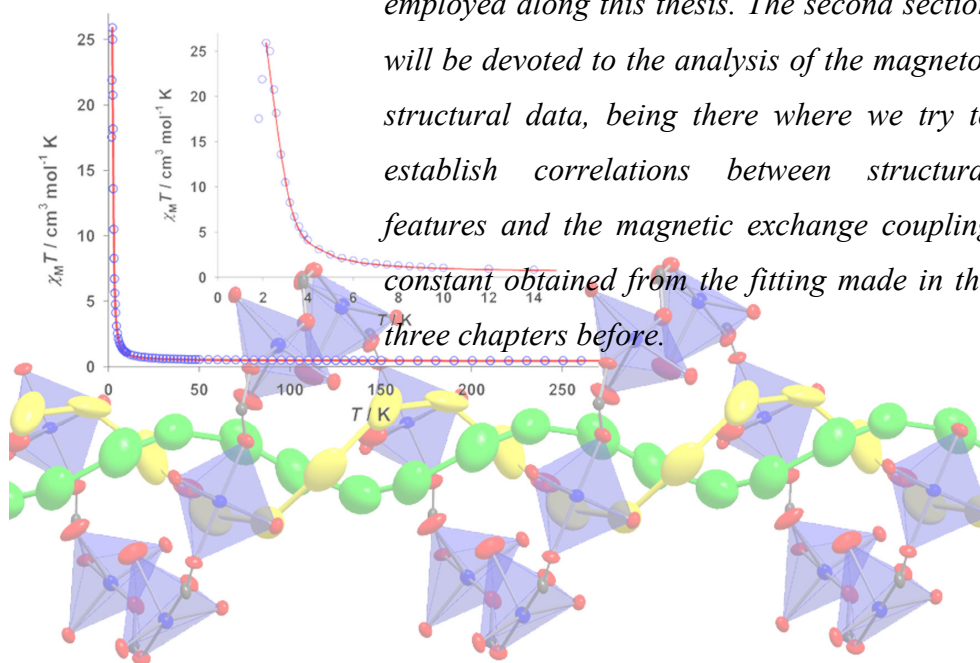
## Chapter IV.

# Structural and Magnetic Discussion

---

---

*This chapter is divided in two different sections, the first one dedicated to the structural discussion and comparison of the three substituted malonate ligands we have employed along this thesis. The second section will be devoted to the analysis of the magneto-structural data, being there where we try to establish correlations between structural features and the magnetic exchange coupling constant obtained from the fitting made in the three chapters before.*



## IV.1. Structural Discussion

### IV.1.1. Introduction

Three different R-malonate ligands (R- being methyl, ethyl and phenyl substituents) have been used along this thesis to synthesize up to thirty-six complexes. It is time now to take them together and make a detailed structural analyses and comparisons between them. The analysis will begin from an aseptic point of view, with a study of the frequency of space groups, copper(II) environments, R-malonate conformations and water motifs present in the complexes. Then, a comparison between the structures of the copper(II)-(R-malonate) complexes with water molecules as unique coligands is presented.

### IV.1.2. Analysis of the Crystal Data

#### IV.1.2.1. Space groups

The analysis of the twelve different space groups the thirty-six copper(II)-(R-malonate) complexes crystallize reveals that the most frequent space group is the  $P2_1/n$  with sixteen compounds (see Table IV.1). These complexes are mainly composed by those which present the square grid of carboxylate bridged copper(II) ions layered structure (eight complexes). There is not predominance of the eleven remaining space groups being remarkably that the different R-malonate copper(II) complexes crystallize in separated space groups depending on the substituent with the only exception of the  $C2cb$  space group.

**Table IV.1.** Space groups in the R-malonate complexes

| Space group           | Compound                                         | Centrosymmetry | R-malonate <sup>a</sup> |
|-----------------------|--------------------------------------------------|----------------|-------------------------|
| $P2_1/n$ (14)         | <b>1,3,4,5,8,9,10,14,17,18,20,21,23,25,31,34</b> | Yes            | Me-(6), Et-(2), Ph-(8)  |
| $P2_1$ (4)            | <b>2, 7, 12</b>                                  | No             | Ph-(3)                  |
| $C2cb$ (41)           | <b>11, 29</b>                                    | No             | Et-(1), Ph-(1)          |
| $Pcab$ (61)           | <b>13, 15</b>                                    | Yes            | Ph-(2)                  |
| $C2/c$ (15)           | <b>22, 26</b>                                    | Yes            | Me-(2)                  |
| $C222_1$ (20)         | <b>28</b>                                        | No             | Et-(1)                  |
| $Pn2_1m$ (31)         | <b>16</b>                                        | No             | Me-(1)                  |
| $Pna2_1, Pc2_1n$ (33) | <b>19, 24</b>                                    | No             | Me-(2)                  |
| $P4_22_12$ (94)       | <b>27</b>                                        | No             | Me-(1)                  |
| $P3_2$ (145)          | <b>30</b>                                        | No             | Et-(1)                  |
| $P-62c$ (190)         | <b>32</b>                                        | No             | Et-(1)                  |
| $Pmnn$ (58)           | <b>35</b>                                        | Yes            | Et-(1)                  |

<sup>a</sup> The number of compounds with the same substituent is given in parenthesis.

## IV.1.2.2. Chirality

The most interesting feature at the sight of Table IV.1 is the apparition of numerous non-centrosymmetrical (NC) space groups, since the R-malonate ligands and the N-donor heterocyclic coligands used in this work were achiral (the twelve complexes exhibiting non-centrosymmetry are listed along with some related structural parameters in Table IV.2). Not all the structures which crystallize in a non-centrosymmetric space group must be chiral, indeed hundred of achiral structures are founded to be resolved in NC space groups.<sup>1,5</sup> The space groups of NC achiral crystal structures belong to the following geometric crystal classes: *m*, *mm2*, *-4*, *-42m*, *4mm*, *3m*, *-6*, *-6m2*, *6mm* and *-43m*, all of which are non-centrosymmetric but contain improper symmetry operations.<sup>1</sup> These crystal structures must have a Flack parameter of 0.5 when they are solved. A close look at Table IV.2 reveals that complexes with Flack parameter<sup>6</sup> around 0.5 belong to the crystal classes referred above. But there are complexes (**2**, **7**, **12**, **13**, **25**, **28** and **30**) which not belong to that crystal classes and hence, the crystal structure must be chiral. Moreover, not only chiral, but homochiral; because the Flack parameter is close to zero in most cases (with the only exception of **13**), the crystal as a whole is chiral and only one of the enantiomers is present in the structure. But, since the initial reagents are achiral, the synthesis affords a racemic mixture of crystals and the x-ray measurement of a statistic number of crystals usually leads to the presence of the two enantiomers in a 50/50 ratio.<sup>2</sup> Let us now, hence, investigate how this chirality arises.

**Table IV.2.** Crystal data for R-malonate non-centrosymmetric complexes.

| Compound  | Space group             | Flack parameter         | Copper(II) environment                          | Bite atoms <sup>a</sup> |
|-----------|-------------------------|-------------------------|-------------------------------------------------|-------------------------|
| <b>2</b>  | <i>P2<sub>1</sub></i>   | 0.09(6)                 | Square pyramidal                                | Eq-eq                   |
| <b>7</b>  | <i>P2<sub>1</sub></i>   | 0.018(11)               | Octahedral                                      | Eq-ap                   |
| <b>12</b> | <i>C2cb</i>             | -0.004(19) <sup>b</sup> | Octahedral                                      | Eq-ap <sup>c</sup>      |
| <b>13</b> | <i>P2<sub>1</sub></i>   | 0.387(12)               | Square pyramidal                                | Eq-ap                   |
| <b>17</b> | <i>Pn2<sub>1</sub>m</i> | 0.51(4)                 | Square pyramidal                                | Eq-eq                   |
| <b>20</b> | <i>Pna2<sub>1</sub></i> | 0.48(5)                 | Octahedral                                      | Eq-eq                   |
| <b>25</b> | <i>Pc2<sub>1</sub>n</i> | 0.019(15)               | Octahedral                                      | Eq-eq                   |
| <b>28</b> | <i>C222<sub>1</sub></i> | 0.076(11)               | Octahedral<br>Trigonal bipyramidal <sup>d</sup> | Eq-ap <sup>e</sup>      |
| <b>29</b> | <i>C2cb</i>             | 0.52(4)                 | Square pyramidal                                | Eq-eq                   |
| <b>30</b> | <i>P3<sub>2</sub></i>   | 0.03(3)                 | Square pyramidal                                | Eq-eq                   |
| <b>32</b> | <i>P-62c</i>            | 0.48(6)                 | Square pyramidal<br>Square planar <sup>d</sup>  | Eq-Eq <sup>e</sup>      |

<sup>a</sup> Atoms of the R-malonate ligand that chelate in the copper coordination sphere; eq and ap stand for equatorial and apical, respectively.

<sup>b</sup> Flack parameter can take negative statistical values (see ref. 5).

<sup>c</sup> The copper environment is statically disordered thorough the crystal (see section I.6).

<sup>d</sup> Two crystallographically different copper atoms with different environments are found for **28** and **32**.

<sup>e</sup> The R-malonate ligand only chelates the copper atom with trigonal bipyramidal (**28**) and square pyramidal (**32**) surroundings.

The ligands used to synthesize the thirty-six complexes of this thesis are achiral, i.e. they can be identical to their mirror images just applying proper symmetry operations (pure rotations and translations). Then, the chirality in these complexes must appear at the metal centre, since its complexation can afford chiral environments. The most common coordination sphere for the R-malonate complexes is the five-coordinated square pyramidal environment (Table IV.3), although other polyhedrons are also formed. The restriction to the chiral structures (**2**, **7**, **12**, **13**, **25**, **28** and **30**) shows that square pyramidal surroundings are as frequent as octahedral (Table IV.2). The complexation of the bidentate R-malonate ligands and the different coligands coordinated to the metal centre will be treated separately for each chiral structure.

**Table IV.3.** Copper(II) surroundings

| Coordination number | Environment          | Complexes                                                                                       |
|---------------------|----------------------|-------------------------------------------------------------------------------------------------|
| 4                   | Square planar        | <b>32</b> <sup>a</sup>                                                                          |
| 5                   | Square pyramidal     | <b>1,2,3,4,5,8,9,10,11,13,14,15,16,17,18,21,22,23,24,26,27,29,30,31,32<sup>a</sup>,33,34,35</b> |
| 5                   | Trigonal bipyramidal | <b>28</b> <sup>a</sup>                                                                          |
| 6                   | Octahedral           | <b>7,12,19,20,25,28<sup>a</sup></b>                                                             |

<sup>a</sup> Two environments are present in **28** and **32**.

[Cu(Isonic)(Phmal)(H<sub>2</sub>O)]<sub>n</sub> (**7**). The copper atom exhibits octahedral environment with the isonicotinamide and water ligands coordinated to equatorial positions. This feature

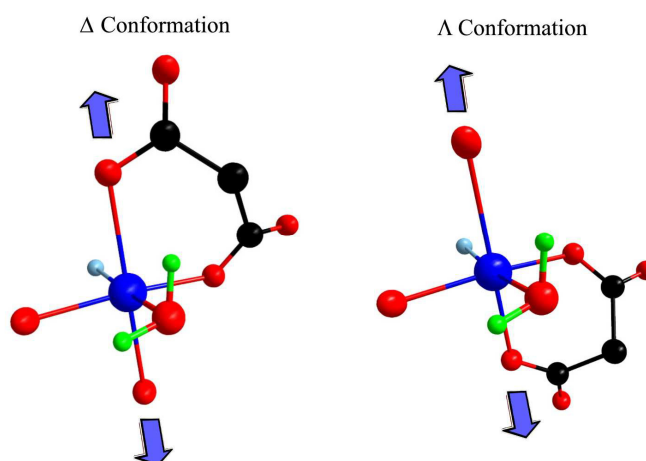


**Fig. IV.1.** Δ (left) and Λ (right) conformations of the copper(II) environment in **7**. The arrows indicate the direction of the pseudo-Jahn-Teller elongation. Phenyl ring of the Phmal ligand and pyridine group are omitted for clarity.

made the phenylmalonate ligand to chelate one equatorial and one apical position, the remaining ones occupied by oxygen atoms from adjacent Phmal ligands (Figure IV.1). If we consider an ideal octahedral environment such a situation is achiral, but since the Jahn-Teller effect distort it from a  $O_h$  to a  $D_{4h}$  point group, this environment becomes chiral. The two ( $\Lambda$  and  $\Delta$ ) conformations are shown in Figure IV.1. An identical situation is found in  $[\text{Cu}(2,4'\text{-bpy})(\text{Phmal})(\text{H}_2\text{O})]_n$  (**11**), but with a static Jahn-Teller disorder within the crystal. The 2,4'-bpy and water ligands occupying the equatorial positions unaffected by the J-T disorder.

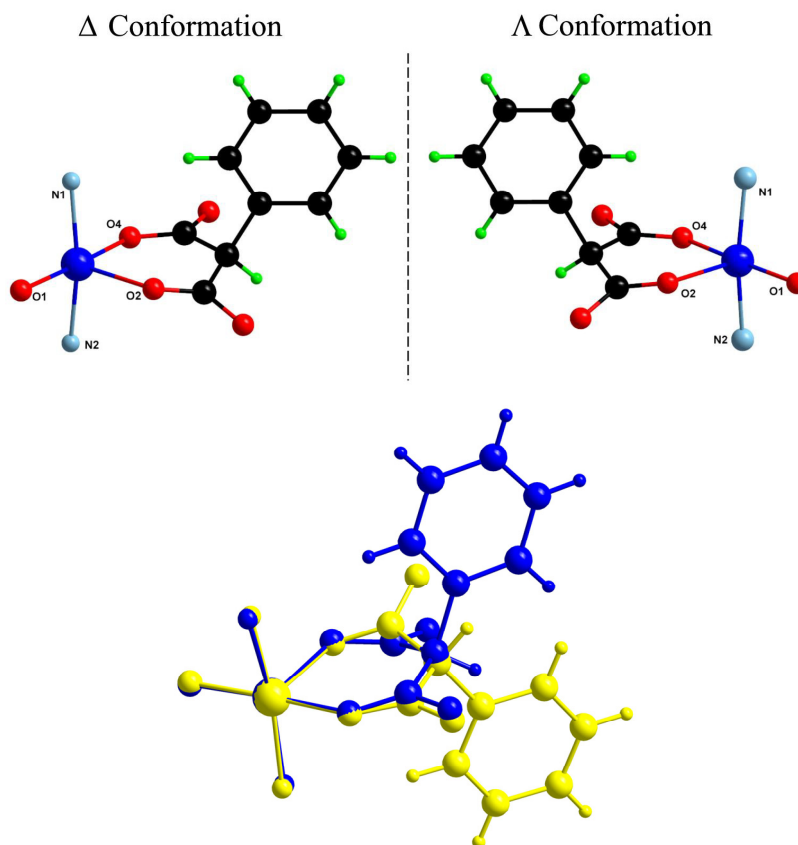


**Fig. IV.2.**  $\Delta$  (up left) and  $\Lambda$  (up right) conformations of the copper(II) environment in **12**. (Bottom) A view of the superposition of the two enantiomers. The pyridine rings have been omitted for clarity.

$[\text{Cu}(4,4'\text{-bpy})(\text{Phmal})]_n \cdot 2n\text{H}_2\text{O}$  (**12**). In **12** the square pyramidal environment of the copper atom is filled with two 4,4'-bpy nitrogen atoms occupying equatorial positions, two

Phmal bidentate oxygen atoms in one equatorial and one apical position and another oxygen atom from an adjacent Phmal ligand in the remaining equatorial position (Figure IV.2). The equatorial-apical chelation and the fact that the Phmal ligand has two different substituents in the central carbon atom of the malonate skeleton (the phenyl ring and the hydrogen atom) account for the chirality. The superposition of the metal environment with its inversion related one shows that the unique difference is the relative situation of the substituents of the methylene carbon atom of the malonate ligand (Figure IV.2).

$\{[\text{Cu}(4,4'\text{-bpy})_2][\text{Cu}(4,4'\text{-bpy})_2(\text{Memal})(\text{NO}_3)(\text{H}_2\text{O})]\}_n \cdot n\text{NO}_3 \cdot 4n\text{H}_2\text{O}$  (**24**). This complex exhibits two crystallographically different copper atoms, both with octahedral environments. From section II.7 one of them are coordinated through the equatorial positions to four 4,4'-bpy ligands and to two methylmalonate ligands through the apical positions. Since the four 4,4'-bpy ligands can be considered equivalents (although crystallographically they do not) there is a mirror plane coplanar with the basal plane and, hence, this metal centre cannot be chiral. The other copper atom is chelated by the Memal ligand at two equatorial positions, the two remaining ones occupied by two 4,4'-bpy ligands, while a nitrate and water molecules fill the apical positions. The superposition of this metal centre with its inverted image (Figure IV.3) reveals that main differences come from the steric repulsion of the 4,4'-bpy ligands which cannot be simultaneously coplanar with the basal plane of the copper atom. However, it seems like the interconversion energy between both enantiomers would not be higher enough to afford the crystallization of enantiopure crystals. The three-dimensional structure of **24** is chiral, as the x-ray crystallography indicates, although the chiral motif has not been found.

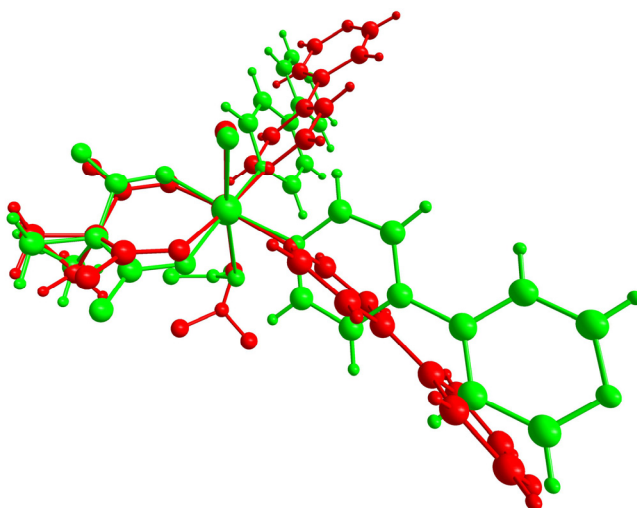
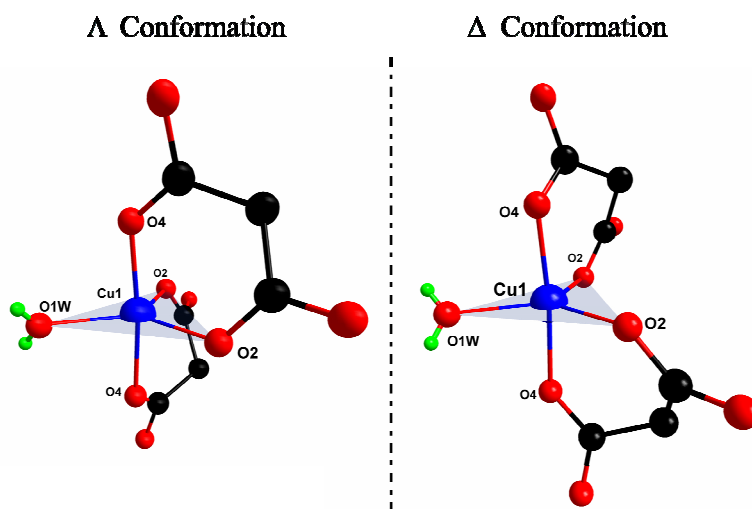


Fig. IV.3. Superposition of the two enantiomers of the pillaring unit of **24**.

$\{[\text{Cu}(\text{H}_2\text{O})_4][\text{Cu}(\text{Etmal})_2(\text{H}_2\text{O})]\}_n$  (**28**). Two different copper environments are present in **28**: (i) an octahedral, with four water molecules occupying the equatorial positions and two ethylmalonate oxygen atoms filling the apical ones. This metal centre, therefore, is not chiral. (ii) a trigonal bipyramidal, with two Etmal acting as equatorial-apical bidentate ligands and the remaining equatorial position filled by a water molecule. This is a chiral environment as it was described in section III.1 (Figure IV.4).



**Fig. IV.4.**  $\Lambda$  (left) and  $\Delta$  (right) conformations of the trigonal bipyramidal copper(II) ion in **28**. The equatorial plane is remarked with a pale blue plane.

$[\text{Cu}(\text{Etmal})(\text{H}_2\text{O})]_n \cdot 1.65n\text{H}_2\text{O}$  (**30**). This is the unique complex which crystallizes in a chiral space group ( $P3_1$ ) and the structure exhibits carboxylate-bridged copper(II) ions in helical arrangement. This feature accounts for the chirality of the three-dimensional structure (see section III.1).

The complex **2** which is also included within the compounds which structure must be chiral, is probably not chiral since its structure is very similar to those of **3**, **4** and **5**. These complexes are centrosymmetric and crystallize in the  $P2_1/n$  space group. Comments on the Flack parameter<sup>3</sup> report that the completeness of Friedel's opposites during the X-ray measurements affects crucially to the obtaining of a meaningful Flack parameter in the structure refinement. Friedel's opposites completeness for **2** is about 20%, and this complex could also be solved in  $P2_1/n$  space group although with a worst R-factor. Compound **2** could probably be achiral and hence crystallize in the centrosymmetric  $P2_1/n$  space group.

Let us remark some important points from these chiral structures: (i) All of the complexes exhibiting the equatorial-apical chelation of the R-malonate ligand, also present



the formation of chiral structures; this feature was not observed previously in copper(II)-malonate complexes. (ii) The square pyramidal geometry of the copper environment does not favour the formation of chiral centres; most of the complexes which exhibit other copper coordination polyhedron crystallize in non-centrosymmetric space groups. (iii) The substituted malonate ligand is able to induce chirality; this is due to the fact that the central carbon of the R-mal ligand is substituted with three different groups (H-, COO<sup>-</sup> and Me-, Et- or Ph-)

#### *IV.1.2.3. R-malonate conformation*

The conformation of the malonate ligand in transition metal complexes [and in particular with copper(II)] has been recently reviewed<sup>7</sup> and some new conformations must be added since they are present in R-malonate-containing copper(II) complexes. The most common conformation is the bidentate-(bis)monodentate (V and VI in Table IV.4), while the two new conformations are IV and VI. The separation between the equatorial-equatorial chelation and the equatorial-apical one has been remarked because the presence of the latter has become significant, whereas in the case of reported malonate-containing copper(II) complexes there only was one example.<sup>8</sup> The coordination of the R-malonate ligand to the copper atom depends on the coligands present in the complex. Although the most common is the bidentate filling two equatorial positions in the copper environment, if the coligands occupy the equatorial positions, the malonate ligand will adopt equatorial-apical bidentate conformations, but always bidentate. This is the reason why conformation VI (Table IV.4) is rare, this is the first example of a copper(II)-R-malonate complex with no malonate-chelation, although there are previous reported examples in zinc(II) complexes.<sup>9</sup> There no evidence for the preference for some kind of conformation depending on the substituent.

**Table IV.4.** Different conformation of the R-malonate ligand in its copper(II) complexes.

| Conformation | Complex                                      | Conformation | Complex                                                                |
|--------------|----------------------------------------------|--------------|------------------------------------------------------------------------|
| I            | 15, 22,<br>23,<br>31, 34,<br>35, 36          | V            | 2, 3, 4,<br>5, 8,<br>9, 10,<br>16, 17,<br>18, 19,<br>24, 29,<br>30, 32 |
| II           | 1 <sup>a</sup> , 13,<br>14,<br>20, 21,<br>26 | VI           | 7, 11                                                                  |
| III          | 12, 28                                       | VI           | 25                                                                     |
| IV           | 1 <sup>a</sup>                               |              |                                                                        |

<sup>a</sup> Two crystallographically different phenylmalonate conformations are present in **1**.

## IV.1.2.4. Water motifs

The review of the formulae of the complexes in this thesis reveals that many compounds have crystallization water molecules, and since there exist cavities, channels or pores in the structure, water molecules can build, by means of hydrogen bonding, a great variety of clusters and motifs. The topology and frequency of these water clusters in organic complexes have been recently reviewed,<sup>10</sup> and also with the H-bond participation of other chemical groups.<sup>11</sup> Among the complexes presented in this thesis there are seven compounds which present water aggregations with a defined pattern. **15**, **35** and **36** exhibit similar two-dimensional patterns involving not only the crystallization water molecules but the copper(II)-malonate entity (Figure IV.5). These three complexes are mononuclear and hence, they have bidentate malonate ligands with two uncoordinated oxygen atoms ready available to act as H-bond acceptors. Another common feature is the blocking N-donor coligands which in the three compounds are bulky aromatic groups, and the crystallization water molecules are most likely located in the hydrophilic areas near the copper atom. Compound **34** exhibits a pure crystallization water cluster which consists of six water molecules aggregated in a hexagon (Figure IV.6). The hexamer is anchored to the host through the coordination water molecule, and through uncoordinated ethylmalonate oxygen atoms (two of the four Etmal oxygen atoms remain uncoordinated available to H-bonding). The water cluster is encapsulated between four  $[\text{Cu}_2(2,2'\text{-bipym})(\text{Etmal})_2(\text{H}_2\text{O})_2]$  units. Also of interest are the infinite water chains, compound **23** exhibits a typical C4 motif (Figure IV.7) with a less usual pendant tetramer formed with the aid of one uncoordinated oxygen atom. Here again, the Memal ligand acts only as bidentate, and the presence of the 2,2'-bpy ligands creates hydrophobic layers between which the water chains are located. One-

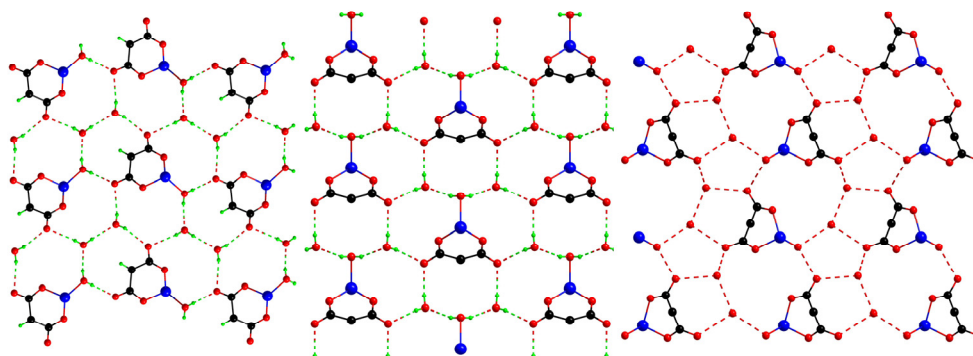


Fig. IV.5. Comparative view of three water patterns formed in the mononuclear complexes **15** (left), **35** (middle) and **36** (right).

dimensional helical water chains are guests of the nanoporous complex **30**. Although the structure of the water motif is disordered and the water molecules are not refined with hydrogen atoms, the unusual presence of the helicity is remarkably enough to be presented here (structural details were given in section III.1). The water motif consists of two helices, with two different diameters following the same screw axis than the carboxylate-bridged copper(II) ions host structure (Figure IV.8). One step further the infinite chains are the water tapes like the water aggregate guest of complex **21**. In this case, the iterative motif along the tape is a pentagon, namely a T5(2) tape because each pentagon share two water molecules with the next (Figure IV.9). The 2,4'-bpy ligands stack together creating channels filled with the water tape which is anchored to the host through H-bonds involving uncoordinated methylmalonate oxygen atoms.

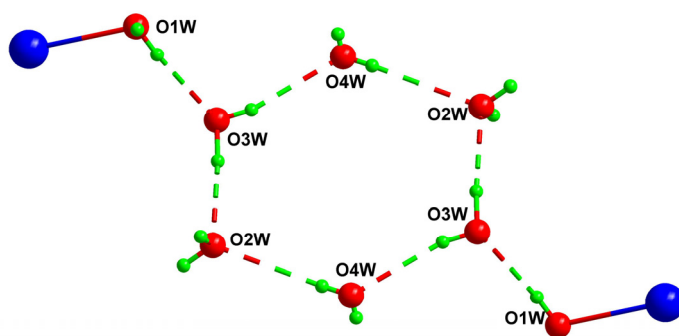


Fig. IV.6. Hexagonal water cluster formed in the compound **34**.

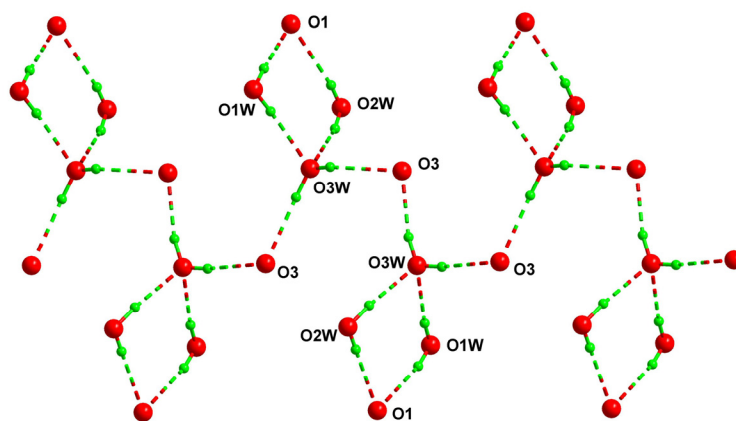


Fig. IV.7. A C4 water chain motif with a pendant water tetramer present in complex **23**.

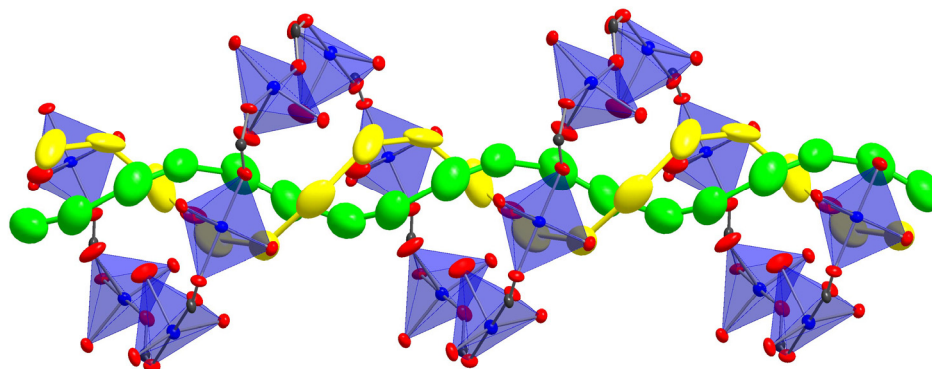


Fig. IV.8. Water helical chains filled the helical pores of the structure of 30.

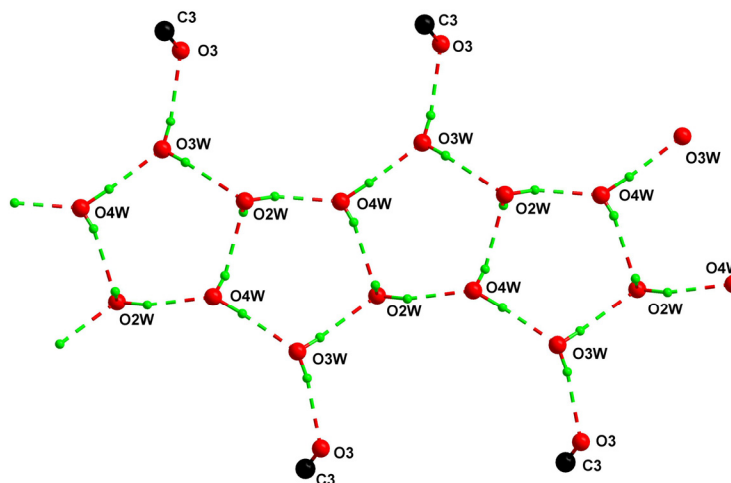


Fig. IV.9. T5(2) tape water motif of complex 21.

The different water motifs in the R-malonate complexes are formed due to the presence of channels and cavities, which are favoured by, not only the presence of aromatic coligands, but the substituent in the malonate ligand.

### IV.1.3. The copper(II)-R-malonate system

There have been synthesized a total of ten R-malonate-containing copper(II) complexes (R- being H-, Ph-, Et- and Me-) with the water molecules as unique coligands (Table IV.5). They show a wide variety of structures ranging from 0D to 3D-networks. The H-malonate

ligand seems to be the most prolific one since five compounds were reported, they are all based on the  $[\text{Cu}(\text{mal})_2(\text{H}_2\text{O})_x]^{2-}$  ( $x$  being 0, 1 or 2; for details see Table IV.5) unit.

**Table IV.5.** The copper(II)-R-malonate system<sup>a</sup>

| Compound                                                                                                                               | Net <sup>b</sup> | Copper(II) <sup>c</sup>  | Space Group | Ref.       |
|----------------------------------------------------------------------------------------------------------------------------------------|------------------|--------------------------|-------------|------------|
| $[\text{Cu}(\text{H}_2\text{O})_6][\text{Cu}(\text{mal})_2(\text{H}_2\text{O})]$                                                       | 0 D              | $\text{O}_h$             | $P-1$       | 12         |
| $[\text{Cu}(\text{H}_2\text{O})_4][\text{Cu}(\text{mal})_2(\text{H}_2\text{O})_2]$                                                     | 0 D              | $\text{O}_h, \text{sp}$  | $Pbcn$      | 13,14      |
| $\{[\text{Cu}(\text{H}_2\text{O})_4][\text{Cu}(\text{mal})_2(\text{H}_2\text{O})_2]\} [\text{Cu}(\text{mal})_2(\text{H}_2\text{O})_2]$ | 0 D              | $\text{O}_h, \text{sp}$  | $C2/c$      | 14         |
| $\{[\text{Cu}(\text{H}_2\text{O})_4]_2[\text{Cu}(\text{mal})_2(\text{H}_2\text{O})_2]\}$                                               |                  |                          |             |            |
| $\{[\text{Cu}(\text{H}_2\text{O})_3][\text{Cu}(\text{mal})_2(\text{H}_2\text{O})]\}_n$                                                 | 1 D              | sp                       | $Pcab$      | 14         |
| $\{[\text{Cu}(\text{H}_2\text{O})_3][\text{Cu}(\text{mal})_2]\}_n \cdot 2n\text{H}_2\text{O}$                                          | 3 D              | sp                       | $Pna2_1$    | 15         |
| $[\text{Cu}(\text{Memal})(\text{H}_2\text{O})]_n$ ( <b>17</b> )                                                                        | 2 D              | sp                       | $Pn2_1m$    | This tesis |
| $\{[\text{Cu}(\text{H}_2\text{O})_4][\text{Cu}(\text{Etmal})_2(\text{H}_2\text{O})]\}_n$ ( <b>28</b> )                                 | 1 D              | $\text{O}_h, \text{tbp}$ | $C222_1$    | This tesis |
| $[\text{Cu}(\text{Etmal})(\text{H}_2\text{O})]_n$ ( <b>29</b> )                                                                        | 2 D              | sp                       | $C2cb$      | This tesis |
| $[\text{Cu}(\text{Etmal})(\text{H}_2\text{O})]_n \cdot 1.65n\text{H}_2\text{O}$ ( <b>30</b> )                                          | 3 D              | sp                       | $P3_2$      | This tesis |
| $\{[\text{Cu}(\text{H}_2\text{O})_3][\text{Cu}(\text{Phmal})_2]\}_n$ ( <b>1</b> )                                                      | 2 D              | sp                       | $P2_1/n$    | This tesis |

<sup>a</sup> The water molecules as unique coligands and the malonate as dianion.

<sup>b</sup> Dimensionality of the covalent network.

<sup>c</sup> Polyhedron of the copper(II) environment.

The simplest one is the mononuclear cationic-anionic salt of formula<sup>12</sup>  $[\text{Cu}(\text{H}_2\text{O})_6][\text{Cu}(\text{mal})_2(\text{H}_2\text{O})_2]$ . Its structure consists of alternating layers of anionic diaquabis(malonato)-copper(II) anions and hexaaqua-copper(II) cations (Figure IV.10). These two units can merge to give a neutral dinuclear entity  $[\text{Cu}(\text{H}_2\text{O})_4][\text{Cu}(\text{mal})_2(\text{H}_2\text{O})_2]$  in which the two copper atoms are linked through a malonate-carboxylate bridge in *anti-syn* conformation (Figure IV.11).<sup>13,14</sup> Another step in this condensation process yields the trinuclear cationic unit  $\{[\text{Cu}(\text{H}_2\text{O})_4]_2[\text{Cu}(\text{mal})_2(\text{H}_2\text{O})_2]\}$  where a central diaquabis(malonato)-copper(II) unit is linked through carboxylate-bridges to two *cis*-tetraaqua-copper(II) units (Figure IV.12).<sup>14</sup> This entity along with the mononuclear and dinuclear units builds a rare compound where the three different species coexist. Variations in the synthetic conditions produce the polymerization of the dimeric units into chains with the triaquacopper(II) units attached in *trans*-positions to the aquabis(malonato)-copper(II) unit affording the one-dimensional complex  $\{[\text{Cu}(\text{H}_2\text{O})_3][\text{Cu}(\text{mal})_2(\text{H}_2\text{O})]\}_n$  (Figure IV.13).<sup>14</sup> More recently, a three-dimensional malonato-containing copper(II) complex has been reported.<sup>15</sup> In this case, the previous chains are linked through apical-equatorial *anti-syn* carboxylate-bridges affording the 3D-complex (Figure IV.14). Therefore, all the malonate-containing copper(II) complexes consist of different degrees of polymerization of the  $[\text{Cu}(\text{mal})_2(\text{H}_2\text{O})_x]^{2-}$  unit. This situation will no longer be applicable to the substituted-malonate complexes.

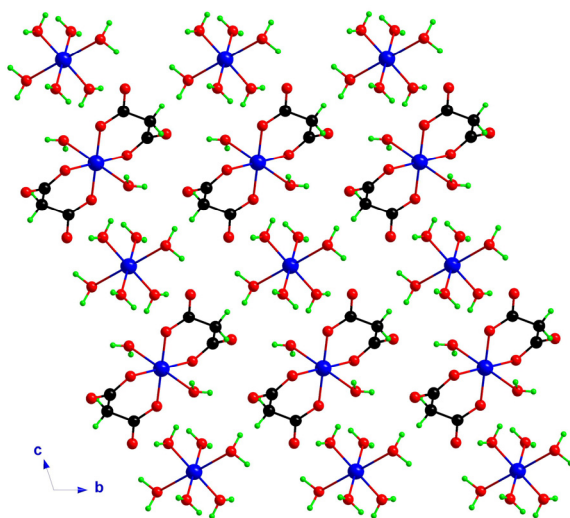


Fig. IV.10. A view along the *a* axis of the alternating layers of [Cu(H<sub>2</sub>O)<sub>6</sub>] cations and [Cu(mal)<sub>2</sub>(H<sub>2</sub>O)] anions in the structure of [Cu(H<sub>2</sub>O)<sub>6</sub>][Cu(mal)<sub>2</sub>(H<sub>2</sub>O)].

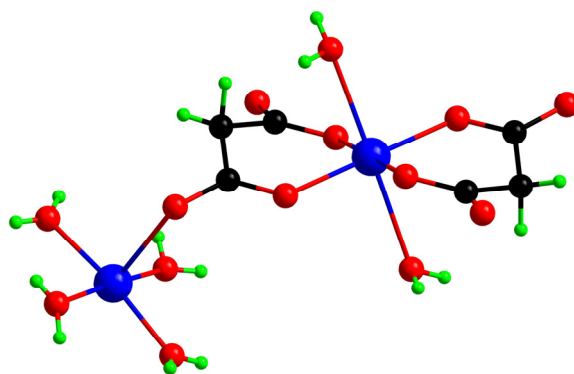


Fig. IV.11. The dinuclear carboxylate-bridged copper(II) unit formed in the complex [Cu(H<sub>2</sub>O)<sub>4</sub>][Cu(mal)<sub>2</sub>(H<sub>2</sub>O)<sub>2</sub>].

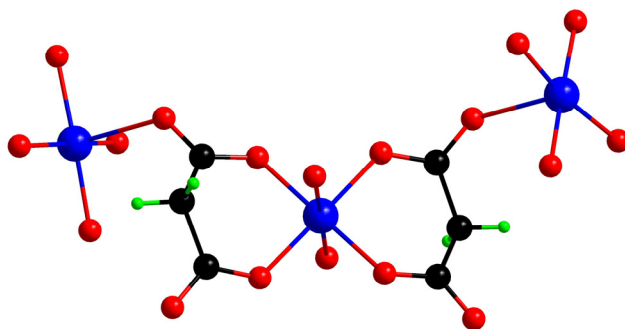


Fig. IV.12. The carboxylate-bridged trinuclear copper(II) unit present in the {[Cu(H<sub>2</sub>O)<sub>4</sub>][Cu(mal)<sub>2</sub>(H<sub>2</sub>O)<sub>2</sub>]} [Cu(mal)<sub>2</sub>(H<sub>2</sub>O)<sub>2</sub>] {[Cu(H<sub>2</sub>O)<sub>4</sub>]<sub>2</sub>[Cu(mal)<sub>2</sub>(H<sub>2</sub>O)<sub>2</sub>]} complex.

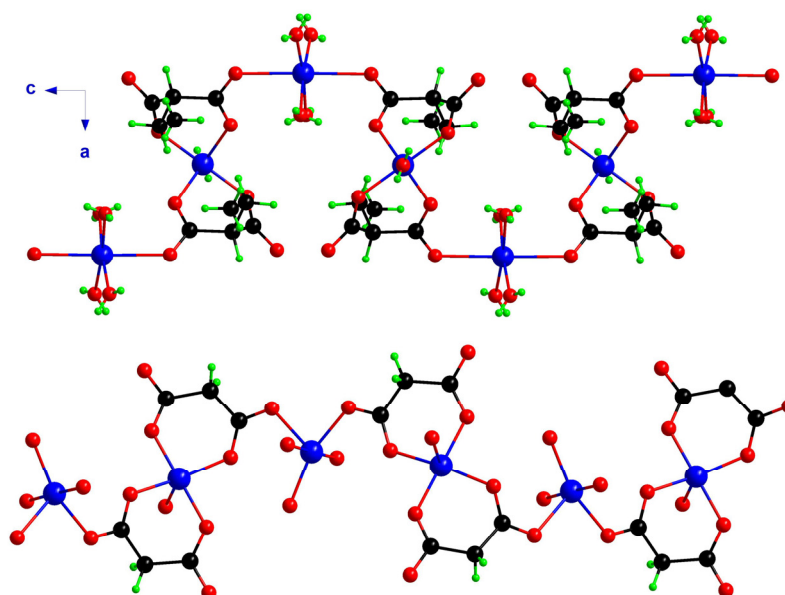


Fig. IV.13. A comparative view of the carboxylate-bridged copper(II) chains formed in the ethylmalonate-containing complex **28** (up) and those built in the malonate compound  $\{[\text{Cu}(\text{H}_2\text{O})_3][\text{Cu}(\text{mal})_2(\text{H}_2\text{O})]\}_n$  (down).

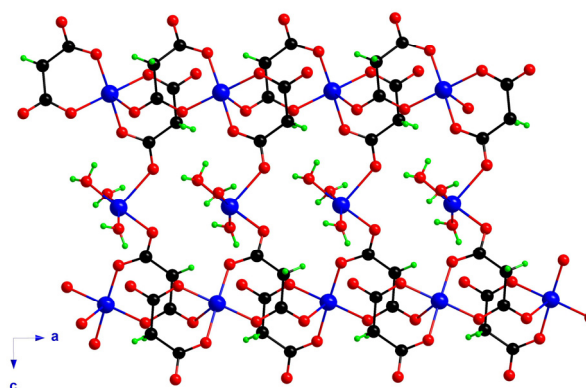
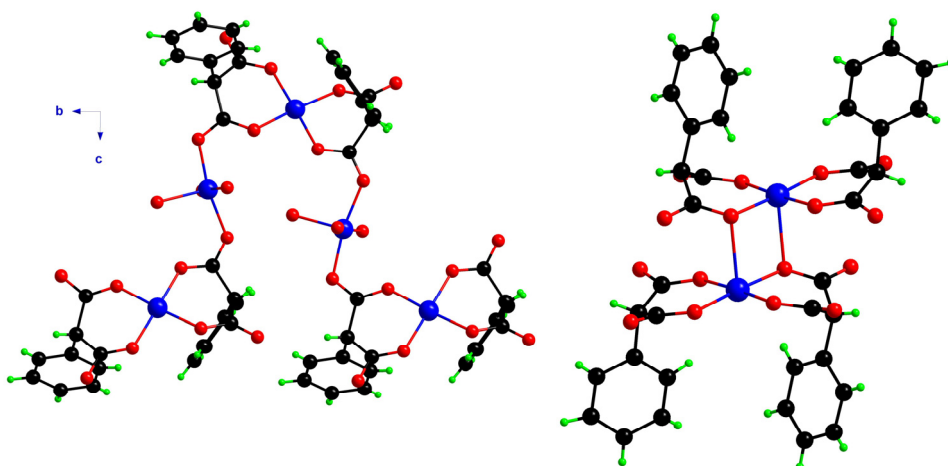


Fig. IV.14. A perspective view along the *b* axis of the three-dimensional malonate-containing copper(II) complex  $\{[\text{Cu}(\text{H}_2\text{O})_3][\text{Cu}(\text{mal})_2]\}_n \cdot 2n\text{H}_2\text{O}$ .

The structural descriptions of the substituted-malonate-containing copper(II) complexes were presented at the beginning of the corresponding chapter. Remarkably, three complexes were obtained with the ethylmalonate ligand (**28**, **29** and **30**), but only one with the phenyl- and methylmalonate ligands (**1** and **16**, respectively; see Table IV.5). Comparing these structures with those of the previously reported malonato-containing copper(II) complexes, the main similarities arise between **28** and the malonate-chain complex. Both compounds are formed by the regular alternation of carboxylate bridged bis(R-malonato)-



copper(II) and tri- or tetraaqua-copper(II) units, although differences appear at copper environments and crystal packing (Figure IV.13). This regular alternation also appears in the layered complex **1**, but the chains being linked to the adjacent ones through  $\mu$ -oxo bridges (Figure IV.15). This more compressed structure is favoured by the formation of hydrophobic layers filled with the phenyl groups of the Phmal ligands, which sandwich the more hydrophilic copper surroundings. Remarkably, these two complexes, **1** and **28**, are the unique of the R-malonate containing copper(II) complexes which exhibit the bis(R-malonato)-copper(II) conformation (see Table IV.5). The three other complexes **16**, **29** and **30** are based on the [Cu(R-mal)] unit with the four oxygen atoms of the R-mal ligand coordinated to copper atoms, two of them (**16** and **29**) affording a layered structure somewhat similar to that of **1** (Figure IV.16). The methyl and ethyl groups of their respective R-malonate ligands build the hydrophobic layer.



**Fig. IV.15.** The two active bridges in **1**. The double  $\mu$ -oxo bridge (left) between two bis(phenylmalonate)cuprate(II) units and the carboxylate-bridge which built up the  $2_1$  chains (right).

The introduction of a substituent in the malonate ligand affects critically to the crystal packing of the copper(II) complexes, and it also allows other conformation modes apart from the bis(malonato)-copper(II) one. The simple substitution by a methyl group produces the formation of a sandwich-like system with the hydrophobic groups (Me-, Et- or Ph-) aggregated in layers. Moreover, the condensation-like behaviour of the H-mal copper(II) system (i.e. the crystallization of the simplest monomeric unit and their subsequent polymerizations) was not observed for none of the substituted-malonate-containing copper(II) complexes. Otherwise, the most amazing behaviour was observed for the ethylmalonate copper(II) system where three complexes of different dimensionality were

synthesized. They are not ordered in a polymeric-condensation as in the malonate system, but the three complexes correspond to different arrangements of the same components

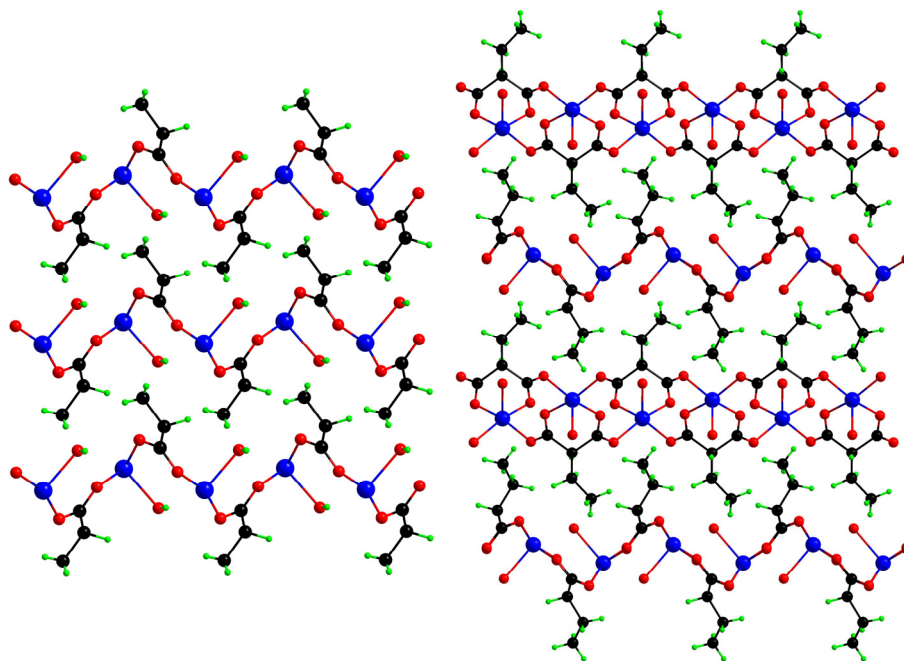


Fig. IV.16. A view of the crystal packing of the methylmalonate (17; left) and ethylmalonate (29; right) layered complexes.

#### IV.1.4. References

- 1 H. D. Flack and G. Bernardinelli, *Cryst. Eng.* **2003**, 6, 213.
- 2 H. D. Flack, *Helv. Chim. Acta* **2003**, 86, 905.
- 3 H. D. Flack and G. Bernardinelli, *Inorg. Chim. Acta* **2006**, 359, 383.
- 4 H. D. Flack and G. Bernardinelli, *Acta Cryst., Sect. A* **1999**, A55, 908.
- 5 H. D. Flack and G. Bernardinelli, *J. Appl. Cryst.* **2000**, 33, 1143.
- 6 H. D. Flack, *Acta Cryst., Sect. A* **1983**, A39, 876.
- 7 F. S. Delgado, *Development of new molecular magnets based on the malonate ion*, Ph.D. thesis work, **2005**.
- 8 F. S. Delgado, J. Sanchiz, C. Ruiz-Pérez, F. Lloret and M. Julve, *Inorg. Chem.* **2003**, 42, 5938.
- 9 (a) A. D. Burrows, R. W. Harrington, M. F. Mahon and C. E. Price, *Dalton Trans.* **2000**, 3845; (b) Y. Zhang, J. Li, J. Chen, Q. Su, W. Deng, M. Nishiura, T. Imamoto, X. Wu and Q. Wang, *Inorg. Chem.* **2000**, 39, 2330.
- 10 L. Infantes and S. Motherwell, *CrystEngComm* **2002**, 4(75), 454.
- 11 L. Infantes, J. Chisholm and S. Motherwell, *CrystEngComm* **2003**, 5(85), 480.
- 12 (a) G. I. Dimitrova, A. V. Ablov, G. A. Kiosse, G. A. Popovich, T. I. Nmalinouskii and I. F. Bourshteyn, *Dokl. Akad. Nauk. SSSR* **1974**, 216, 1055; (b) Y. Rodriguez-Martin, J. Sanchiz, C. Ruiz-Pérez, F. Lloret and M. Julve *CrystEngComm* **2002**, 4, 631.
- 13 D. Chattopadhyay, S. K. Chattopadhyay, P. R. Lowe, C. H. Schwalde, S. K. Mazumder, A. Rana and S. Ghosh, *Dalton Trans.* **1993**, 913.
- 14 C. Ruiz-Pérez, J. Sanchiz, M. Hernández-Molina, F. Lloret and M. Julve, *Inorg. Chem.* **2000**, 39, 1363.
- 15 V. T. Yilmaz, E. Senel and C. Thone, *Transition Met. Chem.* **2004**, 29, 336.

## IV.2. Magneto-structural discussion

This section is devoted to the magneto-structural relationships between the R-malonate-containing copper(II) complexes presented in the previous chapters. Firstly, from a general point of view we discuss briefly about the nature and the magnitude of the magnetic interactions, focusing in our complexes. Then, quite a few complexes will be analyzed and the structural features, which can modify the magnetic interactions from one compound to another, investigated.

### IV.2.1. Nature of the magnetic interaction

The complexes presented in this thesis consist of mono-, di- or polynuclear copper(II) arrangements, all of them exhibiting square pyramidal or octahedral environments (with the only exception of complex **28**, sect. III.1). In this situation, the magnetic orbitals of the copper(II) ions are of the  $d(x^2-y^2)$  character, the  $x$  and  $y$  axes being roughly defined by the equatorial bonds.

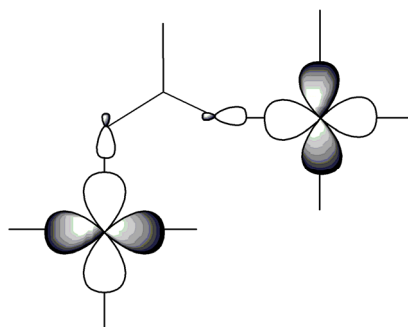
According to the Kahn's natural magnetic orbitals model for a dinuclear system,<sup>1-4</sup> the singlet-triplet energy gap  $J$  for a copper(II) dinuclear system is decomposed in the sum of two contributions, one ferromagnetic and another antiferromagnetic:

$$J = J_F + J_{AF} = 2K_{ab} + 4\beta S - 2S_{ab}^2(2h_a + J_{ab}) - \frac{4[\beta + I - (h_a + J_{ab} + K_{ab})S_{ab}]}{U}$$

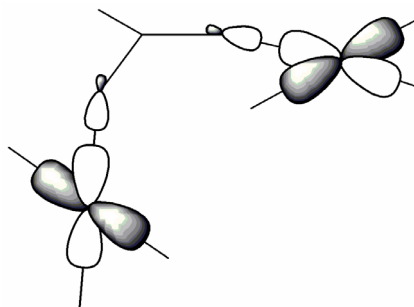
the ferromagnetic contribution corresponds to the two-electron exchange integral  $K_{ab}$  and the main term which stabilizes the singlet state is  $4\beta S$ , proportional to the overlap ( $S$ ) of the magnetic orbitals. Thus, as a consequence of the dependence of the AF contribution with the overlap, *a priori* AF interactions would appear when the interacting magnetic orbitals are of the same type. However, the overlap can be minimized when accidental or strict orthogonality of the magnetic orbitals occur and the ferromagnetic contribution becomes predominant. The strict orthogonality involves the transformation of the orbitals in different irreducible representations of the symmetry group adapted to the system; i.e. different magnetic orbitals, such as  $d(x^2-y^2)$  vs.  $d(xy)$ , which is usually found in heterometallic complexes. The accidental orthogonality deals with the spatial orthogonality of magnetic orbitals of the same type.

Considering our primary objective as the preparation of new ferromagnetic materials based on carboxylate-bridged copper(II) complexes, the strategy to minimize the overlap will consist of achieve an accidental orthogonality of the magnetic orbitals.

Focusing on the compounds described in this thesis, this accidental orthogonality can be reached in two ways: (i) the *anti-syn* conformation of the carboxylate bridge (Scheme IV.1) and (ii) the out-of-plane configuration of the bridge (Scheme IV.2).



Scheme IV.1



Scheme IV.2

(i) The *anti-syn* carboxylate exchange pathway, as an intermediate step between the *anti-anti* and the *syn-syn* ones, presents a poor overlap between the orbitals on the bridge with those bearing the unpaired electrons on each metal atom (Scheme IV.1).<sup>5</sup> This type of bridge has been encountered usually in the related copper(II)-malonate complexes where most of the interactions are ferromagnetic.<sup>6</sup>

(ii) The out-of-plane exchange pathway appears when the basal plane of one of the metal atoms bends to locate out of the carboxylate bridge plane, while the other remains in-plane. The overlap between the magnetic orbitals diminishes as the out-of-plane angle increases, becoming minimum when the equatorial planes of both metal atoms are orthogonal (Scheme IV.2). This situation is similar to that of the *anti-syn* carboxylate bridge and ferromagnetic interactions are expected.<sup>6</sup>

The design of our complexes are directed to the adoption of these two conformations by the carboxylate exchange pathway, which are based on the previous results with the malonate ligand.<sup>6-8</sup> The introduction of steric impediments in the malonate ligand such as the methyl or phenyl groups could favour an out-of-plane configuration, and hence provide the ferromagnetic interactions in our complexes.

#### IV.2.2. Magnitude of the magnetic interaction

The *anti-syn* carboxylate bridge is responsible for the ferro- or antiferromagnetic interactions in the most of the copper(II) complexes presented in this thesis work, depending on the overlap of the magnetic orbitals. However, as explained before, the *anti-syn*

configuration of the exchange pathway precludes a strong overlap of the orbitals and hence, the magnetic interaction will be weak. From this general trend, there exist other factors which can alter the magnitude of the magnetic interaction:

*Nature of the equatorial ligands.* An increase in the electronegativity of the donor atoms in the equatorial terminal ligands results in stronger magnetic couplings for oxalato-bridged compounds.<sup>7</sup> A similar trend is expected for the malonate-bridged complexes. The length of the equatorial bonds also influences the magnetic coupling, being weaker when the Cu–O bond distance increases.

*Nature of the axial ligand.* A change in the axial ligand induces smaller variations in the coupling constant. The general trend is inverted respect to what is observed for the equatorial ligands.<sup>5</sup> Thus, replacement of H<sub>2</sub>O by pyridine-type ligands increases the strength of the magnetic interaction.

*Ion geometry.* The magnetic interactions among copper atoms in D<sub>4h</sub> symmetry are more intense than those with O<sub>h</sub> symmetry. This is probably due to the longer equatorial Cu–O distances observed in the latter symmetry. The distortion in copper centres with D<sub>4h</sub> symmetry diminishes the strength of the interaction due to the mixture of the d(x<sup>2</sup>-y<sup>2</sup>) magnetic orbital which bears the unpaired electron with the d(z<sup>2</sup>) orbital reducing the spin density in the d(x<sup>2</sup>-y<sup>2</sup>) orbital.

### IV.2.3. Magneto-structural relationships in square grid layered Cu(II) complexes

Among the copper(II) complexes presented in the previous three chapters, a structural motif has appeared frequently, that is, the carboxylate-bridged square grid of copper(II) ions which forms layers separated or linked depending on the ligand utilized. This family of compounds seems ideal for the investigation of magneto-structural correlations in this kind of extended systems.

The complexes which are subject of this comparative analysis are displayed in Table IV.6 and IV.7. They all share some structural details apart from the main layered conformation, all the equatorial ligands are oxygen atoms from R-malonate ligands, the carboxylate bridges exhibit the *anti-syn* conformation with a certain degree of out-of-plane configuration, and the axial positions are occupied by pyridine-type or water molecule ligands. In Table IV.6, some square-grid layered compounds have been omitted; they are the complexes **6**, **7**, **8**, **12** and **19**, because of the lack of structural details in complex **8**, and due to the oxygen atoms of the malonate ligand do not occupy all the equatorial positions at the

copper(II) environment in **6**, **7**, **12** and **19** modifying the magnetic properties observed and hence, their magneto-structural correlations (see chapter I).

**Table IV.6.** Copper(II) environment in layered R-malonate complexes.<sup>a</sup>

| Compound                                                                     | Cu–O(1)    | Cu–O(2)   | Cu–O(3)  | Cu–O(4)  | Cu–N(1)                           | $\tau^b$       |
|------------------------------------------------------------------------------|------------|-----------|----------|----------|-----------------------------------|----------------|
| [Cu(pym)(Phmal)] <sub>n</sub> ( <b>2</b> )                                   | 1.982(6)   | 1.936(6)  | 1.979(7) | 1.944(7) | 2.252(10)                         | 0.02           |
| [Cu(pyzy)(Phmal)] <sub>n</sub> ( <b>3</b> )                                  | 1.954(3)   | 1.955(3)  | 1.953(3) | 1.977(3) | 2.242(4)                          | 0.006          |
| [Cu(3-CNpy)(Phmal)] <sub>n</sub> ( <b>4</b> )                                | 1.968(2)   | 1.976(2)  | 1.955(2) | 1.940(2) | 2.250(3)                          | 0.015          |
| [Cu(4-CNpy)(Phmal)] <sub>n</sub> ( <b>5</b> )                                | 2.030(5)   | 2.021(5)  | 1.878(4) | 1.907(5) | 2.236(7)                          | 0.018          |
| [Cu(3-Clpy)(Phmal)] <sub>n</sub> ( <b>9</b> )                                | 1.959(4)   | 1.948(4)  | 1.968(5) | 1.991(5) | 2.239(6)                          | 0.004          |
| [Cu(3-Brpy)(Phmal)] <sub>n</sub> ( <b>10</b> )                               | 1.956(7)   | 1.942(8)  | 1.974(8) | 2.000(7) | 2.239(9)                          | 0.003          |
| [Cu(3-lpy)(Phmal)] <sub>n</sub> ( <b>11</b> )                                | 1.957(5)   | 1.937(5)  | 1.976(5) | 1.992(5) | 2.241(6)                          | 0.018          |
| [Cu(Memal)(H <sub>2</sub> O)] <sub>n</sub> ( <b>17</b> )                     | 1.951(4)   | 1.970(3)  | 1.951(4) | 1.970(3) | 2.231(6) <sup>c</sup>             | 0.0            |
| [Cu(pyzy)(Memal)] <sub>n</sub> ( <b>18</b> )                                 | 1.9578(19) | 1.970(2)  | 1.959(2) | 1.962(2) | 2.292(2)                          | 0.006          |
| [Cu(4-CNpy)(Memal)(H <sub>2</sub> O)] <sub>n</sub> ( <b>20<sup>a</sup></b> ) | 2.052(10)  | 2.031(10) | 2.011(9) | 1.983(9) | 2.237(3)<br>2.323(5) <sup>c</sup> | O <sub>h</sub> |
| [Cu(Etmal)(H <sub>2</sub> O)] <sub>n</sub> ( <b>29</b> )                     | 1.977(5)   | 1.951(6)  | 1.963(5) | 1.946(5) | 2.267(6) <sup>c</sup>             | 0.012          |

<sup>a</sup> The copper(II) ions in all compounds exhibit a square pyramidal environments except in **20** where it presents an octahedral surrounding. Bond distances are expressed in Å.

<sup>b</sup> Distortion from square pyramidal ( $\tau = 0$ ) to trigonal bipyramidal ( $\tau = 1$ ) surroundings (ref. 8).

<sup>c</sup> Values corresponding to Cu–O(1w) bond distances.

Considering the results listed in the Tables IV.6 and IV.7, remarkably, from the eleven compounds investigated, four do not have quantitative values for the magnetic coupling due to the lack of theoretical approaches to treat them. The other seven complexes exhibit magnetic couplings through the carboxylate bridges ranging from  $-0.153$  to  $+5.6$   $\text{cm}^{-1}$ . These values are in agreement with those reported in the literature<sup>5,6</sup> and the theoretical explanation given above about the *anti-syn* carboxylate bridge. However, what is a more difficult task is to evaluate the structural feature responsible for the small changes in the magnetic coupling parameter from one compound to another. Such subtle variations could be due to whatever the structural parameters listed in the Tables IV.6 and IV.7 or a mixture of them.

First of all, we are going to make a structural comparison between the complexes listed in the Tables and the reasons for a specific change to appear.

*Copper environment.* Since all the complexes exhibit square pyramidal surroundings, it is remarkably that **20** presents an octahedral environment. This situation is not unusual and compounds **6**, **7** and **12** show this feature, but in those compounds the water molecule occupies an equatorial position at the copper atom. A close look to the Cu–O bond distances reveals that they subtly vary among the complexes, **5** and **20** exhibit longer equatorial Cu–O bond distances and, in general, they are ranged from 1.878(4) to 2.052(10) Å.

**Table IV.7.** Structural details for layered R-malonate complexes.

| Compound  | $d_1^a / \text{\AA}$   | $\gamma^b / ^\circ$ | $\beta^c / ^\circ$ | $d_2^d / \text{\AA}$                | $J / \text{cm}^{-1}$              | $g$      |
|-----------|------------------------|---------------------|--------------------|-------------------------------------|-----------------------------------|----------|
| <b>2</b>  | 5.100(8)               | 60.57-72.62         | 63.16(2)           | 13.45(4)                            | + 5.6(1) <sup>e</sup>             | 2.12(2)  |
|           | 5.143(7)               | 59.76-71.28         |                    |                                     |                                   |          |
| <b>3</b>  | 5.058(3)<br>5.187(3)   | 53.915(8)-          | 66.761(12)         | 12.413(3)                           | F / AF(-3.6) <sup>f</sup>         | -        |
|           |                        | 68.299(8)           |                    |                                     |                                   |          |
|           |                        | 53.749(8)-          |                    |                                     |                                   |          |
| <b>4</b>  | 4.984(2)<br>5.238(2)   | 67.081(9)           | 71.168(6)          | 13.705(3)                           | +5.4(1) <sup>g</sup><br>-0.70(1)  | 2.212(4) |
|           |                        | 49.694(7)-          |                    |                                     |                                   |          |
|           |                        | 72.921(7)           |                    |                                     |                                   |          |
| <b>5</b>  | 5.022(5)<br>5.229(4)   | 48.941(7)-          | 71.725(14)         | 13.985(8)                           | +4.8(1) <sup>g</sup><br>+0.073(3) | 2.093(4) |
|           |                        | 67.752(7)           |                    |                                     |                                   |          |
|           |                        | 46.772(18)-         |                    |                                     |                                   |          |
| <b>9</b>  | 5.015(5)<br>5.258(6)   | 70.558(18)          | 71.35(14)          | 13.534(7)                           | -0.153(1) <sup>h</sup>            | 2.058(1) |
|           |                        | 47.691(16)-         |                    |                                     |                                   |          |
| <b>10</b> | 4.999(5)<br>5.261(5)   | 73.079(18)          | 71.77(13)          | 13.755(8)                           | F / AF(-1.2) <sup>f</sup>         | -        |
|           |                        | 49.1(5)-67.8(5)     |                    |                                     |                                   |          |
| <b>11</b> | 4.995(4)<br>5.289(3)   | 48.0(5)-73.6(6)     | 71.11(9)           | 14.255(6)                           | F / AF(-1.2) <sup>f</sup>         | -        |
|           |                        | 47.6(5)-68.7(6)     |                    |                                     |                                   |          |
| <b>17</b> | 4.9653(12)             | 29.3(3)-82.4(2)     | 84.44(9)           | 6.203(3)                            | +1.61(1) <sup>e</sup>             | 2.20(3)  |
|           |                        | 43.15(18)-          |                    |                                     |                                   |          |
| <b>18</b> | 5.0226(5)<br>5.2174(5) | 75.95(14)           | 74.71(4)           | 6.6546(5)<br>7.3716(5) <sup>i</sup> | F / AF <sup>f</sup>               | -        |
|           |                        | 43.66(18)-          |                    |                                     |                                   |          |
| <b>20</b> | 5.227(3)<br>5.227(3)   | 68.18(16)           | 85.45(19)          | 11.320(2)                           | +0.25(2) <sup>e</sup>             | 2.258(3) |
|           |                        | 30.1(11)-81.9(8)    |                    |                                     |                                   |          |
| <b>29</b> | 4.971(2)<br>5.0452(18) | 31.0(9)-83.6(5)     | 88.81(13)          | 6.686(2)                            | +1.67(2) <sup>e</sup>             | 2.30(2)  |
|           |                        | 30.0(6)-86.2(5)     |                    |                                     |                                   |          |
|           |                        | 29.0(5)-83.6(5)     |                    |                                     |                                   |          |

<sup>a</sup> Intralayer copper-copper separation through each one of the crystallographically independent carboxylate-bridges.

<sup>b</sup> Dihedral angle between the basal plane of the copper(II) ion and the plane of the carboxylate bridge for each independent pathway [O(1)-C(1)-O(2) and O(3)-C(3)-O(4)]. The second value per bridge refers to the next connected copper atom.

<sup>c</sup> Dihedral angle between the mean basal plane of carboxylate-bridged copper(II) ions.

<sup>d</sup> Shortest interlayer Cu...Cu separation.

<sup>e</sup> From a regression analysis through the 2D-Heisenberg model for a square lattice (ref. 9)

<sup>f</sup> F and AF account for ferro- and antiferromagnetic interactions, respectively. The value in parenthesis is estimated from the magnetization curve.

<sup>g</sup> Values obtained a fit through the Rushbrooke expression for a copper(II) chain (ref. 10) with an additional mean field term.

<sup>h</sup> Value from the fitting through the expression for an isotropic antiferromagnetic square lattice (ref. 11).

<sup>i</sup> Interlayer Cu...Cu separation through the pyrazine bridge.

*Carboxylate bridged copper(II) separations.* The Cu...Cu separations through the carboxylate bridge are slightly different from one compound to another and, interestingly, between the two crystallographically independent carboxylate bridges of the same complex. The average value for the Cu...Cu separation through the carboxylate exchange pathway in these complexes is 5.11 Å [ranging from 4.9653(12) to 5.289(3) Å]. The greatest difference

between the Cu...Cu separations in a given complex occurs in **11**, which represents an extreme situation in the sub-series of the halogen-pyridine complexes where the short and the long bridges decrease and increase in length, respectively, along the series Cl, Br, I. The two independent carboxylate bridge lengths are only equivalent in complexes **17** [4.9653(12) Å] and **20** [5.227(3) Å].

*Conformation of the carboxylate bridge.* The dihedral angle between the basal plane of the copper atom and the carboxylate bridge is always shorter when it chelates (first value of  $\gamma$  in Table IV.7, see Figure IV.17). Moreover, this value is shorter in the complexes of methyl- and ethylmalonate than in those of phenylmalonate (with the exception of **18** where the layers are linked through the pyrazine ligand) (see Figure IV.18). This situation corresponds with the out-of-plane conformation explained above, with an angle between the basal plane of the copper atom in *syn* conformation and the carboxylate bridge ranging from 67.752(7) to 86.2(5)°.

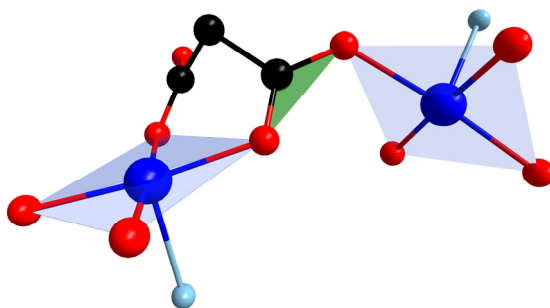


**Fig. IV.17.** *Anti-syn* out-of-plane conformation of the carboxylate-bridge. Equatorial planes of the copper(II) ions are coloured in blue and the carboxylate plane in green.

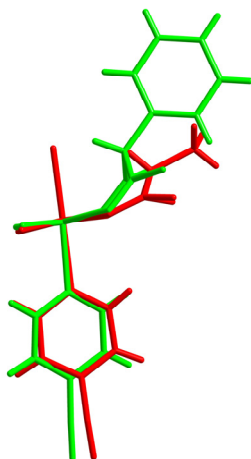


**Fig. IV.18.** Superposition of the copper(II) environment of the two 4-cyanopyridine-containing complexes with the methylmalonate ligand (red) and the phenylmalonate ligand (green).



*Angle between basal planes of carboxylate bridged copper(II) ions.* As a consequence of the out-of-plane configuration of the bridge the basal planes of the copper(II) ions are nearly perpendicular favouring the accidental orthogonality described above. This angle ranges from 63.16(2)° to 88.81(13)°. The large angles [from 84.44(9)° to 88.81(13)°] occur in the methyl- and ethylmalonate complexes (with the exception of **18** where the geometry is modified due to the pyrazine bridge between the layers).

*Interlayer separations.* The shortest Cu...Cu separations between layers are influenced determinately by the coligand involve. Thus, this distance is shorter in **2** (pyrimidine) than in **4** (3-cyanopyridine). The interlayer distance grow according to how bulky is the group attached to the pyridine ring as occur in the series [3-Clpy (**9**), 3-Brpy (**10**) and 3-Ipy (**11**)], also the position of the group in the pyridine ring plays an important role [the separation with the 3-CNpy (**4**) is shorter than that with the 4-CNpy coligand (**5**)]. Of course, interlayer separations in the methyl- and ethylmalonate complexes are shorter than those involving the phenylmalonate ligand.

Concerning the magnetic properties we are going to analyze some examples extracted from the Tables IV.6 and IV.7, and finally, to assign a general trend to the variation of the magnetic properties related to a specific structural parameter. We have to be cautious with the values of the coupling constants listed in Table IV.7 because most of them come from analyses with different theoretical models.

*Complexes 17, 20 and 29.* These are methyl- (**17** and **20**) and ethylmalonate (**29**) complexes (see Table IV.8). The structural parameters of the two compounds with water molecules as coligands (**17** and **29**) are very similar, and hence their coupling constant also does (average  $J$  being +1.64 cm<sup>-1</sup>). According to the out-of-plane configuration of the *anti-syn* carboxylate bridge, a ferromagnetic interaction among the copper(II) ions is observed. However, **20** presents a relative low value of the magnetic coupling, being  $J$  +0.25 cm<sup>-1</sup>. This situation can be explained taking into account the long Cu–O equatorial bond distances of **20**, which lead to a larger Cu...Cu separation through the carboxylate exchange pathway, reducing the magnitude of the ferromagnetic interaction.

*Complexes 9, 10 and 11.* These are phenylmalonate complexes with halogenpyridine coligands. The interaction among the copper(II) ions in **9** is antiferromagnetic, whereas in **10** and **11**, ferro- and antiferromagnetic interactions coexist. The structures of these compounds are very similar with no remarkably changes in the conformation of the bridge, and just an enlargement of the carboxylate exchange pathway and the Cu–O bond distances along the series Cl, Br, I. Where, then, do the differences in the magnetism come

from? As it was suggested in the chapter I, the magnetic behaviour of **9** could also be explained if two interactions of approximately the same magnitude and opposite nature are active. This situation is more similar to that observed in **10** and **11**, with the exception that now the ferromagnetic interaction is strong enough to be observed in the magnetic susceptibility measurements. It is important to remark that we are dealing with very small variations of the coupling constant, since the antiferromagnetic coupling for **9** is  $-0.153 \text{ cm}^{-1}$ . Therefore, only very subtle changes in the structural features are necessary to overcome the ferromagnetism and make the antiferromagnetic contribution to dominate, as occur in **9**.

*Complexes 2-5.* These are the phenylmalonate compounds with pyrimidine, pyrazine and cyanopyridine coligands. There are not many structural differences between these complexes, and they all show moderate ferromagnetic interactions. Weak antiferromagnetic interactions are also present, which in **2** it was assigned to a through-space interlayer interaction and to intralayer exchange pathways in **3** and **4**. This weak contribution becomes ferromagnetic in the complex **5**, but remains extremely weak ( $j$  being  $+0.007 \text{ cm}^{-1}$ ). The reasons for these changes are difficult to found out in the structural parameters listed in the Tables IV.6 and IV.7. We can see how the dihedral  $\gamma$  angle of the chelating carboxylate slightly decreases along the series, pym, pyz, 3-CNpy and 4-CNpy, at the same time the  $\beta$  angle between the two connected copper(II) ions smoothly increases. Probably, **2** was the complex with a more different conformation of the carboxylate bridge (see the  $\gamma$  angles in Table IV.7), and indeed this is the unique complex which exhibits a large magnetic correlation and magnetic ordering below 2.15 K. The Figure IV.19 shows the superposition of fragments of the structure of complexes 2-5. There exist differences, but they are very subtle and involve the location of the phenyl ring of the phenylmalonate ligand and the pyridine ring, being these variations due to supramolecular interactions. Therefore, we can see how the introduction of a specific group which is able to establish supramolecular interactions can modify the structure of the carboxylate exchange pathway and then alter the magnetic properties observed.

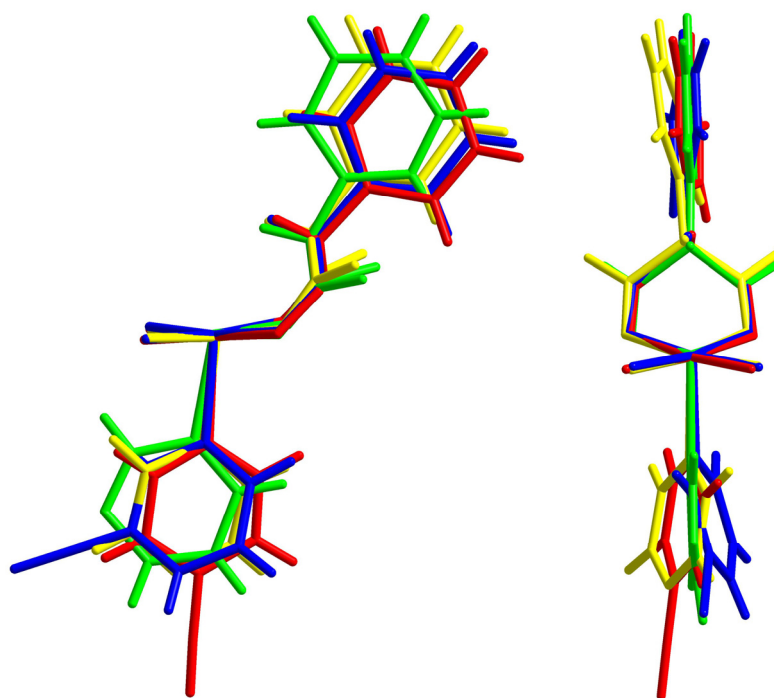


Fig. IV.19. Two views of the superposition of the copper(II) environment for the complexes **2** (green), **3** (yellow), **4** (blue) and **5** (red).

The general study of all the complexes to extract a general trend in the magnetic properties for some structural parameters has been unfruitful. For example, complexes **17**, **20** and **29**, with a greater  $\beta$  and small  $\gamma$  angles than phenylmalonate-containing complexes, which *a priori* should favour the ferromagnetic interactions show lower ferromagnetic coupling constants than the related Phmal-complexes. The reasons responsible for these situations to appear are that there are many structural parameters involved which can vary simultaneously along the series of compounds, some to favour the ferromagnetism and others to increase the antiferromagnetic contribution. Moreover, in our previous analyses describing the main factors which can affect the magnetic coupling, we are restricted to predict the overlap between the magnetic orbitals of the complexes and thus, predict how strong the antiferromagnetic contribution will be according to the Kahn's model. However, we are not able to establish a prediction of the ferromagnetic contribution based on the structural parameters.

#### IV.2.4. References

- 1 O. Kahn, *Molecular Magnetism*, VCH, New York, **1993**.
- 2 J. J. Girerd, Y. Journaux and O. Kahn, *Chem. Phys. Lett.* **1981**, 82, 534.
- 3 O. Kahn and B. Briat, *J. Chem. Soc. Trans. II*, **1976**, 72, 268.
- 4 O. Kahn, *Angew. Chem. Int. Ed.* **1985**, 24, 834.
- 5 A. Rodríguez-Forteza, P. Alemany, S. Alvarez and E. Ruiz, *Chem. Eur. J.* **2001**, 7, 627.
- 6 J. Pasán, F. S. Delgado, Y. Rodríguez-Martín, M. Hernández-Molina, C. Ruiz-Pérez, J. Sanchiz, F. Lloret and M. Julve, *Polyhedron* **2003**, 22, 2143.
- 7 E. Ruiz, P. Alemany, S. Alvarez and J. Cano, *Inorg. Chem.* **1997**, 36, 3683.
- 8 A. W. Addison, T. N. Rao, J. Reedijk, J. van Rijn and G. C. Verschoor, *Dalton Trans.* **1984**, 1349.
- 9 R. Navarro, *Application of High- and Low-Temperature Series Expansions to Two-dimensional Magnetic Systems*, Ed. L. J. de Jongh, Kluwer Academic Publishers, Dordrecht, **1990**.
- 10 G. A. Baker, G. S. Rushbrooke and H. E. Gilbert, *Phys. Rev.* **1964**, 135, A1272.
- 11 G.S. Rushbrooke, G. A. Baker and P. J. Wood in *Phase Transition and Critical Phenomena*, vol. 3, C. Domb and M.S. Green, eds. Academic Press, London, **1972**.

---

---

# Chapter V.

## Perspectives

---

---



## V.1. Molecular Magnetic Materials

### V.1.1. Introduction

The field of investigation opened with the introduction of a substituent in the methylene carbon atom of the malonate ligand has no limits, being the group attached to the malonate ligand the motive of subsequent fruitful ideas. The groups which could be introduced in the malonate ligand have been divided in two sorts; (i) the steric-type substituents which introduce groups involved in weak interactions such long aliphatic chains or bulky aromatic groups, along the line developed in this thesis; (ii) the substituent viewed as an active part of the molecule which can coordinate to the metal atoms, and hence participate in the covalent network, these substituents could be hydroxyl, pyridyl, pyrazolyl groups, etc.

A few complexes were synthesized and their structural and magnetic properties investigated as examples of these two guidelines. Firstly, we present the benzylmalonate ligand as a next step on the Thesis work and also, as an example of the steric-type substituents. Then, we present the copper(II) compounds of a functionalized phenylmalonate ligand with a hydroxyl group, the ketomalonic acid and other more complex ligands sharing the same philosophy.

### V.1.2. Along the Thesis-work line: Copper(II)-Benzylmalonate (**36**)

The benzylmalonate ligand is very similar to the phenylmalonate. The variation introduced here is a methylene group between the aromatic ring and the central carbon atom of the malonate skeleton, which allows certain mobility to the phenyl ring. Previous work on this ligand has been reported,<sup>1-3</sup> although only two mononuclear copper(II) compounds were synthesized (see Section I.9) and they involved other N-donor heterocyclic coligands.<sup>3</sup>

The complex of formula  $[\text{Cu}(\text{Bzmal})(\text{H}_2\text{O})]$  (**36**) was synthesized by adding an aqueous solution (5 cm<sup>3</sup>) of copper(II) nitrate (0.5 mmol, 115 mg) to another one (10 cm<sup>3</sup>) containing a benzylmalonic acid (0.5 mmol; 97 mg) and sodium carbonate (0.5 mmol, 53 mg). The resulting pale blue solution was left to evaporate at room temperature and after a few weeks, deep blue plate-like single crystals of **36** were obtained nearly to dryness. The crystals are poor quality and they were used for both X-ray and magnetic measurements.

The preliminary crystal structure<sup>4</sup> (Figure V.1) reveals the occurrence of a square grid of *anti-syn* carboxylate-bridged copper(II) ions which grow in the *ab* crystallographic plane, similarly to that observed in complexes **2-12**, **17-20** or **29** (Figure V.2). These layers are stacked along the *c* direction, the benzyl groups occupying the interlayer space with a

shortest interlayer copper-copper separation of 12.15 Å (Figure V.3). The benzyl groups are delocalized between two positions for each malonate ligand (Figure V.1).

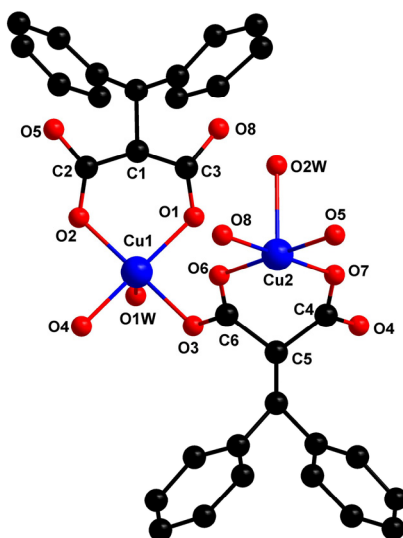


Fig. V.1. A view of a molecular fragment of the structure of **36** along with the numbering scheme.

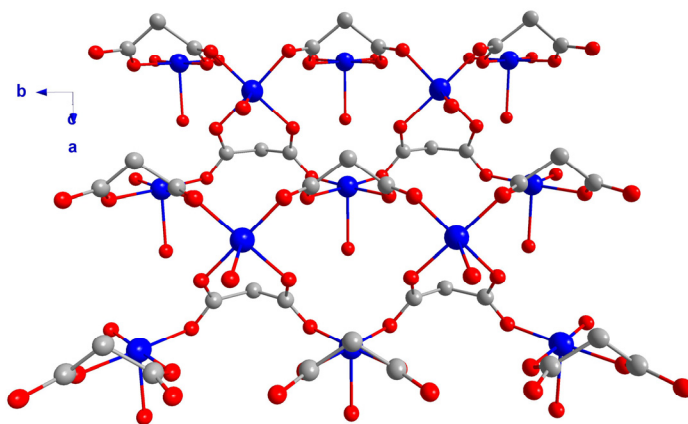


Fig. V.2. Central projection of the carboxylate-bridged square grid of copper(II) ions formed in **36**. The benzyl groups of the benzylmalonate ligand have been omitted for clarity.

Two crystallographically independent copper atoms [Cu(1) and Cu(2)] occur in the structure of **36**. Both copper atoms exhibit a slightly distorted square pyramidal environment with a  $\tau$  value of 0.004. Four benzylmalonate oxygen atoms build the basal plane for Cu(1) and Cu(2) [mean Cu(1)–O(eq) and Cu(2)–O(eq) bond distances being 1.95 Å] while a water molecule occupies the apical positions [2.23 and 2.37 Å for Cu(1)–O(1w) and Cu(2)–O(2w),

respectively]. The two crystallographically independent benzylmalonate ligands adopt simultaneously bidentate and bis-monodentate coordination modes, similarly to what is observed in the related Ph-, Me- and Etmal-containing complexes. The intralayer Cu...Cu separations lay in the range 4.82-4.84 Å, the dihedral angle between the basal planes of adjacent copper(II) ions being 87°.

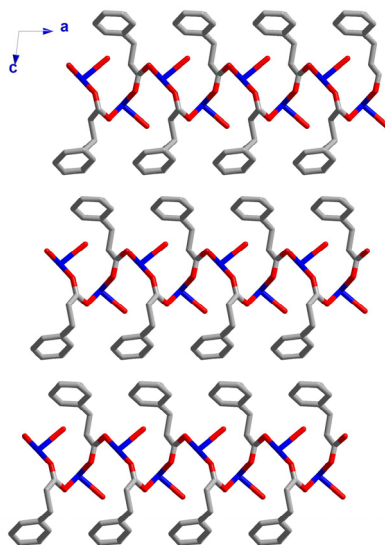
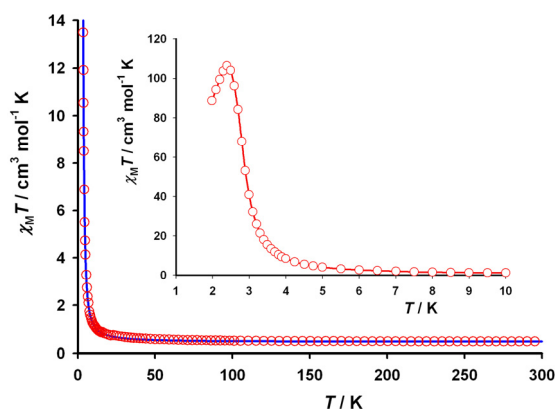


Fig. V.3. A perspective view along the *b* axis of the crystal packing of **36**.

The magnetic properties of complex **36** under the form of  $\chi_M T$  vs  $T$  plot [ $\chi_M$  is the magnetic susceptibility per copper(II) ion] are depicted on Figure V.4. The  $\chi_M T$  value at room temperature is  $0.48 \text{ cm}^3 \text{ mol}^{-1} \text{ K}$ , as expected for a magnetically isolated spin doublet. Upon cooling,  $\chi_M T$  remains almost constant until 90 K and then smoothly increases with a monotonic increment of the slope, being asymptotical at 4.0 K. The  $\chi_M T$  value reaches a maximum of  $106.4 \text{ cm}^3 \text{ mol}^{-1} \text{ K}$  at 2.4 K, and then decreases to a value of  $88.7 \text{ cm}^3 \text{ mol}^{-1} \text{ K}$  at 1.9 K. The magnetization curve (Figure V.5) does not show any hysteresis, and it reaches a saturation value of 1.08 BM at an applied magnetic field of 2 T. No inflexion point was observed at low fields in contrast to what was observed for complex **2**. These features are indicative of an overall ferromagnetic coupling. The occurrence of an out-of-phase susceptibility signal (the maximum has not been observed because it will appear below the minimum temperature available in our device), supports the existence of a ferromagnetic order below a  $T_c$  value of 2.7 K marked as the onset of the  $\chi_M''$  signal (Figure V.6).





**Fig. V.4.**  $\chi_M T$  vs  $T$  plot for **36** under applied fields of 1 T ( $T > 21$  K), 0.01 T ( $7$  K  $< T < 10$  K) and 0.002 T ( $T < 7$  K): (o) experimental data, (—) best fit curve. The inset shows a detail of the low temperature region.

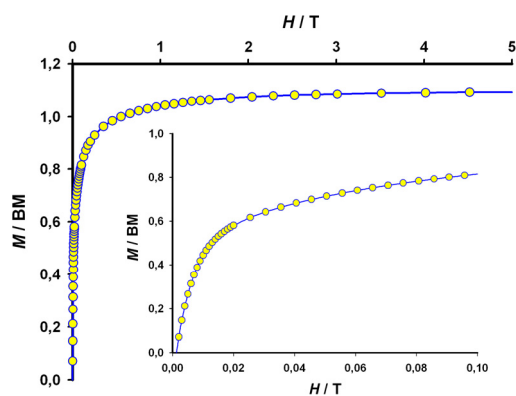


**Fig. V.5.** Magnetization ( $M$ ) vs  $H$  at 2 K; the blue line is only an eye-guide. The inset shows a detail of the low magnetic applied field region.

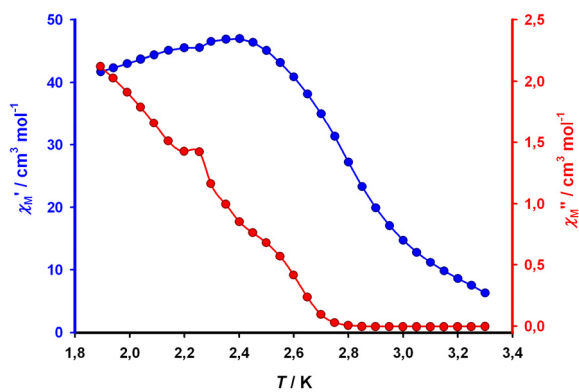


**Fig. V.6.** In-phase (blue) and out-of-phase (red) ac signals of **36** in a 3 G field oscillating at 10 Hz without dc magnetic field: (o,o) experimental data; (—) eye-guide line.

In the light of the above magneto-structural data, its magnetic behaviour would correspond to that of a ferromagnetically coupled square grid of copper(II) ions through carboxylate-bridges in the *anti-syn* conformation, the layers interacting ferromagnetically with the adjacent ones, leading to a magnetic order below  $T_c$ . Thus, the high temperature magnetic data of **36** were analyzed through the expression of the magnetic susceptibility reported by Baker et al. derived from the high-temperature expansion series for an isotropic ferromagnetic square lattice with interacting spin doublets.<sup>6</sup> The spin Hamiltonian is defined as

$$\hat{H} = -J \sum_i \hat{S}_i \cdot \hat{S}_{i+1}$$

and the series takes the form

$$\chi = \left( \frac{N\beta^2 g^2}{3k_B T} S(S+1) \right) \left[ 1 + \sum_{n \geq 1} a_n \frac{x^n}{2^n} \right]$$

with  $N$  the Avogadro's number,  $g$  the Landé factor,  $\beta$  the Bohr magneton,  $k_B$  the Boltzmann's constant,  $x = J/k_B T$ ,  $J$  the in-plane magnetic coupling parameter and the  $a_n$  values are known up to  $n = 10$ . Best least-square fit of the experimental data in the temperature range 4.0–300 K gives  $J = +6.8(1) \text{ cm}^{-1}$ ,  $g = 2.17(1)$  and  $R = 1.0 \times 10^{-3}$ . The calculated curve matches well the experimental data in the 4.0-300 K temperature range (Figure V.4), with a significant deviation in the low temperature extrapolation.

The magnetic coupling constant for this carboxylate-bridged system is the greatest observed in substituted-malonate copper(II) complexes, although there are magnetic coupling parameters greater than this one for copper(II)-malonate complexes.<sup>7,9</sup> The magnetic behaviour of **36** resembles that of **2** (which also exhibits magnetic ordering) and those which share the square grid layered structure (see chapter IV). We establish in the previous chapter that more than one structural parameter can influence the magnetic behaviour. Most likely, the dihedral angle between the basal planes of the carboxylate-connected copper(II) ions, which is closer to the orthogonality in **36** than in the other compounds, together with a non-distorted square pyramidal surroundings, favour the ferromagnetic interaction in **36**.

The magnetic behaviour of this compound reveals that the strategy of introducing a bulky substituent can be highly rewarding when thinking at the magnetic properties.

### V.1.3. The substituent as an ‘active’ part of the ligand

A different approach to obtain molecular magnetic materials based on the malonate ligand consists of the substitution of one- or two hydrogen atoms from the central methylene carbon of the malonate ligand by groups which can coordinate to the metal atoms. This approach implies that the substituent is viewed as an active part of the molecule, which can act as a bridge or as a connector to metal atoms instead of the passive status of the alkyl groups of the R-malonate ligands presented in the previous chapters, in spite of the interesting supramolecular interactions that they establish.

The limit for the substitutions depends only on the imagination of the scientist. Here we have focused on the introduction of a hydroxyl group in the methylene position of the malonate ligand. The OH- group can coordinate to metal atoms and with the aid of the carboxylate groups already present in the malonate ligand can form two adjacent five-member chelate rings bridged by the hydroxyl group. This is a very interesting matter since the hydroxo group is known to mediate strong magnetic interactions, mostly antiferromagnetic. There exists previous work on this kind of ligands, specifically with the 2-hydroxy-malonic acid or tartronic acid.<sup>10</sup>

#### V.1.3.1. 2-Hydroxy-2-

##### phenylmalonate (37)

The 2-hydroxy-2-phenylmalonate (OH-Phmal) ligand is built by the substitution of the remaining hydrogen atom of the central carbon of the phenylmalonate ligand by a hydroxyl group. This group can coordinate with the metal atoms forming five-member chelate rings, somewhat more stable than the six-member chelate ring present in all the R-mal-containing copper(II) complexes.

The compound of formula  $(\text{NH}_4)_2[\text{Cu}_4(\text{O-Phmal})_3(\text{H}_2\text{O})_5]_2 \cdot 7\text{H}_2\text{O}$  (37) was synthesized randomly from a mixture of phenylmalonic acid (0.5 mmol, 90 mg) and copper(II) nitrate (0.5 mmol, 115 mg) in a

**Table V.1.** Crystallographic data for complex 37

| 37                                        |                                                                        |
|-------------------------------------------|------------------------------------------------------------------------|
| Formula                                   | $\text{C}_{54}\text{H}_{68}\text{O}_{45}\text{N}_2\text{Cu}_8$         |
| FW                                        | 1972.32                                                                |
| Crystal system                            | Monoclinic                                                             |
| Space group                               | $P 2_1/n$                                                              |
| $a / \text{\AA}$                          | 12.5443(9)                                                             |
| $b / \text{\AA}$                          | 21.4231(18)                                                            |
| $c / \text{\AA}$                          | 28.297(4)                                                              |
| $\beta / ^\circ$                          | 98.011(8)                                                              |
| $V / \text{\AA}^3$                        | 7530.4(13)                                                             |
| $Z$                                       | 4                                                                      |
| $\mu(\text{Mo K}\alpha) / \text{cm}^{-1}$ | 23.18                                                                  |
| $T / \text{K}$                            | 293(2)                                                                 |
| $\rho_{\text{calc}} / \text{g cm}^{-3}$   | 1.735                                                                  |
| $\lambda / \text{\AA}$                    | 0.71073                                                                |
| Index ranges                              | $-16 \leq h \leq 10,$<br>$-25 \leq k \leq 27,$<br>$-24 \leq l \leq 36$ |
| Indep. reflect. ( $R_{\text{int}}$ )      | 16701 (0.1273)                                                         |
| Obs. reflect. [ $I > 2\sigma(I)$ ]        | 6445                                                                   |
| Parameters                                | 1000                                                                   |
| Goodness-of-fit                           | 1.013                                                                  |
| $R$ [ $I > 2\sigma(I)$ ]                  | 0.1096                                                                 |
| $R_w$ [ $I > 2\sigma(I)$ ]                | 0.1625                                                                 |
| $R$ (all data)                            | 0.2718                                                                 |
| $R_w$ (all data)                          | 0.2137                                                                 |

water/ammonia 50/50 (10 cm<sup>3</sup>) solution. Deep blue plate-like single crystals of **37** were grown after two weeks of slow evaporation of the resulting deep blue solution at room temperature.

The crystal structure of **37** (Table V.1) consists of discrete octanuclear copper(II) anionic entities, ammonium cations and crystallization water molecules. The octanuclear molecule is built by two double oxo(carboxylate)-bridged tetranuclear units, each one being formed by a [Cu<sub>3</sub>(O-Phmal)<sub>3</sub>] core with the addition of a pendant fourth copper atom (Figure V.7). The isolated molecules are packed with the phenyl groups of the O-Phmal ligand forming rectangular hydrophobic channels of dimension 16 x 12 Å<sup>2</sup> along the *a* direction (Figure V.8). The crystallization water and the ammonium cations are located in

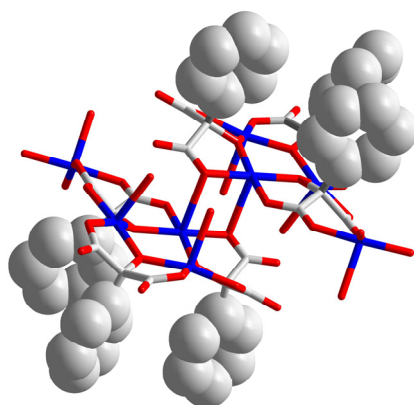


Fig. V.7. A view of the octanuclear copper(II) molecules of the structure of **37**.

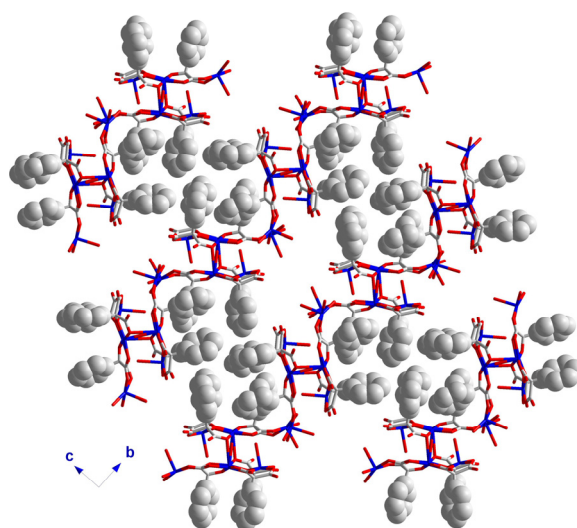
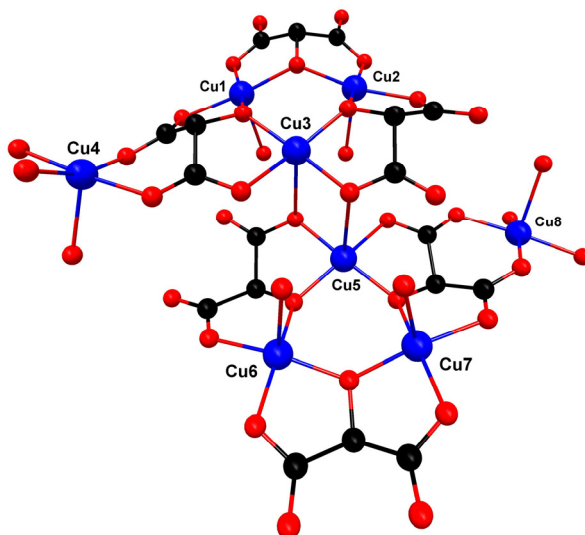


Fig. V.8. A perspective view along the *a* axis of the crystal packing of **37** showing the  $\pi$ -type interactions among the octanuclear units. The crystallization water molecules and the ammonia cations are omitted for clarity.

the intermolecular space forming an extensive hydrogen bond network which stabilizes the structure.

There are eight crystallographically independent copper atoms (Figure V.9), all of them exhibiting square pyramidal environments with  $\tau$  values ranging from 0.02 to 0.22. Cu(1), Cu(2), Cu(6) and Cu(7) share the same surroundings with the four oxygen atoms from the O-Phmal ligands building the basal plane while water molecules occupy the apical positions. Four O-Phmal oxygen atoms also form the basal plane of Cu(3) and Cu(5), but the apical position is occupied by other O-Phmal oxygen atom from the adjacent trinuclear core. The basal plane of the pendant copper atoms Cu(4) and Cu(8) are built by two oxygen atoms from O-Phmal ligands and two water molecules, being the apical positions also occupied by water molecules.



**Fig. V.9.** A view of a octanuclear entity of **37** along with the numbering scheme. The phenyl groups of the OH-Phmal ligand have been omitted for clarity.

There exist six crystallographically independent O-Phmal groups. Four O-Phmal exhibit the same bis-bidentate conformation forming two five-membered chelate rings sharing the central carbon of the malonate skeleton and the deprotonated O- group and two of them present an extra monodentate coordination of one of the carboxylate groups which is responsible for the formation of the  $\mu$ -oxo bridge. The two other O-Phmal ligands exhibit the novel tris-bidentate coordination mode (see Figure V.9).

The deprotonated OH- group is the bridge which links the three copper atoms inside the trinuclear core  $[\text{Cu}_3(\text{O-Phmal})_3]$ , while the fourth pendant copper atom is bridged

through carboxylate in the *anti-anti* conformation to the core (separations and angles between copper atoms are listed in Table V.2).

**Table V.2.** Shortest intramolecular copper-copper separations<sup>a</sup>

|                            | Cu...Cu distance / Å | Cu–O–Cu angle / ° | $\beta$ / ° |
|----------------------------|----------------------|-------------------|-------------|
| Cu(1)···Cu(2)              | 3.4557(19)           | 129.5(4)          | 28.6(2)     |
| Cu(2)···Cu(3)              | 3.435(2)             | 127.8(4)          | 27.1(2)     |
| Cu(3)···Cu(1)              | 3.465(2)             | 127.4(3)          | 29.9(2)     |
| Cu(5)···Cu(6)              | 3.484(2)             | 131.6(4)          | 21.5(2)     |
| Cu(6)···Cu(7)              | 3.5214(18)           | 134.3(4)          | 20.3(2)     |
| Cu(7)···Cu(5)              | 3.461(2)             | 128.2(4)          | 30.4(2)     |
| Cu(3)···Cu(5)              | 3.4819(19)           | 100.2(3)          | 0.9(2)      |
| Cu(1)···Cu(4) <sup>b</sup> | 5.509(2)             | -                 | 40.8(2)     |
| Cu(3)···Cu(4) <sup>b</sup> | 5.495(2)             | -                 | 47.2(2)     |
| Cu(5)···Cu(8) <sup>b</sup> | 5.512(2)             | -                 | 37.7(2)     |
| Cu(7)···Cu(8) <sup>b</sup> | 5.537(2)             | -                 | 32.0(2)     |

<sup>a</sup>  $\beta$  is the angle between the basal planes of the copper atoms involved.

<sup>b</sup> Carboxylate-bridged copper atoms.

The magnetic properties of **37** under the form of both  $\chi_M T$  and  $\chi_M$  vs  $T$  plots [ $\chi_M$  being the susceptibility per four copper(II) ions] are shown in Fig. V.10. At room temperature  $\chi_M T$  is  $1.29 \text{ cm}^3 \text{ mol}^{-1} \text{ K}$ , a value which is lower than that expected for a four magnetically isolated spin doublets. Upon cooling,  $\chi_M T$  continuously decreases to reach a value of  $0.16 \text{ cm}^3 \text{ mol}^{-1} \text{ K}$  at 40 K, indicating an overall antiferromagnetic coupling. The  $\chi_M$  curve exhibits a maximum at 95 K which is indicative of the occurrence of a relatively strong antiferromagnetic interaction.

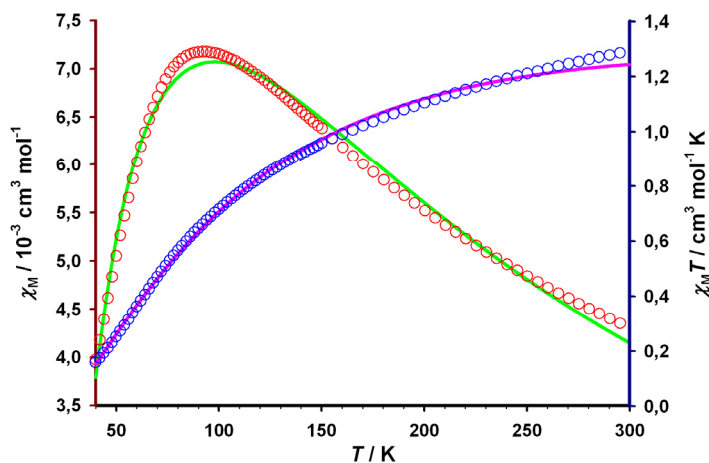


**Fig. V.10.**  $\chi_M$  (left axis, red) and  $\chi_M T$  (right axis, blue) vs  $T$  plot for **37** under an applied field of 1 T: (o) experimental data, (—) best fit curve.

Up to three different exchange pathways can be identified in the crystal structure of **37**; (i) the  $\mu$ -alkoxo bridges in the trinuclear  $\text{Cu}_3\text{O}_3$  core; (ii) the carboxylate bridges in the *anti-anti* conformation which link the trinuclear core with the pendant copper atom and (iii) the double  $\mu$ -oxo bridge which connects the tetranuclear entities in an out-of-plane conformation. Considering the magnetic strength of these bridges, it is well known that the  $\mu$ -alkoxo bridge can mediate of ferro- or antiferromagnetic interactions depending mainly on the value of the angle at the alkoxo bridge molecular geometry [antiferromagnetism is expected for Cu–O–Cu angles above  $98^\circ$  and the larger the angle the stronger the interaction].<sup>11,12,15</sup> Thus, the  $\mu$ -alkoxo as well as the *anti-anti* carboxylate bridge are able to mediate medium to strong antiferromagnetic interactions,<sup>11-15</sup> however, the  $\mu$ -oxo bridge in the out-of-plane exchange pathway mediates weak interactions, usually antiferromagnetic.<sup>16-21</sup> Therefore, we can neglect the double  $\mu$ -oxo exchange pathway in our preliminary magnetic analysis and consider the complex as antiferromagnetically coupled tetranuclear entities (Figure V.11).

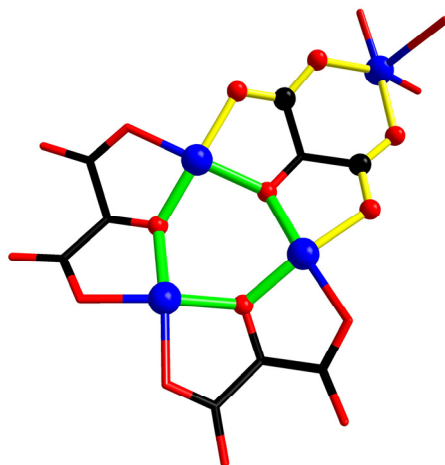


**Fig. V.11.** Active exchange pathways between copper(II) ions in one of the two  $\mu$ -oxo bridged tetranuclear entities of **37**. *Anti-anti* carboxylate-bridges are yellow coloured, while  $\mu$ -alkoxo bridges correspond to the green paths.

In order to simplify the model even more, the same magnetic coupling constant is assumed for the  $\mu$ -alkoxo and the carboxylate exchange pathways. Thus, as seen in Figure V.11, the model proposed is a square of copper(II) ions with the edges and one of the diagonals as active pathways. The Hamiltonian takes the form

$$\hat{H} = -J \left( \hat{S}_1 \cdot \hat{S}_2 + \hat{S}_2 \cdot \hat{S}_3 + \hat{S}_3 \cdot \hat{S}_4 + \hat{S}_4 \cdot \hat{S}_2 + \hat{S}_3 \cdot \hat{S}_1 \right)$$

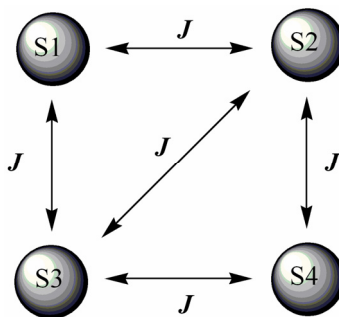
The interpretation of the Hamiltonian can be done with the use of Scheme V.1. The Kambe vector coupling method with  $S_A = S_1 + S_4$  and  $S_T = S_1 + S_2 + S_3 + S_4$  yields the following expression for the energy levels<sup>22</sup>

$$E(S_T, S_A, S_2, S_3) = -\frac{J}{2} [S_T(S_T + 1) - S_A(S_A + 1) - 3/2]$$

Its insertion in the van Vleck equation provides the expression for the molar susceptibility<sup>23</sup>

$$\chi_M = \frac{N\beta^2 g^2}{kT} \frac{\left[ 10 + 2\exp\left(\frac{-J}{kT}\right) + 2\exp\left(\frac{-2J}{kT}\right) \right]}{\left[ 5 + 3\exp\left(\frac{-J}{kT}\right) + 4\exp\left(\frac{-2J}{kT}\right) + \exp\left(\frac{-3J}{kT}\right) \right]}$$

Least-squares fit of the fit of the experimental data through this expression in the temperature range 40-300 K leads the parameters  $J = -79(1)$ ,  $g = 2.24(2)$  and  $R = 3 \times 10^{-3}$ . The curve (solid line in Fig. V.10) roughly matches the experimental data. This is due to the approximation made considering the two exchange pathways with the same coupling parameter and a better model has to be proposed to obtain reliable values for the magnetic couplings involved. However, as a first approximation the value for  $J$  reveals that there exist a strong antiferromagnetic coupling among the copper ions and the tetranuclear model proposed neglecting the double  $\mu$ -oxo bridge is quite reasonable. The  $J$  value obtained is in agreement with previously reported values for copper(II) compounds with  $\mu$ -alkoxo and *anti-anti* carboxylate bridges.<sup>11-15</sup>



Scheme V.1

The structure and magnetic properties of complex **37** could be the source of inspiration for the generation of new high-spin molecules. In fact, the  $\text{Cu}_3\text{O}_3$  core seems to be robust and the pendant copper(II) ions could be substituted by other paramagnetic ions to construct ferrimagnets by design.



### V.1.3.2. Ketomalonic acid (38)

The ketomalonic ligand is very similar to the malonic acid, with the substitution of the two hydrogen atoms of the methylene group by a ketonic group which in the presence of water is transformed into two hydroxyl groups. The use of this ligand comes from the idea of obtaining the  $\text{Cu}_3\text{O}_3$  core which is formed in **37**. This trinuclear core is not unusual and it has been found in about 30 structures according to a CSD database search. Remarkably, a structure very similar to what we are expecting is seen among them; the formed one with the tartronate ligand,<sup>10</sup> which is very similar to the ketomalonate one (with only one hydroxyl group substituted in the methylene carbon atom of the malonic acid). Considering the high prize of the tartronic acid, we focus on the ketomalonic acid and herein we report the synthesis, structural analysis and magnetic properties of the  $\{\text{K}_3[\text{Cu}_3(\text{Ketomal})_3(\text{H}_2\text{O})]\}_n \cdot 4n\text{H}_2\text{O}$  complex (**38**).

The crystal structure of **38** (Table V.3) consists of  $[\text{Cu}_3(\text{Ketomal})_3(\text{H}_2\text{O})]$  trinuclear units which dimerizes through a  $\mu$ -oxo bridge to form hexanuclear entities (Figure V.12). These units are connected through double-carboxylate bridges building chains along the  $a$  direction, which are linked through single-carboxylate bridges to the adjacent chains affording the 3D-network (Figure V.13). The structure exhibit channels of approximately  $10 \times 5 \text{ \AA}^2$  which are filled with hydroxo-bridged potassium ions (Figure V.14) avoiding the presence of crystallization water molecules. Hydrogen bonding among the coordinated water molecules and ketomalonic oxygen atoms contributes to the stabilization of the structure [O...O distances ranging from 2.762(3) to 2.934(6)  $\text{\AA}$ ].

There are three crystallographically independent copper atoms which exhibit square pyramidal [Cu(1);  $\tau = 0.12$ ] and octahedral [Cu(2) and Cu(3);  $s/h$  and  $\phi$  being 1.55 and 53.3° and 1.51 and 53.4°, respectively (the values for an ideal octahedron are  $s/h = 1.22$  and  $\phi = 60^\circ$ )]. The basal plane of the three copper atoms are built by ketomalonate oxygen atoms while the apical positions are occupied by a water molecule [O(1w)] for Cu(1), a water molecule [O(1w)] and a ketomalonate oxygen atom for Cu(2) and two ketomalonate oxygen

**Table V.3.** Crystallographic data for **38**

| <b>38</b>                                 |                                                                       |
|-------------------------------------------|-----------------------------------------------------------------------|
| Formula                                   | $\text{C}_9\text{H}_{13}\text{O}_{23}\text{K}_3\text{Cu}_3$           |
| FW                                        | 797.03                                                                |
| Crystal system                            | Monoclinic                                                            |
| Space group                               | $P 2_1/c$                                                             |
| $a / \text{\AA}$                          | 7.8804(10)                                                            |
| $b / \text{\AA}$                          | 24.870(4)                                                             |
| $c / \text{\AA}$                          | 10.8961(5)                                                            |
| $\beta / ^\circ$                          | 94.315(7)                                                             |
| $V / \text{\AA}^3$                        | 2129.4(4)                                                             |
| $Z$                                       | 4                                                                     |
| $\mu(\text{Mo K}\alpha) / \text{cm}^{-1}$ | 36.71                                                                 |
| $T / \text{K}$                            | 293(2)                                                                |
| $\rho_{\text{calc}} / \text{g cm}^{-3}$   | 2.455                                                                 |
| $\lambda / \text{\AA}$                    | 0.71073                                                               |
| Index ranges                              | $-10 \leq h \leq 5,$<br>$-29 \leq k \leq 32,$<br>$-14 \leq l \leq 13$ |
| Indep. reflect. ( $R_{\text{int}}$ )      | 4634 (0.0216)                                                         |
| Obs. reflect. [ $I > 2\sigma(I)$ ]        | 3950                                                                  |
| Parameters                                | 355                                                                   |
| Goodness-of-fit                           | 1.092                                                                 |
| $R$ [ $I > 2\sigma(I)$ ]                  | 0.0340                                                                |
| $R_w$ [ $I > 2\sigma(I)$ ]                | 0.0796                                                                |
| $R$ (all data)                            | 0.0437                                                                |
| $R_w$ (all data)                          | 0.0833                                                                |

atoms for Cu(3). The potassium atoms are seven- [K(1) and K(3)] and nine-coordinated [K(2)]. The three crystallographically independent ketomalonate ligands act simultaneously as bis-bidentate [through two carboxylate- and one hydroxo-oxygen atoms building the trinuclear  $\text{Cu}_3\text{O}_3$  core] and monodentate [through carboxylate oxygen atoms connecting the trinuclear entity with the adjacent ones].

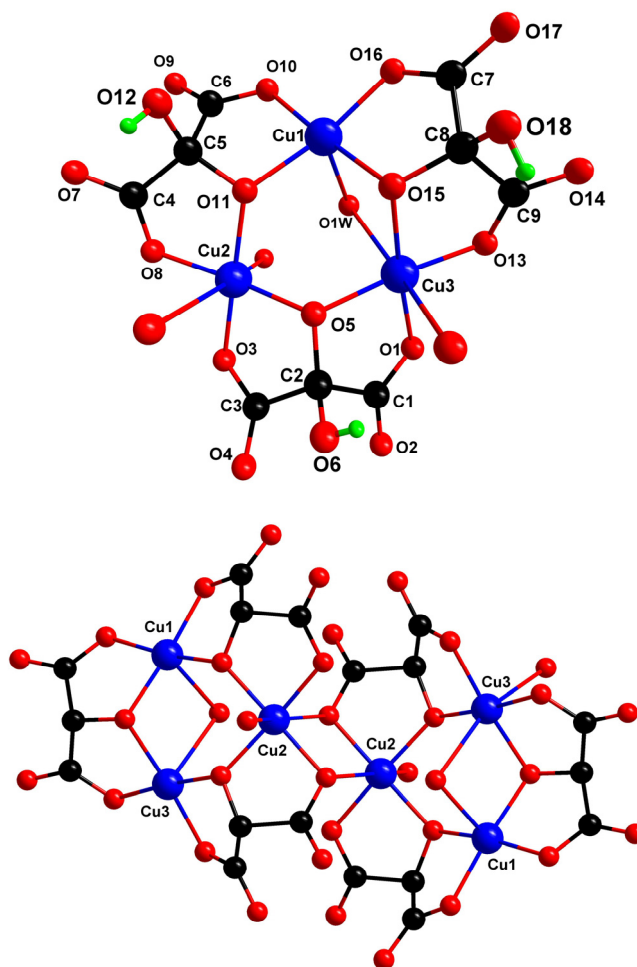


**Fig. V.12.** Central projection view of a fragment of the structure of **38** along with the numbering scheme (up). The hexanuclear entity with the numbering of the copper atoms (bottom) where the oxygen atoms of uncoordinated hydroxo group of the ketomalonic acid were omitted for clarity.

The trinuclear  $\text{Cu}_3\text{O}_3$  core exhibits the conformation of a somewhat distorted isosceles triangle, the  $\text{Cu}(1)\text{--O}(15)\text{--Cu}(3)$  being the different edge [see Table V.4]. The Cu(1) and Cu(3) atoms are also linked through a water molecule occupying the apical position of both atom environments. The  $\text{Cu}_3\text{O}_3$  unit is linked through a  $\mu$ -oxo bridge [O(3)]

to a symmetry-related  $\text{Cu}_3\text{O}_3$  unit, the  $\text{Cu}(2)\text{--O}(3)\text{--Cu}(2a)$  bond angle and the copper-copper separation being  $98.48(9)^\circ$  and  $3.5373(7)$  Å, respectively [(a) =  $-x + 1, -y + 1, -z$ ]. The trinuclear unit is also linked to  $\text{Cu}(2b)$  [(b) =  $-x, -y + 1, -z$ ] through a double equatorial-apical *anti-syn* carboxylate bridge and to  $\text{Cu}(3c)$  [(c) =  $x, -y + 1/2, z + 1/2$ ] through a single equatorial-apical *anti-syn* carboxylate bridge [ $5.2030(9)$  and  $5.8967(10)$  Å for  $\text{Cu}(2)\cdots\text{Cu}(2b)$  and  $\text{Cu}(1)\cdots\text{Cu}(3c)$ , respectively].

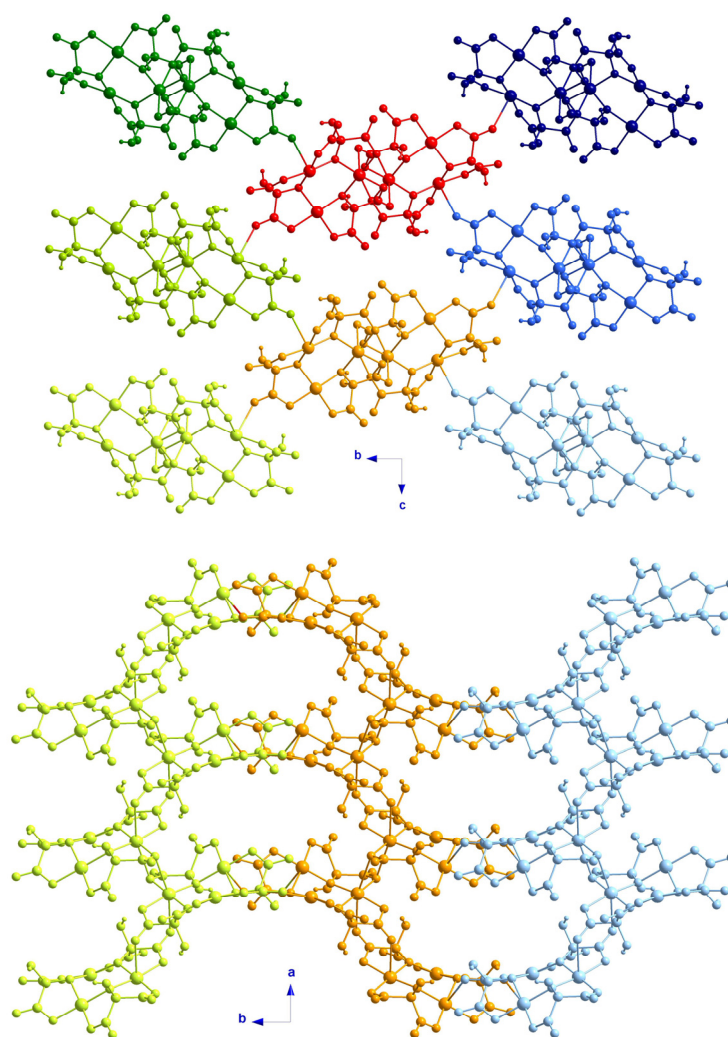


**Fig. V.13.** A perspective view along the *a* (up) and *c* axes (bottom) of the crystal packing of the three-dimensional structure of **38**. The hexanuclear entities are single carboxylate-bridged to the adjacent ones (up) while they are double carboxylate-bridged through the *c* axis (bottom, see text). Colour scheme is maintained through the change of view. Sodium atoms are omitted for clarity.

The structure of **38** is very similar to that of the previously reported<sup>10</sup> copper(II)-tartronate compound commented above. The rubidium ions act as counterions of the  $[\text{Cu}_3(\text{tartronate})_2]^{3-}$  unit in the tartronate-containing complex, but the conformation of this unit is identical to that of **38**. The structure of **37** where a  $[\text{Cu}_3(\text{O-Phmal})_3]^{3-}$  trinuclear motif is also formed, presents great similarities with **38**. The main differences between **37** and **38** include the pendant copper(II) atom coordinated to the  $[\text{Cu}_3(\text{O-Phmal})_3]^{3-}$  unit in **37** and thus, only one ammonium cation is needed to counterbalance the charges. The crystal packing is very different because it is dominated by the supramolecular interactions among the phenyl rings of the O-Phmal ligand in **37**.

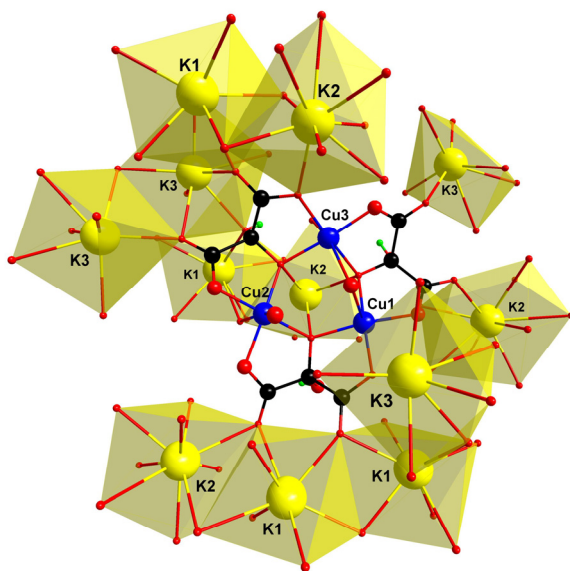


**Fig. V.14.** Central projection view of a fragment of the structure with the sodium atoms which are nearest neighbours of a trinuclear  $[\text{Cu}_3(\text{Ketomal})_3(\text{H}_2\text{O})]$  unit.

**Table V.4.** Relevant structural details for **38**<sup>a</sup>

| <i>Bond angles and lengths in the <math>\text{Cu}_3\text{O}_3</math> unit</i>                         |          |          |             |           |
|-------------------------------------------------------------------------------------------------------|----------|----------|-------------|-----------|
|                                                                                                       | Cu–O / Å | O–Cu / Å | Cu–O–Cu / ° | Cu⋯Cu / Å |
| Cu(1)–O(15)–Cu(3)                                                                                     | 1.937(2) | 1.949(2) | 110.74(11)  | 3.1974(7) |
| Cu(1)–O(11)–Cu(2)                                                                                     | 1.949(2) | 1.920(2) | 129.76(13)  | 3.5034(7) |
| Cu(2)–O(5)–Cu(3)                                                                                      | 1.909(2) | 1.934(2) | 128.31(12)  | 3.4585(8) |
| Cu(1)–O(1w)–Cu(3)                                                                                     | 2.345(3) | 2.592(3) | 80.57(9)    | 3.1974(7) |
| <i>Angles between basal planes of the copper atoms of the <math>\text{Cu}_3\text{O}_3</math> unit</i> |          |          |             |           |
| Cu(1) / Cu(2)                                                                                         |          |          |             | 36.62(7)° |
| Cu(1) / Cu(3)                                                                                         |          |          |             | 57.21(7)° |
| Cu(2) / Cu(3)                                                                                         |          |          |             | 36.82(6)° |
| <i><math>\mu</math>-oxo bridge between adjacent trinuclear units</i>                                  |          |          |             |           |
|                                                                                                       | Cu–O / Å | O–Cu / Å | Cu–O–Cu / ° | Cu⋯Cu / Å |
| Cu(2)–O(3)–Cu(2a)                                                                                     | 1.936(2) | 2.689(2) | 98.48(9)    | 3.5373(7) |

<sup>a</sup> Symmetry operations: (a)  $-x+1, -y+1, -z$ .

The temperature dependence of the  $\chi_M T$  product of **38** is presented in Figure V.15 [ $\chi_M$  is the magnetic susceptibility per three copper(II) ions]. The overall behaviour corresponds to an antiferromagnetically coupled trinuclear system.  $\chi_M T$  at room temperature is  $0.91 \text{ cm}^3 \text{ mol}^{-1} \text{ K}$ , a value which is lower than the  $1.2 \text{ cm}^3 \text{ mol}^{-1} \text{ K}$  expected for three magnetically isolated spin doublets. This feature is indicative that strong antiferromagnetic interactions between the copper atoms occur in this compound. Upon cooling, the  $\chi_M T$  value decreases monotonically up to approximately 70 K when a plateau is reached, the mean value of  $\chi_M T$  being  $0.43 \text{ cm}^3 \text{ mol}^{-1} \text{ K}$ . This value corresponds to that expected for the fully population of a low lying doublet spin state. Below 7.0 K,  $\chi_M T$  slightly decreases due to weak intermolecular antiferromagnetic interactions between the trinuclear entities.

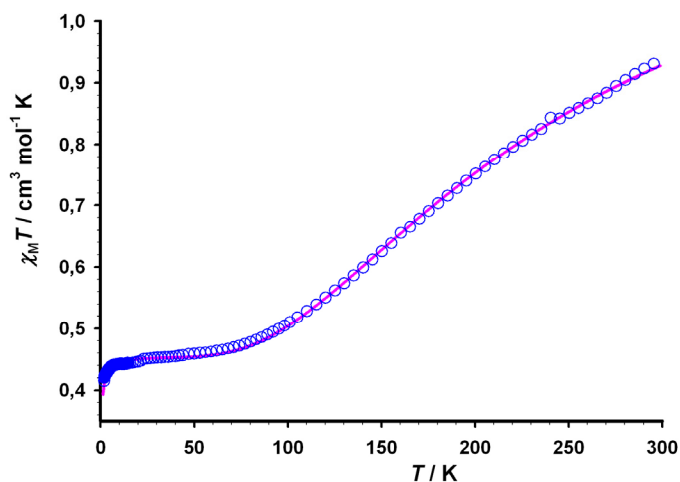


Fig. V.15.  $\chi_M T$  vs  $T$  plot for **38** under applied fields of 1 T ( $T > 22$  K) and 0.05 T ( $T < 22$  K):  
(o) experimental data, (—) best fit curve.

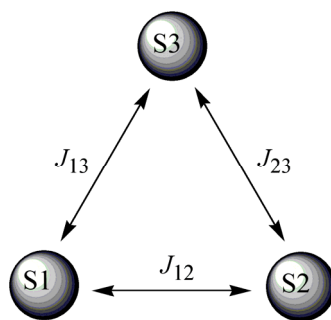
The structure of the trinuclear core of **38** exhibits two different bridges between the copper atoms. Thus, magnetically it can be viewed as an isosceles triangle of local spin doublets. Therefore, the magnetic data of compound **38** were analyzed by means of the expression for an isosceles triangular system on the base of the Hamiltonian (Scheme V.2)<sup>18</sup>

$$\hat{H} = -J_{12}(\hat{S}_1 \cdot \hat{S}_2) - J_{13}(\hat{S}_1 \cdot \hat{S}_3) - J_{23}(\hat{S}_2 \cdot \hat{S}_3) \text{ where } J_{13} = J_{23}$$

The solution of this Hamiltonian and the subsequent introduction of the eigenvalues into the van Vleck formula lead to<sup>17</sup>

$$\chi_M = \frac{N\beta^2 g^2}{4k_B(T - \theta)} \left[ \frac{\exp(-J_{13}/k_B T) + \exp(-J_{12}/k_B T) + 10 \exp(J_{13}/2k_B T)}{\exp(-J_{13}/k_B T) + \exp(-J_{12}/k_B T) + 2 \exp(J_{13}/2k_B T)} \right]$$

A mean molecular field term ( $\theta$ ) is included to evaluate the intermolecular interactions and the other symbols have their usual meanings. Best least-square fit parameters are  $g = 2.20(1)$ ,  $J_{13} = J_{23} = -194(1) \text{ cm}^{-1}$ ,  $J_{12} = -3(4) \text{ cm}^{-1}$ ,  $\theta = -0.20(1) \text{ cm}^{-1}$  and  $R = 3 \times 10^{-5}$ . The calculated curve matches very well the experimental data in the whole temperature range as can be seen in Figure V.15.



Scheme V.2

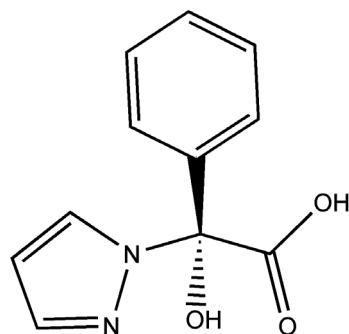
According to the results of the fit, we have two magnetic coupling constants in **38** that differ considerably in intensity. This is in agreement with previous studies performed for hydroxo-bridged copper(II) dinuclear complexes.<sup>11</sup> The magnitude and the nature of the Cu...Cu exchange coupling are strongly dependent on structural parameters such as the Cu–O–Cu angle and the Cu...Cu interatomic distance.<sup>11</sup> These studies have shown that the coupling is ferromagnetic for angles lower than  $98^\circ$  whereas it is antiferromagnetic for greater values. A similar behaviour has been observed for other compounds with other bridges. Compound **38** exhibits two long Cu...Cu distances [3.50 and 3.46 Å] with large Cu–O–Cu angles [ $129.73^\circ$ ,  $128.30^\circ$ ] and a short Cu...Cu distance [3.20 Å] with an aqua- [the Cu–O–Cu angle being  $80.93^\circ$ ] and a  $\mu$ -oxo [the Cu–O–Cu angle is  $110.75^\circ$ ] bridges. According to the literature, the former corresponds to the strong antiferromagnetic coupling.<sup>11</sup> In the latter, the aqua-bridge would lead to a ferromagnetic coupling whereas the  $\mu$ -oxo one would lead to antiferromagnetic coupling, their combination leading to a weak magnetic interaction ( $-3(4) \text{ cm}^{-1}$ ).

The simplicity of this compound has allowed us to determine the value of the magnetic coupling constants and the spin of the ground state of the triangular tricopper system. In this compound, the magnetic coupling is much stronger than those of the previous malonate derivatives. Moreover, this complex has a non-zero ground spin state that is fully populated at  $T < 50 \text{ K}$ . But the more interesting feature is that this compound can potentially act as a hexadentate ligand with oxygen atoms in a good orientation to accept

other paramagnetic centres. So, this trinuclear compound  $[\text{Cu}_3\text{L}_3]^{3-}$  can be seen as a new precursor that opens a new door in the field of molecular magnetism and that may lead to families of molecular magnets similar to those prepared with the tris-oxalato species  $[\text{Cr}(\text{Ox})_3]^{3-}$  and  $[\text{Fe}(\text{Ox})_3]^{3-}$ .<sup>19</sup>

### V.1.3.3. $[\text{Cu}_4(\text{pz})_4(\text{OH-ppac})_2(\text{H}_2\text{O})_4]$ (39).

A next step from the phenylmalonate ligand consists of making it chiral. New phenomena are expected for the optically active magnetic materials and a small magneto-chiral dichroism effect has been observed in a chiral paramagnetic material.<sup>20-21</sup> The transformation of the Phmal into a chiral ligand could be made by the substitution of one of the carboxylate groups, this simple change were argued as the origin of the chiral structures in copper(II) phenylmalonate complexes, as explained in Chapter IV. In this case, a new chiral ligand was synthesized by serendipity and its copper(II) complex was fully characterized. The racemic mixture of 2-hydroxy-2-phenyl-2-(1-pyrazolyl)-acetate (OH-ppac) comes from the substitution of a carboxylate group by a pyrazolyl one and the introduction of a hydroxyl group in the remaining hydrogen atom of the methylene carbon of the phenylmalonate ligand (Scheme V.3). The chiral OH-ppac ligand is apparently formed by a one-pot reaction of sodium phenylmalonate with pyrazole in a mixture of water and methanol in the presence of copper(II) ions. This addition of a group at the position 1 of the pyrazole ring had been observed before. An addition reaction of a ethanoyl group to a pyrazole similar to that found here was reported by Ten Hoedt et al.<sup>22</sup> Moreover, the



Scheme V.3

**Table V.5.** Crystallographic data for **39**

|                                         |                                                                       |
|-----------------------------------------|-----------------------------------------------------------------------|
| Formula                                 | $\text{C}_{17}\text{H}_{18}\text{O}_5\text{N}_6\text{Cu}_2$           |
| FW                                      | 513.42                                                                |
| Crystal system                          | Triclinic                                                             |
| Space group                             | $P-1$                                                                 |
| $a/\text{\AA}$                          | 8.5718 (4)                                                            |
| $b/\text{\AA}$                          | 9.9898 (6)                                                            |
| $c/\text{\AA}$                          | 12.0422 (5)                                                           |
| $\alpha/^\circ$                         | 91.597 (4)                                                            |
| $\beta/^\circ$                          | 91.512 (5)                                                            |
| $\gamma/^\circ$                         | 107.400 (4)                                                           |
| $V/\text{\AA}^3$                        | 982.96 (9)                                                            |
| $Z$                                     | 2                                                                     |
| $\mu(\text{Mo K}\alpha)/\text{cm}^{-1}$ | 22.06                                                                 |
| $T/\text{K}$                            | 293 (2)                                                               |
| $\rho_{\text{calc}}/\text{g cm}^{-3}$   | 1.721                                                                 |
| $\lambda/\text{\AA}$                    | 0.71073                                                               |
| Index ranges                            | $-8 \leq h \leq 11,$<br>$-12 \leq k \leq 10,$<br>$-14 \leq l \leq 15$ |
| Indep. reflect. ( $R_{\text{int}}$ )    | 4420 (0.0315)                                                         |
| Obs. reflect. [ $I > 2\sigma(I)$ ]      | 2974                                                                  |
| Parameters                              | 336                                                                   |
| Goodness-of-fit                         | 1.013                                                                 |
| $R$ [ $I > 2\sigma(I)$ ]                | 0.0442                                                                |
| $R_w$ [ $I > 2\sigma(I)$ ]              | 0.0838                                                                |
| $R$ (all data)                          | 0.0872                                                                |
| $R_w$ (all data)                        | 0.0953                                                                |

electron withdrawing effect of the phenyl group makes the central carbon atom of the phenylmalonate ligand a good candidate for a nucleophilic attack from the pyrazolyl and hydroxyl groups.

The crystal structure of  $[\text{Cu}_4(\text{pz})_4(\text{O-ppac})_2(\text{H}_2\text{O})_4]$  (**39**) (Table V.5) consists of neutral pyrazolate-bridged tetranuclear copper(II) entities (Figure V.16). The tetranuclear copper(II) unit presents a  $C_i$  point group symmetry, thus, only half of the molecule is crystallographically independent and the two enantiomers of the O-ppac ligand are present

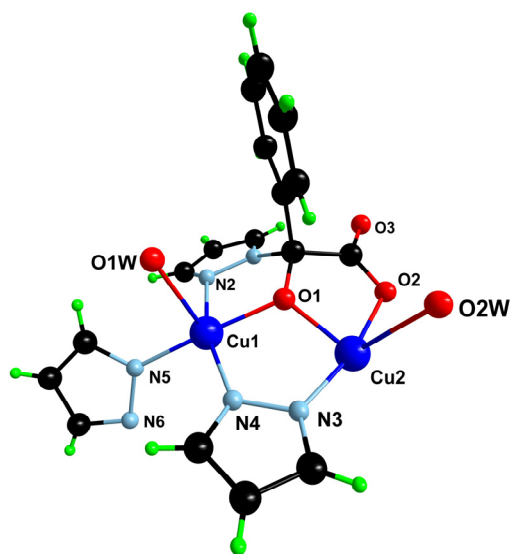


Fig. V.16. A view of the asymmetric unit of the structure of **39** along with the numbering scheme.

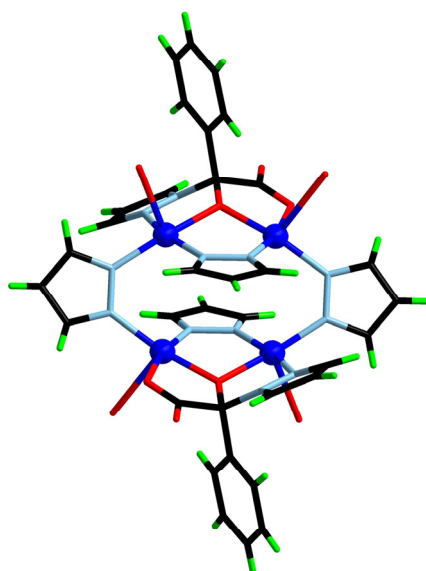


Fig. V.17. A view of the tetranuclear molecules formed by an inversion centre in **39**.



in the same tetranuclear molecule. This asymmetric unit is constituted by a copper(II) dimer simultaneously linked by the deprotonated hydroxo group of the O-ppac ligand and by the pyrazolate ligand. Two dinuclear units are connected through two pyrazolate bridges affording the tetranuclear complex (Figure V.17). The four copper(II) atoms are arranged at the corners of a parallelogram whose edges are 3.2995(2) and 3.5632(2) Å for Cu(1)⋯Cu(2) and Cu(1)⋯Cu(2a), respectively [(a) = -x, -y+2, -z+2]. The angles at the corners are 92.02(1)° [Cu(2)–Cu(1)–Cu(2a)] and 87.98(2)° [Cu(1)–Cu(2)–Cu(1a)]. All four sides are bridged by pyrazolate ligands, being the short ones additionally bridged by the deprotonated hydroxo group of the O-ppac ligand. Weak  $\pi$ -type interactions involving the phenyl and the pyrazolyl groups connect the discrete entities to build a 3D-supramolecular network [(pz)C–H⋯centroid(O-ppac) distances and angle being 2.87(3) Å (H⋯centroid), 3.611(3) Å and 152(3)° (C–H⋯centroid)].

The two crystallographically independent copper(II) ions exhibit somewhat distorted environments, the  $\tau$  values<sup>5</sup> being 0.16 and 0.028 for Cu(1) and Cu(2), respectively. Two nitrogen atoms from two different pyrazolate ligands [N(4) and N(5)] and a O-ppac nitrogen and oxygen atoms [N(2) and O(1)] build the basal plane of Cu(1) [average equatorial bond length for Cu(1) being 1.961(2) Å] while a water molecule occupies the apical position [Cu(1)–O(1w) is 2.465(4) Å]. The basal plane of the Cu(2) is formed by two pyrazolate nitrogen atoms [N(3) and N(6a)] and two O-ppac oxygen atoms [O(1) and O(2); the average equatorial bond length for Cu(2) is 1.948(2) Å] while a water molecule fills the apical position [Cu(2)–O(2w) being 2.624(4) Å]. The copper atoms are shifted toward the apical positions by 0.1286(3) and 0.0793(3) Å for Cu(1) and Cu(2), respectively.

The O-ppac ligand is chiral (see Scheme V.3) both *R*- and *S*-O-ppac being present in the tetranuclear molecule. The O-ppac group acts as a bis-bidentate ligand [through N(2) and O(1) to Cu(1) and through O(1) and O(2) to Cu(2), the bite angles being 80.17(9)° and 82.82(9)°, respectively]. The pyrazolate groups act as bis-monodentate ligands.

The crystal structure of **39** is very similar to those of three related pyrazolate-bridged tetranuclear copper(II) complexes previously reported.<sup>22-24</sup> The structure of the tetranuclear core is close in the three complexes, the four pyrazolate ligands acting as bridges of the four copper(II) ions grouped in two pairs by an alkoxo bridge from a second ligand (OH-ppac (**37**), 1-(1-ethanoyl)-5-methylpyrazolato<sup>22</sup>,...). Surprisingly, in the syntheses reported by Ten Hoedt,<sup>22</sup> and by Manzur,<sup>24</sup> *in situ* additions to the initial reagents occur during the synthetic process, as in **37**.

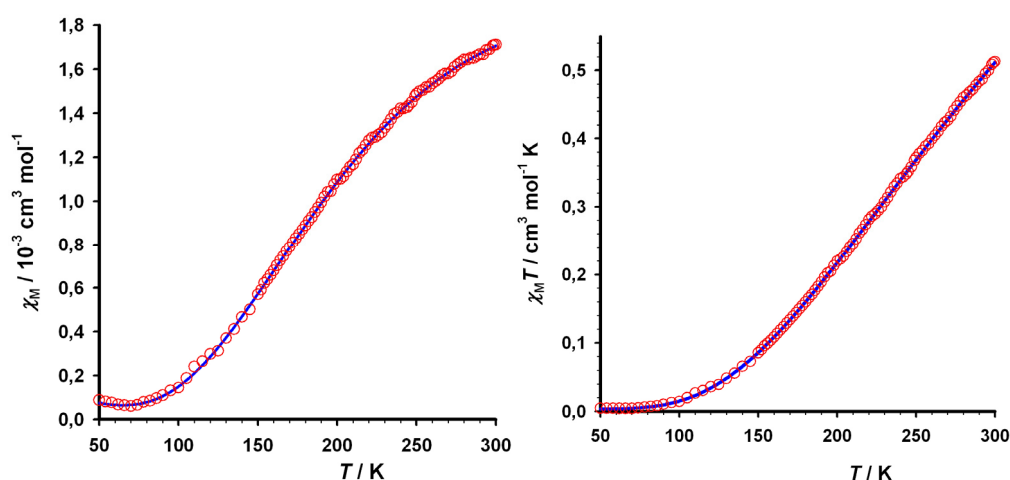
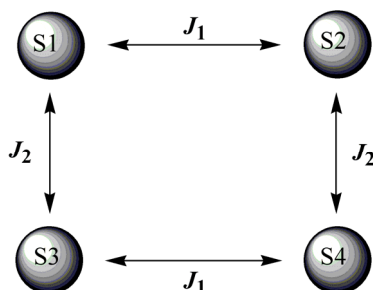


Fig. V.18.  $\chi_M$  (left) and  $\chi_M T$  (right) vs  $T$  plot for **39** under an applied field of 1 T: (o) experimental data, (—) best fit curve (see text).

The magnetic properties of **39** under the form of  $\chi_M$  and  $\chi_M T$  vs.  $T$  plot [ $\chi_M$  is the magnetic susceptibility per four copper(II) ions] are depicted in Figure V.18.  $\chi_M T$  at room temperature is  $0.51 \text{ cm}^3 \text{ mol}^{-1} \text{ K}$ , a value which is much smaller than what is expected for four magnetically isolated spin doublets indicating strong antiferromagnetic coupling between the metal centres. Upon cooling,  $\chi_M T$  decreases monotonically to reach values below  $0.005 \text{ cm}^3 \text{ mol}^{-1} \text{ K}$  at 75 K. This is indicative of an overall antiferromagnetic interaction. The  $\chi_M$  vs.  $T$  plot does not show any maxima. Certainly, it must occur at temperatures above 300 K.

Considering the structure of **39**, one sees tetranuclear entities with two different bridges: (i) a double exchange pathway which consists of a  $\mu$ -alkoxo and a pyrazolate bridge ( $J_1$ ); and (ii) a single pyrazolate bridge ( $J_2$ ). Since the tetranuclear unit is generated by an inversion centre, it could be viewed as a rectangle with two different magnetic coupling parameters (Scheme V.4). The isotropic spin Hamiltonian can be written as



Scheme V.4

$$\hat{H} = -J_1(\hat{S}_1 \cdot \hat{S}_2 + \hat{S}_3 \cdot \hat{S}_4) - J_2(\hat{S}_1 \cdot \hat{S}_3 + \hat{S}_2 \cdot \hat{S}_4)$$

Least-squares fit through a computational diagonalization of this Hamiltonian leads to  $g = 2.08(2)$ ,  $J_1 = -650(5) \text{ cm}^{-1}$ ,  $J_2 = -200(9) \text{ cm}^{-1}$ ,  $\rho = 0.01(1)$  and  $R = 1.0 \times 10^{-3}$ , where the  $\rho$  parameter was included to take into account the paramagnetic impurities (which are responsible for the Curie tail at very low temperatures). The calculated curve matches very well the experimental data in the whole temperature range. It deserves to be noted that the value for  $J_2$  has to be taken with caution because the fit through the Bleaney-Bowers equation for a copper(II) dimer also gave good results. Anyway, the obtained value for  $J_2$  is in agreement with the previous values reported for pyrazolate bridges.<sup>25</sup> The magnetic coupling for the  $\mu$ -alkoxo- $\mu$ -pyrazolate bridge [ $J_1 = -650(5) \text{ cm}^{-1}$ ] also agrees with previously reported values for such bridging unit [ $J$  ranging from  $-164$  to  $-770 \text{ cm}^{-1}$ ].<sup>26-27</sup>

The great difference between the two bridges comes from three factors: (i) the out-of-plane configuration of the pyrazolate in the single bridge ( $J_2$ ) which prevents a better overlap between the magnetic orbitals; (ii) the large Cu–O–Cu angle for the  $\mu$ -alkoxo bridge leads to a strong antiferromagnetic interaction according to the linear dependence between this angle and the magnetic coupling,<sup>11</sup> and (iii) the complementarity between the  $\mu$ -alkoxo and the pyrazolate bridges in the double bridge ( $J_1$ ) could produce that the two strong magnetic interactions were added to provide a stronger one.<sup>27</sup>

Finally, we would like to emphasize the interesting complexes which could be prepared with the OH-ppac ligand, when it will be synthesized in a controlled way and enantiomerically pure. This is a chiral ligand which chelates two metal ions connecting them through a  $\mu$ -alkoxo bridge which is able to mediate strong magnetic interactions. Thus, it could be possible to prepare enantiomerically pure high-spin molecules with this ligand in a very near future.

#### V.1.4. References

- (a) U. Lepore, G. C. Lepore and P. Ganis, *Acta Cryst., Sect. B* **1975**, B31, 2874; (b) Y. Yokomori and D. J. Hodgson, *Int. J. Pept. Protein Res.* **1988**, 31, 289; (c) J. V. Beach and K. J. Shea, *J. Am. Chem. Soc.* **1994**, 116, 379.
- (a) Y. Yokomori and D. J. Hodgson, *Inorg. Chem.* **1988**, 27, 2008; (b) Y. Yokomori, K. A. Flaherty and D. J. Hodgson, *Inorg. Chem.* **1988**, 27, 2300.
- (a) W. Guan, J.-Y. Sun, X.-D. Zhang and Q.-T. Liu, *Chem. J. Chin. Uni.* **1998**, 19, 5; (b) A. Castiñeiras, A. G. Sicilia-Zafra, J. M. González-Pérez, D. Choquesillo-Lazarte and J. Nicolás-Gutiérrez, *Inorg. Chem.* **2002**, 41, 6956.
- More detailed x-ray measurements on better quality crystals are needed since some twinning has been found in the reflections set obtained, and only isotropic refinement could be made. This is the reason why the crystallographic details are not listed in a Table.
- A. W. Addison, T. N. Rao, J. Reedijk, J. van Rijn and G. C. Verschoor, *Dalton Trans.* **1984**, 1349.

- 6 R. Navarro, *Application of High- and Low-Temperature Series Expansions to Two-dimensional Magnetic Systems*, de Jongh, L. J.; Ed., Kluwer Academic Publishers, The Netherlands, **1990**.
- 7 J. Pasán, F. S. Delgado, Y. Rodríguez-Martín, M. Hernández-Molina, C. Ruiz-Pérez, J. Sanchiz, F. Lloret and M. Julve, *Polyhedron* **2003**, *22*, 2143.
- 8 C. Ruiz-Pérez, Y. Rodríguez-Martín, M. Hernández-Molina, F. S. Delgado, J. Pasán, J. Sanchiz, F. Lloret and M. Julve, *Polyhedron*, **2003**, *22*, 2111.
- 9 F. S. Delgado, J. Sanchiz, C. Ruiz-Pérez, F. Lloret and M. Julve, *Inorg. Chem.* **2003**, *42*, 5938.
- 10 A. V. Ablov, G. A. Popovich, G. I. Dimitrova, G. A. Kiosse, I. F. Bourshteyn, T. I. Malinovskii and B. M. Shchedrin, *Dokl. Akad. Nauk SSSR (Proc. Nat. Acad. Sci. USSR)* **1976**, *229*, 611.
- 11 (a) P. J. Hay, J. C. Thibeault and R. Hoffman, *J. Am. Chem. Soc.* **1975**, *97*, 4884. (b) E. Ruiz, P. Alemany, S. Álvarez and J. Cano, *Inorg. Chem.* **1997**, *36*, 3985. (c) E. Ruiz, P. Alemany, S. Álvarez and J. Cano, *J. Am. Chem. Soc.* **1997**, *119*, 1927. (d) W. H. Crawford, H. W. Richardson, J. R. Wasson, D. J. Hodgson and W. E. Hatfield, *Inorg. Chem.* **1976**, *15*, 2107.
- 12 E. Ruiz, S. Alvarez and P. Alemany, *Chem. Commun.* **1998**, 2767.
- 13 M. Inoue and M. Kubo, *Inorg. Chem.* **1970**, *9*, 2311.
- 14 E. Colacio, J. M. Domínguez-Vera, M. Ghazi, R. Kivekäs, M. Klinga and J. M. Moreno, *Eur. J. Inorg. Chem.* **1999**, 441.
- 15 E. Ruiz, S. Alvarez, A. Rodríguez-Fortea, P. Alemany, Y. Pouillon and C. Massobrio, *Magnetism: Molecules to Materials II*, ed. J. S. Miller and M. Drillon, Wiley-VCH Verlag GmbH, Weinheim, Germany, **2001**, pp. 227–279.
- 16 R. Hämäläinen, M. Ahlgren and U. Turpeinen, *Acta Cryst., Sect. B* **1982**, *38*, 1577.
- 17 J. N. Brown and L. M. Trefonas, *Inorg. Chem.* **1973**, *312*, 1730.
- 18 E. Dixon-Estes, W. E. Estes, R. P. N. Scaringe, W. E. Hatfield and D. J. Hodgson, *Inorg. Chem.* **1975**, *14*, 2564.
- 19 J. P. Costes, F. Dahan and J. P. Laurent, *Inorg. Chem.* **1985**, *24*, 1018.
- 20 E. Escrivá, J. Server-Carrió, L. Lezama, J. V. Folgado, J. L. Pizarro, R. Ballesteros and B. Abarca, *Dalton Trans.* **1997**, 2033.
- 21 (a) B. Chiari, J. H. Helms, O. Piovesana, T. Tarantelli and P. F. Zanazzi, *Inorg. Chem.* **1986**, *25*, 2408. (b) B. Chiari, J. H. Helms, O. Piovesana, T. Tarantelli and P. F. Zanazzi, *Inorg. Chem.* **1986**, *25*, 870. (c) B. Chiari, W. E. Hatfield, O. Piovesana, T. Tarantelli and P. F. Zanazzi, *Inorg. Chem.* **1983**, *22*, 1468. (d) L. K. Thompson, S. K. Mandal, S. S. Tandon, J. N. Bridson and M. K. Park, *Inorg. Chem.* **1996**, *35*, 3117. (e) A. Pasini, F. Demartin, O. Piovesana, B. Chiari, A. Cinti and O. Crispu, *Dalton Trans.* **2000**, 3467. (f) Y. Xie, H. Jiang, A. S. C. Chan, Q. Liu, X. Xu, C. Du and Y. Zhu, *Inorg. Chim. Acta* **2002**, *333*, 138.
- 22 K. Kambe, *Phys. Soc. Jpn.* **1950**, *5*, 48.
- 23 J. H. van Vleck, *The Theory of Electric and Magnetic Susceptibilities*, Oxford University Press, Oxford, **1932**.
- 24 (a) S. Ferrer, F. Lloret, I. Bertomeu, G. Alzuet, J. Borrás, S. García-Granda, M. Liu-Gonzalez and J. G. Haasnoot, *Inorg. Chem.* **2002**, *41*, 5821. (b) B. Cage, F. A. Cotton, N. S. Dalal, E. A. Hillard, B. Rakvin and C. M. Ramsey, *J. Am. Chem. Soc.* **2003**, *125*, 5270. (c) I. Gautier-Luneau, D. Phanon, C. Duboc, D. Luneau and J. L. Pierre, *Dalton Trans.* **2005**, 3795. (d) L. Gutierrez, G. Alzuet, J. A. Real, J. Cano, J. Borrás and A. Castineiras, *Eur. J. Inorg. Chem.* **2002**, 2094. (e) X. M. Liu, M. P. de Miranda, E. J. L. McInnes, C. A. Kilner and M. A. Halcrow, *Dalton Trans.* **2004**, 59. (f) H. Lopez-Sandoval, R. Contreras, A. Escuer, R. Vicente, S. Bernes, H. Noth, G. J. Leigh and N. Barba-Behrens, *Dalton Trans.* **2002**, 2648. (g) X. H. Mo, K. M. S. Etheredge, S. J. Hwu and Q. Huang, *Inorg. Chem.* **2006**, *45*, 3478. (h) V. Pashchenko, B. Brendel, B. Wolf, M. Lang, K. Lyssenko, O. Shchegolikhina, Y. Molodtsova, L. Zherlitsyna, N. Auner, F. Schutz, M. Kollar, P. Kopietz and N. Harrison, *Eur. J. Inorg. Chem.* **2005**, 4617. (i) M. P. Suh, M. Y. Han, J. H. Lee, K. S. Min, C. Hyeon, *J. Am. Chem. Soc.* **1998**, *120*, 3819.
- 25 M. Pilkington and S. Decurtins, *Magnetism: Molecules to Materials II*, ed. J. S. Miller and M. Drillon, Wiley-VCH Verlag GmbH, Weinheim, Germany, **2001**, pp. 339–356.
- 26 G. Wagniere and A. Mejer, *Chem. Phys. Lett.* **1984**, *110*, 546.
- 27 G. L. J. A. Rikken and E. Raupach, *Nature* **1997**, *390*, 493.

- 28 R. W. M. ten Hoedt, F. B. Hulsbergen, G. C. Verschoor and J. Reedijk, *Inorg. Chem.*, **1982**, *21*, 2369.
- 29 (a) E. Kavlakoglu, A. Elmali, Y. Elerman and I. Svoboda, *Polyhedron* **2002**, *21*, 1539. (b) Y. Elerman, E. Kavlakoglu and A. Elmali, *Z. Naturforsch.* **2002**, *57a*, 919.
- 30 J. Manzur, A. M. García, M. T. Garland, V. Acuña, O. González, O. Peña, A. M. Atria and E. Spodine, *Polyhedron*, **1996**, *15*, 821.
- 31 (a) M. G. B. Drew, P. C. Yates, F. S. Esho, J. Trocha-Grimshaw, A. Lavery, K. P. McKillop, S. M. Nelson and J. Nelson, *Dalton Trans.* **1988**, 2995. (b) T. Kamiyuki, H. Okawa, N. Matsumoto and S. Kida, *Dalton Trans.* **1990**, 195. (c) T. Kamiyuki, H. Okawa, H. Inoue, N. Matsumoto, M. Kodaera, S. Kida, *J. Coord. Chem.* **1991**, *23*, 201. (d) J. C. Bayon, P. Esteban, G. Net, P. G. Rasmussen, K. N. Baker, C. W. Hahn and M. M. Gumz, *Inorg. Chem.* **1991**, *30*, 2572. (e) J. Pons, X. López, J. Casabó, F. Teixidor, A. Caubet, J. Rius and C. Miravittles, *Inorg. Chim. Acta* **1992**, *195*, 61. (f) F. Degang, W. Guoxiong, Z. Zongyan, Z. Xiangge, *Trans. Met. Chem.* **1994**, *19*, 592. (g) V. P. Hanot, T. D. Robert, J. Kolnaar, J. G. Haasnoot, J. Reedijk, H. Kooijman and A. L. Spek, *Dalton Trans.* **1996**, 4275. (h) H. Matsushima, H. Hamada, K. Watanabe, M. Koikawa and T. Tokii, *Dalton Trans.* **1999**, 971. (i) E. Spodine, A. M. Atria, J. Valenzuela, J. Jalocha, J. Manzur, A. M. García, M. T. Garland, O. Peña, J. Y. Saillard, *Dalton Trans.* **1999**, 3029. (j) M. F. Iskander, T. E. Khalil, W. Haase, R. Werner, I. Svoboda and H. Fuess, *Polyhedron* **2001**, 2787. (k) B. Mernari, F. Abraham, M. Lagrenee, M. Drillon and P. Legoll, *Dalton Trans.* **1993**, 1707. (l) M. K. Ehlert, S. J. Rettig, A. Storr, R. C. Thompson and J. Trotter, *Can. J. Chem.* **1992**, *70*, 2161.
- 32 (a) J. Ackermann, F. Meyer, E. Kaifer and H. Pritzkow, *Chem. Eur. J.* **2002**, *8*, 247. (b) W. Mazurek, B. J. Kennedy, K. S. Murray, M. J. O'Connor, J. R. Rodgers, M. R. Snow, A. Wed and G. P. R. Zwack, *Inorg. Chem.* **1985**, *24*, 3258. (c) T. N. Doman, D. E. Williams, J. F. Banks, R. M. Buchanan, H.-R. Chang, R. J. Webb and D. N. Hendrickson, *Inorg. Chem.* **1990**, *29*, 1058. (d) Y. Nishida and S. Kida, *Inorg. Chem.* **1988**, *27*, 447. (e) K. Nonoyama, W. Mori, K. Nakajima and M. Nonoyama, *Polyhedron*, **1997**, *16*, 3815. (f) H. Nie, S. M. J. Aubin, M. S. Mashuta, R. A. Porter, J. F. Richardson, D. N. Hendrickson and R. M. Buchanan, *Inorg. Chem.* **1996**, *35*, 3325. (g) H. Kara, Y. Elerman and K. Prout, *Z. Naturforsch.* **2000**, *55b*, 796. (h) H. Kara, Y. Elerman and K. Prout, *Z. Naturforsch.* **2001**, *56b*, 719.
- 33 E. Escrivá, J. García-Lozano, J. Martínez-Lillo, H. Nuñez, J. Server-Carrió, L. Soto, R. Carrasco and J. Cano, *Inorg. Chem.* **2003**, *42*, 8328.
- 34 P. J. Hay, J. C. Thibeault and R. Hoffman, *J. Am. Chem. Soc.* **1975**, *97*, 4884. (b) E. Ruiz, P. Alemany, S. Álvarez and J. Cano, *Inorg. Chem.* **1997**, *36*, 3985. (c) E. Ruiz, P. Alemany, S. Álvarez and J. Cano, *J. Am. Chem. Soc.* **1997**, *119*, 1927. (d) W. H. Crawford, H. W. Richardson, J. R. Wasson, D. J. Hodgson and W. E. Hatfield, *Inorg. Chem.* **1976**, *15*, 2107.

## V.2. Porous Materials

Recently, remarkable progress has been made in the area of microporous coordination polymers, because of their diverse topologies and fascinating properties in areas such as gas storage, anion exchange and catalysis.<sup>1</sup> The microporous coordination polymers have unique characteristics: framework regularity, high porosity, flexibility, and designed pore surface, which can create high-performance pores and also unprecedented porous functionalities. Coordination polymers constructed from transition metal ions and bridging organic ligands have afforded new types of robust crystals with high degrees of porosity.<sup>2</sup> In the course of our investigations, we have focused on the development of new metal-organic materials with interesting magnetic properties,<sup>3</sup> whereas the other physical properties our materials could present are considered anecdotic. Recently, we have prepared a series of compounds with a specific coordination framework exhibiting channels, cavities and pores which also retain interesting magnetic behaviour. These multifunctional materials which are able to combine two or more properties in a unique framework could be the first steps for future applications.

Among the complexes presented in this Thesis, a few of them present a great void volume in their structure. The void volume is usually filled by solvent molecules and, to be porous, the framework not only has to be stable after the desolvation, but it has to be able to adsorb reversibly guest molecules. Thus, the complexes presented here are under a porous investigation process, but they suggest a fascinating field for future research. Some examples are:



**25** exhibits channels filled with terminal 4,4'-bpy ligands (Figure V.19).

(ii)  $[\text{Cu}(\text{bpe})(\text{Memal})]_n \cdot 3n\text{H}_2\text{O}$  (**27**) where rectangular pores of dimensions *ca.* 15 x 14 Å<sup>2</sup> occur which are filled by water molecules and being three dimensional it is one of the most promising complexes to present porous properties (Figure V.20).

(iii)  $[\text{Cu}(\text{Etmal})(\text{H}_2\text{O})]_n \cdot 1.65n\text{H}_2\text{O}$  (**30**) which exhibits hydrophilic channels of 9.5 Å diameter (Figure V.21), the surface of the channels being carboxylate bridged copper(II) helices. The pore environment is then chiral, adding an outstanding feature to the material; moreover, this complex exhibits magnetic order, becoming a chiral magnet with high void volume, such a combination of interesting properties makes us to deposit higher expectations on this material.

(iv)  $\text{Na}_6[\text{Cu}(\text{Etmal})_2(\text{H}_2\text{O})]_3 \cdot 5\text{H}_2\text{O}$  (**31**) and  $\{\text{Na}[\text{Cu}(\text{H}_2\text{O})][\text{Cu}(\text{Etmal})_2(\text{H}_2\text{O})]\}_{3n} \cdot n(\text{NO}_3)(\text{H}_2\text{O})(\text{EtO})_2$  (**32**). These two complexes exhibit hydrophobic channels where the ethyl groups of the ethylmalonate ligands form the surfaces of the pores (Figure V.22).

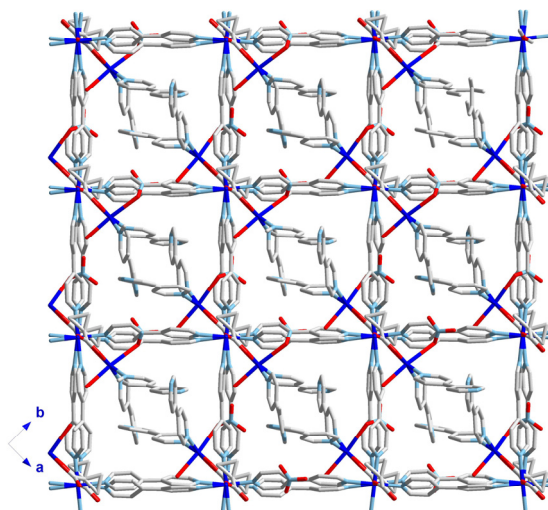


Fig. V.19. A perspective view of the three-dimensional structure of **25**.

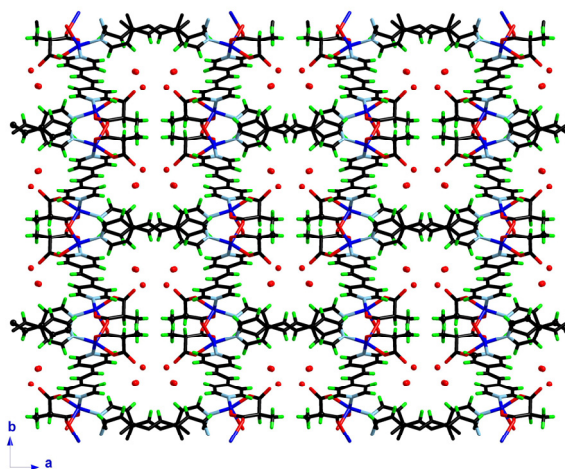


Fig. V.20. A view along the *c* axis of the 3D structure of **27**.

Finally, we can design new coordination polymers from these complexes with interesting topologies varying adequately the ligands used. For example, the replacement of the bpe ligand in **27** by 1,1'-azobispyridine or the more flexible 1,2-bis(4-pyridyl)-ethane, produce the same crystal packing with a different size of the channel. New interesting materials are expected along this line.

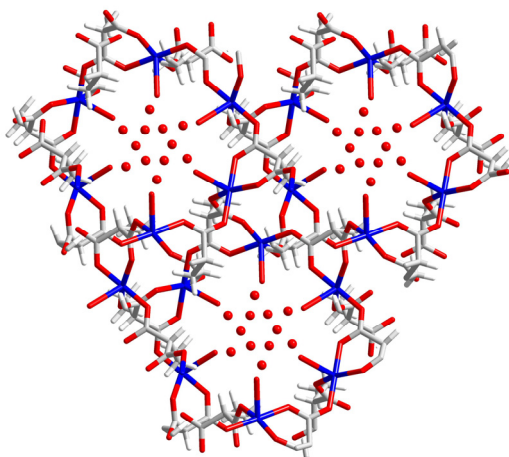


Fig. V.21. A view along the *c* axis of the 3D structure of **30**.

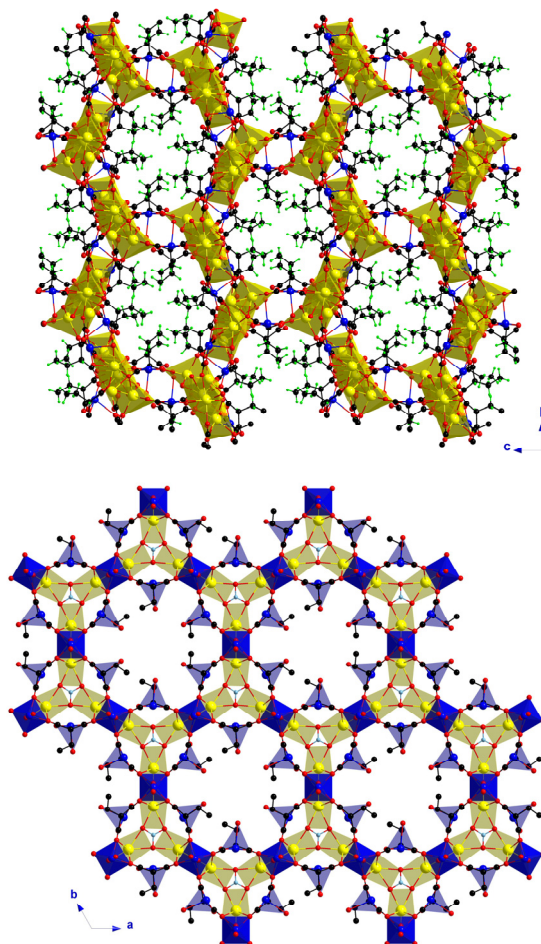


Fig. V.22. Perspective views of the crystal packing of **31** (up) showing the hydrophobic channels running in the *a* direction and the 3D structure of **32** (bottom) with the polyhedra scheme showing the channels running in the *c* direction.



### V.2.1. References

- 1 (a) S. Kitagawa, R. Kitaura and S. Noro, *Angew. Chem. Int. Ed.*, **2004**, *43*, 2334. (b) S. Kitagawa and K. Uemura, *Chem. Soc. Rev.* **2005**, *34*, 109. (c) O. M. Yaghi, H. Li, C. Davis, D. Richardson and T. L. Groy, *Acc. Chem. Res.* **1998**, *31*, 474. (d) S. L. James, *Chem. Soc. Rev.* **2003**, *32*, 276. (e) O. M. Yaghi, M. O’Keeffe, N. W. Ockwig, H. K. Chae, M. Eddaoudi and J. Kim, *Nature*, **2003**, *423*, 705. (f) G. Férey, C. Mellot-Draznieks, C. Serre and F. Millange, *Acc. Chem. Res.* **2005**, *38*, 217. (g) B. Moulton and M. J. Zaworotko, *Chem. Rev.* **2001**, *101*, 1629. (h) D. Bradshaw, J. B. Claridge, E. J. Cussen, T. J. Prior and M. M. Rosseinsky, *Acc. Chem. Res.* **2005**, *38*, 273. (i) E. Y. Lee, S. Y. Jang and M. P. Suh, *J. Am. Chem. Soc.* **2005**, *127*, 6374. (j) C. J. Janiak, *Dalton Trans.* **2003**, 2781. (k) E. Deithers, V. Bulach and M. W. Hosseini, *Chem. Commun.* **2005**, 3906.
- 2 (a) S. S.-Y. Chui, S. M.-F. Lo, J. P. H. Charmant, A. G. Orpen and I. D. Williams, *Science*, **1999**, *283*, 1148. (b) H. Li, M. Eddaoudi, M. O’Keeffe and O. M. Yaghi, *Nature*, **1999**, *402*, 276. (c) H. Li, M. Eddaoudi, T. L. Groy and O. M. Yaghi, *J. Am. Chem. Soc.* **1998**, *120*, 8571. (d) M. Kondo, T. Okubo, A. Asami, S. Noro, T. Yoshitomi, S. Kitagawa, T. Ishii, H. Matsuzaka and K. Seki, *Angew. Chem. Int. Ed.* **1999**, *38*, 140. (e) E. Barea, J. A. R. Navarro, J. M. Salas, N. Masciocchi, S. Galli and A. Sironi, *J. Am. Chem. Soc.* **2004**, *126*, 3014. (f) S. Noro, S. Kitagawa, M. Kondo and K. Seki, *Angew. Chem. Int. Ed.* **2000**, *39*, 2082.
- 3 (a) J. Pasán, F. S. Delgado, Y. Rodríguez-Martín, M. Hernández-Molina, C. Ruiz-Pérez, J. Sanchiz, F. Lloret and M. Julve, *Polyhedron* **2003**, *22*, 2143. (b) C. Ruiz-Pérez, Y. Rodríguez-Martín, M. Hernández-Molina, F. S. Delgado, J. Pasán, J. Sanchiz, F. Lloret and M. Julve, *Polyhedron*, **2003**, *22*, 2111.

### V.3. Chiral Materials

As chirality is an element of life, there is a great interest in the formation of chiral coordination polymers.<sup>1</sup> It is expected that chiral supramolecular architectures play an important role in optical devices and chiral microporous materials are envisioned for enantiomeric separation or chiral synthesis.<sup>2</sup> Recent success in the design and synthesis of novel materials based on metal-organic coordination networks<sup>3</sup> has prompted the examination of supramolecular engineering of noncentrosymmetric solids by exploiting the strong and highly directional metal-ligand coordination bonds. Acentric coordination networks with desired topologies can be rationally designed for applications in second-order non-linear optics which are the key to the future photonics technology.<sup>4</sup>

Among the complexes presented in this thesis, there are some chiral materials which were described and analyzed in the Chapter IV. However, a deep investigation of the potential use of these materials for applications in second-harmonic generation or second-order non-linear optics is compulsory. As mentioned before, it is remarkably that the crystallization of these complexes occurs in acentric space groups being synthesized from achiral ligands. Usually, the two enantiomers grow simultaneously and a racemic mixture is obtained, and further investigations are needed to prepare enantiopure products.

Interesting materials are, for example, those obtained with the ethylmalonate ligand with copper(II) ions (complexes **29-31**). Compounds **29** and **31** are homochiral, the stereogenic centre of the former is a trigonal bipyramidal environment of a metal centre with two chelating ligands whereas in the latter, the structure is made up of helices. These are promising materials for non-linear optics and their properties must be investigated.

#### V.3.1. References

- 1 C. Janiak, *Dalton Trans.* **2003**, 2781.
- 2 (a) C. Janiak, *Angew. Chem. Int. Ed.* **1997**, *36*, 1431. (b) B. Kesanli and W. Lin, *Coord. Chem. Rev.* **2003**, *246*, 305.
- 3 (a) B. Moulton and M. J. Zaworotko, *Chem. Rev.* **2001**, *101*, 1629. (b) P. J. Hagrman, D. Hagrman and J. Zubieta, *Angew. Chem. Int. Ed.* **1999**, *38*, 2638. (c) M. Munakata, L. P. Wu and T. Kuroda-Sowa, *Adv. Inorg. Chem.* **1999**, *46*, 173. (d) J. R. Galan-Mascaros and K. R. Dunbar, *Chem. Commun.* **2001**, 217. (e) J. S. Miller, *Inorg. Chem.* **2000**, *39*, 4392. (f) J. S. Seo, D. Whang, H. Lee, S. I. Jun, J. Oh, Y. J. Jeon and K. Kim, *Nature* **2000**, *404*, 982.
- 4 (a) O. R. Evans and W. Lin, *Acc. Chem. Res.* **2002**, *35*, 511. (b) D. E. Bossi and R. W. Ade, *Laser Focus World* **1992**, *28(1)*, 135. (c) T. V. Higgins, *Laser Focus World* **1992**, *28(1)*, 125.

---

---

# Conclusion

---

---



This Thesis work has illustrated that the coordination chemistry are able to design high-dimensionality molecular systems with interesting magnetic properties. Specifically, the self-assembly of dicarboxylate ligands with transition metal ions has demonstrated to be a good approach to prepare new exciting structures. The substituted-malonate ligands open a wide area of investigation where we can exert some control over the weak interactions such as  $\pi$ - $\pi$  stacking, hydrophobic, steric repulsion, for instance. Since these intermolecular interactions are the leading forces for the aggregation of the molecules in the crystal, we can make some guidance over the crystal packing and hence, over the magnetic properties of the material. This is an exciting idea which deserves to be investigated to the ultimate consequences.

The success of our synthetic strategy which consists of mixing serendipity with rational design provides certain control over the self-assembly process and hence, over the crystal structure. An example of this situation is the series of carboxylate-bridged square grid of copper(II) ions presented in the first chapter.

- The first chapter collected the copper(II) complexes synthesized with the phenylmalonate ligand. Most of them are layered systems with the characteristic square grid of carboxylate-bridged copper(II) ions. The presence of the phenyl ring of the phenylmalonate ligand favours the formation of hydrophobic areas in the crystal structure, the use of aromatic coligands enhance this differentiation as occur in the series with pyrimidine, pyrazine, 3-cyanopyridine, 3-chloropyridine, nicotinamide, etc. Among these complexes the  $[\text{Cu}(\text{pym})(\text{Phmal})]_n$  is particularly interesting because it exhibits metamagnetic-like behaviour with 3D magnetic ordering below 2.15 K. This is based on ferromagnetically coupled layers which establish weakly antiferromagnetic interactions among them. Other complexes of the family as the  $[\text{Cu}(\text{L})(\text{Phmal})]_n$  ( $\text{L} = \text{pyz}$ , 3-CNpy, 3-Fpy, 3-Brpy and 3-Ipy) compounds also exhibit metamagnetic behaviour due to the competition of two interactions of opposite nature within the carboxylate-bridged square grid of copper(II) ions.

- The second chapter is devoted to the preparation and characterization of methylmalonate-containing copper(II) complexes. Again, the presence of the methyl group of the methylmalonate ligand provides the formation of layered systems. The adequate incorporation of rigid bridging ligands such as pyrazine or 4,4'-bipyridine connects the layers affording three-dimensional complexes  $[\text{Cu}(\text{L})(\text{Memal})]_n$  ( $\text{L} = \text{pyz}$  and 4,4'-bpy); however, a large magnetic correlation is not obtained in these compounds. Special interest

## Conclusion

---

presents the crystal structure of  $\{[\text{Cu}(4,4'\text{-bpy})_2][\text{Cu}(4,4'\text{-bpy})_2(\text{Memal})(\text{NO}_3)(\text{H}_2\text{O})]\}_n \cdot n\text{NO}_3 \cdot 4n\text{H}_2\text{O}$  where the methylmalonate acts as a functional pillar unit to the 2D structure of 4,4'-bipyridine-bridged square grid of copper(II) ions.

- The third chapter includes the synthesis, structural characterization and the investigation of the magnetic properties of the ethylmalonate-containing copper(II) complexes. The ethyl group of the ethylmalonate ligand favours the formation of channels and cavities, since up to three complexes present great pores in their crystal structure. The polymorphic system of the copper(II)-ethylmalonate group with water molecules as unique coligands is of particular interest. Their crystal structures are very different and range from the one-dimensional networks to 3D-architectures, being two of them homochiral complexes. In addition, one of them exhibits magnetic order below 3.0 K.

- The fourth chapter describes the most interesting features of the compounds presented in this Thesis from both structural and magnetic points of view. The influence of the R-groups substituted in the R-malonate ligand on the crystal packing is investigated, being remarkable the hydrophobic areas created in the structures of substituted-malonate containing compounds. A survey for magneto-structural correlations was also done, concluding that the conformation of the carboxylate-bridge (*anti-anti*, *anti-syn* and *syn-syn*) and its out-of-plane configuration are the main structural parameters which influence the magnetic behaviour.

- The fifth and last chapter of this Thesis opens new perspectives based on the previous work. The most innovative idea involves the introduction of a substituent in the malonic acid which can take an active part in the coordination to metal ions. The preliminary structures of copper(II) complexes of 2-hydroxy-2-phenyl-malonate and ketomalonate ligands are reported, together with their magnetic behaviour. The porous and non-linear optics applications of the Thesis complexes are also discussed.

The work presented in this Thesis is a continuation of the research done by our investigation group, but in some sense it is the beginning of a new field of interesting exploration. At this respect, not only the selection of some of the compounds presented here could serve as a starting point for future research, but also the ideas presented in the perspectives are very promising.

---

---

# Experimental

---

---



## 1. Materials

The reagents used for all the syntheses presented in this thesis were purchased from commercial sources and used without further purification.

## 2. Physical measurements

### 2.1. Elemental Analysis

The elemental analyses (C, H, N) were performed on a EA 1108 CHNS-O microanalytical analyzer.

### 2.2. Crystallographic Data Collection and Structural Determination

The data collection for the complexes of this thesis were carried out in a Nonius KappaCCD diffractometer using graphite-monochromated Mo-K $\alpha$  radiation ( $\lambda = 0.71073 \text{ \AA}$ ). All the data collections were taken at room temperature, except those indicated in the corresponding section. The structures were solved by direct methods and refined with a full-matrix least-squares technique on  $F^2$  using the SHELXL-97<sup>1</sup> program included in the WINGX<sup>2</sup> software package. In general, all non-hydrogen atoms were refined anisotropically, except when it is indicated specifically in the main text. The hydrogen atoms were usually located from Fourier differences but when it has not been possible, they were positioned geometrically. The final geometrical calculations and graphical manipulations were carried out with PARST97<sup>3</sup> and DIAMOND<sup>4</sup> programs.

### 2.3. Thermal analysis

The thermal analyses were performed on a Perkin Elmer Pyris Diamond, TGA / DTA equipment.

### 2.4. Magnetic measurements

Magnetic susceptibility measurements on polycrystalline samples were performed in the temperature range 1.9-290 K (when it could be possible) with a Quantum Design SQUID magnetometer. Diamagnetic corrections of the constituent atoms were estimated from Pascal's constants.<sup>5</sup> Experimental susceptibilities were also corrected for the temperature-independent paramagnetism [ $60 \times 10^{-6} \text{ cm}^3 \text{ mol}^{-1}$  per Cu(II)] and the magnetization of the sample holder.

## 2.5. EPR measurements

EPR spectra on polycrystalline samples were carried out on a Bruker Elexsys E580 EPR spectrometer operating at Q-band (34GHz) frequency.

## 2.6. References

- 1 G. M. Sheldrick, SHELXL-97, SHELXS-97, Program for Crystal Structure Refinement. Institut für Anorganische Chemie der Universität, Tammanstrasse 4, D-3400 Göttingen, Germany, 1998.
- 2 L. J. Farrugia, *J. Appl. Cryst.*, **1999**, 32, 837.
- 3 M. Nardelli, PARST95, *J. Appl. Crystallogr.* **1995**, 28, 659.
- 4 K. Brandenburg, DIAMOND, 1997-2005 Crystal Impact GbR, Bonn, Germany.
- 5 A. Earnshaw, *Introduction to Magnetochemistry*, Academic Press, London, 1968.

## 3. Supplementary Material

### 3.1. Powder X-ray measurements

The powder X-ray measurement on a polycrystalline sample of **8** was made in a Panalytical X'pert PRO powder diffractometer using monochromated Cu-K $\alpha$  radiation. The well overlap between the experimental pattern of **8** and that calculated for **9** confirms that compound **8** is isostructural with **9-11** (see Fig. Sup.1).

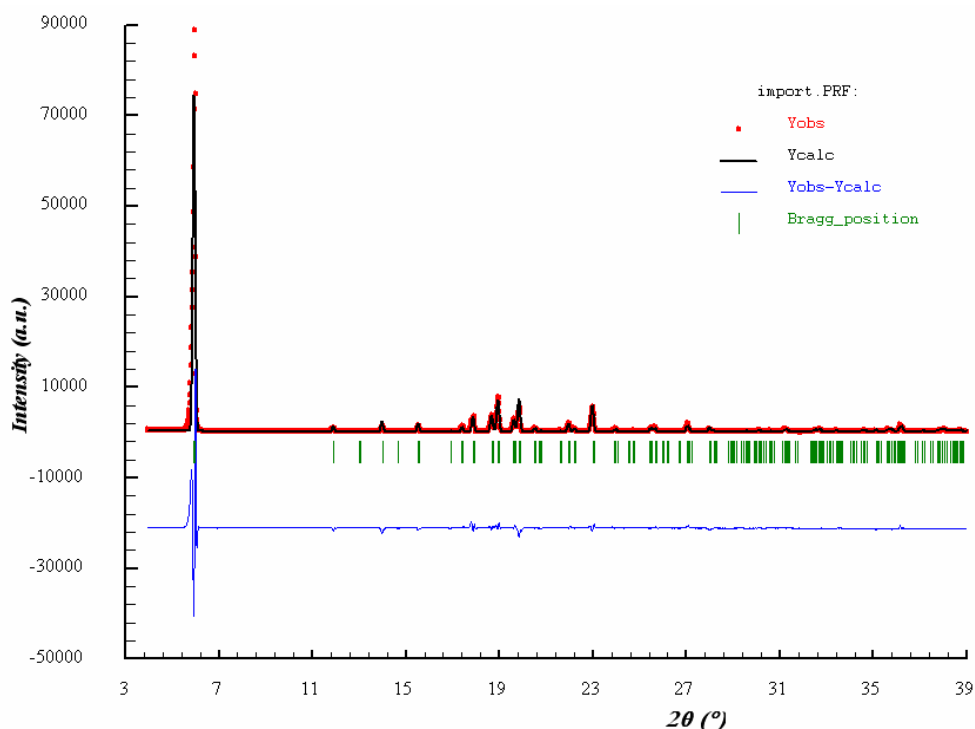


Fig. Sup. 1. Powder diffraction pattern of **8** (red) and the calculated pattern for complex **9** (black).



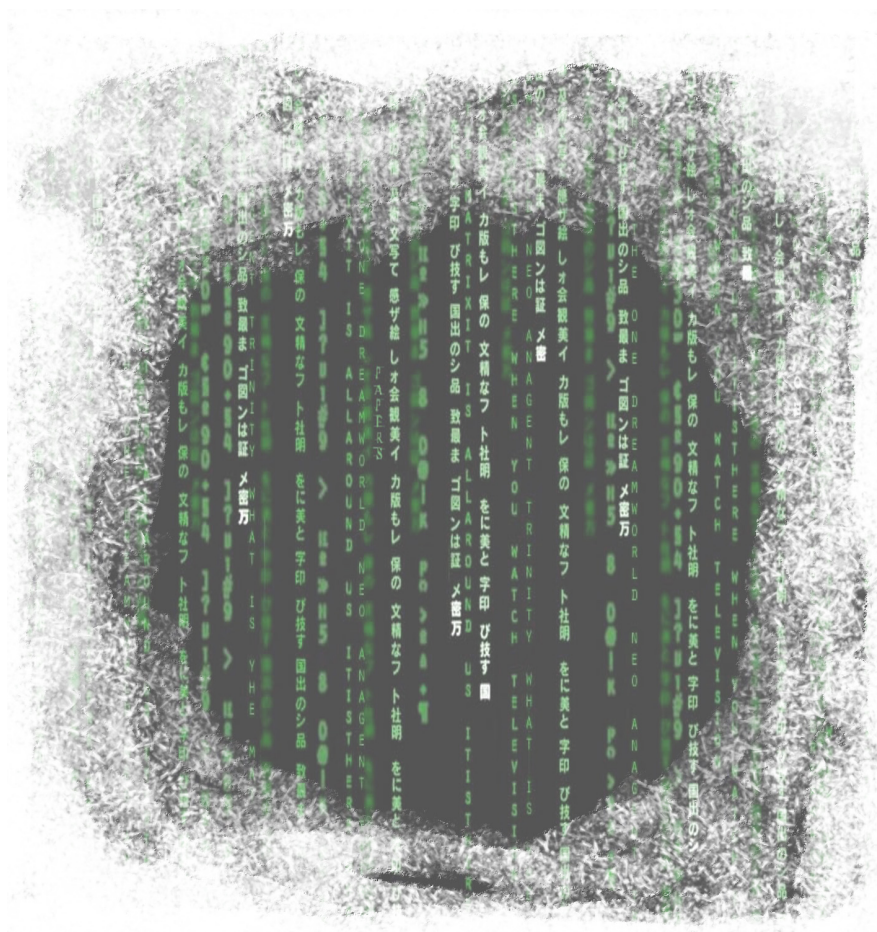
---

---

# Indice

---

---



|                                                                             |           |
|-----------------------------------------------------------------------------|-----------|
| <b>GLOSARIO</b>                                                             | <b>x</b>  |
| <b>INTRODUCCIÓN</b>                                                         | <b>1</b>  |
| <b>1. Materiales Moleculares Magnéticos</b>                                 | <b>3</b>  |
| <b>2. Polímeros de Coordinación: una Vía hacia Imanes Modificables</b>      | <b>4</b>  |
| 2.1. Módulos como ‘Building Blocks’                                         | 5         |
| 2.2. Métodos Sintéticos: Auto-ensamblaje Molecular                          | 8         |
| <b>3. Dicarboxilatos Alifáticos Flexibles</b>                               | <b>10</b> |
| 3.1. El Ácido Malónico                                                      | 10        |
| 3.2. Nuevas Redes de Coordinación basadas en Malonato:                      |           |
| Diseño y Aplicación                                                         | 12        |
| <b>4. Referencias</b>                                                       | <b>14</b> |
| <b>OBJETIVOS</b>                                                            | <b>17</b> |
| <b>CAPÍTULO I. COMPUESTOS DE FENILMALONATO</b>                              | <b>21</b> |
| <b>I.1. Fenilmalonato de Cobre(II) (1)</b>                                  | <b>23</b> |
| I.1.1. Introducción                                                         | 23        |
| I.1.2. Síntesis                                                             | 23        |
| I.1.3. Descripción de la Estructura                                         | 24        |
| I.1.4. Propiedades Magnéticas                                               | 28        |
| I.1.5. Conclusión                                                           | 32        |
| I.1.6. Referencias                                                          | 33        |
| <b>I.2. Pirimidina (2) y Pirazina (3) Fenilmalonato de Cobre(II)</b>        | <b>34</b> |
| I.2.1. Introducción                                                         | 34        |
| I.2.2. Síntesis                                                             | 34        |
| I.2.3. Descripción de la Estructura                                         | 35        |
| I.2.4. Propiedades Magnéticas                                               | 39        |
| I.2.5. Conclusión                                                           | 44        |
| I.2.6. Referencias                                                          | 45        |
| <b>3-Cianopiridina (4) y 4-Cianopiridina (5) Fenilmalonato de Cobre(II)</b> | <b>46</b> |
| I.2.7. Introducción                                                         | 46        |
| I.2.8. Síntesis                                                             | 46        |

|                                                                                                                                   |           |
|-----------------------------------------------------------------------------------------------------------------------------------|-----------|
| I.2.9. Descripción de la Estructura                                                                                               | 47        |
| I.2.10. Propiedades Magnéticas                                                                                                    | 50        |
| I.2.11. Conclusión                                                                                                                | 55        |
| I.2.12. Referencias                                                                                                               | 55        |
| <b>I.3. Nicotinamida (6) e Isonicotinamida (7) Fenilmalonato de Cobre(II)</b>                                                     | <b>56</b> |
| I.3.1. Introducción                                                                                                               | 56        |
| I.3.2. Síntesis                                                                                                                   | 56        |
| I.3.3. Descripción de la Estructura                                                                                               | 57        |
| I.3.4. Propiedades Magnéticas                                                                                                     | 60        |
| I.3.5. Conclusión                                                                                                                 | 63        |
| I.3.6. Referencias                                                                                                                | 63        |
| <b>I.4. 3-Fluoropiridina (8), 3-Cloropiridina (9), 3-Bromopiridina (10),<br/>y 3-Iodopiridina (11) Fenilmalonato de Cobre(II)</b> | <b>65</b> |
| I.4.1. Introducción                                                                                                               | 65        |
| I.4.2. Síntesis                                                                                                                   | 65        |
| I.4.3. Descripción de la Estructura                                                                                               | 66        |
| I.4.4. Propiedades Magnéticas                                                                                                     | 70        |
| I.4.5. Conclusión                                                                                                                 | 74        |
| I.4.6. Referencias                                                                                                                | 74        |
| <b>I.5. 2,4'-Bipiridina (12) Fenilmalonato de Cobre(II)</b>                                                                       | <b>76</b> |
| I.5.1. Introducción                                                                                                               | 76        |
| I.5.2. Síntesis                                                                                                                   | 76        |
| I.5.3. Descripción de la Estructura                                                                                               | 77        |
| I.5.4. Propiedades Magnéticas                                                                                                     | 82        |
| I.5.5. Conclusión                                                                                                                 | 84        |
| I.5.6. Referencias                                                                                                                | 85        |
| <b>I.6. 4,4'-Bipiridina (13) Fenilmalonato de Cobre(II)</b>                                                                       | <b>86</b> |
| I.6.1. Introducción                                                                                                               | 86        |
| I.6.2. Síntesis                                                                                                                   | 86        |
| I.6.3. Descripción de la Estructura                                                                                               | 86        |
| I.6.4. Propiedades Magnéticas                                                                                                     | 90        |
| I.6.5. Conclusión                                                                                                                 | 91        |
| I.6.6. Referencias                                                                                                                | 92        |
| <b>I.7. 2,2'-Bipirimidina (14) y 1,10-Fenantrolina (15)</b>                                                                       |           |

|                                                                              |            |
|------------------------------------------------------------------------------|------------|
| <b>Fenilmalonato de Cobre(II)</b>                                            | <b>93</b>  |
| I.7.1. Introducción                                                          | 93         |
| I.7.2. Síntesis                                                              | 93         |
| I.7.3. Descripción de la Estructura                                          | 94         |
| I.7.4. Propiedades Magnéticas                                                | 98         |
| I.7.5. Conclusión                                                            | 100        |
| I.7.6. Referencias                                                           | 101        |
| <b>I.8. 2,2'-Bipiridina (16) Fenilmalonato de Cobre(II)</b>                  | <b>102</b> |
| I.8.1. Introducción                                                          | 102        |
| I.8.2. Síntesis                                                              | 102        |
| I.8.3. Descripción de la Estructura                                          | 102        |
| I.8.4. Propiedades Magnéticas                                                | 106        |
| I.8.5. Conclusión                                                            | 106        |
| I.8.6. Referencias                                                           | 106        |
| <br>                                                                         |            |
| <b>CAPÍTULO II. COMPUESTOS DE METILMALONATO</b>                              | <b>107</b> |
| <br>                                                                         |            |
| <b>II.1. Metilmalonato de Cobre(II) (17)</b>                                 | <b>109</b> |
| II.1.1. Introducción                                                         | 109        |
| II.1.2. Síntesis                                                             | 109        |
| II.1.3. Descripción de la Estructura                                         | 109        |
| II.1.4. Propiedades Magnéticas                                               | 112        |
| II.1.5. Conclusión                                                           | 115        |
| II.1.6. Referencias                                                          | 115        |
| <b>II.2. Pirazina (18) y 4,4'-bipiridina (19) Metilmalonato de Cobre(II)</b> | <b>117</b> |
| II.2.1. Introducción                                                         | 117        |
| II.2.2. Síntesis                                                             | 117        |
| II.2.3. Descripción de la Estructura                                         | 118        |
| II.2.4. Propiedades Magnéticas                                               | 122        |
| II.2.5. Conclusión                                                           | 124        |
| II.2.6. Referencias                                                          | 125        |
| <b>II.3. 4-Cianopiridina (20) Metilmalonato de Cobre(II)</b>                 | <b>126</b> |
| II.3.1. Introducción                                                         | 126        |
| II.3.2. Síntesis                                                             | 126        |
| II.3.3. Descripción de la Estructura                                         | 127        |

|                                                                                    |            |
|------------------------------------------------------------------------------------|------------|
| II.3.4. Propiedades Magnéticas                                                     | 130        |
| II.3.5. Conclusión                                                                 | 132        |
| II.3.6. Referencias                                                                | 132        |
| <b>II.4. 3-Iodopiridina (21) y 2,4'-bipiridina (22) Metilmalonato de Cobre(II)</b> | <b>133</b> |
| II.4.1. Introducción                                                               | 133        |
| II.4.2. Síntesis                                                                   | 133        |
| II.4.3. Descripción de la Estructura                                               | 134        |
| II.4.4. Propiedades Magnéticas                                                     | 138        |
| II.4.5. Conclusión                                                                 | 140        |
| II.4.6. Referencias                                                                | 141        |
| <b>II.5. 2,2'-Bipirimidina (22) Metilmalonato de Cobre(II)</b>                     | <b>142</b> |
| II.5.1. Introducción                                                               | 142        |
| II.5.2. Síntesis                                                                   | 142        |
| II.5.3. Descripción de la Estructura                                               | 143        |
| II.5.4. Propiedades Magnéticas                                                     | 145        |
| II.5.5. Conclusión                                                                 | 147        |
| II.5.6. Referencias                                                                | 148        |
| <b>II.6. 2,2'-Bipiridina (24) Metilmalonato de Cobre(II)</b>                       | <b>149</b> |
| II.6.1. Introducción                                                               | 149        |
| II.6.2. Síntesis                                                                   | 149        |
| II.6.3. Descripción de la Estructura                                               | 150        |
| II.6.4. Propiedades Magnéticas                                                     | 154        |
| II.6.5. Conclusión                                                                 | 154        |
| II.6.6. Referencias                                                                | 154        |
| <b>II.7. 4,4'-Bipiridina Metilmalonato de Cobre(II) (19, 25 and 26)</b>            | <b>156</b> |
| II.7.1. Introducción                                                               | 156        |
| II.7.2. Síntesis                                                                   | 156        |
| II.7.3. Análisis Cristalográfico                                                   | 157        |
| II.7.4. Descripción de la Estructura                                               | 158        |
| II.7.5. Propiedades Magnéticas                                                     | 166        |
| II.7.6. Conclusión                                                                 | 169        |
| II.7.7. Referencias                                                                | 170        |
| <b>II.8. 1,2-Bis(4-piridil)eteno (27) Metilmalonato de Cobre(II)</b>               | <b>171</b> |
| II.8.1. Introducción                                                               | 171        |

|                                                                                    |            |
|------------------------------------------------------------------------------------|------------|
| II.8.2. Síntesis                                                                   | 171        |
| II.8.3. Descripción de la Estructura                                               | 172        |
| II.8.4. Propiedades Magnéticas                                                     | 175        |
| II.8.5. Conclusión                                                                 | 177        |
| II.8.6. Referencias                                                                | 177        |
| <b>CAPÍTULO III. COMPUESTOS DE ETILMALONATO</b>                                    | <b>179</b> |
| <b>III.1. Etilmalonato de Cobre(II) (28, 29 and 30)</b>                            | <b>181</b> |
| III.1.1. Introducción                                                              | 181        |
| III.1.2. Síntesis                                                                  | 182        |
| III.1.3. Descripción de la Estructura                                              | 184        |
| III.1.4. Propiedades Magnéticas                                                    | 197        |
| III.1.5. Conclusión                                                                | 201        |
| III.1.6. Referencias                                                               | 201        |
| <b>III.2. Etilmalonato de Cobre(II) y Sodio(I) (31 and 32)</b>                     | <b>203</b> |
| III.2.1. Introducción                                                              | 203        |
| III.2.2. Síntesis                                                                  | 203        |
| III.2.3. Descripción de la Estructura                                              | 204        |
| III.2.4. Propiedades Magnéticas                                                    | 211        |
| III.2.5. Conclusión                                                                | 212        |
| III.2.6. Referencias                                                               | 212        |
| <b>III.3. 2,2'-Bipirimidina Etilmalonato de Cobre(II) (33)</b>                     | <b>214</b> |
| III.3.1. Introducción                                                              | 214        |
| III.3.2. Síntesis                                                                  | 214        |
| III.3.3. Descripción de la Estructura                                              | 215        |
| III.3.4. Propiedades Magnéticas                                                    | 217        |
| III.3.5. Conclusión                                                                | 219        |
| III.3.6. Referencias                                                               | 219        |
| <b>III.4. 2,2'-Bipiridina (34) y 1,10-fenantrolina (35) Etilmalonato de Cu(II)</b> | <b>220</b> |
| III.4.1. Introducción                                                              | 220        |
| III.4.2. Síntesis                                                                  | 220        |
| III.4.3. Descripción de la Estructura                                              | 221        |
| III.4.4. Propiedades Magnéticas                                                    | 225        |
| III.4.5. Conclusión                                                                | 225        |

---

|                                                                                                    |            |
|----------------------------------------------------------------------------------------------------|------------|
| III.4.6. Referencias                                                                               | 225        |
| <b>CAPÍTULO IV. DISCUSIÓN ESTRUCTURAL Y MAGNÉTICA</b>                                              | <b>227</b> |
| <b>IV.1. Discusión Estructural</b>                                                                 | <b>229</b> |
| IV.1.1. Introducción                                                                               | 229        |
| IV.1.2. Análisis de los Datos Cristalinos                                                          | 229        |
| IV.1.2.1. Grupos Espaciales                                                                        | 229        |
| IV.1.2.2. Quiralidad                                                                               | 230        |
| IV.1.2.3. Conformaciones del R-malonato                                                            | 234        |
| IV.1.2.4. Motivos de Agua                                                                          | 237        |
| IV.1.3. El Sistema R-malonato de Cobre(II)                                                         | 239        |
| IV.1.4. Referencias                                                                                | 244        |
| <b>IV.2. Discusión Magneto-Estructural</b>                                                         | <b>245</b> |
| IV.2.1. Naturaleza de la Interacción Magnética                                                     | 245        |
| IV.2.2. Magnitud de la Interacción Magnética                                                       | 246        |
| IV.2.3. Relaciones Magneto-Estructurales en Complejos formados<br>por redes cuadradas de Cobre(II) | 247        |
| IV.2.4. Referencias                                                                                | 254        |
| <b>CAPÍTULO V. PERSPECTIVAS</b>                                                                    | <b>255</b> |
| <b>V.1. Materiales Moleculares Magnéticos</b>                                                      | <b>257</b> |
| V.1.1. Introducción                                                                                | 257        |
| V.1.2. En la línea de la Tesis: Bencilmalonato de Cobre(II) (36)                                   | 257        |
| V.1.3. El sustituyente como una parte ‘activa’ del ligando                                         | 262        |
| V.1.3.1. 2-Hidroxo-2-fenilmalonato (37)                                                            | 262        |
| V.1.3.2. Ácido Ketomalónico (38)                                                                   | 268        |
| V.1.3.3. $[\text{Cu}_4(\text{pz})_4(\text{OH-ppac})_2(\text{H}_2\text{O})_4]$ (39)                 | 274        |
| V.1.4. Referencias                                                                                 | 278        |
| <b>V.2. Materiales Porosos</b>                                                                     | <b>281</b> |
| V.2.1. Referencias                                                                                 | 284        |
| <b>V.3. Materiales Quirales</b>                                                                    | <b>285</b> |
| V.3.1. Referencias                                                                                 | 285        |
| <b>CONCLUSIÓN</b>                                                                                  | <b>287</b> |

*Índice*

---

|                     |            |
|---------------------|------------|
| <b>EXPERIMENTAL</b> | <b>291</b> |
| <b>ÍNDICE</b>       | <b>295</b> |
| <b>RESUMEN</b>      | <b>305</b> |
| <b>ANEXO</b>        | <b>321</b> |



---

---

# Resumen

---

---



Esta Tesis tiene como objetivo fundamental la preparación y caracterización tanto estructural como magnética de nuevos materiales moleculares magnéticos y está basada en el trabajo previo de nuestro grupo de investigación en compuestos de coordinación de ácido malónico con metales de transición. La investigación previa utilizando el ligando malonato ha dado buenos resultados, obteniéndose complejos con interesantes propiedades, tanto estructurales como magnéticas. Esto nos ha permitido ir un paso más allá y realizar modificaciones al propio ligando con el fin de obtener cierto control sobre el empaquetamiento cristalino. Para ello, uno de los átomos de hidrógeno del grupo metileno del ácido malónico ha sido sustituido por diferentes grupos funcionales: un grupo metilo (ácido metilmalónico), un grupo etilo (ácido etilmalónico) y un grupo fenilo (ácido fenilmalónico). Estos grupos son capaces de establecer interacciones débiles del tipo  $\pi$ , hidrofóbicas o repulsiones estéricas que pueden modificar el comportamiento estructural del ácido malónico. La influencia que puedan ejercer sobre el proceso de síntesis nos permitirá cierto control sobre el empaquetamiento cristalino del compuesto y, por tanto, sobre sus propiedades magnéticas.

La preparación de compuestos de cobre(II) con diferentes coligandos, su caracterización mediante difracción de rayos X y medidas magnéticas es el principal objetivo de esta Tesis.

## Capítulo I. Complejos de Fenilmalonato

### I.1. Fenilmalonato de cobre(II) (I).

La reacción entre nitrato de cobre(II) y una mezcla de ácido fenilmalónico y carbonato sódico en agua tiene como resultado el compuesto  $\{[\text{Cu}(\text{H}_2\text{O})_3][\text{Cu}(\text{Phmal})_2]\}_n$  (I). Su estructura cristalina es bidimensional formada a partir de cadenas unidas a través de un doble puente  $\mu$ -oxo. Las cadenas están constituidas a su vez por la alternancia regular de aniones  $[\text{Cu}(\text{Phmal})_2]^{2-}$  y cationes  $[\text{Cu}(\text{H}_2\text{O})_3]^{2+}$  unidos por puente carboxilato en conformación *anti-syn*. De este compuesto podemos destacar que: (i) el puente carboxilato en conformación *anti-syn* es capaz de mediar interacciones ferromagnéticas como lo hacía el ligando malonato; (ii) la inclusión del anillo aromático en el esqueleto del ácido malónico hace posible la aparición de interacciones supramoleculares (apilamiento  $\pi$ - $\pi$ ) y el aumento de dimensionalidad estructural (apilamiento  $\pi$ - $\pi$  entre capas); y (iii) finalmente, el fenilo

sustituido induce pequeños cambios en el modo de coordinación del ácido fenilmalónico como el doble puente  $\mu$ -oxo.

### I.2. Pirimidina (2) y pirazina (3).

Los complejos  $[\text{Cu}(\text{pym})(\text{Phmal})]_n$  (2) and  $[\text{Cu}(\text{pyz})(\text{Phmal})]_n$  (3) se prepararon con la intención de unir las redes bidimensionales obtenidas para el compuesto 1 a través de ligandos rígidos del tipo pirazina o pirimidina. La estructura resultante de ambos compuestos, en cambio, sigue siendo bidimensional pero en forma de redes cuadradas de iones cobre(II) unidos a puente carboxilato. Estas redes se encuentran bien separadas por los anillos aromáticos de los coligandos y del fenilmalonato, creando una estructura de tipo sándwich. Aunque la estructura cristalina de los compuestos 2 y 3 es muy similar, sus propiedades magnéticas no lo son. El compuesto 2 presenta un comportamiento metamagnético con orden magnético tridimensional por debajo de la temperatura crítica ( $T_c = 2.15$  K). Este comportamiento es debido a la interacción dominante en la red cuadrada de iones cobre (II) a puente carboxilato es ferromagnética [con una constante de acoplamiento magnético de  $+5.6(1) \text{ cm}^{-1}$ ], mientras que la interacción entre planos es antiferromagnética [con un acoplamiento magnético  $0.01 \text{ cm}^{-1}$ , valor que ha sido estimado de la curva de magnetización]. El compuesto 3 presenta también un comportamiento metamagnético pero, en este caso, dos tipos de interacciones de diferente naturaleza, una ferro- y la otra antiferromagnética, coexisten dentro del plano de iones cobre(II). ¿Qué parámetros estructurales varían del compuesto con pirimidina al de pirazina para observar un cambio tan dramático en el magnetismo? Los siguientes compuestos intentan buscar respuestas a este interrogante.

### I.3. 3-Ciano- (4) y 4-cianopiridina (5).

Los compuestos  $[\text{Cu}(\text{3-CNpy})(\text{Phmal})]_n$  (4) and  $[\text{Cu}(\text{4-CNpy})(\text{Phmal})]_n$  (5) presentan la misma estructura cristalina en capas que 2 y 3 con redes cuadradas de iones cobre(II) a puente carboxilato separadas por áreas hidrofóbicas que contienen los anillos aromáticos de los ligandos. Sin embargo, el comportamiento magnético de estos compuestos difiere un poco del de los anteriores. En 4 coexisten simultáneamente interacciones ferro- y antiferromagnéticas del modo en que lo hacían en 3, mientras que 5 presenta un comportamiento ferromagnético. La posición del grupo ciano o del átomo de nitrógeno de la azina no parece estar relacionada con la aparición de interacciones antiferromagnéticas a través del puente carboxilato, ya que conformaciones *para*- (4) y *orto*- (3) exhiben este tipo de puente. La variación de la naturaleza de las interacciones magnéticas mediadas por el

puente carboxilato debe depender de cambios estructurales mucho más pequeños, y probablemente debe englobar cambios en varios parámetros simultáneamente.

#### **I.4. Nicotinamida (6) e isonicotinamida (7).**

Los compuestos **6** y **7** se prepararon con la intención de que los grupos amido establecieran interacciones a través de puentes de hidrógeno. Sólo se obtuvo la estructura cristalina del compuesto  $[\text{Cu}(\text{isonic})(\text{Phmal})(\text{H}_2\text{O})]_n$  (**7**) que está formado por capas similares a las de los compuestos **2-5**. Los grupos amido del ligando isonicotinamida establecen contactos por puente de hidrógeno entre capas como se esperaba. Sin embargo, el comportamiento magnético de **6** y **7** es diferente del observado en **2-5**. Ello es debido a que en **6** y **7** los puentes carboxilato que forman las redes cuadradas de iones cobre(II) unen posiciones ecuatoriales con apicales de los entornos de los iones cobre(II). La razón para este cambio proviene del hecho de que los ligandos nic e isonic ocupan posiciones ecuatoriales del entorno de los iones cobre(II). Además, una molécula de agua entra en el entorno de coordinación del Cu(II). Por tanto, los cambios que esperábamos observar debido a la introducción de los ligandos nic e isonic han sido suprimidos debido a que han entrado en posiciones ecuatoriales del Cu(II).

#### **I.5. 3-fluoro- (8), 3-cloro- (9), 3-bromo- (10) y 3-iodopiridina (11).**

Los compuestos  $[\text{Cu}(3\text{-Xpy})(\text{Phmal})]_n$  [X = Cl (**9**), Br (**10**) and I (**11**); de **8** no se pudo determinar la estructura cristalina] son isoestructurales con pequeñas variaciones debido a los diferentes radios de van der Waals de los halógenos. La estructura cristalina está formada por capas al igual que los compuestos **2-7**. Las propiedades magnéticas de los cuatro compuestos **8-11** difieren entre sí dependiendo de cuál es la interacción dominante, la ferro- o la antiferromagnética. Los parámetros de acoplamiento observados en **8-11** son débiles ( $J$  aprox.  $|2.5 \text{ cm}^{-1}|$ ) pero dentro del rango para puentes carboxilato en conformación *anti-syn*. Los complejos **8**, **10** y **11** presentan un comportamiento metamagnético, mientras que **9** exhibe un acoplamiento antiferromagnético. Esta situación confirma el hecho de que los cambios estructurales necesarios para observar diferentes propiedades magnéticas son muy sutiles.

#### **I.6. 2,4'-bipiridina (12).**

El compuesto  $[\text{Cu}(2,4'\text{-bpy})(\text{Phmal})(\text{H}_2\text{O})]_n$  (**12**) presenta una estructura cristalina en capas similar a la observada en los compuestos **2-11**, pero con una separación entre ellas mucho mayor que en los compuestos anteriores. Sin embargo, la bipiridina ocupa una posición ecuatorial en el entorno de coordinación del cobre(II) como ocurría en **7**, con la diferencia

que ahora aparece en forma de una distorsión pseudo-Jahn-Teller estática desordenada. Esto condiciona las propiedades magnéticas observadas, que aunque siendo ferromagnéticas, son mucho más débiles que las que presentan los compuestos **2-5**.

#### **I.7. 4,4'-bipiridina (13).**

La estructura cristalina del compuesto  $[\text{Cu}(4,4'\text{-bpy})(\text{Phmal})]_n \cdot 2n\text{H}_2\text{O}$  (**13**) consiste en cadenas de iones cobre(II) a puente carboxilato que se unen a través de la 4,4'-bipiridina formando una red bidimensional. La red cuadrada de iones cobre(II) obtenida en los compuestos **2-12** no se ha reproducido para el caso de la 4,4'-bpy y, por tanto, el propósito principal para incluir este coligando ha fallado. Ello se debe a que el coligando 4,4'-bpy han entrado en posiciones ecuatoriales del entorno del cobre(II). La imposibilidad de los átomos de oxígeno del fenilmalonato para ocupar esas posiciones conduce a la extraña conformación del fenilmalonato en la que actúa como quelante a una posición ecuatorial y otra apical del entorno del cobre(II). La interacción antiferromagnética observada, con un parámetro de acoplamiento de  $-0.59 \text{ cm}^{-1}$  está en acuerdo con la conformación ecuatorial-apical *anti-syn* del puente carboxilato.

#### **I.8. 2,2'-bipirimidina (14) and 1,10-fenantrolina (15).**

Los compuestos  $\{[\text{Cu}(2,2'\text{-bpym})(\text{Phmal})]\}_n$  (**14**) y  $\{[\text{Cu}(\text{phen})(\text{Phmal})]\}_n \cdot 3n\text{H}_2\text{O}$  (**15**) poseen una estructura cristalina formada por cadenas en las que unidades del tipo  $[\text{Cu}(\text{L})\text{Phmal}]$  se encuentran unidas por puentes carboxilato en conformación ecuatorial-apical. La naturaleza ferromagnética de las interacciones a través de puentes carboxilato de fenilmalonato en **14** y **15** es similar a la observada en otros compuestos de malonato con el mismo puente, sin embargo es un poco más débil en magnitud, debido quizás al efecto de electrón-atrayente del grupo fenilo de ligando fenilmalonato.

#### **I.9. 2,2'-Bipiridina (16).**

La estructura cristalina del compuesto  $[\text{Cu}(2,2'\text{-bpy})(\text{Phmal})(\text{H}_2\text{O})] \cdot 2\text{H}_2\text{O}$  (**16**) está formada por entidades mononucleares y presenta varias peculiaridades dignas de ser mencionadas: (i) el anillo del ligando fenilmalonato está inclinado sobre el anillo quelato del ión de cobre(II), algo que no se ha observado previamente en compuestos de fenilmalonato; (ii) la aparición de un patrón (6,3) formado por enlaces de hidrógeno entre átomos de oxígeno de fenilmalonato y moléculas de agua, tanto coordinadas como de cristalización.

## Capítulo II. Complejos de Metilmalonato

### II.1. Metilmalonato de cobre(II) (17).

La estructura cristalina del compuesto  $[\text{Cu}(\text{Memal})(\text{H}_2\text{O})]_n$  (17) está formada por redes cuadradas de iones cobre(II) a puente carboxilato, similares a las observadas en los complejos de fenilmalonato 2-12. Sin embargo, estos compuestos fueron sintetizados con un ligando de tipo piridina, mientras que el compuesto de fenilmalonato con moléculas de agua como único coligando (1) presentaba una estructura muy diferente. Asimismo, los compuestos similares de malonato de cobre(II) no forman este tipo de red cuadrada. Por tanto, parece como si el ligando metilmalonato se comportara en presencia de iones cobre(II) como lo hace el ligando fenilmalonato con coligandos del tipo piridina. Magnéticamente, la interacción entre los centros paramagnéticos en 17 es ferromagnética como ocurre en los compuestos de R-malonato de cobre(II), pero de menor magnitud y, por tanto, sin orden magnético como el que se observa en 2.

### II.2. Pirazina (18) y 4,4'-bipiridina (19).

La estructura cristalina de los compuestos  $[\text{Cu}_2(\text{pyz})(\text{Memal})_2]$  (18) y  $[\text{Cu}_2(4,4'\text{-bpy})(\text{Memal})_2(\text{H}_2\text{O})_2]$  (19) es la prevista, formándose la red cuadrada de iones cobre(II) a puente carboxilato. Los coligandos rígidos pirazina y 4,4'-bipiridina conectan las capas adyacentes para formar una robusta red tridimensional. El hecho de que el grupo metilo sea más pequeño que el fenilo del ligando fenilmalonato permite la unión de las capas a través de ligandos de tipo piridina. Magnéticamente, los dos compuestos presentan aproximadamente el mismo comportamiento que consiste en la aparición simultánea de dos interacciones magnéticas de signo opuesto. De acuerdo con su estructura, las interacciones magnéticas son más débiles en 19 que en 18. Los valores para las constantes de acoplamiento magnético para los puentes carboxilato, pirazina y 4,4'-bipiridina están de acuerdo con los valores reflejados en la bibliografía.

### II.3. 4-Cianopiridina (20).

El compuesto  $[\text{Cu}(4\text{-CNpy})(\text{Memal})(\text{H}_2\text{O})]_n$  (20) presenta una estructura similar a la del complejo de fenilmalonato  $[\text{Cu}(4\text{-CNpy})(\text{Phmal})]_n$  (5) y consiste en redes cuadradas de iones cobre(II) a puente carboxilato. Sin embargo, una molécula de agua ha entrado en la esfera de coordinación de los iones de cobre(II) en 20, dando lugar a una coordinación de tipo 4+2 octahédrica. Además, el espaciado entre capas es más corto en 20, debido al sustituyente más pequeño del ligando metilmalonato. El compuesto 20 exhibe interacciones ferromagnéticas dentro de las capas, al igual que 17; sin embargo, la magnitud de estas

interacciones es más débil que en **5** o **17**, debido a que los enlaces Cu–O ecuatoriales son más largos en **20**.

#### II.4. 3-Iodopiridina (**21**) y 2,4'-bipiridina (**22**).

Los compuestos [Cu(3-Ipy)(Memal)(H<sub>2</sub>O)] (**21**) y [Cu(2,4'-bpy)(Memal)(H<sub>2</sub>O)]·3H<sub>2</sub>O (**22**) no presentan la misma estructura que sus homólogos preparados con el ligando fenilmalonato **11** y **12**, respectivamente. Los ligandos piridínicos se encuentran ocupando posiciones ecuatoriales en la esfera de coordinación de los iones cobre(II) en **21** y **22**, lo que modifica drásticamente la estructura cristalina resultante. La estructura de los compuestos **21** y **22** está formada por cadenas de iones cobre(II) a puente carboxilato que construyen una red supramolecular bidimensional apilada a través de interacciones de tipo  $\pi$ - $\pi$  y puentes de hidrógeno. La estructura tridimensional de **22** presenta canales ocupados por moléculas de agua que forman un patrón de tipo T5(2). Los dos compuestos exhiben interacciones ferromagnéticas a través del puente carboxilato.

#### II.5. 2,2'-Bipirimidina (**23**).

La estructura cristalina del compuesto [Cu<sub>2</sub>(2,2'-bipym)(Memal)<sub>2</sub>(H<sub>2</sub>O)<sub>2</sub>]·3H<sub>2</sub>O (**23**) consiste en moléculas dinucleares y moléculas de agua de cristalización, similar a la presentada por el compuesto homólogo preparado con el ligando malonato, pero diferente de la obtenida para el compuesto de fenilmalonato (**14**). Probablemente, las diferencias entre los compuestos **23** y **14** sean debidas al pequeño tamaño del grupo metilo respecto al del grupo fenilo y la capacidad de éste último para establecer interacciones de tipo  $\pi$  con el coligando 2,2'-bipym. Desde un punto de vista magnético, el compuesto **23** exhibe el comportamiento característico de un compuesto dinuclear de cobre(II) acoplado antiferromagnéticamente [ $J = -155.6(3) \text{ cm}^{-1}$ ]. Este valor está en buen acuerdo con los valores hallados en la bibliografía para complejos dinucleares de cobre(II) a puente 2,2'-bipirimidina.

#### II.6. 2,2'-Bipiridina (**24**).

La estructura cristalina del compuesto [Cu(2,2'-bpy)(Memal)(H<sub>2</sub>O)]·2H<sub>2</sub>O (**24**) consiste en entidades mononucleares y moléculas de agua de cristalización que se encuentran conectadas a través de interacciones débiles para formar una red supramolecular tridimensional. Esta estructura es similar a la obtenida para los compuestos homólogos de malonato y fenilmalonato. Es interesante remarcar la presencia en la estructura de un patrón de tipo C4 a través de puentes de hidrógeno entre moléculas de agua y átomos de oxígeno no coordinados de grupos carboxilato.

### II.7. 4,4'-Bipiridina (25 y 26).

Los dos complejos presentados en esta sección son muy interesantes y, al mismo tiempo, prometedores. El compuesto  $\{[\text{Cu}(4,4'\text{-bpy})_2][\text{Cu}(4,4'\text{-bpy})_2(\text{Memal})(\text{NO}_3)(\text{H}_2\text{O})]\}_n \cdot n\text{NO}_3 \cdot 4n\text{H}_2\text{O}$  (**25**) presenta una estructura inusual. Está construida a partir de redes cuadradas bidimensionales de iones cobre(II) a puente 4,4'-bpy que están conectadas a través de unidades  $[\text{Cu}(4,4'\text{-bpy})_2(\text{Memal})(\text{NO}_3)(\text{H}_2\text{O})]$  a puente carboxilato. Aunque los canales de  $11 \times 11 \text{ \AA}^2$  formados por la red cuadrada  $[\text{Cu}(4,4'\text{-bpy})_2]_n$  están ocupados por ligandos 4,4'-bpy terminales; esta estructura puede verse como un primer paso para la preparación de materiales microporosos con un diseño racional. La estructura cristalina del compuesto  $[\text{Cu}(4,4'\text{-bpy})_2(\text{Memal})(\text{H}_2\text{O})]_n \cdot n\text{H}_2\text{O}$  (**26**) consiste en cadenas de iones cobre(II) a puente metilmalonato. Dos coligandos 4,4'-bpy en posición *trans* y una molécula de agua completan la esfera de coordinación del ión cobre(II). Es interesante observar que el ligando metilmalonato no juega un papel fundamental en la formación de las estructuras de **25** y **26**, al contrario de lo que sucede en, por ejemplo, los compuestos **18** o **19**. La unidad de metilmalonato de cobre en **25** es un conector entre capas y en **26** el metilmalonato no se encuentra quelando al ión cobre(II) y actúa como un simple espaciador. Magnéticamente, ambos compuestos presentan interacciones antiferromagnéticas muy débiles, de acuerdo con el tipo de puente observado en la estructura cristalina.

### II.8. 1,2-Bis(4-piridil)eteno (27).

El compuesto  $[\text{Cu}(\text{bpe})(\text{Memal})]_n \cdot 3n\text{H}_2\text{O}$  (**27**) es tridimensional. Su estructura está formada por cadenas de iones cobre(II) a puente carboxilato unidas a través de coligandos bpe dando lugar a la red 3D. Las moléculas de agua de cristalización rellenan los poros con un tamaño de  $15 \times 14 \text{ \AA}^2$  que aparecen en la estructura. Aunque los resultados obtenidos con el coligando 4,4'-bpy en el compuesto **25** no han sido reproducidos, **26** es un compuesto susceptible de ser investigado por sus propiedades porosas. Las interacciones magnéticas entre los iones de cobre(II) a puente carboxilato son de carácter antiferromagnético con una constante de acoplamiento de  $-1.25 \text{ cm}^{-1}$ .

## Capítulo III. Complejos de Metilmalonato

### III.1. Etilmalonato de cobre(II) (28-30).

Tres complejos se obtienen de la reacción del dianión etilmalonato y el nitrato de cobre(II) en presencia de agua:  $\{[\text{Cu}(\text{H}_2\text{O})_4][\text{Cu}(\text{Etmal})_2(\text{H}_2\text{O})]\}_n$  (**28**),  $[\text{Cu}(\text{Etmal})(\text{H}_2\text{O})]_n$  (**29**) y  $[\text{Cu}(\text{Etmal})(\text{H}_2\text{O})]_n \cdot 1.65n\text{H}_2\text{O}$  (**30**). Las estructuras cristalinas difieren entre ellos y su



dimensionalidad abarca desde la red monodimensional de **28** a la tridimensional de **30**. La estructura de **28** está formada por cadenas en las que se alternan regularmente aniones de  $[\text{Cu}(\text{Etmal})_2]^{2-}$  con entorno de bipirámide trigonal [sin precedentes en complejos de coordinación de R-malonato de cobre(II)] y cationes  $[\text{Cu}(\text{H}_2\text{O})_4]^{2+}$  con entorno octahédrico. El compuesto **29**, en cambio, posee una estructura bidimensional en forma de red cuadrada de iones cobre(II) a puente carboxilato similar a la observada en **2-12** y **17-20**. Finalmente, el compuesto **30** es un compuesto tridimensional formado por iones cobre(II) monohidratados unidos a través de puentes carboxilato de etilmalonato. Esta estructura forma poros de 9.5 Å de diámetro cuya superficie son hélices de iones cobre(II) y que están ocupados por moléculas de agua de cristalización. Magnéticamente, los tres compuestos son muy diferentes, de acuerdo con su estructura. Las cadenas del compuesto **28** presentan un acoplamiento antiferromagnético a través del puente carboxilato, la red cuadrada de iones cobre(II) del compuesto **29** está acoplada ferromagnéticamente de manera similar a como ocurría para el compuesto **17** y finalmente la red tridimensional del compuesto **30** exhibe orden magnético por debajo de 3.0 K.

### III.2. Etilmalonato de cobre(II) y sodio(I) (**31** y **32**)

Las estructuras de los compuestos  $\text{Na}_6[\text{Cu}(\text{Etmal})_2(\text{H}_2\text{O})]_3 \cdot 5\text{H}_2\text{O}$  (**31**) y  $\{\text{Na}[\text{Cu}_3(\text{H}_2\text{O})][\text{Cu}(\text{Etmal})_2(\text{H}_2\text{O})_3]\}_n \cdot n\text{H}_2\text{O}(\text{EtO})_2\text{NO}_3$  (**32**) son muy diferentes. El compuesto **31** es tridimensional y su estructura está formada por entidades aniónicas mononucleares de  $[\text{Cu}(\text{Etmal})_2(\text{H}_2\text{O})]^{2-}$  unidas a través de iones sodio(I), además de moléculas de agua de cristalización. La estructura de **32**, en cambio, es una red tridimensional de iones cobre(II) a puente carboxilato que posee poros y cavidades que alojan iones sodio(I), aniones nitrato y moléculas de etóxido y de agua. La diferencia entre las dos estructuras puede ser explicada en función del papel del ión sodio(I) en la red. En **31**, los iones sodio(I) construyen unidades monodimensionales que unen los monómeros de cobre(II) para dar lugar a la red 3D, mientras que en **32** los iones sodio(I) simplemente ocupan las cavidades de la estructura. Magnéticamente **32** es ferromagnético, sin embargo, el parámetro de acoplamiento no pudo ser determinado.

### III.3. 2,2'-Bipirimidina (**33**).

La estructura cristalina de  $[\text{Cu}_2(2,2'\text{-bipym})(\text{Etmal})_2(\text{H}_2\text{O})_2] \cdot 6\text{H}_2\text{O}$  (**33**) consiste en moléculas dinucleares aisladas y moléculas de agua de cristalización. La estructura es similar a la obtenida para los complejos homólogos con los ligandos malonato y metilmalonato (**23**), aunque diferente de la encontrada para el compuesto de fenilmalonato

(14). El compuesto **33** presenta el comportamiento magnético característico de un dímero de cobre(II) acoplado antiferromagnéticamente con una constante de acoplamiento de  $-132.6(8) \text{ cm}^{-1}$ , en buen acuerdo con los valores hallados para complejos similares.

#### III.4. 2,2'-Bipiridina (**34**) y 1,10-fenantrolina (**35**).

Los dos complejos mononucleares  $[\text{Cu}(\text{L})(\text{Etmal})(\text{H}_2\text{O})] \cdot 3\text{H}_2\text{O}$  [ $\text{L} = 2,2'$ -bpy (**34**) and phen (**35**)] presentan una estructura supramolecular tridimensional debida a puentes de hidrógeno e interacciones de tipo  $\pi$ . Es interesante hacer notar que la red bidimensional de puentes de hidrógeno observada en **34**, lo fue previamente en los complejos homólogos de fenilmalonato y metilmalonato.

## Capítulo IV. Discusión estructural y magnética

### IV.1. Discusión estructural.

#### IV.1.1. Introducción

En esta sección está dividida en dos partes, en la primera se discuten aquellos aspectos más interesantes de las estructuras presentadas en esta tesis desde un punto de vista global, mientras que en la segunda se revisan las estructuras del sistema R-malonato de cobre(II) con el agua como único coligando.

#### IV.1.2. Análisis de los datos cristalinos.

(i) Quiralidad. No existe predominancia por la cristalización en un grupo espacial determinado en las series de complejos. Aunque sí aparecen numerosos grupos no centrosimétricos, hecho remarcable teniendo en cuenta que los ligandos utilizados son todos aquirales. La quiralidad aparece en el entorno de coordinación del metal en muchos de los casos que la presentan, siendo la causa fundamental la aparición de un quelato ecuatorial-apical.

(ii) Modos de coordinación del ligando R-malonato. El modo de coordinación del ligando R-malonato depende del coligando presente en un determinado compuesto, aunque el más común es la coordinación bidentada bis-monodentada. De particular interés por su rareza es la coordinación del compuesto **26** (sólo bis-monodentada) que no tiene precedentes en compuestos de R-malonato de cobre(II).

(iii) Motivos de moléculas de agua. La aparición de moléculas de agua de cristalización que, a través de puentes de hidrógeno, forma un patrón bien definido ha sido de particular interés. Por ejemplo, los compuestos **21**, **23**, **30** y **34** presentan interesantes agregados de moléculas de agua en sus cavidades y poros.

#### IV.1.3. El sistema R-malonato de cobre(II)

La introducción de un sustituyente en el ligando malonato influye decisivamente en el empaquetamiento cristalino de los complejos de cobre(II) y además, permite la aparición de otros modos de coordinación diferentes del de la unidad de bis(malonato) de cobre(II). La simple sustitución de un grupo metilo causa la formación de un sistema estructural en forma de sandwich con los grupos hidrofóbicos (Me-, Et- o Ph-) agregados en capas. El comportamiento de condensación observado en el sistema H-malonato de cobre(II) (es decir, la cristalización de todos los compuestos a partir de la unidad mononuclear más simple en polimerizaciones consecutivas) ya no aparece en los complejos de malonato-sustituido de cobre(II). El aspecto más sobresaliente de este grupo ha sido el observado para el sistema del etilmalonato de cobre(II) donde se sintetizaron tres complejos con tres dimensionalidades diferentes.

#### IV.2. Discusión magneto-estructural.

En todos los compuestos tenemos como especie paramagnética el ión Cu(II) y en la mayoría de los casos en un entorno  $O_h$  o  $D_{4h}$ . Esto hace que la interacción magnética tenga lugar entre orbitales de igual simetría. En general este tipo de interacción nos llevaría a interacciones fuertes y antiferromagnéticas (del orden de  $-100$  a  $-250$   $cm^{-1}$ ). Sin embargo la gran mayoría de los compuestos exhiben interacciones débiles y ferromagnéticas (de  $0$  a  $5.6$   $cm^{-1}$ ), siendo ésta es la gran singularidad de los R-malonato complejos: el carácter débil y ferromagnético de la interacción observada.

Atendiendo al modelo de Kahn, esta singularidad se puede explicar teniendo en cuenta una importante reducción de la contribución antiferromagnética que ocurriría al reducirse la integral de solapamiento entre los orbitales con electrón desapareado y los orbitales del puente; debida fundamentalmente a la conformación *anti-syn* del puente carboxilato y/o al desvío del plano del carboxilato de alguno de los orbitales  $d(x^2-y^2)$  de alguno de los iones Cu(II). Estas dos características son las que tienen un mayor peso en la explicación de las propiedades (y sería las responsables de ese descenso en 2 ordenes de magnitud en los valores de  $J$ ) y las que permiten explicar el comportamiento observado en todos los compuestos.

El hecho de que  $J$  a veces sea positiva (predomina la contribución F) o negativa (predomina la contribución AF), depende de otros factores de menor índole particulares para cada compuesto. No se debe olvidar que esa contribución antiferromagnética no desaparece, sino que se hace del mismo orden que la ferromagnética, por tanto, otros factores pueden

variar levemente el valor de  $J$ . Más difícil es atribuir a un parámetro estructural la responsabilidad de la variación  $J$  desde  $-0.15$  a  $5.6 \text{ cm}^{-1}$ . La naturaleza del ligando ecuatorial, la distorsión trigonal, y las variaciones del ángulo de desvío del plano, así como el mayor o menor carácter *anti-syn* del puente contribuyen en mucha menor medida, pero son las que determinan el valor resultante. Sin embargo su efecto es pequeño y simultáneo y no podemos resolver las contribuciones individuales de cada uno de ellos.

## Capítulo V. Perspectivas

### V.1. Materiales moleculares magnéticos.

#### V.1.1. Introducción

El campo de investigación abierto con la introducción de un sustituyente en el carbono metílico del ligando malonato no tiene límites, puesto que el grupo sustituyente puede modificarse a voluntad. Los grupos que podemos introducir en el ligando malonato pueden dividirse en dos: (i) los de tipo estérico, como cadenas alifáticas o grandes grupos aromáticos capaces de establecer interacciones débiles entre ellos. Estos son del tipo presentado en esta tesis o (ii) los que pueden formar parte activa de la molécula, es decir, grupos capaces de coordinar a los iones metálicos y formar parte de la red covalente de la estructura.

#### V.1.2. En la línea de trabajo de la tesis: *bencilmalonato de cobre(II)* (**36**)

El ligando bencilmalonato es muy similar al fenilmalonato. La estructura de su complejo de cobre(II)  $[\text{Cu}(\text{Bzmal})(\text{H}_2\text{O})]$  (**36**) consiste en redes cuadradas de iones cobre(II) a puente carboxilato similares a las observadas en los compuestos, por ejemplo, **17** al **20**. Las capas están muy separadas por los anillos aromáticos del grupo bencilo del ligando bencilmalonato. El compuesto **36** presenta orden magnético por debajo de  $2.7 \text{ K}$ , un comportamiento similar al observado en **2** con una estructura también muy parecida. El hecho de que este compuesto se ordene magnéticamente nos indica que esta estrategia puede todavía ofrecernos muy interesantes resultados.

#### V.1.3. El sustituyente como parte activa del ligando

En esta sección se incluyen tres compuestos con otros tantos ligandos representativos de esta estrategia que promete ser muy fructífera.

(i) 2-hidroxo-2-fenil-malonato (OH-Phmal). El compuesto  $[\text{Cu}_4(\text{O-Phmal})_3(\text{H}_2\text{O})_5]_2 \cdot 2\text{NH}_4 \cdot 7\text{H}_2\text{O}$  (**37**) fue sintetizado de manera azarosa durante una síntesis con ácido fenilmalónico. Su estructura está formada por moléculas octanucleares que a través de

interacciones de tipo  $\pi$  y puentes de hidrógeno forma una red supramolecular tridimensional. Las entidades octanucleares están constituidas por dos tetranucleares unidas por un doble puente  $\mu$ -oxo; éstas, a su vez, están formadas por una entidad trinuclear a puente  $\mu$ -oxo y un cuarto ion cobre(II) unido a través de un doble puente carboxilato *anti-anti*. Este compuesto es muy interesante por la entidad trinuclear que presenta, en ella el puente  $\mu$ -oxo debe mediar interacciones antiferromagnéticas, dando lugar a frustración de espín. Además puede servir de precursor para el diseño de nuevas moléculas magnéticas.

(ii) ácido ketomalónico (Ketomal). El compuesto  $\{K_3[Cu_3(Ketomal)_3(H_2O)]\}_n \cdot 4nH_2O$  (**38**) está constituido por entidades trinucleares unidas por iones potasio(I) para dar lugar a una red tridimensional. La formación trinuclear es similar a la que aparece en **37** y su comportamiento magnético muestra que posee un estado fundamental  $S \neq 0$  y que está poblado a temperaturas por debajo de 50 K. Este compuesto, además, puede actuar como ligando hexadentado debido a que los átomos de oxígeno del ligando ketomalonato están bien orientados para aceptar otros centros paramagnéticos, y por tanto, servir de precursor para una nueva familia de compuestos importante en el campo del magnetismo molecular.

(iii) 2-hidroxo-2-fenil-2-(N'-pirazolil)-acetato (OH-ppac). El compuesto  $[Cu_4(pz)_4(OH-ppac)_2(H_2O)_4]$  (**39**) fue sintetizado de manera fortuita durante una síntesis con ácido fenilmalónico. La estructura cristalina de **39** consiste en moléculas tetranucleares aisladas en la que los iones cobre(II) se encuentran unidos por puentes pirazol y alkoxo. En cada una de estas moléculas aparecen dos ligandos OH-ppac relacionados por un centro de inversión, por tanto, las dos enantiómeros del ligando OH-ppac están presentes en la misma molécula. El comportamiento magnético de este compuesto es el característico de un complejo dinuclear con gran acoplamiento antiferromagnético que luego interaccionan antiferromagnéticamente también entre ellos. Este compuesto presenta gran interés debido a que podría formar complejos similares a los dos ligandos presentados anteriormente y puesto que el ligando es quiral, presentar también interesantes propiedades ópticas.

## V.2. Materiales porosos.

Los materiales microporosos presentan un gran interés debido a su aplicación en catálisis, intercambio iónico, almacenamiento de hidrógeno, etc. Por ello, el estudio de las propiedades porosas de algunos de los compuestos presentados en esta Tesis debe ser parte de una futura investigación. Algunos como **25**, **30**, **31** ó **32** presentan grandes cavidades y poros que, aunque ocupados por solvente (susceptible de ser evacuado o eliminado reversiblemente), podrían ser utilizados para el almacenamiento de gases.

### **V.3. Materiales quirales.**

Los materiales quirales son interesantes por sus aplicaciones en óptica no-lineal. La gran cantidad de compuestos que cristalizan en grupos espaciales no centrosimétricos nos hace pensar que quizá puedan presentar sorprendentes propiedades ópticas. Un área que merece ser investigada en el futuro.

---

---

# **Annexe**

---

---



Paper

# The flexibility of molecular components as a suitable tool in designing extended magnetic systems†

Yolanda Rodríguez-Martín,<sup>a</sup> María Hernández-Molina,<sup>a</sup> Fernando S. Delgado,<sup>a</sup> Jorge Pasán,<sup>\*a</sup> Catalina Ruiz-Pérez,<sup>\*a</sup> Joaquín Sanchiz,<sup>b</sup> Francesc Lloret<sup>c</sup> and Miguel Julve<sup>c</sup>

<sup>a</sup>Laboratorio de Rayos X y Materiales Moleculares, Departamento de Física Fundamental II, Universidad de La Laguna, Avda. Astrofísico Francisco Sánchez s/n, 38204 La Laguna, Tenerife, Spain. E-mail: caruiz@ull.es

<sup>b</sup>Departamento de Química Inorgánica, Universidad de La Laguna, 38204 La Laguna, Tenerife, Spain

<sup>c</sup>Departament de Química Inorgànica/Institut de Ciència Molecular, Facultat de Química, Universitat de València, Avda. Dr. Moliner 50, 46100 Burjassot, València, Spain

Received 9th April 2002, Accepted 21st May 2002

Published on the Web 19th July 2002

In this work we show how the design of  $n$ -dimensional magnetic compounds ( $nD$  with  $n = 1-3$ ) can strongly benefit from the use crystal engineering techniques, which can give rise to structures of different shapes with different properties. We focus on the networks built by assembling the malonato-bridged tetranuclear copper(II) units  $\text{Cu}_4(\text{mal})_4$  ( $\text{mal}^{2-}$  is the dianion of propanedioic acid,  $\text{H}_2\text{mal}$ ) through the potentially bridging 2,4'-bipyridine (2,4'-bpy), 4,4'-bipyridine (4,4'-bpy) and pyrazine (pyz). The magneto-structural study of the complexes of formula  $[\text{Cu}_4(\text{mal})_4(2,4'\text{-bpy})_4(\text{H}_2\text{O})_4]\cdot 8\text{H}_2\text{O}$  (**1**),  $[\text{Cu}_4(\text{mal})_4(\text{H}_2\text{O})_4(4,4'\text{-bpy})_2]$  (**2**) (this compound was the subject of a previous report but it is included here for comparison) and  $[\text{Cu}_4(\text{mal})_4(\text{pyz})_2]\cdot 4\text{H}_2\text{O}$  (**3**) reveals that the ferromagnetically coupled  $\text{Cu}_4(\text{mal})_4$  unit which occurs in **1-3** is propagated into two- (**2**) and three-dimensions (**3**) by using 4,4'-bpy and pyz as linkers, respectively. Whereas in the case of complex **1**, this tetranuclear unit is magnetically isolated, significant antiferromagnetic interactions between these units mediated by the bridges 4,4'-bpy and pyz occur in **2** and **3**.

## Introduction

Crystal engineering appears to be a suitable tool for the development of rational strategies in designing new crystalline materials, in particular those with functional properties.<sup>1</sup> For example, the specific network topology of a coordination polymer can be controlled by a careful selection of the metal coordination geometry and the organic *spacer*. Indeed, a wide range of one-,<sup>2</sup> two-<sup>3,4</sup> and three-dimensional<sup>5-7</sup> networks ( $nD$ ,  $n = 1-3$ ) which are unknown in naturally occurring compounds have been prepared. A particularly simple example of such a designed and predictable coordination polymer network is the 2D square grid generated when square planar or octahedral metal complexes are linked through the linear *rod* ligand 4,4'-bipyridine (4,4'-bpy).<sup>3</sup> Additionally, more subtle effects such as anion control<sup>8-10</sup> and the use of  $\pi-\pi$  stacking<sup>11</sup> have been seen to have a profound effect upon the network topology.

We are interested in the building-block approach for the network construction of coordination polymers focusing both on the role of the metal-ion geometry and that of the bridging ligand. A survey of the synthetic attempts reveals that most of them deal with rod-like and rigid bridging ligands, and consequently, the use of more flexible spacers deserves to be explored.<sup>12,13</sup> From this respect, the malonate ligand (dianion of the propanedioic acid,  $\text{H}_2\text{mal}$ ) seems a suitable candidate. The occurrence of two carboxylate groups in 1,3-positions allows this ligand to adopt simultaneously chelating bidentate and different carboxylato bridging modes (*syn-syn*, *syn-anti*

and *anti-anti* through one or both carboxylate groups).<sup>14-22</sup> The well known ability of the carboxylato bridge to mediate significant ferro- or antiferro-magnetic interactions<sup>23-27</sup> between the paramagnetic metal ions that it bridges makes the malonate ligand very interesting in the design of extended magnetic systems.

In the context of our magneto-structural research with malonate-bridged homo- and hetero-metallic complexes,<sup>28</sup> we reported very recently the structure and magnetic study of the two-dimensional square network complex  $[\text{Cu}_4(\text{mal})_4(\text{H}_2\text{O})_4(4,4'\text{-bpy})_2]$  (**2**).<sup>29</sup> The replacement of 4,4'-bpy by 2,4'-bpy and pyrazine (pyz) afforded the molecular complex  $[\text{Cu}_4(\text{mal})_4(2,4'\text{-bpy})_4(\text{H}_2\text{O})_4]\cdot 8\text{H}_2\text{O}$  (**1**) and the three-dimensional complex network  $[\text{Cu}_4(\text{mal})_4(\text{pyz})_2]\cdot 4\text{H}_2\text{O}$  (**3**) where malonate, 2,4'-bpy and pyz act as bridging ligands. Their preparation, structural characterization and magnetic properties are presented herein.

## Experimental section

### Materials

Malonic acid (Aldrich), basic copper(II) carbonate  $[\text{CuCO}_3\cdot\text{Cu}(\text{OH})_2]$  (Merck), 2,4'-bipyridine (Aldrich) and pyrazine (Aldrich) were used as received. Elemental analyses (C, H, N) were performed on an EA 1108 CHNS-O microanalytical analyzer.

### Synthesis of $[\text{Cu}_4(\text{mal})_4(2,4'\text{-bpy})_4(\text{H}_2\text{O})_4]\cdot 8\text{H}_2\text{O}$ (**1**)

Malonic acid (0.208 g, 2 mmol) is added to a warm aqueous suspension (30 cm<sup>3</sup>) of basic copper(II) carbonate (0.221 g,

†Based on the presentation given at CrystEngComm Discussion, 29th June–1st July 2002, Bristol, UK.

Dedicated to the memory of Professor Olivier Kahn.



1 mmol) under continuous stirring and heating below 50 °C to generate *in situ* 2 mmol of copper(II) malonate. The solution is filtered and allowed to cool to 34 °C; then, an ethanolic solution (10 cm<sup>3</sup>) of 2,4'-bpy (0.312 g, 2 mmol) is added. The resulting clear blue solution is allowed to stand at 28 °C. Dark-blue cubic crystals of **1** appeared within a few hours. Yield, 0.418 g (55% with reference to the copper). Although the crystals obtained have a nice shape and size they are not air stable undergoing fast disintegration when removed from the mother liquor. It seems that ethanol is clathrated, because even when the crystals are dry there is a strong ethanolic smell. The crystals are left in contact with the mother liquors for *ca.* three weeks, until the ethanol is evaporated from the solution, then the crystals become air stable. All measurements were performed with the air stable crystals. Anal. calc. for C<sub>52</sub>H<sub>64</sub>N<sub>8</sub>O<sub>28</sub>Cu<sub>4</sub> (**1**): C, 41.54; H, 4.26; N, 7.46. Found: C, 41.63; H, 4.32; N, 7.60%. IR (KBr)/cm<sup>-1</sup>: 1608s, 1580s, 1437s, 1367vs and 745s.

### Synthesis of [Cu<sub>4</sub>(mal)<sub>4</sub>(pyz)<sub>2</sub>·4H<sub>2</sub>O (**3**)

This compound is obtained by the reaction of an aqueous solution (40 cm<sup>3</sup>) of 2 mmol of copper(II) malonate generated *in situ* as previously mentioned, with an aqueous solution (10 cm<sup>3</sup>) of pyrazine (0.080 g, 1 mmol). The solution is allowed to stand at 28 °C overnight and dark-blue crystals suitable for X-ray diffraction were obtained. The crystals are air stable and do not lose solvent at room temperature (ethanol was not used in this procedure), and were used for all measurements. Yield, 0.322 g (72% with reference to the copper). Anal. calc. for C<sub>20</sub>H<sub>24</sub>N<sub>4</sub>O<sub>20</sub>Cu<sub>4</sub> (**3**): C, 26.85; H, 2.70; N, 6.26. Found: C, 26.65; H, 2.55; N, 6.77%. IR (KBr)/cm<sup>-1</sup>: 1603s, 1583s, 1440s, 1383vs and 745s.

The Cu(II):mal<sup>2-</sup>:L [L = 2,4'-bpy (**1**) and pyz (**3**)] molar ratio used in the preparations of **1** and **3** are those of their respective formulae. The temperature is a quite critical factor: bad quality crystals are obtained for *T* ≈ 40 °C, whereas the ionic salt [Cu(H<sub>2</sub>O)<sub>6</sub>][Cu(mal)<sub>2</sub>(H<sub>2</sub>O)<sub>2</sub>] is formed when *T* ≈ 20 °C.<sup>19f</sup> The conditions for the best quality crystals of **1** and **3** were those detailed above.

### Physical measurements

IR spectra of **1** and **3** (4000–400 cm<sup>-1</sup>) were recorded on a Bruker IF S55 spectrophotometer with the sample prepared as a KBr pellet. Variable temperature (1.9–300 K) magnetic susceptibility measurements of crushed crystals of **1–3** were carried out in a Quantum Design SQUID magnetometer operating at 100 G (*T* < 50 K) and 1000 G (*T* > 50 K). Diamagnetic corrections of all the constituent atoms were estimated from Pascal's constants<sup>30</sup> as -767.2 × 10<sup>-6</sup> and -343.2 × 10<sup>-6</sup> cm<sup>3</sup> mol<sup>-1</sup>, for **1** and **3**, respectively. Magnetic susceptibility data were also corrected for the temperature-independent paramagnetism [60 × 10<sup>-6</sup> cm<sup>3</sup> mol<sup>-1</sup> per copper(II)] and the magnetization of the sample holder.

### Crystal structure determination

Crystal data and details of measurements for compounds **1** and **3** are reported in Table 1.

Diffraction intensities for **1** were collected at 293 K on a Nonius KappaCCD; for **3** the data were collected on an Enraf-Nonius MACH3 four-circle diffractometer. Both diffractometers were equipped with a graphite monochromator (MoK $\alpha$  radiation,  $\lambda$  = 0.71073 Å). In **3**, intensity data were corrected also for absorption ( $\psi$ -scan method). The maximum and minimum transmission factors were 0.816 and 0.967. All refinements have been carried out on *F*<sup>2</sup> using the SHELXS-97 and SHELXL-97 programs.<sup>31,32</sup> All non-hydrogen atoms were refined anisotropically. For **1** the assignment of N2/C20 atoms in the 2,4'-bpy ligand was carefully checked. However,

**Table 1** Crystallographic data for [Cu<sub>4</sub>(mal)<sub>4</sub>(2,4'-bpy)<sub>4</sub>(H<sub>2</sub>O)<sub>4</sub>]·8H<sub>2</sub>O **1** and [Cu<sub>4</sub>(mal)<sub>4</sub>(pyz)<sub>2</sub>]·4H<sub>2</sub>O **3**<sup>a</sup>

| Parameter                                | <b>1</b>                                                                       | <b>3</b>                                                                       |
|------------------------------------------|--------------------------------------------------------------------------------|--------------------------------------------------------------------------------|
| Formula                                  | C <sub>52</sub> H <sub>64</sub> N <sub>8</sub> O <sub>28</sub> Cu <sub>4</sub> | C <sub>20</sub> H <sub>24</sub> N <sub>4</sub> O <sub>20</sub> Cu <sub>4</sub> |
| <i>M</i>                                 | 1503.29                                                                        | 894.60                                                                         |
| Crystal system                           | Tetragonal                                                                     | Tetragonal                                                                     |
| Space group                              | <i>I</i> 42 <i>d</i>                                                           | <i>P</i> 4 <sub>2</sub> <i>c</i>                                               |
| <i>a</i> /Å                              | 32.760(5)                                                                      | 12.590(2)                                                                      |
| <i>b</i> /Å                              | 32.760(5)                                                                      | 12.590(2)                                                                      |
| <i>c</i> /Å                              | 7.6095(5)                                                                      | 9.188(2)                                                                       |
| <i>V</i> /Å <sup>3</sup>                 | 8167(2)                                                                        | 1456.4(5)                                                                      |
| <i>Z</i>                                 | 4                                                                              | 2                                                                              |
| <i>T</i> /K                              | 293(2)                                                                         | 293(2)                                                                         |
| <i>D<sub>c</sub></i> /g cm <sup>-3</sup> | 1.223                                                                          | 2.040                                                                          |
| Fleck parameter                          | 0.00                                                                           | -0.04(3)                                                                       |
| $\lambda$ /Å                             | 0.71073                                                                        | 0.71073                                                                        |
| $\mu$ (MoK $\alpha$ )/cm <sup>-1</sup>   | 10.98                                                                          | 29.79                                                                          |
| <i>R</i> <sup>b</sup>                    | 0.0907                                                                         | 0.0274                                                                         |
| <i>R<sub>w</sub></i> <sup>c</sup>        | 0.2255                                                                         | 0.0791                                                                         |

<sup>a</sup>Click here for full crystallographic data (CCDC 185258–185260).  
<sup>b</sup>*R* =  $\Sigma||F_o| - |F_c||/\Sigma|F_o|$ . <sup>c</sup>*R<sub>w</sub>* =  $[\Sigma w(|F_o|^2 - |F_c|^2)^2]/\Sigma w|F_o|^2$ <sup>1/2</sup>.

inspection of a disorder over two alternative positions did not improve the refinement. For **3** the high temperature factor on the C(11) and C(12) atoms of the pyrazine group reveals that the molecule can be disordered. A careful inspection of the difference maps and subsequent refinement of the site occupation factors (s.o.f.) did not show two statistical positions for these atoms. The hydrogen atoms for **1** were placed at calculated positions except those on the water molecules. Hydrogen atoms for **3** were located on the difference map except those of the pyrazine molecule which were set in calculated positions and refined with isotropic temperature factors. Analytical expressions of neutral scattering factors were used, and anomalous dispersion corrections were incorporated.<sup>33</sup> The final geometrical calculations and the graphical manipulations were carried out with PARST95<sup>34</sup> and PLATON<sup>35</sup> programs, respectively. Selected interatomic bond distances and angles for **1** and **3** are listed in Table 2.

**Table 2** Selected bond lengths (Å) and angles (°) for compounds **1** and **3**

| Compound <b>1</b> |           |                    |           |
|-------------------|-----------|--------------------|-----------|
| Cu(1)–O(1)        | 1.963(5)  | Cu(1)–O(1W)        | 2.204(6)  |
| Cu(1)–O(2A)       | 1.986(5)  | Cu(1)–N(1)         | 2.024(6)  |
| Cu(1)–O(3)        | 1.939(5)  |                    |           |
| O(1)–Cu(1)–O(2A)  | 90.66(2)  | O(2A)–Cu(1)–N(1)   | 91.18(2)  |
| O(1)–Cu(1)–O(3)   | 88.93(2)  | O(3)–Cu(1)–O(1W)   | 93.25(2)  |
| O(1)–Cu(1)–O(1W)  | 97.74(2)  | O(3)–Cu(1)–N(1)    | 88.07(2)  |
| O(1)–Cu(1)–N(1)   | 166.10(2) | O(1W)–Cu(1)–N(1)   | 100.98(2) |
| O(2A)–Cu(1)–O(3)  | 175.14(2) | Cu(1)–O(1)–C(11)   | 122.07(4) |
| O(2A)–Cu(1)–O(1W) | 91.61(2)  | Cu(1)–O(2A)–C(11A) | 112.44(4) |
| Compound <b>3</b> |           |                    |           |
| Cu(1)–O(1)        | 1.965(3)  | Cu(1)–O(4b)        | 2.250(3)  |
| Cu(1)–O(2a)       | 1.955(3)  | Cu(1)–N(1)         | 2.038(3)  |
| Cu(1)–O(3)        | 1.930(3)  |                    |           |
| O(1)–Cu(1)–O(2a)  | 87.54(1)  | O(3)–Cu(1)–O(4b)   | 88.91(1)  |
| O(1)–Cu(1)–O(3)   | 91.96(1)  | O(3)–Cu(1)–N(1)    | 87.84(1)  |
| O(1)–Cu(1)–O(4b)  | 90.10(1)  | O(4b)–Cu(1)–N(1)   | 94.62(1)  |
| O(1)–Cu(1)–N(1)   | 175.26(1) | Cu(1)–O(1)–C(1)    | 123.60(3) |
| O(2a)–Cu(1)–O(3)  | 171.26(1) | Cu(1)–O(2a)–C(2a)  | 118.00(3) |
| O(2a)–Cu(1)–O(4b) | 99.82(1)  | Cu(1)–O(4b)–C(3b)  | 127.80(3) |
| O(2a)–Cu(1)–N(1)  | 91.94(1)  |                    |           |

Symmetry codes: A = *y*, -*x* + 2, -*z*; a = *y*, -*x* + 1/2, -*z*; b = *y* + 1/2, *x* - 1/2, *z* - 1/2.

## Results and discussion

### Description of the structure of 1

The crystal structure of **1** consists of molecules of water of crystallization and molecules of  $[\text{Cu}_4(\text{mal})_4(2,4'\text{-bpy})_4(\text{H}_2\text{O})_4]$  involving a small planar square with copper(II) cations and malonate anions at each corner and side, respectively. Each copper atom of this tetranuclear unit is linked to a monodentate 2,4'-bpy ligand [Fig. 1(a)]. The molecules are stacked parallel on each other along the tetragonal  $c$  axis [Fig. 1(b)] with an interplanar separation of 3.888(4) Å (1/2 of  $c$  axis) indicating weak  $\pi$ - $\pi$  stacking interactions, exhibiting the ABABAB sequence. Weak hydrogen bonds involving the non-coordinated water molecules ( $\text{C}-\text{H}\cdots\text{OW}$ ) and two malonate oxygens ( $\text{C}-\text{H}\cdots\text{O}$ ) contribute to the stabilization of the crystal structure (see the CIF details in Table 1). The angles at the corners of the square-planar cavity [90.70(2)°] are very close to the ideal square-planar angle of 90°. The dimensions of the square cavities are 4.670(1) × 4.670(1) Å and no solvent molecules are clathrated in them.

Each copper atom exhibits a slightly distorted square pyramidal surrounding, the geometric  $\tau$  value<sup>36</sup> being only 0.15. Three carboxylate-oxygen atoms [O(1), O(3) and O(2a) ( $a = y, -x + 2, -z$ )] from two malonate ligands and one nitrogen atom [N(1)] from the 2,4'-bpy group build the basal plane whereas the apical position is filled by a water molecule.

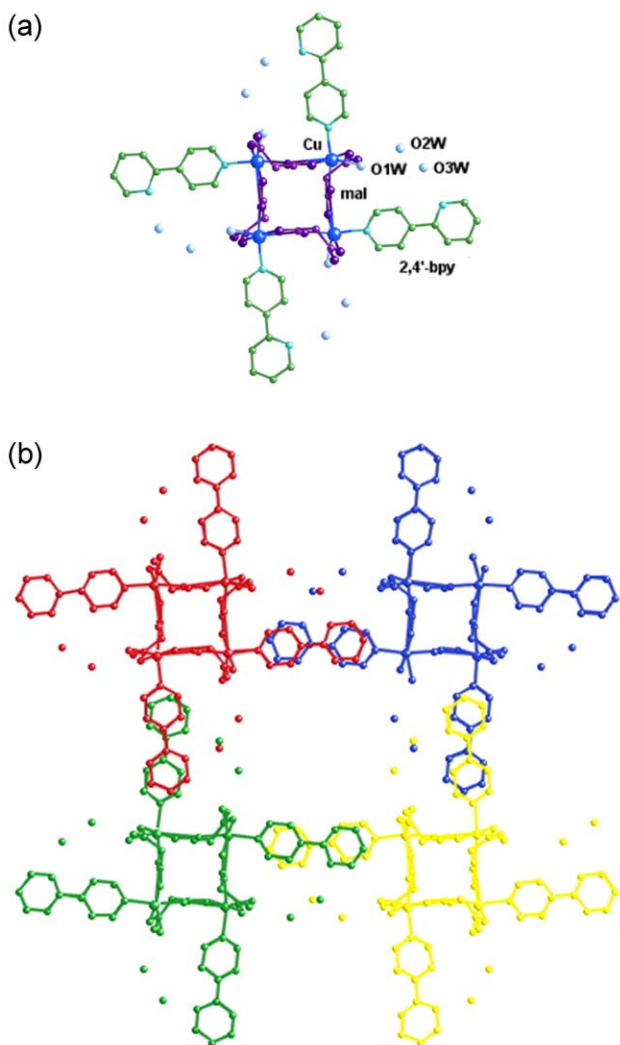


**Fig. 1** (a) Perspective view of the asymmetric unit and three symmetry-related units of **1**; click image or here to access a 3D representation. (b) View of the packing along the tetragonal  $c$  axis; click image or here to access a 3D representation.

The average value of the copper to malonate bond distance [1.963(5) Å] lies within the range observed for other malonate-containing copper(II) complexes.<sup>19,22,28</sup> The copper atom is shifted by 0.161(7) Å from the mean basal plane towards the apical position. The dihedral angle between the equatorial planes of adjacent copper atoms within the malonato-bridged square unit is 70.99(1)°. Each malonate group simultaneously adopts bidentate [through O(1) and O(3) atoms at Cu(1)] and monodentate [through O(2) at Cu(1b)] coordination modes and exhibits a boat conformation with  $\phi = 0.22(5)^\circ$  and  $QT = 0.7798(7)$  Å ( $\phi$  and  $QT$  being the phase angle and total puckering amplitude, respectively).<sup>37</sup> The value of the angle subtended at the copper atom by the bidentate malonato is 89.93(2)°. The average C–O bond distances and O–C–O bond angles are 1.256(9) Å and 122.57(7)°, respectively. The O(1)–C(1)–O(2) carboxylate bridge adopts the *anti-syn* conformation. The value of the dihedral angle between the equatorial plane at Cu(1) and that of the O(1)–C(1)–O(2) bridging carboxylate is 42.19(5)°. The pyridyl rings of the 2,4'-bpy are planar but the ligand as a whole is far from being planar [the dihedral angle between the two pyridyl rings is 29.28(3)°].

### Description of the structure of 2

The structural description of **2** was reported elsewhere<sup>29</sup> and it is briefly recalled here for comparison purposes. The crystal structure of **2** consists of two-dimensional networks involving a small planar square with copper(II) cations and malonate anions at each corner and side, respectively (see Fig. 2). Each copper atom of this tetranuclear unit is linked to another one through a bis-monodentate 4,4'-bpy ligand forming thus a large square in which each edge is shared by one malonate group and one 4,4'-bpy molecule. The layers are stacked parallel but in a staggered manner on each other along the tetragonal  $c$  axis [Fig. 3(a)] with an interplanar separation of 3.850(4) Å (1/2 of  $c$  axis) and an angle of 56.3(2)° indicating weak  $\pi$ - $\pi$  stacking interactions. Hydrogen bonds involving the coordinated water molecule and two malonate oxygens [2.783(9) and 3.014(8) Å for O(1w)⋯O(4c) and O(1w)⋯O(2a), respectively; ( $c = x, -y + 1, -z$ )] contribute to the stabilization of the crystal structure. The small malonate-bridged tetranuclear units fit exactly into the large 4,4'-bpy rings of the adjacent sheet. Parallel sheets stacked on top of each other [the separation is 7.56(3) Å] are laterally displaced so that the copper atoms of the first sheet viewed in the horizontal plane are vertically above those of the 3rd, 5th, 7th, etc., sheets [Fig. 3(b)]. An equivalent stacking of sheets is found in planes parallel to the first. The angles at the corners of the small and large square-planar cavities [89.9(2) and 90.1(2)°, respectively] are very close to the ideal square-planar angle of 90°. The dimensions of the large and small square cavities are 15.784(1) × 15.784(1) Å and 4.644(1) × 4.644(1) Å respectively, and no solvent molecules are clathrated.

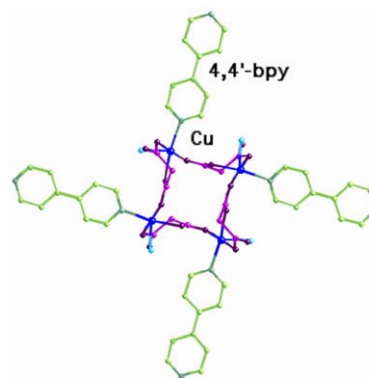


**Fig. 2** Perspective view of the asymmetric unit and three symmetry-related units of **2**.

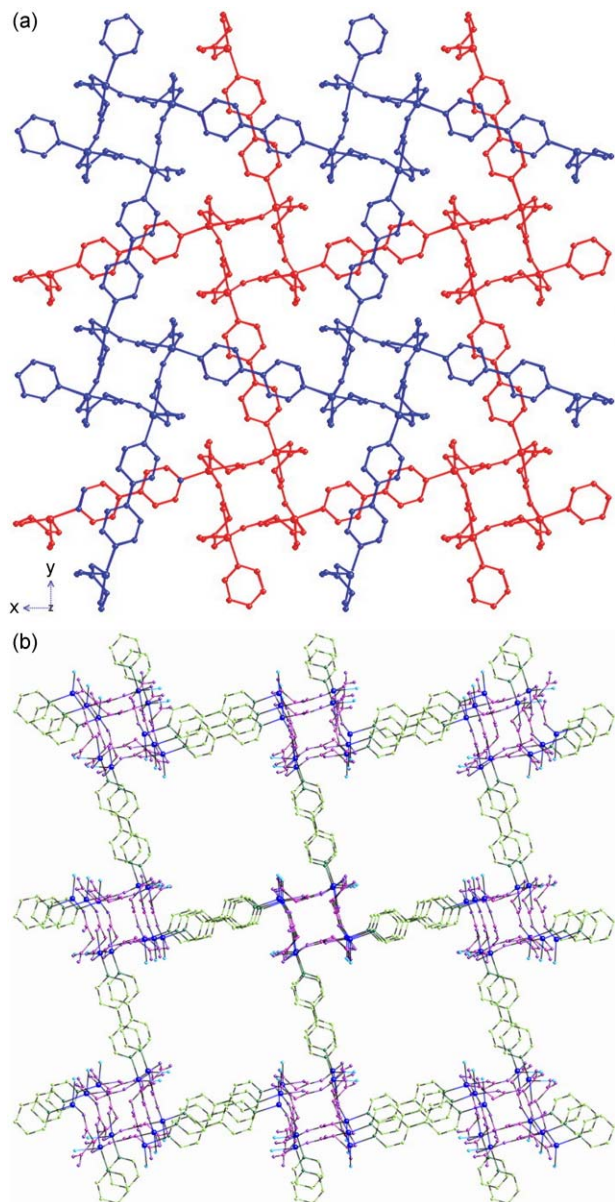


**Fig. 3** (a) View of two adjacent layers of 2 along the *c* axis showing the  $\pi$ - $\pi$  overlap between pairs of 4,4'-bpy molecules. (b) View of the two types of square channels of 2 along the *c* axis when only the odd layers are considered.

### Description of the structure of 3

The crystal structure of complex 3 consists of a three-dimensional arrangement of copper(II) ions bridged by malonate and pyrazine ligands (Fig. 4). The asymmetric unit is shown in Fig. 5(a) with one copper atom at each corner and a malonate anion at each side of a small planar square. Each copper atom of this tetranuclear unit is linked to another one through a bis-monodentate pyrazine ligand forming thus a large square in which each edge is shared by one malonate group and one pyz molecule. The angles at the corners of the small and large square-planar cavities [89.40(2) and 89.90(3)°, respectively] are very close to the ideal square-planar angle of 90°. The dimensions of the large and small square cavities are 11.670(1)  $\times$  11.670(1) Å and 4.842(1)  $\times$  4.842(1) Å, respectively. Within a layer, each malonate acts simultaneously as bidentate [through O(2) and O(3) at Cu(1d); (d) =  $-y + 1, x, -z$ ]. The remaining carboxylate-malonate oxygen [O(4)] is bound to another copper atom [Cu(1c); (c) =  $y + 1/2, -x - 1/2, z + 1/2$ ] from the adjacent layer [the bridging pathway being Cu(1)-O(3)-C(3)-O(4)-Cu(1c)] affording the three-dimensional

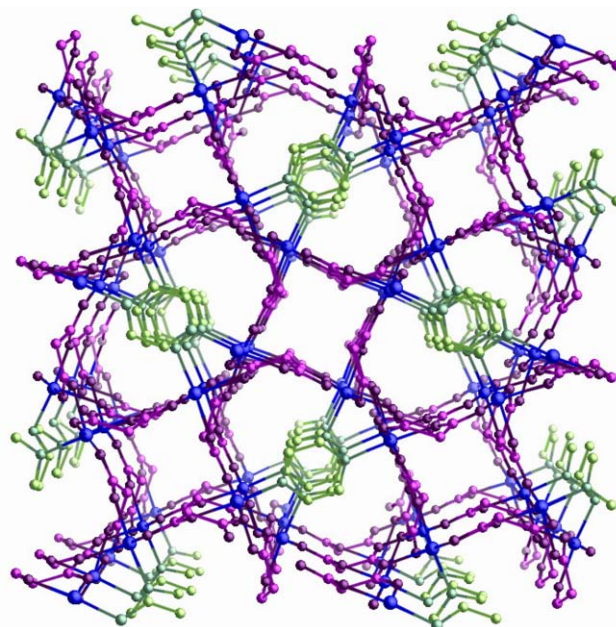


**Fig. 4** View of the 3D structure of 3 along the *c* axis showing the eclipsed arrangement. Click image or [here](#) to access a 3D representation.

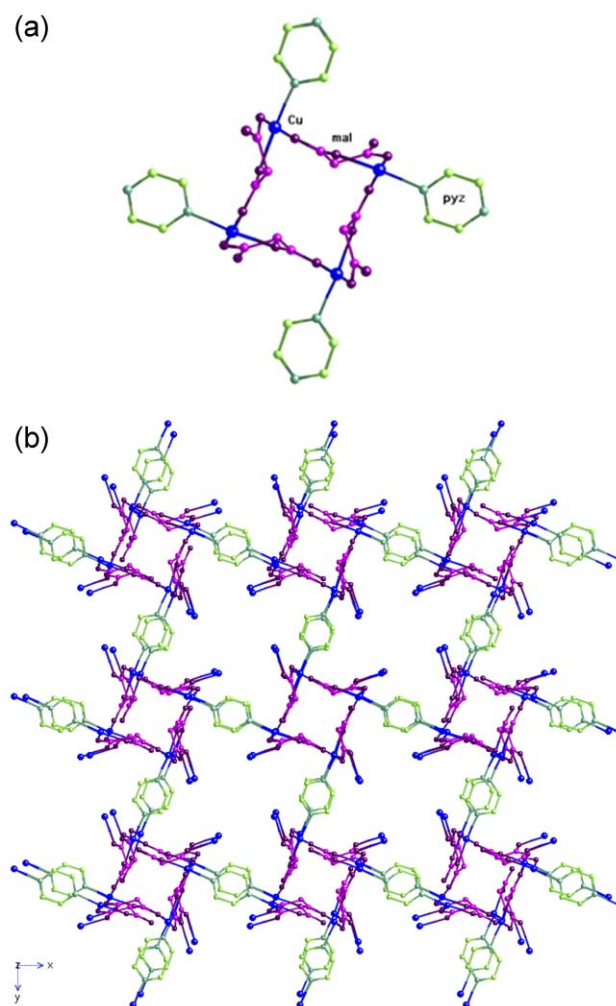


**Fig. 5** (a) Perspective view of the asymmetric unit of 3 showing the bridging role of malonate and pyrazine. (b) View of two adjacent odd layers of 3 along the *c* axis showing the stacking of the square grid layers.

network. The layers are stacked parallel but in a staggered manner on each other along the tetragonal  $c$  axis (the layers exhibiting the ABABAB sequence) with an AB interlayer separation of 4.594(1) Å (1/2 of  $c$  axis) and a twist angle of 44.6(2)°. The small malonate-bridged tetranuclear units of a given layer fit exactly into the large pyz rings of the following one. The copper atoms of the first layer viewed in the horizontal plane are vertically above those of the 3rd, 5th, 7th, etc., sheets [Fig. 5(b)]. Uncoordinated water molecules are clathrated into the small square cavities and they are linked to two malonate oxygens through hydrogen bonds [2.825(6) and 3.168(5) Å for O(1w)⋯O(4) and O(1w)⋯O(3c), respectively] contributing to the stabilization of the crystal structure.

Each copper atom exhibits a nearly perfect square pyramidal surrounding, the geometric  $\tau$  value<sup>36</sup> being only 0.06. Three carboxylate-oxygen atoms [O(1), O(3) and O(2a)] from two malonate ligands and one nitrogen atom [N(1)] from the pyz molecule build the basal plane whereas the apical position is filled by a carboxylate-oxygen atom [O(4b) at 2.250(3) Å] from a different malonate ligand. The average value of the equatorial copper to malonate bond distance [1.947(3) Å] lies within the range observed for other malonate-containing copper(II) complexes.<sup>19,28,29</sup> The Cu–N(py) distance also agrees with those reported for other pyz-bridged copper(II) complexes.<sup>38</sup> The copper atom is shifted by 0.1201(4) Å from the mean basal plane towards the apical position. The dihedral angle between the equatorial planes of adjacent copper atoms [Cu(1) and Cu(1d)] within the square unit is 79.86(1)° whereas that involving the copper atoms which are bridged by the O(3)–C(3)–O(4) [Cu(1) and Cu(1c)] is 68.32(1)°. The malonate ligand exhibits a boat conformation with  $\phi = 119.0(3)^\circ$  and QT = 0.5749(4) Å.<sup>37</sup> The value of the angle subtended at the copper atom by the bidentate malonate is 91.96(1)°. The average C–O bond distances and O–C–O bond angles are 1.257(5) Å and 122.45(4)°, respectively. The O(1)–C(1)–O(2) and O(3)–C(3)–O(4) carboxylate bridges adopt the *anti-syn* conformation. The values of the dihedral angle between the equatorial plane at Cu(1) and that of the O(1)–C(1)–O(2) and O(3)–C(3)–O(4) bridging carboxylates are 32.17(3) and 30.12(4)°, respectively. The copper–copper distances through these bridges are 4.842(1) [Cu(1)⋯Cu(1a)] and 5.276(1) Å [Cu(1)⋯Cu(1c)], values which are much shorter than that across bridging pyrazine [6.843(2) Å for Cu(1)⋯Cu(1e); (e) =  $-x + 1, -y, -z$ ]. This last value is similar to those observed in previous pyrazine-bridged copper(II) complexes.<sup>38c,38f,39,40</sup> The pyrazine ring moiety is practically planar within experimental error. The value of the dihedral angle between the copper equatorial planes across bridging pyz is 49.62(1)°.

### Magnetic properties

The magnetic properties of **1–3** under the form of  $\chi_M T$  versus  $T$  plots [ $\chi_M$  being the magnetic susceptibility per four Cu(II) ions] are shown in Fig. 6. For **1–3** the product  $\chi_M T$  at 290 K ranges from 1.69 to 1.75 cm<sup>3</sup> mol<sup>-1</sup> K, values which are somewhat above that for four magnetically isolated spin doublets (1.65 cm<sup>3</sup> mol<sup>-1</sup> K with  $g = 2.10$ ). Upon cooling,  $\chi_M T$  values exhibit different behavior for each compound, but they are strongly related as discussed hereunder. Compounds **1–3** have in common the square tetranuclear [Cu<sub>4</sub>(mal)<sub>4</sub>L<sub>4</sub>] unit, the difference being the way they are connected to each other. The magnetic properties of **1–3** are governed essentially by those of this square which is isolated in **1** but connected in different fashions in the other two compounds. Although the magnetic properties of **2** were the subject of a previous report we include them here for a better understanding of those of the new compounds **1** and **3**.

The  $\chi_M T$  plot for **1** continuously increases as the temperature is lowered, reaching a plateau at 3.0 K ( $\chi_M T = 3.24$  cm<sup>3</sup> mol<sup>-1</sup> K) which is as expected for a magnetically

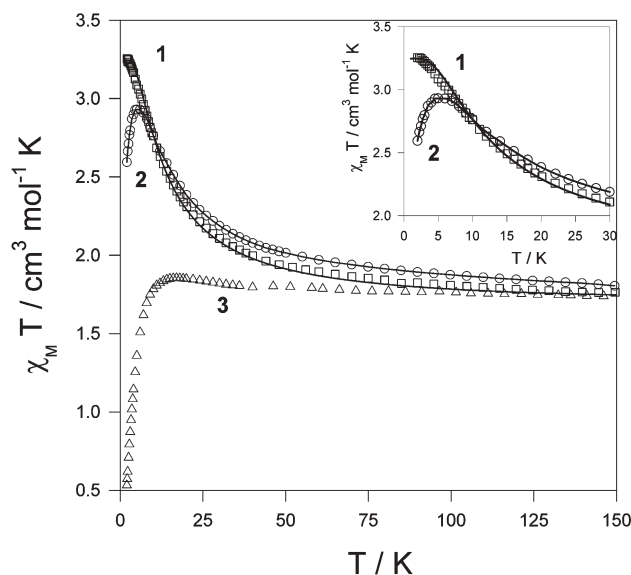


**Fig. 6** Thermal dependence of the  $\chi_M T$  product for complexes **1–3**: (**1**, □; **2**, ○; **3**, △) experimental data; (—) best fit through eqn. (1). The inset shows the  $\chi_M T$  plot in the low temperature region.

isolated square of four spin doublets interacting ferromagnetically (low lying  $S = 2$  accounting for the observed plateau of  $\chi_M T$ ). For compound **2**,  $\chi_M T$  continuously increases, reaches a maximum of 2.93 cm<sup>3</sup> mol<sup>-1</sup> K at 5.5 K and further decreases at lower temperatures. As was previously established, the magnetic behavior of **2** is satisfactorily interpreted considering a quadratic layer of ferromagnetically coupled tetranuclear copper(II) units, which are antiferromagnetically coupled through the bridging 4,4'-bpy. The magnetic coupling within the tetramer is strong and ferromagnetic ( $J = 12.4$  cm<sup>-1</sup>), whereas the coupling through the bridging 4,4'-bpy is antiferromagnetic and very weak ( $J_{\text{eff}} = -0.052$  cm<sup>-1</sup>). In agreement with its structure a similar model can be assumed for **1**, considering the tetramers to be magnetically isolated; thus we can try to fit the magnetic behavior of **1** through the expression for a magnetically isolated square of four spin doublets.

$$\chi_M = (2N\beta^2 g^2 / kT) W / Z \quad (1)$$

where

$$W = 2 + \exp(-J/kT) + 5 \exp(J/kT) \quad (2)$$

and

$$Z = 7 + \exp(-2J/kT) + 3 \exp(-J/kT) + 5 \exp(J/kT) \quad (3)$$

$N$ ,  $\beta$  and  $T$  have their usual meanings,  $J$  is the isotropic spin coupling parameter through bridging malonato in the small square unit [eqn. (4)] and  $g$  is the Landé factor.

$$H = -J[S_1 S_2 + S_2 S_3 + S_3 S_4 + S_1 S_4] \quad (4)$$

The zero-field splitting ( $D$ ) within the ground quintet spin state of four ferromagnetically coupled spin doublets  $S_i = 1/2$  is not introduced. The occurrence of a plateau of  $\chi_M T$  in the low temperature region for **2**, indicates that the squares of copper(II) ions are well isolated magnetically and that there is no significant zero-field splitting in the low lying  $S = 2$  spin state. Least-squares fitting of the data to eqn. (1) gave  $J = 12.3(1)$  cm<sup>-1</sup>,  $g = 2.08(1)$ , and  $R = 6.0 \times 10^{-5}$  ( $R$  is the agreement factor defined as  $\sum_i [(\chi_M T)_{\text{obs}}(i) - (\chi_M T)_{\text{calc}}(i)]^2 / \sum_i [(\chi_M T)_{\text{obs}}(i)]^2$ ), practically the same value of  $J$  that was

obtained for **2**. The calculated  $\chi_M T$  versus  $T$  curve matches very well the experimental data over the whole temperature range. This result is in agreement with that previously reported for **2**, in which the tetranuclear copper(II) units were weakly antiferromagnetically coupled through the 4,4'-bpy leading to the decrease of the  $\chi_M T$  product below 5.5 K. The absence of further bridges in **1** keeps isolated the tetramers leading to the plateau. It is remarkable that the absence of zero-field splitting, which confirms the decrease of the  $\chi_M T$  product below 5.5 K in **2**, is due to weak antiferromagnetic interactions through the 4,4'-bpy as was suggested.

For compound **3** the  $\chi_M T$  plot continuously increases, reaches a maximum of  $1.87 \text{ cm}^3 \text{ mol}^{-1} \text{ K}$  at 17 K, and at lower temperatures rapidly decreases ( $\chi_M T$  is  $0.49 \text{ cm}^3 \text{ mol}^{-1} \text{ K}$  at 1.9 K). A susceptibility maximum is observed at 3.3 K. The shape of the  $\chi_M T$  versus  $T$  plot is as expected for a case where ferro- and antiferro-magnetic interactions coexist.

An inspection of the structure of **3** reveals the tetramers to be connected through a bridging pyrazine in a similar way to that exhibited by the 4,4'-bipy in **2**, leading to layers, but in **3** these layers are additionally interconnected by a carboxylate-malonate oxygen that links the squares in the  $c$  direction, to give a 3D structure. In this compound we have three different exchange pathways: two intralayer (bridging carboxylate-malonate within the small square,  $J_1$ , and bridging pyz,  $J_2$ ) which involve equatorial positions at the copper atoms; and another one connecting the layers linking one equatorial position at one copper atom with an axial one at the other copper atom,  $J_3$ . Unfortunately, there is no model to fit the magnetic properties of this three-dimensional compound with three magnetic interactions, but their values can be roughly evaluated. The structure of the small square is very close to that observed in **1** and **2**, thus a ferromagnetic coupling of *ca.*  $12 \text{ cm}^{-1}$  may also be attributed to  $J_1$  in **3** (see Scheme 1). As far as the other carboxylate-malonate bridging pathway ( $J_3$ ) is concerned, previous magneto-structural studies of malonate-containing copper(II) complexes with the same bridging mode reveal that the magnetic coupling is also ferromagnetic and that it varies between 1 and  $3 \text{ cm}^{-1}$ .<sup>28c</sup> A ferromagnetic coupling within this range can be assumed for  $J_3$ . The greater value of  $J_1$  with respect to that of  $J_3$  can be understood taking into account that the former carboxylate connects equatorial positions of both copper(II) ions, whereas the latter connects an equatorial with an axial position. Finally, magneto-structural studies of pyrazine-bridged copper(II) complexes reveal the occurrence of a weak antiferromagnetic coupling between the copper(II) ions through this bridge (values of  $J$  ranging from  $-2$  to  $-5 \text{ cm}^{-1}$ ).<sup>40</sup> In this sense  $J_2$  would be negative and responsible for the observed maximum of the magnetic susceptibility. The presence of ferro- and antiferro-magnetic interactions in **3** is

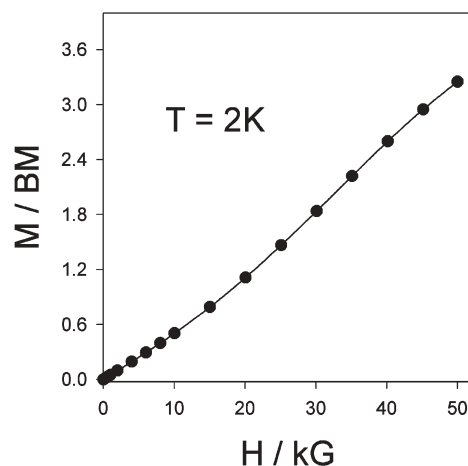
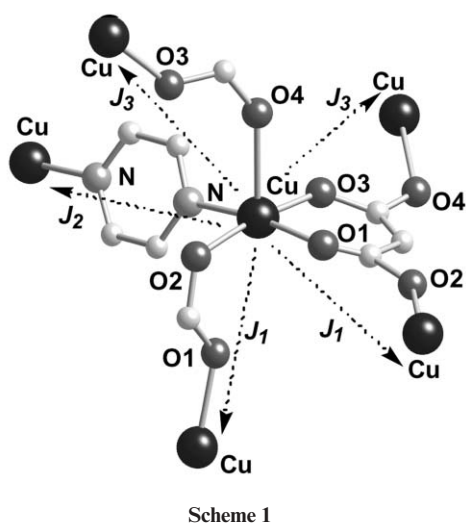


Fig. 7 Field dependence of the magnetization (in Bohr magnetons) at 2.0 K for **3** (the solid line is an eye-guide).

furthermore confirmed by the  $M$  vs.  $H$  curve (Fig. 7). The curve at 2 K has a sigmoidal shape, indicating a pseudo-metamagnetic behavior:  $M$  increases smoothly at low fields, shows an inflexion at about 1.5 T and increases rapidly at greater fields. The expected saturation *ca.* 4 BM (Bohr magneton) is not reached at the highest field applied. The role of this critical field would be to break the antiferromagnetic interaction and to order all the magnetic moments in a parallel way. Thus a value of *ca.*  $-2 \text{ cm}^{-1}$  can be expected for  $J_2$ , in agreement with other reported values for pyrazine-bridged copper(II) ions.<sup>40</sup>

## Conclusions

The present work shows firstly how the combination of simple ligands such as malonate and 2,4'-bpy, 4,4'-bpy and pyz and affords tetrameric rings that can lead to two- and three-dimensional structures with the coexistence of ferro- (through carboxylate-malonate) and antiferro-magnetic (through 4,4'-bpy and pyz) interactions. Secondly, compound **3** illustrates the possibility of the polymerization in three directions of the already known ferromagnetically coupled  $\text{Cu}_4(\text{mal})_4$  building block. The replacement of pyz by other bridging ligands able to transmit ferromagnetic interactions will be investigated in the near future in the search for materials exhibiting magnetic ordering.

## Acknowledgements

The financial support from The Gobierno Autónomo de Canarias through Project PI2000/135 and from the Spanish Ministerio de Ciencia y Tecnología through Project BQU2001-3794 are gratefully acknowledged.

## References

- 1 G. R. Desiraju, *Crystal Engineering: The Design of Organic Solids*, Elsevier, Amsterdam, 1989; J. M. Lehn, *Science*, 2002, **295**, 2400; D. N. Reinhoudt and M. Crego-Calama, *Science*, 2002, **295**, 2403; M. D. Hollingsworth, *Science*, 2002, **295**, 2410.
- 2 For ladders, rail roads and 1D polymers, see: Y. M. Yaghi, H. Li and T. L. Groy, *Inorg. Chem.*, 1997, **36**, 4292; P. Losier and M. J. Zaworotko, *Angew. Chem., Int. Ed. Engl.*, 1996, **35**, 2779; M. Fujita, Y. J. Kwon, O. Sasaki, K. Yamaguchi and J. Ogura, *J. Am. Chem. Soc.*, 1995, **117**, 7287; M. Fujita, Y. J. Kwon, M. Miyazawa and K. Ogura, *J. Chem. Soc., Chem. Commun.*, 1994, 1977.
- 3 For square and rectangular grids, see: R. Gable, B. F. Hoskins and R. Robson, *J. Chem. Soc., Chem. Commun.*, 1990, 1677; M. Fujita, Y. J. Kwon, S. Washizu and K. Ogura, *J. Am. Chem. Soc.*, 1994, **116**, 1151; L. Carlucci, G. Ciani and D. M. Proserpio, *New*

- J. Chem.*, 1998, 1319; L. R. MacGillivray, R. H. Groeneman and J. L. Atwood, *J. Am. Chem. Soc.*, 1998, **120**, 2676; J. Lu, T. Paliwala, S. C. Lim, C. Yu, T. Y. Niu and A. Jacobson, *Inorg. Chem.*, 1997, **37**, 923; C. B. Aakeröy, A. M. Beatty and O. S. Leinen, *Angew. Chem., Int. Ed.*, 1999, **38**, 1815.
- 4 For bilayers, brick walls and herringbones, see: K. N. Power, T. L. Hennigar and M. J. Zaworotko, *New J. Chem.*, 1998, 177; M. A. Withersby, A. J. Blake, N. R. Champness, P. A. Cooke, P. Hubberstey and M. Schröder, *New J. Chem.*, 1999, 573; L. Carlucci, G. Ciani and D. M. Proserpio, *J. Chem. Soc., Dalton Trans.*, 1999, 1799; O. M. Yaghi and G. Li, *Angew. Chem., Int. Ed. Engl.*, 1995, **34**, 207.
- 5 For octahedral and pseudo-octahedral frameworks, see: S. Subramanian and M. J. Zaworotko, *Angew. Chem., Int. Ed. Engl.*, 1995, **34**, 2127; H. Li, M. Eddaoudi, M. O'Keeffe and O. M. Yaghi, *Nature (London)*, 1999, **402**, 276; J. F. Heggin, *Nature (London)*, 1936, **137**, 57; L. Carlucci, G. Ciani, D. M. Proserpio and A. Sironi, *Angew. Chem., Int. Ed. Engl.*, 1995, **34**, 1895.
- 6 For diamondoid structures, see: M. J. Zaworotko, *Chem. Soc. Rev.*, 1994, 283; L. R. MacGillivray, S. Subramanian and M. J. Zaworotko, *J. Chem. Soc., Chem. Commun.*, 1994, 1325; L. Carlucci, G. Ciani and D. M. Proserpio, *J. Chem. Soc., Chem. Commun.*, 1994, 2755.
- 7 For other 3D frameworks, see: F. Robinson and M. J. Zaworotko, *J. Chem. Soc., Chem. Commun.*, 1995, 2413; O. M. Yaghi and H. Li, *J. Am. Chem. Soc.*, 1996, **118**, 295; L. Carlucci, G. Ciani, D. M. Proserpio and A. Sironi, *Chem. Commun.*, 1996, 1393.
- 8 M. A. Withersby, A. J. Blake, N. R. Champness, P. Hubberstey, W. S. Li and M. Schröder, *Angew. Chem., Int. Ed. Engl.*, 1997, **36**, 2327.
- 9 S. R. Batten, B. F. Hoskins and R. Robson, *Angew. Chem., Int. Ed. Engl.*, 1997, **36**, 636.
- 10 K. A. Hirsch, S. R. Wilson and J. S. Moore, *Inorg. Chem.*, 1997, **36**, 2960; L. Ballester, I. Baxter, P. C. M. Duncan, D. M. L. Goodgame, D. A. Grachvogel and D. J. P. Williams, *Polyhedron*, 1998, **17**, 3613.
- 11 A. J. Blake, N. R. Champness, M. Crew, L. R. Hanton, S. Parsons and M. Schröder, *J. Chem. Soc., Dalton Trans.*, 1998, 1533.
- 12 J. Y. Lu, M. A. Lawandy, J. Li, T. Yuen and C. L. Lin, *Inorg. Chem.*, 1999, **38**, 2695.
- 13 M. Fujita, O. Sasaki, T. Mitsuhashi and T. Fujita, *Chem. Commun.*, 1996, 1535.
- 14 R. V. Slone, D. I. Yoon, R. M. Calhoun and J. T. Hupp, *J. Am. Chem. Soc.*, 1995, **117**, 11 813.
- 15 P. Barbaro, F. Ceconi, C. A. Ghilardi, S. Midollini, A. Orlandini, L. Alderighi, D. Peters, A. Vacca, E. Chinea and A. Mederos, *Inorg. Chim. Acta*, 1997, **262**, 187.
- 16 A. Karipides, J. Ault and T. Reed, *Inorg. Chem.*, 1977, **16**, 3299.
- 17 M. L. Post and J. J. Trotter, *J. Chem. Soc., Dalton Trans.*, 1974, 1922; K. H. Chung, E. Hong, Y. Do and C. H. Moon, *J. Chem. Soc., Chem. Commun.*, 1995, 2333.
- 18 N. J. Ray and B. J. Hathaway, *Acta Crystallogr., Sect. B*, 1982, **38**, 770.
- 19 (a) R. Hämäläinen and A. Pajunen, *Suom. Kemistl. B*, 1973, **46**, 285; (b) W. L. Kwik, K. P. Ang, S. O. Chan, V. Chebolu and S. A. Koch, *J. Chem. Soc., Dalton Trans.*, 1986, 2519; (c) D. Chattopadhyay, S. K. Chattopadhyay, P. R. Lowe, C. H. Schawalbe, S. K. Mazumber, A. Rana and S. Ghosh, *J. Chem. Soc., Dalton Trans.*, 1993, 913; (d) A. Tosik, L. Sieron and M. Bukowska-Strzyzewska, *Acta Crystallogr., Sect. C*, 1995, **51**, 1987; (e) E. Suresh and M. H. Bhadbhade, *Acta Crystallogr., Sect. C*, 1997, **53**, 193; (f) G. I. Dimitrova, A. V. Ablov, G. A. Kiosse, G. A. Popovich, T. I. Malinovskii and I. F. Burshtein, *Dokl. Akad. Nauk SSSR*, 1974, **216**, 1055.
- 20 S. M. Saadeh, K. L. Trojan, J. W. Kampf, W. E. Hatfield and V. L. Pecoraro, *Inorg. Chem.*, 1993, **32**, 3034.
- 21 S. Calogero, L. Stievano, L. Diamandescu, D. Mihaila-Tarabasanu and G. Valle, *Polyhedron*, 1997, **16**, 3953.
- 22 I. Gil de Muro, F. A. Mautner, M. Insausti, L. Lezama, M. I. Arriortua and T. Rojo, *Inorg. Chem.*, 1998, **37**, 3243; I. Gil de Muro, M. Insausti, L. Lezama, M. I. Arriortua and T. Rojo, *Inorg. Chem.*, 1998, **37**, 3243; I. Gil de Muro, M. Insausti, L. Lezama, J. L. Pizarro, M. K. Urriaga, M. I. Arriortua and T. Rojo, *J. Chem. Soc., Dalton Trans.*, 2000, 3360.
- 23 C. Oldham, in *Comprehensive Coordination Chemistry*, G. Wilkinson, R. D. Gillard and J. A. McCleverty, ed., Pergamon Press, Oxford, 1987, vol. 2, p. 435 and refs. cited therein.
- 24 D. K. Towle, S. K. Hoffmann, W. E. Hatfield, P. Singh and P. Chaudhuri, *Inorg. Chem.*, 1988, **27**, 394.
- 25 P. R. Levstein and R. Calvo, *Inorg. Chem.*, 1990, **29**, 1581.
- 26 F. Sapiña, E. Escrivá, J. V. Folgado, A. Beltrán, D. Beltrán, A. Fuertes and M. Drillon, *Inorg. Chem.*, 1992, **31**, 3851.
- 27 E. Colacio, J. P. Costes, R. Kivekäs, J. P. Laurent and J. Ruiz, *Inorg. Chem.*, 1990, **29**, 4240; E. Colacio, J. M. Domínguez-Vera, J. P. Costes, R. Kivekäs, J. P. Laurent, J. Ruiz and M. Sundberg, *Inorg. Chem.*, 1992, **31**, 774; E. Colacio, J. M. Domínguez-Vera, R. Kivekäs, J. M. Moreno, A. Romerosa and J. Ruiz, *Inorg. Chem.*, 1993, **32**, 115.
- 28 (a) C. Ruiz-Pérez, J. Sanchiz, M. Hernández-Molina, F. Lloret and M. Julve, *Inorg. Chim. Acta*, 2000, **298**, 202; (b) C. Ruiz-Pérez, M. Hernández-Molina, J. Sanchiz, T. López, F. Lloret and M. Julve, *Inorg. Chim. Acta*, 2000, **298**, 245; (c) C. Ruiz-Pérez, J. Sanchiz, M. Hernández-Molina, F. Lloret and M. Julve, *Inorg. Chem.*, 2000, **39**, 1363; (d) C. Ruiz-Pérez, M. Hernández-Molina, P. A. Lorenzo-Luis, F. Lloret and M. Julve, *Inorg. Chem.*, 2000, **39**, 3845; (e) J. Sanchiz, Y. Rodríguez-Martín, C. Ruiz-Pérez, A. Mederos, F. Lloret and M. Julve, *New J. Chem.*, 2002, in press.
- 29 Y. Rodríguez-Martín, C. Ruiz-Pérez, J. Sanchiz, F. Lloret and M. Julve, *Inorg. Chim. Acta*, 2001, **318**, 159.
- 30 A. Earshaw, *Introduction to Magnetochemistry*, Academic Press, London, 1968.
- 31 G. M. Sheldrick, SHELXS-97, University of Göttingen, Germany, 1997.
- 32 G. M. Sheldrick, SHELXL-97: Program for the Refinement of Crystal Structures, University of Göttingen, Germany, 1997.
- 33 *International Tables for X-Ray Crystallography*, Kynoch Press, Birmingham, UK, 1974, vol. 4, pp. 55, 99 and 149.
- 34 PARST95: M. Nardelli, *J. Appl. Crystallogr.*, 1995, **28**, 659.
- 35 A. L. Spek, *Acta Crystallogr., Sect. A*, 1990, **46**, C-34.
- 36 A. W. Addison and T. N. Rao, *J. Chem. Soc., Dalton Trans.*, **1984**, 1349.
- 37 D. Cremer and J. A. Pople, *J. Am. Chem. Soc.*, 1975, **19**, 1354.
- 38 (a) M.-L. Tong, X.-M. Chen, X.-L. Yu and T. C. W. Mak, *J. Chem. Soc., Dalton Trans.*, 1998, 5; (b) M. A. S. Goher and F. A. Mautner, *J. Chem. Soc., Dalton Trans.*, 1999, 1923; (c) M. A. S. Goher and F. A. Mautner, *Polyhedron*, 1999, **18**, 1805; (d) M. J. Begley, P. Hubberstey and J. Stroud, *J. Chem. Soc., Dalton Trans.*, 1996, 2323; (e) E. Siebel, A. M. A. Ibrahim and R. D. Fischer, *Inorg. Chem.*, 1999, **38**, 2530; (f) S. Kitagawa, M. Munakata and T. Tanimura, *Inorg. Chem.*, 1992, **31**, 1714.
- 39 H. Kuwagai, S. Iwabudu and M. Katada, *Inorg. Chim. Acta*, 1998, **267**, 143.
- 40 C. P. Landee and M. M. Turnbull, *Mol. Cryst. Liq. Cryst.*, 1999, **335**, 193; J. Cano, P. Alemany, S. Alvarez, M. Verdager and E. Rúa, *J. Am. Chem. Soc.*, 1996; J. A. Real, G. de Munno, M. C. Muñoz and M. Julve, *Inorg. Chem.*, 1991, **30**, 2701; J. S. Haynes, S. J. Retting, J. R. Sams, J. Trotter and R. C. Thompson, *Inorg. Chem.*, 1988, **27**, 1237; W. Richardson and W. E. Hatfield, *J. Am. Chem. Soc.*, 1976, **98**, 835.



Highlight

# Structural versatility of the malonate ligand as a tool for crystal engineering in the design of molecular magnets†

Yolanda Rodríguez-Martín,<sup>a</sup> María Hernández-Molina,<sup>a</sup> Fernando S. Delgado,<sup>a</sup> Jorge Pasán,<sup>a</sup> Catalina Ruiz-Pérez,<sup>\*a</sup> Joaquín Sanchiz,<sup>b</sup> Francesc Lloret<sup>c</sup> and Miguel Julve<sup>c</sup>

<sup>a</sup>Laboratorio de Rayos X y Materiales Moleculares, Departamento de Física Fundamental II, Universidad de La Laguna, Avda. Astrofísico Francisco Sánchez s/n, 38204 La Laguna, Tenerife, Spain. E-mail: caruiz@ull.es

<sup>b</sup>Departamento de Química Inorgánica, Universidad de La Laguna, 38204 La Laguna, Tenerife, Spain

<sup>c</sup>Instituto de Ciencia Molecular, Departament de Química Inorgànica, Facultat de Química, Universitat de València, Avda. Dr. Moliner 50, 46100 Burjassot, València, Spain

Received 1st March 2002, Accepted 23rd August 2002

Published on the Web 19th September 2002

The synthesis of ferro- and ferri-magnetic systems with a tunable  $T_c$  and three-dimensional (3-D) ordering from molecular precursors implying transition metal ions is one of the active branches of molecular inorganic chemistry. The nature of the interactions between the transition metal ions (or transition metal ions and radicals) is not so easy to grasp by synthetic chemists working in this field since it may be either electrostatic (orbital) or magnetic (mainly dipolar). Therefore, the systems fulfilling the necessary requirements to present the expected magnetic properties are not so easy to design on paper and realize in the beaker. In this work we show how the design of one-, two- and three-dimensional materials can strongly benefit from the use of crystal engineering techniques, which can give rise to structures of different shapes, and how these differences can give rise to different properties. We will focus on the networks constructed by assembling malonate ligands and

† Dedicated to the memory of Professor Olivier Kahn.

Yolanda Rodríguez-Martín was born in San Andrés y Sauces (La Palma, Spain). In 1997 she received her B.Sc. in Physics from The University of La Laguna. She is currently working towards her Ph.D. at the same University, in the research group of Professor Catalina Ruiz-Pérez, exploring malonate-based molecular magnets.

María Hernández-Molina was born and raised in Santa Cruz de Tenerife (Tenerife, Spain). She obtained a B.Sc. (1994) and a Ph.D. (1999) in Physics at La Laguna University. Her Ph.D. research was performed under the supervision of Professor Catalina Ruiz-Pérez, and involved the synthesis and characterization by X-ray crystallography of coordination polymers with a view to predetermining their topology by judicious choice of ligand and metal ion to obtain interesting magnetic properties. Particular attention was paid to the malonate ligand. She is currently employed in the Laboratorio de Rayos X y Materiales Moleculares on work related to her Ph.D. research.

Fernando S. Delgado was born in Santa Cruz de Tenerife (Tenerife, Spain). In 1999 he received his B.Sc. in Physics from The University of La Laguna while working with Professor Catalina Ruiz-Pérez on X-ray diffraction. He is currently working towards his Ph.D. at the same university and in the same research group, exploring the mechanisms of magnetic interactions in malonate-based coordination compounds.

Jorge Pasán was born in Santa Cruz de Tenerife (Tenerife, Spain). In 2001 he received his B.Sc. in Physics from The University of La Laguna while working with Professor Catalina Ruiz-Pérez on X-ray crystallography. He is currently working towards his Ph.D. at the same university, in the same research group, exploring steric effects in the magnetic behaviour of coordination compounds.



Yolanda Rodríguez-Martín



María Hernández-Molina



Fernando S. Delgado



Jorge Pasán

metal centres. The idea of using malonate (dianion of propanedioic acid, H<sub>2</sub>mal) is that it can give rise to different coordination modes with the metal ions it binds.

Extended magnetic networks of dimensionalities one (1-D), two (2-D) and three (3-D) can be chemically constructed from malonate-bridged metallic complexes. These coordination polymers behave as ferro-, ferri- or canted antiferro-magnets. We are currently trying to obtain analogous compounds using magnetically anisotropic ions, such as cobalt(II), in order to explore how structural differences influence the magnetic properties. In this case the control of the spatial arrangement of the magnetic building blocks is of paramount importance in determining the strength of the magnetic interaction. The possibility of controlling the shape of the networks depends on the coordination bond between the metal ion and the ligands and on supramolecular interactions such as stacking interactions or hydrogen bonding.

## Introduction

### Malonate and dimensionality

Molecular magnetism is an interdisciplinary field of research that congregates physicists and chemists in the design and synthesis of new materials displaying interesting properties.<sup>1</sup>

One of the main challenges in this field is the preparation of compounds exhibiting a spontaneous magnetization with a magnetic hysteresis below a critical temperature.<sup>2</sup> The magnetic ordering is a cooperative phenomenon related to the dimensionality of the solid, high dimensionality being required to achieve the desired property.<sup>3</sup> The target of the scientist consists of optimising the number of chemical links between the

*Catalina Ruiz-Pérez was born in Valencia (Valencia, Spain). She graduated at Valencia University with a B.Sc. degree in Physics in 1982. After completing her Ph.D. in Physics (1987) and a short postdoctoral period with Professor Alfred Gieren at the Max-Planck Institut für Biochemie (Martinsried bei München), she obtained a fellowship in the same year to work at the Instituto Universitario de Bio-Organica (La Laguna, Tenerife). In 1988 she joined the Department of Fisica Fundamental y Experimental at La Laguna University as Assistant Professor of Materials Physics and one year later became Associate Professor within the same department. In 1992 she was awarded an Alexander von Humboldt fellowship to work with Professor Robert Huber at the Max-Planck Institute where she did her Ph.D. work. In 2000 she became Full Professor at the Department of Fisica Fundamental II at the same University. Her research interests deal with X-ray crystallography and the role of the structure in the magnetic properties of coordination compounds. Her work was dedicated initially to complexes derived from polycarboxylate ligands designed to bind pairs, quartets, ... of metal ions and has been extended in recent years to infinite 2D and 3D coordination networks with interesting magnetic interactions.*

*Joaquín Sanchiz was born in Vitoria-Gasteiz (Spain) in 1966. He received his degree in Chemistry in 1989 from the University of Granada and his Ph.D. from the University of La Laguna. In 1997 he participated in postdoctoral work at the Institute the Chimie de la Matière Condensée in Bordeaux (France). There he began his research into the field of molecular magnetism with Professor Olivier Kahn, initiating the synthesis of compounds derived from the [Mo(CN)<sub>7</sub>]<sup>4-</sup> precursor. Currently he is a Senior Lecturer at the University of La Laguna where he continues to pursue his research interests in inorganic crystal engineering and materials chemistry.*

*Francesc Lloret was born in Pego (Alicante, Spain) and gained his B.Sc. in 1977 and his Ph.D. in 1982, both at the University of Valencia under the supervision of Professor Juan Faus Payá and Professor José María Moratall Mascarell. He carried out postdoctoral research for 18 months (1986/87) under the direction of Professor Olivier Kahn at the University of Paris-Sud (France). He was Assistant Professor at different institutions for several years (the CEU San Pablo, University College of Castellón and Department of Inorganic Chemistry of the University of Valencia) prior to becoming Associate Professor in 1986 and Professor in 2000 at the University of Valencia. His research interests deal with coordination chemistry and molecular magnetism. They have included the study of complex formation in water and in non-aqueous solvents and the synthesis and magnetic investigation of mono- and poly-nuclear transition metal complexes. He is specially interested in the design of new spin topologies and magnetic exchange mechanisms.*

*Miguel Julve was born in Moncada (Valencia, Spain) and graduated from the University of Valencia with a B.Sc. degree in Chemistry in 1977. After completing his Ph.D. in inorganic chemistry at the same institution with Professor Juan Faus Payá and Professor José María Moratal Mascarell in 1981, he participated in postdoctoral research for two years under the supervision of Professor Olivier Kahn at the University of Paris-Sud (France). In 1983, he returned to the Department of Inorganic Chemistry of the University of Valencia as Assistant Professor of Inorganic Chemistry. He rose through the ranks to become Associate Professor in 1986 and Professor in 1992 in the same Department. His research interests deal with coordination chemistry and molecular magnetism. They have included the synthesis, structural characterization and magnetic investigation of mono- and poly-nuclear transition metal complexes with special emphasis in the design of mononuclear complexes which can act as ligands, the stepwise formation of extended magnetic lattices, the search for strong magnetic interactions through extended bridging ligands and the preparation of new molecule-based magnets.*



Catalina Ruiz-Pérez



Joaquín Sanchiz

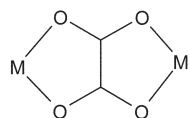


Francesc Lloret



Miguel Julve





two  $\eta^4$  chelates  
*anti-anti* bridging mode

Scheme 1

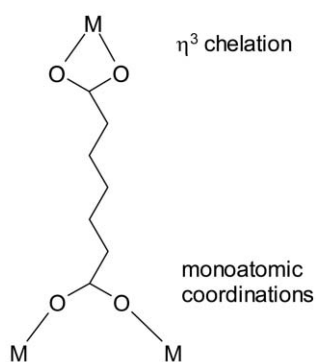
magnetic centres in order to get a greater contribution from intramolecular interactions, and at the same time minimizing the influence of the weaker intermolecular contacts. In this context crystal engineering plays a determining role in the control of the links between the magnetic centres and in the control of the dimensionality of the system.<sup>4</sup>

Dicarboxylic ligands are frequently-used bridging ligands in the design of polynuclear complexes with interesting magnetic properties. The ability of the carboxylato bridge to mediate significant ferro- or anti-ferromagnetic interaction accounts for their use. The most widely studied dicarboxylic ligand is the oxalate ( $C_2O_4$ )<sup>2-</sup> anion in its characteristic coordination mode – the  $\eta^4$ -chelation – acting as a bis(bidentate) ligand, bridging the metal centres in an *anti-anti* fashion<sup>5</sup> (Scheme 1). In addition, other coordination modes have also been observed, but they are not so adequate in the transmission of the magnetic coupling.

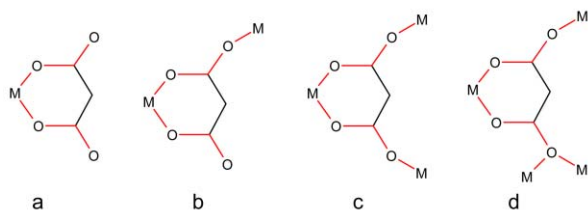
Higher members of the dicarboxylic ligand series exhibit the characteristic chelate coordination of the  $CO_2^-$  group –  $\eta^3$ -chelation – which can be accompanied with one or two monoatomic coordinations, other chelate modes being forbidden for steric reasons<sup>6</sup> (Scheme 2).

Malonate (the dianion of 1,3-propanedioic acid) is a dicarboxylic ligand with a singular behaviour different from the other dicarboxylic ligands. In our investigations we have observed that with the 3d ions it can exhibit different coordination modes such as (a) bidentate [ $\eta^5$ -chelation], (b) bidentate [ $\eta^5$ -chelation] + unidentate, (c) bidentate [ $\eta^5$ -chelation] + bis(unidentate), and (d) bidentate [ $\eta^5$ -chelation] + bis(unidentate) +  $\mu$ -oxo, in which in addition to the bidentate and bis(unidentate) coordination one of the oxygens acts as a  $\mu$ -oxo bridge between two metal centres (Scheme 3).

Other coordination modes, such as the  $\eta^3$ -chelation



Scheme 2



Scheme 3

observed in the higher series, have also been reported by other authors,<sup>6</sup> but are less frequent with 3d metal ions. The bis(bidentate) behaviour analogue to that exhibited by the oxalate is forbidden by steric reasons and this dramatically affects the structure and properties of the malonate complexes. The malonate ligand occupies one or two coordination positions and neutralizes two positive charges of the metallic ion, allowing the inclusion of other ligands in the coordination sphere of the metal. These complementary ligands can act as bridging or blocking ligands contributing to the interconnection or isolation of the spin carriers. Thus, combining the malonate with other bridging and/or blocking ligands we have been able to prepare monomers,<sup>7,8</sup> dimers,<sup>8</sup> trimers,<sup>8</sup> tetramers,<sup>9a</sup> infinite chains,<sup>8,10–12</sup> 2-D<sup>13</sup> and 3D arrays.<sup>9–14</sup>

The magnetic coupling among the magnetic centres is given by the value of  $J$  (the intramolecular exchange interaction),  $J$  being negative or positive depending on the antiferro- or ferro-magnetic character of the coupling, respectively. The magnitude of the interaction depends on the overlap density, thus for the carboxylato bridge, it will be affected by the possible *syn-syn*, *syn-anti* and *anti-anti* bridging modes that it can adopt. The nature of the coupling (ferro- or antiferromagnetic) is dependent upon the nature of the magnetic orbitals of the spin carriers connected by the bridging ligand. We recall that the approximated  $J$  value in the copper(II) dinuclear unit is given by eqn. (1), where  $S$  is the overlap integral between the two magnetic orbitals and  $\beta$  and  $j$  are their monoelectronic resonance and bielectronic exchange integrals, respectively.<sup>1,2</sup>

$$J = 2j + 4\beta S = J^F + J^{AF} \quad (1)$$

$J$  can be seen as the sum of two terms: a ferromagnetic  $J^F$  and an antiferromagnetic  $J^{AF}$  one. Approximately,  $J^{AF}$  is proportional to  $S^2$ , thus the stronger the overlap, the stronger the antiferromagnetic contribution. Usually the antiferromagnetic contributions are much larger than the ferromagnetic ones, but if the overlap integral is neglected either accidentally or by strict orthogonality of the magnetic orbitals of the spin carriers, the ferromagnetic contribution may dominate, leading to ferromagnetism.<sup>1,2</sup> In most of our compounds the magnetic properties can be analyzed under these approximations having a nice explanation of the magnetic properties.

Herein we present a review of our investigations in the magneto-structural correlations of some 3d metal malonate complexes. The study is organized attending to the coordination modes of the malonate and how they govern the dimensionality of the structure, then the magnetic properties can be explained attending to the bridging mode of the carboxylate and the nature of the magnetic orbitals of the paramagnetic centres. Thus, playing with the stoichiometry and with the nature of other complementary ligands very exciting compounds with a controlled dimensionality and with nicely explained magnetic properties have been prepared.

## Structural aspects and properties

### (a) Bidentate (no-bridging)

In this coordination mode two of the oxygens of the malonate coordinate the metal ion, the ligand behaving as  $\eta^5$ -bidentate; the rest of the oxygens may act as acceptors in hydrogen bonding. This mode is analogous to the  $\eta^4$ -bidentate chelate exhibited by the oxalate. The malonate acts as a blocking ligand leading to isolated molecules that are interconnected through hydrogen bonding, exhibiting weak or no magnetic coupling among the metallic centres. As examples we have the bimetallic compounds  $[M^II(H_2O)_6][Cu^II(mal)_2(H_2O)_2]$  (**1**) ( $M = Mn, Co, Ni, Cu$  and  $Zn$ ;  $H_2mal = malonic acid$ )<sup>15</sup> (Fig. 1), the hydrogen bonded polymeric chain  $[Co(H_2O)_2(Hmal)_2]$  (**2**)<sup>9b</sup>

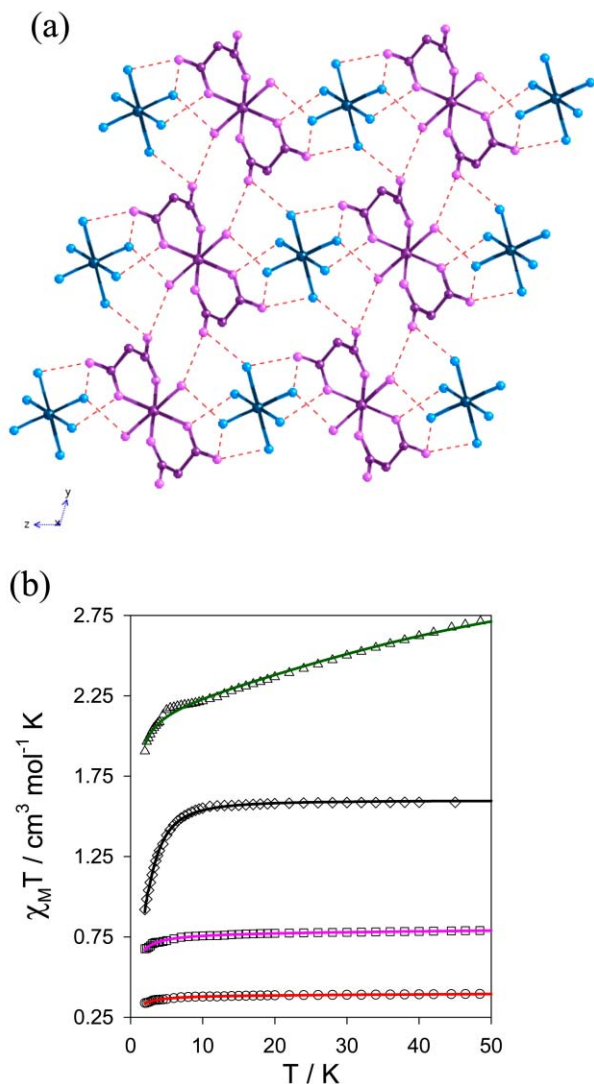


**Fig. 1** (a) The 2-D anion-cation network of hydrogen bonding in complex  $[M^{II}(H_2O)_6][Cu^{II}(mal)_2(H_2O)_2]$  (1) (M = Mn, Co, Ni, Cu and Zn). The six water molecules coordinated to the  $M^{II}$  ion act as space filling to join the neighboring two-dimensional layers of  $[Cu(mal)_2(H_2O)_2]^{2-}$  forming a three-dimensional hydrogen bonding network. (b) Thermal dependence of the  $\chi_M T$  product ( $\chi_M$  being the magnetic susceptibility *per* formula) for the  $[M^{II}(H_2O)_6][Cu^{II}(mal)_2(H_2O)_2]$  (M = Co, Ni, Cu and Zn) complexes.

(Fig. 2), and the discrete species  $[Cu(mal)(bipym)(H_2O)]$  (3)<sup>16</sup> (bipym = 2,2'-bipyrimidine) (Fig. 3),  $[Cu(mal)(phen)(H_2O)]$  (4)<sup>17</sup> (phen = phenanthroline) and  $[Cu_2(mal)_2(H_2O)_2(bipym)]$  (5)<sup>16</sup> (Fig. 4). In 1 and 2 the malonate fills equatorial coordination positions of the metallic ions, the rest of the positions being filled by water molecules. Other ligands may displace water molecules entering in the coordination sphere of the

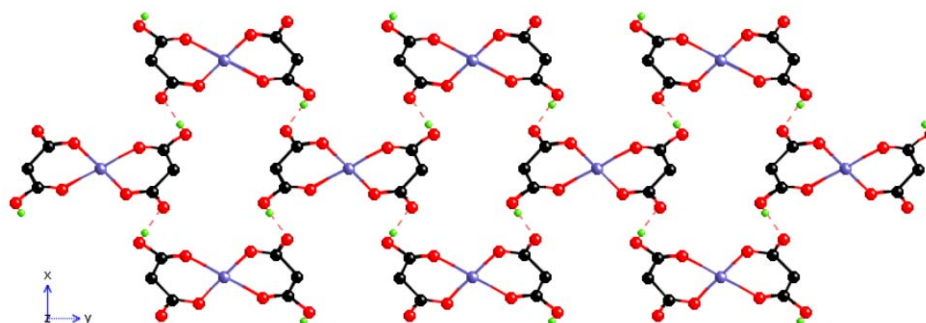


**Fig. 2** Projection of the structure of  $[Co(H_2O)_2(Hmal)_2]$  (2) down the  $c$  axis, showing its sheet-like nature through hydrogen bonding.

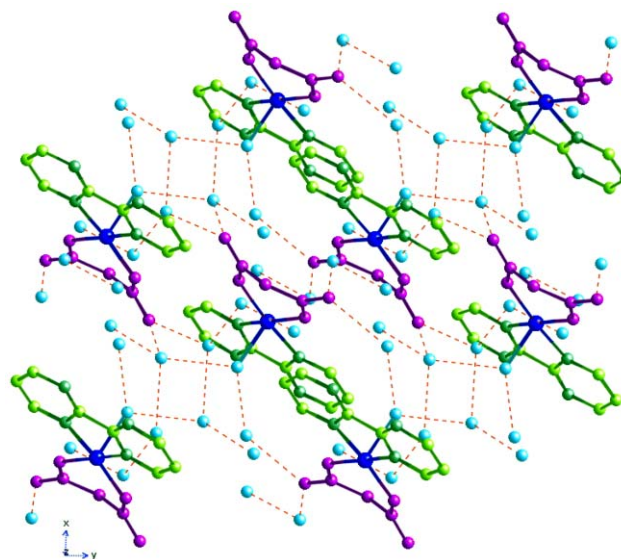


**Fig. 3** Crystal packing pattern of  $[Cu(mal)(bipym)(H_2O)]$  (3), viewed down the crystallographic  $c$  axis showing the extended 3-D network formed through water hydrogen bonding linkages (dashed lines). H atoms have been omitted for clarity.

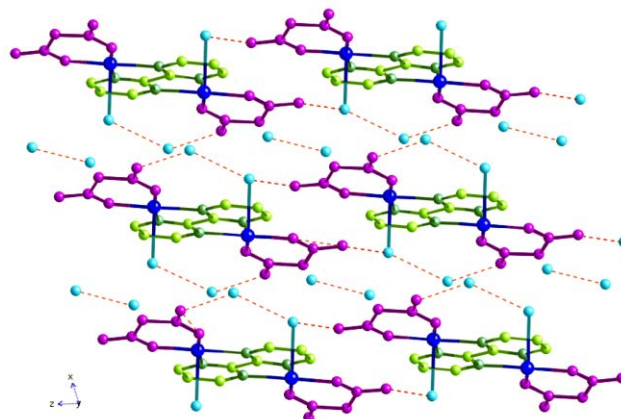


**Fig. 4** Crystal packing of  $[Cu_2(mal)_2(H_2O)_2(bipym)]$  (5), viewed down the crystallographic  $b$  axis showing the extended 2-D network formed through water hydrogen bonding linkages (dashed lines). H atoms have been omitted for clarity.

metal, if they have a large size they may keep the molecules isolated due to steric reasons as in 3 or 4. The magnetic properties of the bimetallic  $[M^{II}(H_2O)_6][Cu^{II}(mal)_2(H_2O)_2]$  (M = Co, Ni, Cu and Zn) compounds are shown in Fig. 1(b) as  $\chi_M T$  vs.  $T$  plots,  $\chi_M$  being the molar magnetic susceptibility and  $T$  the temperature. The magnetic coupling is very weak and is given by the Weiss constant,  $\theta$ , having values of  $-0.317(1)$ ,

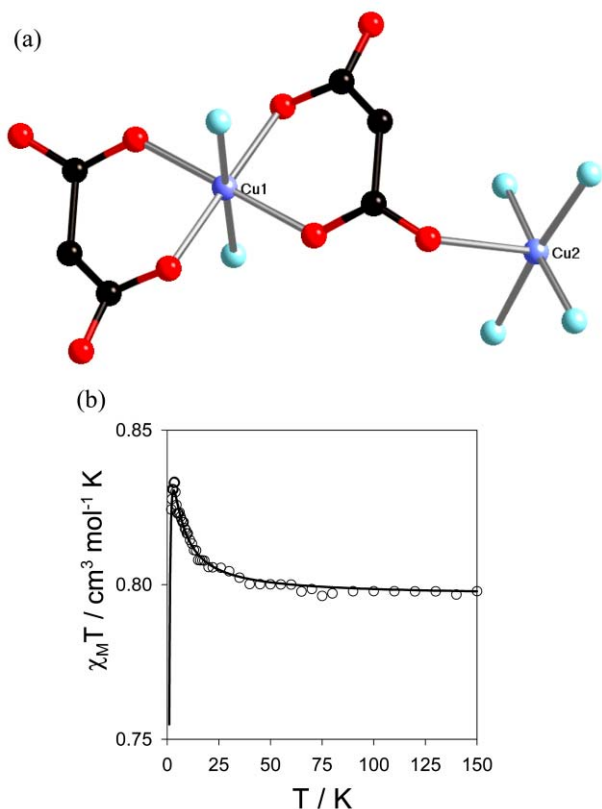


**Fig. 5** (a) Perspective view of the dinuclear copper(II) units of compound  $[(\text{H}_2\text{O})_4\text{Cu}(\mu\text{-mal})\text{Cu}(\text{mal})(\text{H}_2\text{O})_2]$  (**6**) along with the copper(II) numbering scheme. (b) Thermal dependence of the  $\chi_{\text{M}}T$  product for compound **6**.

$-0.47(1)$ ,  $-0.31(2)$ ,  $-0.22(1)$  and  $-0.22(2)$  K for the ZnCu, CuCu, NiCu, CoCu and the MnCu compounds, respectively. The NiCu and the CoCu compounds also exhibit zero-field-splitting,  $|D|$  being  $5.81(4)$  and  $52(1)$   $\text{cm}^{-1}$ , respectively.

Some ligands can bridge the metallic ions, but if the malonate is kept as bidentate the molecules remain isolated as in **5**, where the dimensionality and the magnetic coupling are governed by the complementary ligand.

### (b) $\eta^5$ -Bidentate + unidentate

In this coordination mode two of the oxygens coordinate the same metal and another one is bound to an additional metal as unidentate, the ligand behaving overall as tridentate. The remaining oxygen acts as acceptor in hydrogen bonding blocking the polymerisation in this direction.

The simplest compound exhibiting this coordination mode is the  $[(\text{H}_2\text{O})_4\text{Cu}(\mu\text{-mal})\text{Cu}(\text{mal})(\text{H}_2\text{O})_2]$  dimer (**6**)<sup>8,18</sup> (Fig. 5), in which the Cu(1) and Cu(2) are in octahedral and square pyramidal environments, respectively. The malonate-oxygens fill equatorial positions at Cu(1), the Cu(1)–O distances being shorter, whereas the Cu(2)–O distance is long, the malonate-oxygen filling an apical position with respect to Cu(2). We have observed in this compound that the copper(II) ions are ferromagnetically coupled, the magnetic coupling constant having a value of  $J = 1.8$   $\text{cm}^{-1}$  [Fig. 5(b)]. We can find in the literature that 95% of copper(II) dimers exhibit an antiferromagnetic coupling, but as we will see in our compounds, ferromagnetic behaviour is much more frequent than antiferromagnetic behaviour.

In square pyramidal and octahedral environments the magnetic orbital at each copper(II) atom is defined by the short equatorial (or basal) bonds, and it is of the  $d_{x^2 - y^2}$  type with possibly some mixture of the  $d_{z^2}$  character in the axial position. In **6** the carboxylate couples a  $d_{x^2 - y^2}$  magnetic orbital

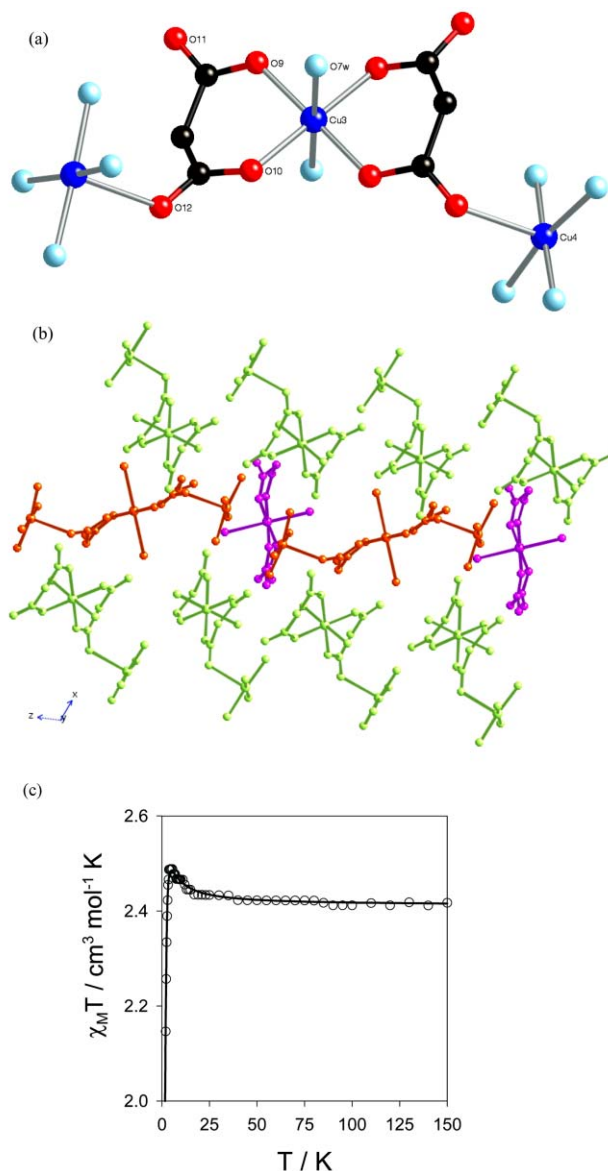


**Fig. 6** (a) Perspective view of the trinuclear copper(II) units of compound  $\{[\text{Cu}(\text{H}_2\text{O})_4]_2[\text{Cu}(\text{mal})_2(\text{H}_2\text{O})]\}\{[\text{Cu}(\text{mal})_2(\text{H}_2\text{O})_2]\}\{[\text{Cu}(\text{H}_2\text{O})_4][\text{Cu}(\text{mal})_2(\text{H}_2\text{O})_2]\}$  (**7**) along with the atom numbering scheme. (b) Contents of the unit cell of complex **7**: monomer (violet), dimer (orange) and trimer (green). (c) Thermal dependence of the  $\chi_{\text{M}}T$  product for compound **7**.

of Cu(1) with a  $d_{z^2}$  orbital of Cu(2), the latter being non-magnetic and orthogonal to its magnetic  $d_{x^2 - y^2}$ . This kind of coupling (basal–apical or equatorial–axial) is repeated in many compounds and it has been found to be ferromagnetic in all of our copper(II) compounds.

The trinuclear cation  $[\text{Cu}_3(\text{mal})_2(\text{H}_2\text{O})_9]^{2+}$  [Fig. 6(a) and 6(b)] present in  $\{[\text{Cu}(\text{H}_2\text{O})_4]_2[\text{Cu}(\text{mal})_2(\text{H}_2\text{O})]\}\{[\text{Cu}(\text{mal})_2(\text{H}_2\text{O})_2]\}\{[\text{Cu}(\text{H}_2\text{O})_4][\text{Cu}(\text{mal})_2(\text{H}_2\text{O})_2]\}$  (**7**)<sup>8</sup> is formed by a central aquabis(malonate)copper(II) entity that is linked to two peripheral tetraaquacopper(II) units through carboxylate bridges which exhibit the *anti-syn* configuration. The coordination around the two crystallographically independent copper atoms [Cu(3) and Cu(4)] is distorted square pyramidal. Four coplanar carboxylate-oxygen atoms from two malonate ligands with nearly identical bond lengths [ $1.938(4)$  and  $1.941(2)$  Å for Cu(3)–O(9) and Cu(3)–O(10), respectively] build the basal plane around Cu(3), whereas a weakly coordinated water molecule [ $2.508(3)$  Å for Cu(3)–O(7w)] occupies the axial position. At Cu(4) four water molecules build the basal plane and a malonate-oxygen occupies the axial position. The

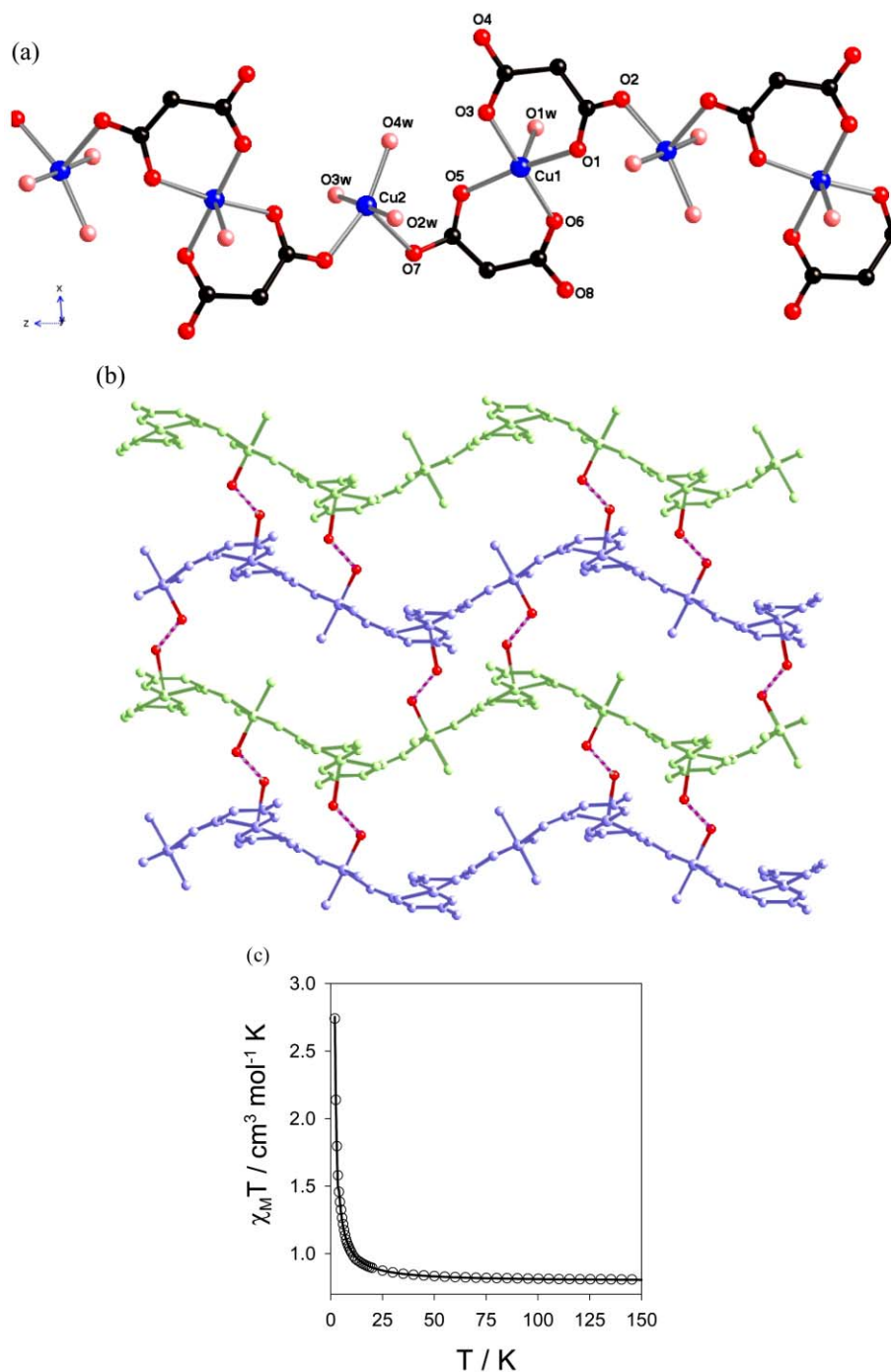


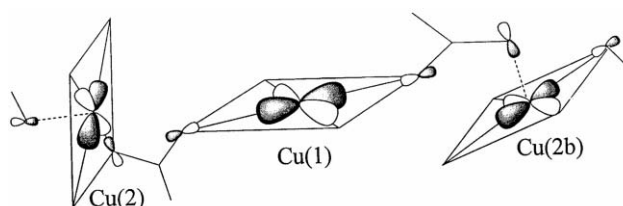
**Fig. 7** (a) Perspective drawing of a fragment of the chain of compound  $\{[\text{Cu}(\text{H}_2\text{O})_3][\text{Cu}(\text{mal})_2(\text{H}_2\text{O})]\}_n$  (**8**). (b) Projection of the structure of compound **8** down the  $a$  axis, showing the sheet-like nature. (c) Thermal dependence of the  $\chi_M T$  product for compound **8**.

magnetic behaviour is shown in Fig 6(c), the copper(II) ions being ferromagnetically coupled ( $J = 1.2 \text{ cm}^{-1}$ ) by the same reasons as previously mentioned for **6**.

The compound  $\{[\text{Cu}(\text{H}_2\text{O})_3][\text{Cu}(\text{mal})_2(\text{H}_2\text{O})]\}_n$  (**8**)<sup>8</sup> [Fig. 7(a) and 7(b)] has a 1-D polymeric structure. It consists of zigzag chains of copper(II) ions that exhibit a regular alternation of aquabis(malonate)copper(II) and triaquocopper(II) units, the former being linked to the latter as bis(monodentate) ligands though two *trans*-malonate-oxygen atoms. The chains run parallel to the  $z$  axis, and they are interconnected through hydrogen bonding. The two crystallographically independent copper(II) ions [Cu(1) and Cu(2)] have distorted square pyramidal surroundings. The four coplanar carboxylate oxygen atoms [O(1), O(3), O(5), and O(6)], which are coordinated to Cu(1), define the basal plane, whereas the apical position is occupied by a weakly coordinated water molecule O(1w).

The three water molecules O(2w), O(3w), and O(4w) and the carboxylate-oxygen O(7) build the basal plane at Cu(2), whereas the other carboxylate-oxygen O(2c) ( $c = -x, 1/2 - y, -1/2 + z$ ) occupies the axial position.

Each malonate simultaneously adopts bidentate [at Cu(1)]



**Scheme 4**

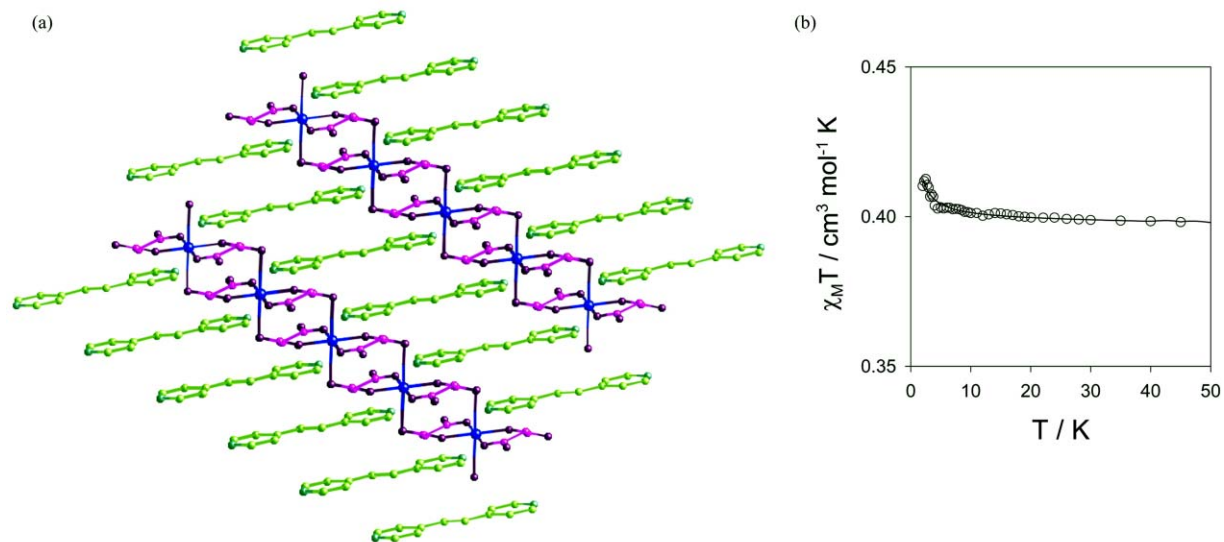


**Fig. 8** (a) Infinite 2-D sheet of compound  $[\text{H}_2\text{bpe}][\text{Cu}(\text{mal})_2]$  (**9**). Adjacent ligands bridge polymeric copper–malonate staircases *via* self-complementary N–H $\cdots$ O hydrogen bonds. (b) Thermal dependence of the  $\chi_{\text{M}}T$  product for compound **9**.

and unidentate [at Cu(2)] coordination modes. Two slightly different carboxylate bridges, that exhibit the *anti-syn* conformation, alternate regularly within each copper(II) chain.

For this compound, the magnetic behavior is shown in Fig. 7(c) and the relative orientation of the metal-centred magnetic orbitals within the chain is depicted in the Scheme 4.

The O(1)–C(1)–O(2) carboxylate connects a basal Cu(1)–O(1) bond with an apical O(2)–Cu(2b) bond, this coupling being weak and ferromagnetic ( $J = 1.9 \text{ cm}^{-1}$ ) as observed in **6**. The O(5)–C(5)–O(7) carboxylate connects two equatorial bonds [Cu(1)–O(5) and Cu(2)–O(7)] but the carboxylate plane and the equatorial plane at Cu(2) [O(2w)O(4w)O(3w)O(7)] are nearly

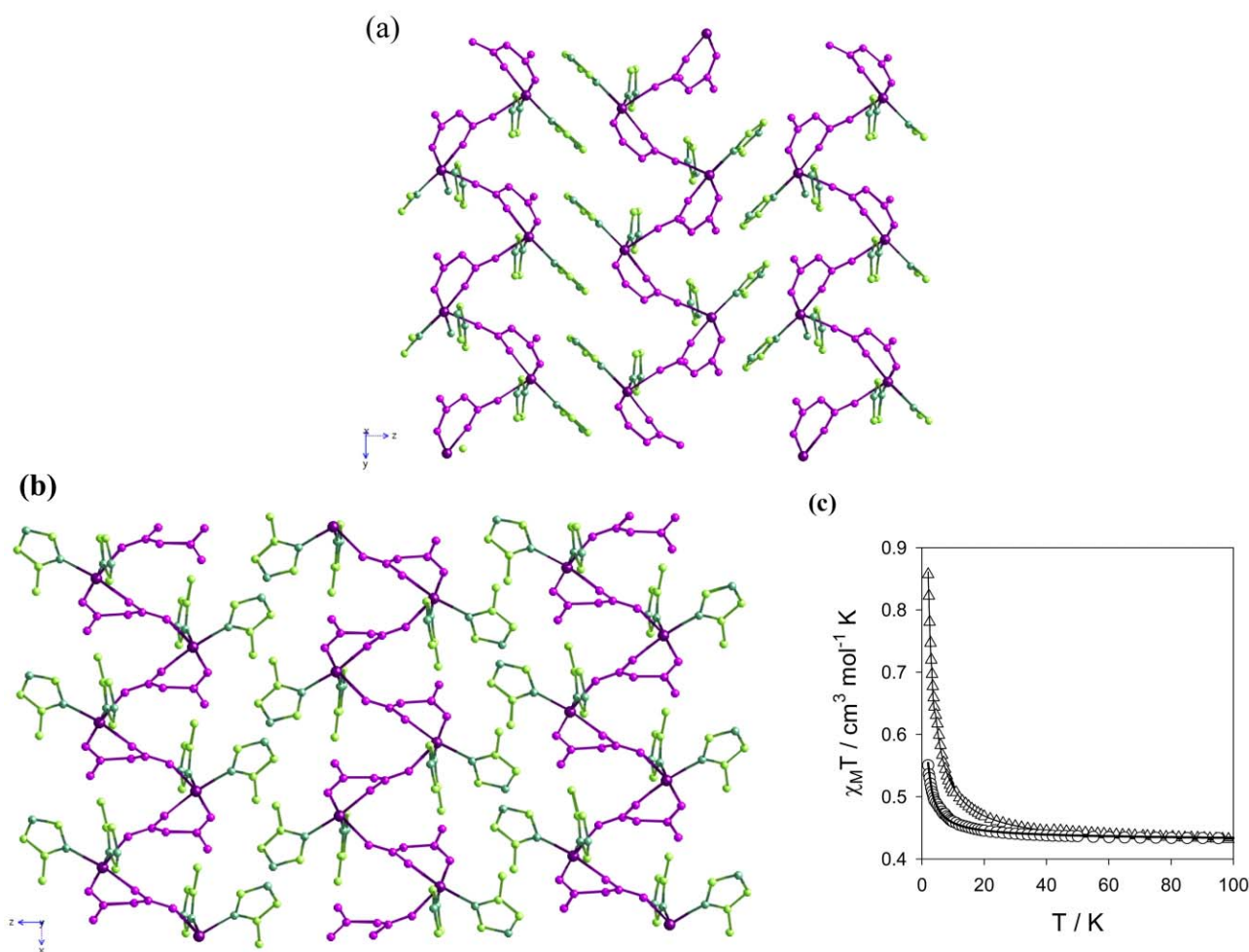


**Fig. 9** (a) Projection of compound  $[\text{Cu}(\text{Im})_2(\text{mal})]$  (**10**) down the *a* axis showing the parallel arrangement of the chains. (b) Projection of compound  $[\text{Cu}(\text{MeIm})_2(\text{mal})]$  (**11**) down the *b* axis showing the parallel arrangement of the chains and the columnar stacking of the 2-MeIm ligands. (c) Thermal dependence of the  $\chi_{\text{M}}T$  product for compounds **10** ( $\Delta$ ) and **11** ( $\circ$ ).

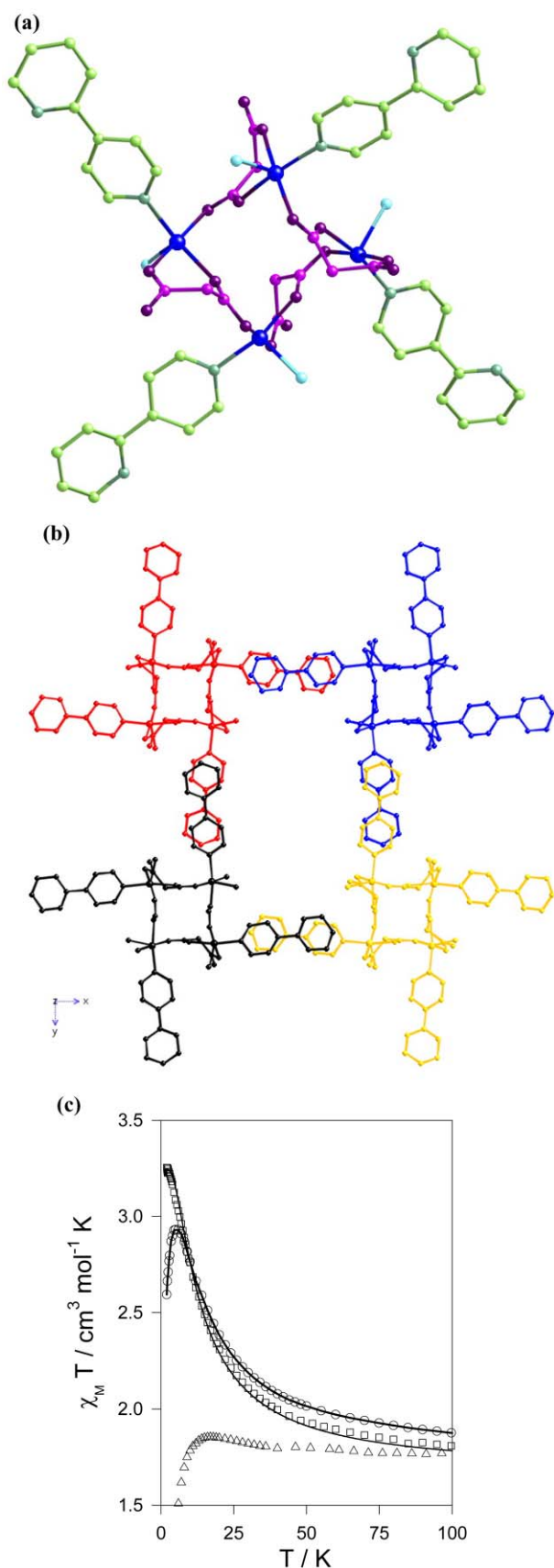


**Fig. 10** (a) Perspective view of the tetramer unit of  $[\text{Cu}_4(\text{mal})_4(\text{H}_2\text{O})_4(2,4'\text{-bipy})_4] \cdot 2\text{H}_2\text{O}$  (**12**), and (b) perspective view of the stacking of the compound along the *c* axis. (c) Thermal dependence of the  $\chi_M T$  product for compounds **12** ( $\square$ ), **13** ( $\circ$ ) and  $[\text{Cu}_4(\text{mal})_4(\text{pyz})_2] \cdot 4\text{H}_2\text{O}$  (*pyz* = pyrazine) ( $\triangle$ ),  $\chi_M$  being the magnetic susceptibility *per* four copper(II) ions.

orthogonal (dihedral angle of  $94.4^\circ$ ), and this may explain this interaction to be ferromagnetic ( $J = 3.0 \text{ cm}^{-1}$ ).

The structure of  $[\text{H}_2\text{bpe}][\text{Cu}(\text{mal})_2]$  (**9**) [bpe = bis(4-pyridyl)-ethylene] consist of polymeric anionic chains spaced by the  $[\text{H}_2\text{bpe}]^{2+}$  cations.<sup>9c</sup> The network is stabilized by extended hydrogen bonding between malonate-oxygens and protonated aromatic nitrogens as illustrated in Fig. 8. Each copper(II) ion is in an elongated octahedral surrounding. The malonate acts as bidentate with respect to a copper(II) filling equatorial positions, and as unidentate with respect to the nearest neighbor, filling an axial position. Although there are two identical exchange pathways among the copper(II) ions, the axial distance is so long that the ferromagnetic coupling within the anionic chain is very weak [Fig. 8(b),  $J = 0.04 \text{ cm}^{-1}$ ].

Combining the malonate with blocking ligands, such as imidazole or methylimidazole, 1-D polymeric structures can be obtained as those observed in compounds  $[\text{Cu}(\text{Im})_2(\text{mal})]$  (**10**) (Im = imidazole) and  $[\text{Cu}(\text{MeIm})_2(\text{mal})]$  (**11**)<sup>10</sup> (MeIm = methylimidazole) [Fig. 9(a) and 9(b)]. In these compounds the copper(II) is in a square pyramidal surrounding. Two malonate-oxygens from a bidentate malonate and two imidazole-nitrogens build the basal plane. The same malonate ligand acts as unidentate towards the neighboring copper(II) filling an apical position with a longer Cu–O distance. The magnetic behaviour is shown in Fig. 9(c), both compounds exhibiting ferromagnetic coupling,  $J = 1.64(1)$  and  $0.39(1) \text{ cm}^{-1}$  for **10** and **11**, respectively, as expected from the apical–equatorial connection.

The crystal structure of  $[\text{Cu}_4(\text{mal})_4(\text{H}_2\text{O})_4(2,4'\text{-bipy})_4] \cdot 2\text{H}_2\text{O}$  (**12**) (2,4'-bipy = 2,4'-bipyridine) consists of tetrameric  $[\text{Cu}_4(\text{mal})_4(\text{H}_2\text{O})_4(2,4'\text{-bipy})_4]$  neutral units, involving a small planar square with copper(II) cations and malonate anions at each corner<sup>9a</sup> [Fig. 10(a) and 10(b)]. Each copper atom exhibits a slightly distorted square pyramidal surrounding. Three carboxylate-oxygen atoms from two malonate ligands and one nitrogen atom from the 2,4'-bipy group build the basal plane whereas the apical position is filled by a water molecule. The network is stabilized by the  $\pi$ – $\pi$  stacking among the 2,4'-bipy ligands of different tetrameric units, and hydrogen bonding between coordinated water molecules and uncoordinated malonate-oxygens. The malonate-oxygens fill only equatorial positions. The 2,4'-bipy acts as a blocking ligand, since the location of the nitrogen in the 2-position does not allow further polymerisation. The magnetic properties of **12** are shown in Fig. 10(c) and correspond to those of magnetically isolated squares of four ferromagnetically coupled spin doublets,  $J = 12.3(1) \text{ cm}^{-1}$ .

$[\text{Cu}_4(\text{mal})_4(\text{H}_2\text{O})_4(4,4'\text{-bipy})_2] \cdot 2\text{H}_2\text{O}$  (**13**) (4,4'-bipy = 4,4'-bipyridine) has a similar structure and magnetic properties [Fig. 10(c)] to those observed for **12**. The main difference is the ability of the 4,4'-bipy to act as a bidentate ligand interconnecting the  $\text{Cu}_4(\text{mal})_4(\text{H}_2\text{O})_4$  tetramers leading to a 2-D network<sup>13</sup> (Fig. 11). This compound illustrates the incrementing of the dimensionality by the introduction of other bridging ligands. The four copper(II) ions are ferromagnetically coupled in the small square [ $J = 12.4(1) \text{ cm}^{-1}$ ] existing as weak antiferromagnetic interactions among the tetramers through the 4,4'-bipy ( $j = -0.05 \text{ cm}^{-1}$ ).

The structure of  $[\text{Mn}^{\text{II}}\text{Cu}^{\text{II}}(\text{mal})_2(\text{H}_2\text{O})_3] \cdot 2\text{H}_2\text{O}$  (**14**)<sup>11</sup> is made up by neutral bimetallic chains that are linked with long weak axial malonate-oxygen to copper bonds, which leads to a corrugated sheet-like structure (Fig. 12). The crystal structure is stabilized by an extensive network of intra- and inter-layer hydrogen bonds involving both coordinated and non-coordinated water molecules and malonate-oxygens. Each malonate group acts simultaneously as a bidentate [through O(1) and O(3) to Cu(1) and through O(6) and O(7) at Cu(2)] and a unidentate [through O(4) and O(5) to Mn(1)] ligand within the chain, the remaining carboxylate-oxygen interacting weakly with the copper atoms of neighboring chains [O(2) and

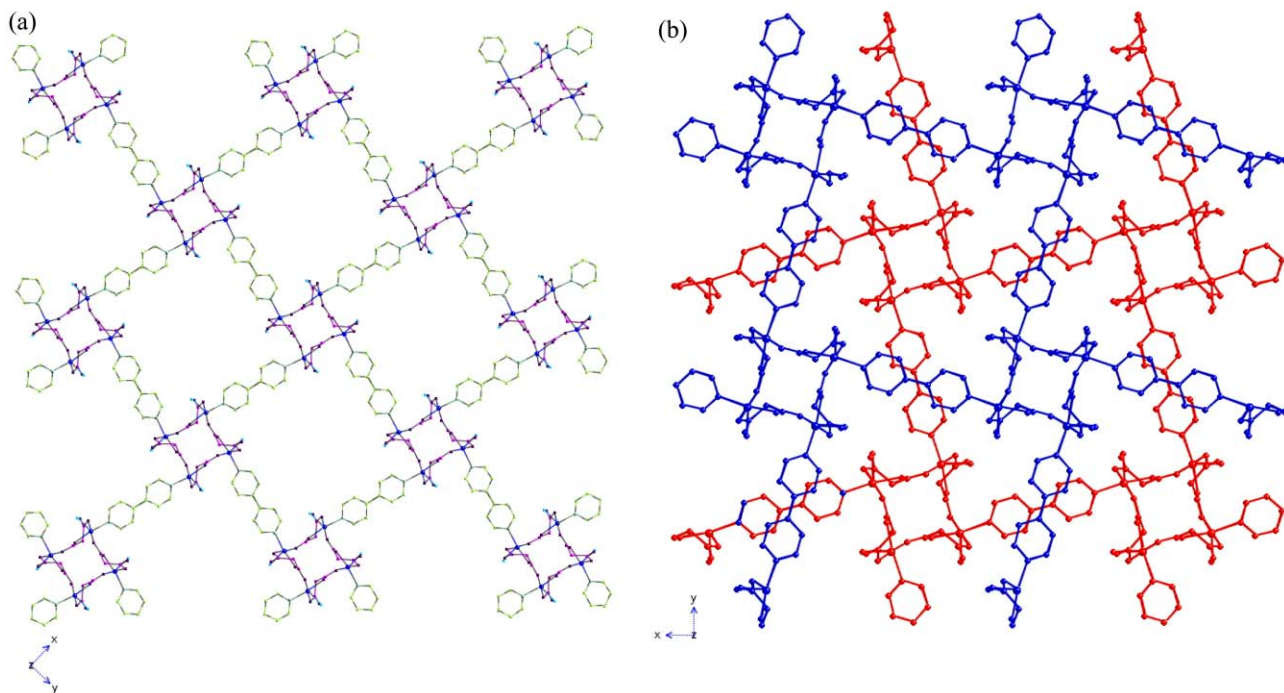


**Fig. 11** (a) View of the two types of square channels of  $[\text{Cu}_4(\text{mal})_4(\text{H}_2\text{O})_4(4,4'\text{-bipy})_2]\cdot 2\text{H}_2\text{O}$  (**13**) along the  $c$  axis when only the odd layers are considered. (b) View of the layers stacked along the tetragonal  $c$  axis.

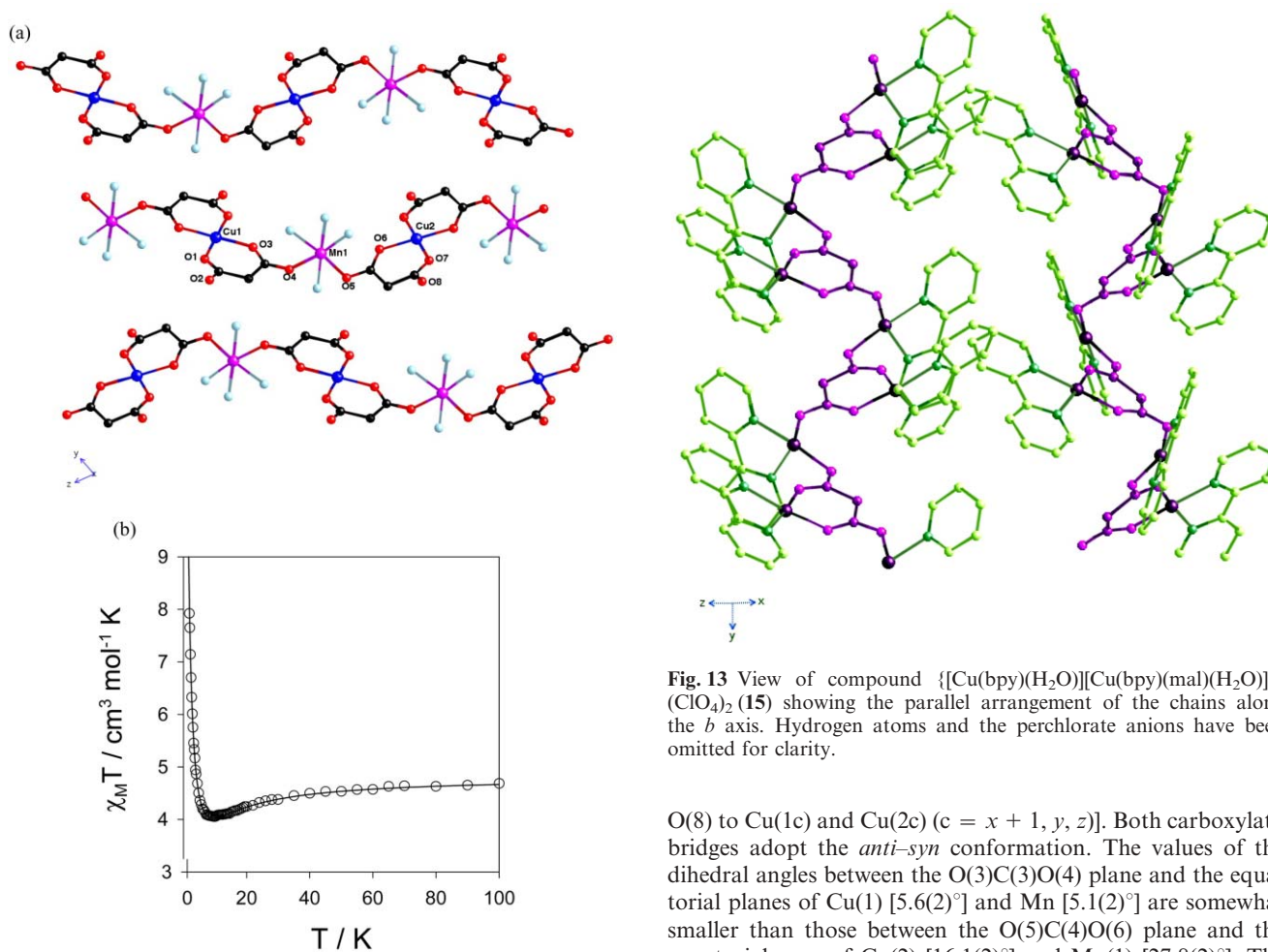


**Fig. 12** (a) Projection of the packing of the chains of  $[\text{Mn}^{\text{II}}\text{Cu}^{\text{II}}(\text{mal})_2(\text{H}_2\text{O})_3]\cdot 2\text{H}_2\text{O}$  (**14**) down the  $a$  axis. Uncoordinated water molecules and hydrogen bonding interactions are not drawn for the sake of clarity. (b) Thermal dependence of the  $\chi_M T$  product for compound **14**.

**Fig. 13** View of compound  $\{[\text{Cu}(\text{bpy})(\text{H}_2\text{O})][\text{Cu}(\text{bpy})(\text{mal})(\text{H}_2\text{O})]\}(\text{ClO}_4)_2$  (**15**) showing the parallel arrangement of the chains along the  $b$  axis. Hydrogen atoms and the perchlorate anions have been omitted for clarity.

O(8) to Cu(1c) and Cu(2c) ( $c = x + 1, y, z$ ). Both carboxylato bridges adopt the *anti-syn* conformation. The values of the dihedral angles between the O(3)C(3)O(4) plane and the equatorial planes of Cu(1) [ $5.6(2)^\circ$ ] and Mn [ $5.1(2)^\circ$ ] are somewhat smaller than those between the O(5)C(4)O(6) plane and the equatorial ones of Cu(2) [ $16.1(2)^\circ$ ] and Mn(1) [ $27.8(2)^\circ$ ]. The shortest interchain metal–metal separations are  $5.234(1) \text{ \AA}$  [Cu(1)⋯Cu(1c) and Mn(1)⋯Mn(1c)].

The magnetic behavior, shown in Fig. 12(b), is characteristic of ferrimagnetic chains without magnetic ordering in the

temperature range explored. Given the special alternating trend  $\dots J_1 - J_1 - J_2 - J_2 - J_1 - J_1 \dots$ , where  $J_1$  and  $J_2$  represent the intra-chain Cu(II)–Mn(II) isotropic magnetic coupling, and the lack of a theoretical model to treat it, we have assumed that the  $J_1$  and  $J_2$  values should be very close and consequently we have treated the experimental data through a regular chain approach. The least square fitting of the data led to  $J_{MnCu} = -4.5 \text{ cm}^{-1}$ .<sup>11</sup>

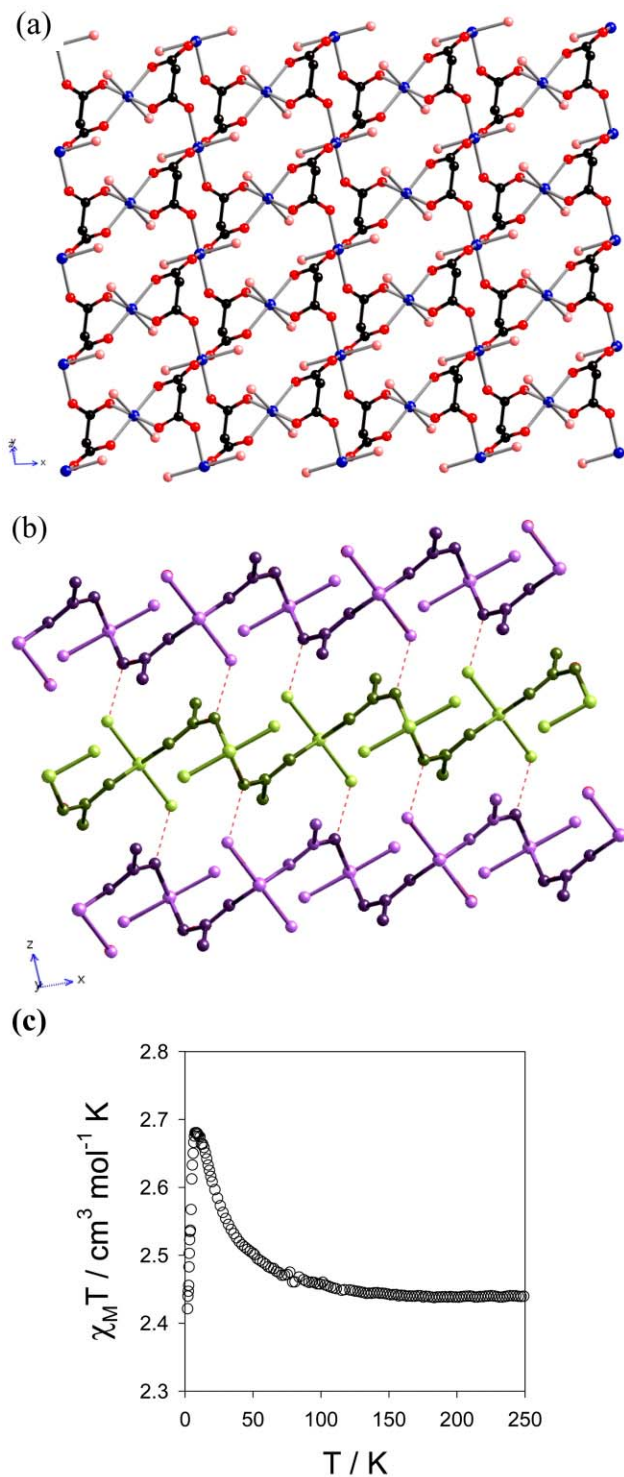


**Fig. 14** (a) Sheet structure of the isostructural  $[\text{M}(\text{H}_2\text{O})_2][\text{M}'(\text{mal})_2(\text{H}_2\text{O})_2]$  ( $\text{M} = \text{Mn}^{\text{II}}, \text{Co}^{\text{II}}, \text{Ni}^{\text{II}}, \text{Zn}^{\text{II}}$ ;  $\text{M}' = \text{Co}^{\text{II}}, \text{Ni}^{\text{II}}, \text{Zn}^{\text{II}}$ ) (16) compounds. (b) Parallel packing of the sheets showing the hydrogen interactions involved in the generation of the framework structure. (c) Thermal dependence of the  $\chi_M T$  product for  $[\text{Ni}(\text{H}_2\text{O})_2][\text{Ni}(\text{mal})_2(\text{H}_2\text{O})_2]$ .

### (c) Bidentate + bis(unidentate)

Two polymorphic, malonate-bridged copper(II) complexes of formula  $\{[\text{Cu}(\text{bpy})(\text{H}_2\text{O})][\text{Cu}(\text{bpy})(\text{mal})(\text{H}_2\text{O})]\}(\text{ClO}_4)_2$  (15) (bpy = 2,2'-bipyridine) (Fig. 13) have been prepared.<sup>12</sup> The structures are made up of uncoordinated perchlorate anions and malonate-bridged zigzag copper(II) chains running parallel to one of the crystallographic axes. These chains are built by a  $[\text{Cu}(\text{bpy})(\text{mal})(\text{H}_2\text{O})]$  unit acting as a bis(unidentate) ligand toward two  $[\text{Cu}(\text{bpy})(\text{H}_2\text{O})]$  adjacent units through its OCCCO skeleton in an *anti-anti* conformation, whereas the carboxylate bridge exhibits the *anti-syn* conformation. These compounds contain four crystallographically independent copper(II) atoms, but the environment of all of them is distorted square

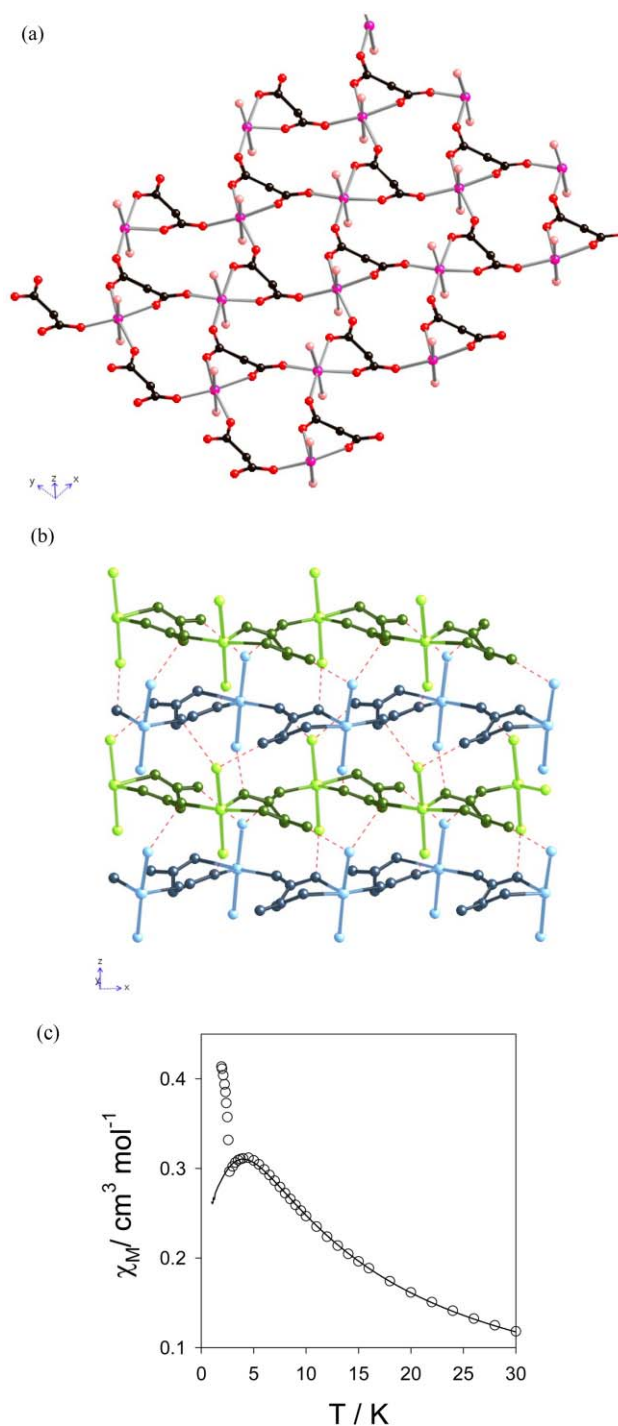


**Fig. 15** (a) Sheet structure of compound  $[\text{Mn}(\text{mal})(\text{H}_2\text{O})_2]$  (17). (b) Parallel packing of the sheets showing the hydrogen interactions involved in the generation of the framework structure. (c) Thermal dependence of the  $\chi_M$  for compound 17.



pyramidal: the axial position is occupied by a water molecule, whereas the equatorial plane is formed by a chelating bpy and either a bidentate malonate or two unidentate carboxylate-oxygens from two malonate ligands. Each malonate acts as bidentate with respect to a copper(II) and as bis(unidentate) to another two. The analysis of the magnetic data indicates the occurrence of a ferro- (through the carboxylate,  $J = 4.6 \text{ cm}^{-1}$ )

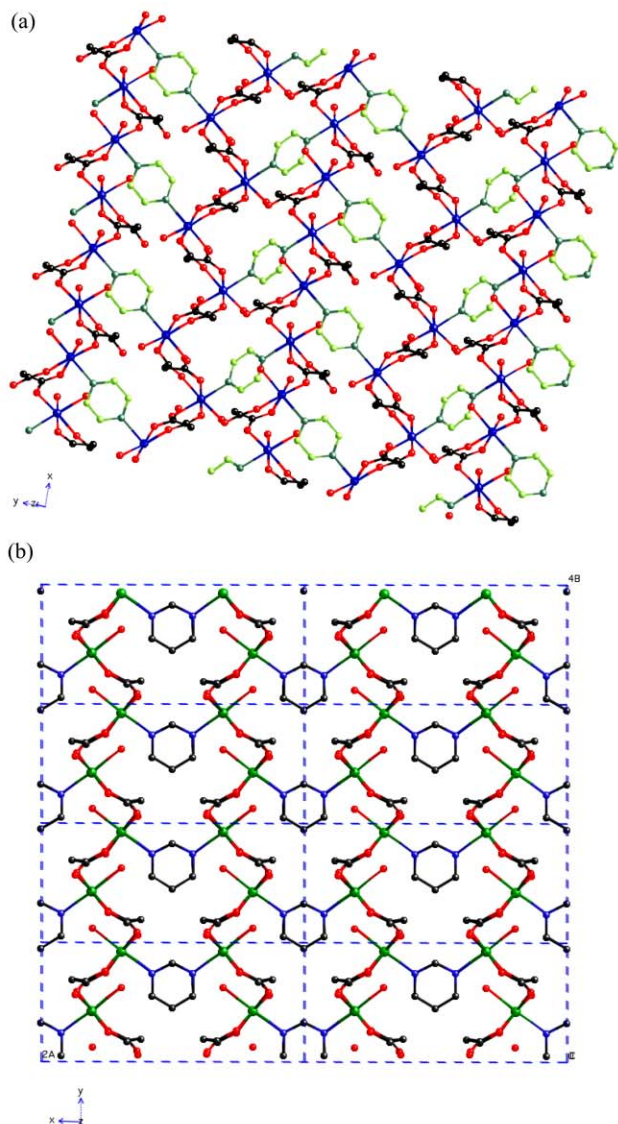


**Fig. 16** A layer of crystal structure showing the  $[\text{M}(\text{mal})(\text{H}_2\text{O})]$  sheets cross-linked by (a) pyrazine ligands  $[\text{M}(\text{mal})(\text{pyz})(\text{H}_2\text{O})]$  ( $\text{M}(\text{II}) = \text{Co}, \text{Zn}$ ), and (b) pyrimidine ligands  $[\text{Mn}(\text{mal})(\text{pym})(\text{H}_2\text{O})]$ . (c) Thermal dependence of the  $\chi_{\text{M}}T$  product for  $[\text{Co}(\text{mal})(\text{pyz})(\text{H}_2\text{O})]$  ( $\square$ ) and  $[\text{Co}(\text{mal})(\text{pym})(\text{H}_2\text{O})]$  ( $\circ$ ).

and an antiferro-magnetic (through the skeleton of the malonate,  $J = -4.2 \text{ cm}^{-1}$ ) coupling.

A family of compounds exhibiting this coordination mode

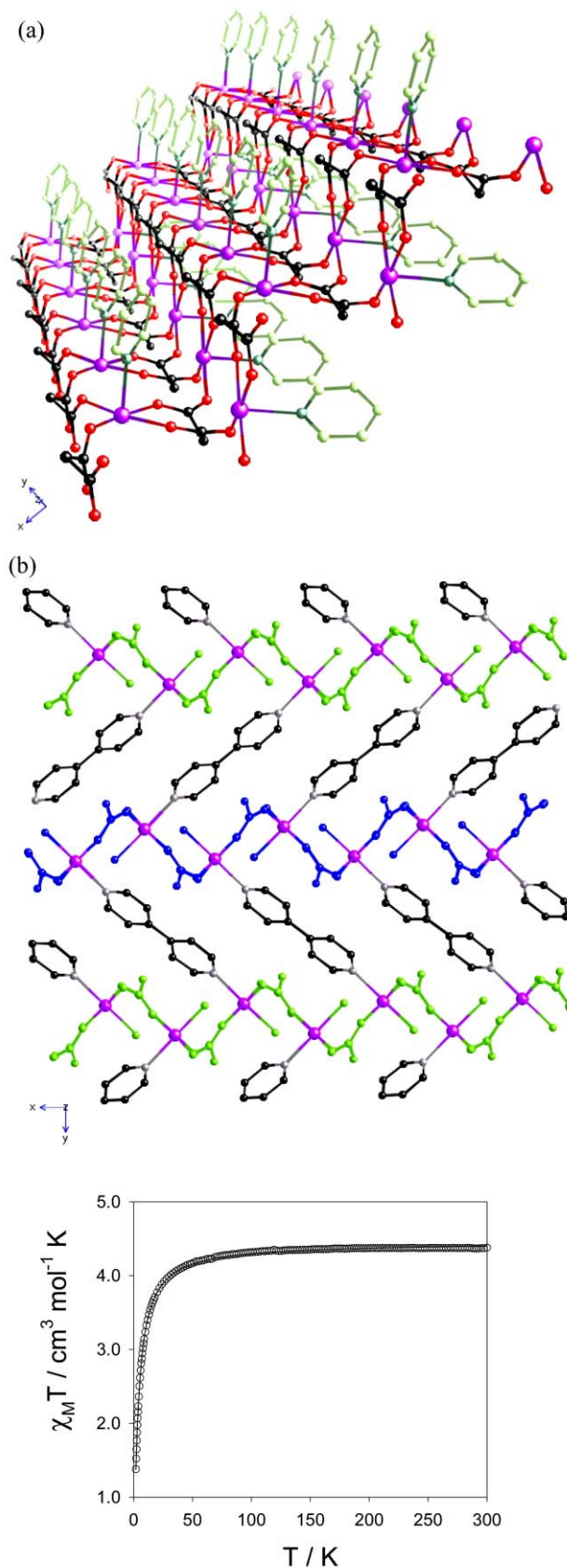


**Fig. 17** (a) View of the zigzag sheet in  $[\text{Mn}(\text{mal})(4,4'\text{-bipy})_{1/2}(\text{H}_2\text{O})]$ , a simplified view of the bridging  $4,4'$ -bipy moieties viewed along the sheet. (b) View of the crystal structure along the  $c$  axis. (c) Thermal dependence of the  $\chi_{\text{M}}T$  product for  $[\text{Mn}(\text{mal})(4,4'\text{-bipy})_{1/2}(\text{H}_2\text{O})]$ .

are the isostructural<sup>9d,19</sup> homo- or hetero-bimetallic malonates of the divalent Co, Ni and Zn:  $[\text{M}(\text{H}_2\text{O})_2][\text{M}'(\text{mal})_2(\text{H}_2\text{O})_2]$  ( $\text{M} = \text{Mn}^{\text{II}}, \text{Co}^{\text{II}}, \text{Ni}^{\text{II}}, \text{Zn}^{\text{II}}; \text{M}' = \text{Co}^{\text{II}}, \text{Ni}^{\text{II}}, \text{Zn}^{\text{II}}$ ) (**16**) (Fig. 14). The simple malonates of the divalent Co, Ni and Zn are isostructural, and their mixed bimetallic malonates behave as solid solutions filling randomly the positions of M and M'. Mn(II) can also be introduced in the network as M, its concentration must be kept below 50% or the mixed malonate is impurified with Mn(II) malonate. These compounds have a corrugated bidimensional structure in which M and M' are in an octahedral environment. Two malonates act as bidentate towards M' filling the equatorial positions, whereas the remaining malonate-oxygens act as unidentate filling equatorial positions of four adjacent M cations. The water molecules fill the axial positions. The magnetic coupling, shown for the Ni(II) complex in Fig. 14(c), is very weak since the malonate exhibits the *anti-syn* configuration, being ferromagnetic and antiferromagnetic for Ni(II) and Co(II), respectively. The mixed malonates are ferrimagnetic, but magnetic ordering is not obtained in any case.

The structure of the Mn(II) malonate (**17**) is made up by the polymerization of  $[\text{Mn}(\text{mal})(\text{H}_2\text{O})_2]$  monomers giving a 2-D array (Fig. 15).<sup>20</sup> The Mn(II) is in an octahedral environment, with the water molecules in the axial positions. Each malonate chelates the metal as bidentate, with the remaining two oxygens bridging to two further adjacent metallic atoms as bis(unidentate). This structure is very original since the two carboxylates of the malonate exhibit two different conformations, *anti-anti* and *anti-syn*, respectively. This feature leads to a spin canting behaviour at low temperatures [Fig. 15(c)].

$[\text{M}(\text{mal})(\text{pyz})(\text{H}_2\text{O})]$  and  $[\text{M}(\text{mal})(\text{pym})(\text{H}_2\text{O})]$  ( $\text{M}(\text{II}) = \text{Co}, \text{Zn}; \text{pym} = \text{pyrimidine}$ ) (**18**)<sup>9c</sup> (Fig. 16), and  $[\text{Co}(\text{mal})(4,4'\text{-bipy})_{1/2}(\text{H}_2\text{O})]$ <sup>21</sup> and  $[\text{Mn}(\text{mal})(4,4'\text{-bipy})_{1/2}(\text{H}_2\text{O})]$  (**19**)<sup>9f</sup> (Fig. 17) have related structures in which layers of octahedrally coordinated metallic atoms bridged by the malonate anions within the layers are interconnected by 4,4'-bipy, pyz or pym molecules leading to a 3-D structure. Each malonate chelates the metal as bidentate, with the remaining two oxygen atoms bridging to two further adjacent metallic atoms as bis(unidentate), thus forming continuous covalently bonded sheets. The metal is then coordinated by three different malonate anions, the remaining two *trans* positions being filled by a terminal  $\text{H}_2\text{O}$  molecule and the nitrogen of the aromatic molecule. All these compounds, except those of Zn, exhibit weak antiferromagnetic coupling [Figs. 16(c) and 17(c)].

The structure of  $[\text{Cu}_4(\text{mal})_4(\text{pyz})_2] \cdot 4\text{H}_2\text{O}$  (**20**)<sup>9a</sup> (Fig. 18) is very similar to that of **13**, in which 2-D layers were obtained by the assemblage of  $\text{Cu}_4(\text{mal})_4$  tetramers by bidentate 4,4'-bipy ligands. In **20** the tetramers are assembled by bidentate pyrazine ligands. Each copper atom is in a quasi perfect square pyramid surrounded by three carboxylate-oxygen atoms from two malonate groups and one nitrogen atom from a pyrazine ligand building the equatorial plane. The main difference with the structure of **13** is the absence of a water molecule filling the apical position of the square pyramidally surrounded copper(II). This position is occupied by a malonate-oxygen of a tetramer of a neighboring layer. By this new link the layers are interconnected leading to a 3-D structure. Each malonate uses its four oxygen atoms to coordinate the copper atoms: within each layer, the malonate adopts simultaneously the bidentate (at one copper atom) and unidentate (at another copper atom) coordination modes, the fourth carboxylate-oxygen acts also as unidentate being bound to a further copper atom from a neighboring layer. The magnetic properties of **20** have been investigated in the temperature range 1.9–300 K and they exhibit an overall weak ferromagnetic behavior which would be the result of a competition between ferromagnetic (through the malonate bridge) and antiferromagnetic (through the pyrazine bridge) interactions, the former being somewhat stronger [Fig. 10(c)].

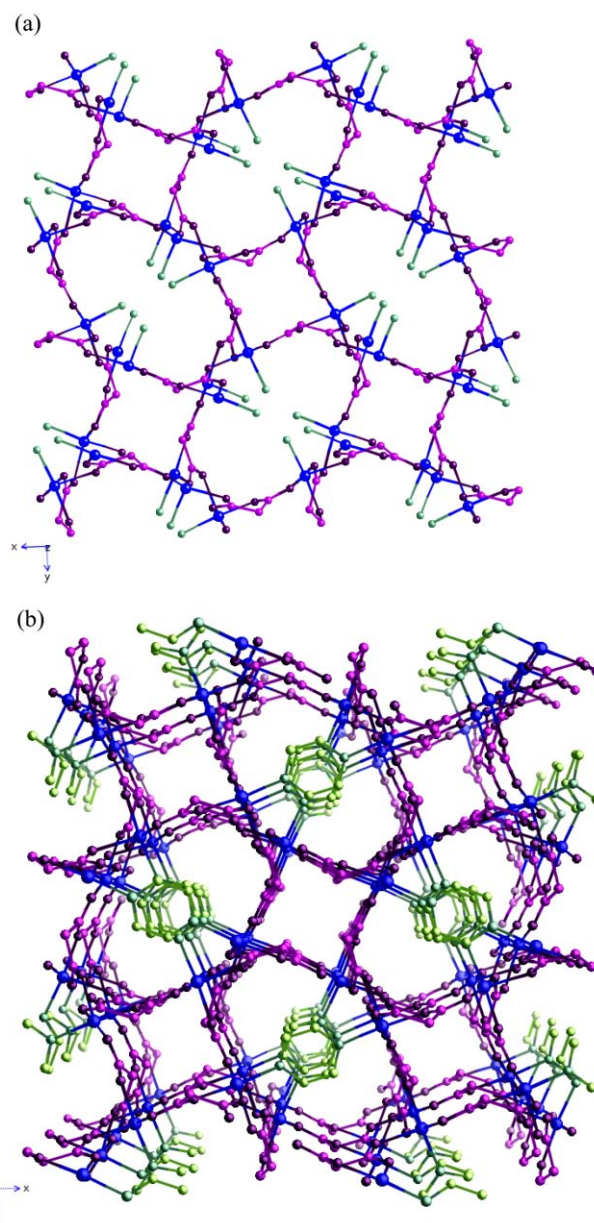


**Fig. 18** (a) The Cu/malonate framework in compound  $[\text{Cu}_4(\text{mal})_4(\text{pyz})_2] \cdot 4\text{H}_2\text{O}$  (**20**) along the *c* axis. (b) A view of the 3-D structure where the square grid layers are stacked along the *c* axis showing the  $\pi$ - $\pi$  overlap between pairs of pyrazine molecules.

#### (d) Bidentate + bis(unidentate) + $\mu$ -oxo

In the compound  $[\text{Cu}_4(\text{mal})_4(\text{bpe})_3]$  (**21**)<sup>9c</sup> we have two crystallographically independent copper(II) ions, Cu(1) and Cu(2) being in square pyramidal and in octahedral surroundings, respectively. The bpe ligands fill basal and equatorial positions of the Cu(1) and Cu(2) coordination polyhedra, respectively. There are two non-equivalent malonate ligands acting as  $\eta^5$ -bidentate ligands chelating the Cu(2), one of them filling two equatorial positions, the other one filling an equatorial and an axial position. This latter malonate has a very special coordination and bridging mode when acting as unidentate with the remaining oxygens. One of them is bound as unidentate to another copper(II) with a long Cu(2)–O distance (2.626 Å) and the last oxygen is bound to two Cu(1) atoms, behaving as a  $\mu$ -oxo bridge (Fig. 19). This compound has a 3-D structure, the copper(II) ions being weakly ferromagnetically coupled [Fig. 19(b)]. In this compound, seven different exchange pathways have been observed, three through the bpe and four through the malonate.

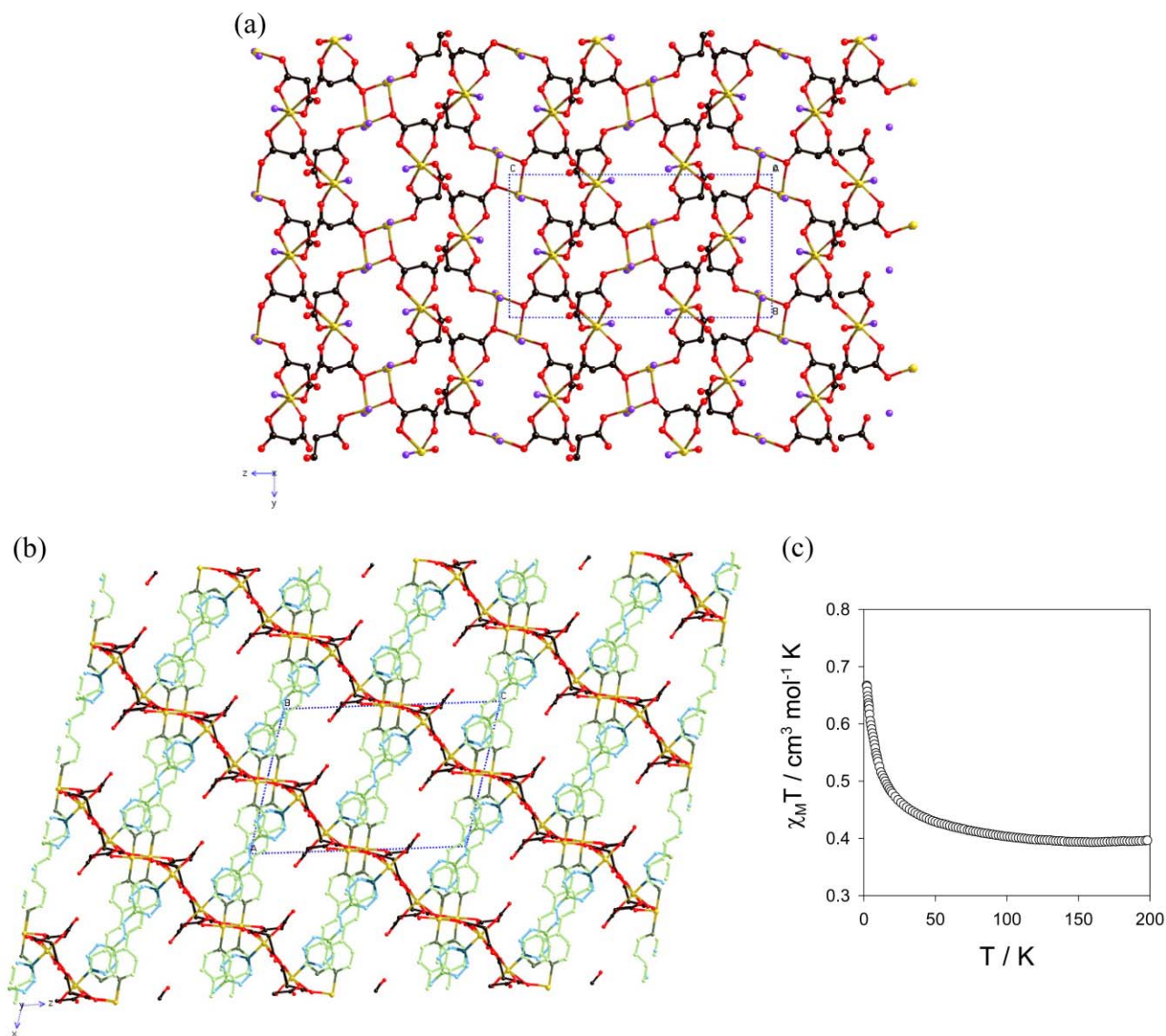


Fig. 19 (a) Structure of a Cu/malonate sheet in compound  $[\text{Cu}_4(\text{mal})_4(\text{bpe})_3]$  (**21**) along the  $a$  axis. (b) View of the crystal packing along the  $b$  axis. (c) Thermal dependence of the  $\chi_M T$  product,  $\chi_M$  being the magnetic susceptibility *per* copper(II) ion.

## Conclusions

The bis(bidentate) coordination mode dominant in the oxalato complexes is sterically forbidden for the malonate, which makes the bidentate + unidentate and the bidentate + bis(unidentate) coordination modes dominate in the chemistry of the malonate. This dramatically affects the structure and the properties of the malonate complexes, with ferromagnetic interactions being much more frequent than in general compounds. The malonate is a dissymmetric ligand. By its bidentate side it is a strong complexing agent (due to the chelate effect), usually filling equatorial or basal positions displaying short M–O distances. By its other side it acts as a unidentate ligand showing weaker interactions and longer M'–O distances. The metallic ion that is chelated usually remains in the same plane of the carboxylato groups with small deviations; on the other hand the unidentate coordinated metal can deviate considerably from the carboxylate plane, reducing notably the overlap between the magnetic orbitals of the paramagnetic centres. This minimizes the antiferromagnetism, and interactions expected to be antiferromagnetic can be turned to ferromagnetic. Another feature of the malonate is the fact that when these latter M'–O distances are long enough, this oxygen becomes axial or apical. Then, as a consequence of the coupling

of orbitals of different symmetry the magnetic interaction is expected to be ferromagnetic in many copper(II) complexes.

Consequently we can conclude that the malonate is a very versatile ligand that is able to generate high dimensionality networks coupling paramagnetic centres ferromagnetically in much higher percentage than other dicarboxylic ligands. The malonate itself cannot lead to a 3-D array, but combined with other ligands the three-dimensional networks can be obtained. We are now in the search of ligands, suitable to be combined with the malonate, capable of coupling ferromagnetically the spin carriers in the remaining dimensions.

## Acknowledgements

The financial support provided by the Gobierno Autónomo de Canarias (Project PI2000/135) and the Spanish Dirección General de Investigación (Ministerio de Ciencia y Tecnología), through project BQU2001-3794, is gratefully acknowledged.

## References

- 1 O. Kahn, *Comments Condens. Matter Phys.*, 1994, **17**, 39; Y. Pei, Y. Journaux and O. Kahn, *Inorg. Chem.*, 1989, **28**, 100.

- 2 O. Kahn, *The Encyclopedia of Advanced Materials*, Pergamon, Oxford, 1994.
- 3 J. S. Miller and A. J. Epstein, *Angew. Chem., Int. Ed. Engl.*, 1994, **33**, 385.
- 4 *Supramolecular Engineering of Synthetic Metallic Materials*, NATO ASI Series, J. Veciana, C. Rovira and D. B. Amabilino, ed., Kluwer Academic Publishers, Dordrecht, 1998, vol. 518.
- 5 M. Hernández-Molina, P. A. Lorenzo-Luis and C. Ruiz-Pérez, *CrystEngComm*, 2001, **3**(16), 60.
- 6 C. Hornick, P. Rabu and M. Drillon, *Polyhedron*, 2000, **19**, 259; P. Rabu, J. M. Rueff, Z. L. Huang, S. Angelov, J. Souletie and M. Drillon, *Polyhedron*, 2001, **20**, 1677.
- 7 M. Hernández-Molina, P. A. Lorenzo-Luis, C. Ruiz-Pérez, F. Lloret and M. Julve, *Inorg. Chim. Acta*, 2001, **313**, 87.
- 8 C. Ruiz-Pérez, J. Sanchiz, M. Hernández-Molina, F. Lloret and M. Julve, *Inorg. Chem.*, 2000, **39**, 1363.
- 9 (a) Y. Rodríguez-Martín, M. Hernández-Molina, F. S. Delgado, J. Pasán, C. Ruiz-Pérez, J. Sanchiz, F. Lloret and M. Julve, *CrystEngComm*, 2002, **4**(73), 440; (b) C. Ruiz-Pérez, J. Sanchiz, Y. Rodríguez-Martín, M. Hernández-Molina, F. S. Delgado, J. Pasán, F. Lloret and M. Julve, *Inorg. Chim. Acta*, 2002, in press; (c) J. Sanchiz, Y. Rodríguez-Martín, C. Ruiz-Pérez, M. Hernández-Molina, F. S. Delgado, J. Pasán, F. Lloret and M. Julve, *Eur. J. Inorg. Chem.*, 2002, submitted; (d) C. Ruiz-Pérez, J. Sanchiz, Y. Rodríguez-Martín, M. Hernández-Molina, F. S. Delgado, J. Pasán, F. Lloret and M. Julve, *Eur. J. Inorg. Chem.*, 2002, submitted; (e) J. Sanchiz, Y. Rodríguez-Martín, C. Ruiz-Pérez, M. Hernández-Molina, F. S. Delgado, J. Pasán, F. Lloret and M. Julve, *Inorg. Chim. Acta*, 2002, submitted; (f) C. Ruiz-Pérez, J. Sanchiz, Y. Rodríguez-Martín, M. Hernández-Molina, F. S. Delgado, J. Pasán, F. Lloret and M. Julve, *Inorg. Chim. Acta*, 2002, submitted.
- 10 J. Sanchiz, Y. Rodríguez-Martín, C. Ruiz-Pérez, A. Mederos, F. Lloret and M. Julve, *New J. Chem.*, 2002, in press.
- 11 C. Ruiz-Pérez, J. Sanchiz, M. Hernández-Molina, F. Lloret and M. Julve, *Inorg. Chim. Acta*, 2000, **298**, 202.
- 12 C. Ruiz-Pérez, M. Hernández-Molina, P. A. Lorenzo-Luis, F. Lloret and M. Julve, *Inorg. Chem.*, 2000, **39**, 3845.
- 13 Y. Rodríguez-Martín, C. Ruiz-Pérez, J. Sanchiz, F. Lloret and M. Julve, *Inorg. Chim. Acta*, 2001, **318**, 159.
- 14 Y. Rodríguez-Martín, C. Ruiz-Pérez, J. Sanchiz, F. Lloret and M. Julve, *New J. Chem.*, submitted.
- 15 J. Sanchiz, Y. Rodríguez-Martín, C. Ruiz-Pérez, M. Hernández-Molina, F. S. Delgado, J. Pasán, F. Lloret and M. Julve, *CrystEngComm*, 2002, submitted; G. I. Bimitrova, A. V. Ablov, G. A. Kiosse, G. A. Popovich, T. I. Nmalinuskii and I. F. Bourshteyn, *Dokl. Akad. Nauk SSSR*, 1974, **216**, 1055.
- 16 Y. Rodríguez-Martín, J. Sanchiz, C. Ruiz-Pérez, F. Lloret and M. Julve, *Inorg. Chim. Acta*, 2001, **326**, 20.
- 17 W.-L. Kwik, K.-P. Ang and H. S.-O. Chan, *J. Chem. Soc., Dalton Trans.*, 1986, 2519.
- 18 D. Chattopadhyay, S. K. Chattopadhyay, P. R. Lowe, C. H. Schwalde, S. K. Mazumder, A. Rana and S. Ghosh, *J. Chem. Soc., Dalton Trans.*, 1993, 913.
- 19 N. J. Ray and B. J. Hathaway, *Acta Crystallogr., Sect. B*, 1982, **38**, 770.
- 20 T. Lis and J. Matuszewski, *Acta Crystallogr., Sect. B*, 1979, **35**, 2212.
- 21 P. Lightfoot and A. Snedden, *J. Chem. Soc., Dalton Trans.*, 1999, 3549.



PERGAMON

Available online at [www.sciencedirect.com](http://www.sciencedirect.com)

SCIENCE @ DIRECT®

Polyhedron 22 (2003) 2143–2153



POLYHEDRON

[www.elsevier.com/locate/poly](http://www.elsevier.com/locate/poly)

# Malonate-based copper(II) coordination compounds: ferromagnetic coupling controlled by dicarboxylates

Jorge Pasán<sup>a</sup>, Fernando S. Delgado<sup>a</sup>, Yolanda Rodríguez-Martín<sup>a</sup>,  
María Hernández-Molina<sup>a</sup>, Catalina Ruiz-Pérez<sup>a,\*</sup>, Joaquín Sanchiz<sup>b</sup>,  
Francesc Lloret<sup>c</sup>, Miguel Julve<sup>c</sup>

<sup>a</sup> *Departamento de Física Fundamental II, Laboratorio de Rayos X y Materiales Moleculares, Universidad de La Laguna, Avda. Astrofísico Francisco Sánchez s/n, 38204 La Laguna, Tenerife, Spain*

<sup>b</sup> *Departamento de Química Inorgánica, Universidad de La Laguna, Tenerife, Spain*

<sup>c</sup> *Departament de Química Inorgànica, Facultat de Química, Institut de Ciència Molecular, Universitat de València, Valencia, Spain*

Received 6 October 2002; accepted 23 December 2002

## Abstract

Studies on structural and magnetic properties of polynuclear transition metal complexes, aimed at understanding the structural and chemical factors governing electronic exchange coupling mediated by multiatom bridging ligands, are of continuing interest to design new molecular materials exhibiting unusual magnetic, optical and electrical properties, bound to their molecular nature. Looking at potentially flexible bridging ligands, the malonate group seems a suitable candidate. The occurrence of two carboxylate groups in the 1,3 positions allows this ligand to adopt simultaneously chelating bidentate and different carboxylato bridging modes (*syn-syn*, *anti-anti* and *syn-anti* through one or two carboxylate groups). In the course of our research we have structurally and magnetically characterized several carboxylato bridged copper(II) complexes. In the present study we start describing briefly the structure and the magnetic behaviour of the compounds, subsequently we analyze the magneto-structural correlations concluding that the parameter that governs, in first order, the magnetic interaction between metal centres is the relative position of the carboxylato bridge of the malonate respect to the copper(II) ions: equatorial–equatorial (strong interaction), equatorial–apical (weak interaction) and apical–apical (negligible interaction). Inside this division another parameters become important such as  $\beta$  (angle between copper(II) basal planes) in the equatorial–equatorial, or the distortion  $t$  in the equatorial–apical.

© 2003 Elsevier Science Ltd. All rights reserved.

**Keywords:** Copper(II) coordination compounds; Malonate ligands; Dicarboxylates; Ferromagnetism

## 1. Introduction

It has long been recognised that carboxylate bridges provide an efficient means for transmitting magnetic information in Cu(II) aggregates as demonstrated by the dinuclear copper acetate system [1–4]. Different coordination and bridging modes favour different forms of cooperative coupling [5–7]. As has been shown previously, a particularly attractive system for investigating how these bridging modes can be used to modulate the

overall magnetic behaviour in coordination compounds involves Cu<sub>4</sub> unit into a cyclic structure [8–13]. In addition, the fact that the Cu(II) centres only carry one unpaired electron makes the interpretation of the magnetic behaviour simpler than in other cases where there are multiple unpaired electrons and several detailed studies of Cu<sub>4</sub> cyclic structures have been reported [14–16].

The malonate (dianion of the propanedioic acid, H<sub>2</sub>mal) is a flexible and versatile ligand. The occurrence of two carboxylate groups in 1,3 positions allow this ligand to adopt simultaneously chelating bidentate and different carboxylato bridging modes (*syn-syn*, *syn-anti* and *anti-anti* through one or both carboxylate

\* Corresponding author. Tel.: +34-922-318-236; fax: +34-922-318-320.

E-mail address: [caruiz@ull.es](mailto:caruiz@ull.es) (C. Ruiz-Pérez).

groups) [17–30]. The ability of the carboxylato bridge to mediate significant ferro- or antiferromagnetic interactions [31–40] between the paramagnetic metal ions it bridges, enhances the interest in this ligand aiming at designing extended magnetic systems. In the context of our magneto-structural research with malonato-bridged homo- and heterometallic complexes [34–40], we have investigated the Cu(II) compounds.

The bisbidentate behaviour analogue to that exhibited by the oxalate is forbidden by steric reasons to malonate and this affects dramatically to the structure and properties of the malonato complexes. The malonate ligand occupies one or two coordination positions and neutralizes two positive charges of the metallic copper ion (Cu(II)), allowing the inclusion of other ligands in the coordination sphere of the metal. These complementary ligands can act as bridging or blocking ligands contributing to the interconnection or isolation of the spin carriers. Thus combining the malonate with other bridging and/or blocking ligands we have been able to prepare monomers, dimers, trimers, tetramers, infinite chains, 2D and 3D arrays.

The magnetic coupling among the magnetic centres is given by the value of  $J$  (the intramolecular exchange interaction), being  $J$  negative or positive depending on the antiferro- or ferromagnetic character of the coupling, respectively. The magnitude of the interaction is governed by the overlap density, thus for the carboxylato bridge, it will be affected by the bridging modes that it can adopt.

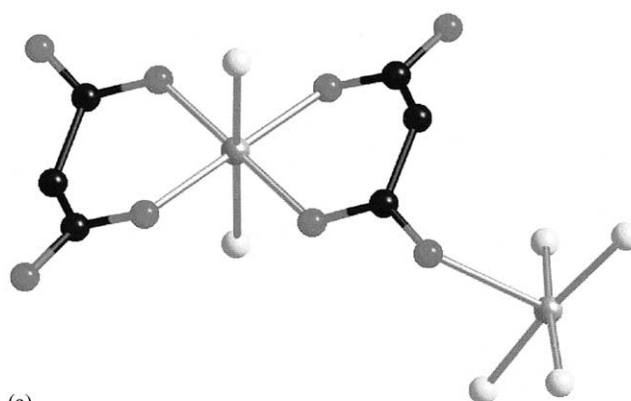
In the course of our research we have structurally and magnetically characterized several carboxylato bridged copper(II) complexes, here we report the main aspects and conclusions of our magneto-structural research in copper(II) malonato complexes. We will start describing briefly the structure and the magnetic behaviour of the compounds, subsequently we will analyze the magneto-structural correlations.

## 2. Structure and magnetic properties

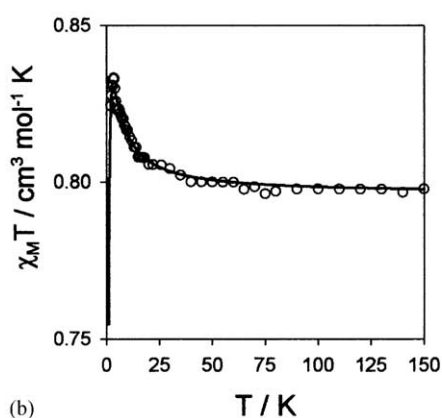
### 2.1. Copper(II)-malonate

#### 2.1.1. $[\text{Cu}(\text{H}_2\text{O})_4][\text{Cu}(\text{mal})_2(\text{H}_2\text{O})_2]$ (**1**)

The dinuclear complex **1** (Fig. 1) was firstly prepared by Chattopadhyay et al. [24]. The magnetic properties were studied by our group [40]. The neutral dinuclear entity consists of a diaquabis(malonato)-cuprate(II) anion and a tetraaquacopper(II) cation connected through a carboxylato group exhibiting the *anti-syn* bridging mode. The environment of the chelated copper(II) ion is octahedral, whereas the coordination of the other is square pyramidal.



(a)



(b)

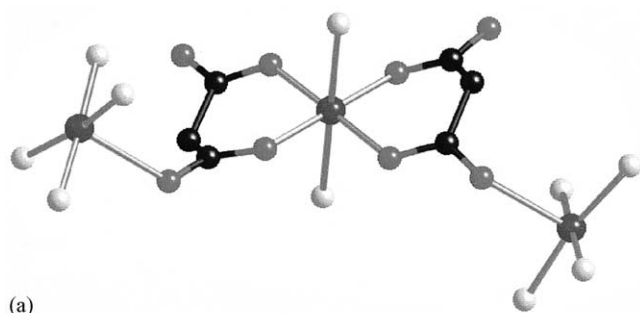
Fig. 1. (a) Perspective view of the dinuclear copper(II) units of compound  $[\text{Cu}(\text{H}_2\text{O})_4][\text{Cu}(\text{mal})_2(\text{H}_2\text{O})_2]$  (**1**) along with the copper(II) numbering scheme. (b) Thermal dependence of the  $\chi_M T$  product for this compound.

The magnetic behaviour is typical of a ferromagnetically copper(II) dimer (intradimer coupling constant of  $J = +1.8 \text{ cm}^{-1}$ ) with a weak intermolecular antiferromagnetic interaction.

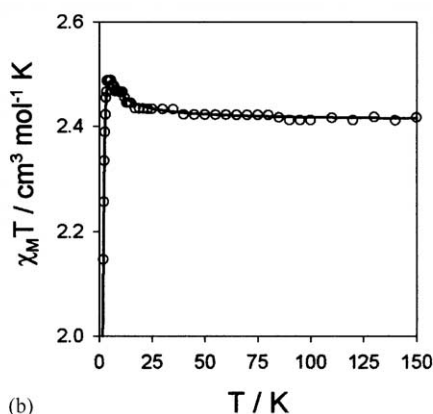
#### 2.1.2. $\{[\text{Cu}(\text{H}_2\text{O})_4]_2[\text{Cu}(\text{mal})_2(\text{H}_2\text{O})]\}; [\text{Cu}(\text{mal})_2(\text{H}_2\text{O})_2]\{[\text{Cu}(\text{H}_2\text{O})_4][\text{Cu}(\text{mal})_2(\text{H}_2\text{O})_2]\}$ (**2**)

The compound **2** is built up by three units of different nuclearity [40]. A neutral entity,  $[\text{Cu}(\text{H}_2\text{O})_4][\text{Cu}(\text{mal})_2(\text{H}_2\text{O})]$  (the dinuclear complex explained previously), an anionic monomer  $[\text{Cu}(\text{mal})_2(\text{H}_2\text{O})_2]$  and a cationic trinuclear unit  $[\text{Cu}(\text{H}_2\text{O})_4]_2[\text{Cu}(\text{mal})_2(\text{H}_2\text{O})_2]$  (Fig. 2). The mononuclear entity is formed by two malonate anions chelating one copper(II) ion. The di-, and trinuclear complexes are built up by joining one and two tetraaquacopper(II) cations to the mononuclear compound via *anti-syn* carboxylato bridging mode, respectively. The chelated copper(II) atom has an octahedral surrounding, and the adjacent Cu(II) have square-pyramidal environments.

The magnetic properties of this compound were explained on the basis of the sum of the magnetic susceptibility of the three units gives the total suscept-



(a)



(b)

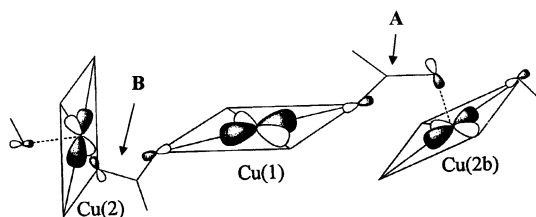
Fig. 2. (a) Perspective view of the trinuclear copper(II) units of compound

$\{[\text{Cu}(\text{H}_2\text{O})_4]_2[\text{Cu}(\text{mal})_2(\text{H}_2\text{O})]\}[\text{Cu}(\text{mal})_2(\text{H}_2\text{O})_2]\{[\text{Cu}(\text{H}_2\text{O})_4][\text{Cu}(\text{mal})_2(\text{H}_2\text{O})_2]\}$  (2) (b) Thermal dependence of the  $\chi_M T$  product for compound 2.

ibility. The coupling constant of the trinuclear unit can therefore be found out and its value is  $J = +1.2 \text{ cm}^{-1}$ .

### 2.1.3. $\{[\text{Cu}(\text{H}_2\text{O})_3][\text{Cu}(\text{mal})_2(\text{H}_2\text{O})]\}_n$ (3)

The structure of **3** [40] (Fig. 3) consists of zigzag chains of copper(II) ions that exhibit a regular alternation of aquabis(malonate)copper(II) and triaquacopper(II) units, the former linked to the latter via two different OCO groups exhibiting the *anti-syn* bridging modes, one involves two equatorial oxygens of the Cu(II) ions (**B**) whereas the other involves an equatorial oxygen at one copper(II) and an apical oxygen at the other (**A**) (see Scheme 1). The two crystallographically independent copper(II) ions have distorted square pyramidal surroundings.



Scheme 1.

The magnetic behaviour of this compound reveals the occurrence of an overall ferromagnetic coupling. The model proposed to explain that magnetic properties is an alternating intrachain magnetic exchange model; with a Hamiltonian of the form:

$$\hat{H} = -J \sum_i [\hat{S}_{2i} \cdot \hat{S}_{2i-1} + \alpha \hat{S}_{2i} \cdot \hat{S}_{2i+1}]$$

where  $\alpha$  is the alternation parameter ( $\alpha J$  equals to  $j$ ).

The analysis of data leads to  $J = +3.0 \text{ cm}^{-1}$  for the B exchange pathway and  $j = +1.9 \text{ cm}^{-1}$  for the A.

## 2.2. Copper(II)–malonate–ligand

Up to now we have seen that the copper(II) malonato complexes have revealed as magnetically interesting materials, so the use of appropriate ligands could enhance the dimensionality of these materials.

There are many copper(II) malonato complexes already prepared with different ligands, such as 1,10-phenantroline [41], 2,4,4'-diaminodiphenylmethane [42], diethylethylenediamine [43], methylethylenediamine [22], 1,3-diaminopropane [44], *N*1-isopropyl-2-methylpropane-1,2-diamine [45], 1,3-diaminopropane [46], triphenylphosphino [47], tricyclohexyl-phosphinol [47], 4,4'-dimethyl-2,2'-bipyridine [48], 5,6-dimethyl-1,10-phenantroline [49], 2,2'-bipyridine [50,34], oxamide oxime [51], benzimidazole [25], 3,5-dimethyl-1H-pyrazole [52], imidazole [35], 2-methylimidazole [35], 4,4'-bipyridine [36], 2,4'-bipyridine [37], pyrazine [37], 2,2'-bipyrimidine [38].

But, most of these compounds are not magnetically characterized or they do not present interesting magnetic behaviours [38], or the malonato bridge does not play an important role in the magnetic exchange pathway [38]. Those compounds will not be analysed in this work.

Mainly the explanation of the magnetic properties of the malonato-bridged copper(II) complexes has been carried out by our group with just an exception [22].

### 2.2.1. $[\text{Cu}(\text{Im})_2(\text{mal})]_n$ (4) and $[\text{Cu}(2\text{-MeIm})_2(\text{mal})]_n$ (5) (*Im* = imidazole and *MeIm* = 2-methylimidazole)

The compounds **4** (Fig. 4) and **5** have a quite similar structure [35]. They consist of regular zig-zag chains that are linked through one malonate carboxylate group exhibiting the *anti-anti* conformation. Each copper(II) ion in **4** and **5** shows a distorted  $\text{CuN}_2\text{O}_3$  square pyramidal geometry and each malonate group adopts simultaneously bidentate and monodentate coordination modes.

The shape of the magnetic  $\chi T$  versus  $T$  curves reveals the occurrence of significant ferromagnetic coupling between the copper(II) ions. The data were analyzed by means of Baker et al. [53] expression for a ferromag-

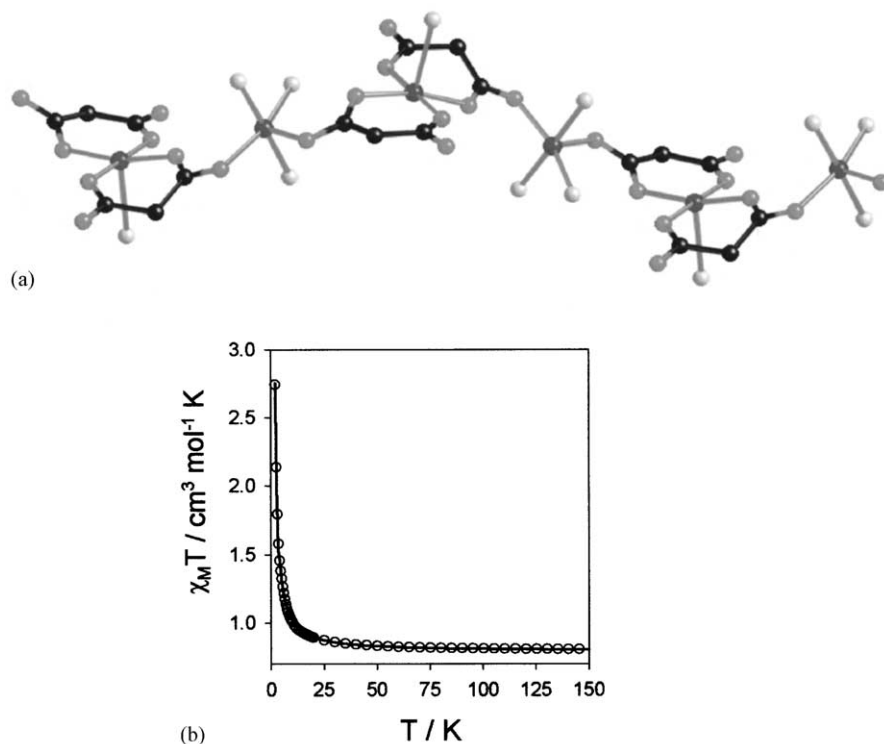


Fig. 3. (a) Perspective drawing of a fragment of the chain of compound  $\{[\text{Cu}(\text{H}_2\text{O})_3][\text{Cu}(\text{mal})_2(\text{H}_2\text{O})]\}_n$  (**3**). (b) Thermal dependence of the  $\chi_M T$  product for compound **3**.

netic copper(II) uniform chain leading, to  $J = +1.64 \text{ cm}^{-1}$  and  $J = +0.39 \text{ cm}^{-1}$  for **4** and **5**, respectively.

### 2.2.2. $\{[\text{Cu}(\text{bpy})(\text{H}_2\text{O})][\text{Cu}(\text{bpy})(\text{mal})(\text{H}_2\text{O})]\}(\text{ClO}_4)_2$ (**6**) (*bpy* = 2,2'-bipyridine)

There are three different malonato-bridged copper(II) complexes with 2,2'-bipyridine (Fig. 5), but only the two polymorphs of **6** have been magnetically characterized [34]. Although their structures and the spatial disposition are different, both can be considered as zig-zag chains with a very similar conformation. The chains exhibit a regular alternating of aqua(2,2'-bipyridyl)-(malonato)copper(II) and aqua(2,2'-bipyridyl)copper(II) units, the former being linked to the latter as a bis-monodentate ligand through two carboxylate-malonate oxygen atoms in a *cis* arrangement with the *anti-syn* coordination mode. The copper(II) ions present a distorted square pyramidal environment.

The magnetic properties of the two polymorphs are practically identical and the shape of the  $\chi T$  versus  $T$  curves is characteristic of the occurrence of weak ferro- and antiferromagnetic interactions in the high- and low-temperature ranges, respectively. Two failed attempts to explain these properties led us to the development of a new model, where two intrachain interactions are considered: one through the carboxylato in the *anti-syn* conformation (the ferromagnetic one) and another through the malonato skeleton in the *anti-anti* conformation (the antiferromagnetic one). According to the

model, the copper(II) chain is made up by isosceles triangles sharing the two vertices of their base, the Hamiltonian describing this situation being:

$$\hat{H} = - \left[ J_1 \sum_{i=1}^n \hat{S}_{2i} \cdot \hat{S}_{2i-1} + J_1 \sum_{i=1}^n \hat{S}_{2i} \cdot \hat{S}_{2i+1} + J_2 \sum_{i=1}^n \hat{S}_{2i-1} \cdot \hat{S}_{2i-1} \right]$$

There is no analytical expression to describe the magnetic behaviour of such a copper(II) chain, so we used a general numerical procedure [54] to obtain the values of the magnetic coupling constants. The results were  $J_1 = +4.6 \text{ cm}^{-1}$  (for the *anti-syn* carboxylato bridge) and  $J_2 = -4.2 \text{ cm}^{-1}$  (through malonato skeleton pathway).

### 2.2.3. $[\text{Cu}_4(\text{mal})_4(2,4'\text{-bpy})_4(\text{H}_2\text{O})_4] \cdot 8\text{H}_2\text{O}$ (**7**) (*2,4'*-*bpy* = 2,4'-bipyridine)

The structure of complex **7** consists of small planar squares with copper(II) ions (Fig. 6) and malonato anions at each corner and side, respectively [37]. The 2,4'-*bpy* acts as a monodentate ligand being located in the same plane of the  $[\text{Cu}_4(\text{mal})_4]$  square. The only crystallographically independent copper(II) ion exhibits a slightly distorted square pyramidal surrounding. The carboxylato bridge in *anti-syn* conformation links the copper(II) ions.



## Self-assembly and magnetic properties of a double-propeller octanuclear copper(II) complex with a *meso*-helicite-type metallacryptand core

Emilio Pardo,<sup>a</sup> Kevin Bernot,<sup>a</sup> Miguel Julve,<sup>a</sup> Francesc Lloret,<sup>\*a</sup> Joan Cano,<sup>a</sup> Rafael Ruiz-García,<sup>b</sup> Jorge Pasán,<sup>c</sup> Catalina Ruiz-Pérez,<sup>c</sup> Xavier Ottenwaelder<sup>d</sup> and Yves Journaux<sup>\*d</sup>

<sup>a</sup> *Departament de Química Inorgànica, Instituto de Ciencia Molecular, Universitat de València, 46100 Burjassot, València, Spain. E-mail: francisco.lloret@uv.es; Fax: +34 963544328*

<sup>b</sup> *Departament de Química Orgànica, Universitat de València, 46100 Burjassot, València, Spain*

<sup>c</sup> *Laboratorio de Rayos X y Materiales Moleculares, Departamento de Física Fundamental II, Universidad de La Laguna, 38204 La Laguna, Tenerife, Spain*

<sup>d</sup> *Laboratoire de Chimie Inorganique, Université Paris-Sud, 91405 Orsay, France.*

*E-mail: jour@icmo.u-psud.fr; Fax: +33 169154754*

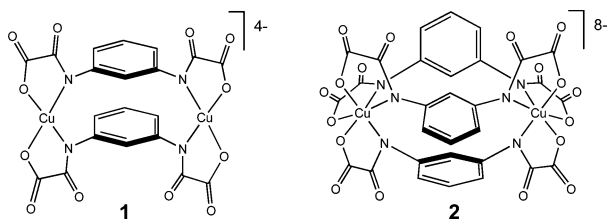
Received (in Cambridge, UK) 9th December 2003, Accepted 20th February 2004

First published as an Advance Article on the web 12th March 2004

**An octanuclear copper(II) complex possessing a dimer-of-tetramers structure self-assembles from a binuclear oxamato-copper(II) metallacryptand of the *meso*-helicite type; its magnetic behaviour is consistent with its unique double-propeller molecular topology.**

The self-assembly of large, well-defined metal cages is one of the foremost topics in modern coordination chemistry.<sup>1</sup> Apart from their fascinating metallo-supramolecular structures and relevant insights into metal-directed self-assembly processes,<sup>2</sup> these poly-metallic species can display unique magnetic properties which result from the assembling topology of the paramagnetic metal ions by the bridging ligands.<sup>3–6</sup>

In the search for rationally designed polynuclear coordination compounds with predetermined spin topologies using oxamate-based ligands, we recently prepared the double-stranded binuclear copper(II) complex **1** from the self-assembly of two Cu<sup>II</sup> ions and two mpba ligands [mpba = *N,N'*-1,3-phenylenebis(oxamate)].<sup>7</sup> Complex **1** has been further used as a building-block for extended two-dimensional bimetallic networks when coordinating four other metal ions at the free carbonyl oxygen atoms of the bidentate oxamate groups.<sup>8</sup> Here, we examine the related triple-stranded binuclear copper(II) complex **2** that results from the self-assembly of two Cu<sup>II</sup> ions and three mpba ligands. Similarly to **1**, complex **2** can coordinate six metal ions with partially blocked coordination sites precluding polymerisation, thus yielding discrete high-nuclearity metal cages such as the octanuclear copper(II) complex Na<sub>2</sub>{[Cu<sub>2</sub>(mpba)<sub>3</sub>][Cu(pmdien)]<sub>6</sub>}(ClO<sub>4</sub>)<sub>6</sub>·12H<sub>2</sub>O **3** (pmdien = *N,N,N',N'',N'''*-pentamethyldiethylenetriamine).



Compound **3** was synthesised in an one-pot reaction from the hexakis-bidentate anionic complex **2** and coordinatively unsaturated [Cu(pmdien)]<sup>2+</sup> cationic complexes.<sup>†</sup> This is a strict self-assembly process since these precursors were not isolated; each was formed *in situ* from a mixture of Cu<sup>2+</sup> and the corresponding ligand in the appropriate stoichiometry. As a matter of fact, all our attempts to isolate **2** have failed, yielding **1** instead.

The structure of **3** consists of octanuclear copper(II) cations with C<sub>3h</sub> molecular symmetry, {[Cu<sub>2</sub>(mpba)<sub>3</sub>][Cu(pmdien)]<sub>6</sub>}<sup>4+</sup>, together with sodium cations, perchlorate anions, and both coordinated and noncoordinated water molecules.<sup>‡</sup> Interestingly, the octacopper cation is bound to two sodium cations through the carboxylate oxygen atoms of the oxamate groups in a *fac* arrangement [Na–O = 2.376(12) Å] (Fig. 1a). These bonding

interactions are likely to stabilise the motif **2** during the metal-directed self-assembly process leading to **3**.

The octacopper cation contains two chiral, oxamato-bridged, propeller-like tetranuclear units that are symmetry-related ( $\Delta$  and  $\Lambda$  enantiomers) (Fig. 1b). Three *m*-phenylenediamide moieties bridge the central Cu(1) and Cu(1<sup>1</sup>) atoms of the tetranuclear units, forming a binuclear metallamacrobicyclic core of the cryptand type (Fig. 1c).<sup>9</sup> Because of the presence of a mirror plane perpendicular to the molecular threefold axis, this achiral metallacryptand is a *meso*-helicite with a strictly zero helicoidal twist angle of the aromatic spacers around the Cu(1)–Cu(1<sup>1</sup>) vector.<sup>10</sup> Within the metallacyclic core unit of **3**, the Cu(1) atom has a six-coordinate trigonally distorted octahedral environment [trigonal twist angle of 11.9(7)°]. The rather long metal–ligand bond lengths [Cu–N =

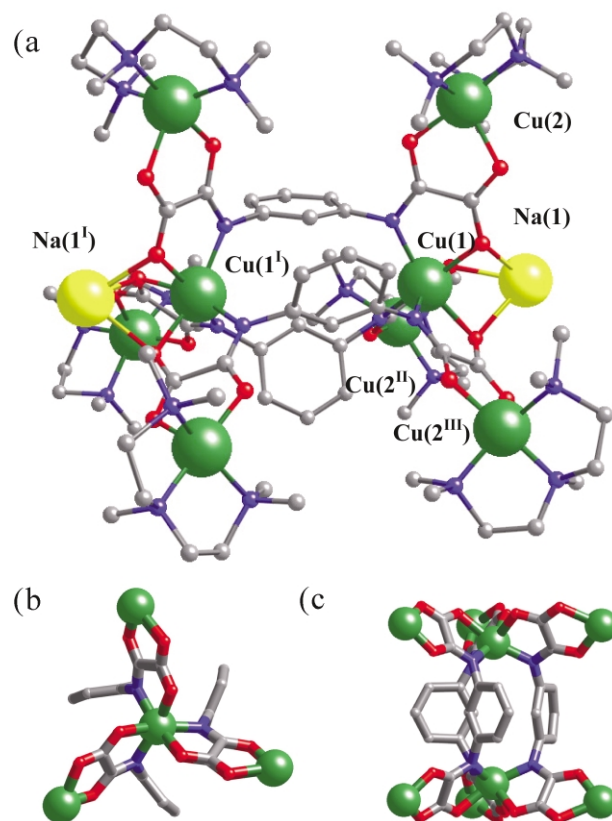


**Fig. 1** (a) Perspective view of the cationic octacopper unit of **3** with the numbering scheme for metal atoms. Selected intermetallic distances (Å) with standard deviations in parentheses: Cu(1)–Cu(2) 5.440(13), Cu(1)–Cu(1<sup>1</sup>) 6.612(7), Cu(2)–Cu(2<sup>II</sup>) 9.307(2) (symmetry codes: I = *x*, *y*, 1/2 – *z*; II = –*y*, *x* – *y*, *z*; III = –*x* + *y*, –*x*, *z*). (b) Side and (c) top views of the octacopper skeleton of **3**.

2.079(12) and Cu–O 2.123(9) Å] compared to those of four-coordinate square-planar metal environment in **1** [average values of 1.95 and 1.96 Å, respectively]<sup>7</sup> suggest a dynamic Jahn–Teller effect whereby the elongation spreads randomly over the three axes.<sup>11</sup> Moreover, unlike those in metallacyclophane **1**, the aromatic groups in **3** are not stacked parallel but disposed edge-to-face [dihedral angle of 60°] with a weak C–H⋯π interaction between neighbouring benzene rings [centroid–centroid distance of 5.366(9) Å].

The magnetic properties of **3** are consistent with its dimer-of-tetramers structure. § Notably, the  $\chi_M T$  versus  $T$  plot,  $\chi_M$  being the molar magnetic susceptibility per octanuclear unit and  $T$  the temperature, presents a minimum at ca. 30 K (Fig. 2). This behaviour is characteristic of antiferromagnetically coupled tetranuclear complexes having a propeller-type topology whereby the spin topology dictates the non-compensation of the spins in the ground state.<sup>12</sup> Accordingly, the model of two magnetically isolated Cu<sup>II</sup><sub>4</sub> molecules with an antiferromagnetic coupling ( $J = -57.0$  cm<sup>-1</sup>) between the Cu(1) and Cu(2) ions through the oxamate bridges fits the experimental data for **3** in the high temperature region (dashed line in Fig. 2). This model predicts a plateau at the lowest temperatures, where only the triplet ground states of the two tetranuclear units ( $S_A = S_B = 1$ ) are thermally populated. However, complex **3** exhibits a different behaviour in the low temperature region, as the  $\chi_M T$  product decreases abruptly below 5 K. This is interpreted as the signature of an antiferromagnetic coupling ( $j = -28.0$  cm<sup>-1</sup>) between the Cu(1) and Cu(1') ions of each tetranuclear unit (solid line in Fig. 2), thus leading to a singlet ground state for **3** ( $S = S_A - S_B = 0$ ). This moderate antiferromagnetic coupling is mediated by the triple *m*-phenylenediamide bridge between the Jahn–Teller distorted octahedral Cu<sup>II</sup> ions within the core **2**. This situation differs dramatically from that of complex **1** which exhibits a ferromagnetic coupling between its square-planar Cu<sup>II</sup> ions through the double *m*-phenylenediamide bridge.<sup>7</sup>

In summary, the binuclear metallacryptand of the *meso*-helicate type **2** can be self-assembled in solution from three aromatic bis(oxamate) ligands and two Cu<sup>II</sup> ions, and then serve as a growing center for high-nuclearity metal cages such as the octanuclear copper(II) complex **3**. We are currently searching for three-dimensional bimetallic networks constructed from the binuclear

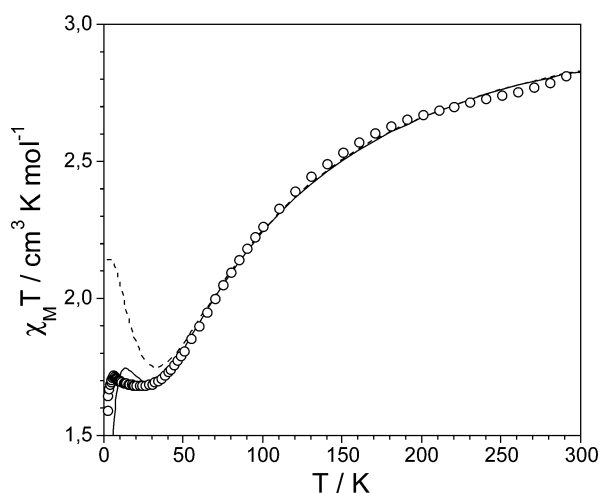


**Fig. 2** Temperature dependence of  $\chi_M T$  for **3**: (o) experimental data; (---) best fit for two isolated Cu<sub>4</sub> molecules, and (—) best fit for a Cu<sub>8</sub> molecule.

precursor **2** and its analogues with paramagnetic first row transition metal ions other than Cu<sup>II</sup> in order to elaborate new supramolecular magnetic materials.

This work was supported by the Ministerio de Ciencia y Tecnología (Spain) through the Plan Nacional de Investigación Científica, Desarrollo e Innovación Tecnológica (Projects BQU2001–2928 and BQU2001–3794). E. P. thanks the Ministerio de Educación, Cultura y Deporte (Spain) for a grant.

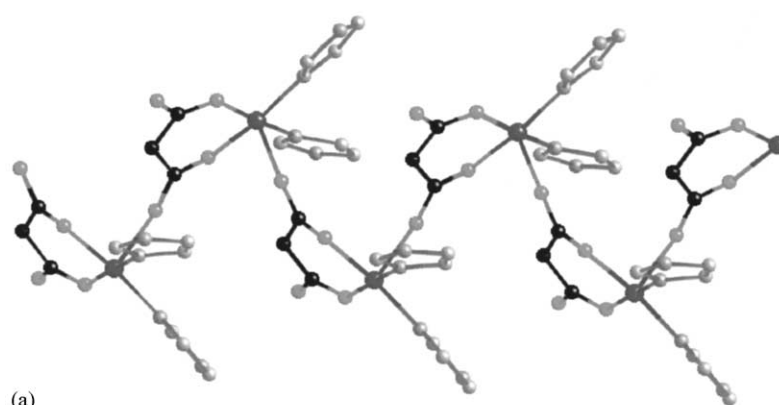
## Notes and references

† *Synthesis and selected data*: To a stirred suspension of H<sub>4</sub>mpba<sup>7</sup> (0.38 g, 1.0 mmol) in 5 mL of water was added a solution of NaOH (0.16 g, 4.0 mmol) in 5 mL of water. After complete dissolution, Cu(ClO<sub>4</sub>)<sub>2</sub>·6H<sub>2</sub>O (0.25 g, 0.67 mmol) dissolved in 5 mL of water was added dropwise under stirring. The resulting deep green solution was then added dropwise to a solution of Cu(ClO<sub>4</sub>)<sub>2</sub>·6H<sub>2</sub>O (0.74 g, 2.0 mmol) and pmdien (0.42 mL, 2.0 mmol) in 10 mL of water under stirring. Blue hexagonal prisms of **3** suitable for single crystal X-ray diffraction were obtained after several hours of standing at room temperature. They were filtered on paper and air-dried (60%).  $\nu(\text{KBr})/\text{cm}^{-1}$  3427vs (O–H) from H<sub>2</sub>O, 3001w and 2971w (C–H) from mpba, 2930w (C–H) from pmdien, 1623vs and 1603 (sh) (C=O) from mpba, 1144 (sh), 1107 (sh) and 1091vs (Cl–O) from ClO<sub>4</sub>.

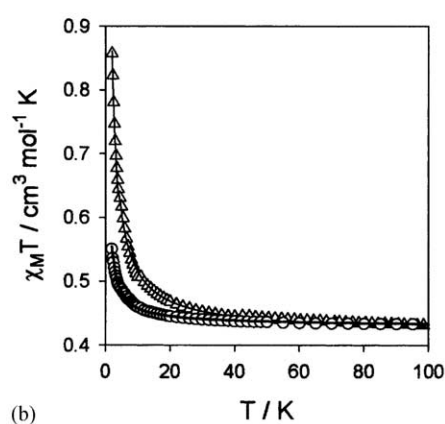
‡ *Crystal data*: C<sub>84</sub>H<sub>174</sub>Cl<sub>6</sub>Cu<sub>8</sub>N<sub>24</sub>Na<sub>2</sub>O<sub>54</sub>,  $M = 3151.47$ , hexagonal,  $a = 17.4169(11)$ ,  $b = 17.4169(11)$ ,  $c = 31.739(2)$  Å,  $U = 8338.1(9)$  Å<sup>3</sup>,  $T = 293(2)$  K, space group  $P6c2$ ,  $Z = 2$ ,  $\mu(\text{Mo–K}\alpha) = 1.179$  mm<sup>-1</sup>, 5026 reflections measured, 2684 assumed as observed with  $I > 2\sigma(I)$ . Hydrogen atoms were calculated and refined with an overall isotropic thermal parameter (except for the water hydrogen atoms which were not found neither calculated). Refinement on  $F^2$  of 271 variables with anisotropic thermal parameters for all non-hydrogen atoms gave  $R = 0.089$  and  $wR = 0.1473$  with  $S = 1.108$  (observed data). CCDC 227333. See <http://www.rsc.org/suppdata/cc/b3/b316081e/> for crystallographic data in .cif format.

§ Variable-temperature (1.8–300 K) magnetic measurements under a magnetic field of 1.0 T were carried out on powdered samples of **3** with a SQUID magnetometer. Least-squares fitting of the magnetic susceptibility data of **3** were performed by full matrix diagonalisation of the isotropic spin Hamiltonian  $H = -J(S_{A1}S_{A2} + S_{A1}S_{A3} + S_{A1}S_{A4} + S_{B1}S_{B2} + S_{B1}S_{B3} + S_{B1}S_{B4}) - jS_{A1}S_{B1} - g\beta(S_{A1} + S_{A2} + S_{A3} + S_{A4} + S_{B1} + S_{B2} + S_{B3} + S_{B4})B$  (with  $S_{A1} = S_{A2} = S_{A3} = S_{A4} = S_{B1} = S_{B2} = S_{B3} = S_{B4} = 1/2$ ) with the VPMAG program.<sup>13</sup>

- R. E. P. Winpenney, *Adv. Inorg. Chem.*, 2001, **52**, 1.
- G. F. Swiegers and T. J. Malefetse, *Chem. Rev.*, 2000, **100**, 3483.
- R. Sessoli, D. Gatteschi, A. Caneschi and M. A. Novak, *Nature*, 1993, **365**, 141.
- K. L. Taft, C. D. Delfs, G. C. Papaefthymiou, S. Forner, D. Gatteschi and S. J. Lippard, *J. Am. Chem. Soc.*, 1994, **116**, 823.
- J. R. Friedman, M. P. Sarachik, J. Tejada and R. Ziolo, *Phys. Rev. Lett.*, 1996, **76**, 3830.
- O. Waldmann, J. Hassmann, P. Müller, G. S. Hanan, D. Volkmer, U. S. Schubert and J. M. Lehn, *Phys. Rev. Lett.*, 1997, **78**, 3390.
- I. Fernández, R. Ruiz, J. Faus, M. Julve, F. Lloret, J. Cano, X. Ottenwaelder, Y. Journaux and M. C. Muñoz, *Angew. Chem., Int. Ed.*, 2001, **40**, 3039.
- C. L. M. Pereira, E. F. Pedroso, H. O. Stumpf, M. A. Novak, L. Ricard, R. Ruiz-García, E. Rivière and Y. Journaux, *Angew. Chem., Int. Ed.*, 2004, **43**, 955.
- R. W. Saalfrank, V. Seitz, D. L. Caulder, K. N. Raymond, M. Teichert and D. Stalke, *Eur. J. Inorg. Chem.*, 1998, 1313.
- M. Albrecht and S. Kotila, *Angew. Chem., Int. Ed. Engl.*, 1995, **34**, 2134; M. Albrecht and S. Kotila, *Chem. Commun.*, 1996, 2309.
- C. R. Rice, S. Worl, J. C. Jeffery, R. L. Paul and M. D. Ward, *J. Chem. Soc., Dalton Trans.*, 2001, 550; C. J. Matthews, S. T. Onions, G. Morata, L. J. Davis, S. L. Heath and D. J. Price, *Angew. Chem., Int. Ed.*, 2003, **42**, 3166.
- A. L. Barra, A. Caneschi, A. Cornia, F. Fabrizi de Biani, D. Gatteschi, C. Sangregorio, R. Sessoli and L. Sorace, *J. Am. Chem. Soc.*, 1999, **121**, 5302.
- J. Cano, VPMAG, University of Valencia, Spain, 2001.



(a)



(b)

Fig. 4. (a) A view of the chain compound  $[\text{Cu}(\text{Im})_2(\text{mal})]$  (**4**) (b) Thermal dependence of the  $\chi_{\text{M}}T$  product for compounds  $[\text{Cu}(\text{Im})_2(\text{mal})]$  ( $\Delta$ ) (**4**) and  $[\text{Cu}(\text{MeIm})_2(\text{mal})]$  ( $\circ$ ) (**5**).

The compound behaves as a magnetically isolated square of four spin doublets interacting ferromagnetically. According to this, the Hamiltonian proposed is:

$$H = -J[S_1S_2 + S_2S_3 + S_3S_4 + S_1S_4]$$

This fit through the expression led to  $J = +12.3 \text{ cm}^{-1}$ .

#### 2.2.4. $[\text{Cu}_2(\text{mal})_2(\text{H}_2\text{O})_2(4,4'\text{-bpy})]$ (**8**) ( $4,4'\text{-bpy} = 4,4'\text{-bipyridine}$ )

The compounds **8** [36] (Fig. 7) is made up by small planar squares as those of complex **7** linked through a bis-monodentate  $4,4'$ -bipyridine ligand to form two-dimensional networks. Copper(II) surrounding and carboxylato bridging mode are also those of **7**.

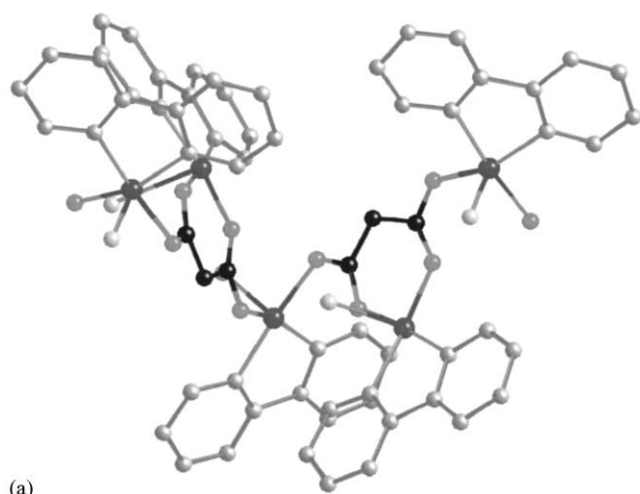
The magnetic properties of compound **8** and **7** are quite similar, except for the antiferromagnetic behaviour coming from the decrease in the  $\chi T$  versus  $T$  curve at low-temperatures. The magnetic behaviour of **8** could be described as a quadratic layer of tetranuclear copper(II) units which are antiferromagnetically coupled through the bridging  $4,4'$ -bpy. Since the value of the spin of the tetranuclear copper(II) unit is large enough as to be considered as a classic one ( $S \geq 1.8$ ), the magnetic susceptibility data can be analyzed by means of the expression for a classic spin model derived by Curély

[55]. This gives  $J = +12.4 \text{ cm}^{-1}$  (for the carboxylate *anti-syn* bridge) and  $j = -0.052 \text{ cm}^{-1}$  (through the  $4,4'$ -bpy).

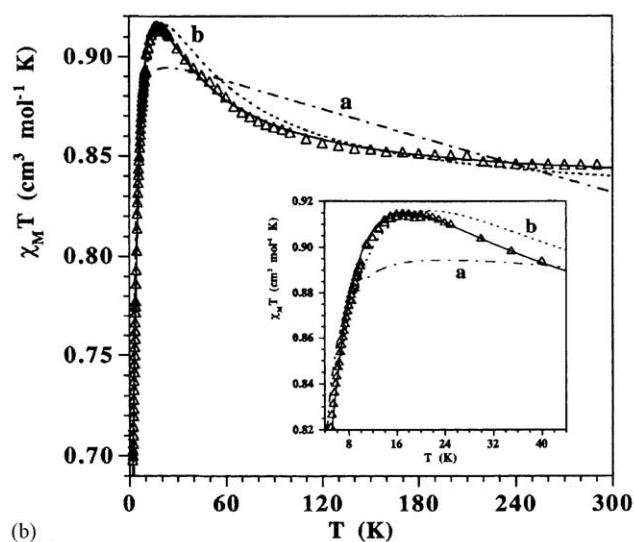
#### 2.2.5. $[\text{Cu}_4(\text{mal})_4(\text{pyz})_2] \cdot 4\text{H}_2\text{O}$ (**9**) ( $\text{pyz} = \text{pyrazine}$ )

The crystal structure of **9** consists of a three-dimensional arrangement of copper(II) ions bridged by malonate and pyrazine ligands [37] (Fig. 8). The 3D arrangement is formed by layers linked via *anti-syn* carboxylate bridges. The layers are made up with small planar squares, similar to those of **7** and **8**, bound through a bis-monodentate pyrazine. Copper(II) surroundings are square pyramidal and the two different bridging modes present the *anti-syn* conformation.

The experimental measurements of the magnetic properties reveal the coexistence of ferro- and antiferromagnetic interactions. According to the structure three different magnetic exchange pathways can be identified, two carboxylate *anti-syn* bridging modes:  $J_1$  (the responsible of the small squares) and  $J_3$  (the pathway that links the layers); and a pyrazine bridge  $J_2$ . However, there is no model to fit the magnetic properties of this three-dimensional compound with three magnetic exchange pathways, although the authors give a roughly evaluation of their magnitude.



(a)

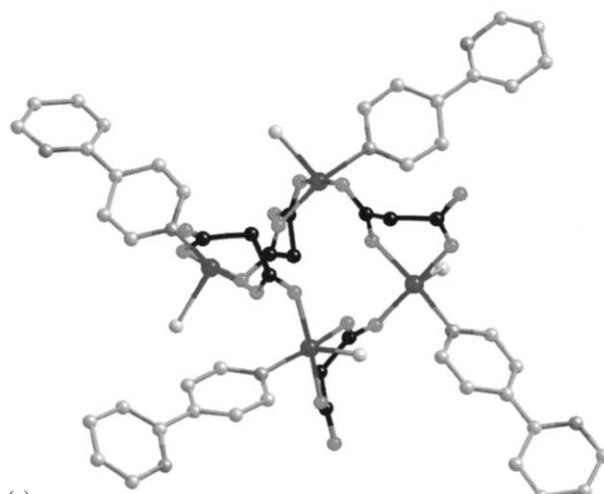


(b)

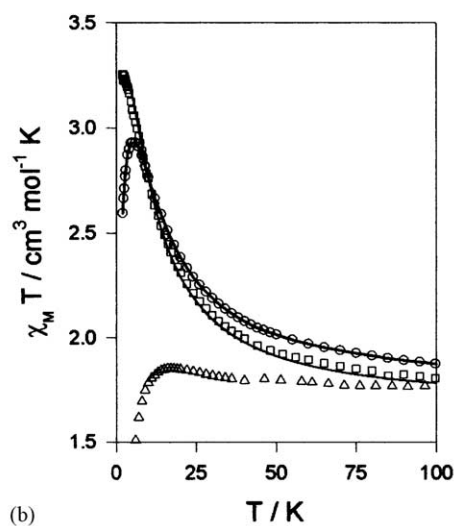
Fig. 5. (a) View of compound  $\{[\text{Cu}(\text{bpy})(\text{H}_2\text{O})][\text{Cu}(\text{bpy})(\text{mal})(\text{H}_2\text{O})]\}(\text{ClO}_4)_2$  (6). Hydrogen atoms and the perchlorate anions have been omitted for clarity. (b) Thermal dependence of the  $\chi_M T$  product for compound 6.

### 3. Magneto-structural correlations

The magnetic orbital at copper(II) atoms is defined by the short equatorial bonds, and it is of the  $d_{x^2-y^2}$  type, with possibly some mixture of the  $d_{z^2}$  character in the axial position when the trigonal distortion defined by the  $\tau$  factor [56] ( $\tau$  ranges from 0, perfect square pyramid, to 1, perfect trigonal bipyramid) becomes important. Following the Kahn's orbital model [57], the magnetic coupling for a copper(II) dimer is decomposed in two terms, one antiferro- and the other ferromagnetic according to  $J = J_{\text{AF}} + J_{\text{F}}$ . The magnitude of the antiferromagnetic term is essentially governed by the square of the overlap integral between the two metal-centred magnetic orbitals, whereas that of the ferromagnetic one is very small.



(a)



(b)

Fig. 6. (a) Perspective view of the tetramer unit of  $[\text{Cu}_4(\text{mal})_4(\text{H}_2\text{O})_4(2,4'\text{-bpy})_4]\cdot 2\text{H}_2\text{O}$  (7). (b) Thermal dependence of the  $\chi_M T$  product for compounds  $[\text{Cu}_4(\text{mal})_4(\text{H}_2\text{O})_4(2,4'\text{-bpy})_4]\cdot 2\text{H}_2\text{O}$  (7) ( $\square$ ),  $[\text{Cu}_4(\text{mal})_4(\text{H}_2\text{O})_4(4,4'\text{-bpy})_2]\cdot 2\text{H}_2\text{O}$  (8) ( $\circ$ ) and  $[\text{Cu}_4(\text{mal})_4(\text{pyz})_2]\cdot 4\text{H}_2\text{O}$  (9) ( $\triangle$ ).

The overlap is minimized when the orthogonality of the magnetic orbitals occurs. This orthogonality could be accidental or strict [57]. The latter involves the transformation of the orbitals in different irreducible representations of the symmetry group adapted to the system (i.e. different magnetic orbitals, such as  $d_{x^2-y^2}$  versus  $d_{xy}$ , which is usually found in heterometallic complexes). However the accidental deals with the spatial orthogonality of the same magnetic orbitals (see Scheme 2).

The magneto-structural correlations of carboxylate-bridged systems have been studied previously, but in the case of dicarboxylates with a mean interest in oxalate bridged complexes [60]. Then the features achieved in these works have been extrapolated to the rest of dicarboxylates with three, four or more carbon atoms.

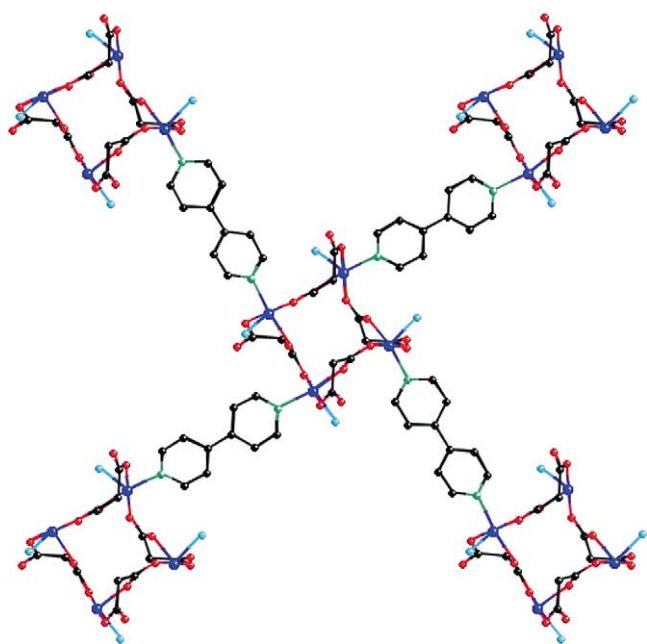


Fig. 7. View of the two-dimensional compound in  $[\text{Cu}_4(\text{mal})_4(\text{H}_2\text{O})_4(4,4'\text{-bpy})_2]\cdot 2\text{H}_2\text{O}$  (**8**)

We are going to analyze first our compounds in the light of these assumptions, and then we will introduce other parameters (see Table 1) that cannot be ignored to explain properly the magnetic properties of the compounds.

### 3.1. On the basis of carboxylate-bridging mode

Carboxylate bridge is a versatile anion that can assume many types of bridging conformations, the most important being *anti-anti*, *anti-syn* and *syn-syn* (Scheme 3). It is assumed that copper(II) complexes with *anti-syn* conformation exhibit very weak magnetic exchange interactions, whereas *syn-syn* and *anti-anti* conformations mediate large and weak to medium antiferromagnetic interactions, respectively [58,59].

According to this, compounds **4** and **5** should exhibit an antiferromagnetic behaviour, but they do not. At the same time, the remaining compounds bridged by a carboxylate in the *anti-syn* conformation should show weak interaction whatever the nature, ranging  $J$  from +3 to  $-45\text{ cm}^{-1}$  [61,62]. But, complexes **6**, **7** and **8** have a magnetic exchange as large as  $J \approx +12.5\text{ cm}^{-1}$ . These wrong conclusions are due to an oversimplification of the system produced by the extrapolation of the results from the oxalate complexes.

### 3.2. On the basis of the relative position of the bridge respect to the copper(II) environment

Attending to the relative positions of the oxygens of the OCO bridge, there are three relative orientations of

Table 1  
List of parameters of the compounds

| Compound  | $\alpha_1$ (°) | $\alpha_2$ (°) | Bridge conformation | $d_1$ (Å) | $d_2$ (Å) | $\beta$ (°) <sup>a</sup> | Position of the oxygen bridge atom in copper(II) environment | $\tau$ (Cu1) <sup>b</sup> | $\tau$ (Cu2) <sup>b</sup> | $J$ (cm <sup>-1</sup> ) |
|-----------|----------------|----------------|---------------------|-----------|-----------|--------------------------|--------------------------------------------------------------|---------------------------|---------------------------|-------------------------|
| <b>1</b>  | 126.0          | 120.5          | <i>anti-syn</i>     | 1.952     | 2.383     | 49.3                     | equatorial-apical                                            | octahedral                | 0.05                      | +1.8                    |
| <b>2</b>  | 126.5          | 124.8          | <i>anti-syn</i>     | 1.941     | 2.381     | 56.5                     | equatorial-apical                                            | octahedral                | 0.12                      | +1.2                    |
| <b>3A</b> | 124.5          | 116.9          | <i>anti-syn</i>     | 1.931     | 2.185     | 85.9                     | equatorial-apical                                            | 0.24                      | 0.28                      | +1.9                    |
| <b>3B</b> | 124.5          | 118.4          | <i>anti-syn</i>     | 1.945     | 1.990     | 85.9                     | equatorial-equatorial                                        | 0.24                      | 0.28                      | +3.0                    |
| <b>4</b>  | 125.7          | 226.9          | <i>anti-anti</i>    | 1.962     | 2.394     | 55.4                     | equatorial-apical                                            | 0.02                      | 0.02                      | +1.6                    |
| <b>5</b>  | 123.8          | 228.1          | <i>anti-anti</i>    | 1.961     | 2.270     | 82.7                     | equatorial-apical                                            | 0.18                      | 0.18                      | +0.4                    |
| <b>6</b>  | 128.5          | 127.6          | <i>anti-syn</i>     | 1.918     | 1.978     | ≈ 80.5                   | equatorial-equatorial                                        | 0.05                      | 0.28                      | +4.6                    |
| <b>7</b>  | 120.9          | 111.0          | <i>anti-syn</i>     | 1.963     | 1.986     | 70.5                     | equatorial-equatorial                                        | 0.15                      | 0.15                      | +12.3                   |
| <b>8</b>  | 121.3          | 109.9          | <i>anti-syn</i>     | 1.984     | 1.957     | 72.6                     | equatorial-equatorial                                        | 0.14                      | 0.14                      | +12.4                   |

The parameters are defined in Scheme 4.

<sup>a</sup> Angle subtended by the basal planes of the copper(II) ions linked by the carboxylate bridge.

<sup>b</sup> Distortion of the copper(II) environment (see text).

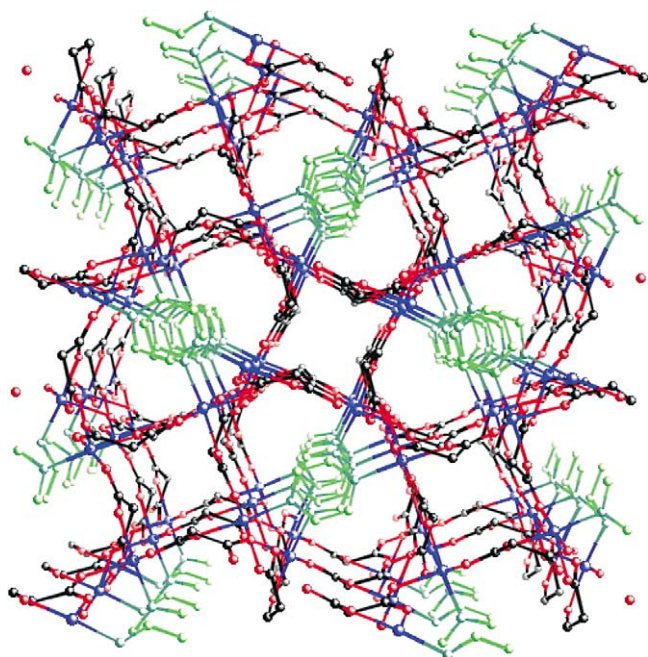


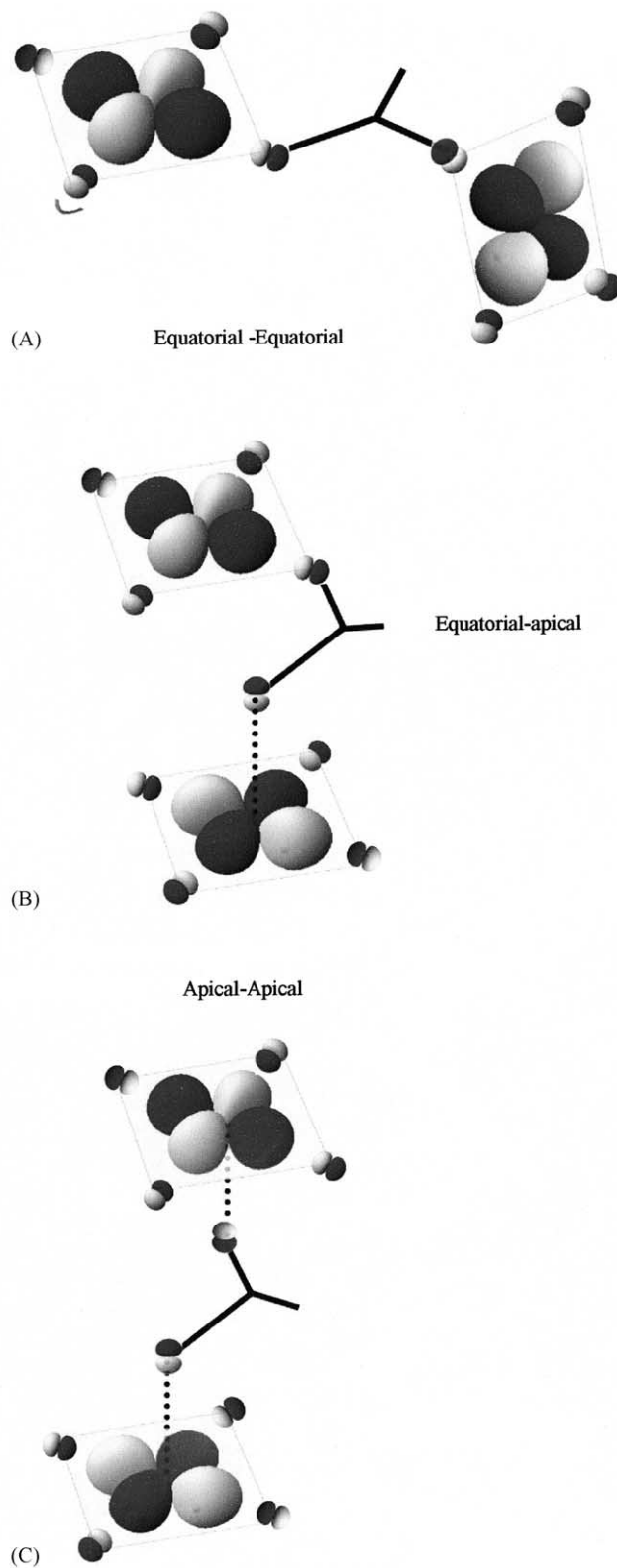
Fig. 8. A view of the 3D structure in compound  $[\text{Cu}_4(\text{mal})_4(\text{pyz})_2] \cdot 4\text{H}_2\text{O}$  (**9**) where the square grids layers are stacked along the  $c$  axis showing the  $\pi$ – $\pi$  overlap between pairs of pyrazine molecules.

the bridge respect to copper(II) ions involved in the Cu–O–C–O–Cu exchange pathway: equatorial–equatorial (most common in the case of oxalates), equatorial–apical and apical–apical (Scheme 2).

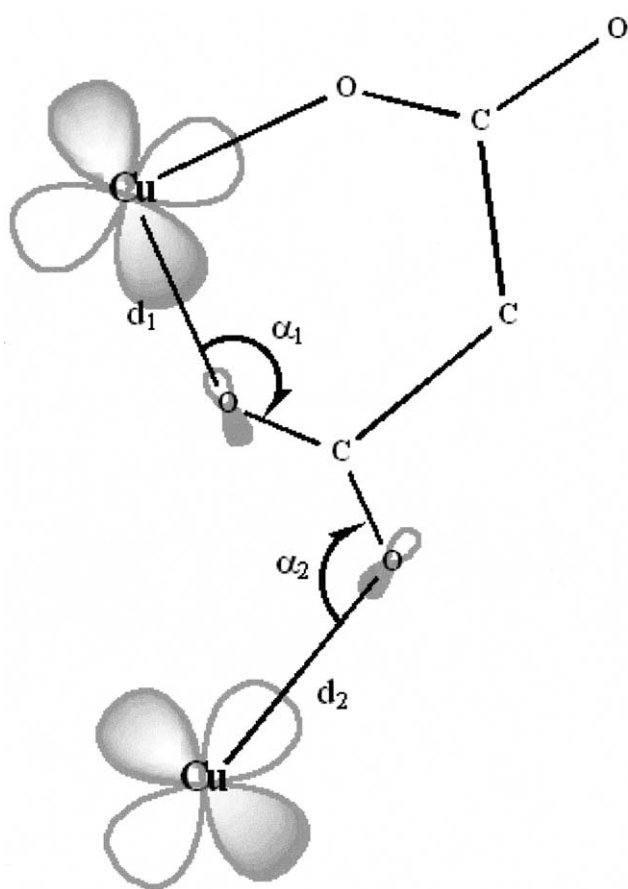
In **6**, **7**, **8** and **3B** the Cu–O–C–O–Cu involves two equatorial oxygen atoms contributing to the largest  $J$ , because the singly occupied orbitals interact directly through the bridge. At the same time  $\beta$  (angle subtended by the basal planes of the interacting copper(II) ions) ranges from  $70$  to  $86^\circ$  making the orbitals to minimize their overlap in such an extent that the ferromagnetic contribution becomes predominant.

The other complexes **1**, **2**, **4**, **5**, and the bridge **3A** involve equatorial–apical pathway. As far as we know this linkage will always give a weak ferromagnetic interaction if the copper(II) environments are not highly distorted. In the light of structural features, it is evident that the  $d_{x^2-y^2}$  copper(II) orbitals are mismatched for interaction to take place between them through the carboxylate group, since the exchange pathway involves an equatorial position on one copper ( $x^2-y^2$  direction) and an axial position on the other copper atom ( $z^2$  direction). Deviations from the idealized symmetry might allow some mixture with the  $d_{z^2}$  orbital, but in any case the overlap would be weak. This would lead to a negligible antiferromagnetic contribution so that the ferromagnetic one becomes predominant.

The apical–apical pathway does not connect the magnetic orbitals of the copper(II) ions, then we expect the interaction to be negligible; although the apical–



Scheme 2.



Scheme 4.

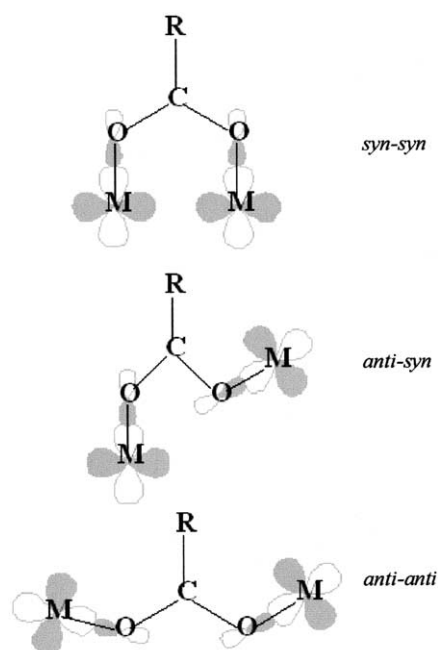
apical pathway has not been yet encountered in our compounds.

### 3.3. On the basis of other structural parameters

The structural parameters  $\beta$ , and  $\tau$  can govern the nature and the magnitude of the interaction.

We can see this focusing on compounds **4** and **5**, in which both exhibit the *anti-anti* and apical–equatorial conformation, leading to a ferromagnetic coupling; but **4** shows a greater  $J$  value than **5**. From Table 1, the distortion parameter ( $\tau$ ) is 0.02 and 0.18 for **4** and **5**, respectively. This leads to a major  $z^2$  character in compound **5**, and hence a larger overlap and a greater value of the antiferromagnetic contribution. A major distortion could cause this term to be greater than the ferromagnetic one, leading to an overall antiferromagnetic interaction, although the magnitude of the interaction is remained weak.

In compounds with equatorial–equatorial linkages the most important structural parameter is  $\beta$ . If  $\beta$  approximates to  $90^\circ$  the magnitude of the interaction decreases and the ferromagnetic term becomes predominant. But when  $\beta$  deviates from that angle, the



Scheme 3.

antiferromagnetic term grows and can be greater than the ferromagnetic one, the coupling becoming stronger.

Other structural parameters could slightly tune the magnitude of the interaction, such as  $\alpha_2$ . Thus a trend in this angle could be stated: decreasing  $\alpha_2$ , (an increase of the *anti-syn* character) a greater value of the ferromagnetic coupling is encountered, as is observed in **3B**, **6**, **7** and **8** (equatorial–equatorial) and in **1**, **2** and **3A** (equatorial–axial).

However, as can be seen in Table 1, many parameters can be simultaneously responsible of the magnitude of the magnetic interaction.

## 4. Conclusion

The malonate is a very versatile ligand, allowing the out-of-plane conformation of the *anti-syn* and *anti-anti* modes. Hence, the magneto-structural assumptions applied to the oxalate bridge cannot be longer extended to more flexible ligands such as malonate, due to the oversimplification it implies.

We can conclude that the parameter that governs, in first order, the magnetic interaction between metal centres is the relative position of the carboxylato bridge of the malonate respect to the copper(II) ions: equatorial–equatorial (strong interaction), equatorial–apical (weak interaction) and apical–apical (negligible interaction). Inside this division another parameters become important such as  $\beta$  (angle between copper(II) basal planes) in the equatorial–equatorial, or the distortion in  $\tau$  the equatorial–apical.

The synthesis and characterization of compounds of this family, and the wideness of this study to other flexible dicarboxylic ligands will allow these remarks to be definitely settled.

### Acknowledgements

The financial support provided by the Gobierno Autónomo de Canarias (Project PI2000/135) and the Spanish Dirección General de Investigación (Ministerio de Ciencia y Tecnología), through project BQU2001-3794, are gratefully acknowledged. J.P. also thanks Ministerio de Educación y Cultura for the predoctoral fellowship AP2001-3322 and F.S.D. thanks the Consejería de Educación, Cultura y Deportes (Gobierno Autónomo de Canarias) for a project-fellowship (PI2000/135).

### References

- [1] B. Bleaney, K.D. Bowers, *Proc. R. Soc. Lond. Ser. A* 214 (1952) 451.
- [2] J. Lewis, F.E. Mabbs, L.K. Royston, W.R. Smail, *J. Chem. Soc. A* (1969) 291.
- [3] R.L. Martin, R.J., Waterman, *J. Chem. Soc.* (1957) 2545.
- [4] P.J. Costes, F. Dahan, J.P. Laurent, *Inorg. Chem.* 24 (1985) 1018.
- [5] A.J. Costa-Filho, O.R. Nascimento, L. Ghivelder, R. Calvo, *J. Phys. Chem.* B105 (2001) 5039.
- [6] E. Colacio, J.M. Domínguez-Vera, M. Ghazi, R. Kivekäs, M. Klinga, J.M. Moreno, *Eur. J. Inorg. Chem.* (1999) 441.
- [7] E. Colacio, J.P. Costes, R. Kivekäs, J.P. Laurent, J. Ruiz, *Inorg. Chim. Acta* 212 (1993) 115.
- [8] E. Colacio, J.P. Costes, R. Kivekäs, J.P. Laurent, J. Ruiz, *Inorg. Chem.* 29 (1990) 4240.
- [9] H. Zhang, D. Fu, F. Ji, G. Wang, K. Yu, T. Yao, *J. Chem. Soc., Dalton Trans.* (1996) 3799.
- [10] E. Colacio, M. Ghazi, R. Kivekäs, J.M. Moreno, *Inorg. Chem.* 39 (2000) 2882.
- [11] Q. Wang, X. Wu, P. Lin, W. Zhang, T. Sheng, H. Yu, L. Chen, J. Li, *Polyhedron* 18 (1999) 1411.
- [12] M. Ahlgren, U. Turpeinen, R. Hämmäläinen, *Acta Crystallogr., Sect. B* 38 (1982) 429.
- [13] M. Murugesu, R. Clérac, B. Pilawa, A. Mandel, C.E. Anson, A.K. Powell, *Inorg. Chim. Acta* (2002), in press.
- [14] J. Rojo, J.M. Lehn, G. Baum, D. Fenske, O. Waldmann, P. Müller, *Eur. J. Inorg. Chem.* (1999) 517.
- [15] Z. Xu, L.K. Thompson, D.O. Miller, *Chem. Commun.* (2001) 1170.
- [16] C.J. Mattheus, K. Avery, Z. Xu, L.K. Thompson, L. Zhao, D.O. Miller, K. Poirier, M.J. Zaworotko, C. Wilson, A.E. Goeta, J.A.K. Howard, *Inorg. Chem.* 38 (1999) 5266.
- [17] R.V. Slone, D.I. Yoon, R.M. Calhoun, J.T. Hupp, *J. Am. Chem. Soc.* 117 (1995) 11813.
- [18] P. Barbaro, F. Cecconi, C.A. Ghilardi, S. Midollini, A. Orlandini, L. Alderighi, D. Peters, A. Vacca, E. Chinea, A. Mederos, *Inorg. Chim. Acta* 262 (1997) 187.
- [19] A. Karipides, J. Ault, T. Reed, *Inorg. Chem.* 16 (1977) 3299.
- [20] (a) M.L. Post, J. Trotter, *J. Chem. Soc., Dalton Trans.* (1974) 1922; (b) K.H. Chung, E. Hong, Y. Do, C.H. Moon, *J. Chem. Soc., Chem. Commun.* (1995) 2333.
- [21] N.J. Ray, B.J. Hathaway, *Acta Crystallogr., Sect. B* 38 (1982) 770.
- [22] R. Hämmäläinen, A. Pajunen, *Suom. Kemistil.* B46 (1973) 285.
- [23] W.L. Kwik, K.P. Ang, S.O. Chan, V. Chebolu, S.A. Koch, *J. Am. Chem. Soc., Dalton Trans.* (1986) 2519.
- [24] D. Chattopadhyay, S.K. Chattopadhyay, P.R. Lowe, C.H. Schawalbe, S.K. Mazumber, A. Rana, S. Ghosh, *J. Chem. Soc., Dalton Trans.* (1993) 913.
- [25] A. Tosik, L. Sieron, M. Bukowska-Strzyzewska, *Acta Crystallogr., Sect. C* 51 (1995) 1987.
- [26] E. Suresh, M.H. Bhadbhade, *Acta Crystallogr., Sect. C* 53 (1997) 193.
- [27] S.M. Saadeh, K.L. Trojan, J.W. Kampf, W.E. Hatfield, V.L. Pecoraro, *Inorg. Chem.* 32 (1993) 3034.
- [28] S. Calogero, L. Stievano, L. Diamandescu, D. Mihaila-Tarabasanu, G. Valle, *Polyhedron* 16 (1997) 3953.
- [29] (a) I. Gil de Muro, F.A. Mautner, M. Insausti, L. Lezama, M.I. Arriortua, T. Rojo, *Inorg. Chem.* 37 (1998) 3243; (b) I. Gil de Muro, M. Insausti, L. Lezama, M.I. Arriortua, T. Rojo, *Inorg. Chem.* 37 (1998) 3243; (c) I. Gil de Muro, M. Insausti, L. Lezama, J.L. Pizarro, M.K. Urtiaga, M.I. Arriortua, T. Rojo, *J. Chem. Soc., Dalton Trans.* (2000) 3360.
- [30] C. Oldham, in: G. Wilkinson, R.D. Gillard, J.A. McCleverty (Eds.), *Comprehensive Coordination Chemistry*, vol. 2, Pergamon Press, Oxford, 1987, p. 435. (and references therein).
- [31] D.K. Towle, S.K. Hoffmann, W.E. Hatfield, P. Singh, P. Chaudhuri, *Inorg. Chem.* 27 (1988) 394.
- [32] P.R. Levstein, R. Calvo, *Inorg. Chem.* 29 (1990) 1581.
- [33] F. Sapiña, E. Escrivá, J.V. Folgado, A. Beltrán, D. Beltrán, A. Fuertes, M. Drillon, *Inorg. Chem.* 31 (1992) 3851.
- [34] C. Ruiz-Pérez, M. Hernández-Molina, P. Lorenzo-Luis, F. Lloret, J. Cano, M. Julve, *Inorg. Chem.* 39 (2000) 3845.
- [35] J. Sanchiz, Y. Rodríguez-Martín, C. Ruiz-Pérez, A. Mederos, F. Lloret, M. Julve, *New J. Chem.*, in press.
- [36] Y. Rodríguez-Martín, C. Ruiz-Pérez, J. Sanchiz, F. Lloret, M. Julve, *Inorg. Chim. Acta* 318 (2001) 159.
- [37] Y. Rodríguez-Martín, M. Hernández-Molina, F.S. Delgado, J. Pasán, C. Ruiz-Pérez, J. Sanchiz, F. Lloret, M. Julve, *Cryst. Eng. Commun.* 4 (2002) 440.
- [38] Y. Rodríguez-Martín, C. Ruiz-Pérez, J. Sanchiz, F. Lloret, M. Julve, *Inorg. Chim. Acta* 326 (2001) 20.
- [39] Y. Rodríguez-Martín, M. Hernández-Molina, F.S. Delgado, J. Pasán, C. Ruiz-Pérez, J. Sanchiz, F. Lloret, M. Julve, *Cryst. Eng. Commun.* (2002) in press.
- [40] C. Ruiz-Pérez, J. Sanchiz, M. Hernández-Molina, F. Lloret, M. Julve, *Inorg. Chem.* 39 (2000) 1363.
- [41] E. Borghi, *Gazz. Chim. Ital.* 117 (1987) 557.
- [42] Y. Zhang, M. Nishiura, L. Jianmin, D. Wei, T. Imamoto, *Inorg. Chem.* 38 (1999) 825.
- [43] A. Pajunen, E. Näsäkkälä, *Finn. Chem. Lett.* (1977) 189.
- [44] A. Pajunen, E. Näsäkkälä, *Finn. Chem. Lett.* (1977) 100.
- [45] J. Kansikas, R. Hämmäläinen, *Finn. Chem. Lett.* (1977) 118.
- [46] R.W. Hay, A. Danby, P. Lightfoot, *Polyhedron* 16 (1997) 3261.
- [47] D.J. Darensbourg, M.W. Holtcamp, B. Khandolwal, K.K. Klausmeyer, J.H. Reibenspies, *Inorg. Chem.* 33 (1994) 2036.
- [48] L. Gasque, R. Moreno-Esparza, E. Mollins, J.L. Briansó-Penalva, L. Ruiz-Ramírez, G. Medina-Dickinson, *Acta Crystallogr., Sect. C* 54 (1998) 1848.
- [49] L. Gasque, R. Moreno-Esparza, E. Mollins, J.L. Briansó-Penalva, L. Ruiz-Ramírez, G. Medina-Dickinson, *Acta Crystallogr., Sect. C* 55 (1999) 158.
- [50] H.-Y. Shen, W.-M. Bu, D.-Z. Liao, Z.-H. Jiang, S.-P. Yan, G.-L. Wang, *Inorg. Chem. Commun.* 3 (2000) 497.



- [51] S. Kawata, S. Kitagawa, M. Machida, T. Nakamoto, M. Kondo, M. Katada, K. Kikuchi, I. Ikemoto, *Inorg. Chim. Acta* 229 (1995) 211.
- [52] Y. Xiong, M. Tong, T. An, H.T. Karlsson, *Acta Crystallogr., Sect. C* 57 (2001) 1385.
- [53] G.A. Baker, G.S. Rushbrooke, H.E. Gilbert, *Phys. Rev. A* 135 (1964) 1272.
- [54] J.J. Borrás-Almenar, E. Coronado, J. Curély, R. Georges, J.C. Gianduzzo, *Inorg. Chem.* 33 (1994) 5171.
- [55] (a) J. Curély, *Europhys. Lett.* 32 (1995) 529;  
(b) J. Curély, *Physica B* 245 (1998) 263.
- [56] A. Addison, T.N. Rao, J. Reedjik, J. van Rijn, G.C. Verschoor, *J. Chem. Soc., Dalton Trans.* (1984) 1349.
- [57] O. Kahn, *Molecular Magnetism*, VCH New York, 1993. (and references therein).
- [58] M. Kato, Y. Muto, *Coord. Chem. Rev.* 92 (1988) 45.
- [59] M. Inoue, M. Kubo, *Inorg. Chem.* 9 (1970) 2310.
- [60] S. Alvarez, M. Julve, M. Verdaguer, *Inorg. Chem.* 29 (1990) 4500.
- [61] O. Castillo, A. Luque, P. Román, F. Lloret, M. Julve, *Inorg. Chem.* 40 (2001) 5526.
- [62] O. Castillo, A. Luque, F. Lloret, P. Román, *Inorg. Chim. Acta* 324 (2001) 141.



PERGAMON

Available online at [www.sciencedirect.com](http://www.sciencedirect.com)

SCIENCE @ DIRECT®

Polyhedron 22 (2003) 2111–2123



POLYHEDRON

[www.elsevier.com/locate/poly](http://www.elsevier.com/locate/poly)

# Malonic acid: a multi-modal bridging ligand for new architectures and properties on molecule-based magnets

Catalina Ruiz-Pérez<sup>a,\*</sup>, Yolanda Rodríguez-Martín<sup>a</sup>, María Hernández-Molina<sup>a</sup>,  
Fernando S. Delgado<sup>a</sup>, Jorge Pasán<sup>a</sup>, Joaquín Sanchiz<sup>b</sup>, Francesc Lloret<sup>c</sup>,  
Miguel Julve<sup>c</sup>

<sup>a</sup> *Laboratorio de Rayos X y Materiales Moleculares, Departamento de Física Fundamental II, Universidad de La Laguna, Avda. Astrofísico Francisco Sánchez s/n, 38204 La Laguna, Tenerife, Spain*

<sup>b</sup> *Departamento de Química Inorgánica, Universidad de La Laguna, La Laguna, Tenerife, Spain*

<sup>c</sup> *Facultat de Química, Departament de Química Inorgànica, Institut de Ciència Molecular, Universitat de València, València, Spain*

Received 6 October 2002; accepted 24 March 2003

In memory of Prof. Oliver Kahn

## Abstract

In this work, we show how the design of one-, two- and three-dimensional materials can strongly benefit from the use of crystal engineering techniques, which can give rise to structures of different shapes, and how these differences can give rise to different properties. We will focus on the networks constructed by assembling malonate ligands and metal centres. The idea of using malonate (dianion of propanedioic acid, H<sub>2</sub>mal) is that they can give rise to different coordination modes with the metal ions bind. Extended magnetic networks of dimensionalities 1 (1D), 2 (2D) and 3 (3D) can be chemically constructed from malonato-bridged metallic complexes. These coordination polymers behave as ferro-, ferri- or canted antiferromagnets. The control of the spatial arrangement of the magnetic building blocks is of paramount importance in determining the strength of the magnetic interaction. It depends on the coordination bond between the metal ion and the ligands, and on supramolecular interactions such as stacking interactions or hydrogen bonds.

© 2003 Elsevier Science Ltd. All rights reserved.

*Keywords:* Malonate; Caboxylate; Magnetic properties; Molecular magnetism

## 1. Introduction

The design of synthetic pathways to obtain systems with desired properties continues to be a challenge for inorganic chemists. In this context, a great interest has been devoted to the development of rational synthetic routes to novel polynuclear compounds of tuneable dimensionality which may have applications as molecu-

lar-based magnetic materials [1–3]. Focusing on the approach of having transition metals as spin carriers, it is the declared target to optimise the number of chemical links between the magnetic centres in order to gain an increased contribution from intramolecular interactions and at the same time, to diminish the influence of the weaker intermolecular contacts.

Along this line, many recent reports have focused on the synthesis and structural characterisation of polymeric transition metal compounds using malonate (mal) [4–9] as blocking and bridging ligand. The use of malonate as bridging ligand in metal complexes has shown the versatility of this ligand [4–9]. The structural complexity diversity of the malonato complexes is due to the versatility of this dicarboxylate ligand which can adopt several chelating bidentate and/or different car-

*Abbreviations:* H<sub>2</sub>mal, malonic acid; bipym, 2,2'-bipyrimidine; phen, phenantroline; Im, imidazole; MeIm, methylimidazole; 2,4'-bipy, 2,4'-bipyridine; 4,4'-bipy, 4,4'-bipyridine; bpy, 2,2'-bipyridine; pyz, pyrazine; pym, pyrimidine.

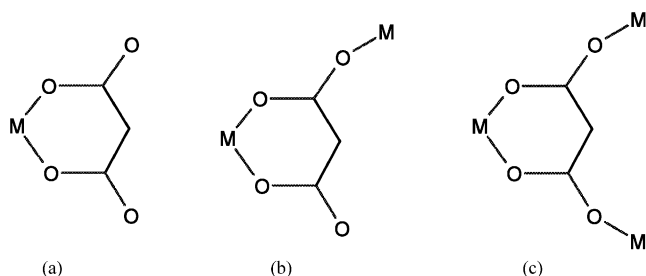
\* Corresponding author. Tel.: +34-922-318-236; fax: +34-922-318-320.

E-mail address: [caruiz@ull.es](mailto:caruiz@ull.es) (C. Ruiz-Pérez).

boxylato-bridging coordination modes. The ability of the carboxylato bridge to mediate significant ferro- or antiferromagnetic coupling [10–14] between the paramagnetic centres enhances the interest in the malonate ligand, aiming at designing extended magnetic systems. Additionally, the carboxylate group provides an efficient pathway that couples the magnetic centres either ferro- or antiferromagnetically [10–14], the coupling constant being influenced by structural aspects such as the conformation of the bridge or the geometry of the metal environment.

The malonate ligand is a dicarboxylic ligand with a singular behaviour different from the other dicarboxylic ligands. In our investigations, we have observed that with 3D ions it can exhibit different coordination modes such as (a) bidentate [ $\eta^5$ -chelation], (b) bidentate [ $\eta^5$ -chelation]+unidentate and (c) bidentate [ $\eta^5$ -chelation]+bis(unidentate).

The malonate ligand occupies one or two coordination positions and neutralises two positive charges of the metallic ion, allowing the inclusion of other ligands in the coordination sphere of the metal. These complementary ligands can act as bridging or blocking ligands, contributing to the interconnection or isolation of the spin carriers. Thus, combining the malonate with other bridging and/or blocking ligands we have been able to prepare monomers, dimers, trimers, tetramers, infinite chains, and 2D and 3D arrays.



Another feature of the carboxylato bridge is the fact that the magnitude of the exchange interaction depends on the possible *syn-syn*, *syn-anti* and *anti-anti* bridging modes that it can adopt. The nature (ferro- or antiferromagnetic) of the interaction being dependent on the nature of the magnetic orbitals of the spin carriers connected by the bridging ligand. In our compounds, these features are nicely in line with theoretical models developed in molecular magnetism, in particular as far as the symmetry rules involving the magnetic orbitals. Thus, playing with the stoichiometry and with the nature of other complementary ligands, very smart several compounds with a controlled dimensionality and with a nicely explained satisfactory explanation of their magnetic properties have been prepared.

Herein, we present an overview of our investigations in the magneto-structural correlations of malonato

complexes. This study is organised attending to the coordination modes of the malonate and how they govern the dimensionality of the structure, then the magnetic properties can be explained attending to the bridging mode of the carboxylate and the nature of the magnetic orbital of the paramagnetic centres.

## 2. Structural aspects and magnetic properties

### 2.1. Bidentate (no-bridging)

In this coordination mode two of the oxygens of the malonate coordinate the metal ion, the ligand behaving as  $\eta^5$ -bidentate, the rest of the oxygens may act as acceptors in hydrogen bonding. This mode is analogue to the  $\eta^4$ -bidentate chelate exhibited by the oxalate. The malonate acts as blocking ligand leading to isolated molecules that are interconnected through hydrogen bonding, exhibiting weak or no magnetic coupling among the metallic centres [15,16].

As examples, we have the bimetallic compounds  $[M^{II}(H_2O)_6][Cu^{II}(mal)_2(H_2O)_2]$  (**1**) ( $M = Mn, Co, Ni, Cu$  and  $Zn$ ) [17] (Fig. 1a). In **1**, the malonate fills equatorial coordination positions of the  $Cu(II)$  ions, the rest of the positions being filled by water molecules. The magnetic properties of the bimetallic compounds (**1**) in the form  $\chi_M T$  vs.  $T$  are shown in Fig. 1b and c,  $\chi_M$  being the molar magnetic susceptibility per each  $Cu(II)M(II)$  couple. At room temperature, the values of  $\chi_M T$  are 4.78(MnCu), 2.98(CoCu), 1.59(NiCu), 0.80(CuCu) and 0.40(ZnCu)  $cm^3 mol^{-1} K$ , as expected for magnetically isolated  $[Cu^{II}(mal)_2(H_2O)_2]^{2-}$  and  $[M^{II}(H_2O)_6]^{2+}$  units. These values slightly decrease upon cooling down except for the complex CoCu where an abrupt decrease is observed. The magnetic behaviour of complexes MnCu, CoCu, NiCu, CuCu and ZnCu is typical of the coexistence of  $[Cu^{II}(mal)_2(H_2O)_2]^{2-}$  and  $[M^{II}(H_2O)_6]^{2+}$  units with very weak antiferromagnetic interactions mediated through hydrogen bonds, in agreement with their structure. Consequently, their magnetic properties were analysed through the Hamiltonian of Eq. (1) with the inclusion of a molecular field correction ( $\theta$ ) accounting for intramolecular interactions. In compound NiCu, the inclusion of an additional term accounting for the zero-field splitting ( $D$ ) of the Ni(II) ion was considered (Eq. (2)):

$$H = g_{Cu}\beta S_{Cu}H + g_M\beta S_MH \quad (1)$$

$$H = g_{Cu}\beta S_{Cu}H + g_M\beta S_MH + S_MDS_M \quad (2)$$

Compound CuZn is the first one we analysed, the least-squares fitting to the experimental data through Eq. (1) leads to  $g_{Cu} = 2.032(1)$ ,  $\theta = -0.317(1)$  K and  $R = 1.85 \times 10^{-5}$ . Given that the geometry of the anion  $[Cu^{II}(mal)_2(H_2O)_2]^{2-}$  remains practically constant for all the compounds, we keep the computed value of  $g_{Cu}$

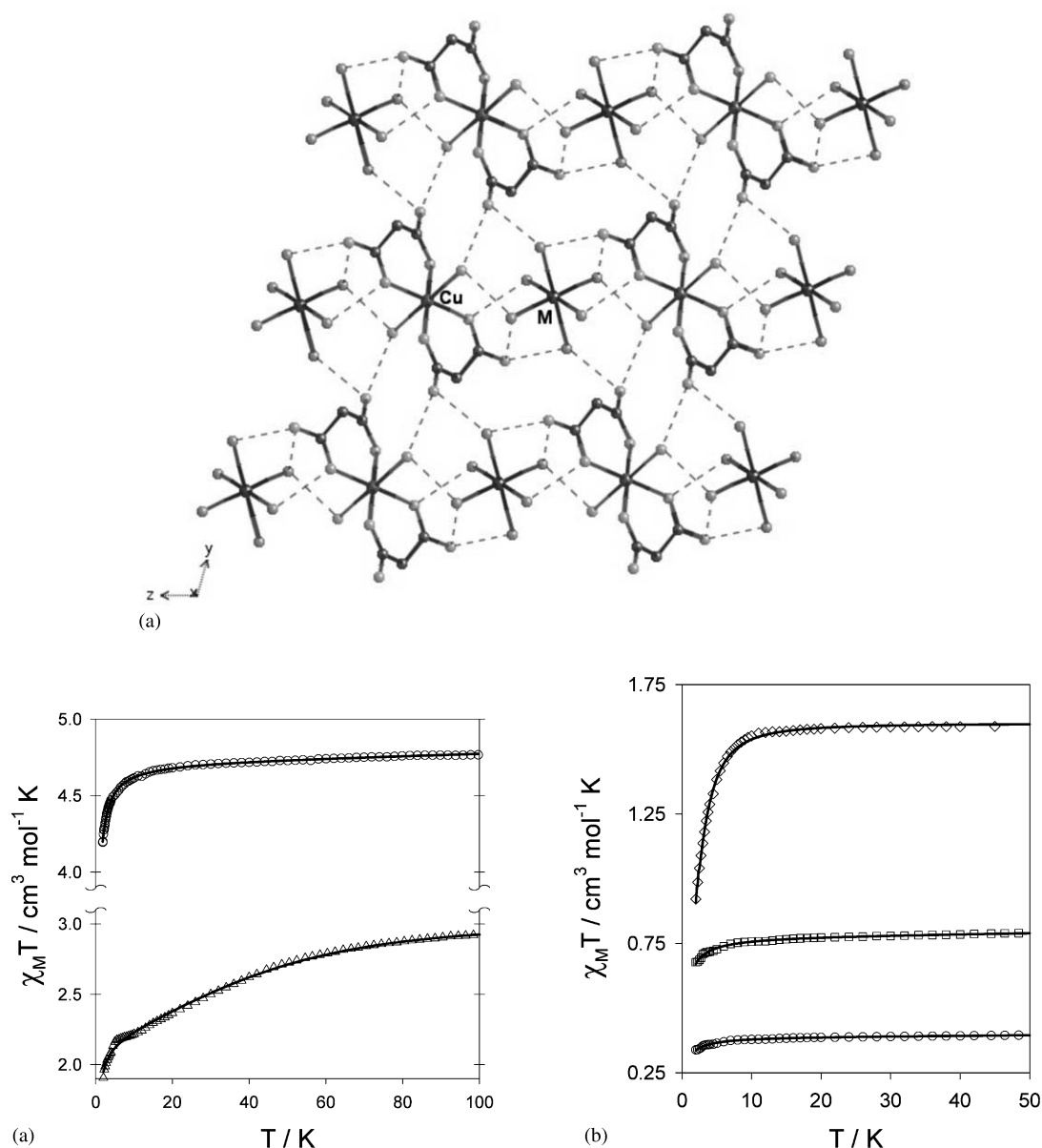


Fig. 1. (a) The 2D anion–cation network of hydrogen bonding in complex  $[\text{M}^{\text{II}}(\text{H}_2\text{O})_6][\text{Cu}^{\text{II}}(\text{mal})_2(\text{H}_2\text{O})_2]$  ( $M = \text{Mn}, \text{Co}, \text{Ni}, \text{Cu}$  and  $\text{Zn}$ ). The six water molecules coordinated to  $M(\text{II})$  ion act as space filling to join the neighbouring 2D layers of  $[\text{Cu}(\text{mal})_2(\text{H}_2\text{O})_2]^{2-}$  forming a 3D hydrogen bonding network. (b) Thermal dependence of the  $\chi_M T$  product ( $\chi_M$  being the magnetic susceptibility per formula) for  $[\text{M}^{\text{II}}(\text{H}_2\text{O})_6][\text{Cu}^{\text{II}}(\text{mal})_2(\text{H}_2\text{O})_2]$  ( $M = \text{Mn}$  (○) and  $\text{Co}$  (△)). The solid lines are the best-fit curve through Eq. (1) (blue line for Mn) and through Eq. (3) (green line for Co). (c) Thermal dependence of the  $\chi_M T$  product for the  $[\text{M}^{\text{II}}(\text{H}_2\text{O})_6][\text{Cu}^{\text{II}}(\text{mal})_2(\text{H}_2\text{O})_2]$  ( $M = \text{Ni}$  (◇),  $\text{Cu}$  (□) and  $\text{Zn}$  (○)). The solid lines are the best-fit curve through Eq. (1) (red line for Zn) and through Eq. (2) (black line for Ni).

for the remaining compounds. The best-fit parameters for complexes MnCu and CuCu are  $g_M = 1.989(1)$  (MnCu) and  $2.075(1)$  (CuCu),  $\theta = 0.22(1)$  (MnCu) and  $-0.47(1)$  (CuCu) K with  $R = 1.21 \times 10^{-6}$  (MnCu) and  $2.15 \times 10^{-5}$  (CuCu). The best-fit parameters for CuNi are  $g_{\text{Ni}} = 2.28(1)$ ,  $\theta = -1.31(1)$  K and  $R = 9.92 \times 10^{-4}$  and  $g_{\text{Ni}} = 2.201(1)$ ,  $|D| = 5.81(4) \text{ cm}^{-1}$  and  $R = 2.78 \times 10^{-5}$ , respectively.

Concerning the magnetic behaviour of complex CoCu (Fig. 1b), once of the contribution of the  $[\text{Cu}(\text{mal})_2(\text{H}_2\text{O})_2]^{2-}$  ion has been removed, the  $\chi_M T$

values continuously decrease on lowering the temperature (values ranging from  $2.42 \text{ cm}^3 \text{mol}^{-1} \text{K}$  at room temperature to  $1.42 \text{ cm}^3 \text{mol}^{-1} \text{K}$  at 2 K). The mononuclear compounds containing a high-spin Co(II) ion in octahedral surrounding present magnetic properties deviating substantially from a Curie–Weiss law. There are several factors influencing the magnetic properties of the Co(II) in  $O_h$  symmetry such as the spin-orbit coupling ( $\lambda$ ), the orbital reduction factor ( $\kappa$ ), the axial crystal field splitting and the Figgis  $T_1$ -term mixing parameter. In a first approximation, we have considered

the Co(II) ion in a pure  $O_h$  symmetry, but all our attempts to fit the experimental data to that model failed, probably due to the distortion around the Co(II) octahedron. In a second approximation, only the two lowest Kramer doublets arising from the  $^4A_2$  state are thermally populated. Then the energy separation ( $D$ ) may be considered as a zero-field splitting within the quartet state, the Hamiltonian (Eq. (3)) to consider being then

$$\mathbf{H} = D(S_z^2 - \frac{5}{4}) + \beta \mathbf{S}g\mathbf{H} \quad (3)$$

Under such approximation (and adding a field correction ( $\theta$ ) to the susceptibility, in order to take into account the intermolecular interactions), the fitting parameters are  $\theta = -0.22$ ,  $g_z = 2.49(1)$ ,  $g_x = g_y = 2.30(1)$ ,  $D = -52(1) \text{ cm}^{-1}$  and  $R = 1.55 \times 10^{-5}$ . The theoretical curve matching very well the experimental data in all temperature range (see Fig. 1b).

Some ligands can bridge the metallic ions, but if the malonate is kept as bidentate the molecules remain isolated as in  $[\text{Cu}_2(\text{mal})_2(\text{H}_2\text{O})_2(\text{bipym})]$  [15], here the dimensionality and the magnetic coupling being governed by the complementary ligand.

## 2.2. $\eta^5$ -Bidentate + unidentate

In this coordination, mode two of the oxygens coordinate the same metal and another one is bound to an additional metal as unidentate, the ligand behaving overall as tridentate. The remaining oxygen acts as acceptor in hydrogen bonding blocking the polymerisation in this direction.

The simplest compound exhibiting this coordination mode is the  $[(\text{H}_2\text{O})_4\text{Cu}(\mu\text{-mal})\text{Cu}(\text{mal})(\text{H}_2\text{O})_2]$  dimer (2) [9,18] (Fig. 2a), in which Cu(1) and Cu(2) are in octahedral and square-pyramidal environments, respectively. The malonate-oxygens fill equatorial positions at Cu(1), the Cu(1)–O distances being shorter, whereas the Cu(2)–O distance is long, the malonate oxygen filling an apical position with respect to Cu(2). We have observed in this compound the copper(II) ions to be ferromagnetically coupled. The magnetic coupling constant having a value of  $J = 1.8 \text{ cm}^{-1}$  (Fig. 2b). We can find in the literature that 95% of copper(II) dimers exhibit an antiferromagnetic coupling, but as we will see in our compounds the ferromagnetic behaviour is much more frequent than the antiferromagnetic one.

In square-pyramidal and octahedral environments, the magnetic orbital at each copper(II) atom is defined by the short equatorial (or basal) bonds, and it is of the  $d_{x^2-y^2}$  type with possible some mixture of the  $d_{z^2}$  character in the axial position. In 2, the carboxylate couples a  $d_{x^2-y^2}$  magnetic orbital of Cu(1) with a  $d_{z^2}$  of Cu(2), the latter being non-magnetic and orthogonal to its magnetic  $d_{x^2-y^2}$ . This kind of coupling (basal-apical

or equatorial-axial) is repeated in many compounds and it has been found to be ferromagnetic in all of our copper(II) compounds.

The trinuclear cation  $[\text{Cu}_3(\text{mal})_2(\text{H}_2\text{O})_9]^{2+}$  (Fig. 2a) present in  $\{[\text{Cu}(\text{H}_2\text{O})_4]_2[\text{Cu}(\text{mal})_2(\text{H}_2\text{O})]\} [\text{Cu}(\text{mal})_2(\text{H}_2\text{O})_2]\{[\text{Cu}(\text{H}_2\text{O})_4][\text{Cu}(\text{mal})_2(\text{H}_2\text{O})_2]\}$  (3) [9] is formed by a central aquabis(malonate)copper(II) entity that is linked to two peripheral tetraaquacopper(II) units through carboxylate bridges which exhibit the *anti-syn* configuration. The coordination around the two crystallographically independent copper atoms (Cu(3) and Cu(4)) is distorted square-pyramidal. Four coplanar carboxylate oxygen atoms from two malonate ligands with nearly identical bond lengths (1.938(4) and 1.941(2) Å for Cu(3)–O(9) and Cu(3)–O(10), respectively) build the basal plane around Cu(3), whereas a weakly coordinated water molecule (2.508(3) Å for Cu(3)–O(7w)) occupies the axial position. At Cu(4), four water molecules build the basal plane and a malonate-oxygen occupies the axial position. The magnetic behaviour is shown in Fig. 2c. The copper(II) ions being ferromagnetically coupled ( $J = 1.2 \text{ cm}^{-1}$ ) by the same reasons as previously mentioned for 2.

The compound  $\{[\text{Cu}(\text{H}_2\text{O})_3][\text{Cu}(\text{mal})_2(\text{H}_2\text{O})]\}_n$  (4) [9] (Fig. 3a) has a 1D polymeric structure. It consists of zigzag chains of copper(II) ions that exhibit a regular alternation of aquabis(malonate)copper(II) and triaquocopper(II) units, the former being linked to the latter as bis-monodentate ligands through two *trans*-malonate oxygen atoms. The chains run parallel to the  $z$ -axis, and they are interconnected through hydrogen bonding. The two crystallographically independent copper(II) ions (Cu(1) and Cu(2)) have distorted square-pyramidal surroundings. The four coplanar carboxylate oxygen atoms (O(1), O(3), O(5), and O(6)), which are coordinated to Cu(1) define the basal plane, whereas the apical position is occupied by a weakly coordinated water molecule O(1w). The three water molecules O(2w), O(3w) and O(4w) and the carboxylate oxygen O(7) build the basal plane at Cu(2), whereas the other carboxylate oxygen, O(2c) ( $c = -x, \frac{1}{2} - y, -\frac{1}{2} + z$ ), occupies the axial position.

Each malonate simultaneously adopts bidentate (at Cu(1)) and unidentate (at Cu(2)) coordination modes. Two slightly different carboxylate bridges, that exhibit the *anti-syn* conformation, alternate regularly within each copper(II) chain.

For this compound, the magnetic behaviour is shown in Fig. 3b. The O(1)–C(1)–O(2) carboxylate connects a basal Cu(1)–O(1) bond with an apical O(2)–Cu(2b) bond; this coupling being weak and ferromagnetic ( $J = 1.9 \text{ cm}^{-1}$ ) as observed in 2. The O(5)–C(5)–O(5) carboxylate connects two equatorial bonds (Cu(1)–O(5) and Cu(2)–O(7)) but the carboxylate plane and the equatorial plane at Cu(2) (O(2w)O(4w)O(3w)O(7))

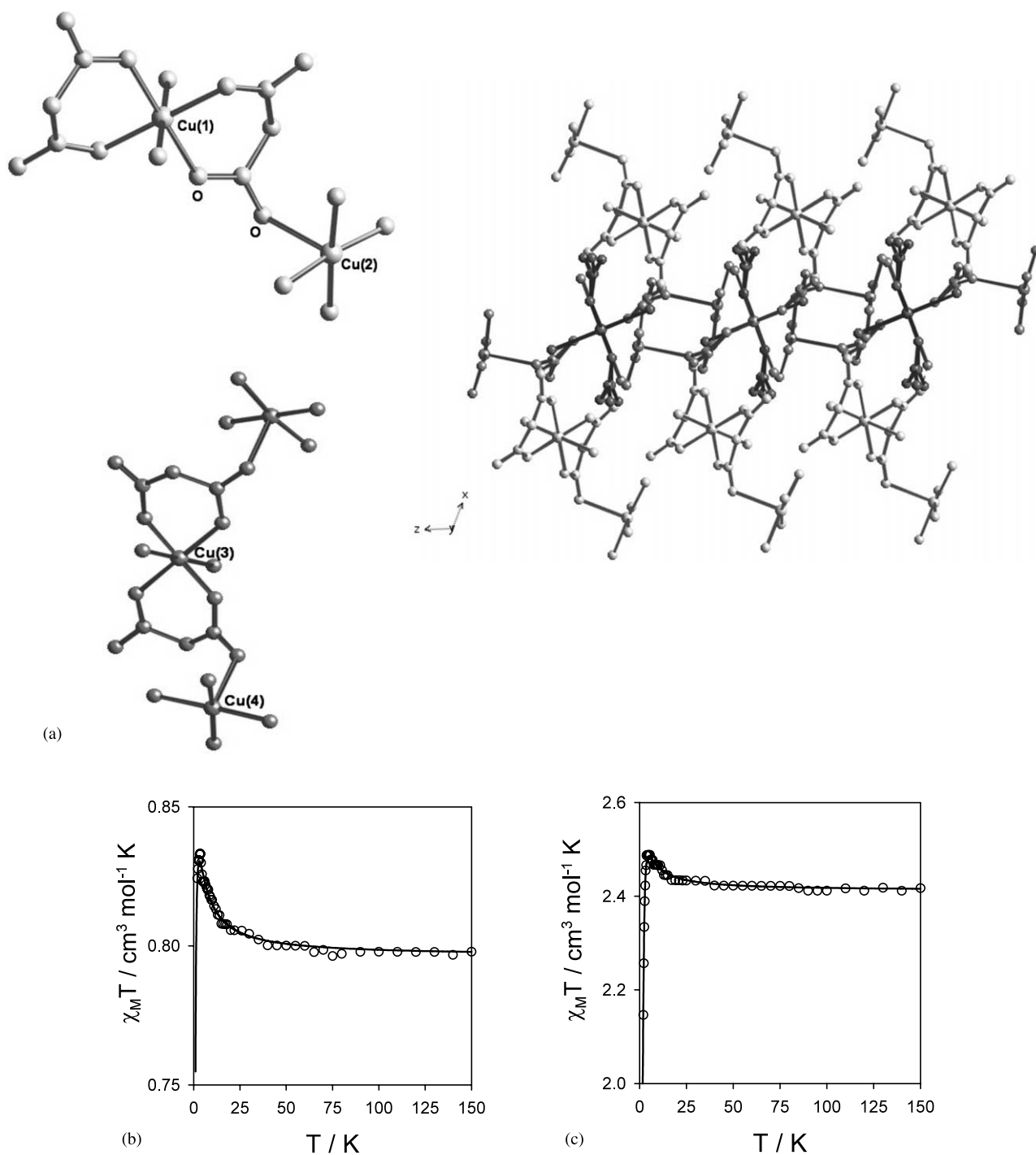


Fig. 2. (a) Perspective view of the trinuclear copper(II) units of compound  $\{[\text{Cu}(\text{H}_2\text{O})_4]_2[\text{Cu}(\text{mal})_2(\text{H}_2\text{O})]\}[\text{Cu}(\text{mal})_2(\text{H}_2\text{O})_2]\cdot\{[\text{Cu}(\text{H}_2\text{O})_4][\text{Cu}(\text{mal})_2(\text{H}_2\text{O})_2]\}$  along the  $b$ -axis. Contents of the unit cell of the complex: monomer (violet), dimer (green) and trimer (orange). (b) Thermal dependence of the  $\chi_M T$  product for compound  $[(\text{H}_2\text{O})_4\text{Cu}(\mu\text{-mal})\text{Cu}(\text{mal})(\text{H}_2\text{O})_2]$  (2) (dimer). Solid line is the best-fit by the appropriate expression through the Hamiltonian  $\mathbf{H} = -J\mathbf{S}_A\mathbf{S}_B + g\beta(\mathbf{S}_A + \mathbf{S}_B)H + \mathbf{S}_A D \mathbf{S}_B$ . (c) Thermal dependence of the  $\chi_M T$  product for compound  $\{[\text{Cu}(\text{H}_2\text{O})_4]_2[\text{Cu}(\text{mal})_2(\text{H}_2\text{O})]\}[\text{Cu}(\text{mal})_2(\text{H}_2\text{O})_2]\cdot\{[\text{Cu}(\text{H}_2\text{O})_4][\text{Cu}(\text{mal})_2(\text{H}_2\text{O})_2]\}$  (3). Solid line is the best-fit derived through the Hamiltonian  $\mathbf{H} = -J(\mathbf{S}_{\text{Cu}3}\mathbf{S}_{\text{Cu}4} + \mathbf{S}_{\text{Cu}3}\mathbf{S}_{\text{Cu}4}) + \sum_{i=1}^3 g_{\text{Cu}_i} \beta \mathbf{S}_{\text{Cu}_i} H$ .

are nearly orthogonal (dihedral angle of  $94.4^\circ$ ), this may explain this interaction to be ferromagnetic ( $J = 3.0 \text{ cm}^{-1}$ ).

Combining the malonate with blocking ligands, such as imidazole or methylimidazole, 1D polymeric struc-

tures can be obtained as those observed in compounds  $[\text{Cu}(\text{Im})_2(\text{mal})]$  (5) and  $[\text{Cu}(\text{MeIm})_2(\text{mal})]$  (6) [19] (Fig. 4a and b). In these compounds, copper(II) is in a square-pyramidal surrounding. Two malonate-oxygens from a bidentate malonate and two imidazole-nitrogens build

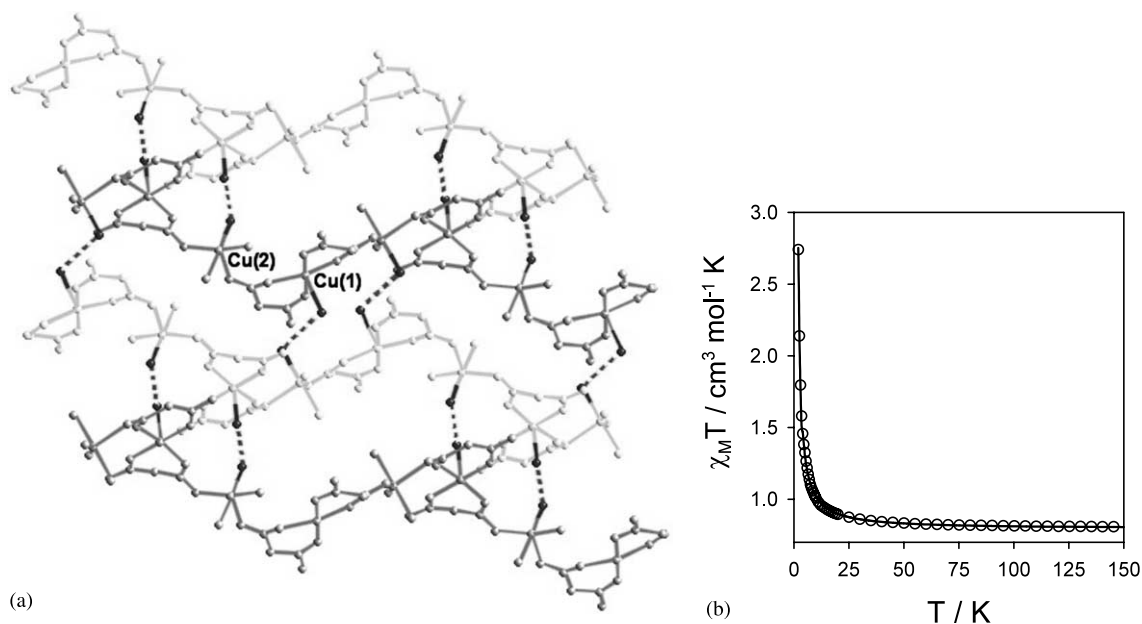


Fig. 3. (a) Projection of the structure of **4** down the *a*-axis, showing the sheet-like nature. (b) Thermal dependence of the  $\chi_M T$  product for compound  $\{[\text{Cu}(\text{H}_2\text{O})_3][\text{Cu}(\text{mal})_2(\text{H}_2\text{O})]\}_n$  (**4**). Solid line is the best-fit derived through the Hamiltonian  $\mathbf{H} = -J\sum_i[\mathbf{S}_{2i}\mathbf{S}_{2i-1} + \alpha\mathbf{S}_{2i}\mathbf{S}_{2i+1}]$ .

the basal plane. The same malonate ligand acts as unidentate towards the neighbouring copper(II) filling an apical position with a longer Cu–O distance. The magnetic behaviour is shown in Fig. 4c, both compounds exhibit ferromagnetic coupling,  $J = 1.64(1)$  and  $J = 0.39(1) \text{ cm}^{-1}$  for **5** and **6**, respectively, as expected from the apical-equatorial connection.

With 2,4'-bipyridine, a tetrameric neutral unit  $[\text{Cu}_4(\text{mal})_4(\text{H}_2\text{O})_4(2,4'\text{-bipy})_4]$  (**7**) can be obtained, involving a small planar-square with copper(II) cations and malonate anions at each corner [20] (Fig. 5a and b). Each copper atom exhibits a slightly distorted square-pyramidal surrounding. The 2,4'-bipy acts as blocking ligand, since the location of the nitrogen in 2 does not allow further polymerisation. The magnetic properties of **7** are shown in Fig. 6 and correspond to those of magnetically isolated squares of four ferromagnetically coupled spin doublets,  $J = 12.3(1) \text{ cm}^{-1}$ . The magnetic properties of **7** under the form of  $\chi_M T$  plot are shown in Fig. 6. The  $\chi_M T$  plot for **7** continuously increases as the temperature is lowered reaching a plateau at 3.0 K ( $\chi_M T = 3.24 \text{ cm}^3 \text{ mol}^{-1} \text{ K}$ ) which is as expected for a magnetically isolated square of four spin doublets interacting ferromagnetically (low-lying  $S = 2$  accounting for the plateau observed for  $\chi_M T$ ).

$[\text{Cu}_4(\text{mal})_4(\text{H}_2\text{O})_4(4,4'\text{-bipy})_2] \cdot 2\text{H}_2\text{O}$  (**8**) has similar structure and magnetic properties to those observed for **7**. The main difference is the ability of the 4,4'-bipy to act as bidentate ligand interconnecting the  $\text{Cu}_4(\text{mal})_4(\text{H}_2\text{O})_4$  tetramers leading to a 2D network [21] (Fig. 7). This compound illustrates the increment of the dimensionality by the introduction of other bridging

ligands. The four copper(II) ions are ferromagnetically coupled in the small square ( $J = 12.4(1) \text{ cm}^{-1}$ ) existing weak antiferromagnetic interactions among the tetramers through the 4,4'-bipy ( $J = -0.05 \text{ cm}^{-1}$ ) (see Fig. 6). For compound **8**,  $\chi_M T$  continuously increases reaching a maximum of  $2.93 \text{ cm}^3 \text{ mol}^{-1} \text{ K}$  at 5.5 K and further decreases at lower temperatures (see Fig. 6). The magnetic behaviour of **8** is satisfactorily interpreted considering a quadratic layer of ferromagnetically coupled tetranuclear copper(II) units, which are antiferromagnetically coupled through the bridging 4,4'-bipy. The magnetic coupling within the tetramer is strong and ferromagnetic ( $J = 12.4 \text{ cm}^{-1}$ ), whereas the coupling through the bridging 4,4'-bipy is antiferromagnetic and very weak ( $J_{\text{eff}} = -0.052 \text{ cm}^{-1}$ ).

Also we obtained heterometallic structures, e.g.,  $[\text{Mn}^{\text{II}}\text{Cu}^{\text{II}}(\text{mal})_2(\text{H}_2\text{O})_3] \cdot 2\text{H}_2\text{O}$  (**9**) [22], made up by neutral bimetallic chains that linked with long weak axial malonate oxygen to copper bonds, which leads to a corrugated sheet-like structure (Fig. 8a). The magnetic behaviour, shown in Fig. 8b, is characteristic of ferrimagnetic chains without magnetic ordering in the temperature range explored. Given the special alternating trend  $\dots J_1 - J_1 - J_2 - J_2 - J_1 - J_1 \dots$  where  $J_1$  and  $J_2$  represent the intrachain Cu(II)–Mn(II) isotropic magnetic coupling and the lack of a theoretical model to treat it, we have assumed that the  $J_1$  and  $J_2$  values should be very close and consequently, we have treated the experimental data through a regular chain approach. The least-square fitting of the data led to  $J_{\text{MnCu}} = -4.5 \text{ cm}^{-1}$  [11].

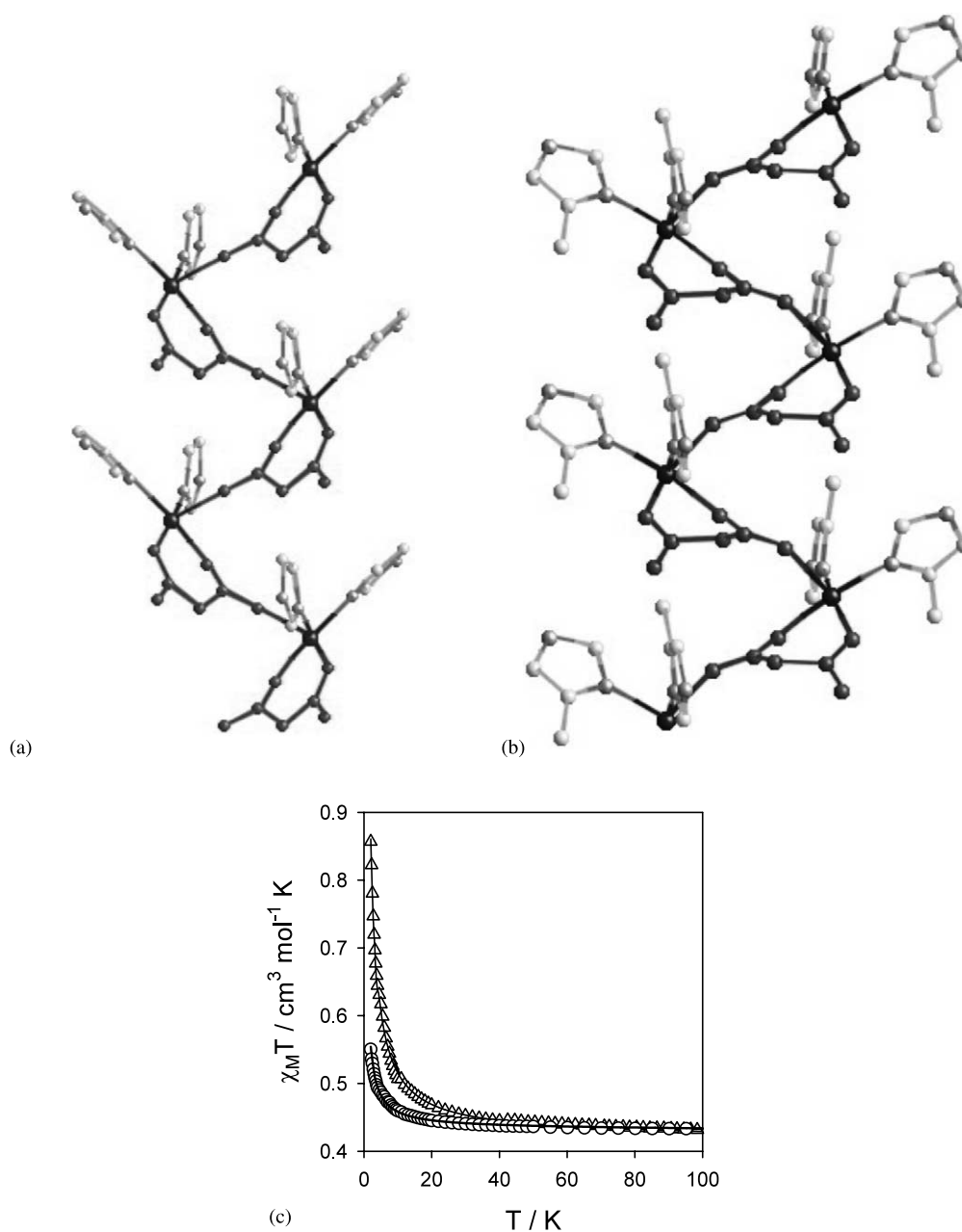


Fig. 4. (a) Projection of compound [Cu(Im)<sub>2</sub>(mal)] (5) down the *a*-axis showing the parallel arrangement of the chains. (b) Projection of compound [Cu(MeIm)<sub>2</sub>(mal)] (6) down the *b*-axis. (c) Thermal dependence of the  $\chi_M T$  product for compounds [Cu(Im)<sub>2</sub>(mal)] ( $\Delta$ ) and [Cu(MeIm)<sub>2</sub>(mal)] ( $\circ$ ). Solid lines are the best-fit through the magnetic susceptibility expression derived from the Hamiltonian  $\mathbf{H} = -J \sum_i \mathbf{S}_i \mathbf{S}_{i+1}$ .

### 2.3. Bidentate + bis(unidentate)

Two polymorphic malonate-bridged copper(II) complexes of formula  $\{[\text{Cu}(\text{bpy})(\text{H}_2\text{O})][\text{Cu}(\text{bpy})(\text{mal})(\text{H}_2\text{O})]\}(\text{ClO}_4)_2$  (**10**) (Fig. 9) have been prepared [8]. The structures are made up of uncoordinated perchlorate anions and malonate-bridged zigzag copper(II) chains running parallel to one of the crystallographic axes. These chains are built by a [Cu(bpy)(mal)(H<sub>2</sub>O)] unit acting as bis-unidentate ligand toward two [Cu(bpy)(H<sub>2</sub>O)] adjacent units through its OCCCO skeleton in

an *anti-anti* conformation, whereas the carboxylate bridge exhibits the *anti-syn* conformation. These compounds contain four crystallographically independent copper(II) atoms, but the environment of all of them is distorted square-pyramidal: the axial position is occupied by a water molecule, whereas the equatorial plane is formed by a chelating bpy and either a bidentate malonate or two unidentate carboxylate-oxygens from two malonate ligands. Each malonate acts as bidentate respect to a copper(II) and as bis(unidentate) to other two. The analysis of the magnetic data indicates the



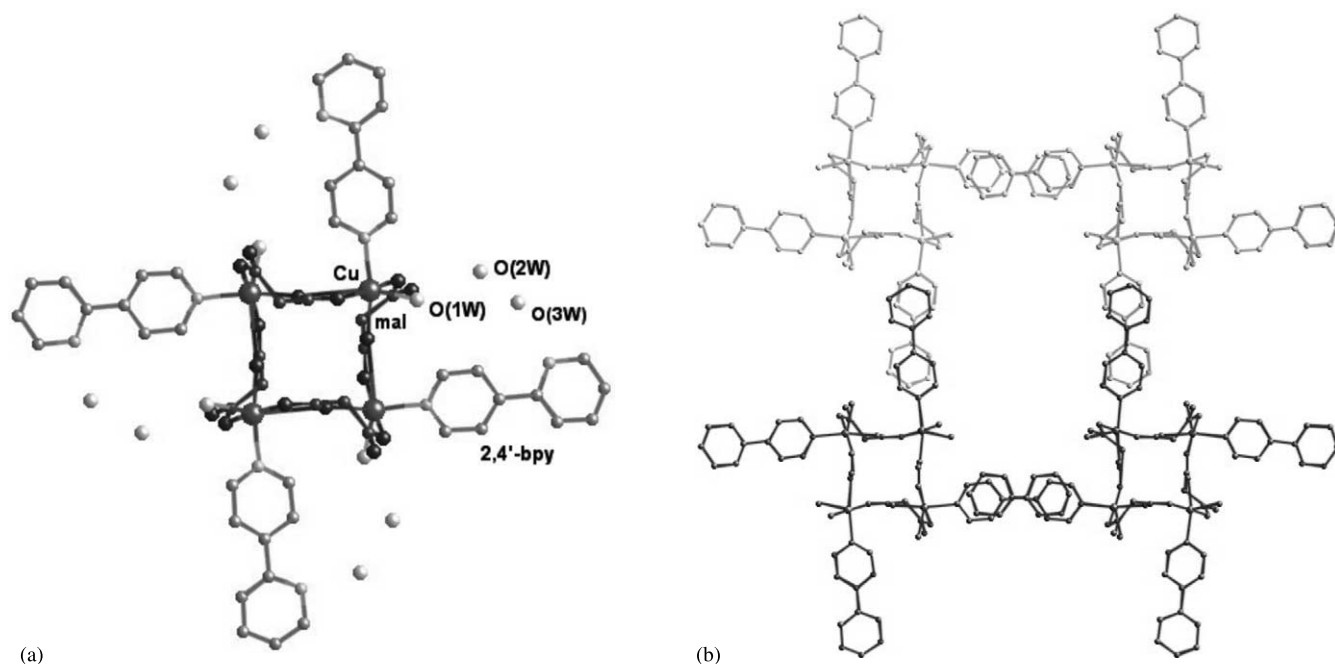


Fig. 5. (a) Perspective view of the tetramer unit of  $[\text{Cu}_4(\text{mal})_4(\text{H}_2\text{O})_4(2,4'\text{-bipy})_4]\cdot 2\text{H}_2\text{O}$  (7). (b) Perspective view of the stacking of the compound along the  $c$ -axis.

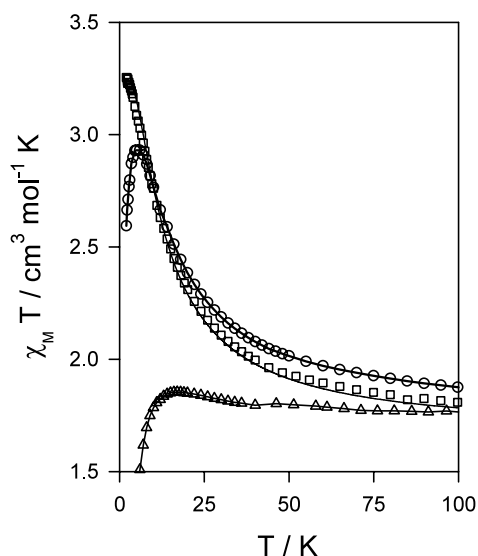


Fig. 6. Thermal dependence of the  $\chi_M T$  product for compounds (7)  $[\text{Cu}_4(\text{mal})_4(\text{H}_2\text{O})_4(2,4'\text{-bipy})_4]\cdot 2\text{H}_2\text{O}$  ( $\square$ ), (8)  $[\text{Cu}_4(\text{mal})_4(\text{H}_2\text{O})_4(4,4'\text{-bipy})_2]\cdot 2\text{H}_2\text{O}$  ( $\circ$ ) and (15)  $[\text{Cu}_4(\text{mal})_4(\text{pyz})_2]\cdot 4\text{H}_2\text{O}$  ( $\triangle$ ),  $\chi_M$  being the magnetic susceptibility per four copper(II) ions. Solid lines are the best-fit by the Hamiltonian  $\mathbf{H} = -J(\text{S}_1\text{S}_2 + \text{S}_2\text{S}_3 + \text{S}_3\text{S}_4 + \text{S}_1\text{S}_4)$ .

occurrence of a ferro- (through the carboxylate,  $J = 4.6 \text{ cm}^{-1}$ ) and antiferromagnetic (through the skeleton of the malonate,  $J = -4.2 \text{ cm}^{-1}$ ) coupling.

A family of compounds exhibiting this coordination mode are the isostructural [23,24] homo or hetero-bimetallic malonates of the divalent Co, Ni and Zn:  $[\text{M}(\text{H}_2\text{O})_2][\text{M}'(\text{mal})_2(\text{H}_2\text{O})_2]$  ( $\text{M} = \text{Mn}^{\text{II}}, \text{Co}^{\text{II}}, \text{Ni}^{\text{II}}, \text{Zn}^{\text{II}}$ ;  $\text{M}' = \text{Co}^{\text{II}}, \text{Ni}^{\text{II}}, \text{Zn}^{\text{II}}$ ) (11) (Fig. 10a and b). The simple malonates of the divalent Co, Ni and Zn are isostruc-

tural, and their mixed bimetallic malonates behave as solid solutions filling randomly the positions of M and M'. Mn(II) can also be introduced in the network as M, its concentration must be kept below 50% or the mixed malonate is impurified with Mn(II) malonate remaining malonate-oxygens act as unidentate filling equatorial positions of four adjacent M cations. The magnetic coupling, shown for the Ni(II) complex in Fig. 10c, is very weak since the malonate exhibits the *anti-syn* configuration, being ferromagnetic and antiferromagnetic for Ni(II) and Co(II), respectively. The mixed malonates are ferrimagnetic, but magnetic ordering is not obtained in any case.

The structure of the Mn(II) malonate (12) is made up by the polymerisation of  $[\text{Mn}(\text{mal})(\text{H}_2\text{O})_2]$  monomers giving a 2D array (Fig. 11a and b) [25]. Mn(II) is in an octahedral environment, with the water molecules in the axial positions. Each malonate chelates the metal as bidentate, with the remaining two oxygens bridging to two further adjacent metallic atoms as bis-unidentate. This structure is very original since the two carboxylates of the malonate exhibit two different conformations, the *anti-anti* and the *anti-syn*, respectively. This feature leads to a spin canting behaviour at low temperatures (Fig. 11c).

$[\text{M}(\text{mal})(\text{pyz})(\text{H}_2\text{O})]$ ,  $[\text{M}(\text{mal})(\text{pym})(\text{H}_2\text{O})]$  ( $\text{M}(\text{II}) = \text{Co}, \text{Zn}$ ) (13) [26], and  $[\text{Co}(\text{mal})(4,4'\text{-bipy})_{1/2}(\text{H}_2\text{O})]$  [21]  $[\text{Mn}(\text{mal})(4,4'\text{-bipy})_{1/2}(\text{H}_2\text{O})]$  (14) [24] have related structures in which layers of octahedrally coordinated metallic atoms bridged by the malonate anions within the layers are interconnected by 4,4'-bipy, pyz or pym molecules leading to a 3D structure. Each malonate

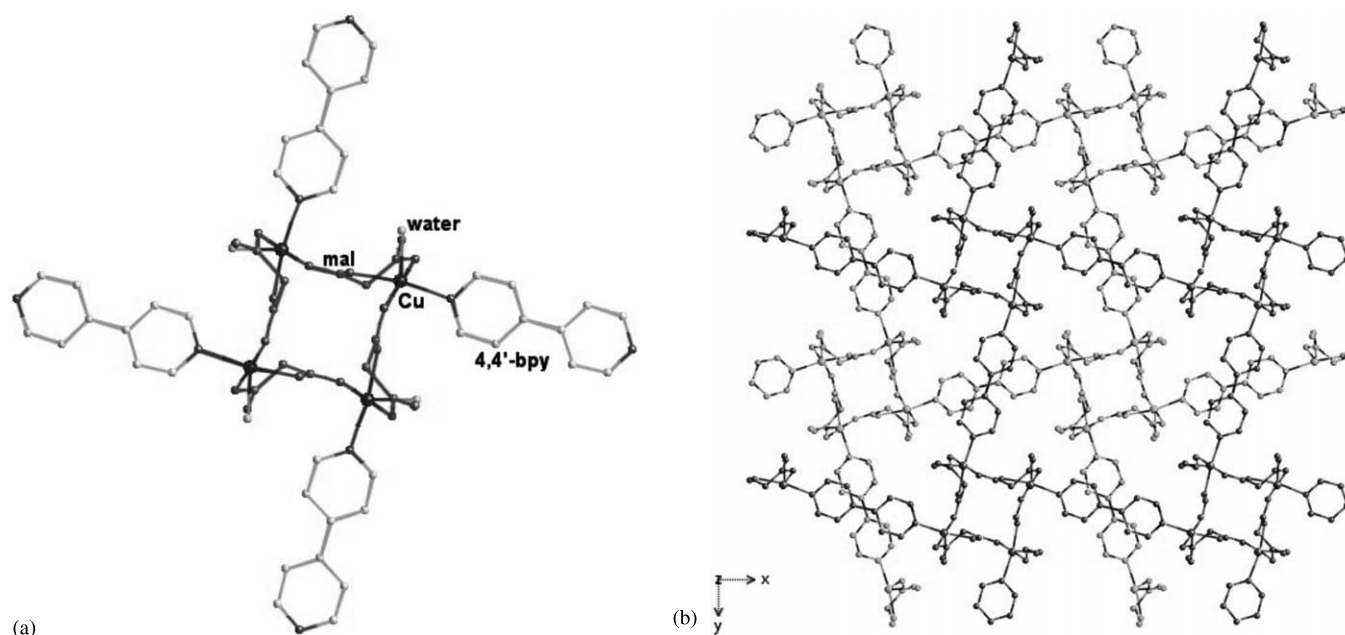


Fig. 7. (a) Perspective view of the tetramer unit of  $[\text{Cu}_4(\text{mal})_4(\text{H}_2\text{O})_4(4,4'\text{-bipy})_2] \cdot 2\text{H}_2\text{O}$  (**8**) along the  $c$ -axis when only the odd layers are considered. (b) View of the layers stacked along the tetragonal  $c$ -axis.

chelates the metal as bidentate, with the remaining two oxygen atoms bridging to two further adjacent metallic atoms as bis-unidentate, thus forming continuous covalently bonded sheets. The metal is then coordinated by three different malonate anions, the remaining two *trans*-positions being filled by a terminal  $\text{H}_2\text{O}$  molecule and the nitrogen of the aromatic molecule. All these compounds, except those of Zn, exhibit weak antiferromagnetic coupling.

The structure of  $[\text{Cu}_4(\text{mal})_4(\text{pyz})_2] \cdot 4\text{H}_2\text{O}$  (**15**) [20] (Fig. 12) is very similar to that of **8**, in which 2D layers were obtained by the assemblage of  $\text{Cu}_4(\text{mal})_4$  tetramers by bidentate 4,4'-bipy ligands. In **15**, the tetramers are assembled by bidentate pyrazine ligands. Each copper atom is in a quasi-perfect square-pyramidal surrounding with three carboxylate-oxygen atoms from two malo-

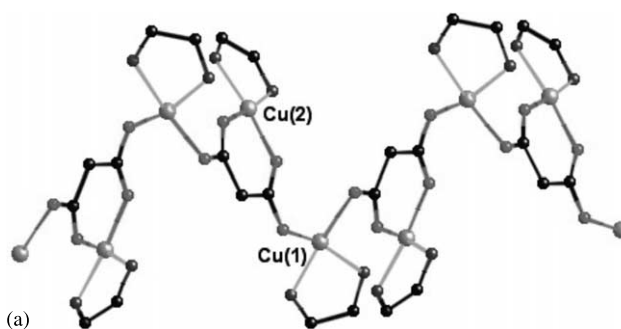


Fig. 9. View of compound  $\{[\text{Cu}(\text{bpy})(\text{H}_2\text{O})][\text{Cu}(\text{bpy})(\text{mal})(\text{H}_2\text{O})]\}(\text{ClO}_4)_2$  (**10**) showing the parallel arrangement of the chains along the  $b$ -axis. 2,2'-Bipyridine ligands, water molecules and the perchlorate anions have been omitted for clarity.

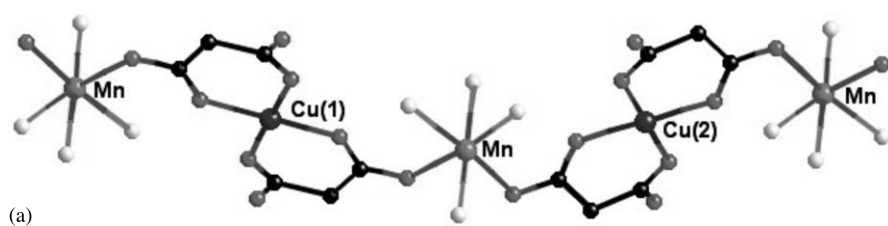
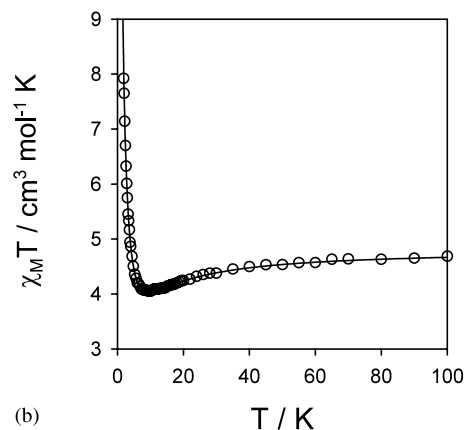


Fig. 8. (a) Perspective drawing of a fragment of the chain of  $[\text{Mn}^{\text{II}}\text{Cu}^{\text{II}}(\text{mal})_2(\text{H}_2\text{O})_3] \cdot 2\text{H}_2\text{O}$  (**9**). (b) Thermal dependence of the  $\chi_{\text{M}}T$  product for compound **9**.



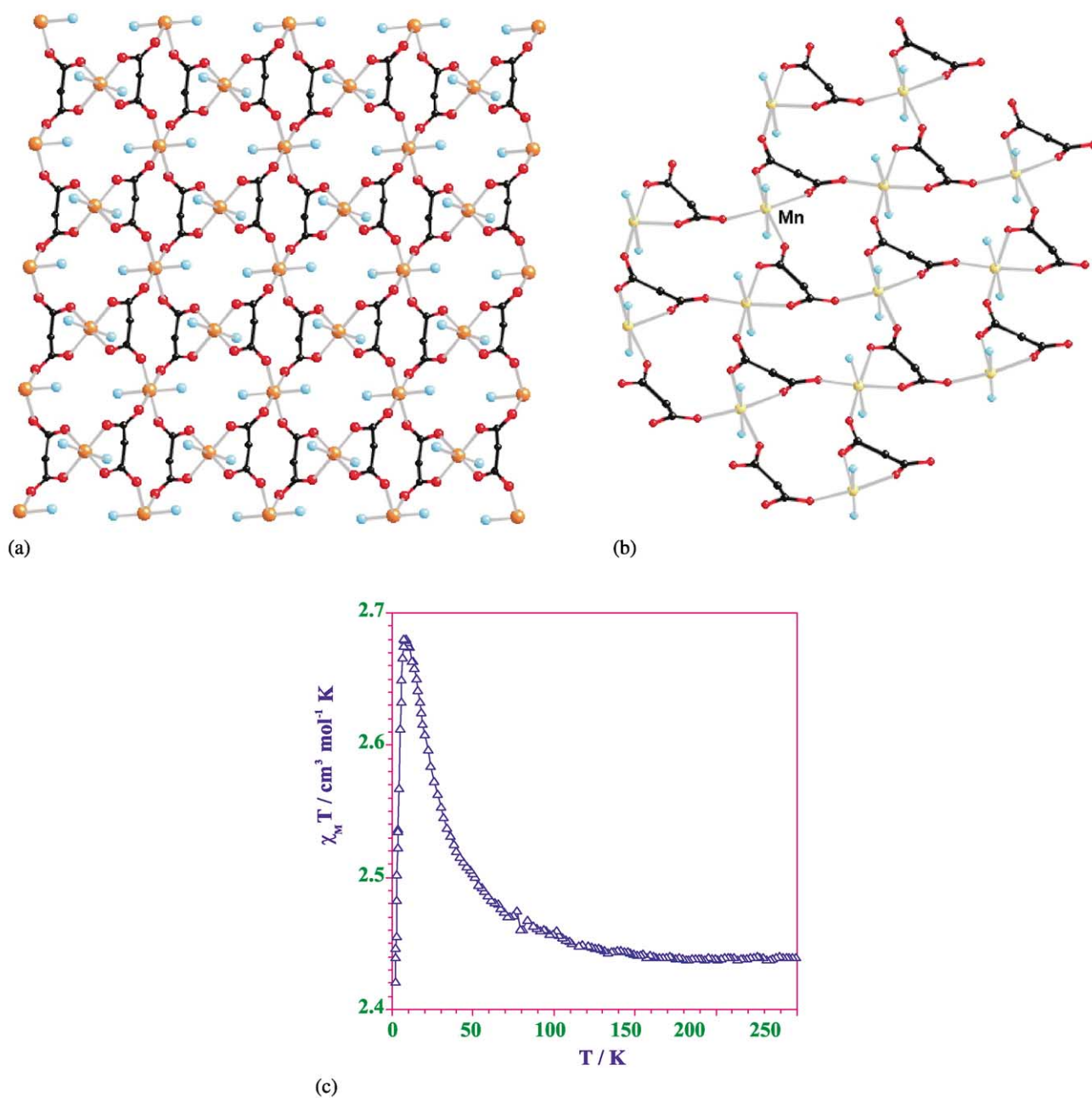


Fig. 10. (a) Layer of  $[M(H_2O)_2][M'(mal)_2(H_2O)_2]$  ( $M = Co^{II}, Ni^{II}, Zn^{II}$ ;  $M' = Co^{II}, Ni^{II}, Zn^{II}$ ) (**11**). (b) Sheet structure of compound  $[Mn(mal)(H_2O)_2]$  (**12**). (c) Thermal dependence of the  $\chi_M T$  product for  $[Ni(H_2O)_2][Ni(mal)_2(H_2O)_2]$ .

nate groups and one nitrogen atom from a pyrazine ligand building the equatorial plane. The main difference with the structure of **8** is the absence of a water molecule filling the apical position of the square-pyramidal surrounded copper(II). This position is occupied by a malonate-oxygen of a tetramer of a neighbouring layer. By this new link, the layers are interconnected leading to a 3D structure. Each malonate uses its four oxygen atoms to coordinate the copper atoms: within each layer, the malonate adopts simultaneously the bidentate (at one copper atom) and uni-

dentate (at another copper atom) coordination modes, the fourth carboxylate-oxygen acts also as unidentate being bound to a further copper atom from a neighbouring layer. The magnetic properties of **15** have been investigated in the temperature range 1.9–300 K and they look like an overall weak ferromagnetic behaviour which would be the result of a competition between ferro- (through the malonate bridge) and antiferromagnetic (through the pyrazine bridge) interactions, the former being somewhat stronger are consistent with the occurrence of a competition between a ferromagnetic

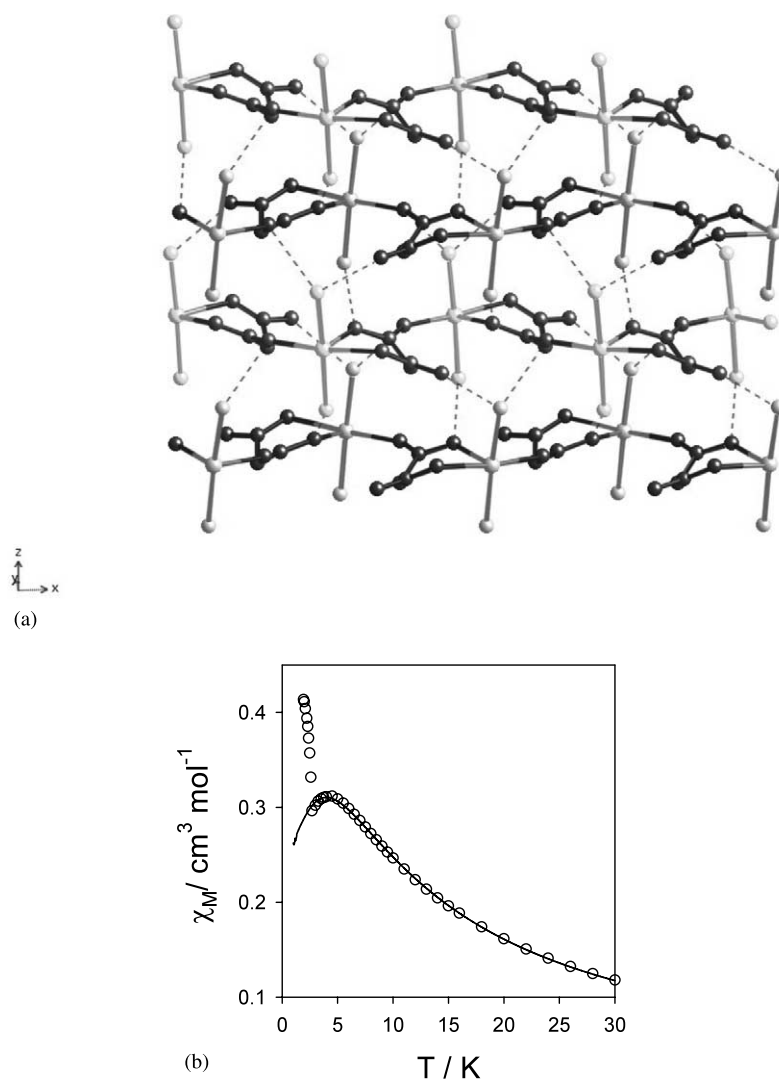


Fig. 11. (a) Parallel packing of the sheets showing the hydrogen interactions involved in the generation of the framework structure in compound **12**. (b) Thermal dependence of the  $\chi_M$  for  $[\text{Mn}(\text{mal})(\text{H}_2\text{O})_2]$ . Solid line is best-fit through the Hamiltonian  $\mathbf{H} = -J\sum_i \mathbf{S}_i \mathbf{S}_{i+1}$ .

coupling through the malonate bridge and an antiferromagnetic one through the pyrazine bridge. However, there is no long-range antiferromagnetic ordering in the temperature range studied (Fig. 6).

### 3. Conclusions

The bis-bidentate coordination mode dominant in the oxalato complexes is sterically forbidden for the malonate, this makes the bidentate+unidentate and the bidentate+bis-unidentate coordination modes to dominate in the chemistry of the malonate. This affects dramatically to the structure and the properties of the malonate complexes, being the ferromagnetic interactions much more frequent than in general compounds. The malonate is a dissymmetric ligand. By its bidentate side, it is a strong complexing agent (due to the chelate effect) and it will be usually filling equatorial or basal

positions displaying short M–O distances. By its other side it acts as unidentate showing weaker interactions and longer M'–O distances. The metallic ion that is chelated usually remains in the same plane of the carboxylate groups with small deviations; on the other hand, the unidentate coordinated metal can deviate considerably from the carboxylate plane, reducing notably the overlap between the magnetic orbitals of the paramagnetic centres. This minimises the antiferromagnetism and interactions expected to be antiferromagnetic can be turned to ferromagnetic. Another feature of the malonate is the fact that when these latter M'–O distances are long enough, this oxygen becomes axial or apical. Then, as a consequence of the coupling of orbitals of different symmetry, the magnetic interaction is expected to be ferromagnetic in many copper(II) complexes.

Consequently, we can conclude that the malonate is a very versatile ligand that is able to generate high

# Phenylmalonate-Containing Copper(II) Complexes: Synthesis, Crystal Structure and Magnetic Properties

Jorge Pasán,<sup>[a]</sup> Joaquín Sanchiz,<sup>[b]</sup> Catalina Ruiz-Pérez,<sup>\*[a]</sup> Francesc Lloret,<sup>[c]</sup> and Miguel Julve<sup>[c]</sup>

**Keywords:** Copper / Magnetic properties / N ligands / O ligands

Three new copper(II) complexes of formula  $[\text{Cu}(2,2'\text{-bpy})(\text{Phmal})(\text{H}_2\text{O})]\cdot 2\text{H}_2\text{O}$  (**1**),  $[\{\text{Cu}(2,2'\text{-bpym})(\text{Phmal})\}]_n$  (**2**) and  $[\{\text{Cu}(\text{phen})(\text{Phmal})\}]_n\cdot 3n\text{H}_2\text{O}$  (**3**) (Phmal = phenylmalonate; 2,2'-bpy = 2,2'-bipyridine; 2,2'-bpym = 2,2'-bipyrimidine; phen = 1,10-phenanthroline) have been prepared and their structures determined by X-ray diffraction techniques. Complex **1** is mononuclear whereas **2** and **3** are uniform chain compounds. The copper atoms in **1–3** are distorted square-pyramidal: two nitrogen atoms from the bidentate nitrogen heterocycle and two carboxylate oxygen atoms from the phenylmalonate ligand build the equatorial plane; the axial position is filled either by a water molecule (**1**) or a carboxylate oxygen atom from another phenylmalonate group (**2** and **3**). The values of the intrachain copper–copper separation through the phenylmalonate-carboxylate bridge in the

*anti-syn* conformation are 4.6853(7) (**2**) and 5.014(3) Å (**3**). The phenyl ring of the Phmal ligand in **1** produces an unusual intramolecular  $\pi$ – $\pi$  stacking interaction with the  $\text{Cu}^{\text{II}}$ –(aromatic 2,2'-bpy) chelate ring. Intrachain edge-to-face phenyl–pyridyl and offset phen–phen-type interactions occur in **2** and **3**, respectively. Magnetic susceptibility measurements of **2** and **3** in the temperature range 1.9–290 K show the occurrence of weak intrachain ferromagnetic interactions between the copper(II) ions through the phenylmalonate-carboxylate bridge [ $J = +0.10(1)$  (**2**) and  $+0.31(1)$   $\text{cm}^{-1}$  (**3**)]. These values are compared with those reported for malonate-containing copper(II) complexes with the same exchange pathway through the *anti-syn* carboxylate bridge.

(© Wiley-VCH Verlag GmbH & Co. KGaA, 69451 Weinheim, Germany, 2004)

## Introduction

The design of synthetic pathways to obtain systems with desired properties continues to be a challenge for inorganic chemists. In this context, a great interest has been devoted to the development of rational synthetic routes to novel polynuclear compounds of tuneable dimensionality which may have applications as molecule-based magnetic materials.<sup>[1–3]</sup> Many recent reports have focused on the synthesis and magneto-structural characterization of polymeric transition metal compounds using malonate (dianion of propanedioic acid,  $\text{H}_2\text{mal}$ ) as both blocking and bridging ligand.<sup>[4–10]</sup> In the framework of our research with malonate-containing metal complexes<sup>[8–13]</sup> we have been able to

prepare a large number of compounds with different structures and properties whose dimensionality goes from zero in the mononuclear species  $[\text{Cu}(\text{mal})(2,2'\text{-bpym})]^{[14]}$  (2,2'-bpym = 2,2'-bipyrimidine) to three in the compound  $[\text{Cu}(\text{mal})(\text{pyz})]_n$  (pyz = pyrazine).<sup>[15]</sup> The variety of the coordination modes of the malonate ligand in these compounds has been reviewed very recently.<sup>[9]</sup> From a magnetic point of view, the parameters governing the nature and magnitude of the magnetic interactions between copper(II) ions are the conformation of the bridge (*anti-anti*, *anti-syn*, *syn-syn*), the environment of the metal atom,<sup>[16,17]</sup> and the relative orientation of the malonate-carboxylate bridge with respect to the metal environment (equatorial-equatorial, equatorial-apical and apical-apical with relatively strong, weak and negligible interactions, respectively), in addition to the Cu–O(carboxylate) distances.<sup>[10]</sup>

More recently, we have started a systematic study on copper(II) complexation by substituted malonate ligands such as phenylmalonate (dianion of phenylmalonic acid,  $\text{H}_2\text{Phmal}$ ). One of the aims of this study is to analyze the influence that factors such as the withdrawing effect, the rigidity and the possibility of specific attractive interactions between phenyl rings can exert on the structure and magnetic coupling of phenylmalonate-containing copper(II) complexes.<sup>[17]</sup> In a previous work, we have observed that

<sup>[a]</sup> Laboratorio de Rayos X y Materiales Moleculares, Departamento de Física Fundamental II, Universidad de La Laguna, Av. Astrofísico Francisco Sánchez s/n, 38206 La Laguna (Tenerife), Spain  
E-mail: caruiz@ull.es

<sup>[b]</sup> Laboratorio de Rayos X y Materiales Moleculares, Departamento de Química Inorgánica, Universidad de La Laguna, Av. Astrofísico Francisco Sánchez s/n, 38204 La Laguna (Tenerife), Spain

<sup>[c]</sup> Departament de Química Inorgànica/Institut de Ciència Molecular, Facultat de Química, Universitat de València, Av. Dr. Moliner 50, 46100 Burjassot (Valencia), Spain

the complex  $[\{\text{Cu}(\text{H}_2\text{O})_3\}\{\text{Cu}(\text{Phmal})_2\}]_n$  has a layered structure induced by the phenyl groups and intralayer ferromagnetic couplings through phenylmalonate-carboxylate and -oxo bridges. Here we show how the structure and magnetic properties of this layered system are modified by the presence of coligands such as 2,2'-bipyridine (2,2'-bpy), 2,2'-bipyrimidine (2,2'-bpym) and 1,10-phenanthroline (phen). These are all aromatic nitrogen heterocycles that, in addition to their good coordinating ability (metal–ligand bonds), can interact with the phenyl ring of the Phmal group (supramolecular interactions), making this system very appropriate to illustrate the effects of both types of interactions.

We report herein the synthesis, crystallographic analysis and magnetic study of the copper(II) complexes of formula  $[\text{Cu}(2,2'\text{-bpy})(\text{Phmal})(\text{H}_2\text{O})]\cdot 2\text{H}_2\text{O}$  (**1**),  $[\{\text{Cu}(2,2'\text{-bpym})(\text{Phmal})\}]_n$  (**2**) and  $[\{\text{Cu}(\text{phen})(\text{Phmal})\}]_n\cdot 3n\text{H}_2\text{O}$  (**3**). Complex **1** is a magnetically isolated mononuclear species whereas **2** and **3** are uniform chains with intrachain ferromagnetic interactions.

## Results and Discussion

### Synthesis of the Complexes

Complexes **1–3** were prepared by reaction of stoichiometric amounts copper(II) phenylmalonate with the appropriate heterocyclic N-donor in a methanol water mixture. X-ray quality crystals of the mononuclear complex **1** and the chain compounds **2** and **3** were grown from concentrated solutions by slow solvent evaporation.

### Description of the Crystal Structures

#### $[\text{Cu}(2,2'\text{-bpy})(\text{Phmal})(\text{H}_2\text{O})]\cdot 2\text{H}_2\text{O}$ (**1**)

The structure of **1** consists of neutral  $[\text{Cu}(\text{Phmal})(2,2'\text{-bpy})(\text{H}_2\text{O})]$  mononuclear entities (Figure 1a) and crystallization water molecules. The molecular units are linked by hydrogen bonding involving the uncoordinated phenylmalonate oxygen atoms and the crystallization water molecules, with O...O distances ranging from 2.667(3) to 2.972(4) Å (see Table 1). A surprising two-dimensional (6,3) net results (Figure 2) which contributes to the stabilization of the whole structure. Adjacent layers are linked by weak offset  $\pi$ – $\pi$ -stacking interactions between pyridyl rings. The shortest offset angle between pyridyl rings is 28.5° while the shortest centroid–centroid contact is 3.966(4) Å, values which are slightly larger than the average values in  $\pi$ – $\pi$  interactions with pyridine-like groups previously reported.<sup>[18]</sup>

The molecular structure of **1** is remarkably similar to that of the recently reported<sup>[19,20]</sup> complexes  $[\text{Cu}(\text{Bzmal})(\text{phen})(\text{H}_2\text{O})]\cdot 3\text{H}_2\text{O}$  and  $[\text{Cu}(\text{Bzmal})(2,2'\text{-bpy})(\text{H}_2\text{O})]\cdot 2\text{H}_2\text{O}$  (Bzmal = 2-benzylmalonate) compounds. The phenyl rings of Bzmal and Phmal are located over the N–C–C–N–Cu chelate ring in the three complexes and metalloaromaticity was pointed out to be the

factor responsible for this structural feature.<sup>[19]</sup> A search in the Cambridge Structural Database has shown the existence of several compounds which present the same conformation (listed in Table 2). The value of the dihedral angle between the mean planes in complex **1** is larger (25.5°) than in the other compounds (1.2–14.5°) due to geometrical constraints that preclude the parallel arrangement of the phenyl group above the chelate ring. All the structures found in the search contain a ligand with the nitrogen atoms inside the aromatic rings (i.e. always 2,2'-bpy or phen but never *N,N'*-ethylenediamine). According to Janiak,<sup>[18]</sup> phenyl rings do not like to stack above each other but to adopt an offset (parallel displaced) arrangement, thus leading to C–H... $\pi$ -type interactions. Therefore, we suggest that this is responsible for the situation of the phenyl group above the chelate ring (i.e. displaced from the stacked position over the pyridyl groups). We can compare this structure with that of the reported mononuclear complex  $[\text{Cu}(2,2'\text{-bpy})(\text{mal})(\text{H}_2\text{O})]\cdot \text{H}_2\text{O}$ ,<sup>[30]</sup> where the monomeric units are distributed in bilayers in the *bc* plane through hydrogen bonds involving the malonate-carboxylate groups and the coordinated and uncoordinated water molecules. The hydrophobic interactions in **1** form layers of different hydrophilic character with the aromatic rings in one and the phenylmalonate oxygen atoms and water molecules in the other one. A remarkable difference between both compounds is the position of the methylene group: it is directed toward the coordinated water molecule in the malonate compound whereas the metalloaromaticity in the case of **1** causes the methylene C–H bond to point towards the opposite side of the coordinated water molecule.

Each copper atom in **1** exhibits a somewhat distorted square-pyramidal environment, with a  $\tau$  value<sup>[31]</sup> of 0.14. The copper atom is bound to two 2,2'-bpy nitrogen atoms [2.001(2) and 1.998(2) Å for Cu(1)–N(1) and Cu(1)–N(2), respectively] and to two carboxylate oxygen atoms from the Phmal ligand [1.954(2) and 1.933(2) Å for Cu(1)–O(2) and Cu(1)–O(4)] in the basal plane, and to a water molecule in the apical position [2.143(2) Å for Cu(1)–O(1w)]. The 2,2'-bpy and Phmal groups in **1** adopt a bidentate coordination mode, the values of the angles subtended at the copper atom by them being 80.53(8)° and 90.09(7)°, respectively. The 2,2'-bpy ligand is practically planar [the value of the dihedral angle between the mean pyridyl planes is 1.1(1)°] and its bond lengths and angles are in agreement with those reported for free 2,2'-bpy.<sup>[32]</sup> The Phmal group exhibits the boat conformation as in  $[\{\text{Cu}(\text{H}_2\text{O})_3\}\{\text{Cu}(\text{Phmal})_2\}]_n$ .<sup>[17]</sup> However, the Phmal group in this last compound simultaneously exhibits bidentate (through two oxygen atoms of the two carboxylate groups) and bis(monodentate) (through two *trans* carboxylate oxygen atoms from two Phmal ligands) coordination modes, leading to a layered structure. The  $[\text{Cu}(\text{Phmal})_2]^{2-}$  units in this compound tend also to align their aromatic rings in the same direction, preventing the occupation of one of the axial positions of the copper(II) coordination sphere, while the other apical site is filled by another  $[\text{Cu}(\text{Phmal})_2]^{2-}$  unit. This also occurs in **1** where the aromatic ring practically fills one of the axial

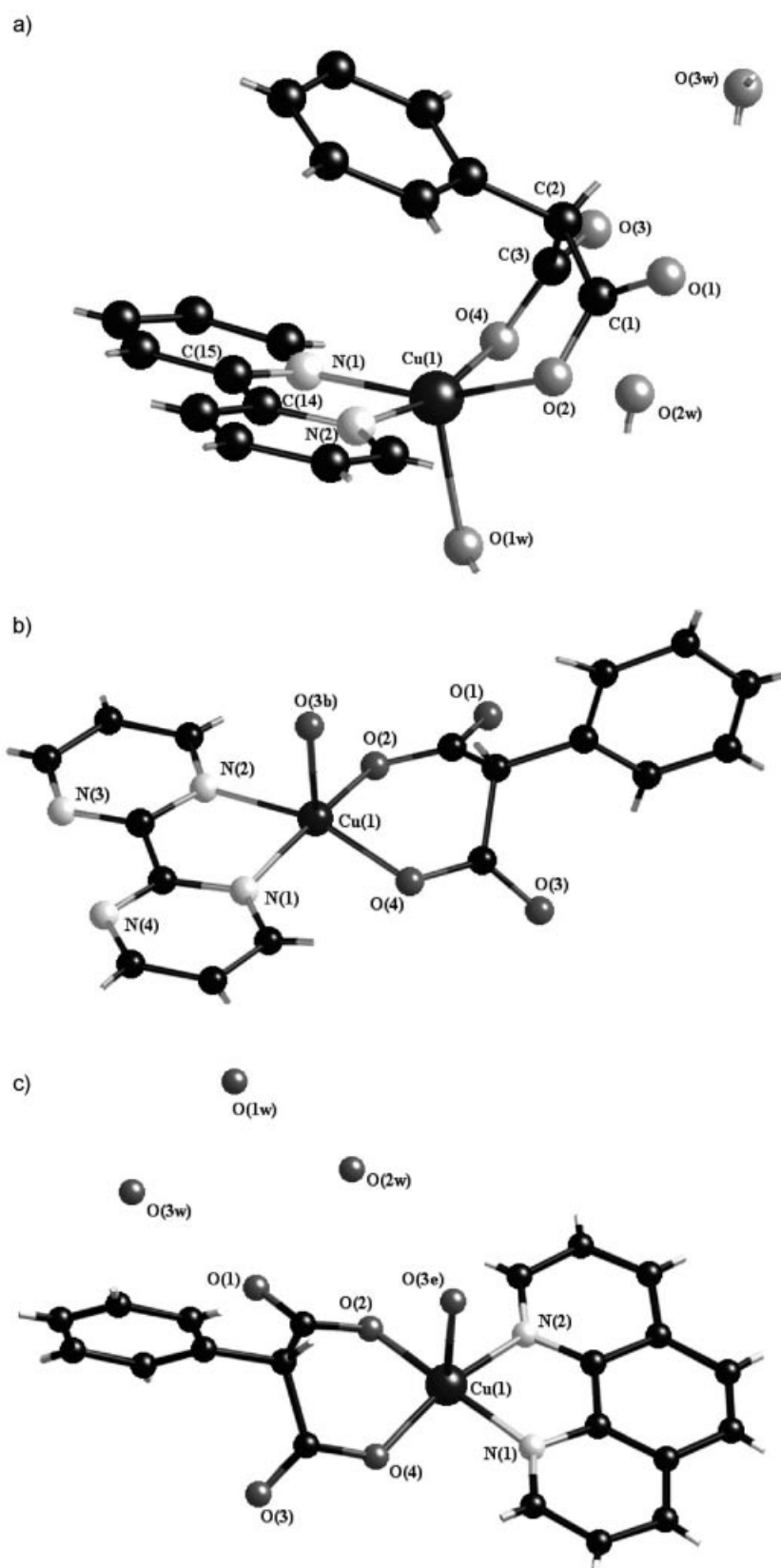


Figure 1. Asymmetric unit of  $[\text{Cu}(2,2'\text{-bpy})(\text{Phmal})(\text{H}_2\text{O})]\cdot 2\text{H}_2\text{O}$  (1) (a) and molecular fragments of  $[\{\text{Cu}(2,2'\text{-bpy})(\text{Phmal})\}]_n$  (2) (b) and  $[\{\text{Cu}(\text{phen})(\text{Phmal})\}]_n\cdot 3n\text{H}_2\text{O}$  (3) (c) with the numbering scheme

Table 1. Hydrogen bonds in complex **1**

| D–H...A <sup>[a]</sup> | D...A    | ∠D–H...A <sup>[b]</sup> | Symmetry operator <sup>[c]</sup> |
|------------------------|----------|-------------------------|----------------------------------|
| O(1w)–H(1wa)···O(2w)   | 2.667(3) | 170(4)                  | $x, y - 1, z + 1$                |
| O(1w)–H(1wb)···O(3)    | 2.735(3) | 172(4)                  | $x + 1/2, -y, -z + 5/2$          |
| O(2w)–H(2wa)···O(1)    | 2.881(4) | 172(6)                  | $x, y + 1/2, -z + 3/2$           |
| O(2w)–H(2wb)···O(3w)   | 2.763(4) | 171(4)                  | $x + 1, y, z$                    |
| O(3w)–H(3wa)···O(3)    | 2.972(4) | 167(5)                  | $x - 1/2, -y + 1/2, z - 1$       |
| O(3w)–H(3wb)···O(1)    | 2.815(3) | 158(5)                  | $x - 1/2, -y + 1, -z + 3/2$      |

<sup>[a]</sup> Values of the distances and angles in Å and °, respectively. <sup>[b]</sup> D = donor and A = acceptor. <sup>[c]</sup> Symmetry operation concerning the acceptor atom.

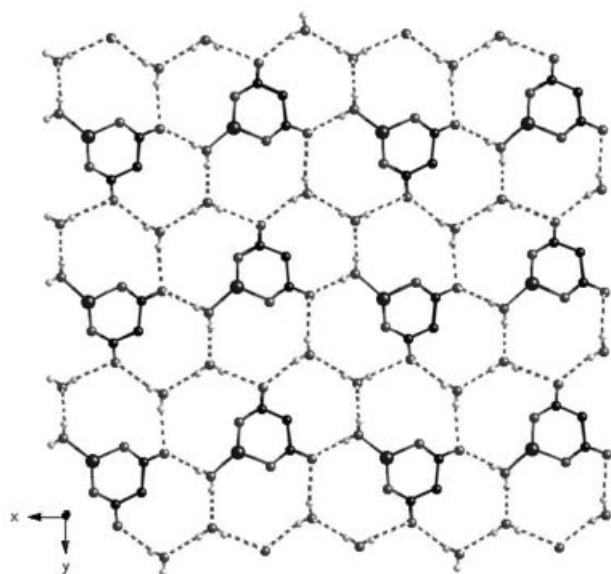


Figure 2. (6,3) pattern formed by hydrogen bonding involving the coordinated and crystallization water molecules and the malonate oxygen atoms; such a regular net contributes to the stabilization of the structure; the 2,2'-bpy ligands have been omitted for clarity

positions of the copper coordination sphere and the other one is occupied by a water molecule. The shortest intermolecular copper–copper separation in **1** is 7.6494(5) Å [Cu(1)–Cu(1a); (a) =  $-x + 2, -y, -z + 2$ ].

### $[Cu(2,2'\text{-bpy})(Phmal)]_n$ (**2**)

The structure of **2** consists of chains of [Cu(2,2'-bpy)(Phmal)] units that are linked through one phenylmalonate-carboxylate group in an *anti-syn* conformation (Figure 1b). These chains run parallel to the *a* axis and interact between themselves by means of  $\pi$ – $\pi$ - and C–H... $\pi$ -type interactions (Figure 3). There are two hydrophobic cavities where 2,2'-bpy molecules and the phenyl rings from the Phmal groups are constrained. The 2,2'-bpy groups are involved in  $\pi$ – $\pi$  interactions, with the shortest centroid–centroid contact being 3.798(6) Å and the shortest parallel displacement angle between pyrimidyl rings being 25.7°, values which are similar to the average ones observed in  $\pi$ – $\pi$  interactions with pyridine-like groups.<sup>[18]</sup> Weak C–H... $\pi$  interactions are also present between the phenyl rings and 2,2'-bpy groups inside the chains and between phenyl groups of different chains, with the shortest H...centroid distance being 2.86(4) Å, and C–H...centroid

Table 2. Stacking parameters of some compounds found in the Cambridge Structural Database with the same conformation as complex **1**

| Compound                                                                     | Stacking parameters <sup>[a]</sup> |                                        |                                         | Ref.      |
|------------------------------------------------------------------------------|------------------------------------|----------------------------------------|-----------------------------------------|-----------|
|                                                                              | $d(c_1 - c_2)$ [Å]/ $a$ [°]        | $d[\perp c_1 - P(2)]$ [Å]/ $\beta$ [°] | $d[\perp c_2 - P(1)]$ [Å]/ $\gamma$ [°] |           |
| [Cu(L1)(L2)]SbF <sub>6</sub> ·CH <sub>2</sub> Cl <sub>2</sub> <sup>[b]</sup> | 3.58/1.2                           | 3.49/13.1                              | 3.49/13.2                               | [21]      |
| [Cu(L3)(L4)(L5)]                                                             | 3.49/7.2                           | 3.45/14.3                              | 3.38/8.2                                | [22]      |
| [Cu(L3)(L4)](NO <sub>3</sub> ) <sub>2</sub> ·3H <sub>2</sub> O               | 3.50/10.2                          | 3.43/18.5                              | 3.32/11.4                               |           |
| catena-[Cu(L4)(L6)]ClO <sub>4</sub> ·H <sub>2</sub> O                        | 3.44/6.46                          | 3.37/8.0                               | 3.41/12.1                               | [23]      |
| [Cu(L7)(L8)H <sub>2</sub> O]BF <sub>4</sub> ·3H <sub>2</sub> O               | 3.39/10.1                          | 3.38/14.2                              | 3.29/4.3                                | [24]      |
| [Cu(L9)(L8)H <sub>2</sub> O]Cl·H <sub>2</sub> O                              | 3.53/14.5                          | 3.32/15.8                              | 3.39/19.7                               | [25]      |
| [Cu(L10)(L4)H <sub>2</sub> O]·3H <sub>2</sub> O                              | 3.49/2.1                           | 3.39/15.5                              | 3.36 /13.9                              | [19]      |
| [Cu(L10)(L8)H <sub>2</sub> O]·2H <sub>2</sub> O                              | 3.51/8.2                           | 3.37/10.7                              | 3.45/16.4                               | [20]      |
| [Cu(L11)(L8)H <sub>2</sub> O]NO <sub>3</sub> ·MeOH·H <sub>2</sub> O          | 3.48/5.2                           | 3.41/15.7                              | 3.35/11.3                               | [26]      |
| [Cu(L9)(L4)H <sub>2</sub> O]ClO <sub>4</sub> ·1.5H <sub>2</sub> O            | 3.38/8.8, 3.38/5.4                 | 3.31/16.6, 3.32/12.0                   | 3.24/11.8, 3.30/10.3                    | [27]      |
| [Cu(L12)(L4)Cl]·3H <sub>2</sub> O                                            | 3.45/6.7                           | 3.41/5.6                               | 3.44/9.2                                | [27]      |
| [Cu(L12)(L8)H <sub>2</sub> O]ClO <sub>4</sub>                                | 3.37/7.4                           | 3.35/13.2                              | 3.28/5.8                                | [28]      |
| [Cu(L9)(L13)H <sub>2</sub> O]ClO <sub>4</sub> ·H <sub>2</sub> O              | 3.42/3.7                           | 3.29/17.1                              | 3.27/16.1                               | [29]      |
| <b>1</b>                                                                     | 3.683/25.5                         | 3.152/31.5                             | 3.562/14.7                              | this work |

<sup>[a]</sup> P(1) = plane 1; P(2) = plane 2;  $c_1$  = centroid of P(1);  $c_2$  = centroid of P(2);  $a$  = angle between mean planes;  $\beta$  = angle between the normal of P(1) and P(2);  $\gamma$  = angle between the normal of P(2) and P(1). <sup>[b]</sup> L1 = (S,S)-2,6-bis(4-phenyl-2-oxazolin-2-yl)pyridine; L2 = benzoyloxyacetaldehyde; L3 = L-4,5-dihydroxyphenylalanine; L4 = 1,10-phenanthroline; L5 = *n*-propanol; L6 = L-tryptophanate; L7 = D,L-2,5-dihydroxytyrosine; L8 = 2,2'-bipyridine; L9 = L-tyrosinate; L10 = 2-benzylmalonate; L11 = L-3-iodotyrosinate; L12 = L-phenylalanine; L13 = 1,4,8,9-tetraazatriphenylene.



groups being almost collinear. The building units of the chain are rotated 90° through the normal axis of the planar 2,2'-bpym group in a twist fashion (i.e. odd units in the same position and even units rotated by 90°; Figure 3).

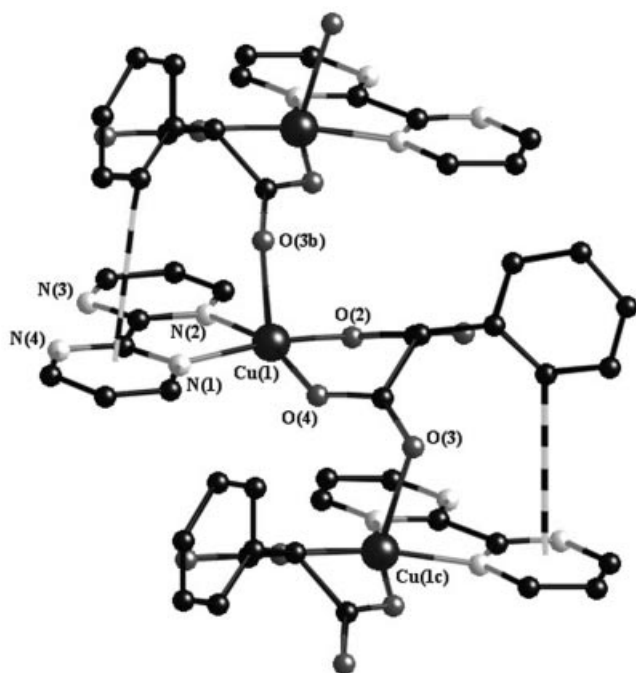


Figure 3. Fragment of the uniform chain of compound **2** showing the rotation of the units by 90° and the intrachain C–H... $\pi$  interaction (dashed line)

Each copper(II) atom has a slightly distorted square-pyramidal surrounding, the  $\tau$  value<sup>[31]</sup> being 0.08. Two nitrogen atoms of the 2,2'-bpym ligand [N(1) and N(2)] and two carboxylate oxygen atoms from the Phmal ligand [O(2) and O(4)] build the basal plane, whereas the symmetry-related carboxylate oxygen atom [O(3b); (b) =  $-1/2 + x, 1/2 - y, z$ ] occupies the apical position. The equatorial bond lengths vary in the range 1.900(3)–2.003(3) Å and the apical bond length is 2.262(3) Å. The 2,2'-bpym ligand is quasi planar [the dihedral angle between the pyrimidyl rings being 3.5(1)°] and it acts as a bidentate ligand through two [N(1) and N(2)] of its four nitrogen atoms. This coordination mode has previously been observed in several mono- and polynuclear 2,2'-bpym-containing copper(II) complexes.<sup>[14,33,34]</sup> The outer N(3) and N(4) 2,2'-bpym nitrogen atoms remain free, the N(3)···N(4) bite distance being somewhat longer [2.811(6) Å] than the N(1)···N(2) one [2.584(5) Å] due to the bidentate coordination of the 2,2'-bpym to the copper atom through N(1) and N(2). The inter-ring carbon–carbon bond length of 2,2'-bpym in **2** [1.480(6) Å for C(13)–C(14)] is close to that found in the free ligand in the solid state [1.497(1) and 1.502(4) Å].<sup>[35]</sup> As in **1**, the Phmal ligand adopts a boat conformation; the phenyl ring in **2** is placed perpendicular to the boat skeleton of the malonate in order to establish the weak intrachain C–H(phenyl)··· $\pi$  (pyrimidyl) interactions mentioned above. Finally, a comparison between the structure of **2** and that of the related mononuclear complex [Cu(2,2'-

bpym)(mal)(H<sub>2</sub>O)]·6H<sub>2</sub>O<sup>[14]</sup> shows once more the structural influence of the hydrophobic phenyl ring of the Phmal ligand. The complexation reaction between the preformed [Cu(2,2'-bpym)]<sup>2+</sup> species and the dicarboxylate mal and Phmal ligands affords neutral hydrated mononuclear (mal) and anhydrous chain (Phmal, **2**) compounds. The structure of the former exhibits extensive hydrogen bonds involving coordinated and uncoordinated water molecules, whereas carboxylate-bridging and supramolecular C–H··· $\pi$ -type interactions counterbalance the lack of hydrogen bonds in the latter.

The shortest intrachain copper–copper separation in **2** is 4.6853(7) Å [Cu(1)···Cu(1c); (c) =  $1/2 + x, 1/2 - y, z$ ], a value which is much shorter than the shortest interchain metal–metal distance [7.3634(8) Å for Cu(1)···Cu(1d); (d) =  $-x, 1 - y, 1 - z$ ].

### [{Cu(phen)(Phmal)}]<sub>n</sub>·3nH<sub>2</sub>O (**3**)

The structure of complex **3** consists of chains of [Cu(phen)(Phmal)] units linked through *anti-syn* carboxylate bridges and crystallization water molecules (Figure 1c). The chains run parallel to the *a* axis and they are linked by pairs along the [011] direction through hydrogen bonds involving the water molecules and noncoordinated carboxylate oxygen atoms [the values of the O···O distance range from 2.338(13) to 3.084(5) Å; Figure 4]. Intrachain offset  $\pi$ – $\pi$  interactions between phen ligands occur, the shortest centroid–centroid distance being 3.907(4) Å and parallel displacement angle being 28.6°, in agreement with previously reported values.<sup>[18]</sup>

Each copper(II) atom presents a slightly distorted square-pyramidal environment, with a  $\tau$  value<sup>[31]</sup> of 0.10. Two carboxylate oxygen atoms from the Phmal ligand [O(2) and O(4)] and the two nitrogen atoms of phen [N(1) and N(2)] form the equatorial plane, whereas a symmetry-related carboxylate oxygen atom [O(3e); (e) =  $x + 1, y, z$ ] occupies the apical position. The equatorial bond lengths vary in the range 1.913(2)–2.026(3) Å and the apical bond amounts to 2.314(3) Å. The angle subtended by the planar bidentate phen ligand at the copper atom is 81.86(11)°. The bond lengths and angles of the phen ligand in **3** agree well with those reported for the free molecule.<sup>[36]</sup> The conformation and coordination mode of the Phmal ligand in **3** are identical to those in **2**. However,  $\pi$ – $\pi$  stacking between phen ligands occurs in **3** instead of the C–H(phenyl)··· $\pi$ (N-heterocycle)-type interaction which occurs in **2**. Moreover, the [Cu(phen)(Phmal)] chain units in **3** are not rotated by 90°, in contrast to what it is observed in **2**; this modification of the crystal packing in **3** is due most likely to the crystallization water molecules which are present in the structure of the latter compound. A comparison between the structure of **3** and that of the mononuclear complex [Cu(phen)(mal)(H<sub>2</sub>O)]·1.5H<sub>2</sub>O<sup>[37]</sup> reveals that weak  $\pi$ – $\pi$  stacking interactions between phen ligands are present in both compounds. However, the mononuclear units are grouped by pairs in the malonato-containing complex, whereas a uniform chain is formed in **3**.

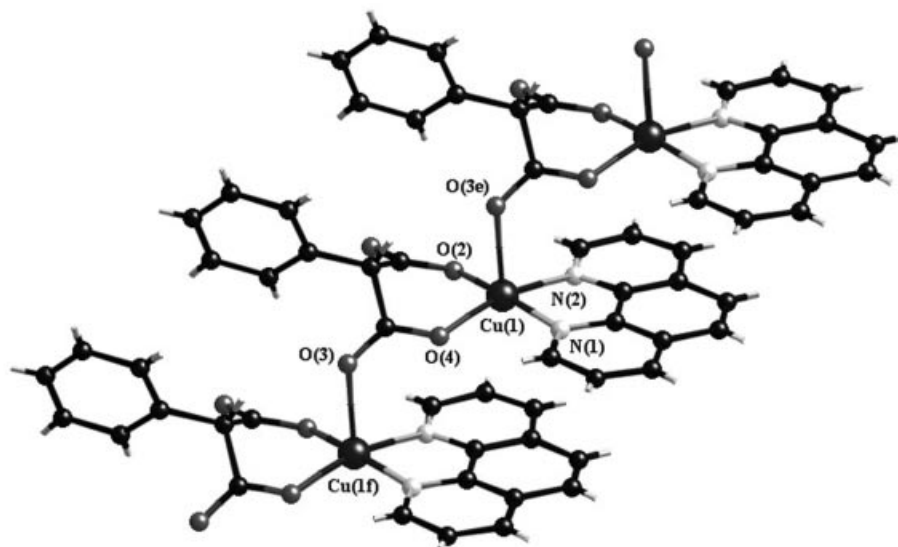


Figure 4. View of the uniform chain of compound **3** showing the phenylmalonate-carboxylate bridge in axial-equatorial *anti-syn* conformation

The shortest intrachain copper–copper separation is 5.014(3) Å [Cu(1)–Cu(1f); (f) =  $-1 + x, y, z$ ], a value which is much shorter than the shortest interchain metal–metal distance [7.5872(16) Å for Cu(1)–Cu(1g); (g) =  $-1/2 + x, 1/2 - y, -1/2 + z$ ].

### Magnetic Properties

The  $\chi_M T$  product of compound **1** obeys the Curie law in the 5–300 K temperature range. Its value is 0.365 cm<sup>3</sup>mol<sup>-1</sup>K, as expected for a magnetically isolated spin doublet of a copper(II) ion. This is in agreement with its mononuclear nature.

The magnetic properties of compounds **2** and **3** in the form of  $\chi_M T$  vs.  $T$  plots [ $\chi_M$  being the molar susceptibility per copper(II) ion] are shown in Figure 5;  $\chi_M T$  at room temperature is 0.41 cm<sup>3</sup>mol<sup>-1</sup>K for both compounds, a value which is as expected for a magnetically isolated spin doublet. Upon cooling,  $\chi_M T$  remains almost constant for compound **2** down to 10 K and then smoothly increases at lower temperatures to reach a value of 0.44 cm<sup>3</sup>mol<sup>-1</sup>K at 1.9 K;  $\chi_M T$  remains constant upon cooling down to 25 K for compound **3** and then it increases at lower temperatures reaching a value of 0.50 cm<sup>3</sup>mol<sup>-1</sup>K at 2.0 K. These features are indicative of an overall weak ferromagnetic coupling between the copper(II) ions in both compounds. Given that the structures of **2** and **3** consist of uniform chains, where the copper(II) ions are bridged by the phenylmalonate-carboxylate group, we analyzed their magnetic properties through the numerical expression proposed by Baker and Rushbrooke<sup>[38]</sup> for a ferromagnetic uniform copper(II) chain [Equation (1)]:

$$\chi_M = (N\beta^2 g^2 / 4kT)(A/B)^{2/3} \quad (1)$$

where

$$A = 1.0 + 5.7979916y + 16.902653y^2 + 29.376885y^3 + 29.832959y^4 + 14.036918y^5 \quad (2)$$

$$B = 1.0 + 2.7979916y + 7.0086780y^2 + 8.6538644y^3 + 4.5743114y^4 \quad (3)$$

and  $y = J/2kT$ , the spin Hamiltonian,  $H$ , being defined as  $\sum_i -J S_i S_{i+1}$ ;  $J$  is the intrachain magnetic-coupling parameter and  $N$ ,  $g$ , and  $\beta$  have their usual meanings.

The best fit obtained using a nonlinear regression analysis leads to  $J = +0.10(1)$  cm<sup>-1</sup>,  $g = 2.091(1)$  and  $R = 2.6 \times 10^{-5}$  for compound **2** and  $J = +0.31(1)$  cm<sup>-1</sup>,  $g = 2.092(1)$  and  $R = 2.1 \times 10^{-6}$  for compound **3** ( $R$  is the agreement factor defined as  $\sum_i [(\chi_M T)_{\text{obsd.}(i)} - (\chi_M T)_{\text{calcd.}(i)}]^2 / \sum_i [(\chi_M T)_{\text{obsd.}(i)}]^2$ ). The calculated curves match very well the experimental data in the whole temperature range, as seen in Figure 5. The fact that the magnetization data of **3** at 2.0 K (see inset of Figure 5) are clearly above the Brillouin function for a magnetically isolated spin doublet (this is also observed for the corresponding plot in **2**) confirms the ferromagnetic nature of the intrachain magnetic coupling.

The weak ferromagnetic interactions in **2** and **3** can be understood in a simple manner by analysing the exchange pathway which is involved and the relative arrangement of the magnetic orbitals. The unpaired electron of the copper(II) ion in **2** and **3** (square-pyramidal environment) lies in the equatorial plane [N(1)N(2)O(2)O(4)] and it is defined by a  $d_{x^2-y^2}$ -type magnetic orbital [the  $x$  and  $y$  axes corre-

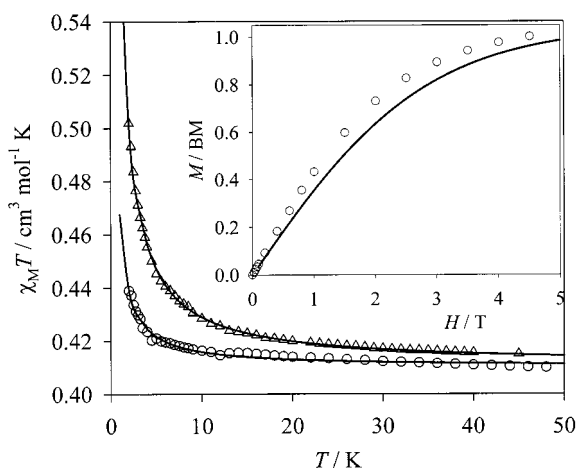
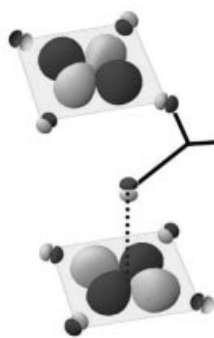


Figure 5. Experimental temperature dependence of the  $\chi_M T$  product of **2** (circles) and **3** (triangles) at  $T < 50$  K; (—) curves calculated from Equation (1); the inset shows the magnetization versus  $H$  plot for **3** at 2.0 K, experimental data (circles), (—) Brillouin function for a magnetically isolated spin doublet with  $g = 2.09$

sponding roughly to the equatorial bonds to the copper atom]. The O(4)C(3)O(3) carboxylate bridge provides the intrachain exchange pathway in **2** and **3**: it links one equatorial position from Cu(1) [O(4)] with the axial one [O(3)] at Cu(1c) (**2**) and Cu(1f) (**3**) (see Scheme 1) adopting the *anti-syn* bridging mode. This exchange pathway produces a very poor overlap between the magnetic orbitals due to the weak spin density in the apical site.<sup>[39]</sup> Thus, the antiferromagnetic contribution, which is proportional to the square of the overlap between the magnetic orbitals, is minimized and the resulting magnetic coupling is most likely ferromagnetic, as observed.<sup>[40]</sup>



Scheme 1

Previous examples of carboxylate-(*anti-syn*)-bridged copper(II) complexes with an axial-equatorial exchange pathway exhibit ferromagnetic couplings with values of  $J$  ranging from  $+0.05$  to  $+1.9$   $\text{cm}^{-1}$  (see Table 3).<sup>[8,10,16,41–43]</sup> The intensity of the magnetic coupling is affected by the Cu–O(axial) distance and the distortion of the metal environment — the longer the distance and the greater the distortion, the weaker the coupling is. The values of  $J$  for **2** and **3** fall in this range, but they are smaller than those with similar structural parameters [distortion and Cu–O(axial) distance]. The low value observed for the coupling constant

for **2** [ $J = +0.10(1)$   $\text{cm}^{-1}$ ] could be due to the greater value of the angle between the apical-oxygen-to-copper vector and the normal to the equatorial mean plane of the copper atom ( $7^\circ$  in **2** and only  $3.6^\circ$  in **3**). In general, this shift influences the effectiveness of the bridge in the transmission of the magnetic coupling because it modifies the overlap between the magnetic orbitals.

Another interesting point looking at the results listed in Table 3 concerns compounds **3** and  $[\{\text{Cu}(\text{mal})(\text{Im})\}]_n$ . Although the structural parameters of **3** are similar to those of  $[\{\text{Cu}(\text{mal})(\text{Im})\}]_n$ , the value of the ferromagnetic coupling for **3** is somewhat smaller. Most likely, the carboxylate group of the phenylmalonate is less effective in the transmission of the magnetic coupling than the carboxylate group of the malonate ligand. The magnetic coupling is essentially an electronic effect and the phenylene ring of the phenylmalonate exerts an electron-withdrawing effect that delocalizes some electron density of the copper(II) towards the aromatic ring, decreasing the electronic delocalization towards the carboxylate bridge. The decrease of the electron delocalization towards the bridge would decrease the size of the magnetic coupling. This could be one of the factors to account for the weaker magnetic interaction between the copper(II) ions in **3** (and also in **2**) through the phenylmalonate-carboxylate bridge with respect to the malonate-carboxylate one.

## Conclusions

Three new compounds have been prepared in which the phenylmalonate ligand acts either as blocking (**1**) or as bridging ligand (**2** and **3**). Weak interactions (hydrogen bonding and  $\pi$ – $\pi$  stacking) govern the structure of the compounds leading to molecular (**1**) and one-dimensional (**2** and **3**) structures. A comparison with the related malonato-containing complexes reveals that the influence of the phenyl group in the Phmal compounds is decisive:  $[\text{Cu}(2,2'\text{-bpy})(\text{mal})(\text{H}_2\text{O})]\cdot\text{H}_2\text{O}$  presents different conformation and crystal packing of the mononuclear units from those in compound **1**; compounds **2** and **3** are uniform chains whereas the malonato-containing copper(II) complexes of 2,2'-bpym and phen are mononuclear compounds. The nature of the magnetic coupling between copper(II) ions through the phenylmalonate-carboxylate bridge (ferromagnetic) is the same as that through the malonate-carboxylate, but its magnitude is somewhat smaller, probably due to the electron-withdrawing effect which is exerted by the phenyl ring. In the near future, magneto-structural studies on phenylmalonate-containing copper(II) complexes will be pursued to check this observation and to gain further insights into the structural possibilities they provide.

## Experimental Section

**General:** Phenylmalonic acid ( $\text{H}_2\text{Phmal}$ ), copper(II) acetate hydrate ( $[\text{Cu}(\text{CH}_3\text{COO})_2\cdot\text{H}_2\text{O}]$ ), 2,2'-bipyridine (2,2'-bpy), 2,2'-bipyrim-

Table 3. Selected magneto-structural data for some (malonate-/phenylmalonate-)carboxylate-bridged copper(II) complexes

| Compound <sup>[a]</sup>                                                                                    | Carboxylate pathway | Cu–(O)ap | $\tau^{[31]}$ Cu1/Cu2                  | $J$ [cm <sup>-1</sup> ] <sup>[b]</sup> | Ref.      |
|------------------------------------------------------------------------------------------------------------|---------------------|----------|----------------------------------------|----------------------------------------|-----------|
| [Cu(H <sub>2</sub> O) <sub>4</sub> ][Cu(mal) <sub>2</sub> (H <sub>2</sub> O) <sub>2</sub> ]                | equatorial-apical   | 2.383    | oct <sup>[c]</sup> /0.05               | +1.8                                   | [8]       |
| [Cu(H <sub>2</sub> O) <sub>4</sub> ][Cu(mal) <sub>2</sub> (H <sub>2</sub> O)] <sup>2+</sup>                | equatorial-apical   | 2.381    | oct <sup>[c]</sup> /0.12               | +1.2                                   | [8]       |
| [{Cu(H <sub>2</sub> O) <sub>3</sub> } <sub>2</sub> {Cu(mal) <sub>2</sub> (H <sub>2</sub> O)}] <sub>n</sub> | equatorial-apical   | 2.185    | 0.24/0.28                              | +1.9                                   | [8]       |
| [Cu(Im) <sub>2</sub> (mal)] <sub>n</sub>                                                                   | equatorial-apical   | 2.394    | 0.02/0.02                              | +1.6                                   | [16]      |
| [Cu(2-MeIm) <sub>2</sub> (mal)] <sub>n</sub>                                                               | equatorial-apical   | 2.270    | 0.18/0.18                              | +0.4                                   | [16]      |
| {(H <sub>2</sub> bpe)[Cu(mal) <sub>2</sub> ]} <sub>n</sub> ·4nH <sub>2</sub> O                             | equatorial-apical   | 2.611    | oct <sup>[c]</sup> /oct <sup>[c]</sup> | +0.049                                 | [41]      |
| <b>2</b>                                                                                                   | equatorial-apical   | 2.262    | 0.08/0.08                              | +0.10                                  | this work |
| <b>3</b>                                                                                                   | equatorial-apical   | 2.314    | 0.10/0.10                              | +0.31                                  | this work |

<sup>[a]</sup> Abbreviations: Im = imidazole; 2-MeIm = 2-methylimidazole; bpe = 1,2-bis(4-pyridyl)ethylene. <sup>[b]</sup> Values of the coupling constant ( $J$ ). <sup>[c]</sup> Octahedral.

idine (2,2'-bpym), 1,10-phenanthroline (phen) and methanol were purchased from Aldrich and used as received. Elemental analyses (C, H and N) were performed with an EA 1108 CHNS-O micro-analytical analyzer. IR spectra (450–4000 cm<sup>-1</sup>) were recorded with a Bruker IF S55 spectrophotometer with the sample prepared as KBr pellets. Magnetic susceptibility measurements on polycrystalline samples of compounds **1–3** were carried out in the temperature range 1.9–290 K with a Quantum Design SQUID magnetometer. Diamagnetic corrections of the constituent atoms were estimated from Pascal's constants<sup>[44]</sup> as  $-228 \times 10^{-6}$ ,  $-189 \times 10^{-6}$  and  $-251 \times 10^{-6}$  cm<sup>3</sup>·mol<sup>-1</sup> for compounds **1**, **2** and **3**, respectively. Experimental susceptibilities were also corrected for the temperature-independent paramagnetism ( $60 \times 10^{-6}$  cm<sup>3</sup>·mol<sup>-1</sup> per Cu<sup>II</sup>) and the magnetization of the sample holder.

**Synthesis:** The general procedure to prepare compounds **1–3** starts with the preparation of an aqueous solution (15 mL) of copper(II) phenylmalonate (1 mmol) which was prepared by adding phenylmalonic acid (0.180 g, 1 mmol) to a warm methanolic solution (20 mL) of copper(II) acetate (1 mmol, 0.200 g) under continuous

stirring. The resulting pale-blue solution was concentrated to dryness in a rotary evaporator. The green solid obtained was washed thoroughly with acetone to remove the acetic acid and then the green product was dissolved in water (15 mL).

**[Cu(2,2'-bpy)(Phmal)(H<sub>2</sub>O)]·2H<sub>2</sub>O (1):** 2,2'-Bipyridine (0.156 g, 1 mmol) was dissolved in methanol/water (50:50, 10 mL) and then an aqueous solution (15 mL) of copper(II) phenylmalonate was added whilst stirring. The solution was allowed to concentrate in a fumehood at room temperature. Prismatic blue single crystals of **1** had grown after a few days. Yield: 0.34 g (75% based on copper). C<sub>19</sub>H<sub>20</sub>CuN<sub>2</sub>O<sub>7</sub> (451.55): calcd. C 50.49, H 4.43, N 6.20; found C 50.41, H 4.40, N 6.05. IR (KBr):  $\nu$ (C–H, =C–H): 3090, 3062, 2950, 2923;  $\nu$ (C=C, COO): 1637, 1605, 1590, 1577, 1445, 1409 cm<sup>-1</sup>.

**[{Cu(2,2'-bpym)(Phmal)}]<sub>n</sub> (2):** Compound **2** was prepared similarly to **1** but using a solution of 2,2'-bipyrimidine (0.158 g, 1 mmol) instead of 2,2'-bipyridine. Prismatic greenish-blue single crystals of **2** were grown after a few days. Yield: 0.24 g (60% based on copper).

Table 4. Crystallographic data for complexes **1–3**

|                                                              | <b>1</b>                                                             | <b>2</b>                                                            | <b>3</b>                                                           |
|--------------------------------------------------------------|----------------------------------------------------------------------|---------------------------------------------------------------------|--------------------------------------------------------------------|
| Empirical formula                                            | C <sub>19</sub> H <sub>20</sub> CuN <sub>2</sub> O <sub>7</sub>      | C <sub>17</sub> H <sub>12</sub> CuN <sub>4</sub> O <sub>4</sub>     | C <sub>21</sub> H <sub>20</sub> CuN <sub>2</sub> O <sub>7</sub>    |
| Formula mass                                                 | 451.91                                                               | 399.85                                                              | 475.88                                                             |
| Crystal system                                               | orthorhombic                                                         | orthorhombic                                                        | monoclinic                                                         |
| Space group                                                  | <i>Pcab</i>                                                          | <i>Pcab</i>                                                         | <i>P2<sub>1</sub>/n</i>                                            |
| <i>a</i> [Å]                                                 | 14.6113(5)                                                           | 8.9331(3)                                                           | 5.014(3)                                                           |
| <i>b</i> [Å]                                                 | 16.1928(4)                                                           | 11.7577(3)                                                          | 26.403(3)                                                          |
| <i>c</i> [Å]                                                 | 16.5067(5)                                                           | 29.8171(4)                                                          | 14.685(3)                                                          |
| $\beta$ [°]                                                  | 90                                                                   | 90                                                                  | 94.75                                                              |
| <i>V</i> [Å <sup>3</sup> ]                                   | 3905.5(2)                                                            | 3131.77(14)                                                         | 1937.3(12)                                                         |
| <i>Z</i>                                                     | 8                                                                    | 8                                                                   | 4                                                                  |
| $\mu$ (Mo- <i>K<math>\alpha</math></i> ) [cm <sup>-1</sup> ] | 11.63                                                                | 14.28                                                               | 11.76                                                              |
| <i>T</i> [K]                                                 | 293(2)                                                               | 293(2)                                                              | 293(2)                                                             |
| $\rho_{\text{calcd}}$ [gcm <sup>-3</sup> ]                   | 1.537                                                                | 1.696                                                               | 1.611                                                              |
| $\lambda$ [Å]                                                | 0.71073                                                              | 0.71073                                                             | 0.71073                                                            |
| Index ranges                                                 | $-18 \leq h \leq 20$<br>$-22 \leq k \leq 22$<br>$-23 \leq l \leq 13$ | $-12 \leq h \leq 9$<br>$-16 \leq k \leq 16$<br>$-41 \leq l \leq 41$ | $-7 \leq h \leq 5$<br>$-32 \leq k \leq 37$<br>$-13 \leq l \leq 20$ |
| Independent reflections ( $R_{\text{int}}$ )                 | 5537 (0.060)                                                         | 4545 (0.132)                                                        | 5284 (0.051)                                                       |
| Observed reflections [ $I > 2\sigma(I)$ ]                    | 3552                                                                 | 2985                                                                | 2872                                                               |
| Parameters                                                   | 343                                                                  | 283                                                                 | 336                                                                |
| Goodness-of-fit                                              | 1.043                                                                | 1.138                                                               | 1.012                                                              |
| $R$ [ $I > 2\sigma(I)$ ]                                     | 0.0429                                                               | 0.0742                                                              | 0.0591                                                             |
| $R_w$ [ $I > 2\sigma(I)$ ]                                   | 0.0837                                                               | 0.1462                                                              | 0.1098                                                             |
| $R$ (all data)                                               | 0.0866                                                               | 0.1217                                                              | 0.1376                                                             |
| $R_w$ (all data)                                             | 0.1004                                                               | 0.1615                                                              | 0.1302                                                             |

C<sub>17</sub>H<sub>12</sub>CuN<sub>4</sub>O<sub>4</sub> (399.55): calcd. C 51.05, H 3.00, N 14.02; found C 51.20, H 3.14, N 14.10. IR (KBr):  $\nu(\text{C-H}, =\text{C-H})$ : 3057, 3027, 2925;  $\nu(\text{C=C}, \text{COO})$ : 1646, 1606, 1578, 1557, 1420, 1403 cm<sup>-1</sup>.

**[{Cu(phen)(Phmal)}]<sub>n</sub>·3nH<sub>2</sub>O (3)**: Compound **3** was prepared similarly to **1** but using a solution of 1,10-phenanthroline (0.180 g, 1 mmol) instead of 2,2'-bipyridine. Prismatic blue single crystals of **3** separated from the mother liquor on standing at room temperature after a week. Yield: 0.38 g (80% based on copper). C<sub>21</sub>H<sub>20</sub>CuN<sub>2</sub>O<sub>7</sub> (475.55): calcd. C 52.99, H 4.21, N 5.89; found C 52.79, H 4.32, N 5.80. IR (KBr):  $\nu(\text{C-H}, =\text{C-H})$ : 3060, 3030, 2923, 2850;  $\nu(\text{C=C}, \text{COO})$ : 1628, 1615, 1595, 1576, 1425, 1405 cm<sup>-1</sup>.

**X-ray Crystallographic Study**: Single crystals of **1–3** were used for data collection with a Nonius KappaCCD diffractometer. The data collection was carried out at 293 K using graphite-monochromated Mo-K $\alpha$  radiation ( $\lambda = 0.71073 \text{ \AA}$ ). A summary of the crystallographic data and structure refinement is given in Table 4 and selected interatomic distances and angles are listed in Table 5. The structures were solved by direct methods and refined with a full-matrix least-squares technique on  $F^2$  using the SHELXL-97<sup>[45]</sup> program included in the WINGX<sup>[46]</sup> software package. All non-hydrogen atoms were refined anisotropically. All hydrogen atoms of structures **1–3** were located from difference maps and refined with isotropic temperature factors, except those of the water molecules of complex **3**. The final geometrical calculations and graphical ma-

Table 5. Selected bond lengths [ $\text{\AA}$ ] and bond angles [ $^\circ$ ] for compounds **1–3**<sup>[a]</sup>

| <b>1</b>         |            |                  |            |
|------------------|------------|------------------|------------|
| Cu(1)–O(2)       | 1.954(2)   | Cu(1)–N(2)       | 1.998(2)   |
| Cu(1)–O(4)       | 1.933(2)   | Cu(1)–O(1w)      | 2.143(2)   |
| Cu(1)–N(1)       | 2.001(2)   |                  |            |
| O(2)–Cu(1)–O(4)  | 90.09(7)   | O(4)–Cu(1)–N(2)  | 166.47(8)  |
| O(2)–Cu(1)–N(1)  | 158.23(8)  | O(4)–Cu(1)–O(1w) | 97.46(9)   |
| O(2)–Cu(1)–N(2)  | 92.89(8)   | N(1)–Cu(1)–N(2)  | 80.53(8)   |
| O(2)–Cu(1)–O(1w) | 96.85(9)   | N(1)–Cu(1)–O(1w) | 104.38(9)  |
| O(4)–Cu(1)–N(1)  | 91.89(8)   | N(2)–Cu(1)–O(1w) | 95.29(9)   |
| <b>2</b>         |            |                  |            |
| Cu(1)–O(2)       | 1.922(3)   | Cu(1)–N(2)       | 1.996(3)   |
| Cu(1)–O(4)       | 1.900(3)   | Cu(1)–O(3b)      | 2.262(3)   |
| Cu(1)–N(1)       | 2.003(3)   |                  |            |
| O(2)–Cu(1)–O(4)  | 92.93(11)  | O(4)–Cu(1)–N(2)  | 162.02(14) |
| O(2)–Cu(1)–N(1)  | 166.90(14) | O(4)–Cu(1)–O(3b) | 100.05(12) |
| O(2)–Cu(1)–N(2)  | 93.31(13)  | N(1)–Cu(1)–N(2)  | 80.53(13)  |
| O(2)–Cu(1)–O(3b) | 106.32(12) | N(1)–Cu(1)–O(3b) | 85.78(12)  |
| O(4)–Cu(1)–N(1)  | 89.79(12)  | N(2)–Cu(1)–O(3b) | 94.33(12)  |
| <b>3</b>         |            |                  |            |
| Cu(1)–O(2)       | 1.913(2)   | Cu(1)–N(2)       | 2.026(3)   |
| Cu(1)–O(4)       | 1.934(2)   | Cu(1)–O(3e)      | 2.314(2)   |
| Cu(1)–N(1)       | 1.992(3)   |                  |            |
| O(2)–Cu(1)–O(4)  | 92.80(9)   | O(4)–Cu(1)–N(2)  | 162.66(10) |
| O(2)–Cu(1)–N(1)  | 168.52(11) | O(4)–Cu(1)–O(3e) | 101.46(9)  |
| O(2)–Cu(1)–N(2)  | 90.63(10)  | N(1)–Cu(1)–N(2)  | 81.86(11)  |
| O(2)–Cu(1)–O(3e) | 92.74(10)  | N(1)–Cu(1)–O(3e) | 96.59(10)  |
| O(4)–Cu(1)–N(1)  | 91.90(10)  | N(2)–Cu(1)–O(3e) | 95.35(10)  |

<sup>[a]</sup> Estimated standard deviations in the last significant digits are given in parentheses. Symmetry codes: (b)  $-1/2 + x, 1/2 - y, z$ ; (e)  $x + 1, y, z$ .

nipulations were carried out with PARST97<sup>[47]</sup> and CRYSTALMAKER<sup>[48]</sup> programs. CCDC-235074 (**1**), -235075 (**2**) and -235076 (**3**) contain the supplementary crystallographic data for this paper. These data can be obtained free of charge at [www.ccdc.cam.ac.uk/conts/retrieving.html](http://www.ccdc.cam.ac.uk/conts/retrieving.html) [or from the Cambridge Crystallographic Data Centre, 12 Union Road, Cambridge CB2 1EZ, UK; Fax: (internat.) + 44-1223-336-033; E-mail: [deposit@ccdc.cam.ac.uk](mailto:deposit@ccdc.cam.ac.uk)].

## Acknowledgments

This work was supported by the Ministerio Español de Ciencia y Tecnología (project BQU2001-3794) and the Gobierno Autónomo de Canarias (project PI2002/175). J. P. acknowledges the Ministerio Español de Educación, Cultura y Deporte for a predoctoral fellowship (ref. AP2001-3322).

- <sup>[1]</sup> D. Gatteschi, O. Kahn, J. S. Miller, F. Palacio, *Magnetic Molecular Materials*, Kluwer Academic Publishers, Dordrecht, The Netherlands, 1991.
- <sup>[2]</sup> *Polyhedron* **2001**, *20* (11–14) entire issue.
- <sup>[3]</sup> *Polyhedron* **2003**, *22* (14–17) entire issue.
- <sup>[4]</sup> D. Chattopadhyay, S. K. Chattopadhyay, P. R. Lowe, C. H. Schwalke, S. K. Mazumber, A. Rana, S. Ghosh, *J. Chem. Soc., Dalton Trans.* **1993**, 913.
- <sup>[5]</sup> I. Gil de Muro, F. A. Mautner, M. Insausti, L. Lezama, M. I. Arriortua, T. Rojo, *Inorg. Chem.* **1998**, *37*, 3243.
- <sup>[6]</sup> C. Ruiz-Pérez, J. Sanchiz, M. Hernández-Molina, F. Lloret, M. Julve, *Inorg. Chim. Acta* **2000**, *298*, 202.
- <sup>[7]</sup> C. Ruiz-Pérez, M. Hernández-Molina, P. Lorenzo-Luis, F. Lloret, J. Cano, M. Julve, *Inorg. Chem.* **2000**, *39*, 3845.
- <sup>[8]</sup> C. Ruiz-Pérez, J. Sanchiz, M. H. Molina, F. Lloret, M. Julve, *Inorg. Chem.* **2000**, *39*, 1363.
- <sup>[9]</sup> Y. Rodríguez-Martín, M. Hernández-Molina, F. S. Delgado, J. Pasán, C. Ruiz-Pérez, J. Sanchiz, F. Lloret, M. Julve, *CrystEngComm* **2002**, *4*, 522.
- <sup>[10]</sup> J. Pasán, F. S. Delgado, Y. Rodríguez-Martín, M. Hernández-Molina, C. Ruiz-Pérez, J. Sanchiz, F. Lloret, M. Julve, *Polyhedron* **2003**, *22*, 2143.
- <sup>[11]</sup> Y. Rodríguez-Martín, M. Hernández-Molina, J. Sanchiz, C. Ruiz-Pérez, F. Lloret, M. Julve, *Dalton Trans.* **2003**, 2359.
- <sup>[12]</sup> C. Ruiz-Pérez, M. Hernández-Molina, J. Sanchiz, T. López, F. Lloret, M. Julve, *Inorg. Chim. Acta* **2000**, *298*, 245.
- <sup>[13]</sup> C. Ruiz-Pérez, Y. Rodríguez-Martín, M. Hernández-Molina, F. S. Delgado, J. Pasán, J. Sanchiz, F. Lloret, M. Julve, *Polyhedron* **2003**, *22*, 2111.
- <sup>[14]</sup> Y. Rodríguez-Martín, J. Sanchiz, C. Ruiz-Pérez, F. Lloret, M. Julve, *Inorg. Chim. Acta* **2001**, *326*, 20.
- <sup>[15]</sup> Y. Rodríguez-Martín, M. Hernández-Molina, F. S. Delgado, J. Pasán, C. Ruiz-Pérez, J. Sanchiz, F. Lloret, M. Julve, *CrystEngComm* **2002**, *4*, 440.
- <sup>[16]</sup> J. Sanchiz, Y. Rodríguez-Martín, C. Ruiz-Pérez, A. Mederos, F. Lloret, M. Julve, *New J. Chem.* **2002**, *26*, 1624–1628.
- <sup>[17]</sup> J. Pasán, J. Sanchiz, C. Ruiz-Pérez, F. Lloret, M. Julve, *New J. Chem.* **2003**, *27*, 1557.
- <sup>[18]</sup> C. Janiak, *J. Chem. Soc., Dalton Trans.* **2000**, 3885.
- <sup>[19]</sup> A. Castiñeiras, A. G. Sicilia-Zafra, J. M. González-Pérez, D. Choquecillo-Lazarte, J. Niclós-Gutiérrez, *Inorg. Chem.* **2003**, *41*, 6956.
- <sup>[20]</sup> W. Guan, J. Y. Sun, X. D. Zhang, Q. T. Liu, *Chem. Res. Chin. Univ.* **1998**, *19*, 5.
- <sup>[21]</sup> D. A. Evans, M. C. Kozlowski, J. A. Murry, C. S. Burgey, K. R. Campos, B. T. Connell, R. T. Staples, *J. Am. Chem. Soc.* **1999**, *121*, 669.
- <sup>[22]</sup> S. Suzuki, K. Yamaguchi, N. Nakamura, Y. Tagawa, H. Kuma, T. Kawamoto, *Inorg. Chim. Acta* **1998**, *283*, 260.

- [23] H. Masuda, O. Matsumoto, A. Odani, O. Yamauchi, *J. Chem. Soc. Jpn.* **1988**, 783.
- [24] N. Nakamura, T. Kohzuma, H. Kuma, S. Suzuki, *J. Am. Chem. Soc.* **1992**, *114*, 6550.
- [25] X. Solans, L. Ruiz-Ramírez, A. Martínez, L. Gasque, R. Moreno-Esparza, *Acta Crystallogr., Sect. C* **1992**, *48*, 1785.
- [26] F. Zhang, T. Yajima, H. Masuda, A. Odani, O. Yamauchi, *Inorg. Chem.* **1997**, *36*, 5777.
- [27] T. Sugimori, H. Masuda, N. Ohata, K. Koiwai, A. Odani, O. Yamauchi, *Inorg. Chem.* **1997**, *36*, 576.
- [28] P. S. Subramanian, E. Suresh, P. Dastidar, S. Waghmode, D. Srinivas, *Inorg. Chem.* **2001**, *40*, 4291.
- [29] X.-Y. Le, M.-L. Tong, Y.-L. Fu, L.-N. Ji, *Acta Chim. Sinica* **2002**, *60*, 367.
- [30] E. Suresh, M. M. Bhadbhade, *Acta Crystallogr., Sect. C* **1997**, *53*, 193.
- [31] A. W. Addison, T. N. Rao, J. Reedijk, J. van Rijn, G. C. Verschoor, *J. Chem. Soc., Dalton Trans.* **1984**, 1349.
- [32] L. L. Merrit, E. D. Schroeder, *Acta Crystallogr.* **1956**, *9*, 801.
- [33] [33a] G. de Munno, G. Bruno, M. Julve, M. Romeo, *Acta Crystallogr., Sect. C* **1990**, *46*, 1828. [33b] L. W. Morgan, W. T. Pennington, J. D. Petersen, R. R. Ruminski, D. W. Bennet, J. S. Rommel, *Acta Crystallogr., Sect. C* **1992**, *48*, 163. [33c] G. De Munno, M. Julve, M. Verdager, G. Bruno, *Inorg. Chem.* **1993**, *32*, 561. [33d] G. De Munno, M. Julve, F. Nicolò, F. Lloret, J. Faus, R. Ruiz, E. Sinn, *Angew. Chem. Int. Ed. Engl.* **1993**, *32*, 613. [33e] I. Castro, J. Sletten, L. K. Glaerum, F. Lloret, J. Faus, M. Julve, *J. Chem. Soc., Dalton Trans.* **1994**, 2777. [33f] I. Castro, J. Sletten, L. K. Glaerum, J. Cano, F. Lloret, J. Faus, M. Julve, *J. Chem. Soc., Dalton Trans.* **1995**, 3207. [33g] S. Decurtins, H. W. Schmalle, P. Schneuwly, L. M. Zheng, *Acta Crystallogr., Sect. C* **1996**, *52*, 561.
- [34] [34a] I. Castro, M. Julve, G. De Munno, G. Bruno, J. A. Real, F. Lloret, J. Faus, *J. Chem. Soc., Dalton Trans.* **1992**, 1739. [34b] M. Julve, M. Verdager, G. De Munno, J. A. Real, G. Bruno, *Inorg. Chem.* **1993**, *32*, 795. [34c] J. A. Real, G. De Munno, R. Chiappetta, M. Julve, F. Lloret, Y. Journaux, J. C. Colin, G. Blondin, *Angew. Chem. Int. Ed. Engl.* **1994**, *33*, 1184. [34d] G. De Munno, M. Julve, F. Lloret, J. Faus, M. Verdager, A. Caneschi, *Inorg. Chem.* **1995**, *34*, 157. [34e] G. De Munno, M. Julve, F. Lloret, J. Cano, A. Caneschi, *Inorg. Chem.* **1995**, *34*, 2048. [34f] G. De Munno, M. G. Lombardi, P. Paoli, F. Lloret, M. Julve, *Inorg. Chim. Acta* **1998**, *282*, 252.
- [35] L. Fernholt, C. Rømming, S. Samdal, *Acta Chem. Scand., Ser. A* **1981**, *35*, 707.
- [36] S. Nishigaki, H. Yoshioka, K. Nakatsu, *Acta Crystallogr., Sect. B* **1978**, *34*, 875.
- [37] [37a] W.-L. Kwik, K.-P. Ang, H. S.-O. Chan, V. Chebolu, S. A. Koch, *J. Chem. Soc., Dalton Trans.* **1986**, 2519. [37b] E. Borghi, *Gazz. Chim. Ital.* **1987**, *117*, 557.
- [38] G. A. Baker, G. S. Rushbrooke, H. E. Gilbert, *Phys. Rev.* **1964**, *135*, A1272.
- [39] A. Rodríguez-Fortea, P. Alemany, S. Álvarez, E. Ruiz, *Chem. Eur. J.* **2001**, *7*, 627.
- [40] O. Kahn, *Molecular Magnetism*, VCH, New York, **1993**.
- [41] F. S. Delgado, J. Sanchiz, C. Ruiz-Pérez, F. Lloret, M. Julve, *Inorg. Chem.* **2003**, *42*, 5938–5948.
- [42] Y. Rodríguez-Martín, C. Ruiz-Pérez, J. Sanchiz, F. Lloret, M. Julve, *Inorg. Chim. Acta* **2001**, *318*, 159–165.
- [43] E. Colacio, J. M. Domínguez-Vera, M. Ghazi, R. Krekäs, M. Klinga, J. M. Moreno, *Eur. J. Inorg. Chem.* **1999**, 441.
- [44] A. Earnshaw, *Introduction to Magnetochemistry*, Academic Press, London, **1968**.
- [45] G. M. Sheldrick, *SHELXL-97, SHELXS-97, Program for Crystal Structure Refinement*, Universität Göttingen, Germany, **1998**.
- [46] L. J. Farrugia, *J. Appl. Crystallogr.* **1999**, *32*, 837.
- [47] PARST95: M. Nardelli, *J. Appl. Crystallogr.* **1995**, *28*, 659.
- [48] CrystalMaker 4.2.1, CrystalMaker Software, P. O. Box 183, Bicester, Oxfordshire, OX26 3TA, UK.

Received March 31, 2004

Early View Article

Published Online August 17, 2004

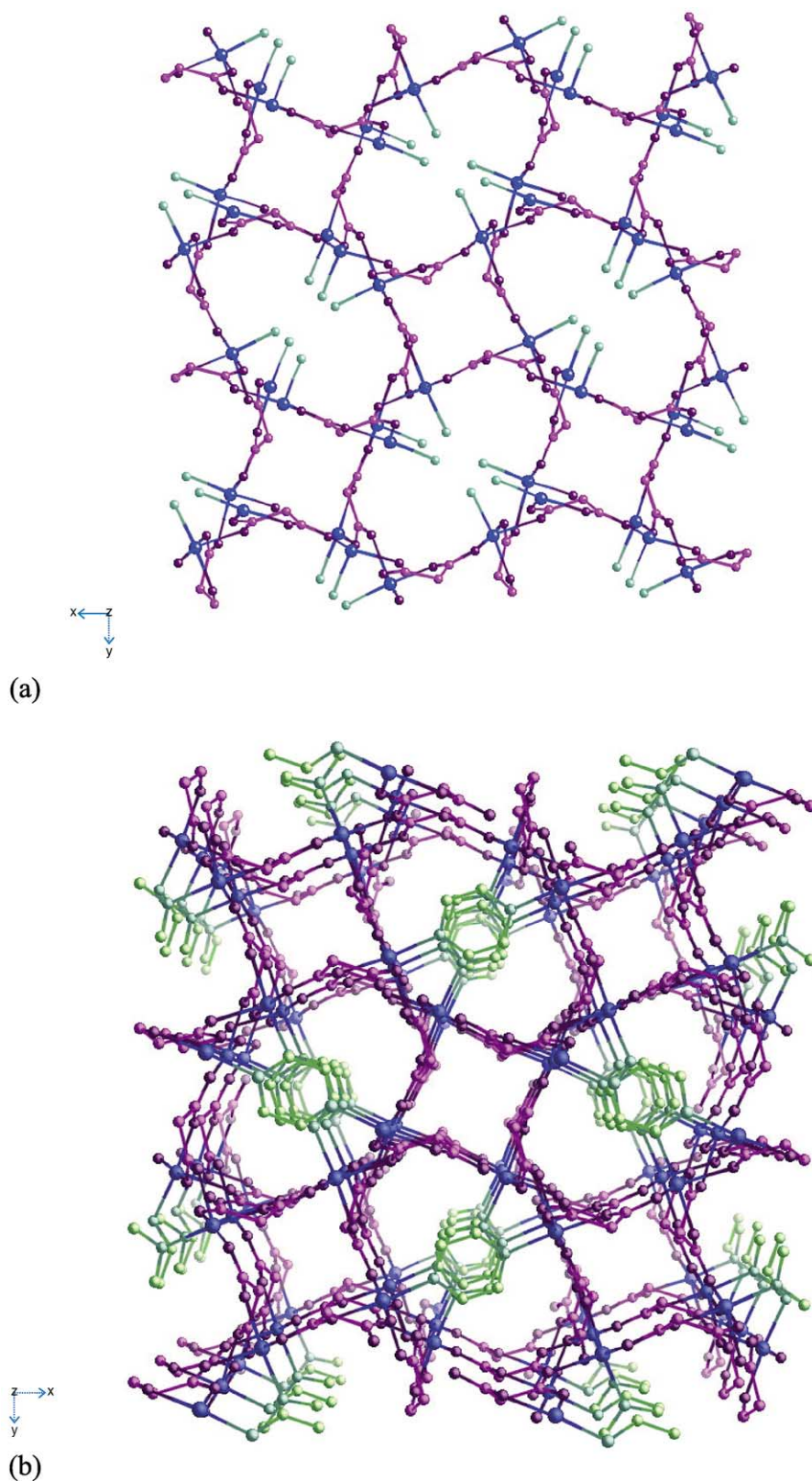


Fig. 12. (a) The Cu/malonate framework in compound  $[\text{Cu}_4(\text{mal})_4(\text{pyz})_2] \cdot 4\text{H}_2\text{O}$  (**15**) along the  $c$ -axis. (b) A view of the 3D structure where the square grids layers are stacked along the  $c$ -axis showing the  $\pi$ - $\pi$  overlap between pairs of pyrazine molecules.

dimensionality networks coupling paramagnetic centres ferromagnetically in much higher percentage than other dicarboxylic ligands. The malonate itself cannot lead to a 3D array, but combined with other ligands the 3D networks can be obtained. We are now in the search of ligands, suitable to be combined with the malonate, capable to couple ferromagnetically the spin carriers in the remaining dimensions.

### Acknowledgements

The financial support provided by the Gobierno Autónomo de Canarias (Project PI2002/175) and the Spanish Dirección General de Investigación (Ministerio de Ciencia y Tecnología), through project BQU2001-3794, is gratefully acknowledged. J.P. thanks Ministerio de Educación y Cultura for a Predoctoral-fellowship AP2001-3322 and F.S.D. thanks the Consejería de Educación, Cultura y Deportes (Gobierno Autónomo de Canarias) for a predoctoral fellowship.

### References

- [1] D. Gatteschi, O. Kahn, J.S. Miller, F. Palacio, *Magnetic Molecular Materials*, Kluwer Academic Publishers, Dordrecht, The Netherlands, 1991.
- [2] H. Iwamura, K. Itoh, M. Kinoshita, *Proceedings of the International Symposium on Chemistry and Physics of Molecular-based Magnetic Materials, Molecular Crystals and Liquid Crystals*, Gordon & Breach, London, 1993.
- [3] J.S. Miller, A.J. Epstein, *Proceedings of the IV International Conference on Molecule-based Magnets, Molecular Crystals and Liquid Crystals*, Gordon & Breach, London, 1995.
- [4] D. Chattopadhyay, S.K. Chattopadhyay, P.R. Lowe, C.H. Schwalke, S.K. Mazumber, A. Rana, S. Ghosh, *J. Chem. Soc., Dalton Trans.* (1993) 913.
- [5] I. Gil de Muro, F.A. Mautner, M. Insausti, L. Lezama, M.I. Arriortua, T. Rojo, *Inorg. Chem.* 37 (1998) 3243.
- [6] C. Ruiz-Pérez, J. Sanchiz, M. Hernández-Molina, F. Lloret, M. Julve, *Inorg. Chim. Acta* 298 (2000) 202.
- [7] E. Suresh, M.H. Bhadbhade, *Acta Crystallogr. C* 53 (1997) 193.
- [8] C. Ruiz-Pérez, M. Hernández-Molina, P. Lorenzo-Luis, F. Lloret, J. Cano, M. Julve, *Inorg. Chem.* 39 (2000) 3845.
- [9] C. Ruiz-Pérez, J. Sanchiz, M. Hernández-Molina, F. Lloret, M. Julve, *Inorg. Chem.* 39 (2000) 1363.
- [10] C. Oldham, in: G. Wilkinson, R.D. Gillard, J.A. McCleverty (Eds.), *Comprehensive Coordination Chemistry*, vol. 2, Pergamon Press, Oxford, 1987, p. 435.
- [11] D.K. Towle, S.K. Hoffmann, W.E. Hatfield, P. Singh, P. Chaudhuri, *Inorg. Chem.* 27 (1988) 394.
- [12] P.R. Levstein, R. Calvo, *Inorg. Chem.* 29 (1990) 1581.
- [13] F. Sapiña, E. Escrivá, J.V. Folgado, A. Beltrán, A. Fuertes, M. Drillon, *Inorg. Chem.* 31 (1992) 3851.
- [14] (a) E. Colacio, J.P. Costes, R. Kivekäs, J.P. Laurent, J. Ruiz, *Inorg. Chem.* 29 (1990) 4240;  
(b) E. Colacio, J.M. Domínguez-Vera, J.P. Costes, R. Kivekäs, J.P. Laurent, J. Ruiz, M. Sundberg, *Inorg. Chem.* 31 (1992) 774;  
(c) E. Ruiz, *Inorg. Chem.* 212 (1993) 115.
- [15] Y. Rodríguez-Martín, J. Sanchiz, C. Ruiz-Pérez, F. Lloret, M. Julve, *Inorg. Chim. Acta* 326 (2001) 20.
- [16] W.-L. Kwik, K.-P. Ang, H.S.-O. Chan, *J. Chem. Soc., Dalton Trans.* (1986) 2519.
- [17] (a) Y. Rodríguez-Martín, J. Sanchiz, C. Ruiz-Pérez, F. Lloret, M. Julve, *Cryst. Eng. Commun.* 4 (2002) 631;  
(b) G.I. Bimitrova, A.V. Ablov, G.A. Kiosse, G.A. Popovich, T.I. Nmalinouskii, I.F. Bourshteyn, *Dokl. Akad. Nauk SSSR* 216 (1974) 1055.
- [18] D. Chattopadhyay, S.K. Chattopadhyay, P.R. Lowe, C.H. Schwalde, S.K. Mazumber, A. Rana, S. Ghosh, *J. Chem. Soc., Dalton Trans.* (1993) 913.
- [19] J. Sanchiz, Y. Rodríguez-Martín, C. Ruiz-Pérez, A. Mederos, F. Lloret, M. Julve, *New J. Chem.* 26 (2002) 1624.
- [20] Y. Rodríguez-Martín, M. Hernández-Molina, F.S. Delgado, J. Pasán, C. Ruiz-Pérez, J. Sanchiz, F. Lloret, M. Julve, *Cryst. Eng. Commun.* 4 (2002) 1.
- [21] Y. Rodríguez-Martín, C. Ruiz-Pérez, J. Sanchiz, F. Lloret, M. Julve, *Inorg. Chim. Acta* 318 (2001) 159.
- [22] C. Ruiz-Pérez, J. Sanchiz, M. Hernández-Molina, F. Lloret, M. Julve, *Inorg. Chim. Acta* 298 (2000) 202.
- [23] C. Ruiz-Pérez, Y. Rodríguez-Martín, J. Sanchiz, M. Hernández-Molina, F.S. Delgado, J. Pasán, F. Lloret, M. Julve, *Eur. J. Inorg. Chem.*, submitted for publication.
- [24] N.J. Ray, B.J. Hathaway, *Acta Crystallogr. B* 38 (1982) 770.
- [25] T. Lis, J. Matuszewski, *Acta Crystallogr. B* 35 (1979) 2212.
- [26] F.S. Delgado, C. Ruiz-Pérez, J. Sanchiz, F. Lloret, M. Julve, *Inorg. Chim. Acta*, in preparation.



Magnetic Anisotropy of a High-Spin Octanuclear Nickel(II) Complex with a *meso*-Helicate CoreEmilio Pardo,<sup>†</sup> Isidoro Morales-Osorio,<sup>†</sup> Miguel Julve,<sup>†</sup> Francesc Lloret,<sup>\*†</sup> Joan Cano,<sup>†</sup> Rafael Ruiz-García,<sup>‡</sup> Jorge Pasán,<sup>§</sup> Catalina Ruiz-Pérez,<sup>§</sup> Xavier Ottenwaelder,<sup>||</sup> and Yves Journaux<sup>\*||</sup>

Departament de Química Inorgànica, ICMOL, and Departament de Química Orgànica, Universitat de València, 46100 Burjassot, València, Spain, Laboratorio de Rayos X y Materiales Moleculares, Departamento de Física Fundamental II, Universidad de La Laguna, 38204 La Laguna, Tenerife, Spain, and Laboratoire de Chimie Inorganique, Université Paris-XI, 91405 Orsay, France

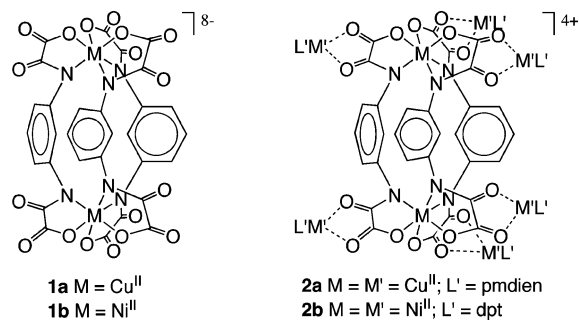
Received July 30, 2004

The octanickel(II) cluster **2b** has been synthesized from the novel ferromagnetically coupled dinickel(II) metallacryptand **1b** assembled from the *m*-phenylene-bis(oxamate) ligand. Complex **2b** exhibits a dimer-of-tetramers structure, with two oxamate-bridged propeller-shaped tetranuclear units connected through three *meta*-substituted phenylenediamidate bridges, giving a metallacryptand core of the *meso*-helicate type. Complex **2b** behaves as a ferromagnetically coupled dimer of two  $S = 2$   $Ni^{II}_4$  units with appreciable magnetic anisotropy.

High-nuclearity coordination clusters of paramagnetic first-row transition metal ions are actively investigated in the field of molecular magnetism for the attainment of single-molecule magnets (SMMs), molecules that exhibit slow relaxation of the magnetization below a blocking temperature ( $T_B$ ).<sup>1,2</sup> The design of an SMM targets the attainment of a ground state with both high spin ( $S$ ) and large negative axial magnetic anisotropy ( $D$ ), properties that ultimately depend on the nuclearity and topology of the cluster, as well as on the nature of the interacting metal centers and the bridging ligands.<sup>3,4</sup> Molecular-programmed self-assembly methods, whereby either a multitopic ligand<sup>5</sup> or a complex<sup>6</sup> coordinates a metal ion with a preferred coordination geometry, emerge as rational synthetic strategies toward the preparation of SMMs.

We have recently demonstrated that a variety of high-nuclearity copper(II) coordination clusters can be rationally designed and synthesized in this way from self-assembled,

Chart 1



exchange-coupled metallacyclic complexes with aromatic oligooxamate ligands.<sup>7</sup> In particular, the binuclear copper(II) complex **1a** resulting from the self-assembly of two Cu<sup>II</sup> ions and three binucleating bridging *N,N'*-1,3-phenylenebis(oxamate) (mpba) ligands (Chart 1, left) is a metallacryptand that can be advantageously used as building block. Through the cis carbonyl oxygen atoms of its oxamate groups, complex **1a** acts as a hexakis(bidentate) ligand toward six other Cu<sup>II</sup> ions with coordination sites partially blocked by tridentate terminal *N,N,N',N'',N'''*-pentamethyldiethylenetriamine (pmdien) ligands, yielding the octanuclear copper(II) complex **2a** (Chart 1, right).<sup>7b</sup> When applied with Ni<sup>II</sup> ions in place of Cu<sup>II</sup> ions, this step-by-step strategy (the so-called “complex-as-ligand” approach) yields the related dinickel(II) metallacryptand  $Na_8[Ni_2(mpba)_3] \cdot 10H_2O$ , **1b**, and the

\* To whom correspondence should be addressed. E-mail: francisco.lloret@uv.es (F.L.), jour@icmo.u-psud.fr (Y.J.).

<sup>†</sup> Departament de Química Inorgànica, Universitat de València.

<sup>‡</sup> Departament de Química Orgànica, Universitat de València.

<sup>§</sup> Universidad de La Laguna.

<sup>||</sup> Université Paris-XI.

- (1) Winpenny, R. E. P. *Adv. Inorg. Chem.* **2001**, *52*, 1.
- (2) Gatteschi, D.; Sessoli, R. *Angew. Chem., Int. Ed.* **2003**, *42*, 268.
- (3) Marvaud, V.; Herrera, J. M.; Barilero, T.; Tuyras, F.; Garde, R.; Scullier, A.; Decroix, C.; Cantuel, M.; Desplanches, C. *Monatsh. Chem.* **2003**, *134*, 149.
- (4) Gatteschi, D.; Sorace, L. *J. Solid State Chem.* **2001**, *159*, 253.

- (5) (a) Saalfrank, R. W.; Trummer, S.; Reimann, U.; Chowdhry, M. M.; Hampel, F.; Waldmann, O. *Angew. Chem., Int. Ed.* **2000**, *39*, 3492. (b) Waldmann, O.; Zhao, L.; Thompson, L. K. *Phys. Rev. Lett.* **2002**, *88*, 066401.
- (6) (a) Marvaud, V.; Decroix, C.; Scullier, A.; Guyard-Duhayon, C.; Vaissermann, J.; Gonnet, F.; Verdagner, M. *Chem. Eur. J.* **2003**, *9*, 1677. (b) Choi, H. J.; Sokol, J. J.; Long, J. R. *Inorg. Chem.* **2004**, *43*, 1606.
- (7) (a) Pardo, E.; Bernot, K.; Julve, M.; Lloret, F.; Cano, J.; Ruiz-García, R.; Delgado, F. S.; Ruiz-Pérez, C.; Ottenwaelder, X.; Journaux, Y. *Inorg. Chem.* **2004**, *43*, 2768. (b) Pardo, E.; Bernot, K.; Julve, M.; Lloret, F.; Cano, J.; Ruiz-García, R.; Pasán, J.; Ruiz-Pérez, C.; Ottenwaelder, X.; Journaux, Y. *Chem. Commun.* **2004**, 920. (c) Ottenwaelder, X.; Cano, J.; Journaux, Y.; Riviere, E.; Brennan, C.; Nierlich, M.; Ruiz-García, R. *Angew. Chem., Int. Ed.* **2004**, *43*, 850.

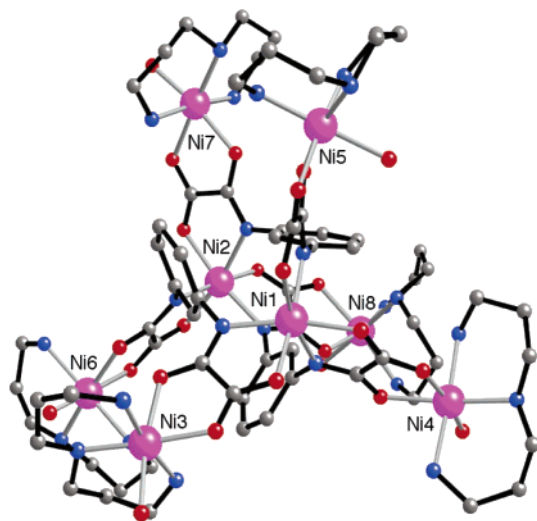


**Figure 1.** Perspective view of the asymmetric cationic octanickel unit of **2b** with the numbering scheme of the metal atoms.

corresponding octanickel(II) complex  $\{[\text{Ni}_2(\text{mpba})_3][\text{Ni}(\text{dpt})(\text{H}_2\text{O})_6]\}(\text{ClO}_4)_4 \cdot 12.5\text{H}_2\text{O}$ , **2b**, reported here, with dipropylene-triamine (dpt) as a tridentate terminal ligand (Chart 1).

Precursor **1b** was synthesized from  $\text{H}_4\text{mpba}$  and  $\text{Ni}(\text{NO}_3)_2$  in a 3:2 stoichiometry in basic ( $\text{NaOH}$ ) aqueous medium. Complex **2b** was then obtained by reaction of **1b** with the coordinatively unsaturated complex  $[\text{Ni}(\text{dpt})]^{2+}$  prepared in situ from a 1:1 mixture of  $\text{Ni}(\text{ClO}_4)_2$  and dpt. The crystal structure of **2b** consists of octanuclear nickel(II) cations,  $\{[\text{Ni}_2(\text{mpba})_3][\text{Ni}(\text{dpt})(\text{H}_2\text{O})_6]\}^{4+}$  (Figure 1), that are well-separated from each other by perchlorate anions and crystallization water molecules.<sup>8</sup>

The octanickel cation exhibits a dimer-of-tetramers molecular structure. Two oxamate-bridged propeller-like tetranickel units are linked by three *m*-phenylene moieties arranged edge-to-face through weak  $\text{C}-\text{H} \cdots \pi$  interactions (average dihedral angle of  $60.0^\circ$  and average centroid-centroid distance of  $4.65 \text{ \AA}$ ). The two central nickel atoms (Ni1 and Ni2) are in a trigonally distorted octahedral  $\text{NiN}_3\text{O}_3$  geometry [trigonal twist angles of  $58.8(6)^\circ$  and  $59.0(6)^\circ$ ] with comparable  $\text{Ni}-\text{N}(\text{amidate})$  and  $\text{Ni}-\text{O}(\text{carboxylate})$  average bond lengths ( $2.08$  and  $2.10 \text{ \AA}$ , respectively). These metal sites have opposite  $\Delta$  and  $\Lambda$  chiralities and are tilted from each other by only  $4.7(5)^\circ$  around the Ni1–Ni2 vector. The binuclear metallacryptand core,  $[\text{Ni}_2(\text{mpba})_3]^{8-}$ , is thus of the *meso*-helicate type and has a pseudo- $C_{3h}$  symmetry. The entire octanuclear cluster, however, has a reduced  $C_1$  symmetry because of the presence among the six peripheral metal atoms of both mer (Ni3, Ni4, Ni6, and Ni7) and fac (Ni5 and Ni8) isomers, with respect to the conformation of the dpt ligand. The peripheral nickel atoms adopt a distorted octahedral  $\text{NiN}_3\text{O}_3$  geometry, with a  $\text{Ni}-\text{O}(\text{water})$  average bond length ( $2.15 \text{ \AA}$ ) larger than the  $\text{Ni}-\text{N}(\text{amine})$  and  $\text{Ni}-\text{O}(\text{carbonyl})$  ones ( $2.09 \text{ \AA}$ ). The distance between the two central nickel atoms is  $6.829(4) \text{ \AA}$ , while those between central and peripheral ones are in the range  $5.446(2)$ – $5.487(6) \text{ \AA}$ .

The temperature dependence of the dc molar magnetic susceptibility ( $\chi_M$ ) of **2b** (Figure 2) is consistent with its

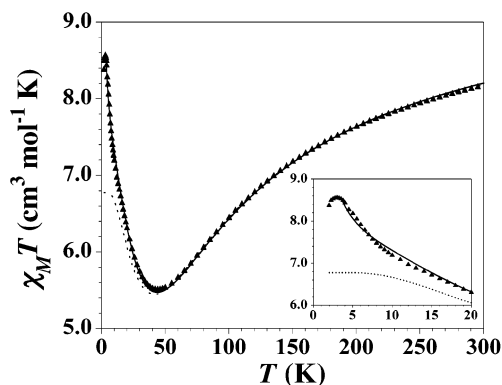


**Figure 2.**  $\chi_M T$  versus  $T$  plot of **2b** under an applied field of 1 T ( $T > 20$  K) and 250 G ( $T < 20$  K). The inset shows the maximum of  $\chi_M T$  in the low-temperature region. Solid and dotted lines are the best-fit curves for a  $[\text{Ni}_4]_2$  molecule and two isolated  $\text{Ni}_4$  molecules with  $J_{\text{eff}} = 0$ , respectively.

dimer-of-tetramers structure. The minimum of  $\chi_M T$  around 45 K is characteristic of a moderately strong antiferromagnetic intratetramer coupling ( $J$ ) between the central and the three peripheral  $\text{Ni}^{\text{II}}$  ions through the oxamate bridges. The propeller-type topology results in an incomplete spin cancellation and thus an  $S = 2$  ground state for each tetranuclear unit. The maximum value of  $\chi_M T$  at 3.0 K ( $8.58 \text{ cm}^3 \text{ K mol}^{-1}$ ) is higher than expected for two isolated  $S = 2 \text{ Ni}_4^{\text{II}}$  units ( $\chi_M T = 6.9 \text{ cm}^3 \text{ K mol}^{-1}$ , with  $g = 2.15$ ). This suggests a weak ferromagnetic intertetramer coupling ( $J_{\text{eff}}$ ) between the  $S = 2$  ground states of the  $\text{Ni}_4^{\text{II}}$  units, yielding an  $S = 4$  ground state for the entire octanuclear molecule. Yet, this maximum of  $\chi_M T$  is lower than expected for an  $S = 4 \text{ Ni}_8^{\text{II}}$  molecule ( $\chi_M T = 11.3 \text{ cm}^3 \text{ K mol}^{-1}$ , with  $g = 2.15$ ). The slight decrease of  $\chi_M T$  below 3.0 K (inset of Figure 2) is most likely due to zero-field splitting (ZFS) effects.

The magnetic susceptibility data of **2b** were fitted according to an effective spin Hamiltonian for a dimer-of-tetramers model that takes into account the coupling between the  $S = 2$  ground state of each  $\text{Ni}_4^{\text{II}}$  unit [ $H = -J(S_{1A}S_{3A} + S_{1A}S_{4A} + S_{1A}S_{5A} + S_{2B}S_{6B} + S_{2B}S_{7B} + S_{2B}S_{8B}) - J_{\text{eff}}S_A S_B + g\beta(S_{1A} + S_{3A} + S_{4A} + S_{5A} + S_{2B} + S_{6B} + S_{7B} + S_{8B})B$ , with  $S_{iA} = S_{jB} = 1$  for  $i = 1, 3-5$ ;  $j = 2, 6-8$ ; and  $S_A = S_B = 2$ ].<sup>9</sup> A least-squares fit gave  $J = -26.6 \text{ cm}^{-1}$ ,  $J_{\text{eff}} = +0.34 \text{ cm}^{-1}$ , and  $g = 2.13$ . The theoretical curve closely follows the experimental data down to 5.0 K (solid line in Figure 2). The small  $J_{\text{eff}}/|J|$  ratio confirms the validity of the perturbational treatment. The  $-J$  value in **2b** is comparable to that reported for related oxalate-bridged ( $22.0$ – $39.0 \text{ cm}^{-1}$ ) and oxamidate-bridged ( $25.0$ – $57.0 \text{ cm}^{-1}$ ) binuclear nickel(II) complexes.<sup>10,11</sup> In this model, the value of  $J_{\text{eff}}$  is related to that of  $J'$  between the two central  $\text{Ni}^{\text{II}}$  ions through the *meta*-phenylenediamidate bridges by  $J_{\text{eff}} = 1/9 J'$ ,<sup>9</sup> that is,  $J' = +3.1$

(8) Crystal data for **2b**:  $\text{C}_{66}\text{H}_{163}\text{Cl}_4\text{N}_{24}\text{Ni}_8\text{O}_{52.5}$ ,  $M = 2744.4$ , triclinic, space group  $P1$ ,  $a = 20.3117(3) \text{ \AA}$ ,  $b = 17.8243(3) \text{ \AA}$ ,  $c = 18.3675(3) \text{ \AA}$ ,  $\alpha = 104.4870(10)^\circ$ ,  $\beta = 115.9840(10)^\circ$ ,  $\gamma = 92.9850(10)^\circ$ ,  $V = 5686.82(16) \text{ \AA}^3$ ,  $Z = 2$ ,  $T = 293(2) \text{ K}$ ,  $\mu(\text{Mo K}\alpha) = 1.487 \text{ mm}^{-1}$ , 25 919 reflections measured, 19 048 assumed as observed with  $I > 2\sigma(I)$ . Refinement on  $F^2$  of 1394 parameters with anisotropic thermal parameters for all non-hydrogen atoms gave  $R = 0.0866$ ,  $R_w = 0.2346$ , and  $\text{GOF} = 1.050$  (observed data).

(9) Aukauloo, A.; Ottenwaelder, X.; Ruiz, R.; Journaux, Y.; Pei, Y.; Riviere, E.; Muñoz, M. C. *Eur. J. Inorg. Chem.* **2000**, 951.

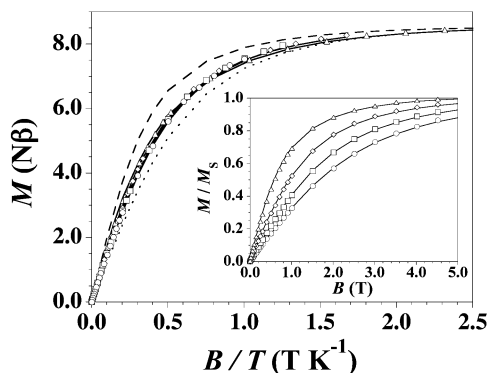


**Figure 3.**  $M$  versus  $B/T$  plot of **2b** at different temperatures: ( $\Delta$ ) 2.0, ( $\diamond$ ) 3.0, ( $\square$ ) 4.0, and ( $\circ$ ) 5.0 K. Dashed and dotted lines are the Brillouin curves for an  $S = 4$  state and two isolated  $S = 2$  states, respectively, with  $D = 0$ . The inset shows the  $M/M_S$  versus  $B$  plot. Solid lines are the best-fit curves for a  $[\text{Ni}_4]_2$  molecule with  $D < 0$ .

$\text{cm}^{-1}$ .<sup>12</sup> The calculated  $J'$  value in **2b** agrees both in sign and in magnitude with that found in the binuclear precursor **1b** ( $+3.6 \text{ cm}^{-1}$ ).<sup>13</sup> This moderate ferromagnetic coupling is likely due to the spin polarization mechanism, as previously observed for related copper(II) complexes.<sup>7a,7c</sup>

The field dependence of the dc magnetization ( $M$ ) of **2b** in the temperature range 2.0–5.0 K (Figure 3) is consistent with a ferromagnetically coupled dimer of two  $S = 2 \text{ Ni}^{\text{II}}_4$  units. At 2.0 K, the saturation magnetization value of 8.49  $N\beta$  is close to the expected one for an  $S = 4$  state ( $M_S = 8.6 \text{ N}$ , with  $g = 2.15$ ). Yet, the various isothermal curves are intermediate between the Brillouin functions of an  $S = 4$  state and two isolated  $S = 2$  states with  $g = 2.15$  and no ZFS. This indicates the proximity of low-lying excited states of smaller spin values that are thermally populated. In the absence of ZFS, because of the relatively small  $J_{\text{eff}}$  value, four lowest excited spin states ( $S = 3$ ,  $S = 2$ ,  $S = 1$ , and  $S = 0$ ) would be close in energy to the  $S = 4$  ground state (at 1.4, 2.4, 3.1, and  $3.4 \text{ cm}^{-1}$ , respectively). On the other hand, the fact that the various isothermal curves in the  $M$  versus  $B/T$  plot do not perfectly superimpose at low  $B/T$  values suggests the presence of weak but nonnegligible ZFS of these low-lying  $S = 4-1$  states.

Accordingly, the low-temperature magnetization data of **2b** were fitted by full-matrix diagonalization of an effective spin Hamiltonian for a dimer model that takes into account the axial magnetic anisotropy of the  $S = 2$  ground state of each  $\text{Ni}^{\text{II}}_4$  unit [ $H = -J_{\text{eff}}S_{\text{A}}S_{\text{B}} + D_{\text{eff}}(S_{\text{zA}}^2 + S_{\text{zB}}^2) + g\beta(S_{\text{A}}$

$+ S_{\text{B}})B$ , with  $S_{\text{A}} = S_{\text{B}} = 2$ ].<sup>14</sup> Least-squares fits with  $J_{\text{eff}} = +0.34 \text{ cm}^{-1}$  fixed, gave  $D_{\text{eff}} = +0.62 \text{ cm}^{-1}$  and  $g = 2.16$  or, alternatively,  $D_{\text{eff}} = -0.54 \text{ cm}^{-1}$  and  $g = 2.15$ . In both cases, the theoretical curves follow the experimental data fairly well (solid lines in the inset of Figure 3). The value of  $|D_{\text{eff}}|$  is of the same magnitude as  $J_{\text{eff}}$ , which ensures a large mixing of the electronic spin states for **2b**. Hence, only the first two low-lying states are well separated from the others states, and according to the wave function composition, they are reminiscent of either the  $M_S = 0, \pm 1$ , levels of an  $S = 4$  state if  $D_{\text{eff}} > 0$ , or the  $M_S = \pm 4, \pm 3$ , levels if  $D_{\text{eff}} < 0$ . The energy spectrum shows the  $M_S = \pm 1$  excited state at  $0.31 \text{ cm}^{-1}$  from the  $M_S = 0$  ground state if  $D_{\text{eff}} > 0$ , and it shows the  $M_S = \pm 3$  excited state at  $1.62 \text{ cm}^{-1}$  from the  $M_S = \pm 4$  ground state if  $D_{\text{eff}} < 0$ . The axial ZFS ( $D$ ) of the  $S = 4$  ground state can then be related to the energy difference ( $\Delta E$ ) between these two lowest levels by  $\Delta E = D$  for  $D_{\text{eff}} > 0$  or  $\Delta E = -7D$  for  $D_{\text{eff}} < 0$ , that is,  $D = +0.31$  or  $-0.23 \text{ cm}^{-1}$ , respectively. The calculated  $|D|$  value ultimately reflects both the single-ion magnetic anisotropy of high-spin  $\text{Ni}^{\text{II}}$  ions in a distorted octahedral coordination geometry and the structural anisotropy of the double-propeller  $[\text{Ni}^{\text{II}}_4]_2$  cluster.<sup>15</sup> Although the calculations do not allow resolution of the ambiguity in the sign of  $D$  for **2b**, a negative  $D$  value can be inferred from ac magnetic susceptibility measurements that revealed a frequency-dependent behavior typical of SMMs with  $T_{\text{B}} \approx 3.0 \text{ K}$ . Yet, the temperature dependence of the magnetic relaxation indicates a complex mechanism for the slow dynamics of the magnetization that is currently under investigation.<sup>16</sup>

In conclusion, the novel octanuclear nickel(II) coordination cluster **2b** is a high-spin and moderately anisotropic molecule built from the oxamate-based binuclear metallacryptand **1b** that acts as a ferromagnetic synthon. This rational complex-as-ligand approach shall lead to a variety of related homo- and heterometallic octanuclear complexes as potential SMMs.

**Acknowledgment.** This work was supported by the MCyT (Spain) (Projects BQU2001-2928 and BQU2001-3794) and the TMR Network “QuEMolNa” (European Union) (Contract MRTN-CT-2003-504880). E.P. and J.P. thank the MECyD (Spain) for grants.

**Supporting Information Available:** Preparation and characterization of **1b** and **2b**, dc magnetic susceptibility data of **1b**, ac magnetic susceptibility data of **2b**, and X-ray crystallographic data of **2b** in CIF format. This material is available free of charge via the Internet at <http://pubs.acs.org>.

IC048965X

- (10) Roman, P.; Guzman-Mirallas, C.; Luque, A.; Beitia, J. I.; Cano, J.; Lloret, F.; Julve, M.; Alvarez, S. *Inorg. Chem.* **1996**, *35*, 3741.
- (11) Lloret, F.; Sletten, J.; Ruiz, R.; Julve, M.; Faus, J.; Verdager, M. *Inorg. Chem.* **1992**, *31*, 778.
- (12) Least-squares fit of the magnetic susceptibility data of **2b** by full-matrix diagonalization of the appropriate spin Hamiltonian for an octamer model [ $H = -J(S_1S_3 + S_1S_4 + S_1S_5 + S_2S_6 + S_2S_7 + S_2S_8) - J'S_1S_2 + g\beta(S_1 + S_2 + S_3 + S_4 + S_5 + S_6 + S_7 + S_8)B$ ] gave  $J = -26.8 \text{ cm}^{-1}$ ,  $J' = +3.2 \text{ cm}^{-1}$ , and  $g = 2.13$ , in excellent agreement with the values obtained through the dimer-of-tetramers model.
- (13) Complex **1b** exhibits a magnetic behavior characteristic of a  $\text{Ni}^{\text{II}}_2$  pair with weak ferromagnetic intrapair coupling ( $J$ ) and appreciable axial ZFS ( $D$ ) of the high-spin  $\text{Ni}^{\text{II}}$  ions (Figure S1, Supporting Information). A least-squares fit of the magnetic susceptibility data to the appropriate analytical expression derived from the spin Hamiltonian  $H = JS_1S_2 + D(S_{1z}^2 + S_{2z}^2) + g\beta(S_1 + S_2)B$  (with  $S_1 = S_2 = 1$ ) gave  $J = +3.6 \text{ cm}^{-1}$ ,  $D = 3.5 \text{ cm}^{-1}$ , and  $g = 2.14$ .

- (14) Wernsdorfer, W.; Aliaga-Alcalde, N.; Hendrickson, D. N.; Christou, G. *Nature* **2002**, *416*, 406.
- (15) Cornia, A.; Fabretti, A. C.; Garrisi, P.; Mortal, C.; Bonacchi, D.; Gatteschi, D.; Sessoli, R.; Sorace, L.; Wernsdorfer, W.; Barra, A. L. *Angew. Chem., Int. Ed.* **2004**, *43*, 1136.
- (16) The relaxation time ( $\tau$ ) of **2b** follows the Arrhenius law characteristic of a thermally activated mechanism,  $\tau = \tau_0 \exp(U/k_{\text{B}}T)$ , with  $\tau_0 = 1.2 \times 10^{-16} \text{ s}$  and  $U = 71.3 \text{ cm}^{-1}$  (Figure S2, Supporting Information). Yet, the calculated preexponential factor ( $\tau_0$ ) is abnormally low compared to those of other SMMs. Moreover, assuming that the slow relaxation stems exclusively from the  $S = 4$  ground state, the  $D$  value of  $-4.5 \text{ cm}^{-1}$  estimated through the expression  $U = |D|S^2$  is far above that derived from dc magnetization data.

## Polymeric Networks of Copper(II) Phenylmalonate with Heteroaromatic N-donor Ligands: Synthesis, Crystal Structure, and Magnetic Properties

Jorge Pasán,<sup>†</sup> Joaquín Sanchiz,<sup>‡</sup> Catalina Ruiz-Pérez,<sup>\*†</sup> Francesc Lloret,<sup>§</sup> and Miguel Julve<sup>§</sup>

Laboratorio de Rayos X y Materiales Moleculares, Departamento de Física Fundamental II, Universidad de La Laguna, Av. Astrofísico Francisco Sánchez s/n, 38206 La Laguna (Tenerife), Spain, Laboratorio de Rayos X y Materiales Moleculares, Departamento de Química Inorgánica, Universidad de La Laguna, Av. Astrofísico Francisco Sánchez s/n, 38204 La Laguna (Tenerife), Spain, and Departament de Química Inorgànica/ Instituto de Ciencia Molecular, Facultat de Química, Universitat de València, Av. Dr. Moliner 50, 46100 Burjassot (València), Spain

Received March 17, 2005

Two new phenylmalonate-bridged copper(II) complexes with the formulas  $[\text{Cu}(4,4'\text{-bpy})(\text{Phmal})]_n \cdot 2n\text{H}_2\text{O}$  (**1**) and  $[\text{Cu}(2,4'\text{-bpy})(\text{Phmal})(\text{H}_2\text{O})]_n$  (**2**) (Phmal = phenylmalonate dianion, 4,4'-bpy = 4,4'-bipyridine, 2,4'-bpy = 2,4'-bipyridine) have been synthesized and characterized by X-ray diffraction. Complex **1** crystallizes in monoclinic space group  $P2_1$ ,  $Z = 4$ , with unit cell parameters of  $a = 9.0837(6)$  Å,  $b = 9.3514(4)$  Å,  $c = 11.0831(8)$  Å, and  $\beta = 107.807(6)^\circ$ , whereas complex **2** crystallizes in orthorhombic space group  $C2cb$ ,  $Z = 8$ , with unit cell parameters of  $a = 10.1579(7)$  Å,  $b = 10.3640(8)$  Å, and  $c = 33.313(4)$  Å. The structures of **1** and **2** consist of layers of copper(II) ions with bridging bis-monodentate phenylmalonate (**1** and **2**) and 4,4'-bpy (**1**) ligands and terminal monodentate 2,4'-bpy (**2**) groups. Each layer in **1** contains rectangles with dimensions of  $11.08 \times 4.99$  Å<sup>2</sup>, the edges being defined by the Phmal and 4,4'-bpy ligands. The intralayer copper–copper separations in **1** through the anti–syn equatorial–apical carboxylate-bridge and the 4,4'-bpy molecule are 4.9922(4) and 11.083(1) Å, respectively. The anti–syn equatorial–equatorial carboxylate bridge links the copper(II) atoms in complex **2** within each layer with a mean copper–copper separation of 5.3709(8) Å. The presence of 2,4'-bpy as a terminal ligand accounts for the large interlayer separation of 15.22 Å. The copper(II) environment presents a static pseudo-Jahn–Teller disorder which has been studied by EPR and low-temperature X-ray diffraction. Magnetic susceptibility measurements of both compounds in the temperature range 2–290 K show the occurrence of weak antiferromagnetic [ $J = -0.59(1)$  cm<sup>-1</sup> (**1**)] and ferromagnetic [ $J = +0.77(1)$  cm<sup>-1</sup> (**2**)] interactions between the copper(II) ions. The conformation of the phenylmalonate–carboxylate bridge and other structural factors, such as the planarity of the exchange pathway in **1**, account for the different nature of the magnetic interaction.

### Introduction

The investigation of properties, such as porosity, guest inclusion, chirality, and magnetism, and their cooperative effects in self-assembled multifunctional molecular materials are of current interest. The design and exploration of new synthetic routes to obtain this type of metal–organic coordination network are topics of the recent research of inorganic chemists.<sup>1–5</sup> In the context of molecular magnetism, the study of the magnetostructural correlations aimed

at understanding the structural and chemical factors that govern the exchange coupling between paramagnetic centers through multiatom bridges are of continuing interest.<sup>3,6–8</sup>

\* To whom correspondence should be addressed. E-mail: caruiz@ull.es.  
<sup>†</sup> Departamento de Física Fundamental II, Universidad de La Laguna.  
<sup>‡</sup> Departamento de Química Inorgánica, Universidad de La Laguna.  
<sup>§</sup> Departament de Química Inorgànica/Instituto de Ciencia Molecular, Universitat de València.

- (1) Picketing, M.; Decurtins, S. *Crystal Design: Structure and Function*; Desiraju, G. R., Ed.; Wiley: Chichester, U.K., 2003.
- (2) (a) Janiak, C. *Dalton Trans.* **2003**, 2781. (b) Moulton, B.; Zaworotko, M. J. *Chem. Rev.* **2001**, *101*, 1629. (c) Zaworotko, M. J. *Chem. Commun.* **2001**, 1.
- (3) *Molecular Magnetism: From Molecular Assemblies to the Devices*; Coronado, E., Delhaès, P., Gatteschi, D., Miller, J. S. Eds.; NATO ASI Series E321; Kluwer: Dordrecht, The Netherlands, 1996.
- (4) *Magnetism: A Supramolecular Function*; Kahn, O., Ed.; NATO ASI Series C484; Kluwer: Dordrecht, The Netherlands, 1996.
- (5) *Supramolecular Engineering of Synthetic Metallic Materials*; Veciana, J., Rovira, C., Amabilino, D. B., Eds.; NATO ASI Series C518; Kluwer: Dordrecht, The Netherlands, 1999.

A reasonable synthetic approach to build three-dimensional structures in crystal engineering consists of connecting layers of transition metal ions through bridging ligands.<sup>1,2</sup> The dimensionality of the structure can be controlled by a careful selection of the metal coordination structure and the organic spacer. Recent reports have focused on the malonate ligand (anion of the malonic acid, hereafter noted mal) as a flexible and fruitful tool for the design of magnetic systems with different dimensionalities when an appropriate coligand is used.<sup>9–11</sup> The introduction of substituents on the methylene group of the malonate ligand could induce different conformations because of geometrical constraints, and it would make possible specific interactions between substituents, which would contribute to the overall stability of the resulting compound. In the first steps of these investigations, we have focused on the phenylmalonate dianion (Phmal), and recent reports were devoted to its complexation of copper(II).<sup>12</sup>

The dimensionality of the structures of the copper(II)–phenylmalonate coordination complexes can be modified with the presence of adequate ligands such as 4,4′-bipyridine (4,4′-bpy) and 2,4′-bipyridine (2,4′-bpy). The efficiency of these ligands stems from their rigidity, which allows for some degree of control to be exerted upon the steric constraints of the assembly process. The use of these ligands has yielded a great variety of coordination polymers, some of them featuring unprecedented physical phenomena (porosity, catalysis, gas and small molecule sorption, magnetism, etc). The current state of the knowledge in this topical area is described in several recent reviews.<sup>2,13</sup>

In previous reports, these ligands were incorporated into copper(II)–malonate complexes producing, for instance, the isolated tetranuclear unit  $[\text{Cu}_4(\text{mal})_4(2,4′\text{-bpy})_4(\text{H}_2\text{O})_4]\cdot 8\text{H}_2\text{O}$  and the two-dimensional compound  $[\text{Cu}_4(\text{mal})_4(4,4′\text{-bpy})_2(\text{H}_2\text{O})_4]_n$ .<sup>14</sup> In addition to the stacking interactions between the pyridyl groups that stabilize the structure in both malonate compounds,  $\pi$ – $\pi$  interactions between the pyridyl and phenyl rings are expected in the Phmal–copper(II) complexes.

We report herein the synthesis, crystallographic study, and magnetic properties of two new phenylmalonate–copper(II) complexes with the formulas  $[\text{Cu}(4,4′\text{-bpy})(\text{Phmal})]_n\cdot 2n\text{H}_2\text{O}$  (**1**) and  $[\text{Cu}(2,4′\text{-bpy})(\text{Phmal})(\text{H}_2\text{O})]_n$  (**2**). Complexes

**1** and **2** are two-dimensional compounds that are structurally very different because of the terminal and bridging coordination modes of the 2,4′-bpy and 4,4′-bpy ligands, respectively. Intralayer antiferromagnetic and ferromagnetic interactions are observed in **1** and **2**, respectively.

## Experimental Section

**Materials.** Phenylmalonic acid ( $\text{H}_2\text{Phmal}$ ), copper(II) acetate hydrate  $[\text{Cu}(\text{CH}_3\text{COO})_2\cdot 2.5\text{H}_2\text{O}]$ , 4,4′-bipyridine (4,4′-bpy), 2,4′-bipyridine (2,4′-bpy), and methanol (MeOH) were purchased from Aldrich and used as received. Elemental analyses (C, H, N) were performed on an EA 1108 CHNS-O microanalytical analyzer.

**Synthesis of  $[\text{Cu}(4,4′\text{-bpy})(\text{Phmal})]_n\cdot 2n\text{H}_2\text{O}$  (**1**).** An aqueous solution of copper(II) phenylmalonate (120 mg, 0.5 mmol), prepared as previously described,<sup>12</sup> was placed into one arm of an H-shaped tube, and a 50/50 MeOH/water solution of the 4,4′-bpy (78 mg, 0.5 mmol) was put into the other arm. A 50/50 MeOH/water solution was added dropwise to fill the H-shaped tube. Rectangular blue single crystals of **1** appeared within a week by slow diffusion at room temperature and were used for all measurements. Anal. Calcd for  $\text{C}_{19}\text{H}_{18}\text{N}_2\text{O}_6\text{Cu}$  (**1**): C, 52.59; H, 4.15; N, 6.46. Found: C, 52.30; H, 4.25; N, 6.38. IR (KBr,  $\text{cm}^{-1}$ ):  $\nu$  1614 vs, 1580 vs, 1494 m, 1430 s, 790 m.

**Synthesis of  $[\text{Cu}(2,4′\text{-bpy})(\text{Phmal})(\text{H}_2\text{O})]_n$  (**2**).** Compound **2** was obtained by following a similar procedure to that of **1**, but 2,4′-bpy was used instead of 4,4′-bpy. Single crystals of **2** as blue rods appeared within a week by slow diffusion at room temperature and were used for all measurements. Anal. Calcd for  $\text{C}_{19}\text{H}_{16}\text{N}_2\text{O}_5\text{Cu}$  (**2**): C, 54.87; H, 3.69; N, 6.74. Found: C, 54.58; H, 3.76; N, 6.72. IR (KBr,  $\text{cm}^{-1}$ ):  $\nu$  1614 vs, 1593 vs, 1452 m, 1410 vs, 788 s.

**Physical Techniques.** IR spectra (450–4000  $\text{cm}^{-1}$ ) of **1** and **2** were recorded on a Bruker IF S55 spectrophotometer with samples prepared as KBr pellets. EPR spectra on a polycrystalline sample of **2** were carried out on a Bruker EleXsys E580 EPR spectrometer operating at Q-band (34 GHz) frequency. Magnetic susceptibility measurements on polycrystalline samples of **1** and **2** were performed in the temperature range of 1.9–290 K with a Quantum Design SQUID magnetometer. Diamagnetic corrections of the constituent atoms were estimated from Pascal's constants<sup>15</sup> to be  $-238 \times 10^{-6}$  and  $-225 \times 10^{-6} \text{ cm}^3 \text{ mol}^{-1}$  for **1** and **2**, respectively. Experimental susceptibilities were also corrected for the temperature-independent paramagnetism [ $60 \times 10^{-6} \text{ cm}^3 \text{ mol}^{-1}$  per Cu(II) ion] and the magnetization of the sample holder.

- (6) *Magnetic Molecular Materials*; Gatteschi, D., Kahn, O., Miller, J. S., Palacio, F., Eds.; Kluwer: Dordrecht, The Netherlands, 1991.
- (7) Kahn, O. *Molecular Magnetism*; VCH: New York, 1993.
- (8) (a) Olivier Kahn Special Issue. *Polyhedron* **2001**, *20* (11–14). (b) Proceedings of the 8th International Conference on Molecule-Based Magnets. *Polyhedron* **2003**, *22* (14–17).
- (9) Rodríguez-Martín, Y.; Hernández-Molina, M.; Delgado, F. S.; Pasán, J.; Ruiz-Pérez, C.; Sanchiz, J.; Lloret, F.; Julve, M. *CrystEngComm* **2002**, *4*, 522.
- (10) Ruiz-Pérez, C.; Rodríguez-Martín, Y.; Hernández-Molina, M.; Delgado, F. S.; Pasán, J.; Sanchiz, J.; Lloret, F.; Julve, M. *Polyhedron* **2003**, *22*, 2111.
- (11) Pasán, J.; Delgado, F. S.; Rodríguez-Martín, Y.; Hernández-Molina, M.; Ruiz-Pérez, C.; Sanchiz, J.; Lloret, F.; Julve, M. *Polyhedron* **2003**, *22*, 2143.
- (12) (a) Pasán, J.; Sanchiz, J.; Ruiz-Pérez, C.; Lloret, F.; Julve, M. *New J. Chem.* **2003**, *27*, 1557. (b) Pasán, J.; Sanchiz, J.; Ruiz-Pérez, C.; Lloret, F.; Julve, M. *Eur. J. Inorg. Chem.* **2004**, 4081.
- (13) (a) Batten, S. R.; Robson, R. *Angew. Chem., Int. Ed.* **1998**, *37*, 1461. (b) Batten, S. R. *CrystEngComm*, **2001**, *3*, 67. (c) James, S. L. *Chem. Soc. Rev.* **2003**, *32*, 276.

- (14) For malonate containing Cu(II) complexes, see: (a) Chattopadhyay, D.; Chattopadhyay, S. K.; Lowe, P. R.; Schwalbe, C. H.; Mazumder, S. K.; Rana, A.; Ghosh, S. *J. Chem. Soc., Dalton Trans.* **1993**, 913. (b) Gil de Muro, I.; Mautner, F. A.; Insausti, M.; Lezama, L.; Arriortua, M. I.; Rojo, T. *Inorg. Chem.* **1998**, *37*, 3243. (c) Ruiz-Pérez, C.; Sanchiz, J.; Hernández-Molina, M.; Lloret, F.; Julve, M. *Inorg. Chim. Acta* **2000**, *298*, 245. (d) Ruiz-Pérez, C.; Sanchiz, J.; Hernández-Molina, M.; Lloret, F.; Julve, M. *Inorg. Chem.* **2000**, *39*, 1363. (e) Ruiz-Pérez, C.; Hernández-Molina, M.; Lorenzo-Luis, P.; Lloret, F.; Cano, J.; Julve, M. *Inorg. Chem.* **2000**, *39*, 3845. (f) Ruiz-Pérez, C.; Sanchiz, J.; Hernández-Molina, M.; Lloret, F.; Julve, M. *Inorg. Chim. Acta* **2000**, *298*, 245. (g) Rodríguez-Martín, Y.; Sanchiz, J.; Ruiz-Pérez, C.; Lloret, F.; Julve, M. *Inorg. Chim. Acta* **2001**, *326*, 20. (h) Rodríguez-Martín, Y.; Ruiz-Pérez, C.; Sanchiz, J.; Lloret, F.; Julve, M. *Inorg. Chim. Acta* **2001**, *318*, 159. (i) Sanchiz, J.; Rodríguez-Martín, Y.; Ruiz-Pérez, C.; Mederos, A.; Lloret, F.; Julve, M. *New J. Chem.* **2002**, *26*, 1624. (j) Rodríguez-Martín, Y.; Hernández-Molina, M.; Delgado, F. S.; Pasán, J.; Ruiz-Pérez, C.; Sanchiz, J.; Lloret, F.; Julve, M. *CrystEngComm* **2002**, *4*, 440. (k) Sain, S.; Maji, T. K.; Mostafa, G.; Lu, T. H.; Chanduri, N. R. *New J. Chem.* **2003**, *27*, 185.
- (15) Earnshaw, A. *Introduction to Magnetochemistry*; Academic Press: London, 1968.

**Table 1.** Crystallographic Data for Complexes **1** and **2**

|                                                             | 1                                                                 | 2                                                                 | 2                                                                 |
|-------------------------------------------------------------|-------------------------------------------------------------------|-------------------------------------------------------------------|-------------------------------------------------------------------|
| formula                                                     | C <sub>19</sub> H <sub>18</sub> O <sub>6</sub> N <sub>2</sub> Cu  | C <sub>19</sub> H <sub>13</sub> O <sub>5</sub> N <sub>2</sub> Cu  | C <sub>19</sub> H <sub>13</sub> O <sub>5</sub> N <sub>2</sub> Cu  |
| fw                                                          | 433.86                                                            | 412.88                                                            | 412.88                                                            |
| cryst syst                                                  | monoclinic                                                        | orthorhombic                                                      | orthorhombic                                                      |
| space group                                                 | <i>P</i> 2 <sub>1</sub>                                           | <i>C</i> 2 <i>cb</i>                                              | <i>C</i> 2 <i>cb</i>                                              |
| <i>a</i> (Å)                                                | 9.0837(6)                                                         | 10.1579(7)                                                        | 10.2178(4)                                                        |
| <i>b</i> (Å)                                                | 9.3514(4)                                                         | 10.3640(8)                                                        | 10.2909(5)                                                        |
| <i>c</i> (Å)                                                | 11.0831(8)                                                        | 33.313(4)                                                         | 32.825(2)                                                         |
| $\beta$ (deg)                                               | 107.807(6)                                                        | —                                                                 | —                                                                 |
| <i>V</i> (Å <sup>3</sup> )                                  | 896.35(10)                                                        | 3507.1(6)                                                         | 3451.6(3)                                                         |
| <i>Z</i>                                                    | 4                                                                 | 8                                                                 | 8                                                                 |
| $\mu$ (Mo K $\alpha$ ) (cm <sup>-1</sup> )                  | 12.59                                                             | 12.84                                                             | 13.01                                                             |
| <i>T</i> (K)                                                | 293(2)                                                            | 293(2)                                                            | 100(2)                                                            |
| $\rho_{\text{calc}}$ (g cm <sup>-3</sup> )                  | 1.593                                                             | 1.642                                                             | 1.612                                                             |
| $\lambda$ (Å)                                               | 0.71073                                                           | 0.71073                                                           | 0.71073                                                           |
| index ranges                                                | -12 ≤ <i>h</i> ≤ 12<br>-13 ≤ <i>k</i> ≤ 12<br>-15 ≤ <i>l</i> ≤ 13 | -14 ≤ <i>h</i> ≤ 13<br>-14 ≤ <i>k</i> ≤ 13<br>-46 ≤ <i>l</i> ≤ 43 | -14 ≤ <i>h</i> ≤ 12<br>-14 ≤ <i>k</i> ≤ 11<br>-46 ≤ <i>l</i> ≤ 36 |
| independent reflns ( <i>R</i> <sub>int</sub> )              | 4940 (0.050)                                                      | 4904 (0.085)                                                      | 4571 (0.079)                                                      |
| observed reflns [ <i>I</i> > 2 $\sigma$ ( <i>I</i> )]       | 4242                                                              | 4224                                                              | 4247                                                              |
| parameters                                                  | 254                                                               | 263                                                               | 263                                                               |
| GOF                                                         | 1.025                                                             | 1.038                                                             | 1.132                                                             |
| <i>R</i> [ <i>I</i> > 2 $\sigma$ ( <i>I</i> )]              | 0.0394                                                            | 0.0485                                                            | 0.0678                                                            |
| <i>R</i> <sub>w</sub> [ <i>I</i> > 2 $\sigma$ ( <i>I</i> )] | 0.0858                                                            | 0.1228                                                            | 0.1807                                                            |
| <i>R</i> (all data)                                         | 0.0525                                                            | 0.0577                                                            | 0.0754                                                            |
| <i>R</i> <sub>w</sub> (all data)                            | 0.0907                                                            | 0.1282                                                            | 0.1905                                                            |

**Crystallographic Data Collection and Structural Determination.** Single crystals of **1** and **2** were used for data collection with a Nonius Kappa CCD diffractometer. The data collection was carried out using graphite-monochromated Mo K $\alpha$  radiation ( $\lambda = 0.71073$  Å) at 293 K, and it was also done at 100 K for compound **2**. A summary of the crystallographic data and structure refinement is given in Table 1. The structures were solved by direct methods and refined with a full-matrix least-squares technique on *F*<sup>2</sup> using the SHELXL-97<sup>16</sup> program included in the WINGX<sup>17</sup> software package. All non-hydrogen atoms were refined anisotropically. The C(13) and C(14) carbon atoms from the 2,4'-bpy ligand in **2** were delocalized between two positions with the *sof* parameter being 0.48 and 0.52. The hydrogen atoms in both structures were set in calculated positions and isotropically refined as riding atoms. The final geometrical calculations and graphical manipulations were carried out with the PARST97<sup>18</sup> and CRYSTALMAKER<sup>19</sup> programs.

### Description of the Structures

**[Cu(4,4'-bpy)(Phmal)]<sub>n</sub>·2*n*H<sub>2</sub>O (**1**).** The structure of complex **1** consists of chains of carboxylate(phenylmalonate)-bridged copper(II) ions which are linked through bis-monodentate 4,4'-bpy ligands to produce a sheetlike polymer growing in the *bc* plane (Figures 1a and 2a). Rectangles with dimensions of 11.08 × 4.99 Å<sup>2</sup> are repeated within each layer, the longer edge corresponding to the 4,4'-bpy ligand (*c* axis), whereas the shorter side is defined by the phenylmalonate-carboxylate group (*b* axis). The separation between adjacent layers is 8.64 Å. The layers are not stacked parallel along the *a* axis but form an angle of 17.807(6)° with the normal plane vector. They are staggered in the ABCABCABC trend and the nearest neighbors are shifted by *c*/3 from each other. Adjacent layers are linked through

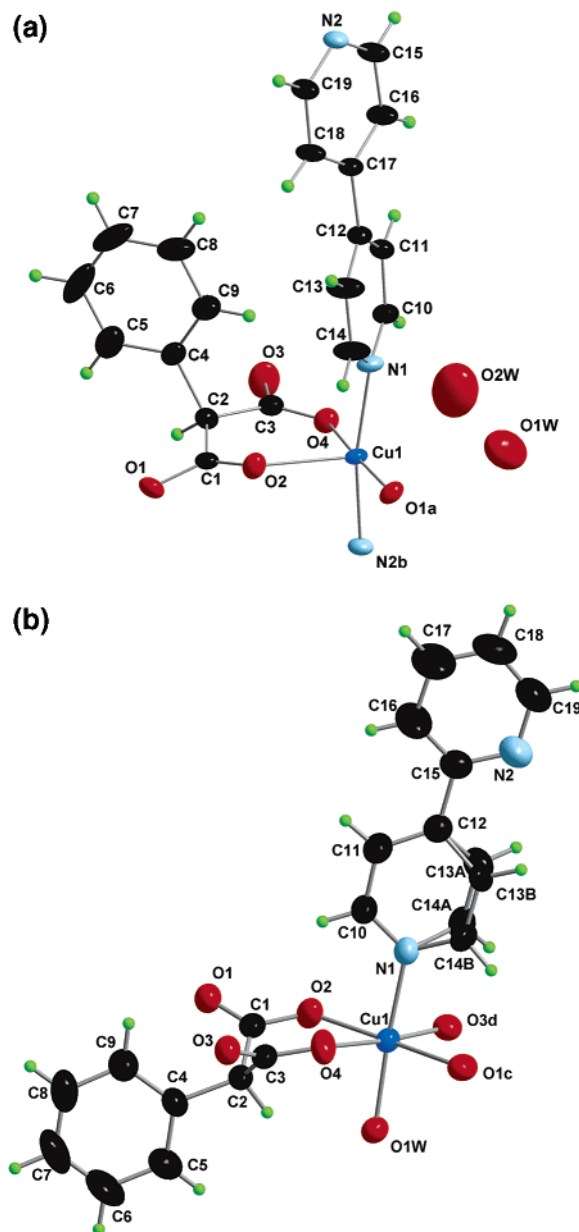


**Figure 1.** View of a fragment of the structures of (a) **1** and (b) **2** with the numbering scheme.

hydrogen bonds involving two carboxylate oxygens [O(1) and O(3)] and the crystallization water molecules (Figure 3); the values of the O...O distances range from 2.839(5) to 3.085(6) Å. It should be noted that the crystallization water molecules are placed between the layers close to the carboxylate groups because of the hydrogen bonds they form. Thus, the water molecules avoid the rectangular cavities because of their hydrophobic character. The  $\pi$ - $\pi$  interactions play an important role in the packing of this structure as observed in previous reports concerning Phmal-containing copper(II) complexes.<sup>12</sup> Several intra- and interlayer C-H... $\pi$  contacts can be identified,<sup>20</sup> the shortest centroid...centroid distance being 4.8781(4) Å, a value which is close to the molecular dynamics calculation for benzene<sup>21</sup> (optimum distance of 4.99 Å between two ring centers in the T-shaped orientation). The values of the dihedral angle between the aromatic rings range from 52.2° to 89.31°.

(16) Sheldrick, G. M. *SHELXL-97* and *SHELXS-97*; Universität Göttingen: Göttingen, Germany, 1998.

(17) Farrugia, L. J. *J. Appl. Crystallogr.* **1999**, *32*, 837.

(18) Nardelli, M. *PARST95*, *J. Appl. Crystallogr.* **1995**, *28*, 659.

(19) *CrystalMaker*, version 4.2.1; CrystalMaker Software: Bicester, U.K.

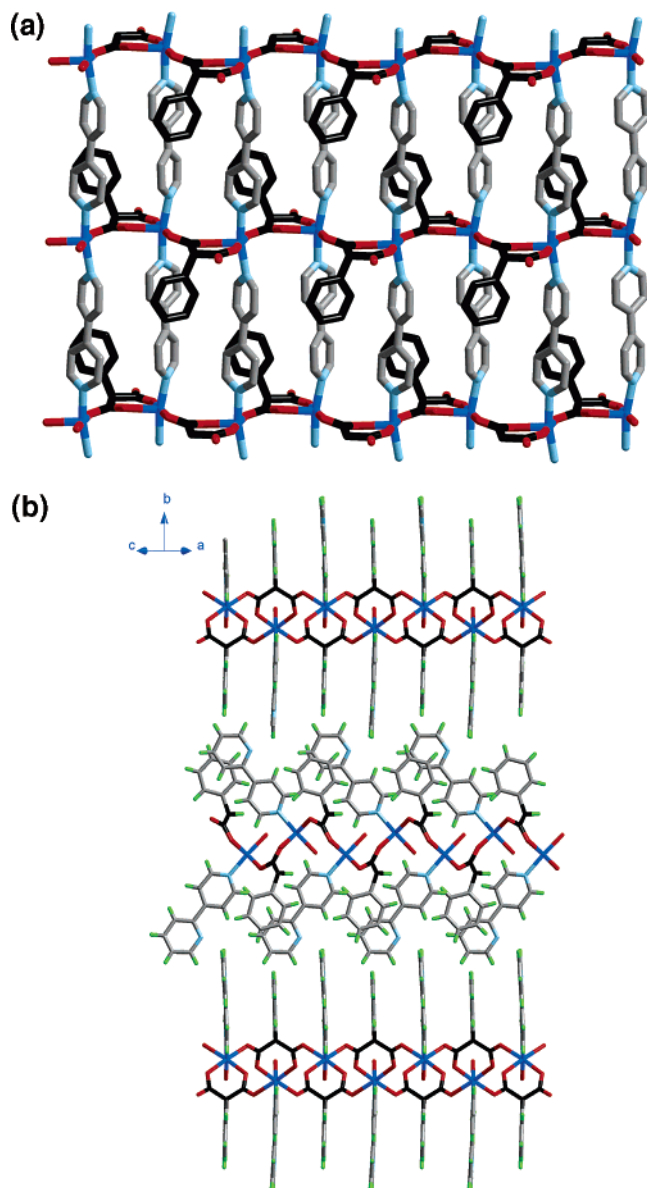


**Figure 2.** (a) View through the [100] direction of a fragment of complex **1**. The 4,4'-bpy ligand connects chains of phenylmalonate-bridged copper(II) ions. Hydrogen atoms are omitted for clarity. (b) Crystal packing of complex **2** with the corrugated layers viewed through the [101] direction.

Each copper atom exhibits a somewhat distorted square pyramidal environment, the geometric  $\tau$  value being 0.13 ( $\tau = 0$  for square pyramidal and  $\tau = 1$  for trigonal bipyramidal).<sup>22</sup> Two nitrogen atoms from the 4,4'-bpy molecule [N(1) and N(2a); (a)  $x, y, z + 1$ ] and two carboxylate-oxygen atoms from the Phmal ligand [O(4) and O(1b); (b)  $-x, y - 1/2, -z$ ] build the basal plane, whereas another carboxylate-oxygen atom [O(2)] occupies the apical position (selected interatomic distances and angles are listed in Table 2). The

(20) For examples of C–H $\cdots\pi$  interactions, see: (a) Janiak, C.; Temizdemir, S.; Dechert, S.; Deck, W.; Girgsdies, F.; Heinze, J.; Kolm, M. J.; Scharmann, T. G.; Zipfel, O. M. *Eur. J. Inorg. Chem.* **2000**, 1229. (b) McNelis, B. J.; Nathan, L. C.; Clark, C. J. *J. Chem. Soc., Dalton Trans.* **1999**, 1831. (c) Biradha, K.; Seward, C.; Zaworotko, M. J. *Angew. Chem., Int. Ed.* **1999**, *38*, 492.

(21) Cox, E. G.; Cruickshank, D. W.; Smith, J. A. S. *Proc. R. Soc. London, Ser. A* **1958**, *247*, 1

(22) Addison, A. W.; Rao, T. N. *J. Chem. Soc., Dalton Trans.* **1984**, 1349.

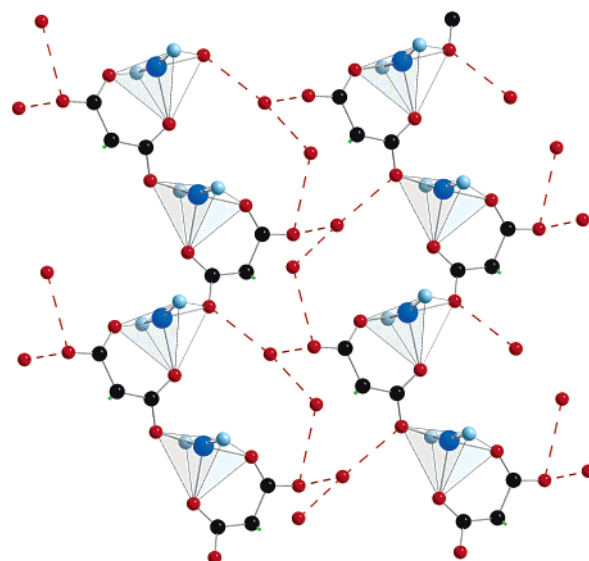


**Figure 3.** Supramolecular layers of phenylmalonate-copper(II) chains bridged through hydrogen bonds with the crystallization water molecules. Phenyl rings of Phmal, carbon atoms of 4,4'-bpy, and hydrogen atoms are omitted for clarity.

**Table 2.** Selected Bond Lengths (Å) and Bond Angles (deg) for Compounds **1** and **2**<sup>a,b</sup>

| <b>1</b>          |            |                   |            |
|-------------------|------------|-------------------|------------|
| Cu(1)–O(1a)       | 1.952(2)   | Cu(1)–N(1)        | 2.041(2)   |
| Cu(1)–O(2)        | 2.185(2)   | Cu(1)–N(2b)       | 2.0220(19) |
| Cu(1)–O(4)        | 1.928(2)   |                   |            |
| O(4)–Cu(1)–O(1a)  | 176.69(9)  | N(2b)–Cu(1)–N(1)  | 168.70(12) |
| O(4)–Cu(1)–N(2b)  | 90.60(9)   | O(4)–Cu(1)–O(2)   | 89.40(8)   |
| O(1a)–Cu(1)–N(2b) | 88.94(9)   | O(1a)–Cu(1)–O(2)  | 93.90(8)   |
| O(4)–Cu(1)–N(1)   | 89.26(9)   | N(2b)–Cu(1)–O(2)  | 94.72(11)  |
| O(1a)–Cu(1)–N(1)  | 90.55(9)   | N(1)–Cu(1)–O(2)   | 95.29(9)   |
| <b>2</b>          |            |                   |            |
| Cu(1)–O(2)        | 2.128(3)   | Cu(1)–O(3d)       | 2.110(3)   |
| Cu(1)–O(4)        | 2.076(3)   | Cu(1)–N(1)        | 2.026(3)   |
| Cu(1)–O(1c)       | 2.208(3)   | Cu(1)–O(1w)       | 2.004(2)   |
| O(1w)–Cu(1)–N(1)  | 176.32(11) | O(4)–Cu(1)–O(2)   | 84.79(14)  |
| O(1w)–Cu(1)–O(4)  | 90.71(12)  | O(3d)–Cu(1)–O(2)  | 90.18(13)  |
| N(1)–Cu(1)–O(4)   | 90.73(12)  | O(1w)–Cu(1)–O(1c) | 89.50(10)  |
| O(1w)–Cu(1)–O(3d) | 91.68(11)  | N(1)–Cu(1)–O(1c)  | 87.13(11)  |
| N(1)–Cu(1)–O(3d)  | 87.19(11)  | O(4)–Cu(1)–O(1c)  | 89.41(13)  |
| O(4)–Cu(1)–O(3)   | 174.49(13) | O(3d)–Cu(1)–O(1c) | 95.57(12)  |
| O(1w)–Cu(1)–O(2)  | 91.59(11)  | O(2)–Cu(1)–O(1c)  | 174.12(14) |
| N(1)–Cu(1)–O(2)   | 91.91(12)  |                   |            |

<sup>a</sup> Estimated standard deviations in the last significant digits are given in parentheses. <sup>b</sup> Symmetry code is as follows: (a)  $-x, y - 1/2, -z$ ; (b)  $x, y, z + 1$ ; (c)  $x, y + 1/2, -z + 1/2$ ; and (d)  $x + 1/2, y, -z + 1/2$ .

equatorial bond lengths vary in the range of 1.928(2)–2.041(2) Å, and the apical bond distance is 2.185(2) Å. The copper atom is shifted by 0.0989(3) Å from the mean basal plane toward the apical position. The copper–copper separation through the phenylmalonate–carboxylate bridge is 4.9922(4) Å, a value which is much shorter than the metal–metal separation through the 4,4'-bpy ligand [11.083(1) Å].

The phenylmalonate ligand simultaneously adopts monodentate [through O(1) to Cu(1e); (e)  $-x, y + 1/2, -z$ ] and bidentate [through O(2) and O(4) to Cu(1)] coordination modes. The bidentate coordination of the Phmal ligand involves one equatorial O(4) bond and one apical O(2) bond, a feature which is unprecedented for Phmal- or malonate-containing copper(II) complexes,<sup>12,14</sup> although it is not

uncommon for copper(II)–oxalate complexes.<sup>23,24</sup> The preference of the copper(II) ion for the nitrogen donor atoms versus the oxygen ones and the fact that the two 4,4'-bpy nitrogen atoms in **1** occupy trans positions in the coordination sphere of the copper atom account for this singularity. The value of the angle subtended at the copper atom by the bidentate Phmal ligand is 89.40(8)°. The pyridyl rings of the 4,4'-bpy molecule are planar, but the ligand as a whole is far from being planar [the dihedral angle between the two pyridyl rings is 19.99(10)°]. As far as we know, there are two recently reported compounds whose structures are very similar to that of **1**: [Cu<sub>3</sub>(μ-ox)<sub>3</sub>(μ-4,4'-bpy)(4,4'-bpy)<sub>2</sub>]<sub>n</sub><sup>24</sup> and {[Cu(Hsal)<sub>2</sub>(4,4'-bpy)]·H<sub>2</sub>O·H<sub>2</sub>sal}<sub>n</sub><sup>25</sup> (ox = oxalate dianion and H<sub>2</sub>sal = salicylic acid). In light of these structures (see Supporting Information), it is clear that the rectangular moiety observed in **1** is not unique, but layered motifs are ensured by the reaction of copper(II) with the appropriate bridging ligand and 4,4'-bpy.

We would like to finish the present structural description with a comparison of the structure of **1** with that of the previously reported malonato copper(II) complex [Cu<sub>4</sub>(mal)<sub>4</sub>(H<sub>2</sub>O)<sub>4</sub>(4,4'-bpy)<sub>2</sub>]<sub>14h</sub> (H<sub>2</sub>mal = malonic acid). This structure consists of layers of tetranuclear entities of carboxylate–malonato-bridged copper(II) ions linked by 4,4'-bpy ligands. The tetranuclear units are small squares with the copper(II) ions at the corners and the bridging-malonato ligand defining the edges. These units are linked by the 4,4'-bpy groups to form large squares of 15.784(1) × 15.784(1) Å<sup>2</sup>. Although the dimensionality of this structure as a whole is identical to that of **1**, the presence of the phenyl ring in **1** provides additional interactions (C–H⋯π- and π–π-type interactions, steric effects, etc.) which account for the new coordination mode of the Phmal ligand and the hydrophobic character in the structure.

[Cu(2,4'-bpy)(Phmal)(H<sub>2</sub>O)]<sub>n</sub> (**2**). The structure **2** consists of a sheetlike arrangement of *trans*-aqua(2,4'-bipyridine)-copper(II) units bridged by phenylmalonate ligands running parallel to the *ac* plane (see Figures 1b and 2b). A corrugated square grid of copper atoms results (Figure 4) where the 2,4'-bpy terminal ligands are alternatively located above and below each layer and, at the same time, inversely to the position of the phenyl group of the Phmal ligand. These sheets are stacked parallel along the *b* axis but rotated 90° through this axis in a twisted fashion (i.e., odd units in the same position and even units rotated by 90°) exhibiting the ABABAB sequence. Intralayer hydrogen bonds involving the coordinated water molecule [O(1w)] and oxygen atoms from the carboxylate–phenylmalonate groups [2.615(4) and

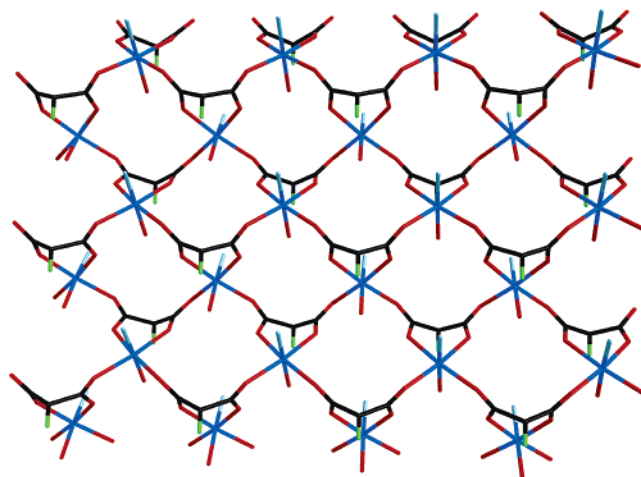


**Figure 4.** View of the corrugated layer of the phenylmalonate-bridged copper(II) atoms of complex **2** forming a square grid. The phenyl (Phmal) pyridyl (2,4'-bpy) rings are omitted for the sake of clarity.

**Table 3.** Bond Distances at Cu(1) and Calculated ΔMSDA Values for Compound **2** at Different Temperatures<sup>a</sup>

| bond        | <i>T</i> = 293 K |                                           | <i>T</i> = 100 K |                                           |
|-------------|------------------|-------------------------------------------|------------------|-------------------------------------------|
|             | <i>d</i> (Å)     | ΔMSDA (×10 <sup>-4</sup> Å <sup>2</sup> ) | <i>d</i> (Å)     | ΔMSDA (×10 <sup>-4</sup> Å <sup>2</sup> ) |
| Cu(1)–O(2)  | 2.128(3)         | 269                                       | 2.111(5)         | 355                                       |
| Cu(1)–O(4)  | 2.076(3)         | 255                                       | 2.087(5)         | 301                                       |
| Cu(1)–O(1c) | 2.208(3)         | 293                                       | 2.187(5)         | 247                                       |
| Cu(1)–O(3d) | 2.110(3)         | 315                                       | 2.156(5)         | 201                                       |
| Cu(1)–O(1w) | 2.004(2)         | 59                                        | 1.992(3)         | 29                                        |
| Cu(1)–N(1)  | 2.026(3)         | 64                                        | 2.014(4)         | 36                                        |

<sup>a</sup> Symmetry code is as follows: (c) *x*, *y* + 1/2, *-z* + 1/2 and (d) *x* – 1/2, *y*, *-z* + 1/2.

2.633(4) Å for O(1w)⋯O(2c) and O(1w)⋯O(4f), respectively; (c) *x*, *y* + 1/2, *-z* + 1/2; (f) *x* – 1/2, *y*, *-z* + 1/2] contribute to stabilize the structure. Weak π-type interactions occur between the phenyl rings and the 2,4'-bpy groups, the shortest centroid⋯centroid distance being 4.154(6) Å and the shortest off-set angle being 29.6°, values which are somewhat larger than the average ones observed in π–π interactions with pyridyl-like groups.<sup>26</sup>

Each copper atom exhibits a six-coordinated environment defined by four carboxylate–phenylmalonate oxygen atoms, one 2,4'-bpy-nitrogen atom, and a water molecule. The CuNO<sub>5</sub> chromophore could be described as an unusual compressed tetragonal octahedron with two short distances [2.004(2) and 2.026(3) Å for Cu(1)–O(1w) and Cu(1)–N(1), respectively] and four long ones [values ranging from 2.076(3) to 2.208(3) Å] (see Table 2). A low-temperature crystallographic study has been carried out to give a clear-cut answer to this compression. In light of Table 3, one can see that the bond distances and angles at 293 and 100 K do not vary significantly, and hence, the presence of a static pseudo-Jahn–Teller disorder could be suspected.<sup>27–30</sup> The

- (23) (a) Oshio, H.; Nagashima, U. *Inorg. Chem.* **1992**, *31*, 3295. (b) Castillo, O.; Luque, A.; Lloret, F.; Román, P. *Inorg. Chim. Acta* **2001**, *324*, 141. (c) Luo, J.; Hong, M.; Liang, Y.; Cao, R. *Acta Crystallogr., Sect. E*, **2001**, *57*, m361. (d) Cavalca, L.; Villa, A. C.; Manfredotti, A. G.; Tomlinson, A. A. G. *J. Chem. Soc., Dalton Trans.* **1972**, 391. (e) Castillo, O.; Luque, A.; Julve, M.; Lloret, F.; Román, P. *Inorg. Chim. Acta*, **2001**, *315*, 9. (f) Castillo, O.; Luque, A.; Román, P.; Lloret, F.; Julve, M. *Inorg. Chem.* **2001**, *40*, 5526. (g) Suárez-Varela, J.; Domínguez-Vera, J. M.; Colacio, E.; Ávila-Rosón, J. C.; Hidalgo, M. A.; Martín-Ramos, D. *J. Chem. Soc., Dalton Trans.* **1995**, 2143. (24) Castillo, O.; Alonso, J.; García-Couceiro, U.; Luque, A.; Román, P. *Inorg. Chem. Commun.* **2003**, *6*, 803. (25) Zhu, L.-G.; Kitagawa, S. *Inorg. Chem. Commun.* **2003**, *6*, 1051.

- (26) Janiak, C. *J. Chem. Soc., Dalton Trans.* **2000**, 3885. (27) Hathaway, B. J. *Struct. Bonding*, **1984**, *57*, 55. (28) Falvello, L. R. *J. Chem. Soc., Dalton Trans.* **1997**, 4463. (29) Halcrow, M. A. *Dalton Trans.* **2003**, 4375. (30) Solanki, N. K.; Leech, M. A.; McInnes, E. J. L.; Mabbs, F. E.; Howard, J. A. K.; Kilner, C. A.; Rawson, J. M.; Halcrow, M. A. *J. Chem. Soc., Dalton Trans.* **2002**, 1295.



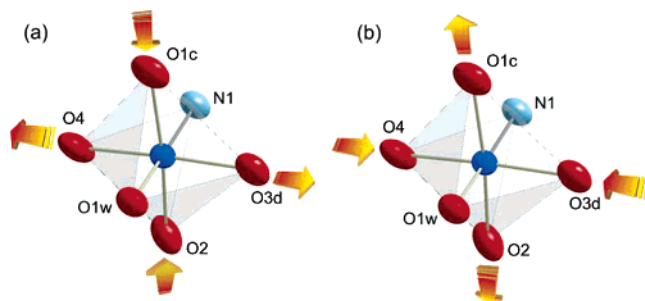


**Figure 5.** Two different copper(II) environments [(a) and (b)] which occur in complex **2** because a static pseudo-Jahn–Teller disorder. Arrows indicate the atoms that fill equatorial (compressed) or apical (elongated) positions at the metal environment.

vibrational amplitudes of the ligand donor atoms along the metal–ligand bonds represented by the quantity  $\langle d^2 \rangle$  or equivalently  $\Delta\text{MSDA}^{27-30}$  are also listed in Table 3. These values correspond to the difference in the mean-square displacements parameters (MSDAs) of a given donor atom and the Cu atom along their common vector (eqs 1 and 2).

$$\text{MSDA} = \frac{\sum_{i=1}^3 \sum_{j=1}^3 U_{ij} n_i n_j}{|n|^2} \quad (1)$$

$$\langle d \rangle^2 = \Delta\text{MSDA} = \text{MSDA}(\text{donor}) - \text{MSDA}(\text{Cu}) \quad (2)$$

where  $U_{ij}$  is an element of the  $3 \times 3$  matrix of thermal parameters and  $n_i$  and  $n_j$  are elements of the vector describing the bond. Values of  $\Delta\text{MSDA}$  are typically found in the range of  $(10-100) \times 10^{-4} \text{ \AA}^2$ .<sup>28</sup> The values of the  $\Delta\text{MSDA}$  for O(1w) and N(1) are within this range but the four carboxylate oxygen atoms present  $\Delta\text{MSDA}$ s in the range of  $(255-315) \times 10^{-4} \text{ \AA}^2$ . This disparity from the “static” values can be attributed to the presence of a static pseudo-Jahn–Teller disorder of two of the three axes of the octahedral copper environment. The shorter bond distances correspond with the Cu(1)–O(1w) and Cu(1)–N(1) bonds indicating that these two atoms belong to the basal plane of Cu(1). The O(2), O(4), O(1c), and O(3d) [(d)  $x + 1/2$ ,  $y$ ,  $-z + 1/2$ ] are statically disordered in pairs between the equatorial and axial positions [two different environments are found within the crystal, one with O(1w), N(1), O(2), and O(1c) in equatorial positions and O(4) and O(3d) in axial positions; the other with O(1w), N(1), O(4), and O(3d) in equatorial positions and O(2) and O(1c) in axial positions] (Figure 5). The analysis of the EPR spectrum at room temperature (see Supporting Information) reveals three different effective  $g$  values ( $g_1 = 2.27$ ,  $g_2 = 2.20$ ,  $g_3 = 2.15$ ) indicating a rhombic environment of the copper(II) ion or, according to our approximation, the averaged values of a static pseudo-Jahn–Teller disorder in the crystal as they appear in the X-ray crystal structure. EPR spectra at low temperatures do not change significantly from the rhombic distortion; the slight variations in the  $g$  values are most likely associated with the spin coupling.

The phenylmalonate ligand acts simultaneously as a bidentate ligand [through O(2) and O(4) to Cu(1)] and as a

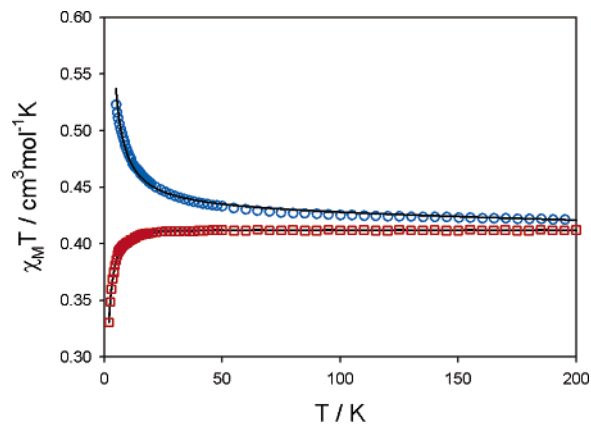


**Figure 6.** Thermal dependence of the  $\chi_M T$  product for complexes **1** and **2** (**1**, red squares; **2**, blue circles). The solid line represents the best fit through eqs 3 and 4 for complexes **1** and **2**, respectively.

bis-monodentate ligand [through O(1) and O(3) to Cu(1 g) and Cu(1d), respectively; (g)  $x$ ,  $y - 1/2$ ,  $-z + 1/2$ ]. The 2,4'-bpy ligand is quasi-planar [the dihedral angle between pyridyl rings is  $4^\circ$ ]. The pyridyl ring formed by the N(1)–C(10)–C(11)–C(12)–C(13)–C(14) set of atoms is slightly distorted, and two crystallographic positions are found for the C(13) and C(14) atoms [0.977(16) and 1.012(15) Å for C(13A)–C(13B) and C(14A)–C(14B), respectively]. These two positions are also found in the low-temperature X-ray study of a different crystal; hence, a static disorder within the crystal could be the responsible for this feature. The copper–copper separations through the two crystallographically independent anti-syn carboxylate bridges are 5.3217(9) and 5.4202(6) Å, values which are much shorter than the interlayer Cu $\cdots$ Cu distance [15.221(2) Å].

The comparison of the structure of **2** with that of the previously reported<sup>31</sup> malonato–manganese(II) complex of formula  $[\text{Mn}(\text{mal})(\text{H}_2\text{O})(2,4'\text{-bpy})]_n$  reveals that both are very similar, fact that cannot be extended to the compound  $[\text{Cu}(\text{mal})_4(2,4'\text{-bpy})_4(\text{H}_2\text{O})_4] \cdot 8\text{H}_2\text{O}$ .<sup>14j</sup> Therefore, from a structural point of view and in the presence of the 2,4'-bpy ligand, the copper(II) ion acts as the manganese(II) cation when the malonate is substituted by the phenylmalonate ligand.

### Magnetic Properties

The magnetic properties of compounds **1** and **2** under the form of the  $\chi_M T$  vs  $T$  plot [ $\chi_M$  is the molar susceptibility per copper(II) ion] are shown in Figure 6. The values of  $\chi_M T$  at room temperature are 0.41 and 0.42  $\text{cm}^3 \text{mol}^{-1} \text{K}$  for **1** and **2**, respectively. These values are as expected for magnetically isolated spin doublets. The  $\chi_M T$  values remains almost constant down to 10 K for compound **1** and then smoothly decreases to 0.34  $\text{cm}^3 \text{mol}^{-1} \text{K}$  at 2.0 K indicating that there is a very weak antiferromagnetic coupling between the copper(II) ions. For compound **2**,  $\chi_M T$  remains almost constant until 30 K and then it increases to reach a value of 0.53  $\text{cm}^3 \text{mol}^{-1} \text{K}$  at 2.0 K, a feature which is indicative of an overall ferromagnetic coupling in **2**.

(31) Rodríguez-Martín, Y.; Hernández-Molina, M.; Sanchiz, J.; Ruiz-Pérez, C.; Lloret, F.; Julve, M. *Dalton Trans.* **2003**, 2359.

Two different magnetic exchange pathways between copper atoms are present in **1**: the 4,4'-bpy bridging ligand and the carboxylate bridge in the anti-syn conformation linking one apical position with an equatorial position at the copper(II) atoms. Since the distance between the copper(II) ions through the 4,4'-bpy bridge is 11.083(1) Å and the values of  $-J$ , from previous reports<sup>14d,32</sup> on 4,4'-bpy-bridged copper dimers, vary in the range of 0.05–0.1 cm<sup>-1</sup>, the magnetic coupling has to be very small compared with that of the anti-syn carboxylate bridge. Therefore, from a magnetic point of view, compound **1** can be seen as uniform chains of antiferromagnetically coupled copper(II) ions, and the magnetic data can be analyzed by means of the following numerical expression:<sup>33</sup>

$$\chi_M = \frac{Ng^2\beta^2}{kT} \frac{0.25 + 0.074975x + 0.075235x^2}{1.0 + 0.9931x + 0.172135x^2 + 0.757825x^3} \quad (3)$$

where  $x = |J|/kT$ , the Hamiltonian is defined as  $\sum_i JS_i \cdot S_{i+1}$ ,  $J$  is the magnetic coupling constant, and  $N$ ,  $g$ ,  $\beta$ , and  $k$  have their usual meaning. Best-fit parameters using a nonlinear regression analysis are as follows:  $J = -0.59(1)$  cm<sup>-1</sup>,  $g = 2.21(2)$ , and  $R = 5.2 \times 10^{-5}$  ( $R$  is the agreement factor defined as  $\sum_i [(\chi_M T)_{\text{obs}}(i) - (\chi_M T)_{\text{calc}}(i)]^2 / \sum_i [(\chi_M T)_{\text{obs}}(i)]^2$ ). The calculated curve matches well the experimental data in the whole temperature range (Figure 6).

According to the square lattice layer defined by the copper(II) ions of compound **2** (Figure 4), its magnetic data were analyzed by the high-temperature series expansion derived from the two-dimensional Heisenberg model for a  $S = 1/2$  ferromagnetic square lattice<sup>34</sup>

$$\chi = [Ng^2\beta^2/(3kT)]S(S+1)(1 + \sum_{n=1}^{10} a_n K^n) \quad (4)$$

with  $K = J/kT$ . The coefficients for the square lattice are represented by  $a_n$ , and  $J$  is the intralayer magnetic coupling between the local spins of the nearest-neighbors with the Hamiltonian of eq 4 defined as

$$H = -\sum_i JS_i \cdot S_{i+1} \quad (5)$$

Best-fit parameters using a nonlinear regression analysis are as follows:  $J = 0.77(1)$  cm<sup>-1</sup>,  $g = 2.22(1)$ , and  $R = 1.2 \times 10^{-5}$  ( $R$  is the agreement factor defined as  $\sum_i [(\chi_M T)_{\text{obs}}(i) - (\chi_M T)_{\text{calc}}(i)]^2 / \sum_i [(\chi_M T)_{\text{obs}}(i)]^2$ ). The calculated curve matches well the experimental data in the temperature range explored (Figure 6). The calculated value of  $g$  is in agreement with that obtained from the EPR spectra.

The analysis of the magnetic data shows that compounds **1** and **2** exhibit weak antiferromagnetic (**1**) and ferromagnetic

(**2**) interactions. Let us try to analyze, first, the magnitude and, second, the nature of the magnetic interaction. The carboxylate group can adopt three different bis-monodentate bridging modes: syn-syn, anti-anti, and anti-syn. From moderate to strong antiferromagnetic coupling is observed for the first two modes, whereas weak either ferromagnetic or antiferromagnetic interactions occur in the third.<sup>35</sup> This ability of the carboxylate group has been substantiated by DFT-type calculations.<sup>36</sup> As the copper(II) ions in compounds **1** and **2** are bridged by carboxylate groups in the anti-syn conformation, the weak values of the magnetic coupling observed are as expected.

In addition to the conformation of the bridge, the relative orientation of the magnetic orbitals centered on the metal ions in both compounds is very unfavorable for a strong magnetic coupling. In the case of compound **1**, the carboxylate bridge links an equatorial position of one copper(II) ion with an axial position of the adjacent copper(II) ion. The magnetic orbital for copper(II) ions in a square pyramidal surrounding is of the  $d_{x^2-y^2}$ -type; the  $x$  and  $y$  axes are roughly defined by the equatorial bonds. Some admixture of the  $d_z^2$  orbital is present as a result of trigonal distortion. The magnetic coupling is very weak because it is the result of the interaction of a  $d_{x^2-y^2}$ -type orbital with a  $d_z^2$ -type orbital, the latter having a very small spin density. In the case of compound **2**, the environment of the copper(II) ion is distorted octahedral and the magnetic orbital also has  $d_{x^2-y^2}$  character. Each copper(II) ion is connected to four other copper(II) ions through anti-syn carboxylate bridges to give a quadratic layer. The magnetic coupling in this compound is also very weak because the equatorial plane of the copper environment (Scheme 1) is quasi-perpendicular to the plane of the bridging carboxylate (the exchange pathway) and only two of the four exchange pathways have important spin density (half of the exchange pathways are inactive). This situation is very unfavorable for a large magnetic interaction and leads to a very weak coupling constant.

We will now try to explain the different nature of the magnetic coupling for compounds with apparently similar chemical and structural features. The exchange constant can be expressed as the sum of two contributions, one ferromagnetic (small and positive) and another antiferromagnetic (negative and proportional to the square of the overlap between the orbitals on the bridge with those of the metal ions bearing the unpaired electrons), in such a way that the lower the overlap is, the smaller the antiferromagnetic contribution [ $J = J_F + J_{AF}$ ].<sup>37</sup> In the case of compound **1**, the copper(II) ions and carboxylate groups lie in a plane with an out-of-plane maximum deviation of 0.321(2) Å for O(2). This situation enhances the overlap between the interacting magnetic orbitals of the metal ions and those of the atoms of the bridge and makes the antiferromagnetic term dominant. On the other hand, the copper(II) ions in compound **2** lie in

(32) (a) Haddad, M. S.; Hendrickson, D. N.; Cannady, J. P.; Drago, R. S.; Bieksza, D. S. *J. Am. Chem. Soc.* **1979**, *101*, 898. (b) Julve, M.; Verdager, M.; Faus, J.; Tinti, F.; Moratal, J.; Monge, A.; Gutiérrez-Puebla, E. *Inorg. Chem.* **1987**, *26*, 3520.

(33) Estes, W. E.; Gavel, D. P.; Hatfield, W. E.; Hodgson, D. *Inorg. Chem.* **1978**, *17*, 1415.

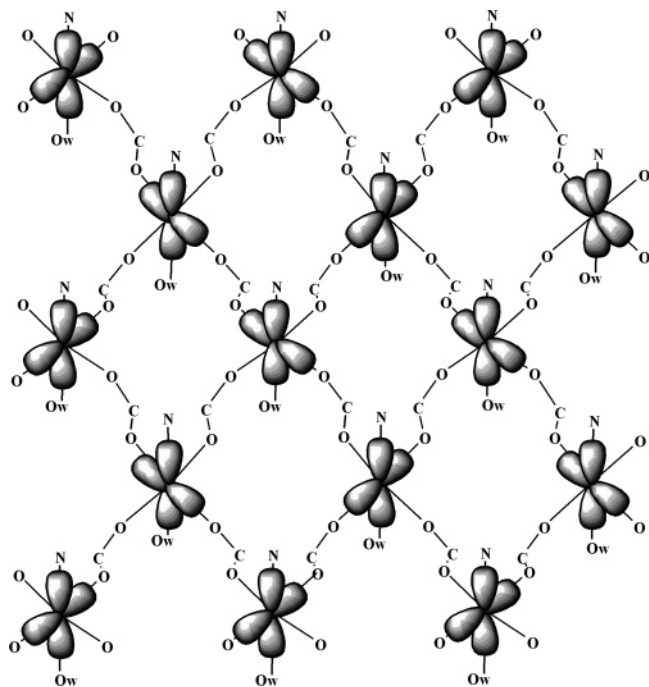
(34) Navarro, R. *Application of High- and Low-Temperature Series Expansions to Two-Dimensional Magnetic Systems*; de Jongh, L. J.; Ed., Kluwer: Dordrecht, The Netherlands, **1990**.

(35) Pasán, J.; Delgado, F. S.; Rodríguez-Martín, Y.; Hernández-Molina, M.; Ruiz-Pérez, C.; Sanchiz, J.; Lloret, F.; Julve, M. *Polyhedron*, **2003**, *22*, 2143.

(36) Rodríguez-Fortea, A.; Alemany, P.; Álvarez, S.; Ruiz, E. *Chem.—Eur. J.* **2001**, *7*, 627.

(37) Kahn, O. *Molecular Magnetism*; VCH: New York, 1993.

Scheme 1



a corrugated layer that makes the magnetic orbitals of the metal ions form an angle of  $87.8(4)^\circ$  in the bridge (Figure 4). This situation leads to a very poor overlap making the antiferromagnetic contribution very small and causing the ferromagnetic contribution to be dominant.

### Conclusions

The compounds  $[\text{Cu}(4,4'\text{-bpy})(\text{Phmal})]_n \cdot 2n\text{H}_2\text{O}$  (**1**) and  $[\text{Cu}(2,4'\text{-bpy})(\text{Phmal})(\text{H}_2\text{O})]_n$  (**2**) were prepared, and their structures and magnetic properties were investigated. Although both compounds are sheetlike polymers, their structures are very different. There are two bridging ligands in **1** (Phmal and 4,4'-bpy), and only one in **2** (Phmal). Addition-

ally, the layers in **1** are almost planar, whereas they are corrugated in **2** with angles of  $87.8^\circ$ . The structures of **1** and **2** are also very different from those of the malonate copper(II) derivatives  $[\text{Cu}(\text{mal})(\text{H}_2\text{O})(4,4'\text{-bpy})_{0.5}]$  and  $[\text{Cu}(\text{mal})(\text{H}_2\text{O})(2,4'\text{-bpy})]$ , demonstrating that the phenyl ring of the phenylmalonate exerts important structural effects. Nevertheless the structure of **2** is similar to that of  $[\text{Mn}(2,4'\text{-bpy})(\text{mal})(\text{H}_2\text{O})]$ .<sup>31</sup>

Under a magnetic point of view, both compounds display very weak interactions mainly caused by the anti-syn conformation of the carboxylate bridge. However, compound **2** exhibits a ferromagnetic coupling between the copper(II) ions, but magnetic ordering down to 2.0 K is not achieved because of the weak magnetic interaction. It seems interesting to determine if other potentially bridging ligands such as pyrazine or pyrimidine lead to similar structures in which the magnetic coupling could be stronger. The work of our group will be oriented in that direction trying to increase the intralayer magnetic coupling and paying attention to the effect of introducing smaller ligands that may lead to a shorter interlayer separation.

**Acknowledgment.** We thank the Ministerio Español de Ciencia y Tecnología (Projects CTQ2004-03633 and BQU2001-3794), the Consejería de Educación, Cultura y Deportes of Gobierno Autónomo de Canarias (Project PI2002/175), and the Ministerio Español de Educación y Ciencia (Project MAT2004-03112) for financial support. J.P. also thanks the Ministerio Español de Educación y Ciencia for a predoctoral fellowship (Ref. AP2001-3322).

**Supporting Information Available:** Crystallographic data in CIF format for **1** (CCDC 266328) and **2** (CCDC 266329) and the Q-band EPR spectra of complex **2** at different temperatures. This material is available free of charge via the Internet at <http://pubs.acs.org>.

IC0503986

**[Fe(bpym)(CN)<sub>4</sub>]<sup>-</sup>: A New Building Block for Designing Single-Chain Magnets**Luminita Marilena Toma,<sup>†</sup> Rodrigue Lescouëzec,<sup>†,§</sup> Jorge Pasán,<sup>‡</sup> Catalina Ruiz-Pérez,<sup>‡</sup> Jacqueline Vaissermann,<sup>§</sup> Joan Cano,<sup>‡</sup> Rosa Carrasco,<sup>†</sup> Wolfgang Wernsdorfer,<sup>||</sup> Francesc Lloret,<sup>†</sup> and Miguel Julve<sup>\*,†</sup>

Contribution from the Departament de Química Inorgànica/Instituto de Ciencia Molecular, Facultat de Química de la Universitat de València, Avda. Dr. Moliner 50, 46100 Burjassot, València, Spain, Laboratorio de Rayos X y Materiales Moleculares, Departamento de Física Fundamental II, Facultad de Física de la Universidad de La Laguna, Avda. Astrofísico Francisco Sánchez s/n, 38204 La Laguna, Tenerife, Spain, Laboratoire de Chimie Inorganique et Matériaux Moléculaires, Université Pierre et Marie Curie, F-75252 Paris, Cedex 05, France, Laboratoire Louis Néel, CNRS, BP 166, 25 Avenue des Martyrs, 38042 Grenoble Cedex 09, France, and Institució Catalana de Recerca i Estudis Avançats(ICREA)/Departament de Química Inorgànica i Centre de Recerca en Química Teòrica, Universitat de Barcelona, Avda. Diagonal 647, 08028 Barcelona, Spain

Received December 12, 2005; E-mail: . miguel.julve@uv.es

**Abstract:** We herein present the preparation, crystal structure, magnetic properties, and theoretical study of new heterobimetallic chains of formula  $\{[\text{Fe}^{\text{III}}(\text{bpym})(\text{CN})_4]_2\text{M}^{\text{II}}(\text{H}_2\text{O})_2\} \cdot 6\text{H}_2\text{O}$  [bpym = 2,2'-bipyrimidine; M = Zn (**2**), Co (**3**), Cu (**4**), and Mn (**5**)] which are obtained by using the building block  $\text{PPh}_4[\text{Fe}(\text{bpym})(\text{CN})_4] \cdot \text{H}_2\text{O}$  (**1**) ( $\text{PPh}_4^+$  = tetraphenylphosphonium) as a ligand toward the fully solvated  $\text{M}^{\text{II}}$  ions. The structure of complex **1** contains mononuclear  $[\text{Fe}(\text{bpym})(\text{CN})_4]^-$  anions. Compounds **2–5** are isostructural 4,2-ribbonlike bimetallic chains where the  $[\text{Fe}(\text{bpym})(\text{CN})_4]^-$  unit acts as a bis-monodenate ligand through two of its four cyanide ligands toward the M atom. Water hexamer clusters (**4**) and regular alternating fused six- and four-membered water rings with two dangling water molecules (**2**, **3**, and **5**) are trapped between the cyanide-bridged 4,2-ribbonlike chains. **1** and **2** behave as magnetically isolated low-spin iron(III) centers. **3** behaves as a single-chain magnet (SCM) with intrachain ferromagnetic coupling, slow magnetic relaxation, hysteresis effects, and frequency-dependent ac signals at  $T < 7$  K). As expected for a thermally activated process, the nucleation field ( $H_n$ ) in **3** increases with decreasing  $T$  and increasing  $\nu$ . Below 1.0 K,  $H_n$  becomes temperature independent but remains strongly sweep rate dependent. In this temperature range, the reversal of the magnetization may be induced by a quantum nucleation of a domain wall that then propagates due to the applied field. **4** and **5** are ferro- and ferrimagnetic chains respectively, with metamagnetic-like behavior (**4**). DFT-type calculations and QMC methodology provided a good understanding of the magnetic properties of **3–5**.

**Introduction**

Magnetic systems that exhibit slow relaxation of the magnetization such as single-molecule magnets (SMMs)<sup>1,2</sup> and single-chain magnets (SCMs)<sup>4–6</sup> are very hot topics in chemistry and materials science because of the interest in them from a fundamental point of view (quantum phenomena and finite-size effects, for instance) and also because of their possible applica-

tions in magnetic devices (nanometric magnetic memory units).<sup>7</sup> A ground state with both high spin ( $S$ ) and large negative axial anisotropy ( $D$ ) together with negligible intermolecular interactions are the requirements to have a double minimum potential for the reversal of the magnetic moment in the so-called SMMs.

<sup>†</sup> Universitat de Valencia.<sup>‡</sup> Universidad de La Laguna.<sup>§</sup> Université Pierre et Marie Curie.<sup>||</sup> ICREA and Universitat de Barcelona.<sup>||</sup> Laboratoire Louis Néel.

- (1) (a) Sessoli, R.; Gatteschi, D.; Novak, M. A. *Nature* **1993**, *365*, 141. (b) Sessoli, R.; Tsai, H.; Schake, A. R.; Wang, S.; Vincent, J. B.; Folting, K.; Gatteschi, D.; Christou, G.; Hendrickson, D. N. *J. Am. Chem. Soc.* **1993**, *115*, 1804.  
 (2) Gatteschi, D.; Sessoli, R. *Angew. Chem., Int. Ed.* **2003**, *42*, 268 and references therein.  
 (3) Winpenny, R. E. P. *Adv. Inorg. Chem.* **2001**, *1*, 52 and references therein.

- (4) (a) Caneschi, A.; Gatteschi, D.; Lalioti, N.; Sangregorio, C.; Sessoli, R.; Venturi, G.; Vindigni, A.; Rettori, A.; Pini, M. G.; Novak, M. A. *Angew. Chem., Int. Ed.* **2001**, *40*, 1760. (b) Caneschi, A.; Gatteschi, D.; Lalioti, N.; Sessoli, R.; Sorace, L.; Tannougouls, V.; Vindigni, A. *Chem. Eur. J.* **2002**, *8*, 286. (c) Caneschi, A.; Gatteschi, D.; Lalioti, N.; Sangregorio, C.; Sessoli, R.; Venturi, G.; Vindigni, A.; Rettori, A.; Pini, M. G.; Novak, M. A. *Europhys. Lett.* **2002**, *58*, 771. (d) Bogani, L.; Caneschi, A.; Fedi, M.; Gatteschi, D.; Massi, M.; Novak, M. A.; Pini, M. G.; Rettori, A.; Sessoli, R.; Vindigni, A. *Phys. Rev. Lett.* **2004**, *92*, 207204.  
 (5) (a) Clérac, R.; Miyasaka, H.; Yamashita, M.; Coulon, C. *J. Am. Chem. Soc.* **2002**, *124*, 12387. (b) Miyasaka, H.; Clérac, R.; Mizushima, K.; Sugiura, K.; Yamashita, M.; Wernsdorfer, W.; Coulon, C. *Inorg. Chem.* **2003**, *42*, 8203.  
 (6) Lescouëzec, R.; Vaissermann, J.; Ruiz-Pérez, C.; Lloret, F.; Carrasco, R.; Julve, M.; Verdager, M.; Dromzee, Y.; Gatteschi, D.; Wernsdorfer, W. *Angew. Chem., Int. Ed.* **2003**, *42*, 1483.  
 (7) (a) Wernsdorfer, W.; Sessoli, R. *Science* **1999**, *284*, 133. (b) Leuenberger, M. N.; Loss, D. *Nature* **2001**, *410*, 789.

The interest in the SCMs has its origin in Glauber's early theoretical work.<sup>8</sup> He suggested that the conditions needed to observe slow magnetic relaxation in a one-dimensional compound were: (i) it must behave as an Ising ferro- or ferrimagnetic chain and (ii) the ratio  $J/J'$  has to be larger than  $10^4$  ( $J$  and  $J'$  being the intrachain and interchain magnetic interactions, respectively). More than three decades were needed to observe this behavior for the first time because of these rather stringent requirements. The ferrimagnetic chain [Co<sup>II</sup>(hfac)<sub>2</sub>(NITPhOMe)] (Hhfac = hexafluoroacetylacetone and NITPhOMe = 4'-methoxy-phenyl-4,4,5,5-tetramethylimidazole-1-oxyl-3-oxide) was the first example of this type of system reported by Gatteschi et al. in 2001.<sup>3a</sup> The alternating current (ac) magnetic susceptibility of this compound is strongly field dependent below 17 K, and the relaxation time ( $\tau$ ) shows a thermally activated (Arrhenius) behavior with  $\tau_0 = 3.0 \times 10^{-11}$  s and an energy barrier ( $E_a$ ) to reverse the magnetization of 107 cm<sup>-1</sup>. The anisotropy of high-spin cobalt(II)-radical intrachain exchange interaction gives the barrier for the reorientation of the magnetization. The first heterometallic SCMs were reported in 2002 by Clérac et al. and they deal with a family of bimetallic chains of general formula [Mn<sup>III</sup><sub>2</sub>(saltmen)<sub>2</sub>Ni<sup>II</sup>(pao)<sub>2</sub>L<sub>2</sub>]A<sub>2</sub> [saltmen<sup>2-</sup> = *N,N'*-(1,1,2,2-tetramethylene)bis(salicylideneimine), pao<sup>-</sup> = pyridine-2-aldoximate, L = nitrogen donor heterocycle, and A<sup>-</sup> = univalent anion] where regular alternating single oximate bridges between Ni<sup>II</sup> and Mn<sup>III</sup> (antiferromagnetic coupling) and double phenolate-oxo bridges between pairs of Mn<sup>III</sup> ions (ferromagnetic coupling) occur.<sup>4</sup> Coercivity and relaxation of the magnetization below 3.5 K are observed in this family. Other more recent examples of SCMs are the homospin helical chain [Co<sup>II</sup>(bt)(N<sub>3</sub>)<sub>2</sub>] (bt = 2,2'-bithiazoline) with double end-on azido bridges between the high-spin cobalt(II) ions,<sup>9</sup> the oxamidato-bridged heterobimetallic chain [Co<sup>II</sup>-Cu<sup>II</sup>(2,4,6-tmpa)<sub>2</sub>(H<sub>2</sub>O)<sub>2</sub>] $\cdot$ 4H<sub>2</sub>O (2,4,6-tmpa<sup>2-</sup> = *N*-2,4,6-trimethylphenylloxamate dianion),<sup>6</sup> the Mn<sub>7</sub> clusters [Mn<sub>7</sub>O<sub>8</sub>(O<sub>2</sub>-SePh)<sub>8</sub>(O<sub>2</sub>CMe)(H<sub>2</sub>O)] and [Mn<sub>7</sub>O<sub>8</sub>(O<sub>2</sub>SePh)<sub>9</sub>(H<sub>2</sub>O)]<sup>10</sup> and the mixed 3d/4f chain compound [LCu<sub>2</sub>Tb(NO<sub>3</sub>)(H<sub>2</sub>O)] [H<sub>3</sub>L = 2-hydroxy-*N*-{2-[(2-hydroxyethyl)amino]ethyl}benzamide].<sup>11</sup>

Our team, among others, is engaged in the extension of the work on SCMs to the cyanide-bearing compounds by using the so-called bottom-up synthetic approach.<sup>6,12-14</sup> Our rational design of SCMs is based on a careful choice of the building block (a paramagnetic cyanide-containing metal complex). In this respect, we prepared the [M<sup>III</sup>(AA)(CN<sub>4</sub>)]<sup>-</sup> mononuclear species (M = Cr and Fe; AA = bidentate nitrogen donor),<sup>15,16</sup> and we explored their use as ligands toward fully solvated first-

row transition metal ions (M')<sup>6,12,15a,b,16</sup> and partially blocked complexes.<sup>15c,17</sup> Among the different cyano-bridged polynuclear compounds obtained, the single and double 4,2-ribbonlike heterobimetallic chains with M = Fe(III) and M' = Co(II) and Cu(II) exhibit intrachain ferromagnetic coupling and the typical behavior of the SCMs.<sup>6,12</sup>

In the present work, we focus on the preparation, crystal structure determination, magnetic investigation, and theoretical study of the new cyanide-bearing precursor PPh<sub>4</sub>[Fe<sup>III</sup>(bpym)(CN)<sub>4</sub>] $\cdot$ H<sub>2</sub>O (**1**) (PPh<sub>4</sub><sup>+</sup> = tetraphenylphosphonium and bpym = 2,2'-bipyrimidine) and of the heterobimetallic chains of formula {[Fe<sup>III</sup>(bpym)(CN)<sub>4</sub>]<sub>2</sub>M<sup>II</sup>(H<sub>2</sub>O)<sub>2</sub>] $\cdot$ 6H<sub>2</sub>O [bpym = 2,2'-bipyrimidine; M = Zn (**2**), Co (**3**), Cu (**4**), and Mn (**5**)]. **3** is a new example of SCM whose reversal of the magnetization is analyzed by a model of thermally activated nucleation on the basis of magnetization measurements on a single crystal at very low temperatures.

## Experimental Section

**Materials.** Chemicals were purchased from commercial sources, and they were used without further purification. Elemental analyses (C, H, N) were carried out at the Microanalytical Service of the Universidad Autónoma de Madrid. Fe/P (**1**), and Fe/M [M = Zn (**2**), Co (**3**), Cu (**4**), and Mn (**5**)] molar ratios of 1:1 (**1**) and 2:1 (**2-5**) were determined by electron probe X-ray microanalysis at the Servicio Interdepartamental de la Universitat de València.

**WARNING.** The severe toxicity of cyanide and most of its compounds must be taken into account in the laboratory. Our syntheses were performed at millimolar scale in a hood, and the samples were handled with great caution.

**Synthesis of the Complexes. PPh<sub>4</sub>[Fe<sup>III</sup>(bpym)(CN)<sub>4</sub>] $\cdot$ H<sub>2</sub>O (**1**).** Compound **1** was prepared by following a procedure similar to that described for the related compounds with 2,2'-bipyridine or 1,10-phenanthroline instead of bpym in refs 15a,b. X-ray-quality dark-red prisms of **1** were obtained by recrystallization of the crude product from a H<sub>2</sub>O/MeOH (1:1) mixture. Yield is 54%. Anal. Calcd for C<sub>36</sub>H<sub>28</sub>FeN<sub>8</sub>OP (I): C, 64.03; H, 4.15; N, 16.59. Found: C, 63.50; H, 4.01; N, 16.25. IR (KBr pellets):  $\nu$  (cyanide stretching) = 2124(m) and 2112-(m) cm<sup>-1</sup>.

{[Fe<sup>III</sup>(bpym)(CN)<sub>4</sub>]<sub>2</sub>M<sup>II</sup>(H<sub>2</sub>O)<sub>2</sub>] $\cdot$ 6H<sub>2</sub>O (**2-5**).

X-ray-quality crystals of compounds **2-4** were obtained by slow diffusion in an H-tube of aqueous solutions of Li[Fe(bpym)(CN)<sub>4</sub>] [isolated by metathetic reaction of **1** and LiClO<sub>4</sub> $\cdot$ H<sub>2</sub>O in a 1:1 molar ratio (0.2 mmol) in acetonitrile] in one arm and the corresponding nitrate salt (0.1 mmol) [Zn(NO<sub>3</sub>)<sub>2</sub> $\cdot$ 6H<sub>2</sub>O (**1**), Co(NO<sub>3</sub>)<sub>2</sub> $\cdot$ 6H<sub>2</sub>O (**3**), Cu(NO<sub>3</sub>)<sub>2</sub> $\cdot$ 3H<sub>2</sub>O (**4**), and Mn(NO<sub>3</sub>)<sub>2</sub> $\cdot$ 4H<sub>2</sub>O (**5**)] in the other arm. The diffusion was allowed to proceed in the dark, and well-shaped orange (**2** and **5**) and brown (**3**) prisms and maroon plates (**4**) were obtained. The yield is practically quantitative after a few weeks. Anal. Calcd for C<sub>24</sub>H<sub>28</sub>Fe<sub>2</sub>N<sub>16</sub>O<sub>8</sub>Zn (**2**): C, 36.51; H, 3.55; N, 28.37. Found: C, 36.28; H, 3.45; N, 28.19. Anal. Calcd for C<sub>24</sub>H<sub>28</sub>CoFe<sub>2</sub>N<sub>16</sub>O<sub>8</sub> (**3**): C, 36.82; H, 3.58; N, 28.62. Found: C, 36.55; H, 3.49; N, 28.48. Anal. Calcd for C<sub>24</sub>H<sub>28</sub>CuFe<sub>2</sub>N<sub>16</sub>O<sub>8</sub> (**4**): C, 36.60; H, 3.55; N, 28.44. Found: C, 36.49; H, 3.43; N, 28.17. Anal. Calcd for C<sub>24</sub>H<sub>28</sub>Fe<sub>2</sub>MnN<sub>16</sub>O<sub>8</sub> (**5**): C, 37.00; H, 3.59; N, 28.75. Found: C, 36.87; H, 3.49; N, 28.61. IR (KBr pellets):  $\nu$  (cyanide stretching) = 2174(m), 2124(w), and 2114(w) (**2**), 2171(m), 2126(w), and 2113(w) (**3**), 2186(m) and 2117(w) (**4**), and 2157(m) and 2132(w) cm<sup>-1</sup> (**5**).

(8) Glauber, R. J. *J. Math. Phys.* **1963**, *4*, 294.

(9) Liu, T. F.; Fu, D.; Gao, S.; Zhang, Y. Z.; Sun, H. L.; Su, G.; Liu, Y. J. *J. Am. Chem. Soc.* **2003**, *125*, 13976.

(10) Chakov, N. E.; Wernsdorfer, W.; Abboud, K. A.; Christou, G. *Inorg. Chem.* **2004**, *43*, 5919.

(11) Costes, J. P.; Clemente-Juan, J. M.; Dahan, F.; Milon, J. *Inorg. Chem.* **2004**, *43*, 8200.

(12) (a) Toma, L. M.; Lescouëzec, R.; Lloret, F.; Julve, M.; Vaissermann, J.; Verdager, M. *Chem. Commun.* **2003**, 1850. (b) Toma, L. M.; Delgado, F. S.; Ruiz-Pérez, C.; Carrasco, R.; Cano, J.; Lloret, F.; Julve, M. *Dalton Trans.* **2004**, 2836.

(13) Wang, S.; Zuo, J. L.; Gao, S.; Song, Y.; Zhou, H. C.; Zhang, Y. Z.; You, X. Z. *J. Am. Chem. Soc.* **2004**, *126*, 8900.

(14) Ferbinteanu, M.; Miyasaka, H.; Wernsdorfer, W.; Nakata, K.; Sugiura, K. I.; Yamashita, M.; Coulon, C.; Clérac, R. *J. Am. Chem. Soc.* **2005**, *127*, 3090.

(15) (a) Lescouëzec, R.; Lloret, F.; Julve, M.; Vaissermann, J.; Verdager, M.; Llugar, R.; Uriel, S. *Inorg. Chem.* **2001**, *40*, 2065. (b) Lescouëzec, R.; Lloret, F.; Julve, M.; Vaissermann, J.; Verdager, M. *Inorg. Chem.* **2002**, *41*, 818. (c) Toma, L. M.; Lescouëzec, R.; Toma, L. D.; Lloret, F.; Julve, M.; Vaissermann, J.; Andruh, M. *J. Chem. Soc., Dalton Trans.* **2002**, 3171.

(16) (a) Toma, L.; Lescouëzec, R.; Vaissermann, J.; Delgado, F. S.; Ruiz-Pérez, C.; Carrasco, R.; Cano, J.; Lloret, F.; Julve, M. *Chem. Eur. J.* **2004**, *10*, 6130. (b) Toma, L.; Lescouëzec, R.; Vaissermann, J.; Herson, P.; Marvaud, V.; Lloret, F.; Julve, M. *New J. Chem.* **2005**, *29*, 210.

(17) Toma, L.; Toma, L. M.; Lescouëzec, R.; Armentano, D.; De Munno, G.; Andruh, M.; Cano, J.; Lloret, F.; Julve, M. *Dalton Trans.* **2005**, 1537.

**Physical Measurements.** Infrared spectra (KBr pellets) were recorded on a Bruker IF S55 spectrometer. Magnetic susceptibility measurements on polycrystalline samples of **1–5** were carried out with a Quantum Design SQUID magnetometer in the temperature range 1.9–295 K and under applied magnetic fields of 50 G to 1 T. The magnetization versus magnetic field measurements on the same samples of **1–5** were performed at 2.0 K in the field range 0–5 T. The ac measurements on a polycrystalline sample of **3** were performed at frequencies ranging from 0.25 to 1200 Hz with an ac field amplitude of 1 G and no dc field applied. Experimental magnetic data were also corrected for the diamagnetic contribution calculated from Pascal constants. Magnetization measurements on single crystals of **3** were performed by using (i) a magnetometer consisting of several Hall-bars<sup>18</sup> and (ii) an array of micro-SQUIDS<sup>19</sup> on top of which a single crystal of the Fe<sup>III</sup><sub>2</sub>Co<sup>II</sup> chain was placed, for higher and lower fields than 1.4 T, respectively. The field can be applied in any direction of the micro-SQUID plane with precision much better than 0.1° by separately driving three orthogonal superconducting coils. The field was aligned with the easy axis of magnetization using the transverse field method.<sup>20</sup> The Hall probes (typically 10 × 10 mm<sup>2</sup>) are made of two-dimensional GaAs/GaAsAl heterostructures and work in the temperature range of 1.5–100 K and in magnetic fields of up to 16 T.

**Computational Details.** All theoretical calculations were carried out with the hybrid B3LYP method,<sup>21–23</sup> as implemented in the GAUSSIAN03 program.<sup>24</sup> Double- $\zeta$  quality basis sets, proposed by Ahlrichs and co-workers, have been used for all atoms.<sup>25</sup> The broken symmetry approach has been employed to describe the unrestricted solutions of the antiferromagnetic spin states.<sup>26–29</sup> The geometries of the studied models [**I** and **II** in Figures S14 (top) and S15(a), respectively] were built from the experimental crystal structures. A quadratic convergence method was used to determine the more stable wave functions in the SCF process. The atomic spin densities were obtained from natural bond orbital (NBO) analysis.<sup>30–32</sup>

**Crystallographic Data Collection and Structure Determination.** Single crystals of compounds **1–5** of dimensions 0.30 mm × 0.35 mm × 0.40 (**1**), 0.09 mm × 0.20 mm × 0.27 (**2**), 0.12 mm × 0.15 mm × 0.20 (**3**), 0.01 mm × 0.04 mm × 0.13 (**4**) and 0.11 mm × 0.12 mm × 0.15 mm (**5**) were mounted on Enraf-Nonius CAD-4 (**1**) and Bruker-Nonius KappaCCD (**2–5**) diffractometers and used for data collection. Intensity data were collected at 295 (**1**) and 293 K (**2–5**) by using graphite monochromated Mo K $\alpha$  radiation source [ $\lambda = 0.71069$  Å (**1**) and 0.71073 Å (**2–5**)] with the  $\omega - 2\theta$  method. Accurate cell dimensions and orientation matrixes were determined by least-squares refinements of 25 accurately centered reflections with  $12 < \theta < 12.3^\circ$  for **1** and through least-squares refinement of the reflections obtained by a  $\theta - \chi$  scan (Dirac/lsq method) for **2–5**. No significant variations were observed in the intensities of two checked reflections (**2–5**) during data collection; for **1**, a decay of 5.52% was observed, and the data were accordingly scaled. Data collection and data reduction for **2–4**

were done with the COLLECT<sup>33</sup> and EVALCCD<sup>34</sup> programs. The data were corrected for Lorentz and polarization effects (**1–5**). Empirical absorption corrections were performed by the use of DIFABS<sup>35</sup> (**1**) and SADABS<sup>36</sup> (**2–5**). The indexes of data collection were  $0 \leq h \leq 40$ ,  $0 \leq k \leq 16$ ,  $-37 \leq l \leq 32$  for **1**,  $-9 \leq h \leq 9$ ,  $-15 \leq k \leq 14$ ,  $-17 \leq l \leq 17$  for **2**,  $-9 \leq h \leq 8$ ,  $-13 \leq k \leq 10$ ,  $-16 \leq l \leq 14$  for **3**,  $-9 \leq h \leq 9$ ,  $-15 \leq k \leq 15$ ,  $-16 \leq l \leq 17$  for **4**, and  $-10 \leq h \leq 10$ ,  $-15 \leq k \leq 15$ ,  $-11 \leq l \leq 17$  for **5**. Of the 11472 (**1**), 5030 (**2**), 3984 (**3**), 4964 (**4**), and 4941 (**5**) measured independent reflections in the  $\theta$  range 1.0–25.0° (**1**), 4.10–30.0° (**2**), 3.21–27.50° (**3**), 4.01–29.99° (**4**) and 5.03–30.00° (**5**), 6213 (**1**), 3744 (**2**), 2521 (**3**), 2538 (**4**), and 3499 (**5**) were considered as observed [ $I \geq 1.5\sigma(I)$  (**1**) and  $I \geq 2\sigma(I)$  (**2–5**)] and used for the refinement of the structures. The structure of **1** was solved by direct methods through SHELX-86<sup>37</sup> and subsequently refined by Fourier recycling. The final full-matrix least-squares refinement on  $F$  for **1** was done by the PC version of CRYSTALS.<sup>38</sup> All calculations for data reduction, structure solution, and refinement for **2–5** were done by standard procedures.<sup>39</sup> The structures of **2–5** were also solved by direct methods and refined with full-matrix least-squares technique on  $F^2$  using the SHELXS-97 and SHELXL-97 programs.<sup>40</sup> All non-hydrogen atoms in **1–5** were refined anisotropically. The hydrogen atoms of the water molecules (**1–5**) were not found, whereas those of the bpm ligand (**1–5**) and the PPh<sub>4</sub><sup>+</sup> cation (**1**) were placed in calculated positions. The hydrogen atoms were refined with isotropic temperature factors for all compounds. The final geometrical calculations and the graphical manipulations for **1–5** were carried out with PARST95<sup>41</sup> and CRYSTALMAKER<sup>42</sup> programs, respectively. The crystal data and details of the structure refinements of **1–5** are summarized in Table S1. Selected bond distances and angles are listed in Tables S2 (**1**), S3 (**2**, **3**, and **5**), and S4 (**4**).

## Results and Discussion

**Synthesis.** Cyanide and bpm are well-known ligands in magnetic studies because of their remarkable ability to mediate strong magnetic interactions between the paramagnetic centers which are bridged by them.<sup>43,44</sup> The coexistence of the two ligands in the stable mononuclear low-spin iron(III) complex [Fe(bpm)(CN)<sub>4</sub>]<sup>−</sup> makes this species a very appealing candidate to build extended magnetic systems. In the present work, we show for the first time how the use of the heteroleptic [Fe(bpm)(CN)<sub>4</sub>]<sup>−</sup> complex as a ligand toward fully solvated divalent first-row transition metal ions [M = Zn (**2**), Co (**3**),

(18) Sorace, L.; Wernsdorfer, W.; Thirion, C.; Barra, A. L.; Pacchioni, M.; Maily, D.; Barbara, B. *Phys. Rev. B* **2003**, *68*, 220407(R).

(19) Wernsdorfer, W. *Adv. Chem. Phys.* **2001**, *118*, 99.

(20) Wernsdorfer, W.; Chakov, N. E.; Christou, G. *Phys. Rev.* **2004**, *B70*, 132413.

(21) Becke, A. D. *Phys. Rev. A* **1988**, *38*, 3098.

(22) Lee, C.; Yang, W.; Parr, R. G. *Phys. Rev. B* **1988**, *37*, 785.

(23) Becke, A. D. *J. Chem. Phys.* **1993**, *98*, 5648.

(24) Frisch, M. J.; et al. *GAUSSIAN 03*, Revision C.03; Gaussian, Inc.: Wallingford, CT, 2004.

(25) Schaefer, A.; Horn, A.; Ahlrichs, R. *J. Chem. Phys.* **1992**, *97*, 2571.

(26) Cano, J.; Alemany, P.; Alvarez, S.; Verdaguier, M.; Ruiz, E. *Chem. Eur. J.* **1998**, *4*, 476.

(27) Ruiz, E.; Cano, J.; Alvarez, S.; Alemany, P. *J. Am. Chem. Soc.* **1998**, *120*, 11122.

(28) Ruiz, E.; Cano, J.; Alvarez, S.; Alemany, P. *J. Comput. Chem.* **1999**, *20*, 1391.

(29) Cano, J.; Ruiz, E.; Alemany, P.; Lloret, F.; Alvarez, S. *J. Chem. Soc., Dalton Trans.* **1999**, 1669.

(30) Carpenter, J. E.; Weinhold, F. *J. Mol. Struct.* **1988**, *169*, 41.

(31) Reed, A. E.; Curtis, L. A.; Weinhold, F. *Chem. Rev.* **1988**, *88*, 899.

(32) Weinhold, F.; Carpenter, J. E. *The Structure of Small Molecules and Ions*; Plenum: New York, 1988; p 227.

(33) Hooft, R. W. W. *COLLECT*; Nonius BV: Delft, The Netherlands, 1999.

(34) Duisenberg, A. J. M.; Kroon-Batenburg, L. M. J.; Schreurs, A. M. M. *J. Appl. Crystallogr.* **2003**, *36*, 220 (EVALCCD).

(35) Walker, N.; Stuart, D. *Acta Crystallogr.* **1983**, *A39*, 156.

(36) *SADABS Empirical Absorption Program*, version 2.03; Bruker AXS Inc.: Madison, WI, 2000.

(37) Sheldrick, G. M. *SHELX-86: Program for Crystal Structure Solution*; University of Göttingen: Göttingen, Germany, 1996.

(38) Watkin, D. J.; Prout, C. K.; Caruthers, J. R.; Betheridge, P. W. *CRYSTALS*; Chemical Crystallography Laboratory, University of Oxford: Oxford, United Kingdom, 1996, Issue 10.

(39) Farrugia, L. J. (*WING*) *J. Appl. Crystallogr.* **1999**, *32*, 837.

(40) Sheldrick, G. M. *SHELX-97: Programs for Crystal Structure Analysis*, Release 97-2; Institut für Anorganische Chemie der Universität: Göttingen, Germany, 1998.

(41) Nardelli, M. *PARST95, J. Appl. Crystallogr.* **1995**, *28*, 659.

(42) *CrystalMaker*, 4.2.1; CrystalMaker Software: Bicester, Oxfordshire X26 3TA, UK.

(43) (a) Verdaguier, M.; Bleuzen, A.; Marvaud, V.; Vaissermann, J.; Seuleiman, M.; Desplanches, C.; Scullier, A.; Train, C.; Garde, R.; Gelly, G.; Lomenech, C.; Rosenman, I.; Veillet, R.; Cartier, C.; Villain, F. *Coord. Chem. Rev.* **1999**, *190–192*, 103 and references therein. (b) Ohba, M.; Okawa, H. *Coord. Chem. Rev.* **2000**, *198*, 313 and references therein.

(44) (a) De Munno, G.; Julve, M. In *Metal Ligand Interactions. Structure and Reactivity*; Russo, N., Salahub, D. R., Eds.; NATO Advanced Study Institute Series 474; Kluwer: Dordrecht, 1996; p 139 and references therein. (b) De Munno, G.; Lloret, F.; Julve, M. In *Magnetism: A Supramolecular Function*; Kahn, O., Ed.; NATO Advanced Study Institute Series 484; Kluwer: Dordrecht, 1996; p 555 and references therein. (c) Vangdal, B.; Carranza, J.; Lloret, F.; Julve, M.; Sletten, J. *Dalton Trans.* **2002**, 566.

Cu (**4**), and Mn (**5**) affords the neutral 4,2-ribbonlike bimetallic chains of formula  $\{[\text{Fe}^{\text{III}}(\text{bpym})(\text{CN})_4]_2\text{M}^{\text{II}}(\text{H}_2\text{O})_2\} \cdot 6\text{H}_2\text{O}$ . The  $[\text{Fe}(\text{bpym})(\text{CN})_4]^-$  unit acts as a bis-monodentate ligand through two cis cyano groups.

This coordination mode as well as the monodentate (across one of the four cyano groups) and tris-monodentate ones (three of the four cyano groups being involved) was previously observed in the parent low-spin iron(III)  $[\text{Fe}(\text{bipy})(\text{CN})_4]^-$  (bipy = 2,2'-bipyridine) and  $[\text{Fe}(\text{phen})(\text{CN})_4]^-$  (phen = 1,10-phenanthroline) units leading to heterobimetallic trinuclear<sup>15b</sup> and tetranuclear<sup>15c,17</sup> compounds and single<sup>5,12b,15a</sup> and double<sup>12b,15b</sup> 4,2-ribbonlike chains. These studies evidenced the relevance of the solvent in the formation of the double 4,2-ribbonlike chains. These double chains can be viewed as the condensation of two single 4,2-ribbonlike chains by the substitution of an axially coordinated water molecule at M by a cyanide-nitrogen atom. In light of these results and keeping in mind the additional coordination possibilities offered by the presence of terminal bpym in the complex  $[\text{Fe}(\text{bpym})(\text{CN})_4]^-$ , its use as a ligand toward either fully solvated metal ions or partially blocked complexes would provide us with a plethora of new heterometallic magnetic species in the very near future.

**Description of the Structures.  $\text{PPh}_4[\text{Fe}^{\text{III}}(\text{bpym})(\text{CN})_4] \cdot \text{H}_2\text{O}$  (**1**).** The crystallographic analysis of **1** shows that its structure consists of mononuclear  $[\text{Fe}(\text{bpym})(\text{CN})_4]^-$  anions (Figure S1), tetraphenylphosphonium cations, and water molecules of crystallization which are linked by electrostatic forces, hydrogen bonds, and van der Waals interactions.

Two crystallographically independent iron atoms [Fe(1) and Fe(2)] occur in **1**, and they are coordinated to two bpym-nitrogen atoms and four cyanide-carbon atoms, taking distorted octahedral geometries. The short bite of the bidentate bpym ligand [80.9(2) and 80.5(2)° at Fe(1) and Fe(2), respectively] is at the origin of this distortion from the ideal geometry. The values of the Fe–N(bpym) bonds in **1** are comprised of those between the low-spin iron(II) unit  $[\text{Fe}(\text{bpym})_3]^{2+}$  in the compounds  $[\text{Fe}(\text{bpym})_3](\text{ClO}_4)_2$  [average value 1.970(5) Å]<sup>45</sup> and  $\text{Fe}(\text{bpym})_3 \cdot \text{Na}(\text{H}_2\text{O})_2\text{Fe}(\text{ox})_3 \cdot 4\text{H}_2\text{O}$  (ox = oxalate) [av value 1.978(4) Å]<sup>46</sup> and those of the high-spin iron(III) complex  $[\text{Fe}(\text{bpym})\text{Cl}_3 \cdot (\text{H}_2\text{O})] \cdot \text{H}_2\text{O}$  [mean value 2.207(3) Å]<sup>47</sup> but they are the same as those found in the low-spin iron(III) complexes  $\text{PPh}_4[\text{Fe}(\text{bipy})(\text{CN})_4] \cdot \text{H}_2\text{O}$  [1.98(2) and 2.00(2) Å]<sup>15b</sup> and  $\text{K}[\text{Fe}(\text{bipy})(\text{CN})_4] \cdot \text{H}_2\text{O}$  [1.991(3) and 1.990(3) Å].<sup>15c</sup> This agreement is also observed between the values of the Fe–C(cyano) bond lengths of **1** [1.915(5)–1.949(6) Å at Fe(1) and 1.910(5)–1.954(5) Å at Fe(2)] and those reported for other cyano-containing mononuclear low-spin iron(III) complexes [1.87(2)–1.95(1) Å].<sup>15,48</sup> The presence of the tetraphenylphosphonium cation in the structure of **1** and the magnetic behavior of this compound demonstrate that it is a low-spin iron(III) complex. Additional support of this low-spin iron(III) character of **1** comes from the values of the higher frequency cyanide stretching in its infrared spectrum [doublet at 2124 and 2112  $\text{cm}^{-1}$ ] which compare very well with those observed in  $\text{PPh}_4[\text{Fe}(\text{bipy})(\text{CN})_4] \cdot \text{H}_2\text{O}$  [2118  $\text{cm}^{-1}$ ]<sup>15b</sup> and  $\text{K}[\text{Fe}(\text{bipy})(\text{CN})_4] \cdot \text{H}_2\text{O}$  [2134 and

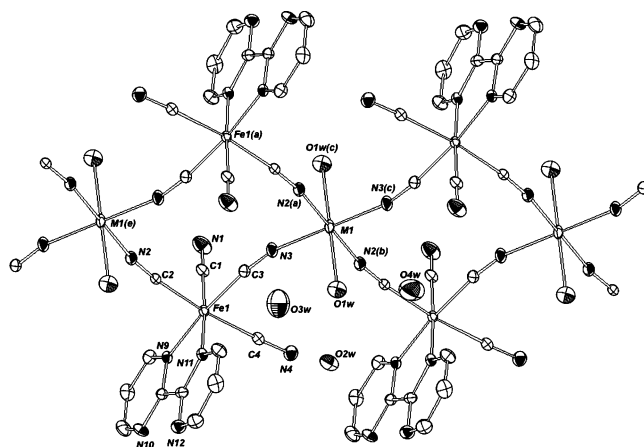


**Figure 1.** Perspective view of a fragment of the 4,2-ribbonlike bimetallic chain of **2** (M = Zn), **3** (M = Co), **4** (M = Cu), and **5** (M = Mn) running parallel to the *a* axis. The hydrogen atoms have been omitted for clarity. Symmetry code: (a) =  $-x, 1-y, 1-z$ ; (b) =  $1+x, y, z$ ; (c) =  $1-x, 1-y, 1-z$ ; (e) =  $-1+x, y, z$ .

2114  $\text{cm}^{-1}$ ].<sup>15c</sup> The two types of  $[\text{Fe}(\text{bpym})(\text{CN})_4]^-$  anions are grouped by pairs through hydrogen bonds involving the crystallization water molecules O(1) and O(2) and the terminal cyanide nitrogens (Figure S2).

The bpym ligands are practically planar, but they are clearly distorted because of their bidentate coordination (see end of Table S2). The value of inter-ring carbon–carbon bond length of the bpym ligands [1.497(8) and 1.472(8) Å for C(15)–C(16) and C(25)–C(26), respectively] is very close to that found in the free molecule in the solid state [1.502(4) and 1.497(1) Å].<sup>49</sup> The triatomic Fe–C–N set of atoms at each cyanide are almost linear. The values of the cyanide C–N bonds agree with those reported for other cyano-containing mononuclear low-spin iron(III) complexes.<sup>15,48,50</sup> The tetraphenylphosphonium cations exhibit the expected tetrahedral shape, and their bond distances and angles are as expected.

**$[\text{Fe}^{\text{III}}(\text{bpym})(\text{CN})_4]_2\text{M}^{\text{II}}(\text{H}_2\text{O})_2 \cdot 6\text{H}_2\text{O}$  [M = Zn (**2**), Co (**3**), and Mn (**5**)].** **2**, **3**, and **5** are isostructural compounds whose structures are made up of neutral cyanide-bridged 4,2-ribbonlike bimetallic chains of formula  $\{[\text{Fe}^{\text{III}}(\text{bpym})(\text{CN})_4]_2\text{M}^{\text{II}}(\text{H}_2\text{O})_2\}$  [M = Zn (**2**), Co (**3**), and Mn (**5**)] with run parallel to the *a* axis (Figure 1). These chains are stacked along the *b* axis through hydrogen bonds (see end of Table S3) involving discrete centrosymmetric water hexameric rings with two dangling water molecules in trans positions [Figure 2 (top)] to form a layered structure (Figure S3). These rings adopt an icelike chair conformation.<sup>51,52</sup>

The iron and M atoms in **2**, **3**, and **5** are six-coordinated: two nitrogen atoms from bpym and four cyanide-carbon atoms around the iron center and two water molecules in trans positions and four cyanide-nitrogen atoms around the M atom build distorted octahedral geometries. The bond distances and angles around the iron atom in the  $[\text{Fe}(\text{bpym})(\text{CN})_4]^-$  unit in **2**, **3**, and **5** agree with those observed for this entity in **1**. The M–O(w1) bond lengths are close to those observed in the related  $\{[\text{Fe}^{\text{III}}(\text{bipy})(\text{CN})_4]_2\text{M}^{\text{II}}(\text{H}_2\text{O})_4\} \cdot 4\text{H}_2\text{O}$  (M = Mn and Zn) trinuclear

(45) De Munno, G.; Julve, M.; Real, J. A. *Inorg. Chim. Acta* **1997**, *255*, 185.

(46) Armentano, D.; De Munno, G.; Faus, J.; Lloret, F.; Julve, M. *Inorg. Chem.* **2001**, *40*, 655.

(47) De Munno, G.; Ventura, W.; Viau, G.; Lloret, F.; Faus, J.; Julve, M. *Inorg. Chem.* **1998**, *37*, 1458.

(48) Lu, T. H.; Kao, H. Y.; Wu, D. I.; Kong, K. C.; Cheng, C. H. *Acta Crystallogr., Sect. C* **1988**, *44*, 1184.

(49) Fernholt, L.; Rømming, C.; Sandal, S. *Acta Chem. Scand., Ser. A* **1981**, *35*, 707.

(50) Vannerberg, N. G. *Acta Chem. Scand.* **1972**, *26*, 2863.

(51) Eisenberg, D.; Kauzmann, W. *The Structure and Properties of Water*; Oxford University Press: Oxford, 1969.

(52) Narten, A. H.; Thiessen, E.; Blum, L. *Science* **1982**, *217*, 1033.

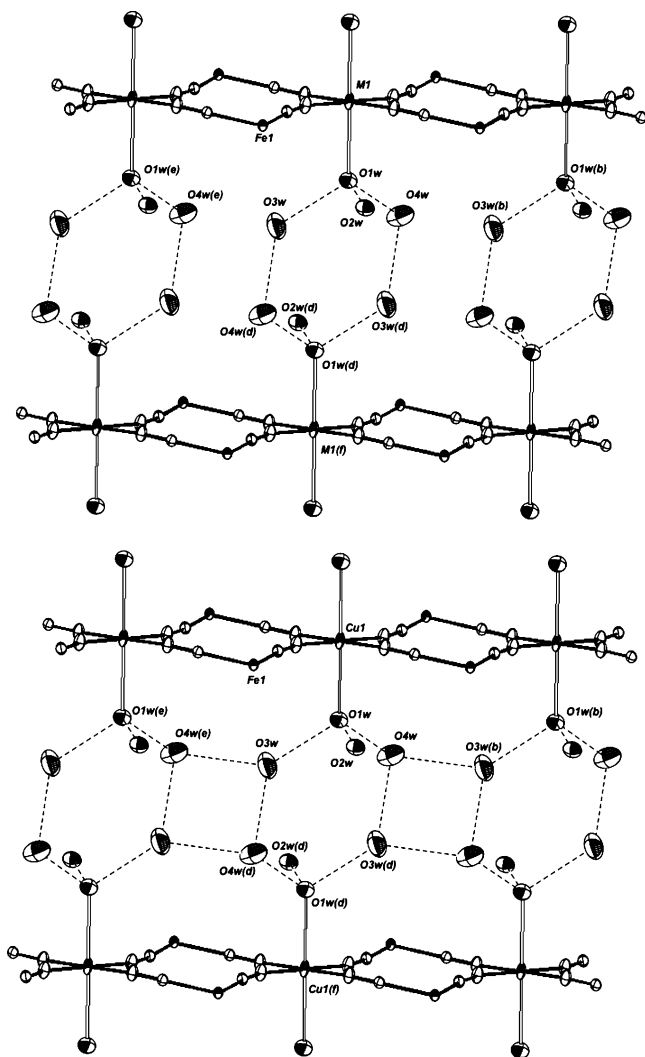


**Figure 2.** Perspective views of the stacking of two fragments of neighboring chains of **2** ( $M = \text{Zn}$ ), **3** ( $M = \text{Co}$ ), and **5** ( $M = \text{Mn}$ ) (top) and **4** ( $M = \text{Cu}$ ) (bottom) showing the interchain linking through hydrogen bonds. The bpym molecules and terminal cyanide ligands have been omitted for clarity. Symmetry code: (b) =  $1+x, y, z$ ; (d) =  $1-x, -y, 1-z$ ; (f) =  $x, -1+y, z$ .

species<sup>15b</sup> and  $\{[\text{Fe}^{\text{III}}(\text{phen})(\text{CN})_4]_2\text{Mn}^{\text{II}}(\text{H}_2\text{O})_4\} \cdot 4\text{H}_2\text{O}$  and  $\{[\text{Fe}^{\text{III}}(\text{L})(\text{CN})_4]_2\text{Co}^{\text{II}}(\text{H}_2\text{O})_2\} \cdot 4\text{H}_2\text{O}$  ( $\text{L} = \text{bipy}$  and  $\text{phen}$ ) 4,2-ribbonlike chains.<sup>5,15a</sup> The  $\text{M}(1)\text{-N}-\text{C}$  angle for the bridging cyanide ligands is largely bent. The  $\text{C}-\text{N}$  bond lengths for terminal cyanide groups in **2**, **3**, and **5** compare well with those observed in **1** and they are very close to those of the bridging cyanide ligands. The CN stretching region of the IR spectrum of **2**, **3**, and **5** is consistent with the occurrence of bridging [medium intensity peaks at 2174 (**2**), 2171 (**3**), and 2157  $\text{cm}^{-1}$  (**5**)] and terminal [weak intensity peaks at 2124 and 2114 (**2**), 2126 and 2113 (**3**), and 2132  $\text{cm}^{-1}$  (**5**)] cyanide ligands.

The bpym ligand as a whole is quasi-planar, and the value of the inter-ring carbon-carbon bond distance [1.486(3) (**2**), 1.470(6) (**3**), and 1.473(3) Å (**5**)] is very close to that observed in **1**. No significant graphite-like interaction between bpym molecules of adjacent chains occur in **2**, **3**, and **5**. The intrachain  $\text{Fe}(1)\cdots\text{M}(1)$  separations through bridging cyanide are 4.9904(5) (**2**), 4.9970(6) (**3**), and 5.0398(5) Å (**5**) [ $\text{Fe}(1)\cdots\text{M}(1)$ ] and 5.0532(5) (**2**), 5.0521(6) (**3**), and 5.0908(5) Å (**5**) [ $\text{Fe}(1)\cdots\text{M}(1e)$ ], values which are much shorter than the metal-metal

separation through the water clusters [10.7418(5) (**2**), 10.7244(5) (**3**), 10.7429(9) Å (**5**)] for  $\text{M}(1)\cdots\text{M}(1f)$ .

$\{[\text{Fe}^{\text{III}}(\text{bpym})(\text{CN})_4]_2\text{Cu}^{\text{II}}(\text{H}_2\text{O})_2\} \cdot 6\text{H}_2\text{O}$  (**4**). The structure of **4** consists of cyanide-bridged crossed  $\text{Fe}^{\text{III}}-\text{Cu}^{\text{II}}$  zigzag chains of formula  $\{[\text{Fe}^{\text{III}}(\text{bpym})(\text{CN})_4]_2\text{Cu}^{\text{II}}(\text{H}_2\text{O})_2\}$  which run also parallel to the  $a$  axis as in **2**, **3**, and **5** (Figure 1), the main difference being the occurrence in **4** of fused four- and five-membered water rings [Figure 2 (bottom)] linking the neutral chains through hydrogen bonds (see end of Table S4) to afford a layered structure (Figure S4). The hexameric ring in **4** exhibits also the chairlike conformation.

As in **2**, **3**, and **5**, the  $[\text{Fe}(\text{bpym})(\text{CN})_4]^-$  unit in **4** acts as a bis-monodentate bridging ligand toward two trans diaquacopper(II) entities through two of its four cyanide groups in cis positions affording a 4,2-ribbonlike bimetallic chain. Each iron atom in **4** is six-coordinated, two bpym-nitrogen and four cyanide-carbon atoms forming a distorted octahedral geometry. The values of the bond lengths at the iron atom and that of the angle subtended by the bidentate bpym agree with those reported for **2**, **3**, and **5**. Each copper atom lies on an inversion center, and it has a distorted, elongated octahedral coordination geometry: four cyanide-nitrogen atoms build the equatorial plane, and two water molecules fill the axial positions. This situation around the copper atom contrasts with that observed in the related 4,2-ribbonlike chain of formula  $\{[\text{Fe}^{\text{III}}(\text{phen})(\text{CN})_4]_2\text{Cu}^{\text{II}}(\text{H}_2\text{O})_2\} \cdot 4\text{H}_2\text{O}$  where the two trans coordinated water molecules and two cyanide-nitrogen atoms define the equatorial positions, whereas the axial ones are filled by other two cyanide-nitrogen atoms.<sup>12b</sup> The  $\text{Fe}-\text{C}-\text{N}$  angles for both terminal and bridging cyanide ligands depart somewhat from the strict linearity, whereas those of the  $\text{Cu}-\text{C}-\text{N}$  units are significantly bent. The occurrence of both terminal and bridging cyanide ligands in **4** is suggested by the presence of two stretching vibrations at 2186m (bridging) and 2117w (terminal) in its IR spectrum.

The heterocyclic bpym ligand is quasi-planar, and no significant  $\pi-\pi$  interactions between bpym ligands are observed. The intrachain iron-copper separations through bridging cyanide in **4** are 4.9268(7) [ $\text{Fe}(1)\cdots\text{M}(1)$ ] and 5.0009(8) Å [ $\text{Fe}(1)\cdots\text{M}(1e)$ ], values which are much shorter than the metal-metal separation through the water cluster [10.8763(8) Å for  $\text{Cu}(1)\cdots\text{Cu}(1f)$ ].

**Magnetic Properties of 1, 2, 4, and 5.** The magnetic properties of complexes **1** and **2** are shown in Figure S5 under the form of  $\chi_{\text{M}}T$  versus  $T$  plot [ $\chi_{\text{M}}$  is the magnetic susceptibility per mole of iron(III)]. The values of  $\chi_{\text{M}}T$  at 300 K are 0.615 (**1**) and 0.644 (**2**)  $\text{cm}^3 \text{mol}^{-1} \text{K}$ . Both  $\chi_{\text{M}}T$  versus  $T$  plots decrease quasi-linearly when cooling, and they reach values of 0.46 (**1**) and 0.455 (**2**)  $\text{cm}^3 \text{mol}^{-1} \text{K}$  at 1.9 K. This is the expected behavior for a magnetically isolated distorted low-spin octahedral iron(III) system with spin-orbit coupling of the  ${}^2T_{2g}$  ground term. The similarity between the magnetic behavior of **2** (4,2-ribbonlike bimetallic chain) and complex **1** shows that the magnetic coupling between iron(III) centers separated by more than 10 Å through the diamagnetic  $-\text{CN}-\text{Zn}-\text{CN}-$  bridging skeleton in **2** must be very small, as expected. At this respect, it deserves to be noted that a weak magnetic coupling of  $J = -1.3 \text{ cm}^{-1}$  [the Hamiltonian being defined as  $\hat{H} = -J\hat{S}_{\text{Fe}(1)} \cdot \hat{S}_{\text{Fe}(2)}$ ] was roughly estimated in the centrosymmetric trinuclear complex  $\{[\text{Fe}^{\text{III}}(\text{bipy})(\text{CN})_4]_2\text{Zn}^{\text{II}}(\text{H}_2\text{O})_4\} \cdot 4\text{H}_2\text{O}$ .<sup>15b</sup>



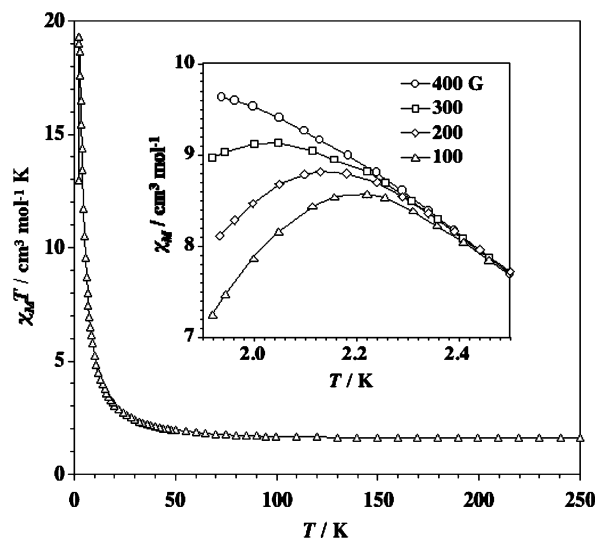


**Figure 3.** Thermal dependence of the  $\chi_{\text{M}}T$  product for complex **4** under an applied magnetic field of 100 G: ( $\Delta$ ) experimental data; (—) eye guideline. (Inset) Field dependence of the magnetic susceptibility of **4** at very low temperatures (the applied magnetic field varying in the range 100–400 G).

For a low-spin iron(III) ion in  $O_h$  symmetry, the  ${}^2T_{2g}$  term is split under a rhombic distortion ( $C_{2v}$  symmetry) into a singlet ground state ( ${}^2A_1$ ) and two excited doublets ( ${}^2B_1 + {}^2B_2$ ) which are separated by an average energy gap ( $\Delta$ ). Consequently, the magnetic data of **1** and **2** were analyzed through the Hamiltonian of eq 1

$$\hat{H} = -\kappa\lambda\hat{L}\hat{S} + \Delta[\hat{L}_z^2 - 2/3] + \beta H[-\kappa\hat{L} + 2\hat{S}] \quad (1)$$

The spin–orbit coupling (first term), an axial distortion (second term), and the Zeeman effect (last term) are considered in this Hamiltonian, and we used  $L = 1$  due to the isomorphism between the  $T_2$  and  $P$  terms ( $[T_2] = -[P]$ ).<sup>53</sup> In this Hamiltonian,  $\lambda$  is the spin–orbit coupling,  $\kappa$  is the orbital reduction factor, and  $\Delta$  is the energy gap between the  $A_1$  singlet and the  $E(B_1 + B_2)$  doublet. Best-fit parameters are  $\lambda = -362 \text{ cm}^{-1}$ ,  $\Delta = 680 \text{ cm}^{-1}$ ,  $\kappa = 0.87$ , and  $R = 2.2 \times 10^{-6}$  for **1** and  $\lambda = -336 \text{ cm}^{-1}$ ,  $\Delta = 578 \text{ cm}^{-1}$ ,  $\kappa = 0.90$ , and  $R = 1.1 \times 10^{-6}$  for **2** where  $R$  is the agreement factor defined as  $\sum_j [(\chi_{\text{M}}T)_{\text{obs}}^j - (\chi_{\text{M}}T)_{\text{calc}}^j]^2 / \sum_j [(\chi_{\text{M}}T)_{\text{obs}}^j]^2$ .

The temperature dependence of the  $\chi_{\text{M}}T$  product for **4** per  $\text{Fe}^{\text{III}}_2\text{Cu}^{\text{II}}$  unit is shown in Figure 3.  $\chi_{\text{M}}T$  at room temperature is  $1.61 \text{ cm}^3 \text{ mol}^{-1} \text{ K}$ , a value which is as expected for one copper(II) and two low-spin iron(III) ions magnetically isolated. Upon cooling,  $\chi_{\text{M}}T$  increases continuously in agreement with an intrachain ferromagnetic coupling between the spin doublets of the copper(II) and low-spin iron(III) centers. The increase is smooth in the high-temperature range and sharp at  $T < 50 \text{ K}$ .  $\chi_{\text{M}}T$  reaches a maximum value of  $19.5 \text{ cm}^3 \text{ mol}^{-1} \text{ K}$  at  $2.5 \text{ K}$  and further decreases to  $13.0 \text{ cm}^3 \text{ mol}^{-1} \text{ K}$  at  $1.9 \text{ K}$  under an applied magnetic field of  $H = 100 \text{ G}$ . The magnetic susceptibility of **4** is field dependent for  $T < 2.5 \text{ K}$  (see inset of Figure 3). A maximum of susceptibility occurs at  $2.2 \text{ K}$  for  $H = 100 \text{ G}$ , revealing the occurrence of a weak antiferromagnetic interaction between the ferromagnetic bimetallic chains in **4**. This maximum is shifted toward lower temperatures when increasing the applied

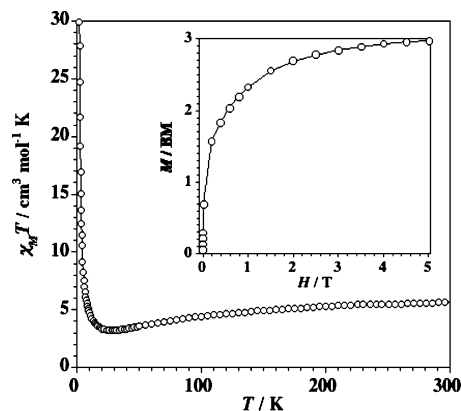


**Figure 4.** Thermal dependence of the  $\chi_{\text{M}}T$  product for complex **5**: ( $\circ$ ) experimental data; (—) eye guideline. (Inset) Magnetization versus  $H$  plot at  $2.0 \text{ K}$ .

magnetic field, and it disappears for  $H \geq 400 \text{ G}$ , suggesting a field-induced transition from an antiferromagnetic to a ferromagnetic ground state. This magnetic behavior of **4** is consistent with its crystal structure: parallel  $\text{Fe}^{\text{III}}_2\text{Cu}^{\text{II}}$  ferromagnetic chains with interchain antiferromagnetic coupling. The magnetization at saturation ( $M_{\text{S}}$ ) tends to a value of  $3.0 \mu_{\text{B}}$  (Figure S5), as expected for a ferromagnetically coupled  $\text{Fe}^{\text{III}}_2\text{Cu}^{\text{II}}$  unit with  $S_{\text{Fe}} = S_{\text{Cu}} = 1/2$ . The sigmoidal shape of the magnetization ( $M$ ) versus  $H$  plot at  $2.0 \text{ K}$  (inset of Figure S6) with an inflection point at  $400 \text{ G}$  gives the order of magnitude of the interchain magnetic interaction, ca.  $0.04 \text{ cm}^{-1}$ . No alternating current (ac) signals were observed for **4** down to  $1.9 \text{ K}$  at  $H = 0 \text{ G}$ . The lack of SCM behavior in **4** in the investigated range of temperatures, [in contrast to what is observed for **3** (see below)], is most likely due to the lower anisotropy of the copper(II) ion compared to that of the high-spin cobalt(II). The lack of an exact model to analyze the magnetic data of the ferromagnetic chain **4** with two intrachain ferromagnetic interactions moved us to use the Monte Carlo methodology to simulate the magnetic data and determine the magnitude of the intrachain magnetic couplings. A value of  $J_{\text{Fe-Cu}} = +20.9 \text{ cm}^{-1}$  was obtained for **4** (see below). DFT-type calculations were also performed on a model fragment of **4** to analyze the exchange pathway and to check the computed value of the exchange interaction obtained through the Monte Carlo methodology (see below).

The temperature dependence of the  $\chi_{\text{M}}T$  product for **5** per  $\text{Fe}^{\text{III}}_2\text{Mn}^{\text{II}}$  unit is shown in Figure 4.  $\chi_{\text{M}}T$  at room temperature is  $5.64 \text{ cm}^3 \text{ mol}^{-1} \text{ K}$ , a value which is as expected for a high-spin manganese(II) and two low-spin iron(III) ions magnetically isolated. As the temperature is lowered,  $\chi_{\text{M}}T$  smoothly decreases, exhibits a minimum at ca.  $25 \text{ K}$  ( $\chi_{\text{M}}T$  being  $3.22 \text{ cm}^3 \text{ mol}^{-1} \text{ K}$ ), and increases sharply to reach a value of  $30.0 \text{ cm}^3 \text{ mol}^{-1} \text{ K}$  at  $1.9 \text{ K}$ . The magnetization curve for **5** at  $2.0 \text{ K}$  is shown in the inset of Figure 4. A value of  $3.0 \mu_{\text{B}}$  is attained at  $5 \text{ T}$  (the maximum available magnetic field in our device). The features observed in Figure 4 are as expected for a ferrimagnetic behavior:<sup>54</sup> the noncompensation between the antiferromagnetically coupled Mn(II) spin sextet and Fe(III) spin doublet across the cyanide bridges in **5** accounts for this well-documented magnetic behavior. As done for **4**, the successful modelization

(53) Herrera, J. M.; Bleuzen, A.; Dromzée, Y.; Julve, M.; Lloret, F.; Verdaguier, M. *Inorg. Chem.* **2003**, *42*, 7052.

(54) (a) Verdaguier, M.; Julve, M.; Michalowicz, A.; Kahn, O. *Inorg. Chem.* **1983**, *19*, 2624. (b) Verdaguier, M.; Gleizes, A.; Renard, J. P.; Seiden, J. *Phys. Rev. B* **1984**, *29*, 5144. (c) Lloret, F.; Julve, M.; Ruiz, R.; Journaux, Y.; Nakatani, K.; Kahn, O.; Sletten, J. *Inorg. Chem.* **1993**, *32*, 27.

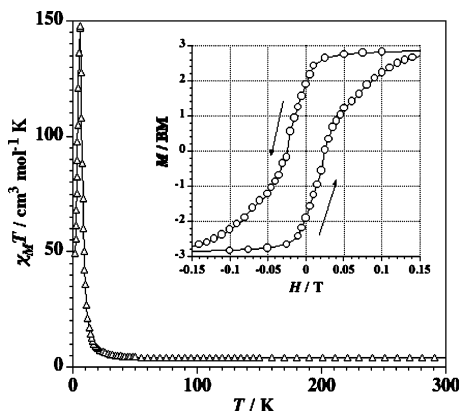


**Figure 5.** Thermal dependence of the  $\chi_M T$  product for complex **3** under an applied magnetic field of 100 G: ( $\Delta$ ) experimental data; (—) eye guideline. (Inset) Hysteresis loop for **3** at 2.0 K.

of the magnetic data of **5** through Monte Carlo methodology allowed us to estimate a value of the magnetic coupling  $J_{\text{Fe-Mn}}$  of  $-10.8 \text{ cm}^{-1}$  which was also substantiated by DFT type calculations (see below).

**Single-Chain Magnet Behavior in 3.** The temperature dependence of the  $\chi_M T$  product for **3** per  $\text{Fe}^{\text{III}}_2\text{Co}^{\text{II}}$  unit is shown in Figure 5. At room temperature, the  $\chi_M T$  product of a polycrystalline sample of **3** per  $\text{Fe}^{\text{III}}_2\text{Co}^{\text{II}}$  unit is  $4.0 \text{ cm}^3 \text{mol}^{-1} \text{K}$  and it corresponds to the presence of one high-spin cobalt(II) ( $S_{\text{Co}} = 3/2$ ) and two low-spin iron(III) ( $S_{\text{Fe}} = 1/2$ ) ions. Upon cooling,  $\chi_M T$  increases continuously in agreement with an intrachain ferromagnetic interaction between  $\text{Co}^{\text{II}}$  and  $\text{Fe}^{\text{III}}$  centers. The increase is smooth in the high-temperature range and sharp at  $T < 40 \text{ K}$ .  $\chi_M T$  reaches a maximum value of  $148 \text{ cm}^3 \text{mol}^{-1} \text{K}$  at  $5.7 \text{ K}$  ( $H = 100 \text{ G}$ ) and further decreases linearly with  $T$  (as the magnetization becomes field-dependent) to a value of ca.  $50 \text{ cm}^3 \text{mol}^{-1} \text{K}$  at  $1.9 \text{ K}$ . The magnetization versus  $H$  plot at  $2.0 \text{ K}$  exhibits an abrupt increase at very low fields, and it reaches a value of  $3.7 \mu_B$  at  $5 \text{ T}$  (the maximum available magnetic field in our device). A hysteresis loop is

observed for **3** at  $2.0 \text{ K}$  (see inset of Figure 5) with values of the coercive field ( $H_c$ ) and remnant magnetization ( $M_r$ ) of  $250 \text{ G}$  and  $2.0 \text{ BM}$ , respectively.

The hysteresis loops were studied in detail with the micro-SQUID technique.<sup>19</sup> A single crystal of **3** was attached on the micro-SQUID array using Apiezon grease. The field was aligned with the easy axis of magnetization using the transverse field method.<sup>20</sup> Typical hysteresis loops are presented in Figures 6 and S7. The chain **3** displays smooth hysteresis loops which are strongly temperature- and field sweep rate-dependent. A detailed study of the temperature and field sweep rate dependences of the coercive fields are presented below. No hysteresis is observed in the magnetization plot at  $3.2 \text{ K}$  as shown in Figure S8. A double-S magnetization curve occurs at small magnetic field loops establishing weak antiferromagnetic interchain interactions. The field derivative of the magnetization curve (inset of Figure S8) allow us to obtain the interaction field of  $0.016 \text{ T}$ .

The slow relaxation of the magnetization of **3** was studied at higher temperatures with ac magnetic susceptibility. A frequency-dependent out-of-phase component ( $\chi''$ ) was observed below  $6.4 \text{ K}$  (Figure 7a). The maximum of  $\chi''$  can be used to get the mean relaxation ( $\tau$ ). The fact that the maximum of  $\chi''$  decreases with decreasing frequency confirms the small interchain coupling. At lower temperatures the relaxation rate becomes too slow for ac magnetic susceptibility measurements, and we used dc relaxation measurements to extract the relaxation time. At a given temperature, the magnetization was first saturated in a high magnetic field. After sweeping the field down to zero with a field sweep rate of  $0.14 \text{ T/s}$ , the magnetization decay was measured as a function of time (Figure S9). Because the decay is not exponential, we used a scaling procedure to obtain the mean relaxation time ( $\tau$ ). The ac and dc relaxation times are plotted into an Arrhenius plot [ $\tau = \tau_0 \exp(E_a/kT)$ ,  $\tau_0$  being the preexponential factor and  $E_a$  the effective energy barrier for spin reversal]. Two regimes are observed in Figure 7 b: (i) above  $3.0 \text{ K}$ , the thermal dependence of the relaxation time follows

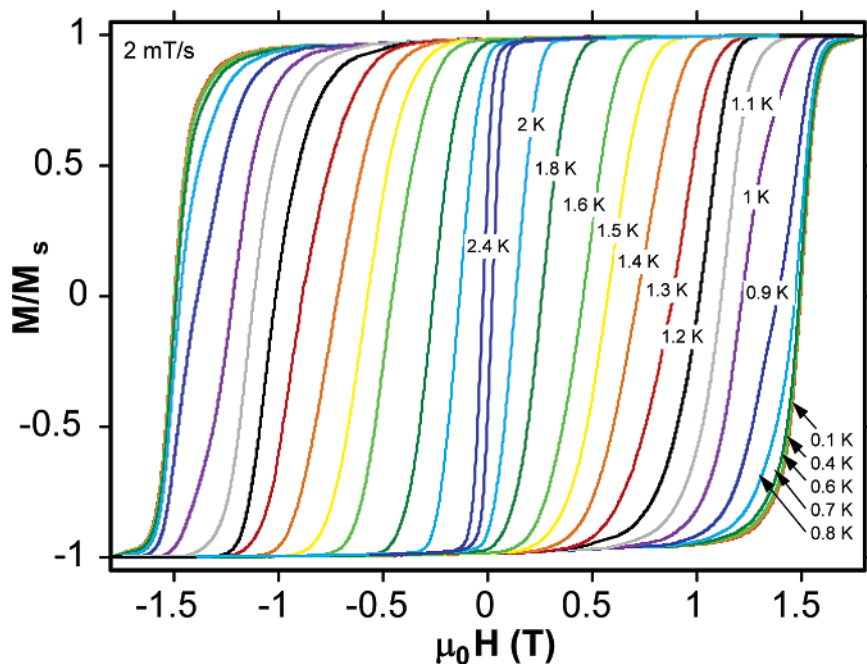


**Figure 6.** Hysteresis loops for a single crystal of **3** at several temperatures and  $0.002 \text{ T/s}$ . The field is aligned with the easy axis of magnetization.

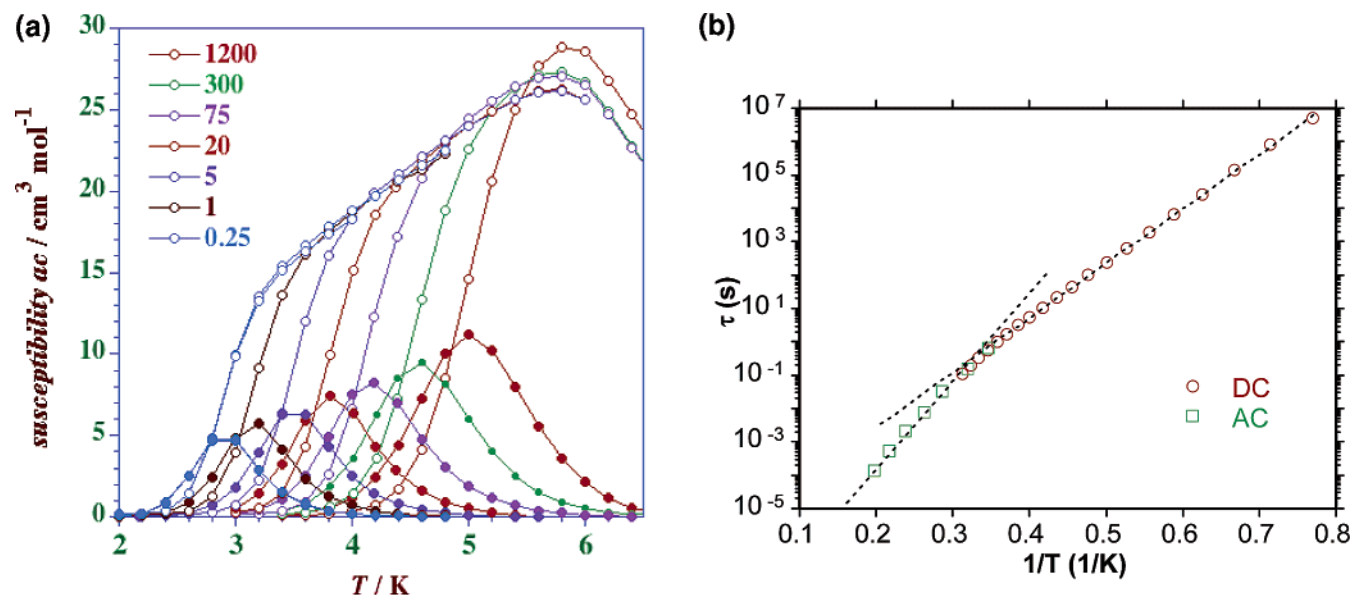


**Figure 7.** (a) In-phase (open circles) and out-of-phase (filled circles) components of the ac susceptibility of **3** at  $T < 6.4 \text{ K}$  in a 1 G field oscillating at different frequencies (0.25–1200 Hz) without dc magnetic field. (b) Plot of  $\ln \tau$  against  $1/T$  for **3**: squares are experimental data from ac susceptibility measurements and circles are from dc decay measurements. The dotted lines are least-squares fits to the Arrhenius law (see text).

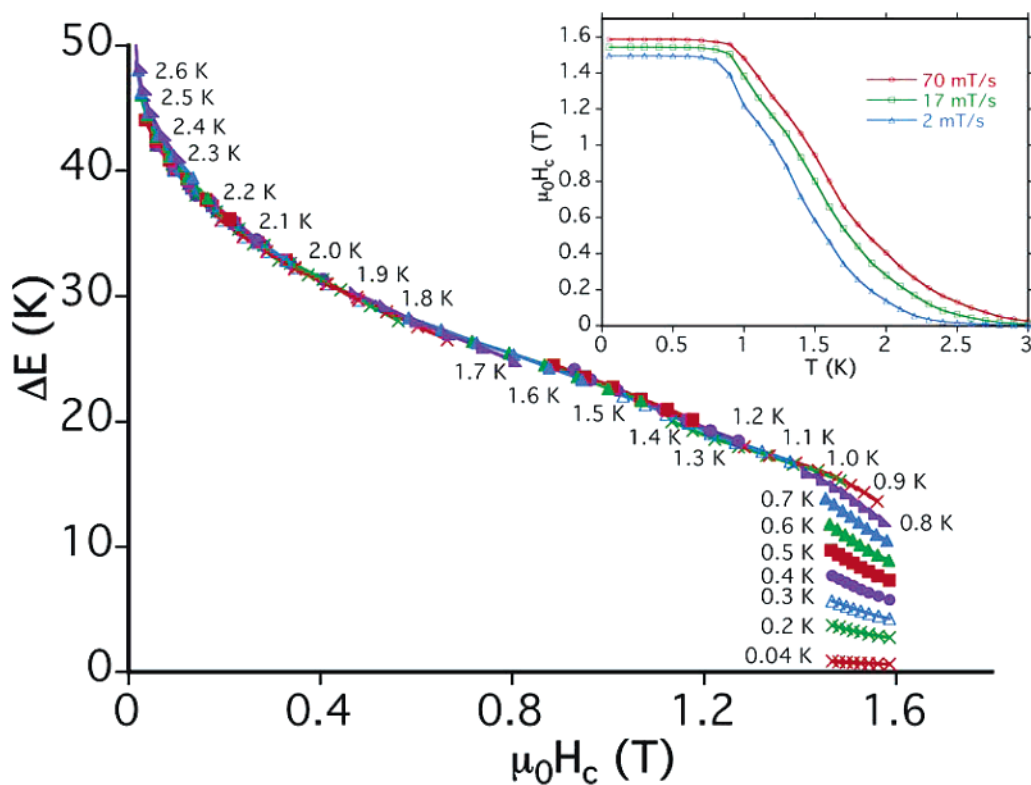


**Figure 8.** Field dependence of the energy barrier of the chain **3** obtained from eq 2 and the set of  $H_c(T, \nu)$  data from Figure S11. (Inset) Coercive field  $H_c$  for the chain **3** as a function of the temperature.

an Arrhenius law with an activation energy of  $E_a/k = 61.4 \text{ K}$  and  $\tau_0 = 7.9 \times 10^{-10} \text{ s}$ ; (ii) below 3 K, a departure from this simple behavior was observed, and a smaller activation energy of 37.8 K and  $\tau_0 = 1.5 \times 10^{-9} \text{ s}$  are found. We interpret the crossover at about 3 K as the manifestation of finite-size effects.<sup>55</sup> Indeed, it has been predicted that the activation energy of the relaxation time should decrease from  $(4J + D)S^2$  to  $(2J + D)S^2$  at the temperature where the correlation length equals the chain length.<sup>55</sup> In our case, a direct application of the model is not possible because of a more complicated coupling scheme

of the spins and the strong spin–orbit coupling of the cobalt centers. However, this interpretation is reasonable because the correlation length becomes extremely long at low temperature. The occurrence of a very small number of defects is therefore limiting the correlation lengths.

The relaxation rate at  $H = 0$  is extremely small below 1.3 K. We applied therefore a magnetic field to study the low-temperature relaxation process. The temperature and field sweep rate dependences of the coercive fields ( $H_c$ ) were measured, and they are plotted in the inset of Figure 8 and in Figure S10.

As expected for a thermally activated process, the values of  $H_c$  increase with the decreasing temperature  $T$  and increasing field sweep rate  $v = dH/dt$ . Furthermore, all our measurements showed an almost logarithmic dependence of  $H_c$  on the field sweep rate (Figure S10).  $H_c$  becomes temperature independent below ca. 0.8 K.

We analyzed the set of  $H_c(T, v)$  data with a model of thermally activated nucleation of magnetization reversal analogous to that of a magnetic single-domain particle. The model was recently applied to SMMs<sup>56</sup> and SCMs<sup>57</sup> and allowed a detailed understanding of the reversal mechanism. Whereas the magnetization relaxation is described at high temperature by the Glauber model, the relaxation at  $H = 0$  at low temperature (below 1.3 K) is extremely small. We applied therefore a magnetic field to drive the relaxation at the low temperatures, that is the anisotropy barrier can be lowered by applying a magnetic field in the opposite direction to that of the chain magnetization. When the applied field is close enough to the nucleation field of a domain wall, thermal fluctuations are sufficient to allow the system to overcome the nucleation barrier, and a domain wall nucleates. Then, due to the applied field, the magnetization of the entire chain reverses via a domain wall propagation process. The domain wall nucleation can be thermally activated at high temperatures or driven by quantum tunneling at low temperatures.<sup>58–61</sup>

This stochastic nucleation process can be studied via the magnetization decay when ramping the applied field at a given rate and measuring the coercive field  $H_c$  which corresponds to the mean nucleation field of a domain wall.  $H_c$  is then measured as a function of the field sweep rate and temperature (inset of Figure 8 and Figure S10). The coercive field of an assembly of identical noninteracting SCMs is given by eq 2

$$H_c(T, v) = H_c^0 (1 - [kT/E_0 \ln(c/v)]^{1/2}) \quad (2)$$

where the field sweeping rate is given by  $v = dH/dt$ ,  $H_c^0$  is the nucleation field at zero temperature,  $E_0$  is roughly the nucleation barrier height at zero applied field and  $c = H_c^0 kT / [2\tau_0 E_0 (1 - H_c/H_c^0)]$ . The validity of eq 2 was tested by plotting the set of  $H_c(T, v)$  values as a function of  $[T \ln(c/v)]^{1/2}$ . If the underlying model is sufficient, all points should collapse onto one straight line by choosing the proper values for the constant  $\tau_0$ . We found that the data of  $H_c(T, v)$  with  $T > 1$  K fell on a master curve provided  $\tau_0 = 2.4 \times 10^{-7}$  s (Figure S11).

At lower temperatures, strong deviation from the master curves are observed. To investigate the possibility that these low-temperature deviations are due to escape from the metastable potential well by tunneling, a common method for classical models is to replace the real temperature  $T$  by an effective temperature  $T^*(T)$  in order to restore the scaling plot.<sup>56,62</sup> In the case of tunneling,  $T^*(T)$  should saturate at low temperatures. Indeed, the ansatz of  $T^*(T)$ , as shown in the inset

of Figure S11 (bottom), can restore unequivocally the scaling plot demonstrated by a straight master curve [Figure S11 (bottom)]. The flattening of  $T^*$  corresponds to a saturation of the escape rate, which is a necessary signature of tunneling. The crossover temperature  $T_c$  can be defined as the temperature where the quantum rate equals the thermal one. The inset of Figure S11 (bottom) gives  $T_c = 0.8$  K. The slope and the intercept of the master curves give  $E_0/k_B = 40.3$  K and  $H_c^0 = 3.8$  T.

This model can be used to find the field dependence of the effective energy barrier [eq 3]<sup>56,57</sup>

$$\Delta E = kT \ln(c/v) \quad (3)$$

The result is plotted in Figure 8. One can see there how  $\Delta E$  decreases with the increasing field. Below ca. 1.0 K, the tunneling reduces the barrier to zero.

In conclusion, the present detailed study of the slow relaxation of the chain **3** shows that the dynamics is Glauber-like at higher temperatures. Below ca. 3.0 K, a transition to finite size Glauber dynamics is observed. The presented low-temperature studies of the field-driven magnetization reversal for the low-temperature region suggest that the magnetization reversal starts by a quantum nucleation of a domain wall followed by domain wall propagation and reversal of the magnetization.

**Monte Carlo Simulation of the Magnetic Properties of 4 and 5.** The simulation of the magnetic properties is an important step for a correct analysis of the magnetic exchange in polynuclear compounds. Procedures based on the exact energy matrix diagonalization are commonly used to do this task, but their applicability is limited by the size of the systems, in particular in the case of the extended ones. Monte Carlo methods are well suited to analyze these latter systems, and they are among the most used ones to perform this work. In a classical spin approach, the implementation of the Monte Carlo algorithms (CMC) is a quite easy task.<sup>63</sup> Nevertheless, this approximation can be applied only to systems with large local spin values, such as high-spin iron(III) or manganese(II) complexes. In the cases of smaller spin values, the local spin moments have to be considered as quantum spins, and consequently, the so-called quantum Monte Carlo (QMC) methods must be used. The main drawbacks associated to the use of the QMC methods are their complexity and time consumption. The occurrence of low-spin iron(III) ( $S_{Fe} = 1/2$ ) in complexes **3–5**, leads us to use the QMC methods to simulate their magnetic properties. Among the possible QMC methods, we have chosen the decoupled Cell Monte Carlo method (DCM) which was proposed by Homma et al. and a modification of such approach from Miyazawa et al. that improves the results at low temperatures (mDCM).<sup>64,65</sup> These QMC methods are applied from the probability that implies a change in the  $m_s$  value (spin flip) for the site placed on the center of a cell or subsystem. This probability is evaluated by the exact diagonalization procedure

(55) Coulon, C.; Clérac, R.; Lecren, L.; Wernsdorfer, W.; Miyasaka, H. *Phys. Rev. B* **2004**, *69*, 132408.

(56) Wernsdorfer, W.; Murugesu, M.; Tasiopoulos, A. J.; Christou, G. *Phys. Rev. B* **2005**, *72*, 212406.

(57) Wernsdorfer, W.; Clérac, R.; Coulon, C.; Lecren, L.; Miyasaka, H. *Phys. Rev. Lett.* **2005**, *95*, 237203.

(58) Stamp, P. C. E. *Phys. Rev. Lett.* **1991**, *66*, 2802.

(59) Chudnovsky, E. M.; Iglesias, O.; Stamp, P. C. E. *Phys. Rev. B* **1992**, *46*, 5392.

(60) Tataru, G.; Fukuyama, H. *Phys. Rev. Lett.* **1994**, *72*, 772.

(61) (a) Braun, H. B.; Kyriakidis, J.; Loss, D. *Phys. Rev. B* **1997**, *56*, 8129. (b) Ansermet, J. Ph.; Maily, D. *Phys. Rev. B* **1997**, *55*, 11552.

(62) (a) Wernsdorfer, W.; Bonet Orozco, E.; Hasselbach, K.; Benoit, A.; Barbara, B.; Demoncey, N.; Loiseau, A.; Boivin, D.; Pascard, H.; Maily, D. *Phys. Rev. Lett.* **1997**, *78*, 1791. (b) Wernsdorfer, W.; Bonet Orozco, E.; Hasselbach, K.; Benoit, A.; Maily, D.; Kubo, O.; Nakano, H.; Barbara, B. *Phys. Rev. Lett.* **1997**, *79*, 4014.

(63) Cano, J.; Journaux, Y. *Magnetism: Molecules to Materials V*; Miller, J. S., Drillon, M., Eds.; Wiley: New York, 2004; Chapter 6.

(64) Homma, S.; Matsuda, H.; Ogita, N. *Prog. Theor. Phys.* **1986**, *75*, 1058.

(65) Miyazawa, S.; Miyashita, S.; Makivic, M. S.; Homma, S. *Prog. Theor. Phys.* **1993**, *89*, 1167.

applied to the mentioned subsystem. Thus, a better description of the spin correlation function is obtained for larger subsystem sizes, allowing the correct application of the method to lower temperatures. In the mDCM methods, the spin flip probability for the paramagnetic center  $i$  is calculated also, taking into account the neighboring subsystems involving it. Thus, the spin correlation function is more correct for the same subsystem size.

In the MC methods, from the spin flip probabilities and using a metropolis algorithm, we can generate a sampling where the states more present are those having a more important contribution in the partition function. This sampling allows us to calculate the average magnetization at a given temperature. The molar magnetic susceptibility can be obtained from the fluctuations in the magnetization through eq 4, where  $\langle M \rangle$  and  $\langle M^2 \rangle$  are the mean values of the magnetization and its square, and  $N$ ,  $\beta$ , and  $k$  have their usual meaning.

$$\chi_M T = \frac{N\beta^2}{k(\langle M^2 \rangle - \langle M \rangle^2)} \quad (4)$$

In all simulations, the number of MC steps for each temperature is  $5 \times 10^6/T$  ( $T$  in K). Thus, we included more steps in the sampling at low temperatures where the correct equilibrium requires more recorded data. Ten percent of the MC steps are employed for the thermalization of the system; thus, we stocked the physical properties when the equilibrium is reached. Models of 90 sites were used for compounds **4** and **5**. Periodic boundary conditions were introduced in all simulations. Deeper details on the MC simulations can be found in ref 63.

As mentioned above, low-spin octahedral iron(III) ions are present in **1–5**. The decrease of  $\chi_M T$  in **1** and **2**, where no significant magnetic coupling is involved, is due to the spin-orbit coupling of the  $^2T_{2g}$  ground term. Consequently, to simulate the magnetic behaviors of **3–5**, we have subtracted first the  $\chi_M T$  data of **2** from those of **3–5** (per two iron atoms). Then,  $0.91 \text{ cm}^3 \text{ mol}^{-1} \text{ K}$  (Curie law term per two noninteracting spin doublets with  $g = 2.20$ , the  $g$  value being calculated from the extrapolated  $\chi_M T$  value of **2** at 0 K) was added to the difference data. The procedure is expected to rule out the orbital contribution of the low-spin iron(III) to the magnetic behavior of **3–5**. However, the additional spin-orbit coupling contribution in **3** due to the presence of high-spin octahedral cobalt(II) ions precludes the simulation of the magnetic data of this compound. This is why we focused only on the QMC simulation of the corrected magnetic data of **4** and **5**.

We have applied the DCM and mDCM methods to a uniform 4,2-ribbonlike chain (only one exchange coupling parameter) where two different local spins occur [ $S_{\text{Fe}} = 1/2$  (**4** and **5**),  $S_{\text{Cu}} = 1/2$  (**4**), and  $S_{\text{Mn}} = 5/2$  (**5**)]. Ferro- (**4**) and ferrimagnetic (**5**) behaviors are observed. Only an intrachain coupling parameter and two decompositions in small cells were used in the simulations (Figure S12). Each decomposition was centered in different metal ions. For **4**, only the three first shells of neighbors were considered in the first decomposition, whereas the fourth nearest-neighbor shell was also introduced in the second one [Figure S12(a)]. However, smaller decompositions were considered for **5** [Figure S12(b)] because of the huge size of the issued energy matrix. Although the interaction topology in these systems is simple, the simulation of the experimental  $\chi_M T$  vs  $T$  plots is a quite complex task due to the presence of a  $g$ -factor

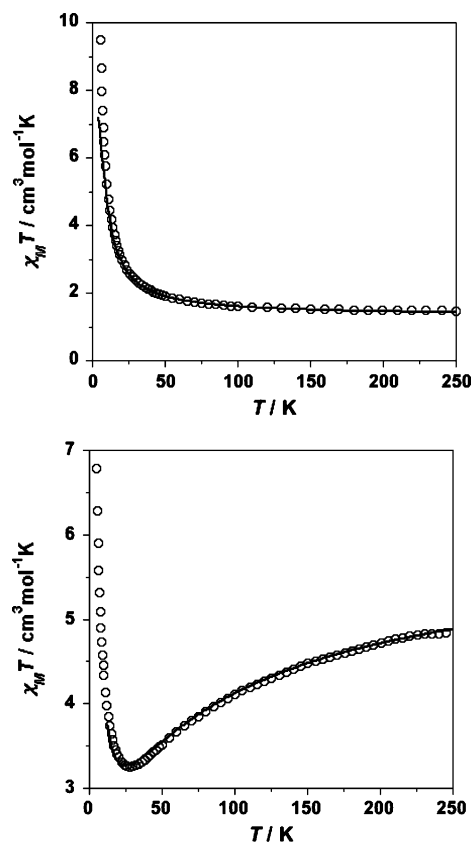


**Figure 9.**  $\chi_M T$  vs  $T$  plots for **4** (top) and **5** (bottom): (O) experimental data; (—) simulated curve through QMC (see text).

for each metal ion. This last fact, that the  $g$ -factors take different values, not only modifies the values of  $\chi_M T$  (including the value in the minimum when the exchange coupling is antiferromagnetic) but also causes a shift of the temperature of the minimum of  $\chi_M T$ . This last comment is visualized in a clearer way in Figure S13 where several sets of  $g$  values are displayed concerning the QMC simulations for **5** with an antiferromagnetic interaction between the local spins ( $S_{\text{Fe}} = 1/2$  and  $S_{\text{Mn}} = 5/2$ ). The temperature ranges of our QMC simulations are  $T/|J| \geq 0.15$  (**4**) and  $0.5$  (**5**).

The simulated curves have been fitted to the corrected  $\chi_M T$  vs  $T$  data, the best-fit parameters being  $g_{\text{Fe}} = 2.20$ ,  $g_{\text{Cu}} = 2.10$ , and  $J_{\text{Fe-Cu}} = +20.9 \text{ cm}^{-1}$  for **4** and  $g_{\text{Fe}} = 2.20$ ,  $g_{\text{Mn}} = 2.00$ , and  $J_{\text{Fe-Mn}} = -10.8 \text{ cm}^{-1}$  for **5** (see Figure 9). A good agreement between the simulated and experimental data is found in both cases. The nature of the magnetic interaction [ferro- (**4**) and antiferromagnetic (**5**)] is as expected, keeping in mind the symmetry of the interacting magnetic orbitals [ $t_{2g}$  vs  $e_g$  (**4**) and  $t_{2g}$  vs  $t_{2g}/e_g$  (**5**); see next section] but the values of the magnetic couplings in them are somewhat above from those reported for other magneto-structurally characterized single cyano-bridged  $\text{Fe}^{\text{III}}$  (low-spin)- $\text{Cu}^{\text{II}}$  [ $J$  values of  $+5.0$  and  $+12.6 \text{ cm}^{-1}$  for  $\{[\text{Fe}^{\text{III}}(\text{phen})(\text{CN})_4]_2\text{Cu}^{\text{II}}(\text{H}_2\text{O})_2\} \cdot 4\text{H}_2\text{O}$  and  $\{[\text{Fe}^{\text{III}}_2\text{Cu}^{\text{II}}_2(\mu\text{-CN})_4(\text{bipy})_6\}(\text{PF}_6)_6 \cdot 4\text{CH}_3\text{CN} \cdot 2\text{CHCl}_3$ , respectively]<sup>12b,66</sup> and  $\text{Fe}^{\text{III}}$  (low-spin)- $\text{Mn}^{\text{II}}$  [ $J$  values of  $-1.3$  and  $-3.0 \text{ cm}^{-1}$  for  $\{[\text{Fe}^{\text{III}}(\text{bipy})(\text{CN})_4]_2\text{Mn}^{\text{II}}(\text{H}_2\text{O})_4\} \cdot 4\text{H}_2\text{O}$  and  $(\mu\text{-bpym})[\text{Mn}^{\text{II}}(\text{H}_2\text{O})_3\text{-}\{[\text{Fe}^{\text{III}}(\text{bipy})(\text{CN})_4]\}_2\} \cdot 12\text{H}_2\text{O}$ ]<sup>15b,c</sup> complexes.

(66) (a) Oshio, H.; Tamada, O.; Onodera, H.; Ito, T.; Ikoma, T.; Tero-Kubota, S. *Inorg. Chem.* **1999**, *38*, 5686. (b) Oshio, H.; Yamamoto, M.; Ito, T. *Inorg. Chem.* **2002**, *41*, 5817.

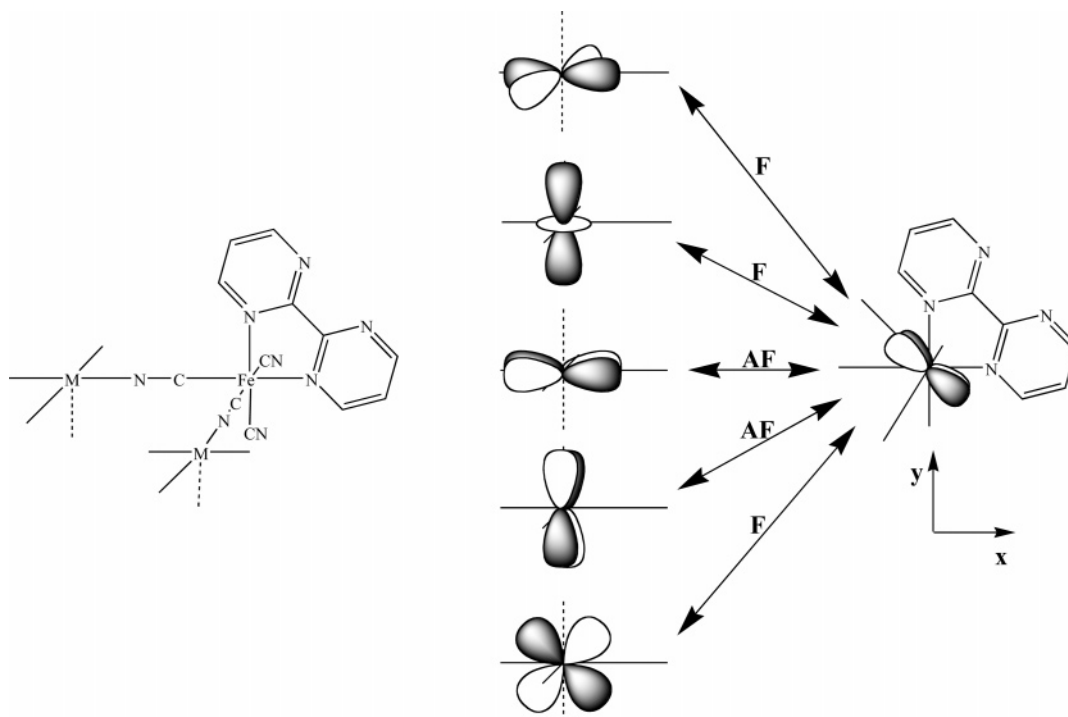


**Figure 10.** Orbital picture showing the different contributions to the magnetic coupling in a dinuclear fragment of **3–5** (F and AF stand for ferro- and antiferromagnetic couplings, respectively).

The different chromophore around the metal ions involved would account for the difference in the values of  $J$ .<sup>67</sup>

**Analysis of the Exchange Pathways in 3–5.** DFT calculations were used as a tool to elucidate the causes of the different magnetic behaviors observed in compounds **3–5** in the framework of the molecular orbital theory. These calculations also allowed us to evaluate the magnitude of the exchange coupling involved in each case. The  $[\text{Fe}(\text{bpym})(\text{CN})_4]^-$  unit [see model **I** in Figure S14 (top)] that has a ground doublet spin state is present in compounds **2–5**. So, the first step was the treatment of this entity to get an orbital picture of the magnetic orbital (that is the molecular orbital which defines its unpaired electron). As in the similar  $[\text{Fe}(\text{phen})(\text{CN})_4]^-$  building block (where bpym is substituted by phen) which was investigated in a previous work,<sup>12b</sup> the spin density map shows that its unpaired electron is described by a  $t_{2g}$ -type orbital. The spin density is mostly localized at the iron atom, the carbon and nitrogen atoms of the cyanide ligands presenting small spin densities whose sign is determined by the spin polarization mechanism. Having in mind the definition of the axes displayed in **I** [the  $x$  and  $y$  axes being roughly defined by the Fe–N(bpym) bonds], this magnetic orbital corresponds to the combination  $d_{xz} - d_{yz}$  [see Figure S14 (bottom)]. The same procedure was applied to the  $[\text{M}(\text{CN})_4(\text{H}_2\text{O})_2]^{2-}$  entity [M = Co (**3**), Cu (**4**), and Mn (**5**)]. The magnetic orbital in the copper unit corresponds to the  $d_{x^2-y^2}$  ( $e_g$ ), whereas the five 3d orbitals act as magnetic orbitals in the manganese one. The analysis for the cobalt unit is more complex, the two  $e_g$  ( $d_{x^2-y^2}$  and  $d_{z^2}$ ) and one  $t_{2g}$  ( $d_{xy}$ ) orbitals playing the role of the magnetic orbitals.

With these results in mind, the prediction of the nature of the magnetic coupling in **3–5** is an easy task. Simple symmetry considerations allow the prediction of a positive value for the

contributions to the magnetic coupling when the  $e_g$  magnetic orbitals of the divalent metal ion interact with the  $t_{2g}$  magnetic orbital of the iron(III) unit. This is a case of strict orthogonality between the magnetic orbitals [see Figure 10] across the bridging cyanide which is equatorially bound to the two metal ions. This case is exemplified by compound **4** which exhibits a ferromagnetic behavior. In compounds **3** and **5**, the occurrence of  $t_{2g}$  magnetic orbitals on the cobalt(II) and manganese(II) ions implies the addition of antiferromagnetic contributions which can be strong or practically nonexistent because of symmetry reasons according to the relative orientation of the magnetic orbitals. Due to the orientation of the magnetic orbital of the low-spin iron(III) ion (the value of the angle between the plane that encompasses it and the  $z$  axis is close to  $45^\circ$ ), only moderate antiferromagnetic (one  $(t_{2g} - t_{2g})$  term) and ferromagnetic (two  $(t_{2g} - e_g)$  terms) contributions are expected (Figure 10) in **3**. The single antiferromagnetic contribution in this compound is not able to cancel the two ferromagnetic terms, and a net ferromagnetic interaction results, as evidenced experimentally. The occurrence in **5** of additional  $(t_{2g} - t_{2g})$  antiferromagnetic contributions leads to a net antiferromagnetic interaction in agreement with its ferrimagnetic behavior.

In previous works with cyano-bridged systems, we have observed that density functional calculations provide a good qualitative evaluation of the exchange coupling constants.<sup>12b,16a,68</sup> However, from a quantitative point of view, the calculated magnetic couplings are overestimated. In this respect, we have concluded that the presence of the charged terminal cyanide ligands (especially in the models where the one-dimensional system is cut, generating a greater number of these ligands) is responsible for the problem in the correct convergence of

(67) Román, P.; Guzmán-Mirallas, C.; Luque, A.; Beitia, J. I.; Cano, J.; Lloret, F.; Julve, M.; Alvarez, S. *Inorg. Chem.* **1996**, *35*, 3741.

(68) Lescouëzec, R.; Toma, M. L.; Toma, L. D.; Vaissermann, J.; Verdaguer, M.; Delgado, F. S.; Ruiz-Pérez, C.; Lloret, F.; Julve, M. *Coord. Chem. Rev.* **2005**, *249*.

calculations and the overestimation of the exchange coupling constants. Although the substitution of cyano groups by ammonia ligands minimizes both problems, it is not enough. A different strategy has been used in the present work. Here we have taken a more extended model which is closer to the 4,2-ribbonlike chain (see **II** in Figure S15). In this model, two iron(III) ions are at the center, and three coordination shells (the first, second, and third metal neighbors) are considered. To simplify the calculations, and taking advantage of the crystal structure of **2**, the third metal neighbor shell is substituted by the diamagnetic zinc(II) ions using the experimental metal-to-ligand distance observed in this compound. With this model, the influence in the modelization on the centered metal ions is minimized. So, the two calculated configurations are the one displaying all local spins aligned in a ferromagnetic manner ( $\Phi_F$ ) and the other one where the spin moments of the centered iron(III) ions are opposite to the rest ( $\Phi_{AF}$ ) [Figure S15(b)]. The spin density map for the most stable configuration of the chain **5** (with local spins arranged in an antiferromagnetic manner) is shown in Figure S16. One can see there the spherical distribution of the spin density around the manganese atom and the perpendicular arrangement of the spin density of the iron atom with respect to the bpym mean plane in agreement with the DFT calculations done for model **I**. Note that the expression used for the evaluation of the exchange coupling constants is given in eq 5:

$$J = \frac{E(\Phi_F - \Phi_{AF})}{4n} \quad (5)$$

with  $n = 2, 1,$  and  $3$  for **3**, **4**, and **5**, respectively.

The calculated results are:  $J_{Fe-Co} = +6.1 \text{ cm}^{-1}$ ,  $J_{Fe-Cu} = +62.9 \text{ cm}^{-1}$ , and  $J_{Fe-Mn} = -11.7 \text{ cm}^{-1}$ . They agree qualitatively with the experimental ones. However, the overestimation of the values of  $J$  remains. Although this overestimation here is reduced when compared to the results in our previous works, due to a better choice of the model, it is not enough for an accurate evaluation. To improve this situation, studies with similar models immersed in a dielectric to simulate the remaining solid are in progress.

### Concluding Remarks

In this paper, the crystal structure of the mononuclear precursor  $\text{PPh}_4[\text{Fe}(\text{bpym})(\text{CN})_4] \cdot \text{H}_2\text{O}$  (**1**) and those of the

bimetallic chains  $\{[\text{Fe}^{\text{III}}(\text{bpym})(\text{CN})_4]_2\text{M}^{\text{II}}(\text{H}_2\text{O})_2\} \cdot 6\text{H}_2\text{O}$  [ $\text{M} = \text{Zn}$  (**2**),  $\text{Co}$  (**3**),  $\text{Cu}$  (**4**), and  $\text{Mn}$  (**5**)] have been determined, and their magnetic behaviors have been investigated as a function of the temperature. Compounds **3** and **4** exhibit intrachain ferromagnetic couplings and weak interchain antiferromagnetic interactions, whereas compound **5** is a ferrimagnetic chain. DFT-type calculations and the Monte Carlo methodology allowed us to analyze the exchange pathways involved and also to simulate the magnetic data. Both dc and ac magnetic measurements demonstrate that compound **3** behaves as a SCM, this compound being the first example of SCM obtained with the use of the new low-spin iron(III) complex  $[\text{Fe}(\text{bpym})(\text{CN})_4]^-$  as a ligand toward fully solvated transition metal ions. This bottom-up synthetic strategy appears to be a safe route to design SCMs with intrachain ferromagnetic coupling. Interestingly, the detailed study of the slow relaxation of the magnetization of the bimetallic chain **3** shows that its magnetization reversal in the low-temperature region starts by a quantum nucleation of a domain wall followed by domain wall propagation and reversal of the magnetization. Complex **3** is the second example of SCM which exhibits quantum effects.

**Acknowledgment.** This work was supported by the European Union through the Network QueMolNa (Project MRTN-CT-2003-504880) and the Magmanet Network of Excellence (Contract 515767-2), el Ministerio Español de Educación y Ciencia (Project CTQ2004-03633 and MAT2004-03112), the Generalitat Valenciana (Grupos 03/197), and the Gobierno Autónomo de Canarias (PI2002/175). Two of us (J.P. and L.M.T.) thank the Ministerio Español de Educación for predoctoral fellowships.

**Supporting Information Available:** Crystallographic tables (Tables S1–S4), additional structural drawings (Figures S1–S4), magnetic plots (Figures S5–S13), models for the theoretical calculations (Figures S14 and S15), spin density map for the model **II** of **5** (Figure 16) and X-ray crystallographic files (CIF) for **1–5** and complete ref 46. This material is available free of charge via the Internet at <http://pubs.acs.org>. The crystallographic files are also available on application to the Cambridge Data Centre, 12 Union Road, Cambridge CB21EZ, U.K. (Fax: (+44) 1223-336-033; e-mail: [deposit@ccdc.cam.ac.uk](mailto:deposit@ccdc.cam.ac.uk)), CCDC 259180 (**1**), 259181 (**2**), 259182 (**3**), 259183, (**4**) and 259184 (**5**).

JA058030V

# Influence of the presence of divalent first-row transition metal ions on the structure of sodium(I) salts of 1,2,3,4-benzenetetracarboxylic acid (H<sub>4</sub>bta)

Oscar Fabelo,<sup>a</sup> Laura Cañadillas-Delgado,<sup>a</sup> Jorge Pasán,<sup>a</sup> Catalina Ruiz-Pérez<sup>\*a</sup> and Miguel Julve<sup>b</sup>

Received 29th November 2005, Accepted 3rd March 2006

First published as an Advance Article on the web 28th March 2006

DOI: 10.1039/b516806f

Three different sodium(I)-containing salts of 1,2,4,5-benzenetetracarboxylic (H<sub>4</sub>bta) of formula [Na<sub>4</sub>(bta)(H<sub>2</sub>O)<sub>12</sub>] (**1**), [Na<sub>2</sub>M(H<sub>2</sub>bta)<sub>2</sub>(H<sub>2</sub>O)<sub>8</sub>]·2H<sub>2</sub>O [M = Mn (**2**) and Ni (**3**)] were synthesized and their structures were solved by single crystal X-ray diffraction methods. Compound **1** crystallises in orthorhombic system, space group *Pc2<sub>1</sub>b* with *a* = 6.9997(4) Å, *b* = 16.4260(9) Å, *c* = 20.3312(18) Å, *V* = 476.30(15) Å<sup>3</sup> and *Z* = 4. Compounds **2** and **3** crystallize in the monoclinic system, space group *C2/m* with *a* = 7.3778(4) Å, *b* = 20.1493(6) Å, *c* = 10.4963(4) Å, *β* = 103.466(8)°, *V* = 1517.5(11) Å<sup>3</sup> and *Z* = 2 for **1** and *a* = 7.2862(4) Å, *b* = 20.1165(7) Å, *c* = 10.4032(3) Å, *β* = 103.366(9)°, *V* = 1483.52(11) Å<sup>3</sup> and *Z* = 2 for **2**. The structure of **1** consists of layers of four crystallographically independent sodium atoms [two six- (Na(O<sub>w</sub>)<sub>6</sub>) and two five- (Na(O<sub>w</sub>)<sub>3</sub>O<sub>2</sub>) coordinated] which are bridged by tetrakismonodentate bta<sup>4-</sup> ligands and single and double water molecules. These layers are interlinked through hydrogen bonds involving some of the coordinated water molecules and free carboxylate-oxygen atoms to afford a 3-D network. Compounds **2** and **3** are isostructural: their structures are made up of chains with regular alternating pairs of Na<sup>+</sup> and single M<sup>2+</sup> cations [M = Mn (**2**) and Ni (**3**)], two water molecules acting as bridges between each pair of metal ions. Two water molecules (at M) and two carboxylate-oxygen atoms from two H<sub>2</sub>bta<sup>2-</sup> ligands (at Na) which are coordinated to the metal ions in *trans* positions build distorted octahedral surroundings. The H<sub>2</sub>bta<sup>2-</sup> group acts as a bimonodentate ligand toward adjacent sodium atoms through 1,3-carboxylate oxygens. These neutral chains are interlinked through hydrogen bonds involving free carboxylate-oxygen atoms and coordinated and crystallization water molecules to afford a 3-D structure.

## Introduction

Crystal engineering of coordination polymers is a very active research field, the potentiality of these compounds as functional materials as well as their flexibility in aspects such as composition and topology being very appealing. The majority of the numerous coordination polymers reported are normally constructed by linking transition metal centres through multidentate bridging ligands.<sup>1</sup> In this context, metal-organic coordination complexes containing a tetradentate ligand such as 1,2,4,5-benzenetetracarboxylate (hereafter noted bta<sup>4-</sup>) represent a highlight due to its versatility as ligand.<sup>2</sup> The coordination chemistry of the deprotonated forms of H<sub>4</sub>bta with up to eight potential oxygen donors and which can act adopt different coordination modes, has been widely studied. Several complexes with deprotonated forms of H<sub>4</sub>bta and transition metal ions [Co(II), Ni(II), Cu(II), Zn(II) and Ag(I)] forming networks of different dimensionality and specific properties have been reported.<sup>3</sup> The design and

exploration of new synthetic routes to prepare this kind of metal-organic coordination networks are important current goals in the field of crystal engineering.

**Table 1** Crystal data and details of structure determination of **1–3**

| Compound                                                 | <b>1</b>                                                        | <b>2</b>                                                           | <b>3</b>                                                           |
|----------------------------------------------------------|-----------------------------------------------------------------|--------------------------------------------------------------------|--------------------------------------------------------------------|
| Formula                                                  | C <sub>10</sub> H <sub>26</sub> Na <sub>4</sub> O <sub>20</sub> | C <sub>20</sub> H <sub>28</sub> Na <sub>2</sub> O <sub>26</sub> Mn | C <sub>20</sub> H <sub>28</sub> Na <sub>2</sub> O <sub>26</sub> Ni |
| <i>M</i>                                                 | 558.27                                                          | 785.34                                                             | 789.11                                                             |
| Crystal system                                           | Orthorhombic                                                    | Monoclinic                                                         | Monoclinic                                                         |
| Space group                                              | <i>Pc2<sub>1</sub>b</i>                                         | <i>C2/m</i>                                                        | <i>C2/m</i>                                                        |
| <i>a</i> /Å                                              | 6.9997(4)                                                       | 7.3778(4)                                                          | 7.2862 (4)                                                         |
| <i>b</i> /Å                                              | 16.4260(9)                                                      | 20.1493(6)                                                         | 20.1165(7)                                                         |
| <i>c</i> /Å                                              | 20.3312(2)                                                      | 10.4963(4)                                                         | 10.4032(3)                                                         |
| <i>α</i> /°                                              | —                                                               | —                                                                  | —                                                                  |
| <i>β</i> /°                                              | —                                                               | 103.466(8)                                                         | 103.366(9)                                                         |
| <i>γ</i> /°                                              | —                                                               | —                                                                  | —                                                                  |
| <i>V</i> /Å <sup>3</sup>                                 | 2337.6(3)                                                       | 1517.46(11)                                                        | 1483.52(11)                                                        |
| <i>Z</i>                                                 | 4                                                               | 2                                                                  | 2                                                                  |
| <i>T</i> /K                                              | 293(2)                                                          | 293(2)                                                             | 293(2)                                                             |
| <i>ρ</i> <sub>calc</sub> /Mg m <sup>-3</sup>             | 1.586                                                           | 1.719                                                              | 1.767                                                              |
| <i>λ</i> (Mo Kα)/Å                                       | 0.71073                                                         | 0.71073                                                            | 0.71073                                                            |
| <i>μ</i> (Mo Kα)/mm <sup>-1</sup>                        | 0.213                                                           | 0.573                                                              | 0.795                                                              |
| <i>R</i> <sub>1</sub> , <i>I</i> > 2σ( <i>I</i> ) (all)  | 0.0589(0.0949)                                                  | 0.0230(0.0253)                                                     | 0.0376(0.0486)                                                     |
| <i>wR</i> <sub>2</sub> , <i>I</i> > 2σ( <i>I</i> ) (all) | 0.1404(0.1582)                                                  | 0.0629(0.0642)                                                     | 0.0812(0.0851)                                                     |
| Measured reflections                                     | 10328                                                           | 3703                                                               | 5114                                                               |
| Independent reflections ( <i>R</i> <sub>int</sub> )      | 4324(0.033)                                                     | 1115(0.015)                                                        | 1728(0.0247)                                                       |

<sup>a</sup>Laboratorio de Rayos X y Materiales Moleculares, Dpto. de Física Fundamental II, Facultad de Física, Universidad de La Laguna, Avda. Astrofísico Francisco Sánchez s/n, E-38204 La Laguna, Tenerife, Spain. E-mail: caruiz@ull.es; Fax: (+34) 922 318320; Tel: (+34) 922318236

<sup>b</sup>Departament de Química Inorgànica/Institut de Ciència Molecular, Facultat de Química de la Universitat de València, Avda. Dr. Moliner 50, 46100-Burjassot, València, Spain



One-dimensional (1-D) coordination polymers are quite common, especially with carboxylate ligands acting as bridges. In this way, the H<sub>4</sub>bta ligand can easily bridge two metal ions to create chains using carboxylate groups in 1,4 positions. Two carboxylate groups are uncoordinated in this conformation mode, but they are usually involved in hydrogen bonding. Alternatively, all four carboxylate groups may participate to form layers or 3-D networks, depending on the coordination mode of tetracarboxylate group.<sup>4</sup>

The work described in this contribution focuses on the preparation and structural characterization of three new compounds of formula [Na<sub>4</sub>(bta)(H<sub>2</sub>O)<sub>12</sub>] (**1**) and [Na<sub>2</sub>M(H<sub>2</sub>bta)<sub>2</sub>(H<sub>2</sub>O)<sub>8</sub>]<sub>2</sub>·2H<sub>2</sub>O [M = Mn(II) (**2**) and Ni(II) (**3**)] aiming at investigating the structure of the Na<sup>+</sup>-bta<sup>4-</sup> complex and the influence which is exerted on this structure by the presence of first-row transition metal ions.

## Experimental

### Materials and methods

The synthetic methods used to obtain X-ray quality crystals of compounds **1–3** are described hereafter. Reagents and solvents used in the syntheses were purchased from commercial sources and used without further purification. Elemental analyses (C, H, N) were performed with an EA 1108 CHNS/O automatic analyzer.

**Synthesis of [Na<sub>4</sub>(bta)(H<sub>2</sub>O)<sub>12</sub>] (**1**).** Aqueous solutions of pyridine (0.079 g, 1 mmol) and H<sub>4</sub>bta (0.25 g, 1 mmol) (10 and 100 cm<sup>3</sup>, respectively) were mixed at room temperature and kept under continuous stirring for *ca.* 2 h. Then, a solution (10 cm<sup>3</sup>) of NaOH (0.16 g, 4 mmol) was added dropwise and the resulting mixture was left to evaporate at room

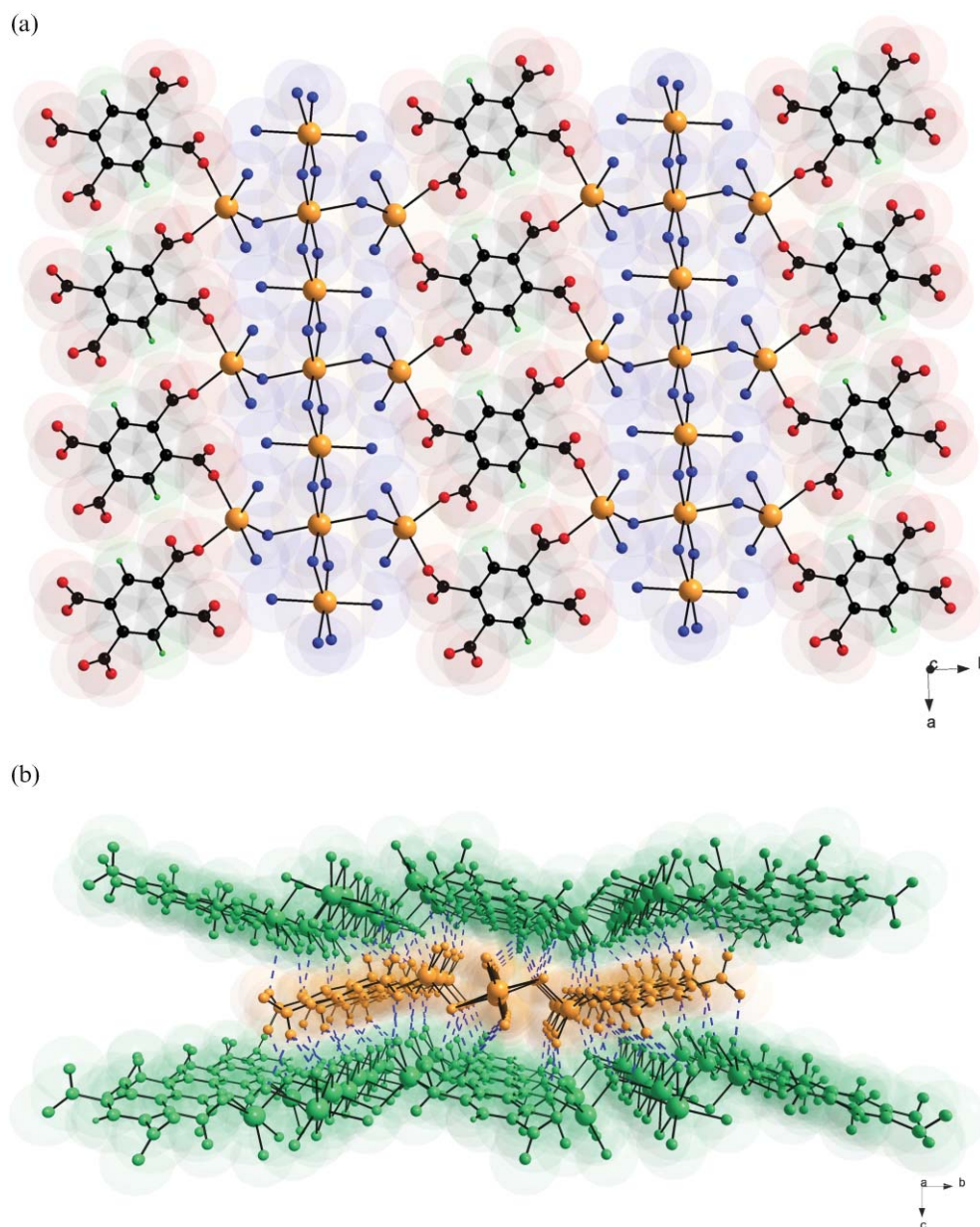


**Fig. 1** (a) Perspective view of a fragment of a layer of **1** growing in the *ab* plane. (b) A projection down the *a*-axis of three adjacent layers of **1** showing the interlayer hydrogen bonds (broken lines).

temperature. The colourless hexagonal crystals which appeared after a few weeks were removed by filtration, washed with water and air dried. Anal. Calcd. for  $C_{20}H_{28}O_{26}Na_4$  (**1**): C, 30.94; H, 3.64%. Found: C, 30.78; H, 3.40%.

**Synthesis of  $[Na_2Mn(H_2bta)_2(H_2O)_8] \cdot 2H_2O$  (**2**).** Single crystals of **2** were grown by slow diffusion using the gel technique. An aqueous solution of NaOH was added dropwise to another aqueous solution (5 cm<sup>3</sup>) of  $H_4bta$  (0.127 g, 0.5 mmol) until pH = 4.5. Then, 0.25 cm<sup>3</sup> of tetramethoxysilane (TMS) was added to the previous solution under vigorous stirring. The gel was formed after standing one day at room temperature. An aqueous solution (3 cm<sup>3</sup>) of  $MnCl_2 \cdot 4H_2O$  (0.098 g, 0.5 mmol) was carefully added over the gel. Needles of colourless crystals of **2** were obtained at room temperature after several weeks. They were mechanically separated, washed with water-methanol and air dried. Anal. Calc. for  $C_{20}H_{28}O_{26}Na_2Mn$  (**2**): C, 30.59; H, 3.59%. Found: C, 30.70; H, 3.40%.

**Synthesis of  $[Na_2Ni(C_{10}H_4O_8)_2(H_2O)_8] \cdot 2H_2O$  (**3**).** This compound is obtained by a similar procedure to that used for **2** but replacing  $MnCl_2 \cdot 4H_2O$  with  $Ni(NO_3)_2 \cdot 6H_2O$ . Light-green crystals of **3** were obtained after a few weeks at room temperature. They were mechanically separated, washed with a 1 : 1 (v/v)  $H_2O$ :MeOH solution and air dried. Anal. Calcd. for  $C_{20}H_{28}O_{26}Na_2Ni$ : C, 30.44; H, 3.52%. Found: C, 30.51; H, 3.48%.

### Crystal structure determination and refinement

Single crystals of five compounds were mounted on a Bruker-Nonius KappaCCD diffractometer. Orientation matrix and lattice parameters were obtained by least-squares refinement of the reflections obtained by a  $\theta$ - $\chi$  scan (Dirax/lsq method). Diffraction data for all compounds were collected at 293(2) K using graphite-monochromated Mo  $K\alpha$  radiation ( $\lambda = 0.71073$  Å). Data collection and data reduction were done with the COLLECT and EVALCCD programs.<sup>5,6</sup> Empirical absorption corrections were carried out using SADABS for all compounds.<sup>7</sup> All calculations for data reduction, structure solution, and refinement were done by standard procedures (WINGX).<sup>8</sup> The structure was solved by direct methods and refined with full-matrix least-squares technique on  $F^2$  using the SHELXS-97 and SHELXL-97 programs.<sup>9</sup> The hydrogen atoms for compound **1** were positioned geometrically and included in the structure-factor calculation, except those of the water molecules. The hydrogen atoms for the compounds **2** and **3** were located from difference Fourier maps and refined with isotropic temperature factors. For all compounds hydrogen atoms were refined with isotropic temperature factors. A summary of the crystallographic data and structure refinement is given in Table 1. The final geometrical calculations and the graphical manipulations were carried out with PARST97<sup>10</sup> and DIAMOND<sup>11</sup> programs, respectively. Crystallographic data (excluding structure factors) for the structures **1–3** have been deposited in the Cambridge Crystallographic Data Centre with CCDC reference numbers 290913–290915. For crystallographic data in CIF or other electronic format see DOI: 10.1039/b516806f

## Results and discussion

### Description of the structures. $[Na_4(bta)(H_2O)_{12}]$ (**1**)

The structure of **1** is made up of layers of sodium(I) cations which are bridged by single and double water molecules and tetrakismonodentate  $bta^{4-}$  anions (Fig. 1a). The layers which grow in the  $ab$  crystallographic plane, are interconnected through extensive hydrogen bonds involving all the carboxylate-oxygens and water molecules (Table 2) to afford a 3-D network (Fig. 1b).

Four crystallographically independent sodium ions [Na(1), Na(2), Na(3) and Na(4)] occur in **1** (Fig. 2a). Two of them [Na(1) and Na(2)] are six-coordinated with six water molecules building a somewhat distorted octahedral environment. The other two sodium atoms [Na(3) and Na(4)] are five-coordinated, three water molecules and two carboxylate-oxygen atoms building a highly distorted square-pyramidal environment (Fig. 2b). Four water molecules [O(7w), O(8w), O(11w) and O(12w) at Na(1) and O(7w), O(8w)<sup>iv</sup>, O(11w)<sup>iv</sup> and O(12w) at Na(2)] in the equatorial plane and other two in the axial positions [O(9w) and O(10w) at Na(1) and O(1w) and O(2w) at Na(2)] form the octahedral surroundings with  $\phi = 95.53^\circ$  [Na(1)] and  $96.11^\circ$  [Na(2)] and  $s/h = 1.217$  [Na(1)] and  $1.216$  [Na(2)] (to be compared to  $90^\circ$  and  $1.22$  for a perfect octahedron).<sup>12</sup> The sodium to water bond distances vary in the ranges  $2.310(4)$ – $2.486(6)$  Å [at Na(1)] and  $2.338(4)$ – $2.495(4)$  Å [at Na(2)] (see Table 3). The axial water molecules at Na(1) act as bridges linking Na(1) with Na(3) and Na(4). Two water molecules and two carboxylate-oxygens in the basal plane [O(5w), O(6w), O(2) and O(4) at Na(3) and O(3w), O(4w), O(8) and O(5) at Na(4)] and another water molecule in the apical position [O(9w) at Na(3) and O(10w) at Na(4)] form the square pyramidal surroundings with values of the distortion parameter  $\tau$  of 0.48 [at Na(3)] and 0.39 [at Na(4)] (square-pyramidal and trigonal-bipyramidal surroundings correspond to  $\tau = 0$  and  $\tau = 1$ , respectively).<sup>13</sup> The Na–Ow bond lengths around Na(3) and Na(4) [values varying in the ranges  $2.351(4)$ – $2.399(4)$  Å (Na(3)) and  $2.319(5)$ – $2.382(4)$  Å (Na(4))]

**Table 2** Intermolecular O...O distances (Å) in **1**<sup>a</sup>

|                               |          |
|-------------------------------|----------|
| O(1)...O(12w) <sup>i</sup>    | 2.764(7) |
| O(1)...O(10w) <sup>i</sup>    | 2.858(5) |
| O(2)...O(4w) <sup>ii</sup>    | 2.728(6) |
| O(3)...O(2w) <sup>iii</sup>   | 2.726(5) |
| O(3)...O(6w) <sup>iv</sup>    | 2.804(5) |
| O(4)...O(3w) <sup>ii</sup>    | 2.737(5) |
| O(5)...O(5w) <sup>iii</sup>   | 2.725(6) |
| O(6)...O(8w) <sup>ii</sup>    | 2.715(5) |
| O(6)...O(11w) <sup>v</sup>    | 3.097(5) |
| O(6)...O(1w) <sup>ii</sup>    | 2.724(5) |
| O(7)...O(9w) <sup>ii</sup>    | 2.755(5) |
| O(7)...O(3w) <sup>iv</sup>    | 2.774(5) |
| O(7)...O(4w) <sup>vi</sup>    | 2.789(6) |
| O(8)...O(2w) <sup>iv</sup>    | 2.890(6) |
| O(8)...O(6w) <sup>i</sup>     | 2.808(5) |
| O(11w)...O(1w) <sup>vii</sup> | 3.139(6) |
| O(10w)...O(1) <sup>i</sup>    | 2.858(5) |
| O(9w)...O(1w) <sup>vii</sup>  | 2.872(5) |

<sup>a</sup> Symmetry codes: (i)  $x + 1, y + 1/2, -z + 1/2$ ; (ii)  $-x, y - 1/2, -z + 1$ ; (iii)  $x, y - 1/2, -z + 1/2$ ; (iv)  $x - 1, y, z$ ; (v)  $-x + 1, y - 1/2, -z + 1$ ; (vi)  $x - 1, y - 1, +z$ ; (vii)  $x + 1, y, z$ .

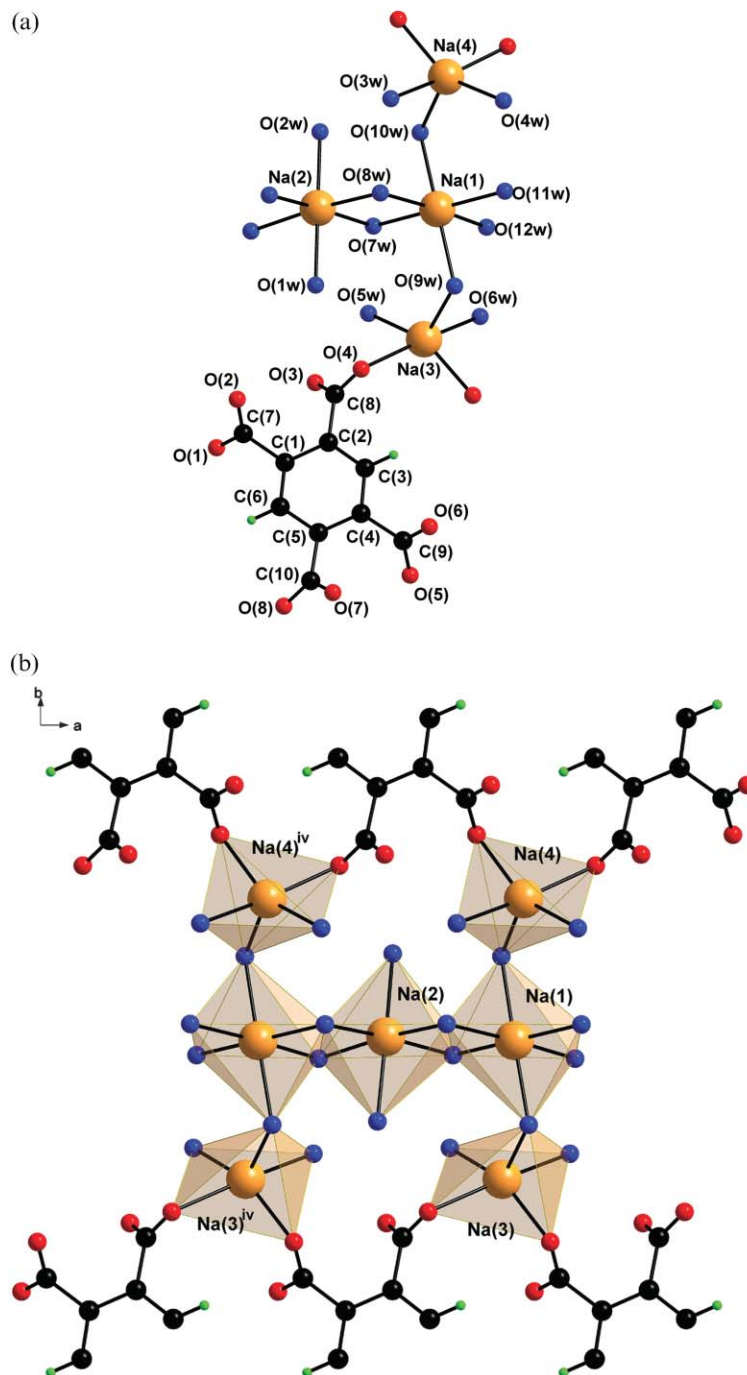


**Fig. 2** (a) Molecular structure and numbering scheme of **1**. (b) View of a fragment of the polymeric structure of **1** with the Na-cluster in the centre.

(Table 3) agree with those observed for the six-coordinated Na(1) and Na(2) atoms. The values of the Na–O(carboxylate) bond distances at Na(3) [2.298(4) and 2.450(4) Å] and Na(4) [2.310(4) and 2.386(4) Å] differ significantly.

The bta group in **1** adopts a tetrakismonodentate coordination mode being bound to four sodium atoms [through O(2), O(4), O(5) and O(8) toward Na(3)<sup>iv</sup>, Na(3), Na(4)<sup>x</sup> and Na(4)<sup>vi</sup>; (x)  $x, -1 + y, z$ ]. The average values for the coordinated and free carbonyl-oxygen are very close [1.251(6) and 1.255(5) Å]. The values of the dihedral angle between the

mean plane of the six-membered benzene ring and the planes of the carboxylate groups are 46.23(19), 55.78(25), 56.40(25), 43.18(18)°. The internal angles in the benzene ring are slightly smaller for the substituted carbon atoms [average value of 119.40(41)° to be compared to 121.19(44)° for the unsubstituted carbon atoms].

The presence of twelve coordinated water molecules (per molecular unit) in **1** leads to an extensive network of hydrogen bonds. All coordination water molecules form hydrogen bonds between themselves or with carboxylate

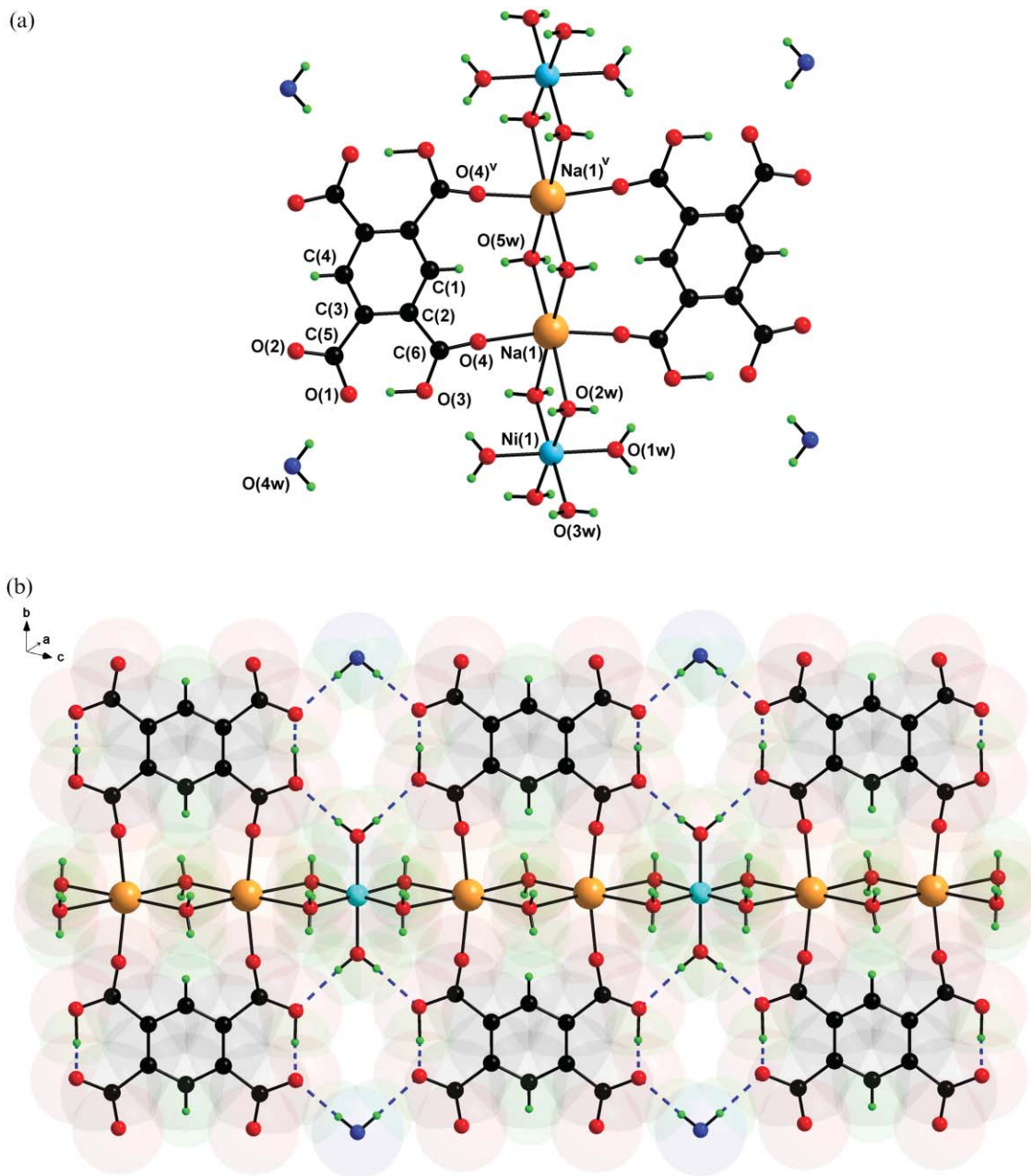


**Fig. 3** (a) Perspective view of a fragment of the structure of **3** with the atom numbering [identical atom labeling was adopted for **2** replacing Ni(1) by Mn(1)]; (b) A view of the chain arrangement growing along the [101] direction in **2** and **3** [the hydrogen bonds are noted by broken lines].

oxygen atoms. All oxygen atoms from carboxylate groups act as acceptors. The most probable hydrogen bonds are gathered in Table 2 and their influence on the packing is shown in Fig. 1b. The values of the sodium–sodium separation through the single water bridge are 3.976(4) [Na(1)⋯Na(3)] and 3.951(4) Å [Na(1)⋯Na(4)] whereas that through the double water bridge is 3.528(3) Å [Na(1)⋯Na(2)].

**[Na<sub>2</sub>M(H<sub>2</sub>bta)<sub>2</sub>(H<sub>2</sub>O)<sub>8</sub>·2H<sub>2</sub>O [M = Mn (**2**) and Ni (**3**)]**

Pyromellitate complexes of formula [Na<sub>2</sub>M(H<sub>2</sub>bta)<sub>2</sub>(H<sub>2</sub>O)<sub>8</sub>·2H<sub>2</sub>O] [M = Co(II), Zn(II)],<sup>14</sup> which have been subject of

previous works, are isostructural with **2** and **3**. The structure of compounds **2** and **3** is made up of chains with regular alternating pairs of Na<sup>+</sup> and single M<sup>2+</sup> cations [M = Mn (**2**) and Ni (**3**)], two water molecules acting as bridges between each pair of metal ions, and water molecules of crystallization. Two water molecules (at M) and two carboxylate-oxygen atoms from two H<sub>2</sub>bta<sup>2-</sup> ligands (at Na), which are coordinated to the metal ions in *trans* positions, build distorted octahedral surroundings (Fig. 3a). The H<sub>2</sub>bta group acts as a bridging ligand between two adjacent sodium ions. The bimetallic Na<sup>+</sup><sub>2</sub>M<sup>II</sup> chains grow along the [101] direction (Fig. 3b) and they are interlinked through hydrogen

**Table 3** Bond lengths (Å) and angles (°) for compound **1**<sup>a</sup>

|                                                  |             |                                    |            |
|--------------------------------------------------|-------------|------------------------------------|------------|
| Na(1)–O(8w)                                      | 2.310(4)    | Na(3)–O(2) <sup>vii</sup>          | 2.298(4)   |
| Na(1)–O(11w)                                     | 2.401(4)    | Na(3)–O(5w)                        | 2.351(4)   |
| Na(1)–O(12w)                                     | 2.402(4)    | Na(3)–O(9w)                        | 2.393(4)   |
| Na(1)–O(9w)                                      | 2.408(4)    | Na(3)–O(6w)                        | 2.399(4)   |
| Na(1)–O(10w)                                     | 2.486(6)    | Na(3)–O(4)                         | 2.450(4)   |
| Na(2)–O(12w) <sup>iv</sup>                       | 2.338(4)    | Na(4)–O(5) <sup>viii</sup>         | 2.310(4)   |
| Na(2)–O(2w)                                      | 2.355(6)    | Na(4)–O(10w)                       | 2.319(5)   |
| Na(2)–O(8w)                                      | 2.367(4)    | Na(4)–O(3w)                        | 2.358(4)   |
| Na(2)–O(7w)                                      | 2.450(5)    | Na(4)–O(4w)                        | 2.382(4)   |
| Na(2)–O(11w) <sup>iv</sup>                       | 2.495(4)    | Na(4)–O(8) <sup>ix</sup>           | 2.386(4)   |
| O(8w)–Na(1)–O(11w)                               | 102.78 (14) | O(2) <sup>iv</sup> –Na(3)–O(5w)    | 149.39(15) |
| O(8w)–Na(1)–O(12w)                               | 170.36 (15) | O(2) <sup>iv</sup> –Na(3)–O(9w)    | 92.50(14)  |
| O(8w)–Na(1)–O(9w)                                | 100.4(2)    | O(2) <sup>iv</sup> –Na(3)–O(6w)    | 88.34(14)  |
| O(8w)–Na(1)–O(10w)                               | 84.3(2)     | O(2) <sup>iv</sup> –Na(3)–O(4)     | 92.94(14)  |
| O(11w)–Na(1)–O(12w)                              | 86.72(14)   | O(5w)–Na(3)–O(9w)                  | 117.81(15) |
| O(11w)–Na(1)–O(9w)                               | 84.3(2)     | O(5w)–Na(3)–O(6w)                  | 87.70(13)  |
| O(11w)–Na(1)–O(10w)                              | 99.0(2)     | O(5w)–Na(3)–O(4)                   | 86.57(12)  |
| O(12w)–Na(1)–O(9w)                               | 82.0(2)     | O(9w)–Na(3)–O(6w)                  | 89.65(15)  |
| O(12w)–Na(1)–O(10w)                              | 92.8(2)     | O(9w)–Na(3)–O(4)                   | 99.38(14)  |
| O(9w)–Na(1)–O(10w)                               | 173.8(2)    | O(6w)–Na(3)–O(4)                   | 170.81(14) |
| O(12w) <sup>iv</sup> –Na(2)–O(2w)                | 99.8(2)     | O(5) <sup>viii</sup> –Na(4)–O(10w) | 97.8(2)    |
| O(12w) <sup>iv</sup> –Na(2)–O(8w)                | 169.4(2)    | O(5) <sup>viii</sup> –Na(4)–O(3w)  | 88.86(14)  |
| O(12w) <sup>iv</sup> –Na(2)–O(7w)                | 100.14(15)  | O(5) <sup>viii</sup> –Na(4)–O(4w)  | 147.3(2)   |
| O(12w) <sup>iv</sup> –Na(2)–O(11w) <sup>iv</sup> | 85.98(14)   | O(5) <sup>viii</sup> –Na(4)–O(8)d  | 91.64(13)  |
| O(2w)–Na(2)–O(8w)                                | 88.4(2)     | O(10w)–Na(4)–O(3w)                 | 89.88(15)  |
| O(2w)–Na(2)–O(7w)                                | 89.0(3)     | O(10w)–Na(4)–O(4w)                 | 114.90(15) |
| O(2w)–Na(2)–O(11w) <sup>iv</sup>                 | 96.0(2)     | O(10w)–Na(4)–O(8) <sup>ix</sup>    | 100.77(14) |
| O(8w)–Na(2)–O(7w)                                | 86.9(15)    | O(3w)–Na(4)–O(4w)                  | 88.97(15)  |
| O(8w)–Na(2)–O(11w) <sup>iv</sup>                 | 86.30(13)   | O(3w)–Na(4)–O(8) <sup>ix</sup>     | 169.16(15) |
| O(7w)–Na(2)–O(11w) <sup>iv</sup>                 | 171.5(2)    | O(4w)–Na(4)–O(8) <sup>ix</sup>     | 84.76(13)  |

<sup>a</sup> Symmetry codes: (iv)  $-1 + x, y, z$ ; (vii)  $1 + x, y, z$ ; (viii)  $x, 1 + y, z$ ; (ix)  $1 + x, 1 + y, z$ .

bonds, involving coordinated [O(2w), O(3w), O(5w)] and uncoordinated [O(4w)] water molecules and carboxylate oxygen atoms [O(1) and O(2)] [Fig. 4 (**2** and **3**) and Tables 4 (**2**) and 7 (**3**)].

The sodium atoms of **2** and **3** lie on a *m* site, and they are coordinated to four water molecules in the equatorial plane [O(2w), O(5w), O(3w) and O(5w)<sup>v</sup>] and to two

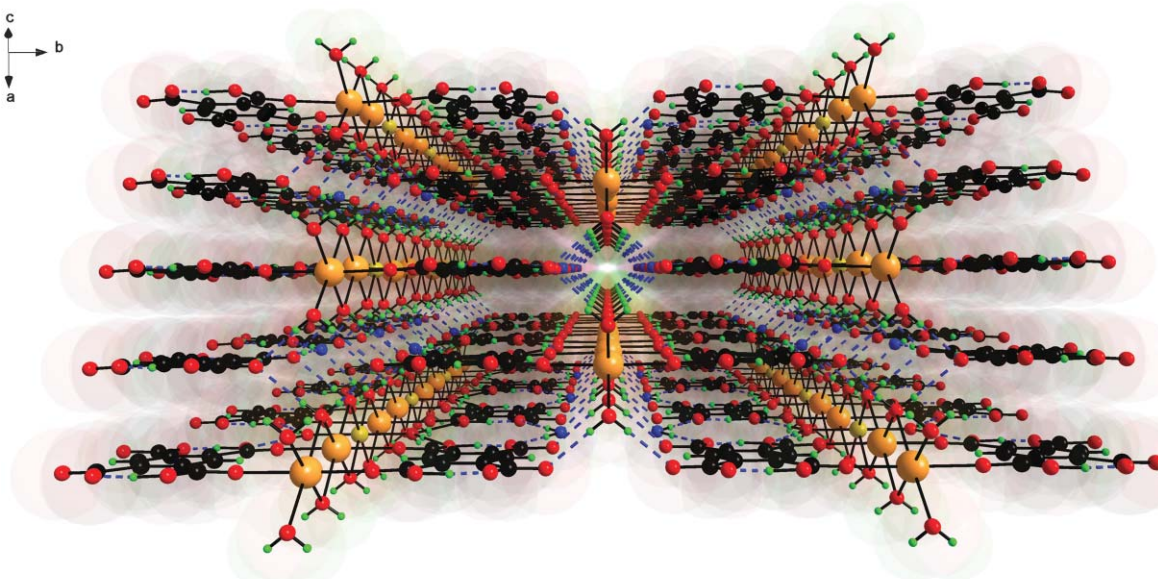


**Fig. 4** A projection of the structure of **2** and **3** down the [101] direction showing the resulting 3-D structure through hydrogen bonds. The hydrogen bonds are noted by blue broken lines.

**Table 4** Hydrogen bonds in **2**<sup>a</sup>

| D–H...A                          | <i>d</i> (D...A)/Å | <i>d</i> (H...A)/Å | ∠(D–H...A)/° |
|----------------------------------|--------------------|--------------------|--------------|
| O(1w)–H(6)···O(3) <sup>iii</sup> | 2.746(2)           | 1.91(2)            | 179(2)       |
| O(2w)–H(5)···O(2) <sup>ii</sup>  | 2.747(2)           | 1.96(2)            | 171(2)       |
| O(3w)–H(7)···O(4w) <sup>ii</sup> | 2.727(2)           | 1.92(2)            | 170(2)       |
| O(3w)–H(7)···O(4w) <sup>iv</sup> | 2.727(2)           | 1.92(2)            | 170(2)       |
| O(4w)–H(8)···O(1)                | 2.770(2)           | 1.92(2)            | 179(2)       |
| O(5w)–H(4)···O(2) <sup>i</sup>   | 2.847(2)           | 2.06(3)            | 168(2)       |
| O(3)–H(3)···O(1)                 | 2.383(2)           | 1.29(3)            | 176(3)       |

<sup>a</sup> Symmetry codes: (i)  $x + 1/2, y - 1/2, z$ ; (ii)  $x - 1/2, y - 1/2, z$ ; (iii)  $-x + 1, -y + 1, -z$ ; (iv)  $-x + 1/2, y - 1/2, -z$ .

**Table 5** Selected bond lengths (Å) and angles (°) for compound **2**<sup>a</sup>

|                                                  |            |                                                   |            |
|--------------------------------------------------|------------|---------------------------------------------------|------------|
| Mn(1)–O(1w)                                      | 2.119(2)   | Na(1)–O(3w) <sup>iii</sup>                        | 2.505(2)   |
| Mn(1)–O(2w)                                      | 2.205(2)   | Na(1)–O(4)                                        | 2.2736(12) |
| Mn(1)–O(3w)                                      | 2.2064(15) | Na(1)–O(5w)                                       | 2.542(2)   |
| Na(1)–O(2w)                                      | 2.591(2)   | Na(1)–O(5w) <sup>viii</sup>                       | 2.444(2)   |
| O(2w)–Mn(1)–O(3w)                                | 95.28(7)   | O(4)–Na(1)–O(3w) <sup>iii</sup>                   | 84.15(4)   |
| O(2w)–Mn(1)–O(3w) <sup>iii</sup>                 | 84.72(7)   | O(4)–Na(1)–O(5w)                                  | 93.75(4)   |
| O(2w) <sup>iii</sup> –Mn(1)–O(3w)                | 84.72(7)   | O(4)–Na(1)–O(5w) <sup>viii</sup>                  | 95.84(4)   |
| O(2w) <sup>iii</sup> –Mn(1)–O(3w) <sup>iii</sup> | 95.28(7)   | O(5w)–Na(1)–O(2w)                                 | 176.04(6)  |
| O(3w) <sup>iii</sup> –Na(1)–O(2w)                | 71.34(6)   | O(5w) <sup>viii</sup> –Na(1)–O(2w)                | 108.48(7)  |
| O(3w) <sup>iii</sup> –Na(1)–O(5w)                | 104.70(6)  | O(5w) <sup>viii</sup> –Na(1)–O(3w) <sup>iii</sup> | 179.82(7)  |
| O(4)–Na(1)–O(4) <sup>ix</sup>                    | 167.40(7)  | O(5w) <sup>viii</sup> –Na(1)–O(5w)                | 75.48(7)   |
| O(4)–Na(1)–O(2w)                                 | 85.91(4)   |                                                   |            |

<sup>a</sup> Symmetry codes: (iii)  $-x + 1, -y + 1, -z$ ; (viii)  $-x + 2, -y + 1, -z + 1$ ; (ix)  $x, -y + 1, z$ .

carboxylate-oxygen atoms in the axial sites [O(4) and O(4)<sup>vi</sup>] the symmetry operation used is a translation with the form (v)  $2 - x, y, 1 - z$ ; (vi)  $x, 1 - y, -z$ ]. The Na–Ow bonds vary in the ranges 2.444(2)–2.591(2) (**2**) and 2.451(3)–2.568(3) Å (**3**) whereas the Na–O<sub>carboxylate</sub> are 2.2736(12) (**2**) and 2.2633(14) Å (**3**), the resulting coordination polyhedron corresponding to a compressed octahedron [see Tables 5 (**2**) and 6 (**3**)]. The values of the  $\phi$  and *s/h* parameters<sup>12</sup> for the sodium atom are 90.60° and 1.1638 (**2**) and 88.63° and 1.1604 (**3**).

**Table 6** Selected bond lengths (Å) and angles (°) for compound **3**<sup>a</sup>

|                                                  |           |                                                   |            |
|--------------------------------------------------|-----------|---------------------------------------------------|------------|
| Ni(1)–O(1w)                                      | 2.019(2)  | Na(1)–O(3w) <sup>iii</sup>                        | 2.503(2)   |
| Ni(1)–O(2w)                                      | 2.074(4)  | Na(1)–O(4)                                        | 2.2633(14) |
| Ni(1)–O(3w)                                      | 2.072(2)  | Na(1)–O(5w)                                       | 2.568(3)   |
| Na(1)–O(2w)                                      | 2.579(2)  | Na(1)–O(5w) <sup>viii</sup>                       | 2.451(3)   |
| O(2w)–Ni(1)–O(3w)                                | 94.16(7)  | O(4)–Na(1)–O(3w) <sup>iii</sup>                   | 84.04(4)   |
| O(2w)–Ni(1)–O(3w) <sup>iii</sup>                 | 85.84(7)  | O(4)–Na(1)–O(5w) <sup>viii</sup>                  | 95.92(4)   |
| O(2w) <sup>iii</sup> –Ni(1)–O(3w)                | 85.84(7)  | O(4)–Na(1)–O(5w)                                  | 92.59(4)   |
| O(2w) <sup>iii</sup> –Ni(1)–O(3w) <sup>iii</sup> | 94.16(7)  | O(5w)–Na(1)–O(2w)                                 | 174.25(7)  |
| O(3w) <sup>iii</sup> –Na(1)–O(2w)                | 67.46(6)  | O(5w) <sup>viii</sup> –Na(1)–O(2w)                | 110.64(8)  |
| O(3w) <sup>iii</sup> –Na(1)–O(5w)                | 106.79(7) | O(5w) <sup>viii</sup> –Na(1)–O(3w) <sup>iii</sup> | 178.10(8)  |
| O(4)–Na(1)–O(4) <sup>ix</sup>                    | 167.94(9) | O(5w) <sup>viii</sup> –Na(1)–O(5w)                | 75.11(8)   |
| O(4)–Na(1)–O(2w)                                 | 86.88(4)  |                                                   |            |

<sup>a</sup> Symmetry codes: (iii)  $-viii + 1, -y + 1, -z$ ; (viii)  $-viii + 2, -y + 1, -z + 1$ ; (ix)  $viii, -y + 1, z$ .

Six water molecules [O(1w), O(2w), O(3w), O(1w)<sup>vii</sup>, O(2w)<sup>vii</sup> and O(3w)<sup>vii</sup>], the symmetry operation used is a translation with the form (vii)  $1 - x, y, -z$  are bound to the M atom [M = Mn (**2**) and Ni (**3**)] in a somewhat distorted octahedral surrounding. The metal centers lie on a two-fold rotation axis with centre of symmetry. The apical positions are occupied by the O(1w) and O(1w)<sup>vii</sup> atoms whereas the four remaining water molecules build the equatorial plane. The average value of the Mn–Ow bond lengths [2.177(1) Å] is somewhat longer than that of the Ni–Ow [2.055(1) Å] as expected due to the decrease of the ionic radius when going from Mn(II) to Ni(II). The values of the  $\phi$  and  $s/h$  parameters are 98.39° and 1.2015 (M = Mn) and 98.57° and 1.2088 (M = Ni). M(1) is linked to Na(1) through a double water bridge, the M(1)⋯Na(1) separation being 3.6991(9) (**2**) and 3.630(1) Å (**3**).

The benzenetetracarboxylate group acts as bimonodentate ligand toward two different sodium atoms [through O(4) toward Na(1) and through O(4)<sup>v</sup> toward Na(1)<sup>v</sup>] in **2** and **3**, the Na(1)⋯Na(1)<sup>v</sup> separation being 3.943(1) (**2**) and 3.979(1) Å (**3**). The whole H<sub>2</sub>bta ligand is generated by a symmetry operation, C(1) and C(4) lying on a two-fold axis. The average values for the C–O bond of the coordinated carbonyl groups are 1.246(2) and 1.246(2) Å in **2** and **3**, respectively. The dihedral angles between the mean plane of the benzene ring and the planes of each carboxylate group are 3.53(12) and 2.74(12)° (**2**) and 2.51(14) and 1.31(13)° (**3**), values which agree with those reported for the corresponding Co(II) and Zn(II) derivatives.<sup>14</sup> However, they are different from those observed in **1** because of the different coordination mode of the tetracarboxylate ligand involved. The values of the internal angles in the benzene ring in both compounds are slightly smaller for the substituted carbon atoms, with average values of 117.46(12) (**2**) and 117.79(14)° (**3**), while for the unsubstituted C atoms the average values are 125.07(12) and 124.41(14)°.

The extensive hydrogen bonding system in **2** and **3** is due to the presence of two water molecules of crystallization and eight aqua ligands (per formula unit). All water molecules and carboxylate oxygen atoms are involved in the hydrogen bonding (see Tables 4 and 7 and Fig. 4). The values of the O⋯O distance vary in the ranges 2.383(2)–2.841(2) Å for **2** and 2.380(2)–2.851(2) Å for **3**. A short intramolecular hydrogen bond also exists between the oxygen atoms of two different

**Table 7** Hydrogen bonds in **3**<sup>a</sup>

| D–H⋯A                          | $d(D\cdots A)/\text{Å}$ | $d(H\cdots A)/\text{Å}$ | $\angle(D-H\cdots A)^\circ$ |
|--------------------------------|-------------------------|-------------------------|-----------------------------|
| O(1w)–H(6)⋯O(3) <sup>iii</sup> | 2.768(2)                | 1.95(2)                 | 175.33(2)                   |
| O(2w)–H(5)⋯O(2) <sup>ii</sup>  | 2.743(2)                | 1.94(3)                 | 167.07(2)                   |
| O(3w)–H(7)⋯O(4w) <sup>ii</sup> | 2.721(2)                | 1.91(2)                 | 170.52(2)                   |
| O(3w)–H(7)⋯O(4w) <sup>iv</sup> | 2.721(2)                | 1.91(2)                 | 170.52(2)                   |
| O(4w)–H(8)⋯O(1)                | 2.759(2)                | 1.91(4)                 | 178.29(3)                   |
| O(5w)–H(4)⋯O(2) <sup>i</sup>   | 2.851(2)                | 2.02(3)                 | 172.23(3)                   |
| O(3)–H(3)⋯O(1)                 | 2.380(2)                | 1.26(3)                 | 166.60(3)                   |

<sup>a</sup> Symmetry codes: (i)  $x + 1/2, y - 1/2, z$ ; (ii)  $x - 1/2, y - 1/2, z$ ; (iii)  $-x + 1, -y + 1, -z$ ; (iv)  $-x + 1/2, y - 1/2, -z$ .

carboxylate groups, with O⋯O distances of 2.383(2) (**1**) and 2.380(2) Å (**2**).

## Acknowledgements

This work was supported by the Ministerio Español de Educación y Ciencia (Projects MAT2004-03112 and CTQ2004-03633), the Gobierno Autónomo de Canarias (PI2002/175) and the Generalitat Valenciana (Grupos 03/197). Predoctoral fellowships from CajaCanarias (L.C.-D.) and Ministerio de Educación y Ciencia (J.P.) are acknowledged. We also thank the Consejería de Industria y Desarrollo Tecnológico del Gobierno Autónomo de Canarias for supporting O.F.

## References

- (a) J. Christoph, *Dalton Trans.*, 2003, 2781; (b) B. Moulton and M. J. Zaworotko, *Chem. Rev.*, 2001, **101**, 1629.
- (a) H. Kumagai, C. J. Kepert and M. Kurmoo, *Inorg. Chem.*, 2002, **41**, 3410; (b) D. Cheng, M. A. Khan and R. P. Houser, *Cryst. Growth Des.*, 2002, **2**, 415.
- (a) D. L. Ward and D. C. Luehrs, *Acta Crystallogr., Sect. C*, 1983, **39**, 1370; (b) B. T. Usualiev, A. N. Shnulin and H. S. Mamadov, *Koord. Khim.*, 1982, **8**, 1535; (c) C. Robl, *Z. Anorg. Allg. Chem.*, 1987, **79**, 54; (d) L. Karanovic, D. Poletti, G. A. Bogdanovic and A. Spasojevic-de Biré, *Acta Crystallogr., Sect. C*, 1999, **55**, 911; (e) D. Poletti, D. R. Stojakovic, B. V. Preslesnik and R. M. Herak, *Acta Crystallogr., Sect. C*, 1988, **44**, 242; (f) D. Poletti and Ij. Karanovic, *Acta Crystallogr., Sect. C*, 1989, **45**, 1716; (g) J. Z. Zou, Q. Liu, Z. Xu, X. Z. You and X. Y. Huang, *Polyhedron*, 1998, **17**, 1863; (h) C. Robl and S. Hentschel, *Mater. Res. Bull.*, 1991, **26**, 1355; (i) S. M. Jessen, H. Küppers and D. C. Luehrs, *Z. Naturforsch., B*, 1998, **47**, 1863; (j) W. Ge-Cheng, J. Zhong, D. Zhin-Bang, Y. Kui-Yue and N. Jia-Zan, *Jiegou Huaxue*, 1991, **10**, 106; (k) P. Chaudhuri, K. Oder, K. Wiegardt, S. Gehring, W. Haase, B. Nuber and J. Weiss, *J. Am. Chem. Soc.*, 1998, **110**, 3657; (l) F. Jaber, F. Charbonnier and R. Faure, *J. Chem. Crystallogr.*, 1997, **27**, 397; (m) C. Robl, *Mater. Res. Bull.*, 1992, **27**, 99; (n) W. Chem, N. Heng Tioh, J.-Z. Zou, Z. Xu and X.-Z. You, *Acta Crystallogr., Sect. C*, 1996, **52**, 46; (o) D. Rochon and G. Massarweh, *Inorg. Chim. Acta*, 2000, **304**, 190.
- (a) J. Kim, B. Chen, T. M. Reineke, H. Li, M. Eddaoudi, D. B. Moler, M. O'Keeffe and O. M. Yaghi, *J. Am. Chem. Soc.*, 2001, **123**, 8239; (b) X. Shi, G. Zhu, Q. Fang, G. Wu, G. Tian, F. Wang, D. Zhang, M. Xue and S. Qiu, *Eur. J. Inorg. Chem.*, 2004, 185.
- R. W. W. Hooft, *COLLECT*. Nonius BV, Delft, The Netherlands, 1999.
- A. J. M. Duisenberg, L. M. J. Kroon-Batenburg and A. M. M. Schreurs, *J. Appl. Crystallogr.*, 2003, **36**, 220 (EVALCCD).
- SADABS, version 2.03. Bruker AXS Inc.: Madison, WI, 2000.
- L. J. Farrugia, *J. Appl. Crystallogr.*, 1999, **32**, 837.

- 9 G. M. Sheldrick, SHELXS-97 & SHELXL-97, Programs for Crystal Structure Analysis (Release 97-2), Institut für Anorganische Chemie der Universität, Tammanstrasse 4, D-3400 Göttingen, Germany, 1998.
- 10 M. Nardelli, *J. Appl. Crystallogr.*, 1995, **28**, 659.
- 11 DIAMOND 2.1d, 2000] DIAMOND 2.1d, Crystal Impact GbR, CRYSTAL IMPACT, K. Brandenburg & H. Putz GbR, Postfach 1251, D-53002 Bonn, Germany, 2000.
- 12 E. I. Stiefel and G. F. Brown, *Inorg. Chem.*, 1972, **11**, 189.
- 13 A. W. Addison, T. N. Rao, J. Reedijk, J. van Rijn and G. C. Verschoor, *J. Chem. Soc., Dalton Trans.*, 1984, 1349.
- 14 (a) L. Karanovic, D. Poleti, G. A. Bogdanovic and A. Spasojevic-de Bire, *Acta Crystallogr., Sect. C*, 1999, **55**, 911; (b) Ch.-D. Wu, D.-M. Wu, C.-Z. Lu and J.-S. Huang, *Acta Crystallogr., Sect. E*, 2001, **57**, m253.

# Chemical Biology

An exciting news supplement providing a snapshot of the latest developments in chemical biology



Free online and in print issues of selected RSC journals!\*

**Research Highlights** – newsworthy articles and significant scientific advances

**Essential Elements** – latest developments from RSC publications

**Free links** to the full research paper from every online article during month of publication

\*A separately issued print subscription is also available

3011053

RSC Publishing

[www.rsc.org/chemicalbiology](http://www.rsc.org/chemicalbiology)

# Metamagnetism in hydrophobically induced carboxylate (phenylmalonate)-bridged copper(II) layers

Jorge Pasán,<sup>a</sup> Joaquín Sanchiz,<sup>b</sup> Catalina Ruiz-Pérez,<sup>\*a</sup> Javier Campo,<sup>c</sup> Francesc Lloret<sup>d</sup> and Miguel Julve<sup>d</sup>

Received (in Cambridge, UK) 14th February 2006, Accepted 22nd May 2006

First published as an Advance Article on the web 14th June 2006

DOI: 10.1039/b602144a

Self-assembly of copper(II) ions, phenylmalonate and pyrimidine yields the layered compound [Cu(pym)(Phmal)]<sub>n</sub> (**1**) where intralayer ferro- and interlayer antiferromagnetic interactions occur with three-dimensional antiferromagnetic ordering at  $T_c = 2.15$  K.

The construction of multidimensional magnetic materials with magnetic ordering is one of the major challenges in magnetochemistry.<sup>1</sup> For such a purpose, the construction of three-dimensional (3D) systems is a good approach, but a deep study of the nature and intensity of the coupling among the paramagnetic centres in these systems is precluded due to the lack of theoretical models to analyze the magnetic ordered state. On the other hand, interesting studies have been performed on 2D systems with different intra- and interlayer magnetic interactions.<sup>2,3</sup> Previous studies by Kahn and co-workers in designing molecule-based magnets have shown that organizing ferromagnetic arrangements in extended 2D or 3D systems is quite a difficult task.<sup>1</sup> The choice of a specifically tailored building block is crucial in the design of systems with tunable dimensionality displaying ferromagnetic coupling.

The malonate-bridged copper(II) complexes show a wide variety of molecular architectures which exhibit ferromagnetic coupling in most cases.<sup>4–8</sup> In previous studies with these compounds, we have observed that the insertion of additional groups in the malonate skeleton (for instance, a phenyl group) modifies the supramolecular interactions and the dimensionality of the coordination polymer, but the ferromagnetic nature of the magnetic coupling is kept as in the compound [Cu(H<sub>2</sub>O)<sub>3</sub>][Cu(Phmal)<sub>2</sub>] (H<sub>2</sub>Phmal = phenylmalonic acid).<sup>9</sup> The use of potentially bridging nitrogen donor heterocycles as coligands has proved to be very appealing because of the construction of supramolecular motifs with varied functions.<sup>10–13</sup> In the present work, we focus on the structure and variable-temperature magnetic study of the layered compound [Cu(pym)(Phmal)]<sub>n</sub> (**1**) (pym = pyrimidine) together with a brief analysis of the supramolecular effects that determine its two-dimensional structure. The compound has a metamagnetic behaviour due to the coexistence of intralayer ferromagnetic and

interlayer antiferromagnetic interactions, the critical magnetic field being  $H_c = 130$  G.

The structure of **1** consists of a sheet-like arrangement of (pym)copper(II) units bridged by carboxylate-phenylmalonate groups growing in the *ab* plane.† Each copper atom is linked to four other symmetry-related copper atoms (Fig. 1) through equatorial–equatorial *anti-syn* carboxylate bridges [the copper–copper separation is 5.121(17) Å]. A corrugated square grid of copper atoms results, the monodentate pym ligand of adjacent metal atoms being located above and below each layer. The pym and phenyl groups of each [Cu(pym)(Phmal)] unit are in the *trans*-position. The neutral sheets are stacked along the *c* axis, the shortest interlayer copper–copper separation being 13.45(4) Å (Fig. 2). Weak interactions between hydrophobic groups of adjacent layers in **1** are the origin of its 2D structure.

Each copper atom exhibits a square-pyramidal environment ( $\tau$  value<sup>14</sup> being 0.02) with four carboxylate-phenylmalonate oxygen atoms [O(1), O(2), O(3) and O(4)] from three different Phmal ligands building the basal plane [mean value for the Cu–O bond distance is 1.960(6) Å] while a nitrogen atom from the pym ligand [N(1)] occupies the axial position [Cu(1)–N(1) = 2.252(3) Å]. The copper atom is shifted by 0.2049(10) Å from the mean basal plane towards the apical position.

The square grid of copper(II) ions occurring in **1** is analogous to those observed for the malonate complexes of cobalt(II) and zinc(II) ions in the presence of N-donor heterocycles as coligands.<sup>15</sup>

The temperature dependence of the  $\chi_M T$  product [ $\chi_M$  being the magnetic susceptibility per copper(II) ion] in the temperature range 1.8–300 K is shown in Fig. 3.‡  $\chi_M T$  at room temperature is 0.42 cm<sup>3</sup> mol<sup>−1</sup> K, a value which is as expected for a magnetically isolated spin doublet. Upon cooling,  $\chi_M T$  continuously increases to reach a value of 25.9 cm<sup>3</sup> mol<sup>−1</sup> K at 2.15 K, and further decreases to 17.5 cm<sup>3</sup> mol<sup>−1</sup> K at 1.8 K. A susceptibility maximum

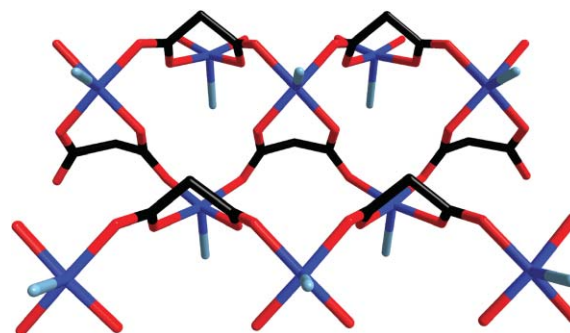


Fig. 1 Central projection of the formation of the square grid of copper(II) ions through the carboxylate-phenylmalonate linkage.

<sup>a</sup>Laboratorio de Rayos X y Materiales Moleculares, Dpto. de Física Fundamental II, Universidad de La Laguna, Avda. Astrofísico Francisco Sánchez s/n, La Laguna, Spain. E-mail: caruiz@ull.es; Fax: +34 922 31 83 20; Tel: +34 922 31 83 00

<sup>b</sup>Laboratorio de Rayos X y Materiales Moleculares, Dpto. de Química Inorgánica, Universidad de La Laguna, La Laguna, Spain

<sup>c</sup>Instituto de Ciencia de Materiales de Aragón, CSIC-Universidad de Zaragoza, 50009 Zaragoza, Spain

<sup>d</sup>Departament de Química Inorgànica/Instituto de Ciencia Molecular, Facultat de Química, Universitat de València, Av. Dr. Moliner 50, 46100 Burjassot (València), Spain



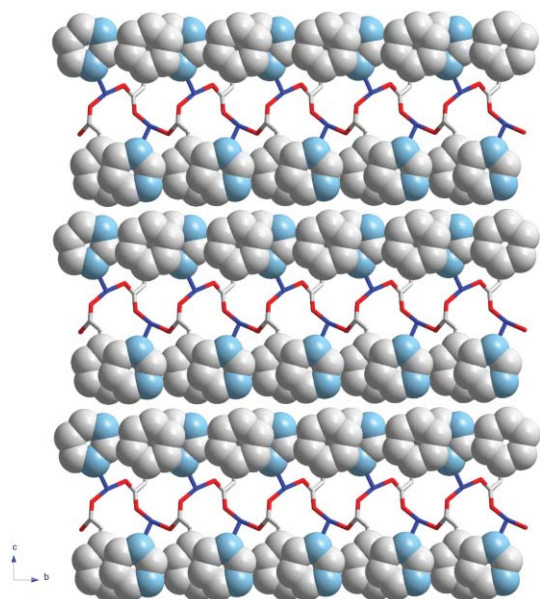


Fig. 2 Projection of the crystal packing of **1** through the *a* axis.

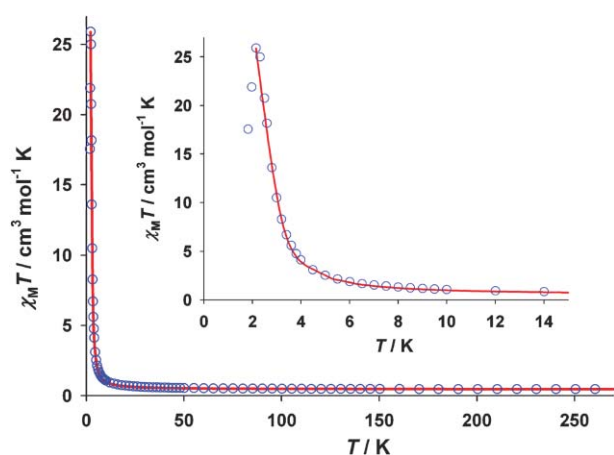


Fig. 3  $\chi_M T$  vs.  $T$  plot for **1** under applied magnetic fields of 1 T ( $T \geq 12$  K) and 100 G ( $T < 12$  K): (○) experimental data; (—) best-fit curve through eqn. (1) (see text). The inset shows a detail of the low temperature region.

is observed at 2.15 K under  $H \leq 130$  G. This maximum disappears for  $H > 130$  G (Fig. 4). These features correspond to a metamagnetic-like behaviour which is due to the coexistence of ferro- and antiferromagnetic interactions, the latter being overcome by an applied field larger than 130 G. The magnetization ( $M$ ) versus  $H$  plot at 1.8 K confirms this metamagnetic behaviour (Fig. 5). The abrupt increase of  $M$  at low fields and the saturation value of 1.06 BM for  $H > 3$  T evidence the presence of a ferromagnetic interaction between the spin doublets. The sigmoidal shape of the magnetization plot at very low fields (see inset of Fig. 5) with a value for the critical field ( $H_c$ ) of 130 G accounts for a weak antiferromagnetic interaction (ca.  $10^{-2}$  cm $^{-1}$ ).

The susceptibility maximum at  $H < H_c$  corresponds to the onset of a long range antiferromagnetic ordering. The value of the ordering temperature ( $T_c = 2.15$  K) is determined by the position of the maximum of the out-of-phase signal ( $\chi_M''$ ) (see Fig. 6).

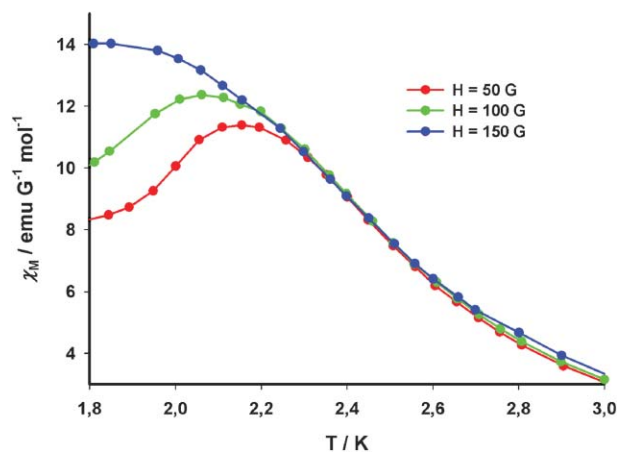


Fig. 4  $\chi_M$  vs.  $T$  plot for **1** at different applied magnetic fields.

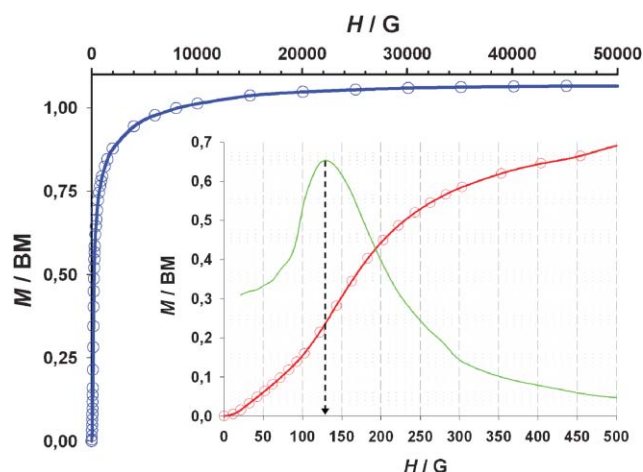


Fig. 5 Magnetization vs.  $H$  plot at 1.8 K. The inset shows the sigmoidal shape of the magnetization in the low field region together with the  $\partial M / \partial H$  (in green).

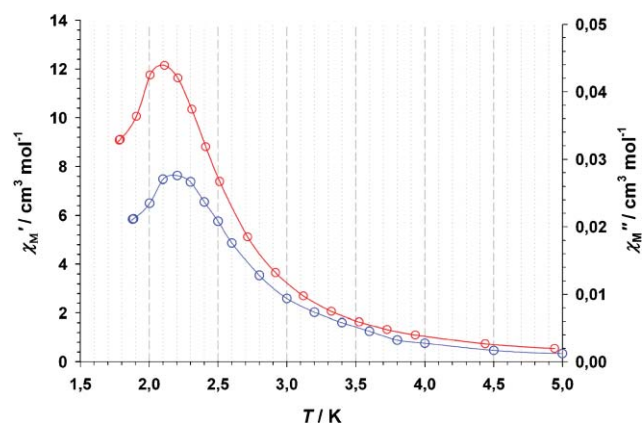


Fig. 6 In-phase (red) and out-of-phase (blue) ac signals of **1** in a 1 G field oscillating at 330 Hz without dc magnetic field: (○, ○) experimental data; (—) eye-guide line.

In the light of the above magneto-structural data of **1**, its magnetic behaviour would correspond to that of a ferromagnetically coupled square grid of copper(II) ions through a carboxylate-bridge in the *anti-syn* conformation, each layer

interacting antiferromagnetically with the adjacent ones. Consequently, the high temperature magnetic data of **1** were analyzed through the expression of the magnetic susceptibility by Baker *et al.* derived from the high-temperature expansion series for an isotropic ferromagnetic square lattice with interacting spin doublets.<sup>16</sup> The spin Hamiltonian is defined as  $\hat{H} = -J \sum_i \hat{S}_i \cdot \hat{S}_{i+1}$  and the series takes the form defined by eqn. (1)

$$\chi_M = \left( \frac{N\beta^2 g^2}{3k_B T} S(S+1) \right) \left[ 1 + \sum_{n \geq 1} a_n \frac{x^n}{2^n} \right] \quad (1)$$

where  $N$ ,  $g$ ,  $\beta$  and  $k_B$  have their usual meaning,  $x = J/k_B T$ ,  $J$  is the intralayer magnetic coupling and  $a_n$  are coefficients which run up to  $n = 10$ . Least-squares fit of the experimental data to eqn. (1) in the temperature range 5–300 K leads to  $J = +5.6(1) \text{ cm}^{-1}$ ,  $g = 2.12(2)$  and  $R = 8.9 \times 10^{-5}$  ( $R$  is the agreement factor defined as  $\sum_i [(\chi_M T)_{\text{obs}}(i) - (\chi_M T)_{\text{calc}}(i)]^2 / \sum_i [(\chi_M T)_{\text{obs}}(i)]^2$ ). The calculated curve matches very well the experimental data in the 5–300 K temperature range. The value of  $J$  for **1** is the largest one observed in the family of carboxylate(phenylmalonate)-bridged copper(II) complexes ( $J$  ranging from  $-0.59(1)$  to  $+4.44(5) \text{ cm}^{-1}$ )<sup>9,17</sup> and it is within the range of previously reported magnetic couplings of *anti-syn* carboxylate(malonate)-bridged copper(II) complexes.<sup>4</sup> The smaller value of  $\tau$  of the copper atom in the case of **1** when compared to other examples with the phenylmalonate ligand reduces the admixture of the  $d_{z^2}$  character in the  $d_{x^2-y^2}$  magnetic orbital and reinforces the magnetic coupling through the equatorial–equatorial exchange pathway, everything being similar.

The weak antiferromagnetic interaction (*ca.*  $10^{-2} \text{ cm}^{-1}$ ) between the ferromagnetically coupled layers of **1** leads to a 3D antiferromagnetic ordering with a  $T_c$  value of 2.15 K and accounts for the observed metamagnetic behaviour of this compound. The small value for the interlayer magnetic interaction is in agreement with the large interlayer metal–metal separation and most likely it is dipolar through-space in origin, given the lack of hydrogen-bonds and  $\pi$ -type interactions between the layers. This situation is similar to that observed in layered compounds of formula  $M_2(\text{OH})_3\text{X}$  [ $M = \text{Cu(II)}$  and  $\text{Co(II)}$ ;  $\text{X} = \text{organic anion}$ ] which exhibit dominant ferromagnetic in-plane interactions, and ferro- or antiferromagnetic inter-plane interactions depending on the interlayer separation. These studies have shown that the large spacings favour spontaneous magnetization.<sup>18</sup>

We can conclude that the introduction of the phenyl group in the malonate carbon skeleton and the presence of coordinated pyrimidine ligand lead to the formation of a hydrophobic layer in which both groups are involved. This aggregation allows the formation of the square grid sheet of carboxylate-bridged copper(II) ions. The analysis of the magnetic properties of **1** shows the occurrence of a metamagnetic behaviour with magnetic ordering below 2.15 K, which arises from the coexistence of intralayer ferro- and interlayer antiferromagnetic interactions.

Further work is planned concerning the preparation of phenylmalonate-copper(II) complexes with pym-like ligands in order to tune the interlayer separation and to correlate it with the nature and magnitude of the interlayer magnetic coupling.

We thank the Ministerio Español de Educación y Ciencia for funding through projects MAT2004-03112 and CTQ2004-03633 and J.P. is grateful for a predoctoral fellowship, AP2001-3322.

## Notes and references

† Synthesis of **1**: A methanolic solution ( $3 \text{ cm}^3$ ) of pyrimidine (0.5 mmol, 40 mg) was added dropwise to an aqueous solution ( $5 \text{ cm}^3$ ) of phenylmalonatecopper(II) (0.5 mmol, 120 mg) prepared as previously described.<sup>9</sup> Poor quality blue plate-like crystals suitable for X-ray diffraction were obtained from the resulting pale blue solution after a few days by slow evaporation at room temperature. Crystal data of **1**: the data collection was carried out on a Bruker-Nonius KappaCCD diffractometer at 293 K, using graphite-monochromated Mo-K $\alpha$  radiation ( $\lambda = 0.71073 \text{ \AA}$ ) by a  $\varphi$ - $\omega$  scan method. The structure was solved by direct methods and refined by least squares procedures on  $F^2$  using SHELX-97 (G. M. Sheldrick, program for the solution and refinement of crystal structures, University of Göttingen, Germany, 1997) incorporated into the WINGX software package (L. J. Farrugia, *J. Appl. Crystallogr.*, 1999, **32**, 659). Crystal dimensions  $0.75 \times 0.30 \times 0.05 \text{ mm}$ ;  $T = 293(2) \text{ K}$ ; monoclinic;  $P2_1$ ;  $a = 6.4460(16)$ ,  $b = 6.4460(12)$ ,  $c = 14.444(3) \text{ \AA}$  and  $\beta = 98.145(12)^\circ$ ;  $V = 594.1(2) \text{ \AA}^3$ ,  $Z = 2$ ; Flack parameter = 0.57(17);  $\rho_{\text{calc}} = 1.799 \text{ g cm}^{-3}$ ,  $2\theta_{\text{max}} = 31.94^\circ$ ; 3279 reflections measured of which 1980 are unique;  $R_1 = 0.1253$ ,  $wR_2 = 0.3153$  for  $I > 2\sigma(I)$ ; residual electron density 7.946 and  $-1.710 \text{ e \AA}^{-3}$ . These high peaks are located at *ca.*  $2.6 \text{ \AA}$  from the copper atoms and can be ascribed to unresolved twinning effects. All non-hydrogen atoms were refined anisotropically. Hydrogen atoms are placed geometrically and refined as a riding model. CCDC 297276. For crystallographic data in CIF or other electronic format see DOI: 10.1039/b602144a

‡ Dc and ac magnetic susceptibility measurements of **1** were performed on polycrystalline samples with a Quantum Design SQUID magnetometer. Corrections for the diamagnetism of the constituent atoms and the sample holder were applied.

- O. Kahn, *Molecular Magnetism*, VCH, New York, 1993 and references therein.
- V. Laget, C. Hornick, P. Rabu, M. Drillon and R. Ziessel, *Coord. Chem. Rev.*, 1998, **180**, 1533.
- M. Drillon, P. Panissod, P. Rabu, J. Souletie, V. Ksenofontov and P. Gutlich, *Phys. Rev. B*, 2002, **65**(10), 4404.
- J. Pasán, F. S. Delgado, Y. Rodríguez-Martín, M. Hernández-Molina, C. Ruiz-Pérez, J. Sanchiz, F. Lloret and M. Julve, *Polyhedron*, 2003, **22**, 2143.
- C. Ruiz-Pérez, Y. Rodríguez-Martín, M. Hernández-Molina, F. S. Delgado, J. Pasán, J. Sanchiz, F. Lloret and M. Julve, *Polyhedron*, 2003, **22**, 2111; J. Sanchiz, Y. Rodríguez-Martín, C. Ruiz-Pérez, A. Mederos, F. Lloret and M. Julve, *New J. Chem.*, 2002, **26**, 1624.
- I. G. de Muro, F. A. Mautner, M. Insausti, L. Lezama, M. I. Arriortua and T. Rojo, *Inorg. Chem.*, 1998, **37**, 3243.
- F. S. Delgado, J. Sanchiz, C. Ruiz-Pérez, F. Lloret and M. Julve, *Inorg. Chem.*, 2003, **42**, 5938.
- T. F. Liu, H. L. Sun, S. Gao, S. W. Zhang and T. C. Lau, *Inorg. Chem.*, 2003, **42**, 4792.
- J. Pasán, J. Sanchiz, C. Ruiz-Pérez, F. Lloret and M. Julve, *New J. Chem.*, 2003, **27**, 1557.
- J. M. Lehn, *Supramolecular Chemistry: Concepts and Perspectives*, VCH, Weinheim, 1995.
- C. Kaes, A. Katz and M. W. Hosseini, *Chem. Rev.*, 2000, **100**, 3553.
- M. Fujita, *Chem. Soc. Rev.*, 1998, **27**, 417.
- D. L. Caulder and K. N. Raymond, *Acc. Chem. Res.*, 1999, **32**, 975.
- A. W. Addison, T. N. Rao, J. Reedijk, J. van Rijn and G. C. Verschoor, *J. Chem. Soc., Dalton Trans.*, 1984, 1349.
- F. S. Delgado, J. Sanchiz, C. Ruiz-Pérez, F. Lloret and M. Julve, *CrystEngComm*, 2003, **5**, 48, 280.
- G. S. Rushbrooke, G. A. Baker and P. J. Wood, *Phase Transitions and Critical Phenomena*, vol. III, ed. C. Domb and M. S. Green, Academic Press, 1974.
- J. Pasán, J. Sanchiz, C. Ruiz-Pérez, F. Lloret and M. Julve, *Eur. J. Inorg. Chem.*, 2004, 4081; J. Pasán, J. Sanchiz, C. Ruiz-Pérez, F. Lloret and M. Julve, *Inorg. Chem.*, 2005, **44**, 7794.
- V. Laget, C. Hornick, P. Rabu, M. Drillon and R. Ziessel, *Coord. Chem. Rev.*, 1998, **178–180**, 1533.